Improving the quality of bio-oil by fast pyrolysis of acid leached and torrefied *Pinus radiata*

A thesis submitted in full fulfilment of the requirements for the Degree of Doctor of Philosophy in Chemical and Process Engineering at the University of Canterbury

Tansy Wigley

University of Canterbury

2015

Table of Contents

Table of Contents **ii**
Acknowledgements **v**
Abstract **vi**
1 Introduction **1**
1.1 Thesis scope and outline 2
2 Literature review of fast pyrolysis **4**
2.1 The basic fast pyrolysis process 4
2.1.1 Reactor types 4
2.1.2 Heat transfer 6
2.1.3 Char removal 6
2.1.4 Vapour condensation and recovery 7
2.2 Fast pyrolysis operating conditions 7
2.2.1 Reactor temperature 8
2.2.2 Residence time and fluidising gas 8
2.2.3 Biomass size and heating rate 9
2.3 Biomass constituents and their role during pyrolysis 10
2.3.1 Pyrolysis of cellulose 11
2.3.2 Pyrolysis of hemicellulose 13
2.3.3 Pyrolysis of lignin 14
2.3.4 Effect of extraneous compounds during pyrolysis 15
2.3.5 Effect of water during pyrolysis 16
2.4 Pyrolysis products 18
2.4.1 Non-condensable gas (NCG) 18
2.4.2 Char 19
2.4.3 Bio-oil 20
2.5 Biomass pretreatments and bio-oil upgrading 26
2.5.1 Biomass pretreatments for improving the bio-oil quality 27
2.5.2 Bio-oil upgrading 34
2.6 Conclusions 41
2.7 References 42
3 Reactor design and experimental development **52**
3.1 Design of a bench scale fast pyrolysis reactor 52
3.1.1 Nitrogen preheating 57
3.1.2 Biomass feeding, heating, and fluidisation 59
3.1.3 Cyclone design 68
3.1.4 Selective condensation 71
3.1.5 Vapour residence time in the pyrolysis reactor 77
3.1.6 Electrostatic precipitator, filters, and gas sampling 77
3.1.7 System control 80
3.2 Analytical techniques 81
3.2.1 Feedstock, pretreated biomass, and char analysis 82
3.2.2 Bio-oil analysis 85
3.2.3 Non-condensable gas analysis 91
3.3 Comparison of yields with other systems 92
3.4 References 93
4 Pretreatment development for bio-oil upgrading **96**

4.1 Inorganic catalysts 96
4.2 Moisture 97
4.3 Acid catalysts 97
4.4 Preliminary experiments to develop pretreatments 98
4.4.1 Removal of one catalyst by leaching or drying 99
4.4.2 Removal of two or more catalysts by leaching and drying 100
4.5 Pretreatment sequence 100
4.6 References 102
5 Pyrolysis of acid leached biomass 105
5.1 Leaching procedures 105
5.1.1 Small scale for leaching optimisation 105
5.1.2 Large scale leaching 106
5.1.3 Leaching procedure at elevated temperatures 107
5.2 Comparison between different leaching reagents 108
5.2.1 Pyrolysis of leached biomass 111
5.3 Effect of leaching temperature 113
5.3.1 Leaching at 90 °C 113
5.3.2 Leaching at 150 °C 116
5.4 Effect of leaching residence time 117
5.5 Effect of acid strength 118
5.6 References 120
6 Pyrolysis of torrefied biomass 122
6.1 Torrefaction procedures 122
6.1.1 Small scale torrefaction for optimisation 122
6.1.2 Large scale torrefaction 124
6.2 Biomass moisture content 125
6.3 Optimising torrefaction residence time 127
6.4 Optimising torrefaction temperature 127
6.4.1 Liquid and NCG composition 131
6.4.2 Pyrolysis of torrefied biomass 135
6.5 References 140
7 Pyrolysis of leached and torrefied biomass 142
7.1 Procedure for combined leaching and torrefaction 142
7.2 Effect of varying leaching conditions but constant torrefaction conditions 143
7.2.1 Leaching and torrefaction of biomass 143
7.2.2 Pyrolysis of leached and torrefied biomass 146
7.3 Effect of constant leaching conditions but varying torrefaction conditions 150
7.3.1 Leaching and torrefaction of biomass 150
7.3.2 Pyrolysis of leached and torrefied biomass 152
7.4 Practical implementation of the biomass pretreatments 158
7.4.1 Recycling torrefaction liquor for acid leaching 159
7.4.2 Replacing biomass rinsing with mechanical dewatering after leaching 160
7.4.3 Pretreatment of larger sized wood chips 161
7.5 Pyrolysis optimisation 164
7.5.1 Improvements to the pyrolysis system 164
7.5.2 Optimising the fluidised bed temperature 166
7.5.3 Optimising the cyclone temperature 171
7.5.4 Optimising the sand volume in the fluidised bed 175
7.6 Extensive analysis of the pyrolysis products from raw and pretreated biomass 179

7.6.1 Bio-oil properties 180
7.6.2 NCG properties 190
7.6.3 Char properties 191
7.7 Leaching leachate regeneration using pyrolysis chars 196
7.8 References 199
8 System balances and economics 202
8.1 Mass and elemental balances 202
8.1.1 Pyrolysis of raw biomass 202
8.1.2 Pyrolysis of pretreated biomass 205
8.2 Energy balances 210
8.2.1 Pyrolysis of raw biomass 211
8.2.2 Pyrolysis of pretreated biomass 212
8.3 Economics for raw and pretreated bio-oil production 213
8.3.1 Capital costs 214
8.3.2 Production costs 215
8.3.3 Sensitivity analysis 218
8.4 References 219
9 Conclusions and recommendations 220
A3 Appendix 3 225
A4 Appendix 4 263
A7 Appendix 7 264
A8 Appendix 8 275

Acknowledgements

I would like to thank my supervisor Prof. Shusheng Pang for his support and guidance over the past three and a half years. He encouraged and trusted me to investigate biomass pretreatments, even though the thesis brief intended catalytic pyrolysis. His generosity in providing me with a scholarship meant I could focus all my attention on research. I am also very thankful that he supported my efforts to attend two international conferences and three domestic conferences. Meeting world renowned pyrolysis experts at the international symposium on analytical and applied pyrolysis in Birmingham was an extremely valuable experience and contributed to improvements in my research.

I would also like to thank my co-supervisor, Dr Alex Yip. Although I did not use catalysts in my research, as intended initially, Alex still provided valuable advice and support. He was especially helpful providing advice for publications.

This research required the construction of a pyrolysis system and extensive analytical equipment. This meant I required wide range of technical and analytical support. From chemical and process engineering: Leigh Richardson, Glenn Wilson, Tim Moore, Stephen Beuzenberg, Dr. Michael Sandridge, Tony Allen, Frank Weerts, and Stephen Hood. From electrical engineering: Paul Agger. From chemistry: Dr. Marie Squire, Dr. Sally Gaw, and Dr. Alexander Goroncy. From mechanical engineering: Mike Flaws. From forestry engineering: Dr. Clemens Altaner and Nigel Pink. From Lincoln University: Lynne Clucas and Jason Breitmeyer. From Scion: Dr. Kirk Torr, Dr. Ferran De Miguel Mercader, and Daniel Van Der Pas. From CRL Energy limited: Dr. Tana Levi.

I would like to thank my family, who provide me with encouragement, a car, meals, and much more during my studies. I would like to thank my friends who diligently listened to my conference rehearsals and provided support over the years. Last but certainly not least, I would like to thank Chris White for leaving his job in Wellington and relocating to Christchurch to be with me while I studied. Your love and support made this an extremely enjoyable time.

Abstract

Fast pyrolysis is a thermochemical process used to convert biomass into a liquid fuel termed bio-oil. The high organic acid, water, oxygen, and inorganic content in bio-oil make it unstable and cause corrosion issues. Consequently, it is widely accepted that bio-oil must be upgraded to be considered a realistic candidate as a large scale transport fuel. Upgrading bio-oil through catalytic cracking and hydrotreating has been extensively researched, but there are high costs and low yields associated with both techniques due to the difficulty in upgrading such a diverse mixture of compounds. Pretreating biomass prior to pyrolysis was investigated in this thesis to improve the bio-oil quality to simplify current upgrading techniques or for direct use as a marine fuel. Three catalytic compounds naturally inherent in biomass were identified to cause undesirable reactions during pyrolysis; these were inorganics, organic acids (acetyl compounds), and water. A pretreatment sequence incorporating both acid leaching and torrefaction was developed to reduce/remove these compounds from biomass prior to pyrolysis.

A fast pyrolysis reactor with a maximum capacity of 1 kgh^{-1} of feed biomass was designed, constructed, commissioned, and used for pyrolysis. The pyrolysis reactor was a fluidised bed with nitrogen as the fluidising gas and silica sand as the fluidising medium. Char was separated in a high efficiency cyclone and bio-oil vapours were condensed in a series of three shell and tube condensers. Remaining aerosols in the vapour stream were collected in an electrostatic precipitator and filter. Pyrolysis at 500 °C of *Pinus radiata* yielded 46.9±0.5 wt% (dry basis) bio-oil, which contained 3.5±0.4 wt% acetic acid and 24.0±1.2 wt% water.

Acid leaching targeted the biomass's inorganic content. The acidic liquor produced during torrefaction was rich in acetic and formic acid; the viability of leaching biomass with this solution was demonstrated by comparing the leaching efficiency of acetic and formic acid to nitric, sulfuric, and hydrochloric acid. Similar leaching efficiencies were achieved for the organic and mineral acids. Therefore, the optimal leaching conditions were summarised as leaching at 30 °C with 1% acetic acid for 4 h. This reduced the biomass's inorganic content from 0.41±0.04 to 0.16±0.02 wt% without altering its structural composition. Pyrolysis of biomass leached at the optimal conditions yielded 54.6 wt% (dry basis) bio-oil, which contained 1.9±0.1 wt% acetic acid and 17.1±1.3 wt% water. This indicates that secondary reactions during pyrolysis were reduced in the inorganic limited environment, which was confirmed by the higher levoglucosan yield of 7.83% for bio-oil from leached biomass, opposed to 2.30% for bio-oil from raw biomass.

Torrefaction targeted the biomass's moisture and acetyl content, and was optimised between 220 and 290 °C. For torrefaction at 290 °C for 20 min, the acetyl content in the biomass was reduced from 1.51 to 0.43 wt% and the oxygen content decreased from 43.1 to 35.7%. However, the mass loss during torrefaction was significant at 38.5 wt%. Therefore, the optimal torrefaction temperature was 270 °C for 20 min; pyrolysis of the torrefied biomass yielded 46.1 wt% bio-oil, which was equivalent to an overall yield of 38.9 wt% bio-oil, taking the into account the mass loss during torrefaction. The bio-oil contained 0.6±0.4 wt% acetic acid and 6.1±0.3 wt% water. It was slightly enriched in levoglucosan (3.64%) and aromatics compared to bio-oil from raw biomass. Torrefaction increased the char yield at the expense of bio-oil due to stable carbon-carbon crosslinks formed by dehydration of biomass polymers during torrefaction.

Acid leaching and torrefaction were integrated and optimised. The optimal pretreatment sequence was summarised as 1% acetic acid leaching at 30 °C for 4 h, followed by torrefaction at 270 °C for 20 min. Next, main pyrolysis operating conditions (pyrolysis temperature, cyclone temperature, and silica sand loading in the fluidised bed) were optimised for raw and pretreated biomass in terms of the pyrolysis yield and operability. The pyrolysis temperature was optimal at 450 °C for both raw and pretreated biomass. Pyrolysis of pretreated biomass required 75 g sand in the fluidised bed to prevent char agglomeration, while pyrolysis of raw biomass only required 25 g. The cyclone was optimal at 400 and 425 °C for pyrolysis of raw and pretreated biomass respectively. Pyrolysis of raw biomass yielded 55.3±2.5 wt% bio-oil, 25.0±1.0 wt%, char, and 12.5±1.2 wt% non-condensable gas, while the corresponding yields from pyrolysis of pretreated biomass were 57.8±1.7 wt% bio-oil, 23.7±2.6 wt%, char, and 11.5±0.7 wt% non-condensable gas.

Mass balances gave a 7.20±0.27 and 6.17±0.49% discrepancy for pyrolysis of raw and pretreated biomass respectively. The discrepancy was due to limitations in measuring the pyrolysis products. Integrating acid leaching and torrefaction as biomass pretreatments significantly reduced undesirable heterogeneous and homogeneous reactions during pyrolysis. This improved the bio-oil's quality in terms of the organic acids (2.46±0.13 to 0.16±0.05%), water content (16.8±1.6 to 3.6±0.3 wt%), aldehydes (1.58±0.04 to 0.50±0.10%), high molecular weight compounds (10.2±4.6 to 4.2±0.4%), inorganics (0.162±0.056 to 0.091±0.030 wt%), and stability. The oxygen content of the bio-oil was only reduced on a wet basis as torrefaction reduced the bio-oil's oxygen content, but acid leaching increased it.

An economic analysis indicated 10.39 MW of bio-oil production from raw biomass required a capital investment of $NZ 53,800,000 and could produce bio-oil at $NZ 29.87 per GJ. To produce 11.44 MW of bio-oil from pretreated biomass required a capital investment of $NZ 46,300,000 and could produce bio-oil at $NZ 29.67 per GJ. Both systems were competitive with price of No. 6 heavy fuel oil at $NZ 30.92 per GJ in the second quarter of 2015, but more expensive than Brent crude oil and WTI crude oil at $NZ 13.78 and 12.78 per GJ respectively. Energy balances indicated that non-condensable gases and a portion of the char would be sufficient to supply the heating requirements during pyrolysis, with an energy surplus of 2.69 and 4.47 MW for pyrolysis of raw and pretreated biomass respectively. It is recommended to investigate the use of calcium oxide in the fluidised bed to reduce the bio-oil's oxygen content, to further improve its stability and energy density.

This study indicated that both acid leaching and torrefaction of biomass were required to limit homogeneous and heterogeneous reactions of pyrolysis vapours, which are catalysed by water, organic acids, and inorganics. Leaching is required as inorganics are highly catalytic during pyrolysis, but leaching is expensive; torrefaction reduces the cost of acid leaching by providing the leaching reagent and eliminating the need for biomass rinsing after leaching. Torrefaction also reduces the biomass grinding costs, which is required to offset the additional process costs for pretreating biomass. Pyrolysis of solely torrefied biomass is constrained by the high torrefaction temperatures required for significant bio-oil improvements, leading to low yields due to the mass loss during torrefaction and increased char formation during pyrolysis. Finally, the reduced thermal conductivity of dry torrefied biomass increases the time for secondary reactions with inorganics during pyrolysis, which become concentrated in torrefied biomass. Therefore, the integration of both pretreatments is required to produce a high quality crude bio-oil cost effectively.

1 Introduction

Since their discovery, fossil fuels have provided humans with an abundant and inexpensive energy source other than primarily biomass. However, there are now concerns over remaining fossil fuel reserves [1, 2], and the combustion of fossil fuels is controversial with many claims that releasing sequestered carbon is causing global warming [3]. The atmospheric carbon dioxide concentration due to emissions from fossil fuel combustion increases by approximately 2% per year [2, 4], and is expected to reach up to 550 ppm by 2050 [5]. Consequently, attention has been focused again on biomass, which has the potential to provide renewable and carbon neutral liquid fuels [3].

Drop-in fuels produced from biomass are likely to be a short to medium term solution as an alternative transport fuel because existing infrastructure can be used; alternative engines may be developed as a long term solution [6]. Utilising existing infrastructure is beneficial for improving the sustainability for biofuel processes [7]. Presently, first generation biofuels are produced at a commercial scale; however corn and sugarcane feedstocks compete with food resources. Second generation biofuels, while not eliminating land usage issues, reduce them significantly as lignocellulosic biomass (wood) is not directly competitive with food production [8, 9].

There are abundant biomass resources in New Zealand due to the fertile soils, the suitable growing climate, and well managed forest plantations. In 20011, 43% of land in New Zealand was used for pasture and arable farming; 24% remained as natural forests; 6% was plantation forests; and the remaining 27% was non-forested land. The 6% as plantation forests equates to 1.7 million hectares (MHA) [10]. Biomass currently provides 10% of New Zealand's energy supply, with the potential to supply 25% of New Zealand's energy requirements and 30% of the transportation fuel requirements by 2040 [11]. The plantation forests in New Zealand are listed Table 1-1 Table 1-1; *Pinus radiata* is the predominant lignocellulose source with over 25 Mm^3 of round wood harvested per year, and of this, 25% becomes wood residues. Wood residues are mainly used within the wood processing industry, but additional forest residues are not extracted from the landing site [12], and are available for bioenergy production. Forest residues are approximately 4-6% of the total harvested volume plus additional cutover trees (trees that break during harvesting and are left at the skid site) [13]. Scion [13] estimated the total energy from biomass not currently used in the wood processing industry in 2008 as 18.3 PJ from forest residues and 8.8 PJ from wood residues. New Zealand already has many sources of renewable electricity (solar, hydro, wind, and geothermal [14, 15]); therefore attention should be focused on producing a transportation fuel from the available wood residues.

Table 1-1: Biomass plantations in New Zealand in 2012, adapted from FOA [10]

Biomass species	Area (Ha)
P. radiata	1,543,000
Douglas-fir	108,000
Cypress Species	10,000
Other exotic softwoods	24,000
Eucalyptus species	23,000
Other exotic hardwoods	13,000

Biofuels produced from woody biomass are normally clean burning fuels due to the naturally low sulfur and nitrogen content in the biomass. Biomass absorbs carbon dioxide via photosynthesis; therefore biofuels can be carbon neutral if petroleum fuels are not used during the growing, collection, transportation, processing, plant construction, development, or decommissioning stages [16]. Using wood residues to produce a biofuel also reduces the amount of waste going into landfills. However, if wood residues are exported from their growing site, soil erosion due to stump removal and nutrient depletion in the soils has to be considered as the continuous large scale production of forest plantations could reduce soil fertility levels, thus leading to increased use of agrichemicals [12].

Lignocellulose biomass can be thermochemically converted into energy via gasification [14, 17, 18], pyrolysis, liquefaction [3, 19], or combustion [14, 20]. Pyrolysis is also the initial process in gasification and combustion; where primary pyrolysis products are then thermally decomposed or combusted [21]. No process currently stands out as the superior option [22], but pyrolysis and liquefaction are the only processes that directly produce a liquid fuel [23, 24]. The high pressure technology associated with liquefaction is thought to be too sophisticated for the thermal conversion of biomass to biofuels [19]; therefore pyrolysis is one of most competitive candidates for production of a second generation liquid fuel, and is the focus of this thesis.

1.1 Thesis scope and outline

The objective of this thesis was to produce a higher quality bio-oil from fast pyrolysis of pretreated biomass. The thesis is broken down into 9 chapters. Chapter 1 covers the introduction and thesis scope and outline. Chapter 2 is an extensive literature review of biomass fast pyrolysis. This investigates reactor types, reactor operating conditions, pyrolysis of biomass constituents, and pyrolysis products. Finally, the literature review introduces techniques used to upgrade the quality of bio-oil. This indicated that upgrading through conventional hydrotreating and catalytic cracking is unlikely to be economical in the short term. Instead, there was potential to pretreat the biomass prior to pyrolysis to prevent the formation of undesirable products. The literature review is broad and comprehensive as all areas associated with pyrolysis must be understood in order to manipulate biomass to improve the bio-oil quality.

Chapter 3 details the fast pyrolysis reactor design, construction, and commissioning. Analytical techniques used for solid, liquid, and gas analysis are detailed next, and then finally, the properties of bio-oil produced using the commissioned system are compared to similar systems in literature.

Chapter 4 is where the innovative research of this thesis begins. This part of the study experimentally investigated biomass pretreatments for the reduction/removal of three naturally occurring biomass catalysts: organic acids, water, and inorganics that were identified in Chapter 2. The aim of removing these catalysts from biomass was to improve the quality of the bio-oil being produced directly from pyrolysis and reduce inconsistencies in the bio-oil related to the variable nature of biomass. The effect of reducing/removing one,

two, or all three biomass catalysts was examined in terms of the bio-oil yield and properties. Results showed the removal of all three catalysts produced a superior bio-oil compared to no pretreatment or the removal of one or two of the catalysts. The techniques used for organic acids water, and inorganic reduction/removal were solely for proof of concept, but were not practical at large scale. Thus, finally in Chapter 4, a pretreatments sequence consisting of acid leaching and subsequent torrefaction was developed to replicate the reduction/removal of these biomass catalysts. The pretreatments were designed to utilise by-products from pyrolysis and minimise waste; therefore lessening additional process costs.

Chapter 5 investigates the effect of solely acid leaching biomass prior to pyrolysis. A high concentration of organic acids is produced during torrefaction; therefore the potential of recycling this stream as the leaching reagent was also studied in this chapter. The efficiency of leaching with typically used mineral acids was compared to leaching with organic acids and the optimal leaching conditions were determined. Chapter 6 investigates the impact of biomass torrefaction on the pyrolysis products and yields, and then predicts the optimal torrefaction conditions. Chapter 7 investigates the effect of combining acid leaching and torrefaction. This firstly used the optimal torrefaction conditions determined in Chapter 6 and varies the acid leaching reagent. Next, acid leaching was held constant at the optimal conditions determined in Chapter 5, while torrefaction was varied. Once the pretreatment sequence was optimised, experiments were carried out to improve their practical implementation, such as pretreating larger wood chips; not rinsing biomass after leaching; and using the actual torrefaction liquor for leaching opposed to a synthetic solution. Next in Chapter 7, bio-oil produced using the optimal pretreatment sequence was compared to raw bio-oil when key pyrolysis conditions are varied. The optimal pyrolysis conditions were reported for pyrolysis of raw and pretreated biomass, and then an extensive analysis on the two optimised systems was carried out. Selective condensation of pyrolysis vapours was investigated for bio-oils produced at the optimal conditions. Finally, in Chapter 7, the use of pyrolysis chars to regenerate leachate produced during acid leaching was examined.

Mass balances for bio-oil produced from both raw and pretreated biomass at the optimal conditions pyrolysis conditions are detailed in Chapter 8. This is followed by an energy balance for both systems and finally an economic analysis was performed to compare the systems. Chapter 9 concludes the thesis, with a summary of key results and recommendations for future research. Additional information for some chapters is located in the appendices which are numbered according to the chapter they refer to.

2 Literature review of fast pyrolysis

Fast pyrolysis of biomass has been extensively studied in the last two decades, but there are still many areas that require additional research [24]. The low quality of crude bio-oil limits its use to direct stationary combustion applications or as a densification technique to reduce transportation costs of shipping wood to a bio-refinery [25, 26]. A recent review by Butler *et al.* [6] concluded that fast pyrolysis is on the verge of commercialisation but upgrading and refining bio-oil to a diesel standard is still confined to laboratory and pilot scale research. Other barriers that restrict large scale production include high plant capital costs, cheaper fossil oil, less developed technology, and a long investment payback period [12]. Further research is required in these areas, especially regarding the development of a higher quality bio-oil at reduced costs, which is the focus of this research. Predicting the bio-oil yield and composition is hard due to the nature of the pyrolysis system: there are many natural catalysts in biomass that affect the products formed. In order to predict how one variable influences pyrolysis, extensive knowledge of whole process is required; therefore this literature review details the influence of the biomass composition and reactor conditions on the pyrolysis process and products formed, followed by analysing potential upgrading procedures. This knowledge was then applied when developing biomass pretreatments.

2.1 The basic fast pyrolysis process

Pyrolysis can be implemented on virtually any biomass source. The process involves heating in the absence of oxygen to produce a liquid (bio-oil), non-condensable gas (NCG), and solid product (char). Heating in an oxygen-free atmosphere that allows biomass polymers to depolymerise but prevents combustion [27]. Traditionally pyrolysis was used to produce charcoal. However, in the last 50 years fast pyrolysis has been developed to target high liquid and low char yields. Fast pyrolysis requires moderate temperatures between 450-550 °C, short vapour residence times of 1-5 s, fast heating rates, and rapid quenching of the vapours [18]. Altering the pyrolysis conditions varies the yield of bio-oil, char, and NCG [28]. Typical yields of these products are 60-75% of bio-oil, 10-20% of char, and 10-20% of NCG. Standard fast pyrolysis systems consist of biomass drying, grinding, pyrolysis, solids separation, vapour condensation, and smoke recovery. Rapid heating of the biomass particles is crucial to obtain fast pyrolysis but temperatures must not be excessive otherwise extensive thermal decomposition of pyrolysis vapours occurs. Bio-oil is normally produced to supplement transportation fuels, but can also be used to densify biomass for later large scale gasification to produce a syngas for liquid fuel synthesis (such as Fischer-Tropsch synthesis); hydrogen production via a water-gas shift reaction; or methanol production via methanol synthesis [3].

2.1.1 Reactor types

The strict requirements of fast pyrolysis makes reactor design challenging. The rapid heating rate mandates a relatively small particle size and limits possible reactor configurations [29]. To reduce secondary reactions, a

short residence time for vapours is required which restricts the reactor height. There is not currently a type of reactor that stands out as the most suitable for fast pyrolysis [6], instead the reactor chosen depends on the specific application. Reactors have been extensively reviewed in this study, but only a summary of possible configurations are listed in Table 2-1. Of these, four are generally used: shallow bubbling fluid bed (fluidised bed), vacuum reactor, ablative plate, and circulating fluid bed [29]. Only fluidised bed and circulating fluid bed reactors have produced bio-oil at a commercial scale to date [6, 22]. Additionally, fluidised bed reactors are most commonly found in literature for laboratory scale system.

Table 2-1: Summary of pyrolysis reactor types

Reactor Type and examples	Status [30]	Comments
Fixed bed [31-33]	Pilot (20 – 200 kgh^{-1})	• Low bio-oil and high char yields [33] • Secondary reactions lead to high water content [32] • Fast pyrolysis conditions are hard to obtain • Heat transfer issues when scaled • Low amounts of inert gas required • Small particles required (<2mm) to improve the heat transfer rate
Fluidised bed [29, 34-40]	Commercial (2 – 20 th^{-1})	• Good char separation produces a bio-oil with consistent quality and high bio-oil yields [18, 20, 41] • Simple, easy to operate, robust and easy to scale [42] • Large amount of inert gas required • Small particles required (<3mm) [3, 20]
Circulating fluid bed [33, 43]	Commercial (2 – 20 th^{-1})	• High bio-oil yields obtained [30], unless char is recycled due to ash build up [3, 29] • Complex hydrodynamics [3]; large amount of inert gas required • High heat transfer and good temperature control [3, 20] • More compact than fluidised beds but higher char abrasion [22, 44]
Ablative [22, 29, 45]	Demonstration (200 -- 2000 kgh^{-1})	• High bio-oil and char yields [3] • Heat is transferred directly from the reactor walls to the biomass [3] • The system is limited by the rate of heat supply to the reactor and the surface area for heat transfer [3, 18] • No fluidising gas required but complex as moving parts at a high temperature [20, 22] • Biomass size is not limited [3, 18]
Entrained flow [46]	Laboratory (1 – 20 kgh^{-1})	• Yields are low if char is used as heat carrier but high if sand is used as the heat carrier [20, 47] • Small particles required (<2mm) and requires a carrier gas • High heat transfer if char is used but medium if carrier gas is the heat transfer mechanism • Heat can also be supplied by directly heating a carrier gas by combustion [33]
Rotating cone [22]	Laboratory (1 – 20 kgh^{-1})	• Bio-oil yields of 60 to 70 wt% can be obtained [20] • Type of ablative plate reactor, thus complex as moving parts at high temperatures • Small particles required (<1mm) [3] • Medium heat transfer rates obtained [48] • Carrier gas requirements are less than for a fluidised bed [20]
Auger [49, 50]	Pilot (20 – 200 kgh^{-1})	• High rate of secondary reactions due to long gas residence times [49] • Moving parts at high temperatures makes the system complex • Larger particles can be used but give a lower quality bio-oil • No or low amounts of carrier gas required • Prone to poor heat transfer rates [49, 50]
Vacuum [44, 51]	Laboratory (1 – 20 kgh^{-1})	• Bio-oil yields of 35 to 50 wt% obtained but with a high water content when compared to bio-oil from a fluidised bed [47]. Char yields were also high [20] • Vapours are removed as soon as they are produced [18] • Complex, expensive to run, and hard to scale up [29, 47] • No carrier gas required [47] • Poor heat and mass transfer, but can be improved by implementing a heat carrier [29, 47] • Bio-oil has a low solids content and less aerosols are produced [44]
Microwave [52]	Laboratory (1 – 20 kgh^{-1})	• High yield of phenols can be obtained with activated carbon catalysts [52] • Induce heat at the molecular level by direct conversion of the electromagnetic field into heat • Complex, expensive to run and hard to scale • No carrier gas required • Good heat transfer rate as heating from the particle centre [52]

2.1.2 Heat transfer

Significant temperature gradients produced within the biomass particle during heating can cause undesirable pyrolysis reactions [53]. The biomass heating rate depends on both the reactor configuration and the dominant mode of heat transfer. Two heat transfer mechanisms must be considered: from the heat source to the heat transfer medium and the from the medium to the biomass particle [54]. The heat transfer medium can be hot gases, heated reactor walls, hot sand, or combinations of these. Typical heat transfer modes for different reactor types are given in Table 2-2. Convective heat transfer using a hot carrier gas is the simplest ways to introduce heat into a pyrolysis reactor [48], although the heat transfer rate between the hot gas and biomass particles (gas-solid heat transfer) is low compared to conductive solid-solid heat transfer rates [55]. Models have been developed to predict the heat required for pyrolysis but data on specific heat capacity of biomass and char is limited above 150-200 °C due to the onset of pyrolysis [55].

Pyrolysis processes can be energy self-sufficient if char and NCGs are combusted to provide the heat required for pyrolysis and biomass drying [23, 41]. The moisture content of the biomass should be reduced to <10 wt% prior to pyrolysis, this improves the heating rates during pyrolysis as it takes 3.43 $MJkg^{-1}$ to heat and evaporate water at the reactor temperature but only 2 $MJkg^{-1}$ is required to heat dry biomass to the pyrolysis temperature [56].

Table 2-2: Heat transfer mode for different reactor configurations, adapted from Bridgwater *et al.* [54]

Reactor type	Conduction (%)	Convection (%)	Radiation (%)
Ablative	95	4	1
Circulating fluid bed	80	19	1
Fluidised bed	90	9	1
Entrained flow	4	95	1

2.1.3 Char removal

Char is carried out of the reactor with the pyrolysis vapours and carrier gas in most systems. It is commonly agreed that char must quickly be separated from the vapours to prevent cracking reactions, as catalytic inorganic minerals become deposited in the char [57, 58]. Cyclones are normally used for the initial separation of char and entrained sand particles [20, 41]. They are generally less effective than other types of separation equipment but are simple, can run at high temperatures, and will not reduce bio-oil yields [59]. High performance cyclones can remove char particles down to 5 µm, and then fines can be captured with hot gas filters or filtered from the bio-oil after condensation [60].

Hot gas filters can reduce the bio-oil solids concentration to 0.005 wt% for fast pyrolysis of *P. radiata*, this also reduces the bio-oil's inorganic content [20, 58], particularly of sodium and magnesium which both have a lower volatility than potassium; therefore are more likely to remain in the char [57]. Build-up of the char cake on hot gas filters increases the vapour residence time, exposes vapours to catalytic char, and causes a significant pressure drop over the filter. Overall this has the potential to reduce the bio-oil yield by 5-20% [20, 57]. Conventional baghouse filters can be used as hot gas filters but pulsing will not effectively remove the sintered char cake from the filter cloth. Oxidative regeneration can be used instead [61], but this leaves

an ash residue that exacerbates the rate of future filter binding [60]. Sintering can be prevented somewhat by removing the preceding cyclone; generating the formation of a less dense filter cake [60], although the throughput of the filter is much higher. Hoekstra *et al.* [57] used the sand entrained in the char to clean the filter and observed no significant pressure drop.

2.1.4 Vapour condensation and recovery

Vapours should be condensed rapidly after char separation to limit thermal cracking reactions [62]. Condensation is inherently difficult because the vapours consist of a complex mixture of aerosols, condensable bio-oil, carrier gas, and NCGs [20]. Aerosols are produced from high molecular weight compounds that are either not a vapour at the gas exit temperature or from compounds that do not have time to vaporise before entrainment in the carrier gas flow [55]. Specialised heat exchangers can initially quench vapours but more sophisticated devices are required to collect the majority of aerosols [41]. Potential heat exchangers include: shell and tube, spiral tube, spiral plate, plate fin, gasket plate, and direct contact [63]. Blockages occur easily from the viscous bio-oil or entrained char in heat exchanges configurations with small or curved vapour paths such as in spiral tubes, plate fin, and spiral plate heat exchangers. Laboratory systems can utilise single pass shell and tube condensers without significant blockages, however for larger systems, direct quenching in an oil or in an immiscible hydrocarbon solvent is widely implemented [20].

Aerosols and vapours which are not condensed in the heat exchangers require additional equipment for capture. Removal of these compounds is commonly accomplished using electrostatic precipitators (ESPs), filters, scrubbers, or demisters [64]. Scrubbers require large volumes of sprayed fluids with high velocities in the active zone of the apparatus [65]. Filters cause pressure drops, have regeneration issues, and are prone to blockages. Cotton, stainless steel, or glass wool filters are commonly used for laboratory scale systems. ESPs are more expensive in relation to the capital and operating costs [60], and the polarity of bio-oil can cause arc-over in the ESP [66]. Charging and removal of the droplets in two separate electric fields can improve the efficiency [65]. Normally a negative corona is produced as this allows for higher voltages before arc-over occurs and can help reduce fouling on the electrode [67, 68].

There are two types of demisters commonly available: a dynamic cyclone and rotational demister. The dynamic cyclone can separate aerosols down to 2 μm [69]. Rotational particle filters can be simulated at a laboratory scale with a centrifuge [42]. Chen *et al.* [70] developed a cyclone shaped rotary demister with an internal rotating element. The separation efficiency was high as droplets were forced to travel a relatively long distance, but the pressure drop was large when the rotational speed was above 2000 rpm or the inlet gas velocity was high.

2.2 Fast pyrolysis operating conditions

Fast pyrolysis yields are affected by the operating temperature, residence time, heating rate, biomass particle size, and gas flow rate. These parameters are examined in detail as the knowledge is essential for the reactor

design and operation. The optimal pyrolysis conditions are normally set to be those that produces the highest liquid yield; however these are not necessarily the conditions for the highest quality bio-oil [35, 71].

2.2.1 Reactor temperature

The temperature of pyrolysis effects yields more than the heating rate or particle size [72]. Changing the temperature dramatically modifies the compounds produced by altering the activation energies reached in the system [73]. The optimum temperature normally ranges from 450-550 °C, with lower temperatures enhancing char formation and higher temperatures increasing secondary vapour cracking reactions and NCG production [34, 74]. The effect of the reactor temperature on the product composition can be minimised with short residence times to reduce secondary reactions [72]. The increased bio-oil yield above 400 °C can be attributed to an increase in lignin derived compounds [35].

From the literature reviewed, the following trends were generalised for bio-oil with respect to pyrolysis temperature: the inorganic content increases with temperature due to inorganic volatilisation [34, 71]; viscosity increases via vapour polymerisation reactions [35, 74]; and the oxygen content decreases due to increased carbon dioxide formation [34, 72]. At higher pyrolysis temperatures the composition of the liquid product is altered with increased aromatics [34, 72], carbohydrates, and polyaromatic hydrocarbons but decreased carbonyls, hydroxyl, and alkyl hydrocarbons [34]. The concentration of phenol and its derivatives can vary with the pyrolysis temperature as higher temperatures tend to increase secondary reactions to break down phenol oligomers but the lignin fraction pyrolysed to a liquid also increases at higher pyrolysis temperatures [35, 72]. The conversion of lignin derived guaiacols to catechols increases, opposed to O-cresols and phenols [34].

2.2.2 Residence time and fluidising gas

A short vapour residence time limits secondary reactions [70]. These occur by pyrolysis vapours reacting homogeneously before condensing, or heterogeneously with inorganics, char, catalysts, or the hot reactor walls. Researchers have purposely extended the vapour residence time and the pyrolysis temperature [29, 66, 75]. Results from these studies indicated that inorganics and the pyrolysis temperature effect yields more than the residence time.

Hoekstra *et al.* [75] varied the amount of sodium (Na) and potassium (K) in biomass to test the influence of alkali metals on heterogeneous reactions. They varied the time and temperature of char and bio-oil vapour hold-up. Results indicated that in the presence of alkali metals, the bio-oil yield was severely affected by char hold-up. However without alkalis present, and thus limited heterogeneous reactions, the bio-oil yield was only affected when the holding temperature was above 400 °C. This applied for vapour residence times of up to 15 s, indicating extended char hold-up did not cause homogeneous cracking reactions below 400 °C. When the char holding temperature was increased to 500 °C, a slight decrease in the bio-oil yield and increase in the NCG yield was observed. This trend was more pronounced when the char holding

temperature was further increased to 550 °C. The study observed a slight change in the bio-oil composition even at holding temperatures of 400 °C, with a decrease in pyrans and an increase in non-aromatic aldehydes. The water and levoglucosan content in the bio-oil was not affected for any holding temperature; therefore dehydration reactions occurred through mainly heterogeneous reactions with inorganic catalysts. The molecular weight and pyrolytic lignin content of the bio-oil decreased slightly with extended char holding times. It was concluded that for systems with low inorganic concentrations, the vapour residence time will not affect the pyrolysis products significantly at 400 °C.

The fluidising gas flow rate determines the residence for biomass, char, and vapours in the pyrolysis reactor. The gas flow rate has to be sufficient to carry the char from the reactor, but not sufficient to remove biomass before it has finished reacting [76, 77]. The minimum fluidisation velocity for bubbling bed reactors depends on the properties and sizes of the bed material as it is denser than the biomass and char. The operational gas velocity can be set based on the minimum fluidisation velocity of the bed material. This generally ranges from 3 to 4.2 times the minimum fluidisation velocity, but should be lower than the terminal velocity of the bed material [71, 78]. The gas flow rate is also influenced by the biomass feed rate: higher feed rates produce more volatiles, which increases the total gas flow rate [40].

2.2.3 Biomass size and heating rate

Particle size effects the heating rate of biomass in a constant heating environment [48]. The low thermal conductivity of biomass generates a greater temperature gradient if larger particles are used as pyrolysis occurs initially at the particle's surface and moves inwards as the particle is heated. Internal vapours have to travel through the outer layer of catalytic char to escape [54, 71]. The char layer can also act as an insulator to reduce further heating [44]. Heat and mass transfer studies show that the fibrous structure of lignocellulosic materials strongly favours transport in the axial direction with thermal conductivities of 0.1 $Wm^{-1}K^{-1}$ (along the grain), compared to the transverse direction with thermal conductivities of 0.05 $Wm^{-1}K^{-1}$ (radial or tangential direction, across the grain) [79]. Rapid heating rates cause concentration and/or pressure gradients of volatiles across the biomass particle. This enhances diffusion and/or forced convection of the volatiles out of the particle to give shorter residence times of the volatiles in the biomass particle [80]. Silica sand is typically used in fluidised systems to increase the heat transfer rate. In an entrained flow reactor, the silica content of the bio-oil increased from 112 to 330 ppm when silica sand was used as the fluidising medium [81].

Comminution of biomass to target given particle sizes can be through milling, grinding, shredding, chipping, kneading, pulverisation, steam explosion, rotary veneer, or crushing of unprocessed biomass [79, 82, 83]. Grinding may affect the cellular structure of biomass which can influence the pyrolysis products [84]. The grinding costs increase nearly exponentially as the size required decreases. To reduce particles to 75 µm, the energy for milling can equal the entire energy content of the biomass feed [79]. Low moisture contents reduce the energy consumption for grinding that can be achieved via shattering (hammer mills), while shearing techniques (rotary veneers) are more efficient for higher moisture contents [82]. Therefore, the

comminution method must consider the moisture content of the biomass. Normally, particle size should not be smaller than 300 μm to prevent fine char particles agglomerating on filters [58]. Commercial scale pyrolysis systems require larger particles due to the grinding cost. The particle size is then limited by the reactor configuration, for example, fluidised beds are limited to particles <3 mm [3, 20]. However, particles under 100 μm are commonly used during laboratory experiments to reduce secondary reactions [85].

2.3 Biomass constituents and their role during pyrolysis

Biomass is a complex biogenic solid consisting of cellulose, hemicellulose, lignin, and extraneous compounds [86]. The bio-oil properties are highly dependent on the content of these constituents; therefore the biomass type [7]. Stem wood is normally utilised as the biomass source for pyrolysis due to the lower concentration of inorganics, and large quantities are produced during log processing. The chemical composition of stem wood varies within forest locations, individual trees, within trees, and with tree age, this decreases the consistently of pyrolysis bio-oil. Woody biomass used for pyrolysis can be from hardwoods or softwoods. Hardwoods are from deciduous (typically) angiosperm trees while softwoods are from coniferous (typically) gymnosperm trees. Softwoods contain relatively more lignin and less hemicellulose compared to hardwoods [87]. Hardwoods generally have a higher methoxyl and acetyl content [88].

Cellulose, hemicellulose, and lignin decompose at different temperature ranges through endothermic and exothermic reactions. These reactions are influenced by the presence of water, extractives, and inorganic minerals [89]. Lignin and hemicellulose can exhibit exothermic behaviour during pyrolysis while cellulose pyrolysis is normally endothermic unless primary products undergo secondary exothermic reactions; for example, the breakdown of levoglucosan [90]. It is also thought that charring is an exothermic process [91].

Interactions between lignin, cellulose, and hemicellulose during pyrolysis remains a topic of debate [92-94]. Some reports indicate that there are no significant interactions and the pyrolysis can be regarded as a simple superposition of the three components [94-96]. However, Williams and Besler [97] stated that pure cellulose and hemicellulose decompose at lower temperatures than woody biomass. This may be due to other major components in the wood having an inhibiting effect on the decomposition reactions. Worasuwannarak *et al.* [93] found the char yield increased for cellulose-lignin and cellulose-hemicellulose blends but not for hemicellulose-lignin blends, indicating that only cellulose interacts with the other components. It was also found that the amount of water formed from the blends was higher than for individual components, and especially for the cellulose mixtures. It should be noted that cellulose contained no inorganics, while the lignin and hemicellulose did. There is the possibility that the interactions were simply from inorganic catalysed pyrolysis of cellulose when blended. Hosoya *et al.* [92] thought the cellulose-lignin interactions were more severe than cellulose-hemicellulose interactions and cellulose may be able to supress char formation from lignin, while lignin can enhance levoglucosan yield from cellulose by inhibiting further decomposition reactions.

The approximate composition of *P. radiata* in New Zealand is 40% cellulose, 31% hemicellulose, 27% lignin, 0.4% inorganic minerals, and 2% extractives [98]. In comparison to other woods, pine has a relatively high oxygen content, low inorganic content, very low sulfur content, and low nitrogen content [44]. The individual components of wood and their roles during pyrolysis are examined in detail below. Detailed knowledge of how the biomasses components react during pyrolysis provides information for what properties are generally problematic, and should be targeted during biomass pretreatments.

2.3.1 Pyrolysis of cellulose

Cellulose is a linear homopolymer with a degree of polymerisation of up to 10,000 anhydroglucose units linked by β-1, 4-glycosidic bonds [99]. Intra- and inter-molecular hydrogen bonds form between hydroxyl (OH) and hydrogen (H) groups to produce its crystalline structure, and help form and maintain a flat, linear conformation [3]. There are some amorphous regions along the cellulose chain. The amorphous regions are more susceptible to chemical attack; however the degree of crystallinity is generally not important if inorganics are present to catalyse degradation [96]. If inorganics are not present, the crystalline regions are thought to cause inter-ring crosslinking to promote char formation [100].

Cellulose pyrolysis has been studied in detail as it is the simplest compound in biomass, due to its repetitive structure. Even then, degradation of cellulose is complex and there has been much debate on the actual mechanism: whether compounds are formed via competitive reactions or by secondary reactions of levoglucosan. Luo *et al.* [101] found that secondary reactions of levoglucosan did not occur below 610 °C unless a catalyst was present, signifying competitive reaction pathways. Cellulose has a high oxygen content of around 49 wt% [48], this is reflected in the highly oxygenated products produced from cellulose pyrolysis, including acetic acid, water, sugar derivatives, and possibly furans and phenols [102]. Furans are thought to be primary products that easily undergo secondary reactions as they are only detected in systems with negligible residence times [103]. The main sugar derivative is levoglucosan, which is normally formed as a primary product. Secondary reactions may occur by oligomerisation to produce larger compounds or further degradation to produce light oxygenates such as organic acids, hydroxyacetaldehyde, and 1-hydroxy-2-propanone [99, 103].

Based on various theories reported in literature, four mechanisms for cellulose pyrolysis were simplified and combined to form Figure 2-1, which gives an overview of proposed reaction pathways. Additional details of each pathway can be found in literature by Shen and Gu [99], Evans and Milne [96], Piskorz *et al.* [104], and Luo *et al.* [101].

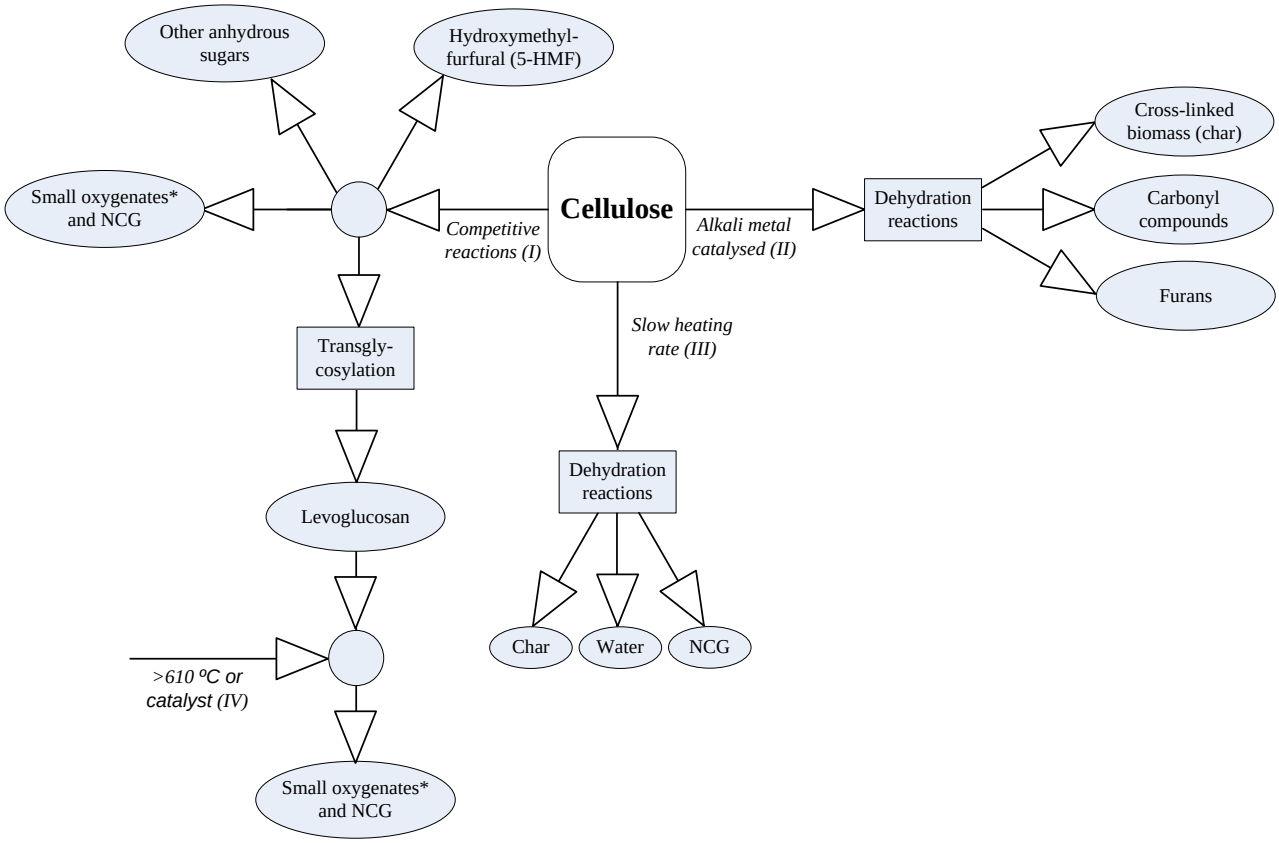

**Small oxygenates are mainly represented by organic acids, hydroxyacetaldehyde (HAA), hydroxyactone (HA), pyruvic aldehyde (PA), glyceraldehyde (GA), 5-hydroxymethyl-furfural (5-HMF), and furfural (FF)*

Figure 2-1: Collaboration of cellulose pyrolysis pathways: (I): Shen and Gu [99], (II): Evans and Milne [96], (III): Piskorz *et al.* [104], and (IV): Luo *et al.* [101].

When pure cellulose is heated in an inert atmosphere, physical water desorption and thermal dehydration are the dominant mechanisms until 220 °C. Higher temperatures cause chemical elimination of water through dehydration reactions [105]. Pyrolysis reactions occur between 240-350 °C [66], initiated by reactive dehydration and polymer depolymerisation (cleavage of the β-1, 4-glycosidic linkages). Dehydration reactions stabilise the remaining carbon polymer as elimination of the OH group results in a sable carbon-carbon crosslink perpendicular to the chain direction. Thus, dehydrated cellulose is less accessible to cleavage than the original polymer [106]. Low temperatures, slow heating rates, the presence of moisture, and inorganics favour dehydration reactions over depolymerisation reactions [99, 105].

Pyrolysis of pure cellulose may not produce any char during degradation if no moisture is present to catalyse charring reactions. Water exhibits auto-catalytic activity by enhancing vapour-solid reactions that have been identified as the main source for char formation through the removal of OH groups from cellulose [107]. The effect of metal salts was examined by impregnating cellulose with metal salts [94]. Metal salts normally lower the cellulose degradation temperature and enhance dehydration reactions [108]. Alkali metals inhibit the formation of levoglucosan through disruption of intramolecular condensation (transglycosylation). Glycosidic rupture becomes more prominent with crosslinks, substituted furans, and carbonyl groups formed

through dehydration reactions [96]. Alkaline earth metals favour depolymerisation reactions over dehydration reactions [105], but enhance vapour cracking reactions. Conversely, the presence of an acid increases pyrolytic water through increased dehydration reactions at the expense of depolymerisation reactions [105, 108].

2.3.2 Pyrolysis of hemicellulose

Hemicellulose has a degree of polymerisation of 100-200, consisting of heterogeneously linked five and six carbon anhydrosugars. The composition of anhydrosugars varies between softwoods and hardwoods [109]. In softwoods, up to 20 wt% of the polymers are *O*-acetyl-galactoglucomannan [110, 111], which are present in two forms: a water soluble form (glucomannan) and water insoluble form, having galactose:glucose:mannose ratios of 0.1:1:4 and 1:1:3, respectively. The bond between galactose and the main chain can be easily depolymerised with an acid but the acetyl groups are more easily cleaved by alkali than an acid. The xylan content in softwoods ranges from 7-15 wt% and it is not associated with acetyl groups but is more highly branched than hardwood xylan. The side branches can be removed under mildly acidic conditions without affecting the xylan backbone as arabinose groups stabilise xylan against degradation. Hardwoods comprise of predominantly glucuronoxylan groups with smaller amounts of glucomannan. The xylan chain contains uronic acids and acetyl side branches [111]. *P. radiata* contains an average of 15% galactoglucomannan, 10% arabinoglucuronoxylan, and 4% arabinogalactan [112].

Hemicellulose has a high oxygen content of around 54 wt% [48]. The highly oxygenated side branches are relativity easy to remove during pyrolysis [91], thus hemicellulose is the initial fraction in biomass to decompose, with degradation normally occurring between 180-320 °C [32, 66, 110, 113]. There are normally higher char yields associated with pyrolysis of hemicellulose compared to cellulose [114]. The abundance of acetyl groups makes acetic acid one of the main products, in addition to other organic acids, sugars, and furans [102, 115].

Xylan has been widely used as a model compound for pyrolysis of hemicellulose. Fewer studies have been reported in literature for pyrolysis of glucomannan and galactoglucomannan (softwood hemicelluloses), thus pyrolysis data is limited compared to xylan pyrolysis. Branca *et al.* [109] found that the products were similar from both anhydrosugars, with acetic acid the main product and CO_2 the primary gas. Alén *et al.* [95] reported that volatiles released during pyrolysis of glucomannan were mainly CO, CO_2, acetic acid, hydroxyacetacetaldehyde (glycolaldehyde), 1-hydroxy-2-propanone (acetol), and certain <C5 hydrocarbons and/or their derivatives. During pyrolysis, the total volatiles released from glucomannan were less than those produced from xylan pyrolysis. Xylan released mainly CO, CO_2, formic acid, acetic acid, hydroxyacetaldehyde, and 1 -hydroxy-2-propanone. Prins *et al.* [116] also noticed that larch (a softwood) reacted at a slower rate than hardwoods during pyrolysis.

2.3.3 Pyrolysis of lignin

Lignin is normally the second most abundant component in woody biomass. It is the only source of renewable aromatics in nature [76]. Lignin consists of three dimensional polymers that act as the "cementing material" in the wood to strengthen and protect cellulose and hemicellulose [83]. It crosslinks plant polysaccharides by covalently linking to hemicellulose, this gives mechanical strength to the cell wall [117]. The polymer structure depends on the wood type and growth environment but the major polymers are guaiacyl alcohols in softwoods and guaiacyl-syringyl alcohols in hardwoods [111]. Polymers contain side branches that have random hydroxyl and methoxy substituted phenylpropane units [66]. Lignin is mostly insoluble in water, common organic solvents, and acids (the acid insoluble fraction is referred to as Klason lignin [118]). The acid soluble fraction is generally <1% for softwoods and 3-4% for hardwoods [119]. Lignin is partly soluble in alkali solutions and is readily attacked and solubilised by strong oxidising agents such as hydrogen peroxide, nitric acid, sulfuric acid, and formic acid [120].

Lignin is the hardest component of biomass to pyrolyse, with degradation of pure lignin occurring over a large temperature range of 160-900 °C. Char yields from lignin pyrolysis can reach 46 wt% [91]; these are increased in the presence of alkali metals as these metals (such as Na) are believed to promote demethoxylation, demethylation, and dehydration of lignin [121]. The bio-oil produced from lignin pyrolysis is referred to as pyroligneous acid which typically consists of about 20% aqueous compounds and 15% tar [122]. The majority of heavy compounds present in bio-oil originate from pyrolysis of lignin. Pyrolysis of biomass with high lignin content generally leads to a less stable bio-oil as the compounds in the pyroligneous acid decrease the bio-oil's stability, independent of the inorganic content of the bio-oil. As the inorganic content in a biomass increases, the lignin content generally decreases. Fahmi *et al.* [123] found that high inorganic but low lignin feedstocks produced a more stable bio-oil, although yield was lower, the water content was higher, and the oxygen content was higher.

There is a much smaller number of free OH groups in lignin compared to cellulose and hemicellulose; this means the pyrolysis mechanism is different as dehydration reactions are not so prominent [121]. The products from lignin pyrolysis have a lower oxygen content than products from cellulose and hemicellulose pyrolysis as lignin's oxygen content is between 12-29 wt% [48]. Common products from lignin pyrolysis include: guaiacols, syringols, and other substituted phenols [102, 110, 115], with smaller quantities of aromatic hydrocarbons, methanol, organic acids, and aromatic acids. Methanol and organic acids can be produced directly from the decomposition of aromatic carboxyl groups and carboxyl side branches [124]. This can lead to a decrease in the bio-oil's pH [123]. Short vapour residence times are required to prevent secondary breakdown of pyrolysis vapours, but very short residence times can produce a less homogeneous bio-oil due to incomplete depolymerisation of lignin [125].

2.3.4 Effect of extraneous compounds during pyrolysis

In woody biomass, extraneous compounds include extractives, fats, oils, proteins, pectin, and inorganic minerals. Extractives are soluble in water or an organic solvent. These constitute up to 1.5% of *P. radiata* [112] and include primary tannins (phenols); resins (fats, fatty acids, alcohols, resin acids, and phytosterols); terpenes (isoprene alcohols and ketones); and starches [79, 99]. The type and amount of extractives depends on the heartwood content of the tree (wood near the stem centre which is formed at a young age), and therefore the tree's age. The extractive composition in heartwood and sapwood for *P. radiata* is given in Table 2-3. Pyrolysis of pure extractives is thought to produce 50% char [126]. The removal of extractives has minimal effect on pyrolysis yields but can alter the product composition. Extractive-free biomass produces a bio-oil with approximately 25% less acetic acid, 50% less formic acid, and can increase the levoglucosan yield from 1 wt% to 10 wt% [127]. Carrier *et al.* [128] noticed that the pyrolytic water decreased for ethanol extracted biomass but increased when acetone extraction techniques were implemented, indicating that either the solvent influences pyrolysis or that acetone cannot remove the catalytic extractives.

Table 2-3: Extractive composition for *P. radiata* heartwood and sapwood, obtained from Uprichard and Lloyd [112]

Compound	Heartwood (% of tot. ext.)	Sapwood (% of tot. ext.)
Fatty acids (free)[1]	2	1
Fatty acid esters	11	41
Resin acids[2]	71	41
Phenols	6	3
Unsaponifiables (neutrals)[3]	10	14

[1]Present mainly as glycerides (oleic and linoleic), [2]Present mainly as prmaric, isopimaric, levopimaric, sandaracopimaric, neoabietic, abietic, and dehydroubietic acids, [3]Present mainly as sterols, alcohols, and hydrocarbons

Woody biomass, in general, has a low inorganic (ash) content. Inorganic minerals can be present as hydroxides, silicates, carbonates, sulfates, chlorides, and phosphates [100, 129]. Some of the inorganics may exist in the wood as soluble salts or cations bound to reactive sites in wood, probably as functionalities of cellulose or of acid groups [130]. The inorganics detected in *P. radiata* are listed in Table 2-4; the main inorganic elements are Si, K, Ca, Mg and Na respectively [100, 115]. Inorganic minerals exhibit catalytic activity during pyrolysis [130, 131], by increasing the reactivity of biomass, thus lowering the activation energies [132]. Ring opening reactions are catalysed through fragmentation, depolymerisation, and cracking reactions of primary pyrolysis vapours. This causes liquid yields to decrease while increasing acetic acid, water, and formaldehyde yields [115]. Silica sand used for the fluidising medium can cause low-melting eutectic mixtures of alkali compounds and silica to form [133, 134], which may lead to bed agglomeration [129].

Most alkali metals remain in the char fraction following pyrolysis, although a portion of the metals may volatise during pyrolysis. The presence of certain inorganics such as Cl facilitate volatilisation of other inorganics as KCl and NaCl [129]. Olsson *et al.* [135] found that Cl only increased alkali volatilisation above 500 ℃. Studies with surface ionisation techniques have shown the main release of alkali metals

during pyrolysis is between 200-500 °C, with a peak at 300-400 °C [134]. Alkalis can be re-deposited as discrete particles or disperse in the char matrix [115]. The fraction released when temperatures are below 500 °C is only a small percentage of the total alkalis [136]. Biomass/char has a second release of alkali metals above 600 °C. This is only applicable if char is burnt for process heat as pyrolysis temperatures are typically below 600 °C. The second release of alkali metals seems to be easily removed during water or acid leaching of the biomass, with water leaching able to reduce the secondary release by 90% [134, 135]. If char is combusted for process heat, the ash from combustion has the potential to be used as a fertiliser, although compounds such as Ca can increase the soil's pH; therefore application must be carefully analysed to avoid harming the soil's flora. Combustion of char should be below 900 °C to minimise nutrient volatilisation and fly ash should be collected and disposed of separately due to the Cd, Cr, Cu, Pb, and As content [137].

Table 2-4: Periodic groups for elements detected in wood [100, 115]

Element group	Elements detected in *Pinus radiata*
Alkali Earth	Lithium (Li), sodium (Na), potassium (K)
Alkaline Earth	Magnesium (Mg), calcium (Ca), barium (Ba)
Transition Metals	Chromium (Cr), copper (Cu), iron (Fe), manganese (Mn), nickel (Ni), zinc (Zn), cadmium (Cd), cobalt (Co)
Other metals	Aluminium (Al), lead (Pb)
Non-metals	Phosphorus (P), sulfur (S), nitrogen (N), silica (Si), arsenic (As), boron (B)
Halogens	Chlorine (Cl)

To examine the effect inorganics on pyrolysis yields and bio-oil composition, biomass can be impregnated with catalysts. Encinar *et al.* [138] impregnated biomass with NaCl, LiCl, KCl, $FeCl_3{\cdot}6H_2O$, $AlCl_3{\cdot}6H_2O$, and $ZnCl_2$. All catalysts increased char yield and decreased the bio-oil yield. $FeCl_3{\cdot}6H_2O$ decreased the bio-oil yield the most and KCl the least. Di Blasi *et al.* [139] also obtained similar results, with KOH and K_2CO_3 having less effect on the bio-oil yield than NaOH and Na_2CO_3, respectively. This contradicts claims by Nowakowski *et al.* [115] who found that K had the greatest catalytic effect. Discrepancies between these studies could be due to the impregnation method or the lignin content in the raw biomass as inorganics do not catalyse lignin pyrolysis as severely as cellulose and hemicellulose pyrolysis [124]. Some inorganics may have the ability to increase the accessibility of reactions in the biomass by weakening the rigid lignin structure and function as a catalyst to increase the thermo-conversion rate of biomass. Decreasing the inorganic content normally increases the bio-oil's viscosity. This is by decreasing the water content and increasing the average molecular weight with of compounds through reduced vapour cracking reactions [123]. Reducing the inorganic content of bio-oil does not appear to prevent aging reactions, indicating that their catalytic effect in bio-oil is not significant as so many other potential catalysts are present, such as acids, alcohols, aldehydes phenols, and other unsaturated compounds [57].

2.3.5 Effect of water during pyrolysis

Biomass is a hygroscopic material; therefore it readily re-absorbs moisture following complete drying. Pyrolysis must take place immediately after drying or biomass should be stored in a desiccator to maintain the low moisture content. It is commonly recommended that the biomass moisture content should be reduced

to <10% prior to pyrolysis to prevent phase separation of the bio-oil [54, 140] and microbial degradation of the biomass during storage [141]. Raw biomass can have a moisture content of 60-85 wt% (dry basis), this can be reduced slightly by mechanical pressing and to around 20 wt% via air drying [141]. High temperature drying using air as the drying medium is required for further moisture reductions. Microwave drying gives higher efficiencies and faster drying rates but the costs of drying are high. Following microwave drying, the pyrolysis products are slightly altered as the rapid moisture removal enhances the surface area of biomass creating more pathways for volatiles to escape. However, there is minimal change compared to conventional drying for woody biomass species [140].

During pyrolysis, water delays the reaction propagation due to the additional time required to heat and vaporise water from the biomass [136]. Physical desorption of water (free water) occurs between 25-150 °C, and thermal dehydration (bound water) occurs between 150-220 °C. Most research suggests that below 220 °C water is not chemically produced [105]. Free water can aid heat transfer and fragmentation when water explosively vaporises during pyrolysis [50, 122]. However, water is typically the most abundant compound in bio-oil, ranging from 15-35 wt%, which is undesirable. Reducing the water content in bio-oil is normally desirable as it improves the energy density, transportation costs, stability, and acidity of bio-oil. However, water can lower the viscosity, limit NO_X emissions, and ensure a uniform temperature distribution in cylinders [142].

Water displays an auto-catalytic effect during pyrolysis of biomass [107], but does not actually participate as a reactant; therefore any water in the biomass prior to pyrolysis will be reflected in the water content of bio-oil [23]. Some authors reported an increase in pyrolytic water production for pyrolysis of oven-dry biomass [142], while others reported a decrease in pyrolytic water production [143, 144]. The effect of the biomass moisture content on the char, NCGs, and bio-oil seems to vary, but generally the organic yield decreases. This is especially for primary products such as levoglucosan [142, 143, 145]. The varying results could be related to the inorganic content of biomass. To investigate this, Gary *et al.* [146] looked at the combined effect of inorganic-free and oven-dry biomass. Gary *el al.* found that the bio-oil yield increased significantly when inorganics and moisture were both removed. It was thought that the presence of moisture would increase the quantity of volatiles escaping the biomass particle, increase wood permeability, increase surface area through swelling, and reduce vapour pressure in biomass. The presence of moisture may also enhance bubble formation through reduced viscosity of the biomass glass transition melt, thus decreasing secondary reactions. However, inorganic-free biomass with a higher moisture content produced less volatiles and more char, signifying that a chemical interaction with water occurred. Gary [143] proposed that there could be reactions between free radicals and moisture: with tar molecules becoming trapped in the solid phase due to the free radical reactions.

2.4 Pyrolysis products

The yields and composition of bio-oil, char, and NCG formed during biomass pyrolysis are determined by the pyrolysis operating conditions and the process variables [31]. The process variables include: the type of feedstock and its properties, scale of operation, reactor type, solids separation, and condensation system. Biomass properties such as density, permeability, size, and shape influence vapour mitigation, and therefore the rate of secondary reactions. The effect of biomass size was reviewed in Section 2.2.3. It is hard to define a relationship between biomass density, permeability for the yield of char but high wood permeability is normally associated with lower char yields [147]. Permeability varies during pyrolysis as extractives are initially deposited in vessels and block flow passages; however these decompose and are removed when the wood is heated during pyrolysis to unblocks the passages. The quantity of vessels in wood may be related to the biomass density, with the diffusion resistance of volatiles increasing with density as the components of the biomass are packed more tightly. Although high wood densities increase the biomass's thermal conductivity, which facilitates heat and mass transfer into the interior of the biomass particle, it is thought that higher wood density leads to additional char formation. *P. radiata* is a softwood with a relatively low density and produces less char during pyrolysis compared to other wood species with a higher density [147].

2.4.1 Non-condensable gas (NCG)

Pyrolysis volatiles not condensed at ambient conditions are referred to as NCGs. These normally consist of carbon dioxide (CO_2), carbon monoxide (CO), hydrogen (H_2), methane (CH_4), ethane (C_2H_6), and ethylene (C_2H_4). Pyrolysis systems can combust the NCGs for process energy or recycle them directly through the pyrolysis reactor. It is not currently economical to use NCGs for synthetic gas production due to the low energy density and dilution from the fluidising gas if N_2 is used.

NCG formation occurs during primary and secondary cracking reactions [48, 99]. Table 2-5 provides detailed data on the NCG formation at different pyrolysis temperatures [32, 48]; the data indicates that CO_2 is mainly produced during primary reactions while CO is mainly produced during secondary reactions, especially through secondary reactions of low molecular weight compounds, thus the CO concentration can give an indication of the degree of secondary reactions. Increasing the pyrolysis temperature above 500 °C increases volatile cracking reactions to produce higher portions of CO, H_2, and CH_4 in the NCG, overall increasing the NCG's lower heating value (LHV) but lowering the bio-oil's LHV [32, 148, 149].

Table 2-5: Gas evolution from primary and secondary reactions during pyrolysis

	Primary gas [48]	**Secondary gas [48]**	**Temp. of maximum evolution (°C) [32]**
Carbon dioxide (wt%)	53	9	350
Carbon monoxide (wt%)	36	63	350
Hydrocarbons (wt%)	6.7	27	425
Hydrogen (wt%)	0.8	1.4	700-750
LHV ($MJ.nm^{-3}$)	11	20	

2.4.2 Char

Char yield and its characteristics are influenced by the pyrolysis temperature, heating rate, reaction pressure, and biomass properties [147, 148]. Primary chars produced at low pyrolysis temperatures or low heating rates are unstable and can undergo secondary reactions to form a stable char and additional volatiles [150]. Char produced at low temperatures exhibits a higher oxygen and hydrogen content than char produced at higher temperatures [148]. In an experimental study, Shen *et al.* [114] varied the heating rate for pure cellulose and hemicellulose pyrolysis. When the heating rate was increased from 5 to 60 °Cmin^{-1}, the char yield increased from 10.2 to 24.5% for hemicellulose pyrolysis but decreased from 10.1 to 7.5% for cellulose pyrolysis. Cellulose is known to form carbon-carbon crosslinks when heating rates are lower, leading to increased char yields. Char formed from hemicellulose at low heating rates is less stable than char produced at higher heating rates, and undergoes secondary reactions to reduce the total char yield. Contradictorily experimental studies by Gao-Jin *et al.* [113] found that corn stalk hemicellulose did not show a variation in the final char yield when heating rates were increased from 10 to 50 °Cmin^{-1}.

Char is thought to catalyse vapour cracking reactions, probably due to the reactive inorganics present in char. Large char particles can 'float' in the freeboard section above fluidised beds, catalysing exiting vapours [44]. The char particle size is highly dependent on the initial biomass particle size and abrasion in the reactor. Biomass particles shrink up to 50% when char is formed [151]. Raw biomass particles do not appear to agglomerate during pyrolysis but may do once the char is cooled below the vapour dew point in transfer lines [48]. However, Brown [152] reported agglomeration from pyrolysis of passivated biomass, which may indicate that inorganic-free biomass can agglomerate in the pyrolysis reactor. Cellulose char retains a memory of the initial cellulose structure after pyrolysis; even though x-ray diffraction patterns show an amorphous structure forms during pyrolysis. Thus, demonstrating the strong tendency for char layers to form with an orientation analogous to the original cellulose chain direction [153]. Solid residue without the original lignocellulose structure is generally defined as either coke or soot [96]. Coke is a four carbon network, formed through polycondensation and polymerisation reactions of the primary vapours as they mitigate to the surface of the biomass particle.

Char can be combusted to supply process heat but a high ash content lowers the heating value [154], and can cause alkali vapour deposition and corrosion during combustion [155]. Hot chars are extremely flammable due to the small particle size and high volatility (auto-ignition temperature ranges between 200-250 °C [48]). Oxygen containing functional groups on the hydrophilic surface of chars indicate it is suitable for removing metal ions and other pollutants from a waste water stream. Char can be modified to have both an alkaline and acidic surface to improve ion removal [156]. Other char uses include upgrading to activated carbon, carbon fibres, carbon molecular sieves, fertiliser supports, catalyst supports, smokeless briquette, or for soil mitigation [106, 133, 148]. Char utilisation in soil mitigation renders pyrolysis of biomass a carbon sink instead of simply carbon neutral [157]. Furthermore, it improves soil texture, returns inorganics to the soil, retains, and slowly releases nutrients and water. It acts as a support for beneficial micro-organisms [22].

However, fast pyrolysis chars have less bio-available carbon compared to slow pyrolysis chars, which could potentially lead to nutrient immobilisation [158, 159].

2.4.3 Bio-oil

Bio-oil formed during pyrolysis is a complex mixture of polymer fragments and reacted compounds produced from cellulose, hemicellulose, and lignin. The fragments consist of molecules that escape the pyrolysis environment by volatilising or as aerosols (normally oligomeric compounds) that small enough to become entrained from the reactor [48]. Bio-oil is highly oxygenated, which increases its polarity and makes it hydrophilic; therefore, holding water in solution. When the water content is above approximately 40 wt%, bio-oil becomes heterogeneous and separates into two phases. The top layer (aqueous phase) contains organic acids, alcohols, water, and sugars while the bottom layer (non-aqueous phase or tar) consists of various oxygenated compounds and pyrolytic lignin [148].

2.4.3.1 General bio-oil properties

The quality of bio-oil largely originates from the biomass's composition [3]. Common bio-oil characteristics include: low pH, high viscosity, high density, high water content, high oxygen content, dark brown colour, smoky smell, and medium heating value [18, 160]. Table 2-6 lists typical bio-oil properties; the properties for heavy fossil oil are also given for a comparison. Biomass's high oxygen content is reflected in the bio-oil's elementary composition, subsequently decreasing its heating value to approximately half that of petroleum fuels. The water content in bio-oil is a combination of free water from the biomass source and pyrolytic water. The pyrolytic water is mainly produced via dehydration of cellulose and hemicellulose, with only a small amount associated with lignin degradation [71]. Water acts as a solvent in the bio-oil to help reduce polymeric interactions; therefore the water content significantly influences the bio-oil's viscosity. Westerhof *et al.* [142] found the viscosity of bio-oil increased exponentially when the water content was below 15 wt%.

The acidity of bio-oil causes corrosion issues. Carboxylic acids contribute to 60-70% of the acidity; these are produced principally from hemicellulose pyrolysis. Phenolic compounds, fatty acids, resin acids, and hydroxyl acids can also affect the acidity. Oasmaa *et al.* [161] noticed that the acidity did not appear to change during storage or when bio-oil was aged. The inorganic content in bio-oil is normally associated with entrained char particles. Even filtering to 0.1 μm does not remove all the inorganics; therefore they may be associated with smaller char particles or leached into the bio-oil by acidic compounds [162]. Elliott [81] looked at the distribution of inorganics in the non-aqueous and aqueous phases, and reported no clear separation was observed between the aqueous and non-aqueous phases. However the non-aqueous fraction contained more inorganics, probably as the char becomes concentrated in the tar fraction, except K as it is typically more water soluble.

Table 2-6: Properties of bio-oil and their effect on the quality

Property	Pyrolysis oil [3, 54]	Heavy fossil oil [3]	Effect on the quality in terms of fuel use
HHV ($MJkg^{-1}$)	14-20	40	Larger volumes required [163]
Water content (wt%)	15-30	0.1	Lowers the heating value, viscosity, density, and ignition rate [16, 164]
pH	2.5	-	Corrosive to pipes and vessels: compounding at elevated temperatures [16, 164]
Solids (wt%)	0.2-1	1	May enhance bio-oil aging, corrosion, and equipment blockages [164]
Inorganics	0-0.2	0.1	High temperature corrosion, hard deposits, and bio-oil aging [16, 129]
Viscosity (cP at 50 °C)	40-100	180	High pressure drop which increases equipment costs, leakages, and ruptures [164]
Density [18] (kgL^{-1})	1.2	0.85	Higher density can cause pumping issues [163]
Oxygen content (wt%)	30-48		Immiscible with petroleum based fuels [16]
Safety (flammable class)	3	3	Potentially harmful [36]

2.4.3.2 Chemistry and reactions of crude bio-oil

The chemistry of compounds in bio-oil and their interactions must be understood in order to predict fuel characteristics and to be able to implement biomass pretreating techniques, bio-oil upgrading, and final refining of the upgraded bio-oil. Bio-oil can contain around 400 compounds produced through hydrolysis, dehydration, isomerisation, dehydrogenation, aromatisation, retro-condensation, and charring reactions [3]. Due to the variety and complexity of bio-oils, it is necessary to group compounds into major chemical groups such as water, organic acids, aldehydes, ketones, furans, sugars, guaiacols, syringols, alcohols, phenols, esters, and light oxygenates [165]. Based on the mass of components in the bio-oil, approximately one third is phenols, one third is neutral components, and rest is a mix of organic acids, aldehydes, ketones, esters, and water [23, 166]. Guaiacols and syringols originate from lignin, whereas the light oxygenates, sugars, organic acids, alcohols, and furans originate from cellulose and hemicellulose. Secondary reactions of oxygenates, sugars, and furans probably produces esters, organic acids, alcohols, ketones, and aldehydes [3]. The significant organics produced during pyrolysis are listed below:

- *Organic acids*: Acetic acid is the major organic acid, formed mainly from acetyl braches of hemicellulose [99, 167]. Acetic acid is also produced during the secondary reactions of volatiles, such as the dehydration of an aldehyde alcohol to a ketone and then rehydration to an acidic product [44]. Smaller quantities of formic, lactic, and oxalic acid are formed mainly during the secondary reactions.

- *Anhydrosugars*: Levoglucosan (anhydroglucose, 1,6-anhydro-β-D-glucopyranose) is the main anhydrosugars formed. It is a primary product, which is probably formed by a mechanism involving intramolecular condensation and sequential depolymerisation of glycosidic units [3]. The yields can be up to 20 wt% if biomass is pretreated to reduce the inorganic and hemicellulose content [3, 104, 164], as levoglucosan is stable at pyrolysis conditions when no catalyst is present [101, 168]. In the presence of catalysts, levoglucosan can breakdown to substituted furans and pyran derivatives [50]. Levoglucosan is not suitable as a fuel, as combustion at 527 °C will not cause vaporisation [165], but it can be used as a building block for producing other compounds. Hydrolysis of levoglucosan gives glucose, this can be converted to fructose, then hydroxymethylfurfural (HMF), which is a precursor to 2,5-dimethylfuran (DMF): a potential biofuel [169, 170].

- *Light oxygenates*: Normally in pyrolysis, the system can be set to produce either high yields of levoglucosan or light oxygenates. Production of light oxygenates is thought to occur during sequential decomposition of levoglucosan or through parallel reactions [104]. Higher temperatures, longer residence times, or the presence of catalysts (such as fructose, inorganics, chloride, and zinc chloride) enhance hydroxyacetaldehyde (glycolaldehyde), 1-hydroxy-2-propanone, hydroxyacetone, and 5-hydroxymethly-furfural formation over levoglucosan [44, 101, 164, 168].

- *Polycyclic aromatic hydrocarbons (PAHs)*: Aromatic compounds can be formed through secondary and tertiary cracking reactions. These involve pyrolysis of alkanes to produce alkenes which are subsequently aromatised through Diels-Alder type reactions to form a single ring aromatic compound that can further react to form PAHs [97]. The concentration of PAHs increases with the pyrolysis operating temperature [72, 75]. They are normally not detectable below 500 °C and only become significant in the tar fraction above 700 °C. Some PAHs may be carcinogenic and/or mutagenic, causing fuel handling issues. Examples of PAHs include naphthalene, phenanthrene, and fluorene and their alkylated substituents.

- *Phenols*: These are produced primarily from lignin during pyrolysis. Phenolic compounds are produced between pyrolysis temperatures of 200-350 °C, following radical C-O and C-C bond cleavage [102]. As phenols are potentially high value compounds, different methods have been used to separate or extract phenols from bio-oil including alkaline extraction; partition into different solvents or adsorption on different packed materials; liquid chromatography; and steam distillation [102].

- *Oligomeric compounds*: Also defined as pyrolytic lignin, and can make up 20-30 wt% of the bio-oil. This high molecular weight fraction cannot be vaporised and rapidly forms tar, then eventually char when heated to over 100 °C [171]. Pyrolytic lignin can be produced during the secondary reactions or sudden entrainments of small wood polymers as aerosol, before they have time to full depolymerise [172]. Their molecular weight is normally between 650-1300 $gmol^{-1}$; therefore increases the bio-oil's viscosity.

- *Alcohols*: Methanol is the primary alcohol formed during pyrolysis from the cleavage of methyl branches and from the breakdown of methyl esters and/or ethers. The addition of 5% methanol to bio-oil can reduce the viscosity by 35% via partial oxidation reactions [16, 167], and reducing polymeric interactions.

- *Furans*: 5-hydroxmethyl furfural (5-HMF) can be produced during pyrolysis of hemicellulose. Alternatively, a glucose monomer from cellulose can be converted to a five membered structure via a ring opening step [151]. This has the potential to be upgraded to 2,5-dimethylfuran (DMF) through triple dehydration, which is a potential biofuel [173].

Short residence times and rapid quenching during pyrolysis means that vapours do not reach thermodynamic equilibrium; therefore they may react during storage until thermodynamic stability is obtained [16]. The bio-oil's viscosity is often used as a measure for stability [48, 60, 174], as it tends to increase upon storage or upon heating through polymerisation, condensation, esterification, and polycondensation reactions. A homogeneous bio-oil can separate into layers during storage as low molecular weight compounds (such as water and alcohols) are released during polymerisation reactions [174]. If bio-oil separates into two phases, the heavy bottom phase undergoes polymerisation and condensation reactions during storage, increasing the bio-oil's viscosity [174].

It is important to understand potential reactions in bio-oil to be able to enhance desirable ones and prevent undesirable ones. Possible reactions are listed in Table 2-7, from which it can be seen that the carbonyl compounds (especially aldehydes) are highly active in bio-oil and can lead to polymerisation reactions [175]. Inorganics and/or organic acid catalysts are required for many reactions. Other reactions possible are methoxy (R-O-CH_3) compounds being polymerisation precursors [25], and pyrolytic lignin reacting with other pyrolytic lignin or other compounds (especially carbonyl compounds).

Table 2-7: Possible reactions in bio-oil [3, 162]

Reaction	Reactants	Products	Thermodynamics
Esterification 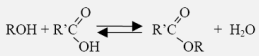	Alcohols, organic acids	Esters, water	Thermodynamically favoured, reversible reaction. Can also react with olefins to from iso-esters
Trans-esterification 	Esters	Esters	Exchange of alcohol and acid groups
Homo-polymerisation 	Aldehydes, furfurals	Polyacetal oligomers and polymers	Thermodynamically favoured in an acidic environment. Normally irreversible
Hydration 	Aldehydes or ketones, water	Hydrates (glycol)	Reversible, aldehydes will form more hydrates than ketones at equilibrium
Hemiacetal formation 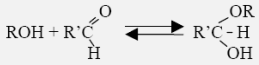	Aldehyde, alcohols	Hemiacetals	Quick reaction, reversible, does not require a catalyst. Water and methanol stabilise aldehydes, preventing the formation of polyaldehyde resins
Acetalisation 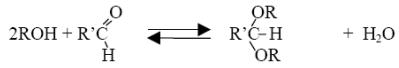	Aldehydes, alcohols	Aldehydes, alcohols, or a cyclic diether	Reversible, 100 times faster reaction for primary alcohols and aldehydes than secondary and unsaturated compounds
Trans-acetalisation 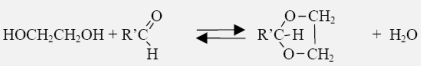	Aldehydes, alcohols	Aldehydes, alcohols	Reactions between aldehydes and alcohols
Phenols 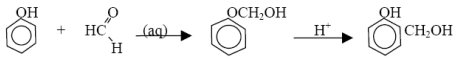	Phenols, aldehydes	hemiformal	React like alcohols with no catalyst present
Polymerisation 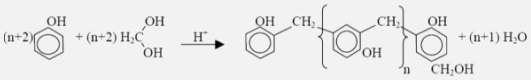	Phenols, aldehydes	Novolak resins, water	Normally irreversible, requires metal or acid catalysts for fast reaction
Condensation	Furan derivatives	Furan polymers	Catalysed by a strong acid
Olefinic condensation	Unsaturated compounds	Polyolefins	Catalysed by a carboxylic acid
Oxidation	Air, alcohols, aldehydes	Carboxylic acids, hydroperoxides, alkylperoxides	
Decarboxylation 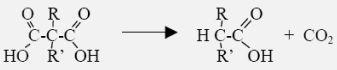	Carboxylic acids	Mono-acids, carbon dioxide	Moderate temperatures required

2.4.3.3 Combustion of bio-oil

Bio-oil is normally produced as a liquid fuel for combustion, thus its combustion properties must be evaluated. Bio-oil requires preheating before most applications to decrease the viscosity and to increase atomisation to avoid ignition delay [165]. Preheating may change the composition through enhanced aging reactions at elevated temperatures. Instead, cetane improvers can be added to improve ignition problems, but are costly and the polarity of bio-oil makes mixing without emulsifiers difficult. If the bio-oil is to be used as a diesel fuel substitute, the following properties must be considered: ignition quality, chemical composition, heating value, density, viscosity, lubricating properties, Conradson carbon residue, sulfur content, and heavy-metal content.

The power and speed of an engine are also critical aspects as smaller engines have lower manufacturing tolerances, with requirements for short ignition delay. These become more constringent as the engine speed increases [160]. Water in bio-oil delays the onset of micro-explosions, but improves droplet shattering due to its large vapour expansion rate [176]. Decreasing the water content and increasing the thermal cracking rate would improve engine performance [165]. Char in bio-oil can cause early micro-explosions but reduce the effectiveness of the micro-explosion shattering. Char can also enhance coke formation. Volatile compounds such as methanol reduce the time before micro-explosions occur due to their volatility [176]. One documented benefit is that bio-oil degrades faster than petroleum oil, indicating mitigating an oil spill may be easier compared to crude oil spills [54].

Bio-oil can be blended directly with diesel to create an emulsion. Since bio-oil is not soluble in petroleum based fuels, blending can only be accomplished by using expensive surfactants [3, 16]. Storage or heating of an emulsion can destabilise it [177]. Yang *et al.* [178] tested an emulsification of diesel and pyrolysis oil from coffee bean residue in a 12 kW power generation system. When the bio-oil content was increased to 10%, the viscosity and ignition delay increased while the heating value decreased. NO_x were reduced but in some cases, smoke produced from the engine was denser. Bio-oil has also been tested in turbines and furnaces, with a number of issues reported: filters blocking from char deposits, pumping issues due to the high viscosity, and corrosion [164]. The alkali content should be reduced to under 0.5 ppm for turbine use [61]. In summary, it is widely accepted that the bio-oil from fast pyrolysis cannot be considered as a realistic candidate for liquid transport fuel substitution at large scale unless it is upgraded [6].

2.4.3.4 Chemical production from bio-oil

The extraction and recovery of chemicals from pyrolysis oil has been well researched to improve the overall economics of pyrolysis systems. It is generally hard to recover high purity compounds due to the low concentration of most individual components; therefore recovering fractional groups with similar functionalities and chemical properties is commonly practised. Also, the pyrolysis process can be altered to increase the yield of specific compounds of high value. Phenols, levoglucosan, levoglucosenone, hydroxyacetaldehyde, food flavourings, hydrogen, wood preservatives, slow release fertilisers (by reaction with ammonia, urea, or other NH_2 containing materials), sugars, and organic acids are all of particular interest [20, 164, 179]. Food flavourings from phenolic derivatives are currently the only commercially produced chemicals from bio-oil. The recovery of potentially valuable chemicals could be an important way of improving the overall economics of fast pyrolysis, especially if the compounds removed have a detrimental effect on the bio-oil quality or combustion; therefore making refining easier [164].

Organic acid removal with calcium oxide, anion exchange resins, distillation, or selective condensation improves the quality of bio-oil while producing a chemical commodity [180]. Germany used a similar technique to produce glacial acetic acid in the 1910's, but nowadays, it is commonly produced from a petroleum source. Levoglucosan can be hydrolysed to glucose and then fermented to bioethanol [181]. Aqueous extraction using water initially separates the bio-oil into a top aqueous layer from which

levoglucosan can be separated [182]. This can also be used to separate the phenols into the organic fraction. The organic fraction is then dissolved in ethyl acetate and washed with aqueous sodium bicarbonate to remove strong acids as water soluble sodium salt. The organic material remaining in the ethyl acetate solution consists of phenolic and neutral components [166]. Phenols have extensive use in the production of resins. Syringol and guaiacol both can be used in the production of biodegradable polyesters and polyethers [72]. Dynamotive Corporations developed BioLime by reacting bio-oil with lime. This is used to capture SO_x emissions from coal combustion with a 90-98% efficiency.

2.5 Biomass pretreatments and bio-oil upgrading

There are readily available renewable sources for producing electricity in New Zealand; therefore bio-oil would be intended as a diesel fuel substitute. Crude bio-oil cannot be used directly in a diesel combustion engine as discussed in Section 2.4.3.3 [48]. This implies that upgrading and subsequent refining steps are required to improve the bio-oil's quality and stability before its commercial use as a liquid fuel [183]. The multi-scale structure and complex composition of biomass make fundamental predictions of bio-oil properties challenging [151], thus it is hard to define the general severity of upgrading required. The objective of this research was to improve the bio-oil quality through pretreatments of biomass; literature to date is reviewed in this section.

It needs to be established what the 'ideal' pyrolysis bio-oil would constitute. It was initially be thought that upgraded bio-oil should be comparably to petroleum fuels standards but the use of ethanol as a motor fuel demonstrated that such stringent chemical requirements are not necessary [27]. The main criteria would be to produce a stable liquid fuel that can be directly substituted into current combustion engines, Table 2.2-8 designates properties that must be considered for compatibility. The positive and negative attributes of the chemical compounds present in the bio-oil have to be considered and establish the compounds desirable after upgrading.

Fast pyrolysis is associated with high liquid yields, but the yield from bio-oil upgrading process remains low due to coke, tar, and char formation [171]. An obstacle for the bio-oil upgrading is the bio-oil's instability, leading to coke formation on the upgrading catalysts. Carbonyl compounds (aldehydes, ketones, carboxylic acids, and esters), inorganics, char, and pyrolytic lignin are thought to be responsible for many of the polycondensation reactions that cause bio-oil aging [164, 175, 184]. Hydrocarbons and alcohols are traditionally acceptable compounds for fuels. Levoglucosan is desirable as alternative products are NCGs and small oxygenated compounds. Phenols are also desirable due to the high commercial value if extracted [184].

Table 2.2-8: Criteria for upgraded bio-oil, data obtained from Diebold *et al.* [185]

Properties	Description	Criteria
Flash point	Volatility of the fuel as well as ease of ignition	The flash point of bio-oils is normally between 50-100 °C, which is in the bracket of what is commonly required by petroleum fuels
Distillation temperature	Volatility of the fuel	It is important that a fuel can be completely distilled if it is necessary to have complete volatilisation before burning
Viscosity and density	Pumping and atomising [164]	The viscosity should not increase during storage and when heated, indicating that the bio-oil is stable
Inorganic content	Corrosion of equipment	The inorganic content should be low enough to minimise the particulate content in the exhaust gas and to prevent corrosion to materials
Sulfur and nitrogen content	NO_x and SO_x emissions during combustion	Both are naturally low in woody biomass but nitrogen content is higher in green biomasses
Pour point	The minimum temperature at which the oil can be pumped without heating	Depends on fuel use
Cetane number	Measure of the ease of auto-ignition of a fuel in a diesel engine	Reference oils fuels are n-hexadecane (100 cetane) and methyl naphthalene (0 cetane)
Heating Value	Indicates the heat released during combustion	Indicates the fuel's energy density and requirements depend on the application
pH	Indicates acidity of oil	Bio-oil should not cause corrosion to standard pipes, vessels, and engines

2.5.1 Biomass pretreatments for improving the bio-oil quality

Pretreating biomass has been identified as one of the most promising routes for improving the bio-oil's quality [186]. Some pretreatment methods have the potential to reduce the variations between different biomass species [126]. Techniques for pretreating lignocellulosic biomass prior to pyrolysis include: mechanical comminution, alkali swelling, demineralisation (acid leaching), dry torrefaction, hydrothermal torrefaction, and exposure to supercritical fluids. If the quality of bio-oil produced directly from pyrolysis is improved through pretreating the biomass, it will reduce the extent of secondary upgrading required [187]. The additional energy required for the pretreatments has to be offset by the benefits; therefore is dependent on the biomass type and pretreatment implemented. In some cases, hardwoods have a higher permeability along the grain compared to softwoods, this is due to long vessels in the hardwood matrix and allows pretreating agents easier passage [79].

2.5.1.1 Alkali swelling

Alkali swelling with sodium hydroxide (NaOH) is traditionally used during bioethanol production to increase the digestibility of cellulose and remove lignin [79, 188]. The swelling mechanism is thought to be through saponification reactions breaking uronic ester bonds crosslinking hemicellulose to other polymeric materials (such as lignin) [79, 189]. Glucoside bonds are also weakened through depolymerisation of the pyranose ring [190]. After the pretreatment, a portion of the sodium ions become incorporated into the biomass matrix [188], either in carboxyl groups [79], present as sodium acetate, or as salts in the free water. Sodium acetate is formed through saponification of hemicellulose acetate [189]. Leaching with water after alkali swelling can remove most of the sodium salts present in the water and the sodium acetate but ion exchange with an acid is required to remove the sodium ions associated with carboxyl groups. Alkali swelling without subsequent acid washing will decrease the bio-oil yield during pyrolysis as the catalytic inorganic content of Na is increased.

Higher lignin contents reduce the efficiency alkali swelling, thus pretreating hardwoods is more efficient compared to softwoods for ethanol production [189]. Alkali swelling as a pretreatment for pyrolysis could enhance bio-oil yields by breaking crosslinks that enhance secondary and charring reactions. The main sugar in softwood hemicellulose is O-acetyl-galactoglucomannan; the acetyl side-branches are much more easily cleaved by alkali than by acid [111]. Removal of acetyl groups from biomass reduces the bio-oil's organic acid content after pyrolysis. Hassan *et al.* [191] leached pine wood with sodium hydroxide, calcium hydroxide, and ammonium hydroxide. It was found that the pretreatments decreased the total acid number the bio-oils, which was thought to be due to reduced acetyl compounds and possibly reduced uronic acid groups.

2.5.1.2 Demineralisation

As reviewed in Section 2.3.4, the inorganic constituents in biomass catalyse dehydration and cracking reactions during pyrolysis, lowering the bio-oil quality and yield. Inorganics are problematic during pyrolysis, vapour condensation, bio-oil storage, final upgrading, and end use [192]. Demineralisation involves leaching biomass in water or in a dilute acid to reduce the inorganic fraction. Leaching is typically carried out at either room temperature or at elevated temperature up to 150 °C. High temperatures or strong acidic solutions may depolymerise the biomass polysaccharides, especially hemicellulose. Demineralisation is a relativity expensive step when producing a low value fuel; therefore the pretreatment must be carried out in a fashion that minimises costs such as heating and acid usage [130]. Environmental issues concerning the disposal of the mobile phase after leaching must be considered due to possible traces of hazardous elements [193]. Inorganic regulatory limits for fuels may require bio-oil processing to reduce the content, increasing the attractiveness of biomass leaching.

The detrimental inorganics are normally considered as the alkali and alkaline earth metals (AAEMs). Encinar *et al.* [138] impregnated biomass with NaCl, LiCl, KCl, $FeCl_3 \cdot 6H_2O$, $AlCl_3 \cdot 6H_2O$, and $ZnCl_2$. The transition metals actually decreased the bio-oil yield more than the AAEMs tested. Therefore, the inorganics targeted for removal during demineralisation requires clarification: demineralisation will be considered as a reduction of the total inorganic fraction instead of only the AAEMs. Only silica is considered inert at pyrolysis temperatures [124], but has been reported to be catalytic at higher temperatures such as those during gasification [100].

The biomass inorganics can be reduced by 70-75% through water leaching [107, 194]. Water leaching also removes water soluble extractives, while hot water washing removes biomass starches [136]. 80% of potassium and sodium is commonly removed during water leaching, chlorine removal can reach 90%, whereas sulfur and phosphorus are partially removed [129]. Deionised water (DI) washing reduces the salts present in biomass while tap water washing can actually deposit additional ions such as calcium onto the biomass [107].

Leaching in an acidic solution will remove additional inorganics in comparison to those targeted by water leaching. This suggests that inorganics present in biomass in multiple forms: probably as soluble salts and

cations bound to reactive sites in wood, which act as functionalities of cellulose or acid groups in lignin and hemicellulose. Cations would be expected to exchange ions with an acid during leaching [130]. When the soluble salts are removed though water washing, there is no significant effect on the bio-oil yield or composition. However, removing the acid soluble ions generally decreases pyrolytic water, increases bio-oil yields, and significantly alters the bio-oil composition [130, 194]. This is because the acid soluble ions are bound closer to the cellulose, hemicellulose, and lignin; therefore are more likely to interact during pyrolysis by catalysing fragmentation and charring reactions rather than depolymerisation reactions [130, 194]. However, a portion of the inorganics remain in the biomass even after severe acid leaching, indicating that some inorganics are strongly bound to the biomass [134], such as silicates.

Table 2-9 presents a summary of previous research on biomass leaching using various leaching reagents. The change in yield is given as a percentage relative to the initial mass. The results from these studies vary significantly amongst from different researchers, with possible reasons including:

- Different leaching reagents
- Severe leaching altering the biomass's morphology
- Different types of biomass having different chemical compositions
- Varying analytical techniques
- Different leaching conditions
- Mineral acid ions may become incorporated into the biomass after leaching, which may catalyse reactions during pyrolysis
- Different pyrolysis conditions.

Bio-oil produced from the leached biomass is normally higher in viscosity and can also have a higher molecular weight due to reduced fragmentation reactions [123]. The pH of the bio-oil normally increases due to reduced secondary reactions [115, 130], although Hassan *et al.* [191] found it decreased due to the removal of AAEMs in the biomass. Inorganics reduction can also alter the char morphology by increasing the surface area by an average of 30% [100]. Removing inorganics deposited in biomass pores may cause the increase in surface area [195].

Table 2-9: Summary of data from leaching biomass prior to pyrolysis

Leaching conditions				**Change in yields based on pyrolysis of the pretreated biomass compared to raw biomass, times reduced**								
Reagent	Time (min)	Temp. (°C)	Biomass type	Inor-ganics	Orga-nics	Gas	Char	Water	Levog-lucosan	Glycol-aldehyde	Acetic acid	Formic acid	Ref.
5% H_2SO_4	-	25	Wheat Chaff	-	0.24	-0.14	-0.41	-24	11.25	-1.00	-	-	[166]
5% H_2SO_4	120	100	Poplar	-10.5	0.12	-0.41	-0.18	-48	84.4	-0.91	-0.97	-0.54	[104]
3.7% HCl	120	100	Poplar	-10.3	0.30	-0.19	-0.29	-100	47.6	-0.35	-	-	[104]
0.5% HCl	6	165	Poplar	-9.8	0.19	-0.30	0.31	-76	0.48	-0.09	-	-	[104]
5% H_2SO_4	330	90	Cellulose	-10	0.15	-0.50	-0.76	-44	3.54	-0.60	-0.98	-0.66	[104]
1% H_2SO_4	60	100	Loblolly pine	0.74[1]	0.17	-0.37	0.06	32	0.40	-	-	-	[188]
0.5% H_2SO_4	60	100	Loblolly pine	0.82[1]	0.17	-0.37	0.06	42	-0.20	-	-	-	[188]
5% H_2SO_4	360	90	Poplar	-	0.06	-0.41	0.21	-66	0.70	1.26	-0.04	0.11	[196]
1% H_2SO_4	1140 (19h)	90	Poplar	-	0.19	-0.63	-0.22	-78	4.16	-0.47	-0.73	-0.18	[196]
Hot water	330	90	Poplar	-	0.21	-0.69	-0.13	-95	9.01	-.0.96	-0.97	-0.54	[196]
0.1% HNO_3	42	30	Poplar	-0.99	0.13	-0.32	-0.30	16	4.70	-0.80	-0.76	-	[130]
3% H_3PO_4	60	100	loblolly pine	-	-0.40	-	-	5.3	-0.71	-	-	-	[191]
2.1% H_2SO_4	60	100	loblolly pine	-	-0.38	-	-	11.8	-0.54	-	-	-	[191]
Water	60	25	Sugarcane bagasse	-0.31	0.65	-0.14	-0.19	-6.7	-	-	-	-	[195]
5M HCl	60	25	Sugarcane bagasse	0.16[1]	1.15	-0.17	-0.10	-30.8	-	-	-	-	[195]
3% HF	60	25	Sugarcane bagasse	-0.98	1.46	-0.34	-0.45	-38.3	-	-	-	-	[195]

[1]*The inorganic content appeared to increase either because the pretreatment removed a portion of the hemicellulose or additional ions from the acid became incorporated into the biomass*

2.5.1.3 Torrefaction

Torrefaction is regarded as a mild version of slow pyrolysis, characterised by slow heating rates, long residence times and temperatures between 200-320 °C. The main product is a solid, with minor amounts of liquid and NCG produced. The use of torrefaction as a pyrolysis pretreatment is relatively new, with the original development aimed at increasing the energy density of biomass for palletising [107, 197-199]. Torrefaction softens lignin to improve the pallet strength as the lignin acts as a binder. The weakened biomass structure decreases the pressure and energy required during palletisation by a factor of 2 for palletisation at 225 °C. The heating value of the pellets also increases by 70-80%, which is similar to some coals [117]. In recent years, torrefaction has increasingly been used as a biomass pretreatment prior to pyrolysis. Torrefaction reactors are much simpler than pyrolysis reactors as the vapour residence time is not crucial, allowing larger biomass particles to be used. Auger reactors are commonly used but other types reported include fixed beds and rotary drier configurations [199].

Biomass's fibrous structure is destroyed during torrefaction, which reduces biomass grinding costs of the solid product by up to 90% [200]; although biomass can become too friable with severe torrefaction [197]. Torrefied biomass exhibits increased particle spherically when ground, improving flow characteristics, and higher bulk density [117, 198, 201, 202]. The liquid product produced mainly contains water and acetic acid. Lignin can decompose slightly to produce phenolic compounds [117], and methanol (if the lignin contains methoxy groups [203]). The NCG mainly consists of CO_2, CO with minor amounts of CH_4. CO_2 is produced mainly through decarboxylation of carboxyl groups in hemicellulose. The CO yield increases with the inorganic content of biomass and temperature of torrefaction, indicating that it is probably linked to secondary reactions [204]. These include decarbonylation of compounds formed during torrefaction or secondary reactions of CO_2 with steam and char [203].

Residence time and reactor temperature determine the severity of torrefaction. Chen and Kuo [205] examined torrefaction of individual biomass components. Results suggested that hemicellulose decomposes at a relatively low temperature, followed by cellulose at higher temperatures. Key results from this study are shown in Table 2-10. These findings were confirmed by Zheng *et al.* [206], who found that the cellulose weight percentage in torrefied biomass first increased from 46.4 to 46.7 wt% at 240 °C to a maximum of 51.3 wt% at 260 °C, and then decreased to 36.4 wt% at 320 °C as the cellulose started to depolymerise. Complete cellulose and hemicellulose removal in pine wood can be accomplished by torrefaction at 300 °C for 4 h, with lignin partially remaining [207]. Three torrefaction classes are classified as:

- *Mild torrefaction (<220 °C)*: Non-reactive drying and particle shrinkages occurs initially followed by reactive drying; bond breaking (hydrogen, C-O and C-C); and volatising of lipophilic extractives and other light compounds [197].
- *Moderate torrefaction (220-250 °C)*: Distinguished by water, CO, CO_2, CH_4, light volatile, and organic acid release [200].
- *Severe torrefaction (>250 °C)*: Removal of the majority of hemicellulose. Cellulose and lignin decomposition initiates when residences times are prolonged [107]. Temperatures over 300 °C are normally associated with severe biomass loss and are not recommended for biomass pretreating [117].

Table 2-10: Torrefaction of individual biomass components at different temperatures, obtained from Chen and Kuo [205]

Torrefaction temp. (°C)	**Percentage decomposed (wt%)**		
	Cellulose	Hemicellulose	Lignin
230	1.1	2.7	1.5
260	4.4	38.0	3.1
290	44.8	58.3	7.0

The content of inorganics, moisture, hemicellulose, and the biomass's polymeric structure all influence the torrefaction severity for a given temperature and residence time [207]. Medic *et al.* [208] examined the effect of biomass moisture content between 30-50 wt%. The study found that high biomass moisture tends to

increase the severity of torrefaction and lower the solids yield. This was thought to be due to expansion of water vapour inside the biomass polymer matrix during the temperature ramping stage which would loosen the material and make it less resistant to mass transfer. When heating rates were below 50 °Cmin^{-1}, it was proposed that the reaction limiting parameter was the kinetics not the heat transfer rate through the particle. Therefore, the change in total solid yields could be due to interactions with the organic acids produced and the biomass as the water vapour in the particle enhances acid interactions. Torrefaction affects the crystallinity of biomass. Chang *et al.* [203] noted that up to 300 °C, the crystallinity of the biomass increased, due to decomposition of amorphous regions, but after 300 °C, severe biomass decomposition occurred and the crystallinity decreased. Zheng *et al.* [186] reported a similar trend.

2.5.1.3.1 Pyrolysis of torrefied biomass

Torrefaction as a pretreatment prior to pyrolysis has the potential to reduce the oxygen, moisture, and acetyl content of biomass, and therefore the content of these components in the pyrolysis oil. During torrefaction, free and bound water is removed and non-polar unsaturated structures are formed that cause biomass to become more hydrophobic [209]. Removing oxygen is relativity easy during torrefaction because oxygen-containing functional groups such as methyl and acetyl groups with a high activity and low activation energies are easily removed as light oxygenates, CO, and CO_2 [207, 209]. Higher temperatures and longer residence times improve the oxygen removal, with around a 60 wt% reduction possible for biomass at 290 °C for 1 hour [198]. The trade-off of high oxygen removal is severe biomass loss, carbon-carbon crosslinking, and hydrogen loss as small hydrocarbons [209].

Various authors have looked at torrefaction as a pretreatment for pyrolysis [107, 186, 200, 203, 210, 211] [186]. It was reported that pyrolysis of torrefied biomass increases char yield at the expense of bio-oil. Torrefaction below 275 °C and with residence times shorter than 30 min marginally increased the char yield during pyrolysis [212]. Bio-oil yields from pyrolysis of torrefied biomass normally decrease due to carbon-carbon crosslinks forming in cellulose during torrefaction. These can undergo further polycondensation reactions to form char during pyrolysis [186]. Carbon-carbon crosslinks are created when an adjacent hydroxyl groups is removed to produce water. Worasuwannarak *et al.* [93] thought crosslinks also occur between lignin and cellulose to form water and an ester. The degree of crosslinking can be determined by the increase in acid insoluble fibres during biomass hydrolysis as torrefaction produces compounds that act like lignin in the fibre analysis, alternatively Fourier transform infrared spectroscopy (FTIR) can be used to analysis chemical bonds [203, 213].

Westerhof *et al.* [211] investigated pyrolysis of torrefied pine and noticed that for torrefaction below 290 °C, the sum of the pyrolysis oil and the torrefaction liquid were approximately equal to the yield of bio-oil from pyrolysis of raw biomass. Conversely, Zheng *et al.* [206] showed that when the torrefaction temperature of pine increased from 240 to 320 °C, the total liquid from torrefaction plus pyrolysis oil decreased from 58.8 to 38.9%. Both studies used same feedstock of pine and both researchers used fluidised beds pyrolysis

reactors, these results indicate there are still some unknown parameters, thus more research is required to determine why there were discrepancies between the results.

Bio-oil produced from pyrolysis of torrefied biomass contains less water, oxygen, organic acids, and light components [210]. Zheng *et al.* [186] noticed that for torrefied biomass, the water, furfural, and acetic acid content decreased after pyrolysis while the carbonyl content increased. Chang *et al.* [203] found that the levoglucosan yield increased with torrefaction, speculated to be caused by the slightly disturbed wood structure reducing catalytic interactions between the wood components. However, it is more likely that the disturbed wood structure and the enhanced biomass pore size facilitated volatile removal during pyrolysis [117]. In raw biomass, cellulose and hemicellulose are sealed by lignin, thus during pyrolysis primary products such as levoglucosan are diffusionally restricted from escaping the reaction zone [83]. Meng *et al.* [200] reported that the bio-oil from torrefied biomass was rich in pyrolytic lignin, anhydrosugars, and low in light oxygenates and aldehydes. The increased pyrolytic lignin content could be detrimental for secondary upgrading as it is thought to be a precursor to coke formation, although Hilten *et al.* [214] reported decreased coke, char, and tar yields during catalytic upgrading of bio-oil using common HZSM-5 catalysts.

2.5.1.3.2 Hydrothermal torrefaction

Hydrothermal torrefaction occurs in a water environment, under significant pressure so that water remains a liquid at elevated temperatures. The process was traditionally used as a biomass pretreatment during ethanol production. When operated at similar temperatures as dry torrefaction (normally torrefaction), the energy densification is better and reactions more severe [79, 173], as water can penetrate the biomass channels into the axial direction providing uniform conductive heat transfer; opposed to primarily convective heat transfer during dry torrefaction.

During hydrothermal torrefaction, acetic acid is formed from degradation of the acetyl branches in hemicellulose, giving a mild acid hydrolysis reaction and slight inorganic removal. Stephanidis *et al.* [215] found that the pretreatment at 190 °C under autogenous pressure (approximately 1.24 MPa) for 8 min lead to 13 wt% higher organic yield during pyrolysis and 5 wt% less pyrolytic water was produced. The acetic acid content in the bio-oil was reduced from 14.4 to 3.9 wt%. Wang *et al.* [188] reported the opposite trend and noted that pyrolytic water increased after the hydrothermal torrefaction at 190 °C under 1.3 MPa of pressure for 10 minutes. During hydrothermal torrefaction, the pyrolytic water is probably partially being reduced due to the removal of some inorganics; therefore results would depend on the acetyl content in the hemicellulose fraction of the raw biomass. Hydrothermal torrefaction in the presence of an acid was investigated by Chaiwat *et al.* [216], who examined the structure of cellulose after hot phosphoric and sulfuric acid (200 °C and 1% acid solution) and hot water (240 °C) pretreatments. Acid pretreatments changed cellulose into a partly crosslinked loose structure leading to high a bio-oil yield (especially levoglucosan). On the other hand, the hot water washing had the opposite effect by producing a random and

highly crosslinked cellulose structure. It was thought that acid addition favoured depolymerisation reactions over crosslinking reactions.

Yan *et al.* [213] compared dry torrefaction to hydrothermal torrefaction for lobby pine. Key results from this study are given in the Table 2-11, it was found that hydrothermal torrefaction was more severe compared to dry torrefaction, and had a higher rate of oxygen removal for similar solid yields. One reason for the higher biomass yields from hydrothermal torrefaction was that aqueous solubles remained stuck in the biomass pores. Hydrothermal torrefaction at 200 °C gave the same oxygen reduction as dry torrefaction at 300 °C, but the biomass yield was 70.6% for hydrothermal torrefaction compared to 60.5% for dry torrefaction. It was also observed that the inorganic content was lower and hydrogen content higher for hydrothermal in comparison with dry torrefaction. Wet torrefaction may give better results but these would have to be offset by the high capital and operational costs.

Table 2-11: Comparison between dry and hydrothermal torrefaction of loblolly pine, data obtained from Yan *et al.* [213]

Pretreatment	Temp. (°C)	Mass yield (%)	Carbon (%)	Hydrogen (%)	Oxygen (%)	Hemi-cellulose (%)	Cellulose (%)	Lignin (%)	Aqueous solubles (%)	Ash (%)
Raw biomass	-	-	50.3	6.0	43.3	12	54	25	9	0.4
Hydrothermal torrefaction	200	88.7	54.7	6.0	39.1	0.4	47	28	24	0.5
	230	70.6	56.1	5.9	37.9	0	41	30	25	0.4
	260	57.0	72.1	4.9	22.9	0	34	34	32	0.5
Dry torrefaction	250	83.8	50.7	6.2	42.9	9	51	34	5	0.5
	275	74.2	52.3	6.1	41.5	7	53	37	4	0.6
	300	60.5	54.8	5.9	39.1	2	33	62	2	0.7

2.5.2 Bio-oil upgrading

Pretreatments are aimed at improving the quality of crude bio-oil by reducing the water, oxygen, organic acid, char, and inorganic content in bio-oil. Further bio-oil upgrading and refining is required to produce a fuel to current transportation standards. This includes increasing the calorific value, removing all acids, and further reducing the water, oxygen, inorganic, and solids content. Upgrading techniques include phase separation, reduction, esterification, supercritical upgrading, hydrotreating, catalytic processing, catalytic pyrolysis, hydropyrolysis, or combinations of these. These are typically applied to crude bio-oil but implementation is limited by the high pressures and/or temperatures, complicated equipment, catalyst deactivation rates, hydrogen requirements, and high reactor clogging rates [3, 16, 164, 217]. It is possible to combine hydroprocessing and catalytic cracking with the intention of increasing overall efficiency. Hydrotreating initially can serve as a stabilisation step for bio-oil before catalytic cracking, but the economics are still unfavourable [217].

Compounds that limit the efficiency during bio-oil upgrading should be targeted during the pretreatments. Important characteristics are the molecular weight distribution, oxygen content, acidity, stability, and hydrogen to carbon ratio [218]. High molecular weight compounds such as pyrolytic lignin are generally unstable and form tar or coke when heated. Their low volatility hinders upgrading procedures that require compounds to volatise. Oxygen reduction is a primary objective of bio-oil upgrading; the bond dissociation

energies required during deoxygenation are given in Table 2-12. High bond energies indicate higher activation energies required to break these bonds, thus catalysts are implemented to reduce activation energies. Generally, phenol is hard to deoxygenate [7]. Ether compounds can polymerise during upgrading. Decarboxylation of organic acids requires large activation energies and is prone to coke formation compared to deoxygenation of other compounds such as alcohols [7]. Aldehyde and ketone deoxygenation is also prone to coke formation.

Table 2-12: Bond dissociation energy required during deoxygenation [7]

Bond	Dissociation energy ($kJmol^{-1}$)
C-O	1076.5
C=O	749
C-C	610.0
O-H	430.0
C-H	338.4

2.5.2.1 Fractionation

Bio-oil fractionation can be implemented to separate water and water soluble compounds such organic acids. These can be separated through selective condensation of pyrolysis vapours or after condensation with specialised distillation, centrifuging, drying agents, or by water addition.

Selective condensation reduces additional process equipment. It separates pyrolysis vapours either by the components' dew point or latent heat of condensation. Water is condensed in either the first or last fraction depending on the condenser temperatures [78, 219]. If the temperature exiting the first condenser is above 100 °C, heavy compounds condense while water and other light oxygenates remain in the vapour phase [220].

Bio-oil cannot be distilled using traditional processes due to its thermal instability and solids content. Other distillation techniques such as molecular, flash, and distillation with inert gases and steam have been tested instead [221, 222]. Flash, inert gas, and steam distillation prevents secondary reactions due to the short residence time but are only suitable for pre-separation, where high purities are not required [102, 221]. Molecular distillation gives higher yields than other techniques [221, 223], but coking and polymerisation reactions occur at elevated temperatures [221]. Removal of char particles prior to molecular distillation and an operational temperature below 80 °C can prevent coking [224], although a residue remains. Using these distillation techniques, water, organic acids, and other light oxygenates are initially vaporised and collected. The second fraction is normally considered the bio-oil fraction with both a low water content and oxygen content and improved stability [221, 222].

Drying agents can be used for separation of bio-oil compounds; drying agents include molecular sieves, sodium sulphate anhydrous adsorbents, and calcium oxide. Sodium sulphate anhydrous adsorbents are expensive and not as effective as molecular sieves but there are regeneration issues with molecular sieves as bio-oil needs to be combusted for removal. Calcium oxide forms a cake that nearly half the bio-oil becomes immersed within, reducing yields significantly [66].

Phase separation of bio-oil occurs at around 30 to 45 wt% water [182]. The aqueous phase contains compounds such as levoglucosan, organic acids, and light oxygenates while the viscous inorganic phase contains mainly lignin derived components [182, 225]. The organics in the aqueous phase should be recovered to prevent loss of yields [142]. Activated carbon adsorption (produced from char) can purify the water for disposal and remove the organic compounds [155].

2.5.2.2 Chemical reduction, esterification, and supercritical solutions

Ketones and aldehydes are highly active compounds in bio-oil; therefore reduction (hydrogenation) to alcohols or hydrocarbons will improve the bio-oil's stability. Partial reduction of carboxylic acids to aldehydes and ketones is beneficial as these are easier to deoxygenate further [7]. The reagents used must be able to donate a proton. Formic acid in the presence of a metal catalyst (nickel, platinum, or palladium) or in a hydrothermal environment can reduce ketones to alcohols. Between 260-300 °C, water has a lower dielectric constant; fewer and weaker hydrogen bonds; and a higher isothermal compressibility than ambient liquid water [226]. Indicating water molecules may act as catalysts and directly participate in the transition state by producing a hydrogen-bond ring network with the ketone, acid, and water [227]. Small quantities of formic acid are produced during pyrolysis but high acid to ketone ratios are required (around 2:1), restricting the use of this technique as formic acid is more expensive than transport fuels per unit volume.

Esterification is normally done by adding an alcohol (methanol, ethanol, or propanol) to the non-aqueous fraction of bio-oil [162]. Carboxylic acids react with the alcohol at room temperature to form the corresponding ester. However, esterification of bio-oil components in the presence of a catalyst increases reaction rates and reduces the reaction residence time. The alcohol can also have a stabilising effect by converting reactive aldehydes to hemiacetals and acetals [162, 228].

Another possible upgrading technique is to use supercritical solutions, which have been used in petroleum and coal processing industries to upgrade shale oil, coal tar, heavy fuel oils, and tested for algae bio-oil upgrading [229]. The use of supercritical solution is less researched for bio-oil from woody biomass. Supercritical ethanol can be used to help solubilise oligomers into monomers. This requires a catalyst to upgrade bio-oil to prevent tar formation. Supercritical ethanol upgrading can improve bio-oil and stabilise it by reducing acids, phenols, aldehydes, and ketones [171]. Zhang *et al.* [230] upgraded bio-oil using supercritical ethanol in a hydrogen atmosphere at 260 °C, using the bifunctional catalyst $Pt/SO_4^{2-}/ZrO_2$/SBA-15. Reactions were dominate by esterification to give a bio-oil rich in esters, ethers, and ethanol and depleted in organic acids, aldehydes, phenols, ketones, PAHs, and sugars.

2.5.2.3 Hydroprocessing

Hydroprocessing is commonly used in the petroleum industry for hydrodesulfurisation and hydrodenitrogenation of crude oil [231]. The same process has been applied to bio-oil for hydrodeoxygenation: either directly as vapours are produced (on-line) or after condensation (off-line) [162, 232-234]. On-line hydroprocessing reduces heating and cooling energy requirements but larger reactors are

required due to the inert gas and water vapour present [232]. Initial phase separation of the bio-oil for off-line upgrading reduces the reaction severity and the catalyst deactivation rate [234].

Hydroprocessing is non-selective for products, requires high pressures, uses complicated equipment, requires hydrogen, and experiences problems with catalyst deactivation and reactor clogging [3, 16, 164, 217]. Catalyst deactivation is caused by water attacking the support, alkali metals, coking, and loss of sulphide from the catalyst [164]; therefore a sulfur supply is required for sulfide catalysts [7]. Acetic acid can enhance coke formation when hydrotreating glucose, while the presence of acetaldehyde and acetone alter reactions pathways to alter the products formed [235]. The presence of guaiacol compounds may also lead to catalyst deactivation [3]. Several researchers have looked at producing hydrogen *in-situ* via water gas shift reactions of the aqueous phase [234], or by consuming a portion of the bio-oil in the presence of a catalysts to make a hydrogen rich syngas [236].

A bio-oil hydroprocessing environment is carbon limited, giving a maximum stoichiometric yield of 56-58 wt%. During hydrotreating process, 20-30 wt% of the carbon in bio-oil is converted into gas-phase carbon, decreasing the maximum overall yield of bio-oil to around 40 wt% [3]. Mild hydrotreating increases the liquid yield but will reduce the rate of deoxygenation [237], and can increases the bio-oil's viscosity dramatically [162]. A second hydrocracking stage can further reduce the viscosity and the bio-oil's oxygen content, with typical conditions given in Table 2-13. Two stage hydroprocessing may reduce coke formation as the rate of coke formation is low below 150 °C, even in the presence of an acid [235]. Researchers have also investigated the effect of additives (such as tetralin) with the idea that these additive could enhance hydrogen transfer from the gas phase to the radical fragments, thus increase the bio-oil yield [232].

Table 2-13: The two stages of hydroprocessing

	Stage 1: hydrotreating	**Stage 2: hydrocracking**
Temperature (°C)	250-400 [41]	350-450 [164]
Pressure (MPa)	7-10 [41]	10-14
H_2 consumption	Low, 5 wt%	High, 700 Lkg^{-1} bio-oil
Purpose	Stabilisation, reduces coking	Breaks down heavy molecules [41]
Possible catalyst	Cobalt-molybdenum	Nickel-molybdenum
Products	Levoglucosan, ketones, and aldehydes converted to alcohols	Alcohols and acids converted to hydrocarbons

2.5.2.4 Catalytic processing

Extensive research has been done on catalytic upgrading of bio-oil. Catalysts can crack the pyrolysis vapours on-line [77, 184, 238-240], or off-line [241-245]. On-line upgrading gives higher liquid yields and improves product quality compared to off-line upgrading as additional coke is formed during bio-oil revaporisation [77]. In catalytic upgrading, bio-oil compounds are cracked on the catalyst's surface, followed by synthesis of compounds in the zeolites pores to convert oxygenated compounds in bio-oil into lighter hydrocarbons [164]. Bio-oil is deoxygenated via three main reactions: dehydration, decarboxylation, and decarboylation, which release H_2O, CO_2, and CO, respectively, as well as direct molecular cracking [246].

Catalytic processing is normally operated at atmospheric pressures and at temperatures between 350-500 °C. Fluid catalytic cracking (FCC) catalysts commonly used is Zeolite Socony Mobil-5 (ZSM-5). The quality of the catalytically upgraded bio-oil is relativity low with high water, coke, and gas production [217, 239]. The nanopore structure (about 5.4 to 5.5 A) of ZSM-5 allows for hydrocarbons production in the petrol range but leads to rapid pore blockage [7]. Compounds in bio-oil that are thought to limit the efficiency of catalytic processing and lead to pore blockages or catalysts deactivation include:

- Oxyphenols and furfurals which can deactivate zeolites [3]
- Aldehydes, oxyphenols, acids, furfurals, and lignin derived compounds may contribute to coke formation [214]
- Heavy metals and sulfur which are major factors responsible for FCC catalyst deactivation [217]
- Water (steam) which can cause high coke yields and dealumunation of the zeolite [231], which can irreversible deactivate it [246]
- Water formed during dehydration reactions which can adsorb onto acids sites in the catalyst to decrease its activity [7]
- Highly oxygenated compounds tend to produce coke when reactively dehydrated, while dehydration of lower oxygen content compounds produces more hydrocarbons [247]
- Coke which once produced, causes reversible catalyst deactivation [246]

Catalytic upgrading is a hydrogen limited process, with a maximum stoichiometric yield of 42 wt%. Multi-functional catalysts should have the ability to generate hydrogen *in-situ* by shifting the CO in the gas product to give a maximum possible yield of 55 wt%; however practical yields would only be about half this due to tar and coke formation [164]. Upgrading bio-oil by blending with petroleum oil can reduce coking (not linearly linked to the ratio of bio-oil to petroleum oil, indicating interactions occur) [246]. Primary upgrading of bio-oil can improve the efficiency of catalytic processing. For example, bio-oil produced from torrefied biomass and upgraded using HZSM-5 produced less coke and tar as the bio-oil contained less acids, aldehydes (5-HMF and furfural), and oxyphenols (guaiacol, creosol) [214, 248].

Various catalysts previously studied for bio-oil upgrading are shown in Table 2-14. From the table, it can be seen that catalyst selectivity still requires modification and improvement, possibly by manufacturing new multi-functional catalysts [24]. Zhang *et al.* [16] stated that after reviewing catalysts commonly used, a catalyst with good performance of high conversion and little coking tendency would require highly sophisticated technology.

Table 2-14: Cracking catalysts used for upgrading bio-oil

Catalysts tested	Upgrading temp. (°C)	Bio-oil yields (wt%)	Ref
Off-line			
HZSM-5, H-Y, H-mordenite, silica, and silica alumina	370	27.9, 14.1, 4.4, 5.0, 13.2	[241, 242]
HZSM-5 and H-Y	450	18.8, 49.2	[243]
Red mud	350	To reduce acids	[245]
On-line			
Al-MCM-41, FCC, siliceous SBA-15, and Al-SAB-15	500	13.1, 19.5, 16.9, 19.3 (organic yields)	[184]
AI-MSU-F, MI-575, and ZSM-5	500	ZSM-5 produced 3 fold more light phenolic compounds	[239]
ZnO			[240]
ZnO, MgO, dolomite, and limestone	500	57 (raw), 51, 36, 26, 32	[249]
FCC, HZSM-5, and H-mordenite	500, 450, 500	61 (raw), 39, 46, 34 (carbon basis)	[250]

2.5.2.5 Catalytic pyrolysis

To directly improve the bio-oil quality, catalytic pyrolysis of biomass has been studied. It has the potential to improve the bio-oil's stability before hydroprocessing and improve overall upgrading efficiency [251]. Catalytic pyrolysis reduces process equipment compared to on-line catalytic processing and eliminates revaporisation required for off-line catalytic processing [43]. A suitable pyrolysis catalyst would enhance cracking reactions of heavy molecules to give a lighter and less viscous bio-oil and reduce reactive oxygenated species, especially carbonyl compounds [239]. The catalyst can be embedded in the biomass particles or the biomass can be mixed with the catalyst particles through abrading, kneading, or grinding [83]. Catalysts can also be added directly to the pyrolysis reactor.

Various catalysts tested in previous studies are given in Table 2-15. Most catalysts increase char, coke, water, and NCG yields while decreasing the yield of primary pyrolysis products (such as levoglucosan) through dehydration and cracking reactions. It is beneficial to remove oxygen as CO_2 or CO as this reduces the concentration of acids and aldehydes, whereas dehydration can cause double bonded compounds to form [172]. ZSM-5 and FCC catalysts give low bio-oil yields while only slightly improving the bio-oil's quality, possible due to the strong acid groups incorporated into the catalysts; therefore these are not recommended. Stephanidis *et al.* [215] confirmed this observation by comparing H-ZSM-5, Al-MCM-41, and silicalite catalysts (with less acid groups). It was concluded that the presence of strong acids decreases bio-oil yields. Torri *et al.* [172] tested 31 catalysts using Py-GC-MIP-AED and stated that the best catalysts were the bulk metal oxides (ZnO, Fe_2O_3, and CuO compared to ZSM-5 type catalysts).

Table 2-15: Summary of past research on catalytic pyrolysis

Catalysts	Biomass	Effect on yields				Bio-oil	Ref.
		Liq	Char	NCG	Water		
H_3PO_4 and $(NH_3)_3PO_4$	Miscanthus, cellulose, xylan, lignin	↓	↑			Levoglocosenone: ↑, furfural:↑	[252]
HZSM-5	Pine	↓	↓	↑	↑	Oxygen: ↓(36.4→23.7%), acids: ↓, ketones: ↓, aldehydes: ↓, alcohols: ↓, phenols: ↓	[238]
ZSM-5	Pine					Aromatics: ↑ (15.5%)	[253]
CaO	Pine powder	↑	↑	↓	↑	Oxygen: ↓(39→31%), organics: ↓, levoglucosan: ↓, formic acid: ↓, acetic acid: ↓, furfural: ↑, furfuryl alcohol: ↑, hydroxymethylfurfural: ↑, 2(5H)-furanone: ↑	[183]
CaO	Aspen-poplar	S				Ethylene: ↑, methane: ↑. Lowered the temperature for maximum liquid production by around 50 °C	[254]
ZSM-5	Forest thinnings	↓			↑	Oxygen: ↓(34→19%)	[255]
NaOH and NaCl		↓	↑	↑	↑	Phenols: ↑, sugar derivatives: ↓, acetic acid: ↑, Hydroxyacetaldehyde: ↑	[139]
KCl	Xylan	↓	↑				[124]
KCl	Cellulose		↑		↑		[124]
$(NH_4)_2HPO_4$ and $(NH_4)_2SO_4$ (release H_2SO_4)	Fir	↓	↑		↑		[256]
CaO, and calcinated dolomite (CaO,MgO)	Pine chips	S	S	S		Oxygen: ↓, acidity: ↓, stability: ↑	[257]
Alumina (Al_2O_3)	Corncorb	↑				Oxygen: ↓(20.2→19.7%)	[73]
MgO	Cotton seed	↓	↑	↑		Calorific value: ↑, oxygenated compounds: ↓. Hydrocarbon distribution improved	[258]
$Fe(NO_3)_3$, Al-$(NO_3)_3$, $Ca(NO_3)_2$, K_2CO_3, $Mg(NO_3)_2$, and Na_2CO_3	Pine bark		↑			Oxygen: S. Al most severe catalyst	[133]
NaCl, KCl, $MgCl_2$, $CaCl_2$, $Ca(OH)_2$, $Ca(NO_3)_2$, $CaCO_3$, $CaHPO_4$, and switchgrass ash	Cellulose		↑	↑	↑	Low molecular weight compounds: ↑, sugar derivatives: ↓	[259]
H-beta zeolites with varying SiO_2/Al_2O_3 ratios	Pine	↓	↑	↑	↑	Aldehydes: ↓, ketones: ↓, phenols: ↓. levoglucosan: ↓, PAH: ↑	[110]
Al-MCM-41, FCC, pure siliceous SBA-15, and Al-SBA-15	Spruce		↓	↑		Aqueous yield: ↑, hydrocarbons: ↑, PAHs: ↑, phenols: ↑, furans: ↑, carbonyl compounds: ↓, acids: ↓, heavy compounds: ↓, alcohols: ↓	[184]
Na_2CO_3, NaOH, NaCl, and Na_2SiO_3	Pine, cotton, and fir		↑			↓pyrolysis temp.	[21]
TiO_2 and HZSM-5	Pine, cotton, and fir		↓				[21]

N.B: Some references were investigating the effect of inorganics during pyrolysis, rather than catalytic pyrolysis. S is the same yield

2.5.2.6 Reactive carrier gases

Some pyrolysis systems use an inert gas (typically nitrogen) as the gas carrier for fluidisation and as a heat carrier to supply heat to the reactor. However, the added inert gas dilutes the NCG stream, thus making the condensation and NCG use more complicated. Alternatively, NCG's produced during biomass pyrolysis (H_2, CO, CO_2, H_2O, and CH_4) can be recirculated into the reactor as the fluidisation gas and heat carrier [260]. CO_2 produces a mildly oxidative atmosphere while CO and H_2 produce a reducing atmosphere. Zhang *et al.* [25] tested pyrolysis NCGs individually and compared the results to N_2 as the fluidising gas. The liquid yields were 49.6, 57.1, 55.3, 58.7, and 56.4% when using CO, N_2, CO_2, CH_4, and H_2 respectively. It appeared that each gas suppressed the production of itself slightly, but promoted the production of other gases. For example, CO promoted the conversion of oxygen from the bio-oil fraction into CO_2, while H_2 promoted oxygen conversion to water. O_2 is commonly used in gasification systems, but less often for pyrolysis. When biomass is decomposed in the presence of O_2, oxidation and secondary reactions are

accelerated, lowering the bio-oil yield but increasing depolymerisation of biomass polymers. It may also increase the rate of CO_2 and CO production from polysaccharides [261].

Pyrolysis in a hydrogen atmosphere is referred to as fast hydropyrolysis. The hydrogen partial pressure helps address the hydrogen deficiency associated with pyrolysis. Insufficient hydrogen results in disproportionate reactions to form hydrogen depleted coke and undesirable recombined oligomeric tar compounds [27]. Producer gas can be steam reformed to produce H_2 for the system [19], or higher proportions of H_2 and CO can be supplied through coal, pyrolysis char, or biomass gasification. The use of *in-situ* water-gas shift catalysts in the reactors could also provide a way to control the H_2 partial pressure during pyrolysis [17].

Pyrolysis systems have been pressurised up to 15 MPa and operated in batch mode with extended residence times. Generally, the organic bio-oil yield decreases with increasing pressure but the products are lighter, more aromatic, and less oxygenated [262]. Extensive cracking increases the NCG yield and re-polymerisation reactions produce coke. Catalysts can be added to hydropyrolysis systems, certain catalysts such as iron-sulfur reduce char formation and aid in further oxygen removal [263]. Table 2-16 gives a summary of previously researched hydropyrolysis systems. Reducing reagents can also be used to provide a hydrogen environment. For example, with formic acid present, oxygen is efficiently removed as water to produce high quality bio-oil. Any excess formic acid is decomposed at the reaction conditions (2-54 h at 380 °C) [8, 27].

Table 2-16: Hydropyrolysis conditions from previous studies

Pressure (MPa)	Temperature (°C) and RT	Catalyst	Yields	Ref.
4	450, 100 s	None	5% higher liquid yields, slightly less oxygenated	[262]
6	475	Palladium on activated charcoal	37 wt% bio-oil produced	[19]
6	380 - 480, 1 h	Pyrrhotite and haematite	Slightly improved bio-oil yields	[264]
10	520	Colloidal FeS	Bio-oil yield 40-50 wt%, oxygen content low (11% minimum)	[263]
15	400 - 600	None	41.5 wt% bio-oil	[265]
10	500	None	Carbon yields increased from 55% to 75% compared to fast pyrolysis	[266]
Atm.	-	Zinc Oxide	Increased hydrocarbons	[240]

2.6 Conclusions

While there has been a large amount of research in the area of fast pyrolysis, the low quality of pyrolysis oil restricts its direct use and upgrading is required. The cellulose, hemicellulos, and lignin content in biomass influence the basic composition of the bio-oil produced; while inorganics, water, extractives, and organic acids in biomass alter the bio-oil's composition by either changing the primary reaction pathways or catalysing undesirable secondary reactions. The variable composition of biomass sources means literature on pyrolysis systems are hard to compare, and bio-oil has highly variable properties.

Bio-oil must be upgraded before it can be used as a transportation fuel. The most promising upgrading techniques are hydroprocessing and catalytic cracking; however both techniques are prone to coke formation, low yields, and rapid catalyst deactivation. The development of multifunctional catalysts may improve the efficiently and yields when upgrading crude bio-oil, but suitable catalysts would need to be regeneratable and cheap to manufacture. Bio-oil properties that cause these issues during upgrading include the acidity, water content, inorganic content, pyrolytic lignin content, and the instability. Pretreating biomass prior to pyrolysis to control the pyrolysis reactions has the potential to limit the content of these detrimental compounds in the bio-oil, possibly allowing for common catalysts such as ZSM-5 or bulk metal oxides to be used during upgrading procedures.

Researchers have investigated acid leaching of biomass prior to fast pyrolysis, results clearly indicate inorganics naturally inherent in biomass alter primary pyrolysis pathways and cause secondary reactions of pyrolysis vapours to produce undesirable products such as water, organic acids, and small oxygenates. Disposal of the waste produced during acid leaching and neutralisation of the solution remain issues. Torrefaction has only been research recently as a biomass pretreatment. Pyrolysis of torrefied biomass can reduce the bio-oil's content of water, oxygen, organic acid, and other light components. However, the char yield increases at the expense of bio-oil as significant improvements in the bio-oil properties are limited by the carbon-carbon crosslinks formed in the biomass carbohydrates during torrefaction. Past research has shown the benefit of acid leaching and torrefaction of biomass to improve the bio-oil properties, although both processes require further investigation before they could be economically implemented at large scale.

2.7 References

1. IEA. (2011). *Key world energy statistics*. Pais, France: International Energy Agency.
2. Haoxi, B., & Ragauskas, A. J. (2012). Torrefaction of loblolly pine. *Green Chemistry, 14*(1), 72-76.
3. Huber, G. W., Iborra, S., & Corma, A. (2006). Synthesis of transportation fuels from biomass: chemistry, catalysts, and engineering. *Chemical Reviews, 106*(9), 4044-4098.
4. Pimchuai, A., Dutta, A., & Basu, P. (2010). Torrefaction of agriculture residue to enhance combustible properties. *Energy & Fuels, 24*(9), 4638-4645.
5. Marsh, K. (2013). Energy: past, present, and future. Unpublished Presentation. The University of Western Australia.
6. Butler, E., Devlin, G., Meier, D., & McDonnell, K. (2011). A review of recent laboratory research and commercial developments in fast pyrolysis and upgrading. *Renewable and Sustainable Energy Reviews, 15*(8), 4171-4186.
7. Gunawardena, D. A., & Fernando, S. D. (2013). *Methods and applications of deoxygenation for the conversion of biomass to petrochemical products* (Vol. 16).
8. Kleinert, M., & Barth, T. (2008). Towards a lignincellulosic biorefinery: direct one-step conversion of lignin to hydrogen-enriched biofuel. *Energy & Fuels, 22*(2), 1371-1379.
9. Schuck, S. (2008). *Bioenergy from forestry - status and opportunities*. Paper presented at the Asia Pacific Forest Industries Climate Change Conference.
10. FOA. (2012/2013). New Zealand plantation and forest industry: facts and figures. In N. Z. F. O. Association (Ed.) (pp. 1-46). Wellington: New Zealand Forest Owners Association.
11. Bioenergy-Association-of-New-Zealand. (2015). Bioenergy association. Retrieved 10.8.2015, 2015
12. Roughton, E. (2001). *Energy from woody biomass in New Zealand*. Wellington: Energy Efficiency and Conservation Authority.
13. Scion. (2008). *Bioenergy options for New Zealand*: Scion.
14. McKendry, P. (2002). Energy production from biomass (part 2): conversion technologies. *Bioresour Technol, 83*(1), 47-54.
15. Bertram, G., & Clover, D. (2010). Kicking the fossil-fuel habit: New Zealand's ninety percent renewable target for electricity. 1-40. Retrieved from http://www.mfe.govt.nz

16. Zhang, Q., Chang, J., Wang, T., & Xu, Y. (2007). Review of biomass pyrolysis oil properties and upgrading research. *Energy Conversion and Management, 48*(1), 87-92.
17. Agrawal, R., & Singh, N. R. (2009). Synergistic routes to liquid fuel for a petroleum-deprived future. *AIChE Journal, 55*(7), 1898-1905.
18. Bridgwater, A. V. (1999). An introduction to fast pyrolysis of biomass for fuels and chemicals. In A. V. Bridgwater (Ed.), *Fast Pyrolysis of Biomass: A Handbook* (Vol. 1, pp. 1-13). Newbury: CPL Press.
19. Meier, D., Berns, J., & Faix, O. *Pyrolysis and hydropyrolysis of biomass and lignins - activities at the institute of wood chemistry in hambury, Germany*. Germany: Institute of Wood Chemistry and Chemical Technology of Wood.
20. Bridgwater, A. V. (2003). Renewable fuels and chemicals by thermal processing of biomass. *The Chemical engineering journal, 91*(2), 87.
21. Wang, J., Zhang, M., Chen, M., Min, F., Zhang, S., Ren, Z., et al. (2006). Catalytic effects of six inorganic compounds on pyrolysis of three kinds of biomass. *Thermochimica Acta, 444*(1), 110-114.
22. Briens, C., Piskorz, J., & Berruti, F. (2008). *Biomass valorization for fuel and chemicals production - a review* (Review No. 1542-6580).
23. Marosky, A. (2008). *Liquid fuels from woody biomass pyrolysis.* University of Canterbury, Berlin.
24. Bridgwater, A. V. (1991). Conclusions and recommendations. In A. V. Bridgwater & G. Grassi (Eds.), *Biomass Pyrolysis Liquids Upgrading and Utilisation* (Vol. 1, pp. 351-362). London Elsevier Applied Science.
25. Zhang, H., Xiao, R., Wang, D., He, G., Shao, S., Zhang, J., et al. (2011). Biomass fast pyrolysis in a fluidized bed reactor under N2, CO2, CO, CH4 and H2 atmospheres. *Bioresour Technol, 102*(5), 4258-4264.
26. Badger, P. C., & Fransham, P. (2006). Use of mobile fast pyrolysis plants to densify biomass and reduce biomass handling costs - a preliminary assessment. *Biomass and Bioenergy, 30*(4), 321-325.
27. Barth, T., & Kleinert, M. (2008). Motor fuels from biomass pyrolysis. *Chemical Engineering & Technology, 31*(5), 773-781.
28. Bridgwater, A. V. (2012). Review of fast pyrolysis of biomass and product upgrading. *Biomass and Bioenergy, 38*, 68-94.
29. Scott, D. S., Majerski, P., Piskorz, J., & Radlein, D. (1999). A second look at fast pyrolysis of biomass - the RTI process. *Journal of Analytical and Applied Pyrolysis, 51*(1–2), 23-37.
30. Elliott, D., Bridgwater, T., Meier, D., Oasmaa, A., & van de Beld, B. (2009). IEA Bioenergy. *Task 34 - Pyrolysis* Retrieved 22/07/13, 2013, from http://www.pyne.co.uk/?_id=18
31. Zanzi, R., Sjostrom, K., & Bjornbom, E. (1997). Rapid pyrolysis of straw at high temperature. In A. V. Bridgwater & D. G. B. Boocock (Eds.), *Developments in Thermochemical Biomass Conversion* (Vol. 1, pp. 61-67). Great Britain: IEA Bioenergy.
32. Wang, Z., Cao, J., & Wang, J. (2009). Pyrolytic characteristics of pine wood in a slowly heating and gas sweeping fixed-bed reactor. *Journal of Analytical and Applied Pyrolysis, 84*(2), 179-184.
33. Diebold, J. P. (1991). Development of pyrolysis reactor concepts in the USA. In A. V. Bridgwater & G. Grassi (Eds.), *Biomass Pyrolysis Liquids Upgrading and Utilisation* (Vol. 1, pp. 341-350). London: Elsevier Applied Science.
34. DeSisto, W. J., Hill, N., Beis, S. H., Mukkamala, S., Joseph, J., Baker, C., et al. (2010). Fast pyrolysis of pine sawdust in a fluidized-bed reactor. *Energy & Fuels, 24*(4), 2642-2651.
35. Garcia-Perez, M., Wang, X. S., Shen, J., Rhodes, M. J., Tian, F., Lee, W.-J., et al. (2008). Fast pyrolysis oil of mallee woody biomass: effect of temperature on the yield and quality of pyrolysis products. *Industrial & Engineering Chemistry Research, 47*(6), 1846-1854.
36. Dynamotive. (2012). *Dynamotive BioOil*. Canada: Dynamotive Energy Systems Corporation.
37. Boateng, A. A., Daugaard, D. E., Goldberg, N. M., & Hicks, K. B. (2007). Bench-scale fluidized-bed pyrolysis of switchgrass for bio-oil production. *Industrial & Engineering Chemistry Research, 46*(7), 1891-1897.
38. Scott, D. S. (1984). The continuous flash pyrolysis of biomass. *Canadian journal of chemical engineering, 62*(3), 404-412.
39. Kaushal, P., & Abedi, J. (2010). A simplified model for biomass pyrolysis in a fluidized bed reactor. *Journal of Industrial and Engineering Chemistry, 16*(5), 748-755.
40. Luo, Z., Wang, S., & Cen, K. (2005). A model of wood flash pyrolysis in fluidized bed reactor. *Renewable Energy, 30*(3), 377-392.
41. Wright, M. M., Daugaard, D. E., Satrio, J. A., & Brown, R. C. (2010). Techno-economic analysis of biomass fast pyrolysis to transportation fuels. *Fuel, 89, Supplement 1*(0), S2-S10.
42. Aguado, R., Olazar, M., San José, M. J., Aguirre, G., & Bilbao, J. (2000). Pyrolysis of sawdust in a conical spouted bed reactor. Yields and product composition. *Industrial & Engineering Chemistry Research, 39*(6), 1925-1933.
43. Lappas, A. A., Samolada, M. C., Iatridis, D. K., Voutetakis, S. S., & Vasalos, I. A. (2002). Biomass pyrolysis in a circulating fluid bed reactor for the production of fuels and chemicals. *Fuel, 81*(16), 2087-2095.
44. Isahak, W. N. R. W., Hisham, M. W. M., Yarmo, M. A., & Yun Hin, T.-y. (2012). A review on bio-oil production from biomass by using pyrolysis method. *Renewable and Sustainable Energy Reviews, 16*(8), 5910-5923.
45. Peacocke, G. V. C., & Bridgwater, A. V. (1994). Ablative plate pyrolysis of biomass for liquids. *Biomass & bioenergy, 7*(1-6), 147-154.
46. Bohn, M. S., & Benham, C. B. (1984). Biomass pyrolysis with an entrained flow reactor. *Industrial & Engineering Chemistry Process Design and Development, 23*(2), 355-363.

47. Piskorz, J. W., CA), Majerski, Piotr (Waterloo, CA), Radlein, Desmond (Waterloo, CA). (1998). United States Patent No.
48. Bridgwater, A. V., & Diebold, J. P. (1999). Overview of fast pyrolysis of biomass for the production of liquid fuels. In A. V. Bridgwater (Ed.), *Fast Pyrolysis of Biomass: A Handbook* (Vol. 1, pp. 14-32). Newbury: CPL Press
49. Liaw, S.-S., Wang, Z., Ndegwa, P., Frear, C., Ha, S., Li, C.-Z., et al. (2012). Effect of pyrolysis temperature on the yield and properties of bio-oils obtained from the auger pyrolysis of Douglas Fir wood. *Journal of Analytical and Applied Pyrolysis, 93*(0), 52-62.
50. Ingram, L., Mohan, D., Bricka, M., Steele, P., Strobel, D., Crocker, D., et al. (2007). Pyrolysis of wood and bark in an auger reactor: physical properties and chemical analysis of the produced bio-oils. *Energy & Fuels, 22*(1), 614-625.
51. Roy, C., & Chornet, E. (1984). Canada Patent No. 1163595.
52. Bu, Q., Lei, H., Ren, S., Wang, L., Zhang, Q., Tang, J., et al. (2012). Production of phenols and biofuels by catalytic microwave pyrolysis of lignocellulosic biomass. *Bioresour Technol, 108*, 274-279.
53. Meier, D., & Faix, O. (1999). State of the art of applied fast pyrolysis of lignocellulosic materials - a review. *Bioresour Technol, 68*(1), 71-77.
54. Bridgwater, A. V., Meier, D., & Radlein, D. (1999). An overview of fast pyrolysis of biomass. *Organic Geochemistry, 30*(12), 1479-1493.
55. Piskorz, J. (1999). IEA pyrolysis fundamentals review. In A. V. Bridgwater (Ed.), *Fast Pyrolysis of Biomass: A Handbook* (Vol. 1, pp. 33-50). Newbury: CPL Press
56. Shaw, K. (2009). *Heat self sufficient biomass pyrolysis system.* Canterbury University.
57. Hoekstra, E., Hogendoorn, K. J. A., Wang, X., Westerhof, R. J. M., Kersten, S. R. A., van Swaaij, W. P. M., et al. (2009). Fast pyrolysis of biomass in a fluidized bed reactor: In situ filtering of the vapors. *Industrial & Engineering Chemistry Research, 48*(10), 4744-4756.
58. Park, H. J., Park, Y.-K., & Kim, J. S. (2008). Influence of reaction conditions and the char separation system on the production of bio-oil from radiata pine sawdust by fast pyrolysis. *Fuel Processing Technology, 89*(8), 797-802.
59. Economopoulou, A. A., & Economopoulos, A. P. (2002). Rapid performance evaluation and optimal sizing of dry cyclone separators. *Journal of Environmental Engineering*, 275-285.
60. Scahill, J., P. Diebold, J. P., & Feik, C. (1998). Removal of residual char fines from pyrolysis vapors by hot gas filtration. *Fuel and Energy Abstracts, 39*(4), 286.
61. Agblevor, F. A., & Besler, S. (1996). Inorganic compounds in biomass feedstocks. 1. Effect on the quality of fast pyrolysis oils. *Energy & Fuels, 10*(2), 293-298.
62. Bridgwater, A. V., & Peacocke, G. V. C. (2000). Fast pyrolysis processes for biomass. *Renewable and Sustainable Energy Reviews, 4*(1), 1-73.
63. Chan, R. (2011). *Development of a condenser for the developed marine florae pyrolysis reactor.* Unpublished Masters, University of San Carlos, University of San Carlos.
64. Xu, R., Ferrante, L., Chaplin, G., Berruti, F., & Briens, C. (2010). Development of a new rotary demister. *Chemical Engineering and Processing: Process Intensification, 49*(2), 183-191.
65. Bedmutha, R. J., Ferrante, L., Briens, C., Berruti, F., & Inculet, I. (2009). Single and two-stage electrostatic demisters for biomass pyrolysis application. *Chemical Engineering and Processing: Process Intensification, 48*(6), 1112-1120.
66. Xu, R. (2010). *Development of advanced technologies for biomass pyrolysis.* Unpublished PhD, Univeristy of Western Ontario, London.
67. Surati, H. S., Beltran, M. R., & Raigorodsky, I. (1981). Tubular electrostatic precipitators of two-stage design. *Environment International, 6*(1–6), 239-244.
68. Parker, K. R. (1997). *Applied electrostatic precipitation* (1 ed.). UK: Blackie academic & Professional.
69. Jiao, J., Zheng, Y., Wang, J., & Sun, G. (2008). Experimental and numerical investigations of a dynamic cyclone with a rotary impeller. *Chemical Engineering and Processing: Process Intensification, 47*(9–10), 1861-1866.
70. Chen, G., Andries, J., Luo, Z., & Spliethoff, H. (2003). Biomass pyrolysis/gasification for product gas production: the overall investigation of parametric effects. *Energy Conversion and Management, 44*(11), 1875-1884.
71. Salehi, E., Abedi, J., & Harding, T. (2011). Bio-oil from sawdust: effect of operating parameters on the yield and quality of pyrolysis products. *Energy & Fuels, 25*(9), 4145-4154.
72. Horne, P. A., & Williams, P. T. (1996). Influence of temperature on the products from the flash pyrolysis of biomass. *Fuel, 75*(9), 1051-1059.
73. Ateş, F., & Işıkdağ, M. A. (2009). Influence of temperature and alumina catalyst on pyrolysis of corncob. *Fuel, 88*(10), 1991-1997.
74. Westerhof, R. J. M., Brilman, D. W. F., van Swaaij, W. P. M., & Kersten, S. R. A. (2009). Effect of temperature in fluidized bed fast pyrolysis of biomass: oil quality assessment in test units. *Industrial & Engineering Chemistry Research, 49*(3), 1160-1168.
75. Hoekstra, E., Westerhof, R. J. M., Brilman, W., Van Swaaij, W. P. M., Kersten, S. R. A., Hogendoorn, K. J. A., et al. (2012). Heterogeneous and homogeneous reactions of pyrolysis vapors from pine wood. *AIChE Journal, 58*(9), 2830-2842.
76. Nowakowski, D. J., Bridgwater, A. V., Elliott, D. C., Meier, D., & de Wild, P. (2010). Lignin fast pyrolysis: results from an international collaboration. *Journal of Analytical and Applied Pyrolysis, 88*(1), 53-72.

77. Li, H.-y., Yan, Y.-j., & Ren, Z.-w. (2008). Online upgrading of organic vapors from the fast pyrolysis of biomass. *Journal of Fuel Chemistry and Technology, 36*(6), 666-671.
78. Zhang, H., Xiao, R., Wang, D., Zhong, Z., Song, M., Pan, Q., et al. (2009). Catalytic fast pyrolysis of biomass in a fluidized bed with fresh and spent fluidized catalytic cracking (FCC) catalysts. *Energy & Fuels, 23*(12), 6199-6206.
79. McMillan, J. D. (1994). Pretreatment of lignocellulosic biomass *Enzymatic Conversion of Biomass for Fuels Production* (Vol. 566, pp. 292-324): American Chemical Society.
80. Okuno, T., Sonoyama, N., Hayashi, J.-i., Li, C.-Z., Sathe, C., & Chiba, T. (2005). Primary release of alkali and alkaline earth metallic species during the pyrolysis of pulverized biomass. *Energy & Fuels, 19*(5), 2164-2171.
81. Elliott, D. C. (1994). Water, alkali and char in flash pyrolysis oils. *Biomass and Bioenergy, 7*(1–6), 179-185.
82. Dooley, J. H., Lanning, D. N., & Lanning, C. J. (2012). Woody biomass size reduction with selective material orientation. *Biofuels, 4*(1), 35-43.
83. Bartek, R., Brady, M., & Stamires, D. (2012). United States Patent No.
84. Shen, J., Wang, X.-S., Garcia-Perez, M., Mourant, D., Rhodes, M. J., & Li, C.-Z. (2009). Effects of particle size on the fast pyrolysis of oil mallee woody biomass. *Fuel, 88*(10), 1810-1817.
85. Carpenter, D., Westover, T. L., Czernik, S., & Jablonski, W. (2014). Biomass feedstocks for renewable fuel production: a review of the impacts of feedstock and pretreatment on the yield and product distribution of fast pyrolysis bio-oils and vapors. [10.1039/C3GC41631C]. *Green Chemistry, 16*(2), 384-406.
86. Vassilev, S. V., Baxter, D., Andersen, L. K., & Vassileva, C. G. (2010). An overview of the chemical composition of biomass. *Fuel, 89*(5), 913-933.
87. Behrendt, F., Neubauer, Y., Oevermann, M., Wilmes, B., & Zobel, N. (2008). Direct liquefaction of biomass. *Chemical Engineering & Technology, 31*(5), 667-677.
88. Rowell, R. M. (2005). *Handbook of wood chemistry and wood composites* (Vol. 2). Boca Raton, Fla. : CRC Press.
89. Rath, J., Wolfinger, M. G., Steiner, G., Krammer, G., Barontini, F., & Cozzani, V. (2003). Heat of wood pyrolysis. *Fuel, 82*(1), 81-91.
90. Arseneau, D. F. (1971). Competitive reactions in the thermal decomposition of cellulose. *Canadian Journal of Chemistry, 49*(4), 632-638.
91. Yang, H., Yan, R., Chen, H., Lee, D. H., & Zheng, C. (2007). Characteristics of hemicellulose, cellulose and lignin pyrolysis. *Fuel, 86*(12–13), 1781-1788.
92. Hosoya, T., Kawamoto, H., & Saka, S. (2007). Cellulose-hemicellulose and cellulose-lignin interactions in wood pyrolysis at gasification temperature. *Journal of Analytical and Applied Pyrolysis, 80*(1), 118-125.
93. Worasuwannarak, N., Sonobe, T., & Tanthapanichakoon, W. (2007). Pyrolysis behaviors of rice straw, rice husk, and corncob by TG-MS technique. *Journal of Analytical and Applied Pyrolysis, 78*(2), 265-271.
94. Yang, H., Yan, R., Chen, H., Zheng, C., Lee, D. H., & Liang, D. T. (2005). In-depth investigation of biomass pyrolysis based on three major components: hemicellulose, cellulose and lignin. *Energy & Fuels, 20*(1), 388-393.
95. Alén, R., Kuoppala, E., & Oesch, P. (1996). Formation of the main degradation compound groups from wood and its components during pyrolysis. *Journal of Analytical and Applied Pyrolysis, 36*(2), 137-148.
96. Evans, R. J., & Milne, T. A. (1987). Molecular characterization of the pyrolysis of biomass. *Energy & Fuels, 1*(2), 123-137.
97. Williams, P. T., & Besler, S. (1996). The influence of temperature and heating rate on the slow pyrolysis of biomass. *Renewable Energy, 7*(3), 233-250.
98. Green, A. (2009). *Fixed bed pyrolysis optimisation, part 1*. University of Canterbury: Chemical and Process Engineering.
99. Shen, D. K., & Gu, S. (2009). The mechanism for thermal decomposition of cellulose and its main products. *Bioresour Technol, 100*(24), 6496-6504.
100. Raveendran, K., Ganesh, A., & Khilar, K. C. (1995). Influence of mineral matter on biomass pyrolysis characteristics. *Fuel, 74*(12), 1812-1822.
101. Luo, Z., Wang, S., Liao, Y., & Cen, K. (2004). Mechanism study of cellulose rapid pyrolysis. *Industrial & Engineering Chemistry Research, 43*(18), 5605-5610.
102. Murwanashyaka, J. N., Pakdel, H., & Roy, C. (2002). Fractional vacuum pyrolysis of biomass and separation of phenolic compounds by steam distillation. In A. V. Bridgwater (Ed.), *Fast Pyrolysis of Biomass: A Handbook Volume 2* (Vol. 2, pp. 407-418). Newbury, UK: IEA Bioenergy.
103. Patwardhan, P. R., Dalluge, D. L., Shanks, B. H., & Brown, R. C. (2011). Distinguishing primary and secondary reactions of cellulose pyrolysis. *Bioresour Technol, 102*(8), 5265-5269.
104. Piskorz, J., Radlein, D. S. A. G., Scott, D. S., & Czernik, S. (1989). Pretreatment of wood and cellulose for production of sugars by fast pyrolysis. *Journal of Analytical and Applied Pyrolysis, 16*(2), 127-142.
105. Scheirs, J., Camino, G., & Tumiatti, W. (2001). Overview of water evolution during the thermal degradation of cellulose. *European Polymer Journal, 37*(5), 933-942.
106. Brunner, P. H., & Roberts, P. V. (1980). The significance of heating rate on char yield and char properties in the pyrolysis of cellulose. *Carbon, 18*(3), 217-224.
107. Kasparbauer, R. D. (2009). *The effects of biomass pretreatments on the products of fast pyrolysis.* Iowa State University, Ames, Iowa.

108. Dobele, G., Rossinskaja, G., Telysheva, G., Meier, D., & Faix, O. (1999). Cellulose dehydration and depolymerization reactions during pyrolysis in the presence of phosphoric acid. *Journal of Analytical and Applied Pyrolysis, 49*(1–2), 307-317.
109. Branca, C., Di Blasi, C., Mango, C., & Hrablay, I. (2013). Products and kinetics of glucomannan pyrolysis. *Industrial & Engineering Chemistry Research, 52*(14), 5030-5039.
110. Aho, A., Kumar, N., Eränen, K., Salmi, T., Hupa, M., & Murzin, D. Y. (2007). Catalytic pyrolysis of biomass in a fluidized bed reactor: influence of the acidity of H-beta zeolite. *Process Safety and Environmental Protection, 85*(5), 473-480.
111. Hayes, D. (2013). Advanced biomass research for beyond the petroleum age. *Important Compositional Parameters* Retrieved 07/09/2013, 2013, from http://www.carbolea.ul.ie/composition.php
112. Uprichard, J. M., & Lloyd, J. A. (1980). Influence of tree age on the chemical composition of radiata pine. *New Zealand Journal of Forestry Science, 1*(3), 551-557.
113. Gao-Jin, L., Shu-Bin, W., & Rui, L. (2010). Kinetic study of the thermal decomposition of hemicellulose isolated from corn stalk. *Bioresources, 5*(2).
114. Shen, D. K., Gu, S., & Bridgwater, A. V. (2010). The thermal performance of the polysaccharides extracted from hardwood: Cellulose and hemicellulose. *Carbohydrate Polymers, 82*(1), 39-45.
115. Nowakowski, D., Jones, J., Brydson, R., & Ross, A. (2007). Potassium catalysis in the pyrolysis behaviour of short rotation willow coppice. *Fuel, 86*(15), 2389-2402.
116. Prins, M. J., Ptasinski, K. J., & Janssen, F. J. J. G. (2006). Torrefaction of wood: part 1. Weight loss kinetics. *Journal of Analytical and Applied Pyrolysis, 77*(1), 28-34.
117. Boardman, R. D., Hess, J. R., Sokhansanj, S., Tumuluru, J. S., & Wright, C. T. (2011). A review on biomass torrefaction process and product properties for energy applications. [Report]. *Industrial Biotechnology, 7*(5), 384+.
118. Carrier, M., Loppinet-Serani, A., Denux, D., Lasnier, J.-M., Ham-Pichavant, F., Cansell, F., et al. (2011). Thermogravimetric analysis as a new method to determine the lignocellulosic composition of biomass. *Biomass and Bioenergy, 35*(1), 298-307.
119. Maekawa, E., Ichizawa, T., & Koshijima, T. (1989). An evaluation of the acid-soluble lignin determination in analyses of lignin by the sulfuric acid method. *Journal of Wood Chemistry and Technology, 9*(4), 549-567.
120. Speaks, J., Campbell, R., & Veal, M. (1997). 5698667 United States Patent.
121. Sharma, R. K., Wooten, J. B., Baliga, V. L., Lin, X., Geoffrey Chan, W., & Hajaligol, M. R. (2004). Characterization of chars from pyrolysis of lignin. *Fuel, 83*(11–12), 1469-1482.
122. Mohan, D., Pittman, C. U., & Steele, P. H. (2006). Pyrolysis of wood/biomass for bio-oil: a critical review. *Energy & Fuels, 20*(3), 848-889.
123. Fahmi, R., Bridgwater, A. V., Donnison, I., Yates, N., & Jones, J. M. (2008). The effect of lignin and inorganic species in biomass on pyrolysis oil yields, quality and stability. *Fuel, 87*(7), 1230-1240.
124. Jensen, A., Dam-Johansen, K., Wójtowicz, M. A., & Serio, M. A. (1998). TG-FTIR study of the influence of potassium chloride on wheat straw pyrolysis. *Energy & Fuels, 12*(5), 929-938.
125. Bridgwater, A. V. (1999). Principles and practice of biomass fast pyrolysis processes for liquids. *Journal of Analytical and Applied Pyrolysis, 51*(1–2), 3-22.
126. Várhegyi, G., Grønli, M. G., & Di Blasi, C. (2004). Effects of sample origin, extraction, and hot-water washing on the devolatilization kinetics of chestnut wood. *Industrial & Engineering Chemistry Research, 43*(10), 2356-2367.
127. Roy, C., Pakdel, H., & Brouillard, D. (1990). The role of extractives during vacuum pyrolysis of wood. *Journal of Applied Polymer Science, 41*(1-2), 337-348.
128. Carrier, M., Neomagus, H. W., Görgens, J., & Knoetze, J. H. (2012). Influence of chemical pretreatment on the internal structure and reactivity of pyrolysis chars produced from sugar cane bagasse. *Energy & Fuels, 26*(7), 4497-4506.
129. Dayton, D. C., Jenkins, B. M., Turn, S. Q., Bakker, R. R., Williams, R. B., Belle-Oudry, D., et al. (1999). Release of inorganic constituents from leached biomass during thermal conversion. *Energy & Fuels, 13*(4), 860-870.
130. Scott, D. S., Paterson, L., Piskorz, J., & Radlein, D. (2001). Pretreatment of poplar wood for fast pyrolysis: rate of cation removal. *Journal of Analytical and Applied Pyrolysis, 57*(2), 169-176.
131. Hallen, R. T., Sealock, L. J., & Cuello, R. (1985). Influence of alkali carbonates on biomass volatilization. In R. P. Overend, T. A. Milne & L. K. Mudge (Eds.), *Fundamentals of Thermochemical Biomass Conversion* (pp. 157–166): Elsevier Applied Science Publishers.
132. Saddawi, A., Jones, J. M., Williams, A., & Le Coeur, C. (2011). Commodity fuels from biomass through pretreatment and torrefaction: Effects of mineral content on torrefied fuel characteristics and quality. *Energy & Fuels, 26*(11), 6466-6474.
133. Liu, C., Liu, X., Bi, X. T., Liu, Y., & Wang, C. (2011). Influence of inorganic additives on pyrolysis of pine bark. *Energy & Fuels, 25*(5), 1996-2003.
134. Davidsson, K. O., Korsgren, J. G., Pettersson, J. B. C., & Jäglid, U. (2002). The effects of fuel washing techniques on alkali release from biomass. *Fuel, 81*(2), 137-142.
135. Olsson, J. G., Jäglid, U., Pettersson, J. B. C., & Hald, P. (1997). Alkali metal emission during pyrolysis of biomass. *Energy & Fuels, 11*(4), 779-784.

136. Davidsson, K. O., Stojkova, B. J., & Pettersson, J. B. C. (2002). Alkali emission from birchwood particles during rapid pyrolysis. *Energy & Fuels, 16*(5), 1033-1039.
137. Pitman, R. M. (2006). Wood ash use in forestry – a review of the environmental impacts. *Forestry, 79*(5), 563-587.
138. Encinar, J. M., Beltrán, F. J., Ramiro, A., & González, J. F. (1997). Catalyzed pyrolysis of grape and olive Bagasse. influence of catalyst type and chemical treatment. *Industrial & Engineering Chemistry Research, 36*(10), 4176-4183.
139. Di Blasi, C., Galgano, A., & Branca, C. (2009). Influences of the chemical state of alkaline compounds and the nature of alkali metal on wood pyrolysis. *Industrial & Engineering Chemistry Research, 48*(7), 3359-3369.
140. Wang, X., Chen, H., Luo, K., Shao, J., & Yang, H. (2007). The influence of microwave drying on biomass pyrolysis. *Energy & Fuels, 22*(1), 67-74.
141. Brown, R. C. (2003). *Biorenewable resources: engineering new products from agriculture*: Iowa State Press.
142. Westerhof, R. J. M., Kuipers, N. J. M., Kersten, S. R. A., & van Swaaij, W. P. M. (2007). Controlling the water content of biomass fast pyrolysis oil. *Industrial & Engineering Chemistry Research, 46*(26), 9238-9247.
143. Gary, M. (1984). *The effect of moisture and ash content on the pyrolysis of a wood derived material.* California Institute of technology, Pasadena.
144. Demirbas, A. (2004). Effect of initial moisture content on the yields of oily products from pyrolysis of biomass. *Journal of Analytical and Applied Pyrolysis, 71*(2), 803-815.
145. Kawamoto, H., Saito, S., Hatanaka, W., & Saka, S. (2007). Catalytic pyrolysis of cellulose in sulfolane with some acidic catalysts. *Journal of Wood Science, 53*(2), 127-133.
146. Gray, M. R., Corcoran, W. H., & Gavalas, G. R. (1985). Pyrolysis of a wood-derived material. Effects of moisture and ash content. *Industrial & Engineering Chemistry Process Design and Development, 24*(3), 646-651.
147. Connor, M. A., & Viljoen, M. H. (1997). Relationships between woody density, wood permeability and charcoal yield. In A. V. Bridgwater & D. G. B. Boocock (Eds.), *Developments in Thermochemical Biomass Conversion* (Vol. 1, pp. 82-96). Great Britain: IEA Bioenergy.
148. Yanik, J., Kornmayer, C., Saglam, M., & Yüksel, M. (2007). Fast pyrolysis of agricultural wastes: characterization of pyrolysis products. *Fuel Processing Technology, 88*(10), 942-947.
149. Xu, R., Ferrante, L., Briens, C., & Berruti, F. (2009). Flash pyrolysis of grape residues into biofuel in a bubbling fluid bed. *Journal of Analytical and Applied Pyrolysis, 86*(1), 58-65.
150. Demirbas, A. (2004). Effects of temperature and particle size on bio-char yield from pyrolysis of agricultural residues. *Journal of Analytical and Applied Pyrolysis, 72*(2), 243-248.
151. Mettler, M. S., Vlachos, D. G., & Dauenhauer, P. J. (2012). Top ten fundamental challenges of biomass pyrolysis for biofuels. *Energy & Environmental Science, 5*(7), 7797-7809.
152. Brown, R. C. (2014). *Selective thermal depolymerisation of biomass.* Paper presented at the 20th International Symposium on Analytical and Applied Pyrolysis, Birmingham, UK.
153. Bacon, R., & Tang, M. M. (1964). Carbonization of cellulose fibers-II. Physical property study. *Carbon, 2*(3), 221-225.
154. Maschio, G., Koufopanos, C., & Lucchesi, A. (1992). Pyrolysis, a promising route for biomass utilization. *Bioresour Technol, 42*(3), 219-231.
155. Xu, R., Ferrante, L., Briens, C., & Berruti, F. (2011). Bio-oil production by flash pyrolysis of sugarcane residues and post treatments of the aqueous phase. *Journal of Analytical and Applied Pyrolysis, 91*(1), 263-272.
156. Savova, D., Apak, E., Ekinci, E., Yardim, F., Petrov, N., Budinova, T., et al. (2001). Biomass conversion to carbon adsorbents and gas. *Biomass and Bioenergy, 21*(2), 133-142.
157. Marris, E. (2006). Putting the carbon back: black is the new green. [10.1038/442624a]. *Nature, 442*(7103), 624-626.
158. Brewer, C. E., Hu, Y.-Y., Schmidt-Rohr, K., Loynachan, T. E., Laird, D. A., & Brown, R. C. (2012). Extent of pyrolysis impacts on fast pyrolysis biochar properties. *J. Environ. Qual., 41*(4), 1115-1122.
159. Xu, R., Ferrante, L., Hall, K., Briens, C., & Berruti, F. (2011). Thermal self-sustainability of biochar production by pyrolysis. *Journal of Analytical and Applied Pyrolysis, 91*(1), 55-66.
160. Solantausta, Y., Nylund, N.-O., Westerholm, M., Koljonen, T., & Oasmaa, A. (1993). Wood-pyrolysis oil as fuel in a diesel-power plant. *Bioresour Technol, 46*(1–2), 177-188.
161. Oasmaa, A., Elliott, D. C., & Korhonen, J. (2010). Acidity of biomass fast pyrolysis bio-oils. *Energy & Fuels, 24*(12), 6548-6554.
162. Diebold, J. P. (2000). *A review of the chemical and physical mechanisms of the storage stability of fast pyrolysis bio-oils*. Lakewood, Colorado: National Renewable Energy Laboratory.
163. Oasmaa, A., Kuoppala, E., & Solantausta, Y. (2003). Fast pyrolysis of forestry residue. 2. Physicochemical composition of product liquid. *Energy & Fuels, 17*(2), 433-443.
164. Bridgwater, A. V. (1996). Production of high grade fuels and chemicals from catalytic pyrolysis of biomass. *Catalysis Today, 29*(1–4), 285-295.
165. Zhang, L., & Kong, S.-C. (2012). Multicomponent vaporization modeling of bio-oil and its mixtures with other fuels. *Fuel, 95*(0), 471-480.
166. Stoikos, T. (1991). Upgrading of biomass pyrolysis liquids to high value chemicals and fuel additives. In A. V. Bridgwater & G. Grassi (Eds.), *Biomass Pyrolysis Liquids Upgrading and Utilisation* (Vol. 1, pp. 227-242). London: Elsevier Applied Science.

167. Güllü, D., & Demirbaş, A. (2001). Biomass to methanol via pyrolysis process. *Energy Conversion and Management, 42*(11), 1349-1356.
168. Mettler, M. S., Paulsen, A. D., Vlachos, D. G., & Dauenhauer, P. J. (2012). Pyrolytic conversion of cellulose to fuels: levoglucosan deoxygenation via elimination and cyclization within molten biomass. [10.1039/C2EE21305B]. *Energy & Environmental Science, 5*(7), 7864-7868.
169. Choudhary, V., Burnett, R. I., Vlachos, D. G., & Sandler, S. I. (2012). Dehydration of glucose to 5-(hydroxymethyl)furfural and anhydroglucose: thermodynamic insights. *The Journal of Physical Chemistry C, 116*(8), 5116-5120.
170. Thananatthanachon, T., & Rauchfuss, T. B. (2010). Efficient production of the liquid fuel 2,5-dimethylfuran from fructose using formic acid as a reagent. *Angewandte Chemie International Edition, 49*(37), 6616-6618.
171. Tang, Z., Lu, Q., Zhang, Y., Zhu, X., & Guo, Q. (2009). One step bio-oil upgrading through hydrotreatment, esterification, and cracking. *Industrial & Engineering Chemistry Research, 48*(15), 6923-6929.
172. Torri, C., Reinikainen, M., Lindfors, C., Fabbri, D., Oasmaa, A., & Kuoppala, E. (2010). Investigation on catalytic pyrolysis of pine sawdust: catalyst screening by Py-GC-MIP-AED. *Journal of Analytical and Applied Pyrolysis, 88*(1), 7-13.
173. Lynam, J. G. (2011). *Pretreatment of lignocellulosic biomass with acetic acid, salts, and ionic liquids.* Unpublished 1505147, University of Nevada, Reno, United States -- Nevada.
174. Chaala, A., Ba, T., Garcia-Perez, M., & Roy, C. (2004). Colloidal properties of bio-oils obtained by vacuum pyrolysis of softwood bark: aging and thermal stability. *Energy & Fuels, 18*(5), 1535-1542.
175. Meier, D. (1999). New methods for chemical and physical characterization and round robin testing. In A. V. Bridgwater (Ed.), *Fast Pyrolysis of Biomass: A Handbook* (Vol. 1, pp. 92-101). Newbury Berkshire UK: CPL Press.
176. Shaddix, C. R., & Tennison, P. J. (1998). Effects of char content and simple additives on biomass pyrolysis oil droplet combustion. *Symposium (International) on Combustion, 27*(2), 1907-1914.
177. Chiaramonti, D., Bonini, M., Fratini, E., Tondi, G., Gartner, K., Bridgwater, A. V., et al. (2003). Development of emulsions from biomass pyrolysis liquid and diesel and their use in engines-part 1 : emulsion production. *Biomass and Bioenergy, 25*(1), 85-99.
178. Yang, S. I., Hsu, T. C., Wu, C. Y., Chen, K. H., Hsu, Y. L., & Li, Y. H. (2014). Application of biomass fast pyrolysis part II: The effects that bio-pyrolysis oil has on the performance of diesel engines. *Energy*(0), 172-180.
179. Czernik, S., & Bridgwater, A. V. (2004). Overview of applications of biomass fast pyrolysis oil. *Energy & Fuels, 18*(2), 590-598.
180. Sukhbataar, B., Steele, P. H., Ingram, L. L., & Kim, M. G. (2009). An exploratory study on the removal of acetic and formic acids from bio-oil. *BioResources, 4*(4), 1319-1329.
181. Li, Q., Steele, P. H., Mitchell, B., Ingram, L., & Yu, F. (2013). The addition of water to extract maximum levoglucosan from the bio-oil produced via fast pyrolysis of pretreated loblolly pinewood. *BioResources, 8*(2), 1868-1880.
182. Bennett, N. M., Helle, S. S., & Duff, S. J. B. (2009). Extraction and hydrolysis of levoglucosan from pyrolysis oil. *Bioresour Technol, 100*(23), 6059-6063.
183. Lin, Y., Zhang, C., Zhang, M., & Zhang, J. (2010). Deoxygenation of bio-oil during pyrolysis of biomass in the presence of CaO in a fluidized-bed reactor. *Energy and Fuels, 24*(10), 5686-5695.
184. Adam, J., Antonakou, E., Lappas, A., Stöcker, M., Nilsen, M. H., Bouzga, A., et al. (2006). In situ catalytic upgrading of biomass derived fast pyrolysis vapours in a fixed bed reactor using mesoporous materials. *Microporous and Mesoporous Materials, 96*(1–3), 93-101.
185. Diebold, J. P., Milne, T. A., Czernik, S., Oasmaa, A., A.V, B., Cuevas, A., et al. (1999). Proposed specifications for various grades of pyrolysis oils. In A. V. Bridgwater (Ed.), *Fast Pyrolysis of Biomass: A Handbook* (Vol. 1, pp. 102-114). Newbury Berkshire UK: CPL Press.
186. Zheng, A., Zhao, Z., Chang, S., Huang, Z., Wang, X., He, F., et al. (2012). Effect of torrefaction on structure and fast pyrolysis behavior of corncobs. *Bioresour Technol, 128*(0), 370–377.
187. Gutierrez, A., & Domine, M. (2007). *Co-processing of upgraded bio-liquids in standard refinery units* Paper presented at the European Biomass Conference and Exhibition, Florence, Italy.
188. Wang, H., Srinivasan, R., Yu, F., Steele, P., Li, Q., & Mitchell, B. (2011). Effect of acid, alkali, and steam explosion pretreatments on characteristics of bio-oil produced from pinewood. *Energy & Fuels, 25*(8), 3758-3764.
189. Tarkow. (1969). Cellulases and their applications a mechanism for improving the digestibility of lignocellulosic materials with dilute alkali and liquid ammonia. *Advances in Chemistry*(95), 197-218.
190. Rustamov, V. R., Abdullayev, K. M., & Samedov, E. A. (1998). Biomass conversion to liquid fuel by two-stage thermochemical cycle. *Energy Conversion and Management, 39*(9), 869-875.
191. Hassan, M., Steele, P. H., & Ingram, L. (2009). Characterization of fast pyrolysis bio-oils produced from pretreated pine wood. *Appl Biochem Biotechnol, 154*(1-3), 3-13.
192. Oudenhoven, S. R. G., Westerhof, R. J. M., Aldenkamp, N., Brilman, D. W. F., & Kersten, S. R. A. (2013). Demineralization of wood using wood-derived acid: towards a selective pyrolysis process for fuel and chemicals production. *Journal of Analytical and Applied Pyrolysis, 103*(0), 112-118.

193. Vassilev, S. V., Baxter, D., Andersen, L. K., Vassileva, C. G., & Morgan, T. J. (2012). An overview of the organic and inorganic phase composition of biomass. *Fuel, 94*(0), 1-33.
194. Mourant, D., Wang, Z., He, M., Wang, X. S., Garcia-Perez, M., Ling, K., et al. (2011). Mallee wood fast pyrolysis: effects of alkali and alkaline earth metallic species on the yield and composition of bio-oil. *Fuel, 90*(9), 2915-2922.
195. Das, P., Ganesh, A., & Wangikar, P. (2004). Influence of pretreatment for deashing of sugarcane bagasse on pyrolysis products. *Biomass and Bioenergy, 27*(5), 445-457.
196. Radlein, D., Piskorz, J., Grinshpun, A., & Scott, D. S. (1987). *Fast pyrolysis of pre-treated wood and cellulose*. Ontario: University of Waterloo.
197. Westover, T. L., Phanphanich, M., Clark, M. L., Rowe, S. R., Egan, S. E., Zacher, A. H., et al. (2012). Impact of thermal pretreatment on the fast pyrolysis conversion of southern pine. *Biofuels, 4*(1), 45-61.
198. Chen, W.-H., Cheng, W.-Y., Lu, K.-M., & Huang, Y.-P. (2011). An evaluation on improvement of pulverized biomass property for solid fuel through torrefaction. *Applied Energy, 88*(11), 3636-3644.
199. Kolokolova, O. (2011). Experimental investigation into torrefaction and pyrolysis treatment of woody biomass for gasification. Canterbury University.
200. Meng, J., Park, J., Tilotta, D., & Park, S. (2012). The effect of torrefaction on the chemistry of fast-pyrolysis bio-oil. *Bioresour Technol, 111*(0), 439-446.
201. Wang, G., Luo, Y., Deng, J., Kuang, J., & Zhang, Y. (2011). Pretreatment of biomass by torrefaction. *Chinese Science Bulletin, 56*(14), 1442-1448.
202. Deng, J., Wang, G.-j., Kuang, J.-h., Zhang, Y.-l., & Luo, Y.-h. (2009). Pretreatment of agricultural residues for co-gasification via torrefaction. *Journal of Analytical and Applied Pyrolysis, 86*(2), 331-337.
203. Chang, S., Zhao, Z., Zheng, A., He, F., Huang, Z., & Li, H. (2012). Characterization of products from torrefaction of sprucewood and bagasse in an auger reactor. *Energy & Fuels, 26*(11), 7009-7017.
204. Prins, M. J., Ptasinski, K. J., & Janssen, F. J. J. G. (2006). Torrefaction of wood: part 2. Analysis of products. *Journal of Analytical and Applied Pyrolysis, 77*(1), 35-40.
205. Chen, W.-H., & Kuo, P.-C. (2011). Torrefaction and co-torrefaction characterization of hemicellulose, cellulose and lignin as well as torrefaction of some basic constituents in biomass. *Energy, 36*(2), 803-811.
206. Zheng, A., Zhao, Z., Chang, S., Huang, Z., He, F., & Li, H. (2012). Effect of torrefaction temperature on product distribution from two-staged pyrolysis of biomass. *Energy & Fuels, 26*(5), 2968-2974.
207. Chew, J. J., & Doshi, V. (2011). Recent advances in biomass pretreatment – torrefaction fundamentals and technology. *Renewable and Sustainable Energy Reviews, 15*(8), 4212-4222.
208. Medic, D., Darr, M., Shah, A., Potter, B., & Zimmerman, J. (2012). Effects of torrefaction process parameters on biomass feedstock upgrading. *Fuel, 91*(1), 147-154.
209. Chen, Q., Zhou, J., Liu, B., Mei, Q., & Luo, Z. (2011). Influence of torrefaction pretreatment on biomass gasification technology. *Chinese Science Bulletin, 56*(14), 1449-1456.
210. Wannapeera, J., & Worasuwannarak, N. (2012). Upgrading of woody biomass by torrefaction under pressure. *Journal of Analytical and Applied Pyrolysis, 96*(0), 173-180.
211. Westerhof, R. J. M., Brilman, D. W. F., Garcia-Perez, M., Wang, Z., Oudenhoven, S. R. G., & Kersten, S. R. A. (2012). Stepwise fast pyrolysis of pine wood. *Energy & Fuels, 26*(12), 7263–7273.
212. Wannapeera, J., Fungtammasan, B., & Worasuwannarak, N. (2011). Effects of temperature and holding time during torrefaction on the pyrolysis behaviors of woody biomass. *Journal of Analytical and Applied Pyrolysis, 92*(1), 99-105.
213. Yan, W., Acharjee, T. C., Coronella, C. J., & Vásquez, V. R. (2009). Thermal pretreatment of lignocellulosic biomass. *Environmental Progress & Sustainable Energy, 28*(3), 435-440.
214. Hilten, R. N., Speir, R. A., Kastner, J. R., Mani, S., & Das, K. C. (2013). Effect of torrefaction on bio-oil upgrading over HZSM-5. Part 1: product yield, product quality, and catalyst effectiveness for benzene, toluene, ethylbenzene, and xylene production. *Energy & Fuels, 27*(2), 830-843.
215. Stephanidis, S., Nitsos, C., Kalogiannis, K., Iliopoulou, E. F., Lappas, A. A., & Triantafyllidis, K. S. (2011). Catalytic upgrading of lignocellulosic biomass pyrolysis vapours: effect of hydrothermal pre-treatment of biomass. *Catalysis Today, 167*(1), 37-45.
216. Chaiwat, W., Hasegawa, I., Kori, J., & Mae, K. (2008). Examination of degree of crosslinking for cellulose precursors pretreated with acid/hot water at low temperature. *Industrial & Engineering Chemistry Research, 47*(16), 5948-5956.
217. Samolada, M. C., Baldauf, W., & Vasalos, I. A. (1998). Production of a bio-gasoline by upgrading biomass flash pyrolysis liquids via hydrogen processing and catalytic cracking. *Fuel, 77*(14), 1667-1675.
218. Westerhof, R. J. M., Brilman, D. W. F., Garcia-Perez, M., Wang, Z., Oudenhoven, S. R. G., van Swaaij, W. P. M., et al. (2011). Fractional condensation of biomass pyrolysis vapors. *Energy & Fuels, 25*(4), 1817-1829.
219. Chen, T., Deng, C., & Liu, R. (2010). Effect of selective condensation on the characterization of bio-oil from pine sawdust fast pyrolysis using a fluidized-bed reactor. *Energy & Fuels, 24*(12), 6616-6623.
220. Lin, R. W. S. L., TX, US). (2011). United States Patent No.
221. Wang, S., Gu, Y., Liu, Q., Yao, Y., Guo, Z., Luo, Z., et al. (2009). Separation of bio-oil by molecular distillation. *Fuel Processing Technology, 90*(5), 738-745.

222. Zheng, J.-L., & Wei, Q. (2011). Improving the quality of fast pyrolysis bio-oil by reduced pressure distillation. *Biomass and Bioenergy, 35*(5), 1804-1810.
223. Guo, X., Wang, S., Guo, Z., Liu, Q., Luo, Z., & Cen, K. (2010). Pyrolysis characteristics of bio-oil fractions separated by molecular distillation. *Applied Energy, 87*(9), 2892-2898.
224. Guo, Z., Wang, S., Gu, Y., Xu, G., Li, X., & Luo, Z. (2010). Separation characteristics of biomass pyrolysis oil in molecular distillation. *Separation and Purification Technology, 76*(1), 52-57.
225. Ba, T., Chaala, A., Garcia-Perez, M., & Roy, C. (2003). Colloidal properties of bio-oils obtained by vacuum pyrolysis of softwood bark. Storage stability. *Energy & Fuels, 18*(1), 188-201.
226. Shen, Z., Jin, F.-m., Zhang, Y.-l., Wu, B., & Cao, J.-l. (2009). Hydrogen transfer reduction of ketones using formic acid as a hydrogen donor under hydrothermal conditions. *Journal of Zhejiang University SCIENCE A, 10*(11), 1631-1635.
227. Shen, Z., Zhang, Y., Jin, F., Zhou, X., Kishita, A., & Tohji, K. (2010). Hydrogen-transfer reduction of ketones into corresponding alcohols using formic acid as a hydrogen donor without a metal catalyst in high-temperature water. *Industrial & Engineering Chemistry Research, 49*(13), 6255-6259.
228. Mahfud, F. H., Melin-Cabrera, I., Manurung, R., & Heeres, H. J. (2007). Upgrading of flash pyrolysis oil by reactive distillation using a high boiling alcohol and acid catalysts. *Process Safety and Environmental Protection, 85*(5), 466-472.
229. Duan, P., & Savage, P. E. (2011). Upgrading of crude algal bio-oil in supercritical water. *Bioresour Technol, 102*(2), 1899-1906.
230. Zhang, J., Luo, Z., Dang, Q., Wang, J., & Chen, W. (2011, 9-11 Sept. 2011). *Upgrading of bio-oil in supercritical ethanol.* Paper presented at the 2011 International Conference on Electronics, Communications and Control (ICECC).
231. Wang, H., Male, J., & Wang, Y. (2013). Recent advances in hydrotreating of pyrolysis bio-oil and its oxygen-containing model compounds. *ACS Catalysis, 3*(5), 1047-1070.
232. Zhang, S., Yan, Y., Li, T., & Ren, Z. (2005). Upgrading of liquid fuel from the pyrolysis of biomass. *Bioresour Technol, 96*(5), 545-550.
233. Şenol, O. İ., Viljava, T. R., & Krause, A. O. I. (2005). Hydrodeoxygenation of methyl esters on sulphided NiMo/γ-Al2O3 and CoMo/γ-Al2O3 catalysts. *Catalysis Today, 100*(3–4), 331-335.
234. Vispute, T. P., & Huber, G. W. (2009). Production of hydrogen, alkanes and polyols by aqueous phase processing of wood-derived pyrolysis oils. *Green Chemistry, 11*(9), 1433-1445.
235. Wildschut, J., Arentz, J., Rasrendra, C. B., Venderbosch, R. H., & Heeres, H. J. (2009). Catalytic hydrotreatment of fast pyrolysis oil: model studies on reaction pathways for the carbohydrate fraction. *Environmental Progress & Sustainable Energy, 28*(3), 450-460.
236. Ammendola, P., Lisi, L., Piriou, B., & Ruoppolo, G. (2009). Rh-perovskite catalysts for conversion of tar from biomass pyrolysis. *Chemical Engineering Journal, 154*(1–3), 361-368.
237. Elliott, D. C., & Neuenschwander, G. G. (1998). Liquid fuels by low-severity hydrotreating of biocrude. *Fuel and Energy Abstracts, 39*(4), 611-621.
238. Olazar, M., Aguado, R., Bilbao, J., & Barona, A. (2000). Pyrolysis of sawdust in a conical spouted-bed reactor with a HZSM-5 catalyst. *American Institute of Chemical Engineers. AIChE Journal, 46*(5), 1025-1025.
239. Pattiya, A., Titiloye, J. O., & Bridgwater, A. V. (2008). Fast pyrolysis of cassava rhizome in the presence of catalysts. *Journal of Analytical and Applied Pyrolysis, 81*(1), 72-79.
240. Nokkosmäki, M. I., Kuoppala, E. T., Leppämäki, E. A., & Krause, A. O. I. (2000). Catalytic conversion of biomass pyrolysis vapours with zinc oxide. *Journal of Analytical and Applied Pyrolysis, 55*(1), 119-131.
241. Adjaye, J. D., & Bakhshi, N. N. (1995). Production of hydrocarbons by catalytic upgrading of a fast pyrolysis bio-oil. Part I: conversion over various catalysts. *Fuel Processing Technology, 45*(3), 161-183.
242. Adjaye, J. D., & Bakhshi, N. N. (1995). Production of hydrocarbons by catalytic upgrading of a fast pyrolysis bio-oil. Part II: comparative catalyst performance and reaction pathways. *Fuel Processing Technology, 45*(3), 185-202.
243. Vitolo, S., Seggiani, M., Frediani, P., Ambrosini, G., & Politi, L. (1999). Catalytic upgrading of pyrolytic oils to fuel over different zeolites. *Fuel, 78*(10), 1147-1159.
244. Luque, R., Clark, J. H., Yoshida, K., & Gai, P. L. (2009). Efficient aqueous hydrogenation of biomass platform molecules using supported metal nanoparticles on Starbons. *Chemical Communications*(35), 5305-5307.
245. Karimi, E., Gomez, A., Kycia, S. W., & Schlaf, M. (2010). Thermal decomposition of acetic and formic acid catalyzed by red mud - implications for the potential use of red mud as a pyrolysis bio-oil upgrading catalyst. *Energy & Fuels, 24*(4), 2747-2757.
246. Al-Sabawi, M., Chen, J., & Ng, S. (2012). Fluid catalytic cracking of biomass-derived oils and their blends with petroleum feedstocks: a review. *Energy & Fuels, 26*(9), 5355-5372.
247. French, R., & Czernik, S. (2010). Catalytic pyrolysis of biomass for biofuels production. *Fuel Processing Technology, 91*(1), 25-32.
248. Hilten, R. N., Speir, R. A., Kastner, J. R., Mani, S., & Das, K. C. (2012). Effect of torrefaction on bio-oil upgrading over HZSM-5. Part 2: byproduct formation and catalyst properties and function. *Energy & Fuels, 27*(2), 844-856.
249. Nokkosmäki, M. I., Krause, A. O. I., Leppämäki, E. A., & Kuoppala, E. T. (1998). A novel test method for catalysts in the treatment of biomass pyrolysis oil. *Catalysis Today, 45*(1), 405-409.

250. Nokkosmäki, M. I., Kuoppala, E. T., Leppämäki, E. A., & Krause, A. O. I. (1998). A novel test method for cracking catalysts. *Journal of Analytical and Applied Pyrolysis, 44*(2), 193-204.
251. Wang, Y., He, T., Liu, K., Wu, J., & Fang, Y. (2012). From biomass to advanced bio-fuel by catalytic pyrolysis/hydro-processing: hydrodeoxygenation of bio-oil derived from biomass catalytic pyrolysis. *Bioresource Technology, 108*, 280-284.
252. Nowakowski, D. J., Woodbridge, C. R., & Jones, J. M. (2008). Phosphorus catalysis in the pyrolysis behaviour of biomass. *Journal of Analytical and Applied Pyrolysis, 83*(2), 197-204.
253. Jae, J., Coolman, R., Mountziaris, T. J., & Huber, G. W. (2014). Catalytic fast pyrolysis of lignocellulosic biomass in a process development unit with continual catalyst addition and removal. *Chemical Engineering Science, 108*(0), 33-46.
254. Scott, D. S., Piskorz, J., & Radlein, D. (1985). Liquid products from the continuous flash pyrolysis of biomass. *Industrial & Engineering Chemistry Process Design and Development, 24*(3), 581-588.
255. Paasikallio, V., Agblevor, F., Oasmaa, A., Lehto, J., & Lehtonen, J. (2013). Catalytic pyrolysis of forest thinnings with ZSM-5 catalysts: effect of reaction temperature on bio-oil physical properties and chemical composition. *Energy & Fuels, 27*(12), 7587-7601.
256. Di Blasi, C., Branca, C., & Galgano, A. (2008). Thermal and catalytic decomposition of wood impregnated with sulfur- and phosphorus-containing ammonium salts. *Polymer Degradation and Stability, 93*(2), 335-346.
257. Veses, A., Aznar, M., Martínez, I., Martínez, J. D., López, J. M., Navarro, M. V., et al. (2014). Catalytic pyrolysis of wood biomass in an auger reactor using calcium-based catalysts. *Bioresour Technol, 162*(0), 250-258.
258. Pütün, E. (2010). Catalytic pyrolysis of biomass: effects of pyrolysis temperature, sweeping gas flow rate and MgO catalyst. *Energy, 35*(7), 2761-2766.
259. Patwardhan, P. R., Satrio, J. A., Brown, R. C., & Shanks, B. H. (2010). Influence of inorganic salts on the primary pyrolysis products of cellulose. *Bioresour Technol, 101*(12), 4646-4655.
260. Steinberg, M., Fallon, P. T., & Sundaram, M. S. (1986). Flash pyrolysis of biomass with reactive and non-reactive gas. *Biomass, 9*(4), 293-315.
261. Butt, D. A. E. (2006). Formation of phenols from the low-temperature fast pyrolysis of radiata pine (Pinus radiata): part I. Influence of molecular oxygen. *Journal of Analytical and Applied Pyrolysis, 76*(1–2), 38-47.
262. Pindoria, R. V., Lim, J.-Y., Hawkes, J. E., Lazaro, M.-J., Herod, A. A., & Kandiyoti, R. (1997). Structural characterization of biomass pyrolysis tars/oils from eucalyptus wood waste: effect of H2 pressure and sample configuration. *Fuel, 76*(11), 1013-1023.
263. Dilcio Rocha, J., Luengo, C. A., & Snape, C. E. (1999). The scope for generating bio-oils with relatively low oxygen contents via hydropyrolysis. *Organic Geochemistry, 30*(12), 1527-1534.
264. Sharypov, V. I., Beregovtsova, N. G., Kuznetsov, B. N., Baryshnikov, S. V., Cebolla, V. L., Weber, J. V., et al. (2006). Co-pyrolysis of wood biomass and synthetic polymers mixtures: part IV: Catalytic pyrolysis of pine wood and polyolefinic polymers mixtures in hydrogen atmosphere. *Journal of Analytical and Applied Pyrolysis, 76*(1–2), 265-270.
265. Pütün, A. E., Gerçel, H. F., Koçkar, Ö. M., Ege, Ö., Snape, C. E., & Pütün, E. (1996). Oil production from an arid-land plant: fixed-bed pyrolysis and hydropyrolysis of Euphorbia rigida. *Fuel, 75*(11), 1307-1312.
266. Pütün, A. E., Koçkar, Ö. M., Yorgun, S., Gerçel, H. F., Andresen, J., Snape, C. E., et al. (1996). Fixed-bed pyrolysis and hydropyrolysis of sunflower bagasse: product yields and compositions. *Fuel Processing Technology, 46*(1), 49-62.

3 Reactor design and experimental development

Chapter 3 covers the design, construction, and commissioning of a bench scale fast pyrolysis reactor, as well as the development of analytical procedures. Equations used for the reactor design are generally presented in a table format for brevity, as these were all previously published in literature. During the commissioning stage, the reactor's performance was compared to similar systems in terms of the bio-oil, char, and non-condensable gas (NCG) yield. Analytical procedures were developed to determine the composition and properties of the biomass, bio-oil, char, and NCG.

3.1 Design of a bench scale fast pyrolysis reactor

Two pyrolysis reactors pre-existed in the Chemical and Process Engineering Department (CAPE) at the University of Canterbury. However these systems were both batch, fixed bed reactors, and could only achieve slow pyrolysis due to low the heating rate, [1-3]. Figure 3-1 displays one of these fixed bed reactors reactor which consisted of a stainless steel (SS) tube, 38.1 mm in diameter and 490 mm long. A heating rate of 21 °Cmin^{-1} was accomplished by placing the tube in a 1500 W electric tubular furnace with a Eurotherm 3216 temperature controller [2]. Cold nitrogen was fed through the top of the reactor, which further limited heating rates. The reactor's capacity was 10 g of sawdust per run; restricted by the heat transfer rate and gas collection system. A condenser with a surface area of 126 cm^2 was used to quench the pyrolysis vapours, and it was noted that this may not be sufficient to cool the pyrolysis vapours as smoke was observed in the bio-oil collection container. The maximum bio-oil yield obtained was 36.5 wt% at 500 °C, when using biomass particles between 45-150 μm [3].

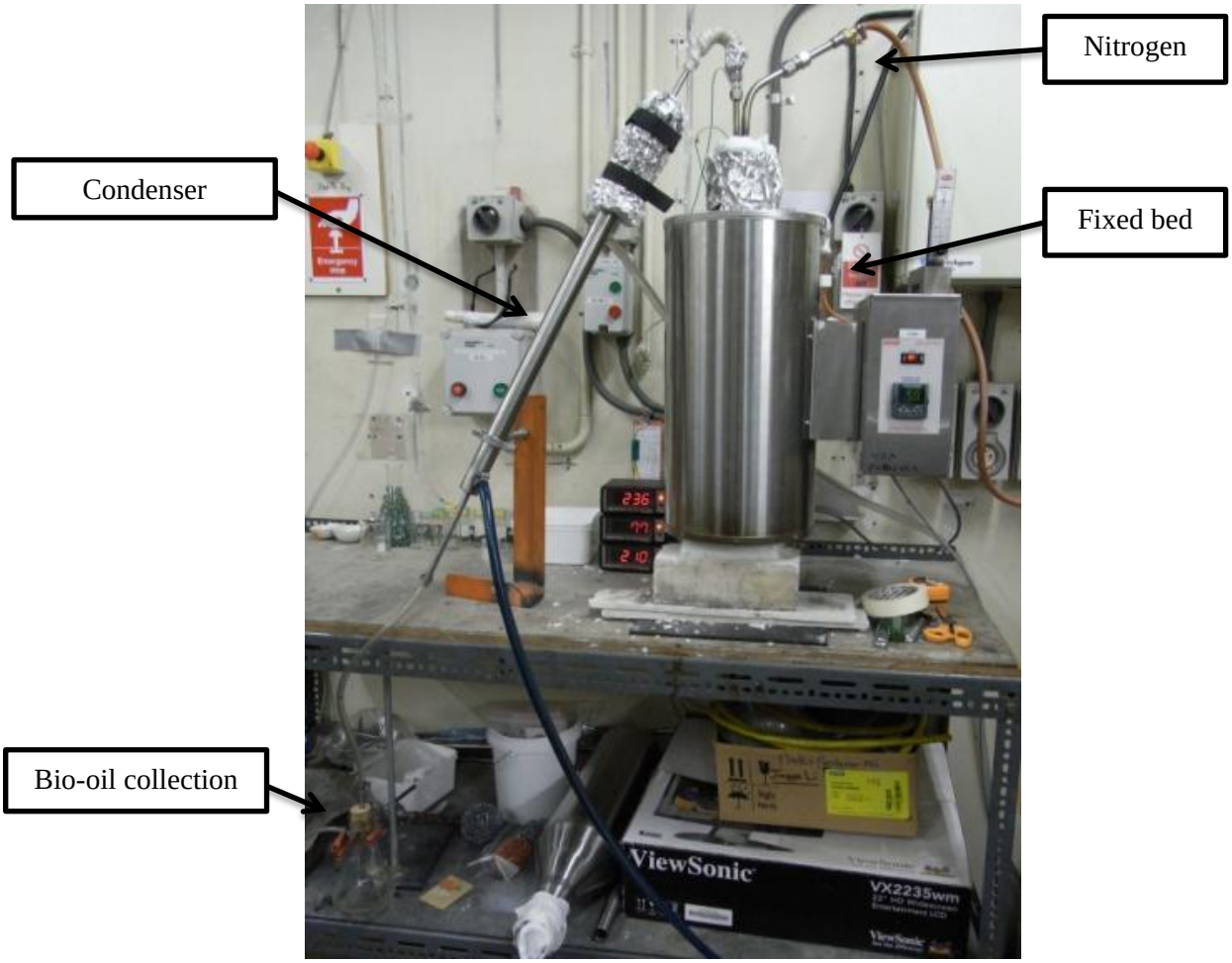

Figure 3-1: Original fixed bed pyrolysis reactor at the University of Canterbury

The reactor requirements for this research were a continuous system that could accomplish fast pyrolysis and process larger biomass particles. It was decided that the system in Figure 3-1 could not be modified to accomplish these targets. The tubular furnace was salvaged to preheat nitrogen in the new system and the condenser was modified for torrefaction vapour collection. Criteria for the new system included:

- Achieve fast pyrolysis
- Continuously feed biomass and remove char
- Able to process biomass particles up to 2 mm
- Have a maximum biomass flow rate of 1 kgh^{-1}
- Able to preheat nitrogen to the operational temperature.

The ability for a system to achieve fast pyrolysis does not solely depend on heating rate or vapour residence time, thus can be considered as the conditions that produce the highest liquid yield [4]. Considering the above requirements, a fluidised bed reactor was chosen as the reactor type as it achieves fast pyrolysis, is simple, robust, easy to scale, and well developed [5]. Fluidised bed reactors can achieve uniform fluid flow and temperature distribution; therefore can process biomass samples with an irregular texture, variable

particle size distributions, and a range of moisture contents [5]. Fluidised bed reactors have been used extensively amongst other pyrolysis researchers and have been built to commercial scale [6, 7].

A picture of the system developed in this study is given in Figure 3-2 and a piping and instrumental diagram of the system is given in Figure 3-3. In brief, biomass was stored in the hopper and fed into the fluidised bed via dual augers. Nitrogen was fed into the hopper to prevent backpressure from the pyrolysis vapours; it was also fed into the fluidised bed to convectively heat the biomass and sand. Nitrogen designated for the reactor was preheated before entering the fluidised bed. The nitrogen flow rate was precisely controlled with a digital flow controller, which was required for overall mass balance calculations. Char and pyrolysis vapours exited the fluidised bed and were transferred to the cyclone. Char was separated in the cyclone and was captured in a storage vessel below the vortex beaker, while pyrolysis vapours were carried out the cyclone's top to a series of three condensers before entering the electrostatic precipitator (ESP) and then a filter. A slip-stream exiting the filter was used for NCG analysis, while the rest of the NCGs were vented. 316 stainless steel (SS) was used for construction, unless otherwise stated.

Figure 3-2: The continuous fluidised bed reactor for fast pyrolysis of biomass, constructed at the University of Canterbury

To design the system, a model based on mass and energy balances was developed, which was used to determine the operations conditions for targeted outputs. The system was broken down into the following sections in the modelling and design: nitrogen preheating; biomass feeding, heating and fluidising; char separation in the cyclone; vapour cooling and condensation; aerosol capture in the ESP; final vapour filtering and gas sampling; and pressure and temperature control. The input parameters to the model were:

- Pyrolysis temperature of 450 °C
- Room temperature of 25 °C

- Biomass flow rate: although the system could process up to 1 $kghr^{-1}$, it was typically operated at 330 ghr^{-1}
- Biomass moisture content of 10% (dry basis).

All data that varies with temperature was calculated using interpolation, with raw data given in Appendix 3.1 and 3.2. The biomass and char particle size distribution was determined experimentally. For each sieve fraction, the average particle diameter was used, as indicated in Table 3-1.

Table 3-1: Biomass particle size distribution used in calculations

Diameter range (µm)	**Ave. diameter (µm)**	**Size distribution (%)**	
		Biomass	*Char*
<295	147.5	4.5	6.38
295-500	397.5	11.8	22.16
500-710	605	20.9	38.17
710-1000	855	36.9	31.77
1000-1400	1200	25.4	1.52
1400-2000	1700	0.4	0.00

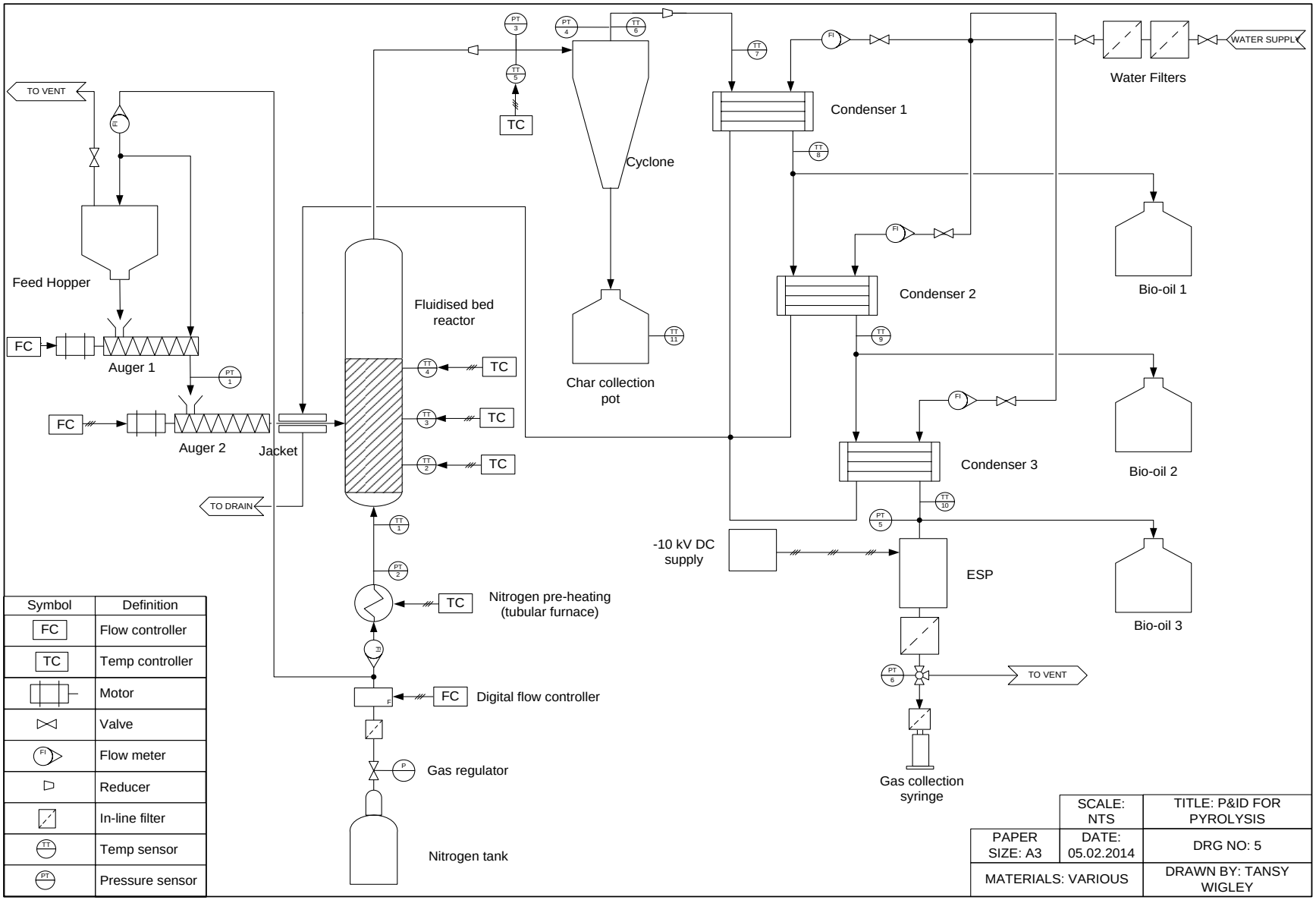

Figure 3-3: Piping and instrumental diagram for the fast pyrolysis system

3.1.1 Nitrogen preheating

The total N_2 flow rate into the system was precisely controlled using an Alicat Mass Controller. An electric tubular furnace was used for N_2 heating with a 38.1 mm OD and 490 mm long SS tube inside, this was packed with 304-SS pot scrub to increase the heating rate. The mass of scrub required was theoretically calculated by assuming forced convection around wires (assumed as the pot scrub). A temperature profile of the furnace containing the preheating tube was experimentally determined when the furnace temperature set at 570 °C, with the given in Figure 3-4. The temperatures at the bottom and top of the furnace were lower than the set-point, while the temperature near the mid-length of the furnace reached 619 °C. The temperature profile of N_2 up the height of the tube was modelled assuming this temperature profile, but that it did not drop below 450 °C in the top half of the furnace due to heat from the fluidised bed.

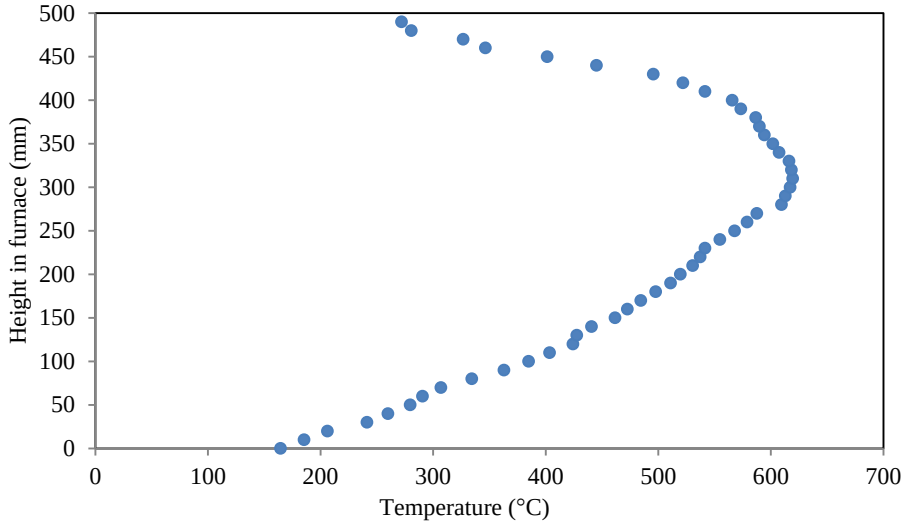

Figure 3-4: Temperature profile up the preheater furnace, with a set-point of 570 °C

The nitrogen temperature was calculated at 10 mm increments up the preheating tube. At each increment, the heat transfer from the pot scrub to the N_2 was calculated based on equations given in Holman [8] for a forced-convective heat transfer over a cylinder. Equations and values at three increments are given in Table 3-2.

Calculation assumptions:

- SS pot scrub was represented by wires
- Furnace operated at 570 °C
- Wire temperature equalled the temperature given in Figure 3-4
- Wires had an average length of 5000 mm, although length did not affect results
- Temperature of the preheater did not drop below 450 °C in the top half
- The boundary layer was not effected by surrounding wires
- The N_2 flowrate required was calculated in the fluidisation calculations.

Table 3-2: Constants and variables used to determine the packing required in the preheater

Calculating the amount of pot scrub (wires) required							
Constants	**Sym.**	**Units**	**Equation**	**Value**			
Tube OD	OD	m	*1 1/2" tube*	0.0381			
Tube wall thickness	W_t	m	-	0.0015			
Tube ID	ID	m	ID=OD-2×W_t	0.0351			
Tube length	L_{tube}	m	-	0.49			
Cross-sectional area tube	A_{cross}	m^2	$A_{cross} = \frac{\pi \times ID^2}{4}$	0.000968			
Mass flow raw of N_2	$\dot{m}$	kgs^{-1}	*System input – from fluidisation*	0.00044			
Diameter of one wire	D_{wire}	m	-	0.000215			
Length of one wire	L_{wire}	m	-	5			
Volume one wire	V_{wire}	m^3	$V_{wire} = \frac{\pi \times L_{wire} \times D_{wire}^2}{4}$	1.82×10^{-7}			
Density of stainless steel	ρ_{ss}	kgm^{-3}	-	7850			
Mass of wire	m_{wire}	kg	*Found by solver*	0.253			
Number of wires in tube	N_{wires}	-	$N_{wires} = \frac{m_{wire}}{\rho_{ss} \times V_{wire}}$	177.5			
Determining the N_2 temperature exiting the preheater							
Variables	**Sym.**	**Units**	**Equation**	**Example of values**			
Height up furnace	-	mm	-	0	10	20	450
N_2 temp.	T_{N2}	°C	$T_{N2}=T_{N2}(previous)+T_{inc}$	25.0	35.9	47.5	449.5
Furnace temp.	T_{fur}	°C	From Figure 3-4	164.4	185.3	206.1	450.0
Film temp.	T_f	°C	$T_f = \frac{T_{fur}+T_{N2}}{2}$	94.7	110.6	126.8	449.8
N_2 viscosity	μ_{N2}	$kgm^{-1}s^{-1}$	*Interpolation at* T_f	0.000013	0.000013	0.000012	0.000033
N_2 density	ρ_{N2}	kgm^{-3}	*Interpolation at* T_f	0.87	0.81	0.74	0.48
N_2 thermal conductivity	k_{N2}	$Wm^{-1}K^{-1}$	*Interpolation at* T_f	0.03	0.03	0.03	0.05
Prandtl no.	Pr	-	*Interpolation at* T_f	1.10	1.19	1.28	0.69
Superficial N_2 velocity	v_S	$m.s^{-1}$	$v_s = \frac{\dot{m}}{A_{cross}\times\rho_{N2}}$	0.52	0.56	0.61	0.95
Reynolds no.	Re	-	$Re = \frac{v_s\times D_{wire}\times\rho_{N2}}{\mu_{N2}}$	7.78	7.82	7.86	2.98
C constant for Nusselt no.	C	-	*Interpolation at* Re	0.91	0.91	0.91	0.99
n constant for Nusselt no.	*n*	-	*Interpolation at* Re	0.39	0.39	0.39	0.33
Nusselt no.	Nu	-	$Nu = C \times Re^n \times Pr^{\frac{1}{3}}$	2.07	2.13	2.19	1.25
Heat transfer coff.	h	$Wm^{-2}K^{-1}$	$h = \frac{Nu \times k_{N2}}{D_{wire}}$	305.8	327.4	349.9	306.1
Heat transfer per height increment	$\frac{q}{L}$	$Wm^{-1}K^{-1}$	$\frac{q}{L} = \frac{\pi\times D_{wire}\times L_{wire}\times h\times(T_f-T_{fur})\times N_{wire}\times.01}{L_{tube}}$	260.8	299.2	339.5	0.9
N_2 heat capacity	C_p	$kJkg^{-1}K^{-1}$	*Interpolation at* T_f	1040.8	1040.8	1040.8	1096.9
N_2 increase in temp per sec	ΔT_{ps}	Ks^{-1}	$\Delta T_{ps} = \frac{q/L}{C_p\times v_s\times\rho_{N2}\times A_{cross}}$	569.7	653.5	741.5	1.8
Time to pass through section	t_s	S	$t_s = \frac{10}{v_s}$	0.019	0.018	0.016	0.010
Actual increase in temp.	T_{inc}	°C	$T_{inc}=t_s\times\Delta T_{ps}$	10.90	11.59	12.09	0.019

The mass of SS pot scrub required to heat the N_2 to 450 °C was 0.253 kg, determined using Excel's solver function. Heating tests were conducted to validate the calculations; however these indicated that 0.115 kg was required. The theoretical calculations did not take into account the increase in residence time for N_2 when packing was added to the preheater due to turbulence. Additionally, the model assumed the tube was packed with stainless steel wires with the superficial velocity was perpendicular to the wires. Packed scrub may have altered the transverse velocity as flow was also not perpendicular to all wires, and thus affected the boundary layer.

3.1.2 Biomass feeding, heating, and fluidisation

3.1.2.1 Feeding system

For a given system, the biomass size distribution determines the particle heating rate, reaction time, and char removal. Biomass particles in the upper range for fluidised beds (0.295-2 mm) were used to represent realistic pyrolysis conditions. The fraction of biomass particles below 0.295 mm was not used during experiments, thus was ignored in the system design. Biomass was fed into the bottom of the fluidised bed using the dual auger feeding system in Figure 3-5, which was constructed by Andar Holdings located in Timaru, New Zealand.

Figure 3-5: Biomass feeding system for the pyrolysis reactor

The hopper was designed to hold at least 4 kg of biomass, and was sealed using four G-clamps. The augers were constructed from square bar coiled around rod. Auger 1 was located at the bottom of the biomass hopper, as indicated in Figure 3-6(a), this determined the biomass feed rate with a variable speed drive, which then dropped biomass into auger 2. Auger 2 operated constantly at 48 rpm to pump the biomass into the reactor before it started to pyrolyse, the auger was also water jacketed to prevent premature biomass heating. Figure 3-6(b) and Figure 3-6(c) indicate how auger 2 connected to the fluidised bed, with the cooling jacket permanently attached to the fluidised bed: this allowed for auger cleaning and inspection after each experiment. The water jacket utilised recycled waste water from the condensers; therefore the flow was dependant on the total flow rate through the three condensers. There was a N_2 purge on the hopper and

another before the second auger, as recommended by Salehi *et al.* [9] to prevent back pressure from the reactor. Numerical details of the feeding system are summarised in Table 3-3.

Figure 3-6(a-b): (a) Auger 1 at the bottom of the hopper, (b) Connection between auger 2 and the fluidised bed, (c) The feeding system and the fluidised bed connected

Table 3-3: Basic properties of the biomass feeding system

Description	**Units**	**Value**	
Overall height	mm	555	
Overall length	mm	750	
Overall width	mm	450	
Hopper height	mm	300	
Hopper width	mm	450	
Hopper length	mm	300	
Hopper volume	m^3	0.024	
Maximum biomass capacity	kg	4.36	
		Auger 1	**Auger 2**
Auger diameter	mm	30	18
Diameter of inner rod	mm	20	10
Flight thickness (square rod)	mm	5	4
Length of auger	mm	450	150
Maximum speed	rpm	10	48
Maximum biomass transfer	$kghr^{-1}$	1.37	2.23

3.1.2.2 Biomass heating in the pyrolysis reactor

The pyrolysis reactor was a fluidised bed with a diameter equal to that of the N_2 preheater tube, with an OD of 35.1 mm and ID of 31.8 mm. The preheater was connected to the fluidised bed by 6 bolts through 10 mm thick flanges. A copper gasket was used between the flanges and a SS wire mesh with a pore size of 56 µm was used for the gas distributor to help prevent slugging [10]. Figure 3-7 indicates how the preheater and the fluidised bed were connected.

The total heating requirements for pyrolysis was the sum of the energy required to heat and vaporise the water in biomass; the energy required to heat the biomass; the energy required for pyrolysis reactions; and the energy to compensate for heat loss. The energy required for pyrolysis varies dependant on the initial biomass composition, moisture content, residence time, and pyrolysis temperature. These parameters affect the pyrolysis yields, and in turn, affect the heating requirements for pyrolysis. For example, char formation

is an exothermic reaction, while bio-oil and NGC formation are typically endothermic reactions. Rath *et al.* [11] developed a basic correlation for spruce wood assuming a competitive lumped reaction model to form volatiles and char. The correlation estimates the heat of pyrolysis based on the final char yield. Since the composition is similar to that of pine, this correlation was adopted in the present study. Calculations given in Table 3-4 suggest the total energy requirement was 529.3 W, excluding heat losses. In the fluidised bed, heat is firstly transferred from the heating source (electric heating elements and hot N_2 gas) to the heating medium (sand and reactor walls), then the heating medium transfers heat to the biomass. To achieve fast heating rates, heat supply was designed to be in excess with a total of 2500 W. This was supplied by five, 500 W Watlow heating bands clamped directly to the outside of the fluidised bed. Bands were tightened to 10.8 Nm to ensure direct heat transfer between the heating band and the fluidised bed.

The time to heat biomass particles of varying sizes was estimated in Table 3-4. Heat transfer to the biomass particle in a fluidised bed is 90% conduction with hot sand and the reactor walls, 9% convection with the hot N_2, and 1% radiation [12]. To calculate the radiative heat transfer, the emissivity and Stefan-Boltzmann constant must be assumed. Considering the low contribution of radiative heat transfer, the time to heat biomass particles to the required temperature was estimated based on the conductive and convective heat transfer only. The conductive heat transfer was calculated assuming a 2D system at steady state. It was modelled around a sphere buried in a heated medium (the sand), using equations given by Holman [13]. The convective heat transfer to the biomass particles was assumed to be forced convection over a sphere [8]. The model estimated the time for the biomass to reach the pyrolysis temperature ranged between 0.31 s for 0.148 mm particles and 4.63 s for 1.700 mm particles. The large variance in heating times indicates why small particles are beneficial in reducing secondary reactions compared to larger particles.

Additional assumptions:

- Moisture in biomass evaporated rapidly; therefore the biomass heat capacity was for oven-dry biomass
- Biomass particle were spherical
- Biomass was heated uniformly in the radial, tangential, and axial direction
- Char formation did not occur until the pyrolysis temperature was reached, thus did not affect the biomass's heat capacity
- N_2 remained at a constant temperature, equal to that of gas exiting the preheater
- Sand temperature was the same as the operation temperature
- 1 $Lmin^{-1}$ N_2 was fed through the feeding system to maintain a positive pressure. This stream of N_2 was assumed to be heated to the operation temperature in the fluidised bed.

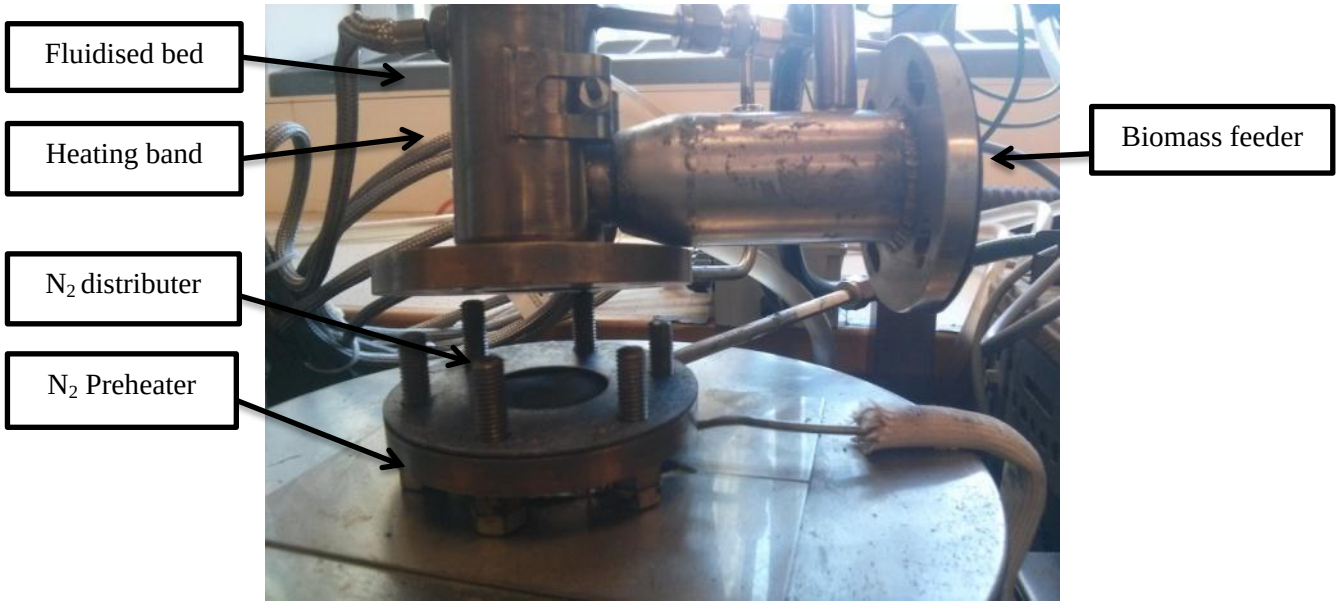

Figure 3-7: Preheater attachment to the fluidised bed

Table 3-4: Calculating the heat required for pyrolysis and the time to heat biomass particles

Energy requirements for heating and reacting biomass				
Constants	**Sym.**	**Units**	**Equation**	**Value**
Biomass temp.	T_{bio}	°C	*System input*	25
Reactor temp.	T_R	°C	*System input*	450
Film temp.	T_f	°C	$T_f = \frac{T_R + T_{bio}}{2}$	238
N_2 temp.	T_{N2}	°C	*Output from nitrogen preheating*	450
Biomass feed rate	$\dot{m}_{bio}$	kgs^{-1}	*System input*	0.000278
Ave. biomass heat capacity	$C_{p\text{-}bio}$	$Jkg^{-1}K^{-1}$	$C_{P-bio} = 1113.68 + 4.8567(T_f - 271.15)$ [11]	2267.1
Heat for biomass	q_{bio}	W	$q_{bio} = \dot{m}_{bio} \times C_{p-bio}(T_R - T_{bio})$	267.9
Char yield	Y_{char}	%	*System input*	15
Heat of pyrolysis[1]	q_{py}	W	$q_{pr} = (-3827Y_{char} + 1277(1 - Y_{char}))1000\dot{m}_{bio}$	142.2
Biomass moisture	MC	%	*System input*	10
Water in biomass	$\dot{m}_{water}$	kgs^{-1}	$\dot{m}_{water} = MC \times \dot{m}_{bio}$	0.000028
Specific heat of water	$C_{p\text{-}water}$	$Jkg^{-1}K^{-1}$	*Interpolation at* T_f	4780
Latent heat of water	L_{water}	Jkg^{-1}	*System input*	$2.26E^{6}$
Heat for water	q_{water}	W	$q_{water} = \dot{m}_{water}\left(L_{water} + C_{p-water} \times (T_R - T_{bio})\right)$	119.2
Total heat required	q_{tot}	W	$q_t = q_{bio} + q_{py} + q_w$	529.3
Time to heat the biomass particles				
Constants	**Sym.**	**Units**	**Equation**	**Value**
Biomass thermal conductivity	k_{bio}	$Wm^{-1}K^{-1}$	*System input* [14]	0.30
Density biomass	ρ_{par}	kgm^{-3}	*System input – from experiments*	430.7
Superficial N_2 velocity	v_S	$m.s^{-1}$	*Calculated in nitrogen preheating*	0.955
N_2 viscosity	μ_{N2}	$kgm^{-1}s^{-1}$	*Interpolation at* T_R	0.000032
N_2 density	ρ_{N2}	kgm^{-3}	*Interpolation at* T_R	0.48
Prandtl no.	Pr_{N2}	-	*Interpolation at* T_R	0.69
Viscosity at particle wall	μ_{wall}	$ks.ms^{-1}$	*Interpolation at* T_R	0.0000136
N_2 thermal conductivity	k_{N2}	$Wm^{-1}K^{-1}$	*Interpolation at* T_R	0.05123

Table 3-5 continued

Variables	Sym.	Units	Equation	Values for biomass diameter range					
Ave. particle diameter	D_{par}	mm	*Average of the diameter range*	0.148	0.400	0.605	0.855	1.200	1.700
Mass distribution	-	%	*System input – from experiments*	4.5	11.8	20.9	36.9	25.4	0.40
Particle mass	m_{par}	kg	$m_{par} = \left(\frac{3}{4} \times \pi \times \mathrm{D}_{\mathrm{par}}^3\right) \times \rho_{par}$	$7.0E^{-10}$	$1.4E^{-8}$	$4.8E^{-8}$	$1.4E^{-7}$	$3.8E^{-7}$	$1.1E^{-6}$
Particle surface area	A_{par}	m^2	$\mathrm{A}_{\mathrm{par}} = \pi \times \mathrm{D}_{\mathrm{par}}^2$	$6.8E^{-8}$	$5.0E^{-7}$	$1.1E^{-6}$	$2.3E^{-6}$	$4.5E^{-6}$	$9.1E^{-6}$
Mass of water in particle	m_{water}	kg	$m_{water} = MC \times m_{par}$	$6.8E^{-9}$	$5.0E^{-8}$	$1.1E^{-7}$	$2.3E^{-7}$	$4.5E^{-7}$	$9.1E^{-7}$
Conductive heat transfer to biomass[2]									
Shape factor	S	-	$S = 4 \times \pi \times \frac{\mathrm{D}_{\mathrm{par}}}{2}$	$9.3E^{-4}$	$2.5E^{-3}$	$3.8E^{-3}$	$5.4E^{-3}$	$7.5E^{-3}$	$1.1E^{-2}$
Conductive heat transfer	q_{cond}	W	$\mathrm{q}_{\mathrm{cond}} = k \times S \times (T_R - T_{bio})$	0.12	0.32	0.48	0.68	0.96	1.36
Convective heat transfer to biomass[3]									
Variables	**Sym.**	**Units**	**Equation**	**Value for biomass diameter range**					
Reynolds no.	Re_{par}	-	$\mathrm{Re}_{\mathrm{par}} = \frac{v_s \times \mathrm{D}_{\mathrm{par}} \times \rho_{N2}}{\mu_{N2}}$	2.1	5.6	8.5	12.1	17.0	24.0
Nusselt no.	Nu_{par}	-	$\mathrm{Nu}_{\mathrm{par}} = 2 + \left(0.4\mathrm{Re}_{\mathrm{par}}^{0.5} + 0.06\mathrm{Re}_{\mathrm{par}}^{2/3}\right) \times \mathrm{Pr}_{\mathrm{N2}}^{0.4} \left(\frac{\mu_{N2}}{\mu_{wall}}\right)^{\frac{1}{4}}$	2.72	3.22	3.52	3.82	4.18	4.63
Heat transfer coff.	h_{par}	$Wm^{-2}K^{-1}$	$h_{par} = \mathrm{Nu}_{\mathrm{par}} \times \left(\frac{k_{N2}}{\mathrm{D}_{\mathrm{par}}}\right)$	945.3	414.4	297.9	229.1	178.6	139.5
Convective heat transfer	q_{conv}	W	$\mathrm{q}_{\mathrm{conv}} = h_{par} \times \mathrm{A}_{\mathrm{par}} \times (T_R - T_{bio})$	0.027	0.087	0.146	0.224	0.343	0.538
Total heat transfer to biomass									
Heat of pyrolysis per particle	$q_{py\text{-}par}$	W	$\mathrm{q}_{\mathrm{py-par}} = \frac{m_{par}}{\dot{m}_{bio}} \times (q_{py} + q_{bio}) + \frac{m_{water}}{\dot{m}_{water}} \times \mathrm{q}_{\mathrm{water}}$	$3.6E^{-4}$	$7.0E^{-3}$	0.025	0.070	0.19	0.55
Time to heat particles[4]	t_{par}	s	$t_{par} = \frac{\mathrm{q}_{\mathrm{py-par}}}{\mathrm{q}_{\mathrm{cond}}} \times 90\% + \frac{\mathrm{q}_{\mathrm{py-par}}}{\mathrm{q}_{\mathrm{conv}}} \times 10\%$	0.34	0.92	1.43	2.09	3.06	4.63

[1]Predicition given by Rath et al. [11], [2]2D steady state conduction model [13], [3]forced convection over a sphere [8], [4]assuming 90% conductive heat transfer and 10% convective heat transfer [12]

3.1.2.3 Fluidisation

Determining the minimum fluidising gas velocity and the terminal gas velocity in the pyrolysis reactor was needed to ensure the bed operated in the desired bubbling fluidised bed regime. These were calculated over the size distribution for biomass, char, and silica sand. The minimum fluidisation velocity occurs when the drag force of the fluidising N_2 equals the weight of the particles, while the terminal gas velocity occurs when solid particles are carried out of the reactor by the fluidising gas. The minimum fluidisation velocity was calculated using Equation 3.1, given by Kunii and Lvenspiel [15], but was re-arranged in the present study as the quadratic form in Equation 3.2 to solve for the minimum fluidising velocity (v_{mf}):

$$\frac{D_{par}^3 \rho_{N2}(\rho_{par} - \rho_{N2})g}{\mu_{N2}^2} = \frac{1.75}{\varepsilon_{mf}^3 \emptyset_{par}} \left(\frac{D_{par} v_{mf} \rho_{N2}}{\mu_{N2}}\right)^2 + \frac{150(1-\varepsilon_{mf})}{\varepsilon_{mf}^3 \emptyset_{par}^2} \left(\frac{D_{par} v_{mf} \rho_{N2}}{\mu_{N2}}\right) \quad (3.1)$$

$$0 = v_{mf}^2 \left(\frac{1.75 \rho_{N2}}{\varepsilon_{mf}^3 \emptyset_{par} D_{par}}\right) + v_{mf} \left(\frac{150(1-\varepsilon_{mf})\mu_{N2}}{\varepsilon_{mf}^3 \emptyset_{par}^2 D_{par}^2}\right) - g(\rho_{par} - \rho_{N2}) \quad (3.2)$$

Symbols descriptions and calcualtions of the variables in Equation 3.2 are given in Table 3-7. The terminal velocity of particless was calcualted in Table 3-7, based on the terminal free-fall velocity for biomass particles in the fluidised bed. This equation was developed by Haider and Levenspiel [16].

Determining the minimum fluidisation velocity allowed the superficial velocity in the fluidised bed to be predicated, and thus, the N_2 flow rate required. The superficial gas velocity in the pyrolysis reactor should be higher than the terminal velocity of the char particles for their removal but should be less than the terminal velocity of the biomass and sand particles. Based on the data in Table 3-7, the superficial velocity was set at 0.955 ms^{-1}, this was also plotted in Figure 3-9 for clarity. Accordingly, char particles 0.86 mm and larger will not be removed from the reactor (33% of the total char). The superficial N_2 velocity cannot be increased further without removing biomass from the reactor before it has time to react; therefore the char particles over 0.86 mm will recirculate within the reactor and abrade until the diameter is sufficient for entrainment, or form a freeboard section above the fluidised bed.

Once the fluidising gas velocity was determined, the corresponding particle size of sand was calculated so that the bed operated within the bubbling fluidisation regime. Incorrectly sized particles may lead to slugging, sand carry-over, or insufficient fluidisation. Using the data in Table 3-7, sand with an average particle size of 655 µm was chosen, this equates the sieve screens between 600 and 710 µm. The superficial velocity was 3.2 times higher than the minimum fluidising velocity for the sand, which is in the typical range of 3 to 4.2 times the minimum fluidisation velocity [9, 17]. Similar particles have been used by other researcher [18], although smaller sand sizes are more typical due to the smaller biomass particles used.

For high heat transfer from the sand particles to the biomass, high mass ratios of the sand to the biomass are normally used. Bridgewater [12] reported that silica sand to biomass mass ratios at large scale are typically 20:1; however 75:1 was used in the present study to ensure fast heating rates. Larger ratios were used in previous studies by Patwardhan *et al.* [19], Meng *et al.* [20], and Salehi *et al.* [9], who used sand to biomass mass ratios between 3460:1, 3200:1 and 1750:1, respectively.

The fluidised bed height becomes a limiting factor when scaling-up traditional fast pyrolysis reactors as shallow beds are required for short vapour residence times to prevent secondary reactions. This increases the fluidising gas requirements as the superficial velocity must be sufficient to remove char [21-23]. It also restricts the biomass particles size to <3 mm [24, 25]. Since the diameter of the fluidised bed was set to equal that of the preheating tube (35.1 mm ID), the height was calculated as 72.2 mm, using equations in Table 3-7. The fluidised bed was built to be 315 mm in height, as displayed in Figure 3-8, which was longer than the required 72.2 mm considering the following factors:

- It is easier to construct a longer reactor and reduce it if need be
- Allows for higher sand to biomass ratios to be tested
- Biomass particles >0.40 mm have a terminal velocity lower than the superficial velocity in the reactor; therefore a longer reactor allows enough time for them react as they are entrained
- It would be beneficial if longer residence times for vapours was possible as it increases the ease when scaling-up reactors.

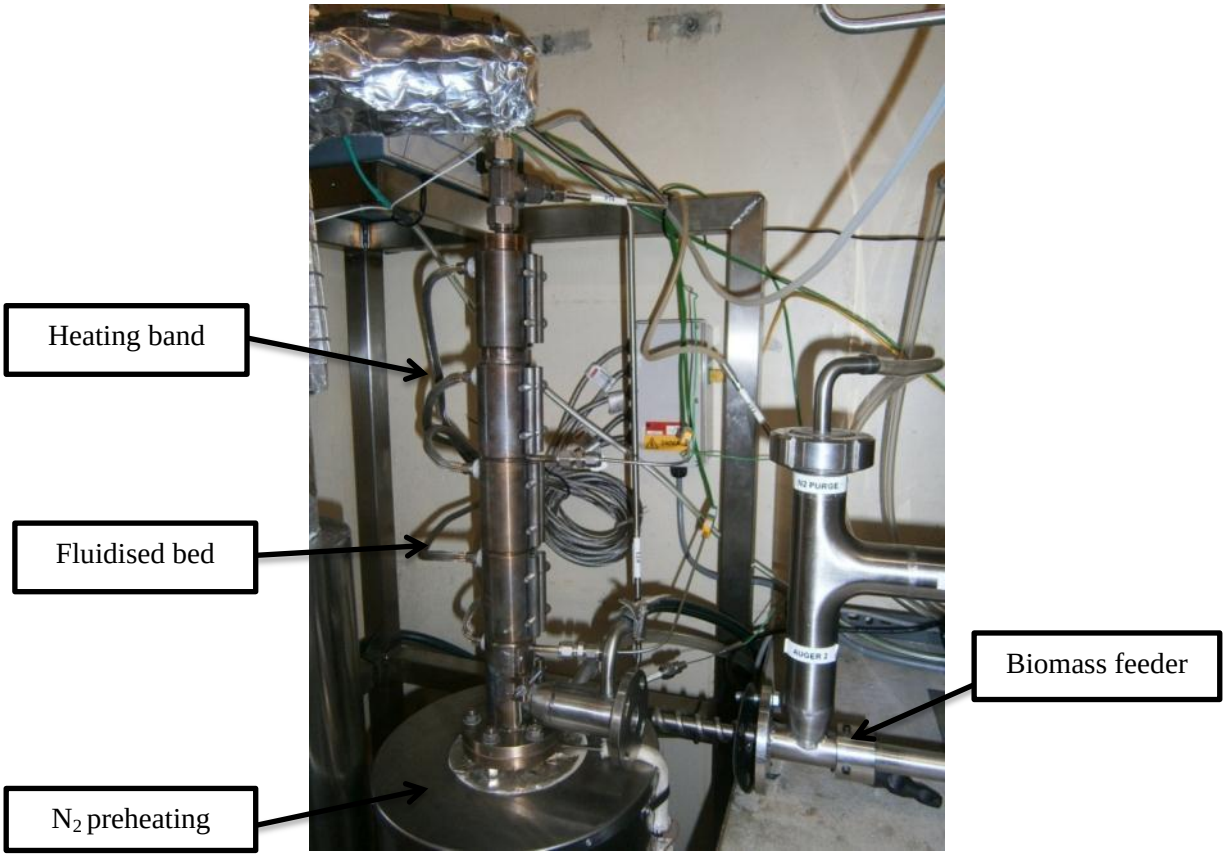

Figure 3-8: Fluidised bed reactor with heating bands attached

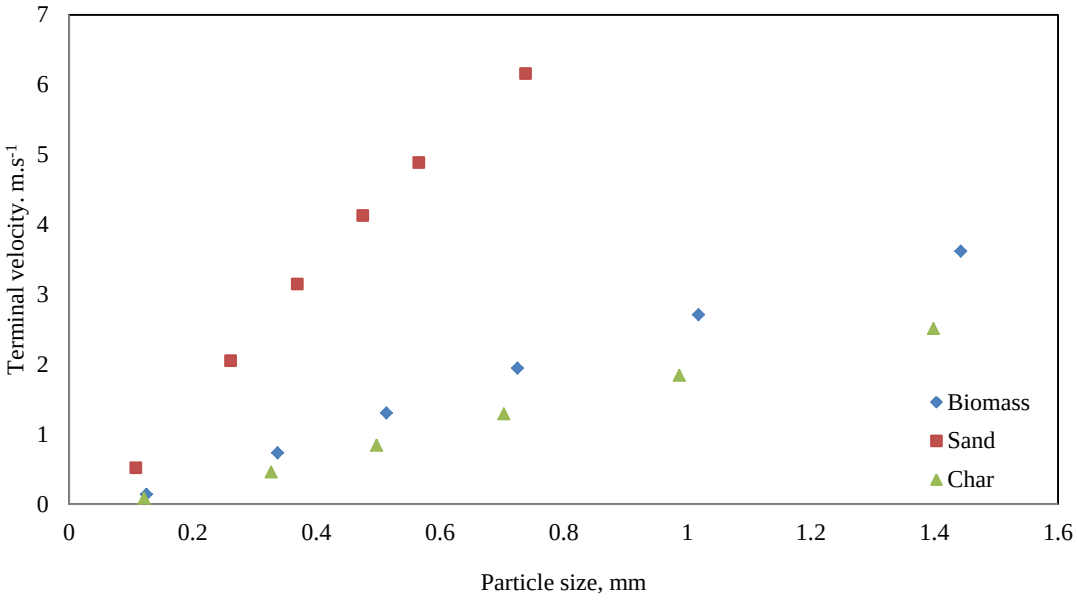

Figure 3-9: Criteria for entrainment from the fluidised bed for sand, biomass, and char particles

Table 3-6: Calculating the minimum fluidising and terminal velocity for biomass, char, and sand

Pressure drop over the bed and vapour residence time in the bed									
Constants	**Sym.**	**Units**	**Equation**	**Value**					
Biomass temp.	T_{par}	°C	*Output from biomass heating*	450					
N_2 density	ρ_{N2}	kgm^{-3}	*Interpolation at* T_{par}	0.48					
N_2 viscosity	μ_{N2}	$kgm^{-1}s^{-1}$	*Interpolation at* T_{par}	0.000032					
Voidage at min fluid vel.	ε_{mf}	-	*System input – from experiments*	0.48					
Gravity	g	$m.s^{-2}$	*System input*	9.81					
Mass flow rate of N_2	$\dot{m}_{N2}$	kgs^{-1}	*Set based on terminal vel of char*	0.00044					
Superficial N_2 vel.	v_S	$m.s^{-1}$	*Set based on terminal vel of char*	0.955					
Ave. time for particles to heat to T_{par}	$t_{par\text{-}ave}$	s	*System input – from biomass heating*	1.99					
Biomass flow rate	$\dot{m}_{bio}$	kgs^{-1}	*System input*	0.000278					
Ave. biomass in the reactor	$m_{bio-ave}$	kg	$m_{bio-ave} = \dot{m}_{bio} \times t_{par-ave}$	0.00055					
Sand required	m_{sand}	kg	*Sand to biomass ratio of 75:1*	0.041					
Bulk density of biomass	ρ_{par-b}	kgm^{-3}	*System input – from experiments*	182.7					
Bulk density of sand	ρ_{sand-b}	kgm^{-3}	*System input – from experiments*	1370.2					
Total volume in reactor	V_R	m^3	$V_R = \frac{m_{bio-ave}}{\rho_{par-h}} + \frac{m_{sand}}{\rho_{sand-b}}$	0.0000333					
Cross-sectional area reactor	A_{cross}	m^2	*Calculated in nitrogen preheating*	0.000968					
Bed height	H_{bed}	m	*Measured*	0.0722					
Vapour RT in bed	RT_{bed}	s	$RT_{bed} = \frac{\rho_{N2}(H_{bed}A_{cross} - V_R)}{\dot{m}_{N2}}$ [26]	0.04					
Minimum fluidising and terminal velocity for biomass									
Variables	**Sym.**	**Units**	**Equation**	**Value**					
Vol. expansion of biomass	VE_{par}	%	*System input*	1.18					
Sphericity of biomass	$\emptyset_{par}$	-	*System input – from experiments*	0.84					
Particle density of biomass at T_{par}	ρ_{par-h}	kgm^{-3}	*System input*	415.6					
Variables	**Sym.**	**Units**	**Equation**	**Values for particle size range**					
Ave. particle diameter	D_{par}	m	*Average of the diameter range*	$0.148E^{-3}$	$0.40E^{-3}$	$0.61E^{-3}$	$0.86E^{-3}$	$1.20E^{-3}$	$1.70E^{-3}$
Particle diameter at T_{par}	$D_{par\text{-}h}$	m	$D_{par\text{-}h} = D_{par} \times VE_{par}$	$0.149E^{-3}$	$0.40E^{-3}$	$0.61E^{-3}$	$0.87E^{-3}$	$1.21E^{-3}$	$1.72E^{-3}$
Mass distribution	-	%	*System input - from experiments*	4.5	11.8	20.9	36.9	25.4	0.4
From Eq 3.2 for v_{mf}^2	A	-	$A = \left(\frac{1.75\rho_{N2}}{\varepsilon_{mf}^3 \emptyset_{par} D_{par-h}}\right)$	1524606	209927	90621	45374	23035	11477
From Eq 3.2 for v_{mf}	B	-	$B = \left(\frac{150(1-\varepsilon_{mf})\mu_{N2}}{\varepsilon_{mf}^3 \emptyset_{par}^2 D_{par-h}^2}\right)$	61645	22874	15029	10635	7577	5349
Constant for Eq 3.2	C	-	$C = -g(\rho_{par-h} - \rho_{N2})$	-4072	-4072	-4072	-4072	-4072	-4072
Min. fluidising vel[1]	v_{mf-p}	$m.s^{-1}$	$0 = v_{mf-p}^2 A + v_{mf-p} B + C$ solving for v_{mf-p}	0.0026	0.0193	0.0440	0.0870	0.1670	0.3090
Dimensionless particle size	D^*_{par-h}	-	$D^*_{par-h} = D_{par-h}\left(\frac{\rho_{N2} g(\rho_{par-h} - \rho_{N2})}{\mu_{N2}^2}\right)^{1/3}$	1.82	4.89	7.45	10.52	14.77	20.92
Dimensionless vel.	v^*_{t-p}	-	$v^*_{t-p} = \left(\frac{18}{(D^*_{par-h})^2} - \frac{2.335 - 1.744\emptyset_{par}}{(D^*_{par-h})^{1/2}}\right)^{-1}$	0.16	0.87	1.55	2.32	3.23	4.31
Terminal vel.[2]	v_{t-p}	$m.s^{-1}$	$v_{t-p} = v^*_{t-p}\left(\frac{\mu_{N2} g(\rho_{par-h} - \rho_{N2})}{\rho_{N2}^2}\right)^{1/3}$	0.14	0.73	1.30	1.94	2.71	3.62
Particles removed at v_S?	-	-	$\text{IF}(v_{t-p} > v_s, \text{Yes}, \text{No})$	Yes	Yes	No	No	No	No
Variables	**Sym.**	**Units**	**Equation**	**Value**					
Vol. expansion of char	VE_{char}	%	*System input*	1.18					
Sphericity of char	$\emptyset_{char}$	-	*System input – from experiments*	0.81					
Particle density of char at T_{par}	ρ_{char-h}	kgm^{-3}	*System input*	241.2					

Table 3-6 continued

Variables	Sym.	Units	Equation	Values for particle size range					
Ave. particle diameter	D_{char}	m	*Average of the diameter range*	$0.148E^{-3}$	$0.40E^{-3}$	$0.61E^{-3}$	$0.86E^{-3}$	$1.20E^{-3}$	$1.70E^{-3}$
Particle diameter at T_{par}	D_{char-h}	m	$D_{par-h}= D_{par}\times VE_{par}$	$0.149E^{-3}$	$0.40E^{-3}$	$0.61E^{-3}$	$0.87E^{-3}$	$1.21E^{-3}$	$1.72E^{-3}$
Mass distribution	-	%	*System input from experiments*	6.4	22.2	38	32	2	0
From Eq 3.2 for v_{mf}^2	A	-	$A = \left(\frac{1.75\rho_{N2}}{\varepsilon_{mf}^3 \emptyset_{char} D_{char-h}}\right)$	1622326	223382	96430	48283	24511	12213
From Eq 3.2 for v_{mf}	B	-	$B = \left(\frac{150(1-\varepsilon_{mf})\mu_{N2}}{\varepsilon_{mf}^3 \emptyset_{char}^2 D_{char-h}^2}\right)$	63590	23596	15503	10970	7816	5517
Constant for Eq 3.2	C	-	$C = -g(\rho_{char-h} - \rho_{N2})$	-2362	-2362	-2362	-2362	-2362	-2362
Min. fluidising vel[1]	v_{mf-c}	$m.s^{-1}$	$0 = v_{mf-c}^2 A + v_{mf-c} B + C$ solving for v_{mf-c}	0.0014	0.0105	0.0243	0.0480	0.0930	0.1780
Dimensionless particle size	D^*_{char-h}	-	$D^*_{char-h} = D_{char-h}\left(\frac{\rho_{N2} g(\rho_{char-h}-\rho_{N2})}{\mu_{N2}^2}\right)^{1/3}$	1.51	4.08	6.21	8.78	12.32	17.45
Dimensionless vel.	v^*_{t-c}	-	$v^*_{t-c} = \left(\frac{18}{(D^*_{char-h})^2} - \frac{2.335 - 1.744\emptyset_{char}}{(D^*_{char-h})^{1/2}}\right)^{-1}$	0.12	0.65	1.20	1.84	2.63	3.59
Terminal vel.[2]	v_{t-c}	$m.s^{-1}$	$v_{t-c} = v^*_{t-c}\left(\frac{\mu_{N2} g(\rho_{char-h}-\rho_{N2})}{\rho_{N2}^2}\right)^{1/3}$	0.08	0.46	0.84	1.29	1.84	2.51
Particles removed at v_S?	-	-	$IF(v_{t-c} > v_s, Yes, No)$	Yes	Yes	Yes	No	No	No

Minimum fluidising and terminal velocity sand

Variables	Sym.	Units	Equation	Value
Vol. expansion for sand	VE_{sand}	%	*System input*	0.41
Sphericity of sand	$\emptyset_{sand}$	-	*System input – from experiments*	0.86
Particle density of sand	ρ_{sand}	kgm^{-3}	*System input – from experiments*	2397.9

Variables	Sym.	Units	Equation	Values for particle size range					
Ave. particle diameter	D_{sand}	m	*Average of the diameter range*	$0.125E^{-3}$	$0.30E^{-3}$	$0.43E^{-3}$	$0.55E^{-3}$	$0.66E^{-3}$	$0.86E^{-3}$
particle diameter at T_{par}	D_{sand-h}	m	$D_{par-h}= D_{par}\times VE_{sand}$	$0.13E^{-3}$	$0.30E^{-3}$	$0.43E^{-3}$	$0.55E^{-3}$	$0.66E^{-3}$	$0.86E^{-3}$
From Eq 3.2 for v_{mf}^2	A	-	$A = \left(\frac{1.75\rho_{N2}}{\varepsilon_{mf}^3 \emptyset_{sand} D_{sand-h}}\right)$	2050059	350055	175273	105891	74663	43818
From Eq 3.2 for v_{mf}	B	-	$B = \left(\frac{150(1-\varepsilon_{mf})\mu_{N2}}{\varepsilon_{mf}^3 \emptyset_{sand}^2 D_{sand-h}^2}\right)$	71483	29538	20901	16246	13642	10451
Constant for Eq 3.2	C	-	$C = -g(\rho_{sand} - \rho_{N2})$	-23519	-23519	-23519	-23519	-23519	-23519
Min. fluidising vel.[1]	v_{mf-s}	$m.s^{-1}$	$0 = v_{mf-s}^2 A + v_{mf-s} B + C$ solving for v_{mf-s}	0.011	0.066	0.132	0.215	0.298	0.481
Dimensionless particle size	D^*_{sand-h}	-	$D^*_{sand-h} = D_{sand-h}\left(\frac{\rho_{N2} g(\rho_{sand}-\rho_{N2})}{\mu_{N2}^2}\right)^{1/3}$	2.74	6.63	9.37	12.05	14.35	18.73
Dimensionless vel.	v^*_{t-s}	-	$v^*_{t-s} = \left(\frac{18}{(D^*_{sand-h})^2} - \frac{2.335 - 1.744\emptyset_{sand}}{(D^*_{sand-h})^{1/2}}\right)^{-1}$	0.34	1.36	2.09	2.74	3.25	4.09
Terminal vel.[2]	v_{t-s}	$m.s^{-1}$	$v_{t-s} = v^*_{t-s}\left(\frac{\mu_{N2} g(\rho_{sand}-\rho_{N2})}{\rho_{N2}^2}\right)^{1/3}$	0.52	2.05	3.15	4.13	4.89	6.16
Particles removed at v_S?	-	-	$IF(v_{t-s} > v_s, Yes, No)$	Yes	No	No	No	No	No

[1]Equations to calculate the minimum fluidising velocity from Kunii and Lvenspiel [15] [2]equations to calculate the terminal velocity from Haider and Levenspiel [16]

3.1.2.4 Validating sand particle fluidisation in the pyrolysis reactor

To validate the calculations of the sand particles bubbling fluidisation regime in the pyrolysis reactor, 41 g of silica sand with particles sizes between of 600 and 710 µm was fluidised in a glass tube. In the tests, N_2 was used as the fluidising agent. The superficial velocity of the N_2 was increased from 0-0.85 $m.s^{-1}$, and then decreased from 0.6-0 $m.s^{-1}$. Figure 3-10 shows that as the N_2 superficial velocity increase, the flow regime of the sand particles changed from a static bed (Figure 3-10(a)) to bubbling fluidisation (Figure 3-10(b)) and then to slugging flow (Figure 3-10(c)). The minimum fluidisation velocity was experimentally estimated as 0.283 $m.s^{-1}$ from Figure 3-11, and theoretically calculated as 0.298 $m.s^{-1}$ from Table 3-6, which indicates the calculations were acceptable.

The pressure drop over the glass tube was measured during the N_2 superficial velocity increase and decrease. The pressure verses superficial velocity is plotted in Figure 3-11. This displays the classical relationship between the pressure drop and the superficial gas velocity, with a high pressure drop plateau after the N_2 flow rate increased to the minimising fluidisation velocity (0.298 to 0.589 $m.s^{-1}$). This is due to be "unlocking" of the fixed bed as the voidage increased to the critical gas velocity at the minimum fluidisation velocity. After the minimum fluidising velocity was reached, pressure drop only increased slightly with further increases in the N_2 flow rates as the gas-solid phase was already aerated and can be deformed with minimal resistance [15]. The bed increased from initially 40 mm in height to 45 mm after the fluidisation experiments, giving a bed expansion of 13%.

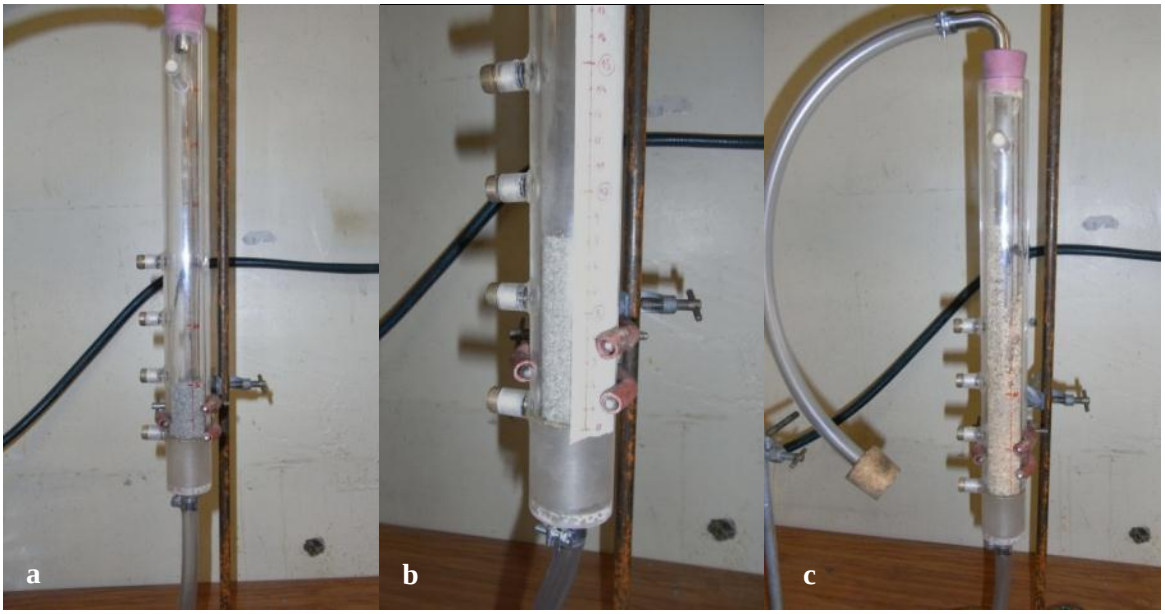

Figure 3-10(a-c): Fluidisation of sand particles in a glass tube, for a static bed (a), bubbling bed (b), and slugging (c)

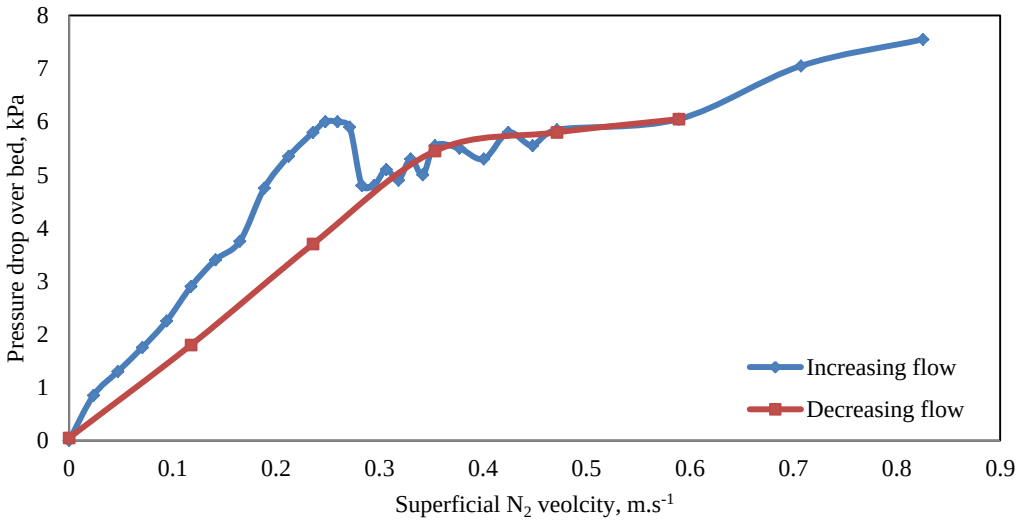

Figure 3-11: Pressure drop over the fluidised bed when increasing and decreasing N_2 flow rate

3.1.3 Cyclone design

Design of the cyclone and condensers was based around 16 model molecules/compounds which are typically formed during pyrolysis; these compounds are given in Table 3-7. The overall pyrolysis yields were

estimated on a wet basis as 15 wt% char, 15 wt% NCG, and 70 wt% bio-oil (containing 25 wt% water). Bio-oil compounds used in the models were representatives for typical bio-oil chemical families [27]. The NCG composition and yield used were adopted from a previous study by Green [2]. The density and viscosity of each model molecule/compound was interpolated at the cyclone temperature of 400 °C to give an overall gas stream density leaving the fluidised bed of 0.749 kgm^{-3} and an average viscosity of $2.68E^{-5}$ $kgm^{-1}s^{-1}$.

Table 3-7: Compounds exiting fluidised bed reactor after pyrolysis

Compound	Flow rate×E^{-6} (kgs^{-1})	Fraction in stream (wt%)	Overall fraction (wt%)	Density[1] (kgm^{-3})	Viscosity[1]×E^{-5} ($kgm^{-1}s^{-1}$)
NCGs, 15% wet basis yield					
Hydrogen, H_2	1.00	2.39	0.14	0.041	1.43
Methane, CH_4	3.41	8.18	0.48	0.292	2.07
Carbon monoxide, CO	15.89	38.10	2.21	0.507	3.20
Carbon dioxide, CO_2	20.59	49.37	2.87	0.796	2.93
Ethane, C_2H_6	0.82	1.96	0.11	0.544	1.90
Nitrogen, N_2 (from feed)	439.93	-	61.27	0.569	2.91
Condensable vapours, 70% wet basis yield					
Water vapour	48.66	25.00	6.78	0.796	2.93
Hydroxyacetaldehyde	54.94	28.23	7.65	0.832	2.15
Acetic Acid	14.02	7.20	1.95	1.088	1.98
Hydroxypropanone	30.56	15.70	4.26	1.343	1.72
Levoglucosan	23.60	12.12	3.29	1.960	1.47
Furfural	5.92	3.04	0.82	1.741	1.70
Isoeugenol	4.01	2.06	0.56	1.960	1.47
Phenol	0.26	0.13	0.04	1.705	1.67
Syringol	12.67	6.51	1.76	1.960	1.47
Solids, 15% wet basis yield					
Char	41.71	15	5.81	-	-
Average				0.749	2.68

[1]*Densities and viscosities were at the cyclone temperature of 400 °C*

There is a trade-off between the separation efficiency and the pressure drop over cyclones. Char has a low particle density; therefore either a high gas flow rate or smaller diameter cyclone is required to increase the centrifugal force. The cyclone was sized based on the high efficiency Swift model [28], basic dimensions are calculated in Table 3-8 with parameters displayed in Figure 3-12(a) the actual cyclone covered with insulation is displayed in Figure 3-12(b). The circular to rectangular transition for the cyclone entrance had confining and expanding angles of 12.3°. The transition was 100 mm before the cyclone's entrance to reduce any boundary layer separation or turbulent flow caused by the transition [29]. The solids outlet was extended by 93 mm to act as a vortex breaker. The chars were filtered into a cylindrical vessel with an approximate capacity of 8.3 L, enough to hold 0.94 kg of char. The cyclone was trace heated using a 2.5 M long, fibre-glass Hotwatt trace heater with a maximum capacity of 450 W.

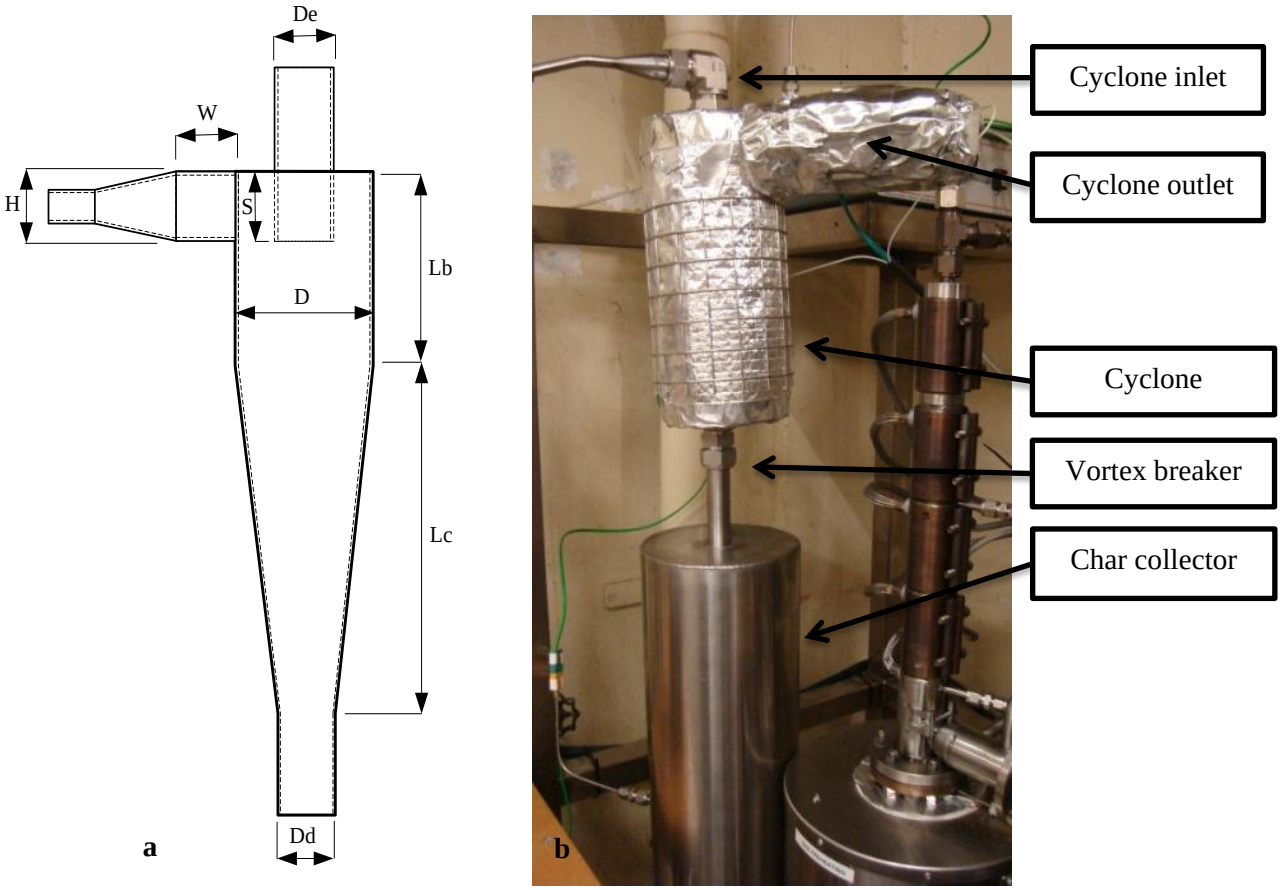

Figure 3-12(a-b): (a) cyclone parameters for sizing, (b) cyclone with trace heating and insulation

The cyclone's diameter was set based on the char separation using the Leith and Licht efficiency model [30]. The Leith and Licht efficiency model estimates all char particles used in the fluidisation calculations will be removed. Abrasion may lead to smaller char particles; therefore it is important to consider the removal efficiency for wider range of char particles. Efficiency calculations are given for a few representative char particle sizes in Table 3-8, but plotted over the entire particle range in Figure 3-13. This indicates 99% removal efficiency for particles over 46 µm. The residence time for vapours in the cyclone was estimated to be 0.719 s and the pressure drop over the cyclone was calculated as 145.5 Pa.

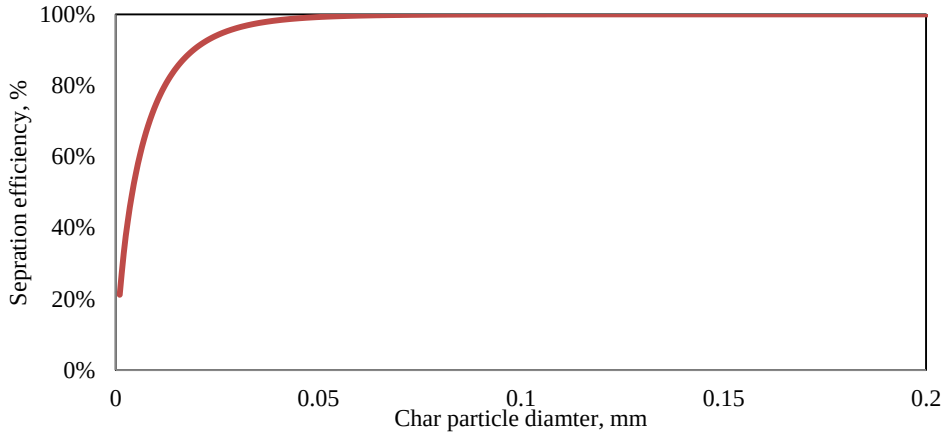

Figure 3-13: Char removal efficiency as a function of particle size based on the Leith and Licht efficiency model [30]

Table 3-8: Calculating the cyclone size, pressure drop, vapour residence time, and efficiency

Dimensions for the Swift cyclone										
Constants	**Sym.**	**Units**	**Geometric ratio[1]**	**Equation, refer to Figure 3-12**	**Value**					
Cylinder diameter	D	mm	1	*Set, based on efficiency*	47.1					
Inlet height	H	mm	0.44	$H = D \times 0.44$	20.7					
Inlet width	W	mm	0.21	$W = D \times 0.21$	9.9					
Gas exit diameter	De	mm	0.4	$De = D \times 0.4$	18.8					
Body length	Lb	mm	1.4	$Lb = D \times 1.4$	65.9					
Cone length	Lc	mm	2.5	$Lc = D \times 2.5$	117.7					
Overall length	L	mm	3.9	$L = D \times 3.9$	183.6					
Vortex finder	S	mm	0.5	$S = D \times 0.5$	23.5					
Outlet diameter	Dd	mm	0.4	$Dd = D \times 0.4$	18.8					
Pressure drop over the cyclone										
Constants	**Sym.**	**Units**	**Equation**		**Value**					
Mass flow of vapours entering cyclone	$\dot{m}_{in-cy}$	kgs^{-1}	*Sum of vapours flow rates from Table 3-7*		0.00068					
Ave. density of vapour	$\rho_{vap-ave}$	kgm^{-3}	*From Table 3-7*		0.749					
Ave. viscosity of vapour	$\mu_{vap-ave}$	$kgm^{-1}s^{-1}$	*From Table 3-7*		$2.68E^{-5}$					
Inlet vapour velocity	v_{in-cy}	$m.s^{-1}$	$v_{in-cy} = \frac{\dot{m}_{in-cy} H \times W}{\rho_{vap-ave}}$		4.41					
Constant	$K_{\Delta P_{cy}}$	-	*Given in [30]*		3.2					
Inlet velocity heads	N_H	-	$N_H = K_{\Delta P_{cy}} \left(\frac{D}{De}\right)^2$		20.0					
Pressure drop over cyclone	ΔP_{cy}	Pa	$\Delta P_{cy} = \frac{\rho_{vap-ave} v_{in-cy}^2 N_H}{2}$		145.6					
Removal efficiency of char										
Particle density of char	ρ_{char-h}	kgm^{-3}	*System input*		241.2					
Temp. in cyclone	T_{cy}	°C	*System input*		400					
Variable M_1	M_1	-	$M_1 = 1 - (1 - 0.67D^{0.14}) \left(\frac{T_{cy}}{283}\right)^{0.3}$		0.270					
Variable M_2	M_2	-	$M_2 = \frac{1}{M_1 + 1}$		0.788					
Variables	**Sym.**	**Units**	**Equation**		**Values for char size range**					
Char particle diameter	$D_{char-cy}$	m	*Example of char particles*		$1.0E^{-6}$	$5.0E^{-6}$	$1.1E^{-5}$	$5.0E^{-5}$	$1.0E^{-4}$	$2.0E^{-4}$
Cunningham slip factor	C'	-	$C' = 1 + \frac{6.6E^{-8}}{D_{char-cy}} \left(2.514 + 0.8EXP\left(-0.55 \frac{D_{char-cy}}{6.6E^{-8}}\right)\right)$		1.17	1.03	1.02	1.00	1.00	1.00
Variable φ	φ	-	$\varphi = 2\left(\frac{699.2 C' \rho_{char-h} C (M_1 + 1)}{18 \mu_{vap-ave} D}\right)^{M_2/2}$		12640	12052	11969	11914	11906	11902
Collection efficiency	ϵ	%	$\epsilon = 1 - exp\left(-\varphi D_{char-cy}^{M_2}\right)$ [31]		21.2	55.3	77.4	99.2	100.0	100.0
Vapour residence time in the cyclone										
No. of effective turns	N_e	-	$N_e = \frac{1}{H}\left(Lb + \frac{Lc}{2}\right)$ [30]		6.02					
Ave. diameter of cyclone	D_{ave}	m	$D_{ave} = \left(\left(\frac{D + De}{2}\right) Lc + D \times Lb\right)/L$		0.038					
Vapour residence time	RT_{cy}	s	$RT_{cy} = N_e \times D_{ave} \times \pi$		0.719					

[1]*Geometric ratio for a high efficiency Swift cyclone, given by Economopoulou and Economopoulos [28]*

3.1.4 Selective condensation

Heat exchangers can selectively condensate pyrolysis vapours based on their dew points by maintaining certain temperatures exiting the condenser [32]. Alternatively, vapours can be selectively condensed by initially dropping the vapour temperature to atmospheric, and then separating based on the compounds latent heat. Selectivity is generally better with the dew point technique, thus selective condensation was used in this study. Maintaining a high vapour temperature in the first two condensers means minimal water, acetic

acid, and other light compounds are condensed. Although prolonging the vapour residence time at higher temperatures can induce secondary reactions to alter the product composition [33].

A train consisting of three single pass shell and tube heat exchangers in series was modelled assuming film condensation inside horizontal tubes, with water as the as the cooling agent. The formation of a smooth condensate film impedes heat transfer while condensed droplets that fall in a random fashion (drop-wise condensation) maintain heat transfer rates close to ideal values. Wet surfaces cause film condensation; therefore it is hard to avoid this phenomena, but inclining the condensers 20° relative to the horizon optimises heat transfer in a single pass heat exchanger as the condensation film stretches and thins down the length of the tube [34].

Most condenser models assume the vapour is simply water [3, 32], thus underestimating the efficiency as the latent heat of most bio-oil components is lower than that of water. Using the 15 model compounds given in Table 3-7 (excluding char) gives a better representation of the actual pyrolysis vapour condensation. Calculations were done iteratively: an initial condenser length was estimated and used to calculate the heat transfer coefficient for the cooling water and vapours not condensing, and then the model was iterated to determine the actual length. The model outputs for the condenser lengths, temperature drops, water flow rates, and product separation are given in Table 3-9 while full calculations for condenser 1 are given in Table 3-10 and in Appendix 3.3 for condensers 2 and 3. Thermal properties for liquids and vapours were taken from Handbook of Heat Exchanger Design [35] and SciFinder [36].

Table 3-9: Theoretical separation of pyrolysis vapours using selective condensation

Operating conditions	**Condenser 1**	**Condenser 2**	**Condenser 3**
Inlet vapour temperature (°C)	400	200	120
Outlet vapour temperature (°C)	200	120	40
Condenser length (with 30% extra) (m)	0.102	0.136	0.465
Water flow rate ($Lmin^{-1}$)	0.5	0.5	2.0
Products condensed ($kghr^{-1}$)			
Water	0	0	0.175
Hydroxyacetaldehyde	0	0.198	0
Acetic Acid	0	0	0.050
Hydroxypropanone	0	0.110	0
Levoglucosan	0.085	0	0
Furfural	0	0	0.021
Isoeugenol	0.014	0	0
Phenol	0	0.0009	0
Syringol	0.046	0	0
Total	*0.145*	*0.309*	*0.247*

The condensers lengths were 30% longer than the model estimated to allow for flexibility in operation as each condenser had a separate water source. The model could be updated and the vapour temperature drop over each condenser altered by varying the water flow rate when actual yields and products were known. The inner condensers were 3/8 inch 316-SS tubes. SS was selected for welding purposes; ideally a metal with a higher thermal conductivity would be used. Condensers were connected in series using Swagelok union tees, with glass containers to collect products after each condenser. The condensation train after construction is displayed in Figure 3-14.

Model assumptions:

- ❖ All char was removed in the cyclone
- ❖ Complete condensation of vapours
- ❖ Did not take into account the presence of aerosols
- ❖ Evenly mixed water and vapour stream.

Figure 3-14: Selective condensation of pyrolysis vapours

Table 3-10: Determining the condenser length

Determining the condenser lengths						
Constants	**Sym.**	**Units**	**Equation**	**Value**		
Bio-oil yield	Y_{oil}	wt%	*System input*	70		
NCG yield	Y_{NCG}	wt%	*System input*	15		
Biomass feed rate	$\dot{m}_{bio}$	kgs^{-1}	*System input*	0.000278		
Mass flow NCG	$\dot{m}_{NCG}$	kgs^{-1}	$\dot{m}_{NCG} = \dot{m}_{bio} \times Y_{NCG}$	0.000042		
Mass flow rate N_2	$\dot{m}_{N2}$	kgs^{-1}	*Set in fluidisation*	0.00044		
Mass flow bio-oil	$\dot{m}_{oil}$	kgs^{-1}	$\dot{m}_{oil} = \dot{m}_{bio} \times Y_{oil}$	0.000195		
Dimensions of condensers tubes						
Inner tube OD	OD_{in}	m	*3/8" tubing*	0.00953		
Inner tube wall thickness	W_{in}	m	-	0.0012		
Inner tube ID	ID_{in}	m	$ID_{in}=OD_{in}-2\times W_{in}$	0.00713		
Outer tube OD	OD_{out}	m	*3/4" tubing*	0.0191		
Outer tube wall thickness	W_{out}	m	-	0.0015		
Outer tube ID	ID_{out}	m	$ID_{out}=OD_{out}-2\times W_{out}$	0.0161		
Variables	**Sym.**	**Units**	**Equation**	**Cond. 1**	**Cond. 2**	**Cond. 3**
Vap. flow in cond.	$\dot{m}_{in-c}$	kgs^{-1}	*Cond. 1 from Table 3-8. Cond. 2 and 3 from $\dot{m}_{out-c}$ of preceding cond.*	0.00068	0.00064	0.00055
NCG in vap.	M_{NCG}	%	$M_{NCG} = \frac{\dot{m}_{NCG}}{\dot{m}_{in-c}}$	6.2	6.6	7.6
N_2 in vap.	M_{N2}	%	$M_{N2} = \frac{\dot{m}_{N2}}{\dot{m}_{in-c}}$	65.1	69.2	80
Bio-oil in vap.	M_{oil}	%	$M_{oil} = 100\% - M_{N2} - M_{NCG}$	29	24	12
Inlet vap. temp.	T_{in-c}	°C	*Cond. 1 from Table 3-8. Cond. 2 and 3 from T_{out-c} of preceding cond.*	400	200	120
Outlet vap. temp.	T_{out-c}	°C	*System input*	200	120	40
Film temp.	T_{f-c}	°C	$T_{f-c} = \frac{T_{in-c} + T_{out-c}}{2}$	300	170	80

Heat required to cool vapours over condensers 1				**Bio-oil vapours**									**NCG**					
Variables	**Sym.**	**Units**	**Equation**	Water	Hy. ace.	Ace. acid	Hy. Prop.	Levo.	Furf.	Iso.	Phen.	Syrin.	H_2	CH_4	CO	CO_2	C_2H_6	N_2
Comp. fraction in stream	F_c	%	*From Table 3-11*	25.0	28.2	7.2	15.7	12.1	3.0	2.1	0.1	6.5	2.4	8.2	38.1	49.4	2.0	-
Boiling point	bp	°C	*System input*	100	132	118.5	145.5	384	86.7	266	181.7	261	-	-	-	-	-	-
Molecular weight	MW	$gmol^{-1}$	*System input*	18.0	60.1	60.1	74.1	162.0	84.1	164.2	94.1	154.2	2.0	16.0	28.0	44.0	30.1	14.0
Heat of vap.	h_v	Jkg^{-1}	*System input [36]*	$2.3E^{6}$	$7.2E^{5}$	$3.9E^{5}$	$6.0E^{5}$	$4.5E^{5}$	$5.2E^{5}$	$3.2E^{5}$	$4.6E^{5}$	$3.4E^{5}$	-	-	-	-	-	-
Comp. flow in	$\dot{m}_{in-c}$	kgs^{-1}	$\dot{m}_{in-c} = IF(bp < T_{in-c}, \dot{m}_{oil} \times F_c, 0)$ OR $\dot{m}_{in-c} = \dot{m}_{NCG} \times F_c$	$4.9E^{-5}$	$5.5E^{-5}$	$1.4E^{-5}$	$3.1E^{-5}$	$2.4E^{-5}$	$5.9E^{-6}$	$4.0E^{-6}$	$2.6E^{-7}$	$1.3E^{-5}$	$1.0E^{-6}$	$3.4E^{-6}$	$1.6E^{-5}$	$2.1E^{-5}$	$8.2E^{-7}$	$4.4E^{-4}$
Comp. flow out	$\dot{m}_{out-c}$	kgs^{-1}	$\dot{m}_{out-c} = IF(bp < T_{out-c}, \dot{m}_{oil} \times F_c, 0)$ OR $\dot{m}_{out-c} = \dot{m}_{NCG} \times F_c$	$4.9E^{-5}$	$5.5E^{-5}$	$1.4E^{-5}$	$3.1E^{-5}$	0	$5.9E^{-6}$	0	$2.6E^{-7}$	0	$1.0E^{-6}$	$3.4E^{-6}$	$1.6E^{-5}$	$2.1E^{-5}$	$8.2E^{-7}$	$4.4E^{-4}$
Fraction of conden.	F_{con}	%	$F_{con} = \frac{(\dot{m}_{in-c} - \dot{m}_{out-c})}{\dot{m}_{con}}$	0	0	0	0	58.6	0	9.9	0	31.5	-	-	-	-	-	-

Table 3-10 continued

Comp. heat capacity at T_{f-c}	Cp_c	$Jkg^{-1}K^{-1}$	*Value lookup at* T_{f-c}	2798	1638	1704	1958	844	1335	1916	1833	1788	14489	3210	1094	1077	2854	1056
Heat required	q_c	W	$q_c = \dot{m}_{in-c}(Cp_c(T_{in-c} - T_{out-c}) + IF(\dot{m}_{out-c} = 0, h_v, 0)$	27.2	18.0	4.8	12.0	14.6	1.6	2.8	0.1	8.8	2.9	2.2	3.5	4.4	0.5	92.9
Determining the heat transfer coefficient for water[2]																		
Ave. temp. water	T_{in-w}	°C	*System input*	20														
Heat capacity of water at T_{in-w}	Cp_{in-w}	$Jkg^{-1}K^{-1}$	*Value lookup at* T_{in-w}	4182														
Cross section area cond. for water	A_w	m^2	$A_w = \frac{\pi ID_{out}^2}{4} - \frac{\pi OD_{in}^2}{4}$	$1.31E^{-4}$														
Hydraulic dia.	D_h	m	$D_h = \frac{(ID_{out}^2 - OD_{in}^2)}{OD_{in}}$	0.0175														
Variables	**Sym.**	**Units**	**Equation**	**Cond. 1**			**Cond. 2**			**Cond. 3**								
Total heat req. to cool stream	q_{tot-c}	W	$q_{tot-c} = \sum q_{co\ comp.}$	196.3			138.6			171.3								
SS thermal conductivity	k_{ss}	$Wm^{-1}K^{-1}$	*Value lookup at* T_{f-c}	18.9			17.21			16.04								
Flow of water	$\dot{m}_w$	kgs^{-1},	*Set based on cond. Length desired*	0.0084 (0.5 $Lmin^{-1}$)			0.0084 (0.5 $Lmin^{-1}$)			0.033 (2.0 $Lmin^{-1}$)								
Temp. water out of cond.	T_{out-w}	°C	$T_{out-w} = \frac{q_{tot-c}}{\dot{m}_w Cp_{in-w}} + T_{in-w}$	25.6			24.0			21.2								
Film temp. water	T_{f-w}	°C	$T_{f-w} = \frac{T_{in-w} + T_{out-w}}{2}$	22.8			22.0			20.6								
Density of water	ρ_w	kgm^{-3}	*Value lookup at* T_{f-w}	998			998			998								
Viscosity of water	μ_w	$kgm^{-1}s^{-1}$	*Value lookup at* T_{f-w}	0.010			0.010			0.010								
Water thermal conductivity	k_w	$Wm^{-1}K^{-1}$	*Value lookup at* T_{f-w}	0.61			0.61			0.61								
Superficial water vel.	v_{s-w}	$m.s^{-1}$	$v_{s-w} = \frac{\dot{m}_w}{\rho_w A_w}$	0.064			0.064			0.252								
Reynolds no.	Re_w	-	$Re_w = \frac{\rho_w v_{s-w} D_h}{\mu_w}$	1113			1113			4398								
Prandtl no.	Pr_w	-	$Pr_w = \frac{Cp_{in-w}\mu_w}{k_w}$	6.9			6.9			6.9								
Nusselt no.	Nu_w	-	$Nu_w = 3.66 + \frac{0.0668 Re_w Pr_w (D_h/L_c)}{1 + 0.04(Re_w Pr_w (D_h/L_c))^{2/3}}$	20.7			18.4			*20.2 - Nu all for laminar flow as* Re_w*>10,000*								
Heat transfer coff.	h_w	$Wm^{-2}K^{-1}$	$h_w = \frac{Nu_w k_w}{D_h}$	714.5			636.8			697.4								
Calculating the condenser length[3]																		
Angle of the cond.	θ	°	*System input*	20 - *relative to the horizon*														
Gravity	g'	$m.s^{-2}$	$\theta' = 9.81 \sin\theta$	8.96 - *correction for inclined condensers*														
Heat transfer coefficient of the remaining vapours over condenser 1				**Bio-oil vapours**									**NCG**					
Variables	**Sym.**	**Units**	**Equation**	Water	Hy. ace.	Ace. acid	Hy. Prop.	Levo.	Furf.	Iso.	Phen.	Syrin.	H_2	CH_4	CO	CO_2	C_2H_6	N_2
Vap. density	ρ_{vap}	kgm^{-3}	*Value lookup at* T_{f-c}	0.93	0.98	1.28	1.58	2.30	2.05	2.30	2.00	2.30	0.05	0.34	0.60	0.93	0.64	0.68
Vap. viscosity	μ_{vap}	$kgm^{-1}s^{-1}$	*Value lookup at* T_{f-c}	$2.9E^{-5}$	$2.2E^{-5}$	$2.0E^{-5}$	$1.7E^{-5}$	$1.5E^{-5}$	$1.7E^{-5}$	$1.5E^{-5}$	$1.7E^{-5}$	$1.5E^{-5}$	$1.4E^{-5}$	$2.1E^{-5}$	$3.2E^{-5}$	$2.9E^{-5}$	$1.9E^{-5}$	$2.9E^{-5}$

Table 3-10 continued

Vap. thermal conductivity	k_{vap}	$Wm^{-1}K^{-1}$	*Value lookup at* T_{f-c}	0.038	0.036	0.037	0.036	0.033	0.032	0.033	0.035	0.033	0.272	0.079	0.043	0.038	0.064	0.040
Superficial vap. Vel.	$v_{s\text{-}vap}$	$m.s^{-1}$	$v_{s-vap} = \frac{4\dot{m}_{out-c}}{\rho_{vap}\pi ID_{in}^2}$	1.31	1.41	0.28	0.49	0	0.07	0	0.003	0	0.51	0.25	0.67	0.55	0.03	16.17
Reynolds no.	Re_{vap}	-	$Re_{vap} = \frac{\rho_{vap} v_{s-vap} ID_{in}}{\mu_{vap}}$	296.8	456.7	126.5	317.5	0	62.2	0.0	2.8	0	12.5	29.5	88.7	125.6	7.7	2701
Prandtl no.	Pr_{vap}	-	$Pr_{vap} = \frac{Cp_c \mu_{vap}}{k_{vap}}$	1.53	0.98	0.91	0.94	0.38	0.71	0.85	0.87	0.80	0.76	0.84	0.81	0.83	0.85	0.68
Nusselt no.	Nu_{vap}	-	$Nu_{vap} = 3.66 + \frac{0.0668 Re_{vap} Pr_{vap}(ID_{in}/L_c)}{1+0.04\left(Re_{vap} Pr_{vap}(ID_{in}/L_c)\right)^{2/3}}$ *if* $Re_{vap-c} < 2300$, *else* $Nu_{vap} = 0.023 Re_{vap}^{0.8} Pr_{vap}^{0.4}$	5.52	5.49	4.24	4.98	3.66	3.90	3.66	3.67	3.66	3.72	3.80	4.04	4.19	3.70	10.99
Vap. heat transfer coff.	h_{vap}	$Wm^{-2}K^{-1}$	$h_{vap} = \frac{Nu_{vap} k_{wvap}}{ID_{in}}$	29.4	27.7	22.0	25.2	0	17.5	0	18.1	0	141.8	42.1	24.4	22.4	33.2	61.4
Heat transfer coefficient of the condensing compounds for condenser 1																		
Overall film temp.	T_{f-o}	°C	$T_{f-o} = \frac{(T_{f-c} + T_{f-w})}{2}$	161.4	161.4	161.4	161.4	161.4	161.4	161.4	161.4	161.4	-	-	-	-	-	-
Conden. density	ρ_{con}	kgm^{-3}	*Value lookup at* T_{f-o}	958.1	1108.0	960.0	911.0	930.0	1020.0	930.0	931.0	930.0	-	-	-	-	-	-
Conden. viscosity	μ_{con}	$kgm^{-1}s^{-1}$	*Value lookup at* T_{f-o}	$2.8E^{-4}$	$5.4E^{-4}$	$4.6E^{-4}$	$4.5E^{-4}$	$5.7E^{-4}$	$3.8E^{-4}$	$5.7E^{-4}$	$6.7E^{-4}$	$5.7E^{-4}$	-	-	-	-	-	-
Conden. thermal conductivity	k_{con}	$Wm^{-1}K^{-1}$	*Value lookup at* T_{f-o}	0.680	0.232	0.142	0.136	0.135	0.142	0.135	0.130	0.135	-	-	-	-	-	-
Conden. heat transfer coff.	h_{con}	$Wm^{-2}K^{-1}$	$h_{con} = 0.555\left(\frac{\rho_{con}^2 g' k_{con}^3 (h_v + 0.68 Cp_c(bp - T_{out-c}))}{\mu_{con} ID_{in}(bp - T_{f-0})}\right)^{1/4} F_{con} M_{oil}$	-	-	-	-	173.0	-	32.8	0.0	105.4	-	-	-	-	-	-

Variables	**Sym.**	**Units**	**Equation**	**Cond. 1**	**Cond. 2**	**Cond. 3**
Total heat transfer coff.	h_{tot}	$Wm^{-2}K^{-1}$	$h_{tot} = \sum(h_{con} + h_{vap})$	780.2	836.0	876.9
Log mean temp. diff.	ΔT_{log}	°C	$\Delta T_{log} = \frac{(T_{in-c} - T_{out-w}) - (T_{out-c} - T_{in-w})}{ln(T_{in-c} - T_{out-w})/(T_{out-c} - T_{in-w})}$	265.4	142.7	49.3
Vapours condensed	$\dot{m}_{con}$	kgs^{-1}	$\dot{m}_{con} = \sum(\dot{m}_{in-c} - \dot{m}_{out-c})$	0.00064	0.00055	0.00048
Bio-oil condensed	-	%	-	21	44	35
Condenser length	L_c	m	$L_c = \frac{q_{tot-c}}{\pi \Delta T_{log}}\left(\frac{1}{OD_{in} h_w} + \frac{LN\left(\frac{OD_{in}}{ID_{in}}\right)}{2k_{ss}} + \frac{1}{ID_{in} h_{tot}}\right)$	0.079	0.105	0.357

N.B. value lookup tables can be found in Appendix 3 [1]Caluclation for heat required was from Chan [34] [2]Calculations based on those given by Holman [8] [3]following the procedure in Holman [37], but developed by Chato [38]

3.1.5 Vapour residence time in the pyrolysis reactor

The total vapour residence time (RT) of the pyrolysis vapours in the pyrolysis reactor, cyclone, and transfer lines is given in Table 3-12. These times can be used to predict possible chemical and physical changes to the vapours. Long residence times can encourage secondary reactions; therefore the total vapour RT should be kept under 2 s. The vapour residence time varies with the pyrolysis conditions as these affects the vapour density, thus the superficial velocity in the reactor and consequently the vapour residence time. The N_2 flow rate, biomass feed rate, volatile yield, reactor temperature, and cyclone temperature are key parameters that affect the total vapour residence time.

Table 3-12: Vapour residence time in the pyrolysis reactor

Reactor part	Sym.	Time (s)
Vapour RT in fluidised bed	RT_{bed}	0.04 *(From Table 3-6)*
RT exiting reactor	RT_R	0.307
Transfer RT to the cyclone	$RT_{tr\text{-}cy}$	0.026
RT in cyclone	RT_{cy}	0.719 (*From Table 3-8*)
Transfer RT to condensers 1	$RT_{tr\text{-}c1}$	0.041
Total vapour RT	$\boldsymbol{RT_{tot}}$	**1.133**

3.1.6 Electrostatic precipitator, filters, and gas sampling

3.1.6.1 Electrostatic precipitator

Gas exiting the cyclone contains condensable vapours, nitrogen, NCG, and aerosols. Suspended aerosol are condensed droplets of bio-oil entrained in the gas stream, accordingly, cannot be condensed during selective condensation and instead require collision for capture. An electrostatic precipitator (ESP) was used to collect aerosols since alternative methods such as solvent scrubbers contaminate the bio-oil with the solvent and demisters can cause large pressure drops [39].

ESPs used for bio-oil collection negatively ionise vapours, then collect ionised aerosols on a positively charged electrode [40]. High voltages are required to produce an adequate corona discharge for vapour ionisation. Bedmutha *et al.* [41] investigated the efficiency for varying voltages and found it only increased from 99.7 to 99.9% when the voltage increased from 9 to 13 kV (total of ESP and inertial impaction efficiency). Based on this, a -10 kV DC Glassman power supply was used to produce the corona, as it was already available at this University. The constructed ESP is displayed in Figure 3-15. Its two stage design initially charges vapours with an electrode constructed of 6 mm threaded rod with a ball on the end to prevent voltage drainage, and then collects vapours in the second stage. Two stage precipitation improves the efficiency [41], and the threaded rod improves the corona discharge. Polypropylene (PP) pipe was used in the charging section to prevent voltage drainage and spark-over occurring, as indicated in Figure 3-16. The lower section was constructed from SS pipe and was grounded to provide the positive electrode. Amperage was measured during pyrolysis experiments to indicate the ESP efficiency.

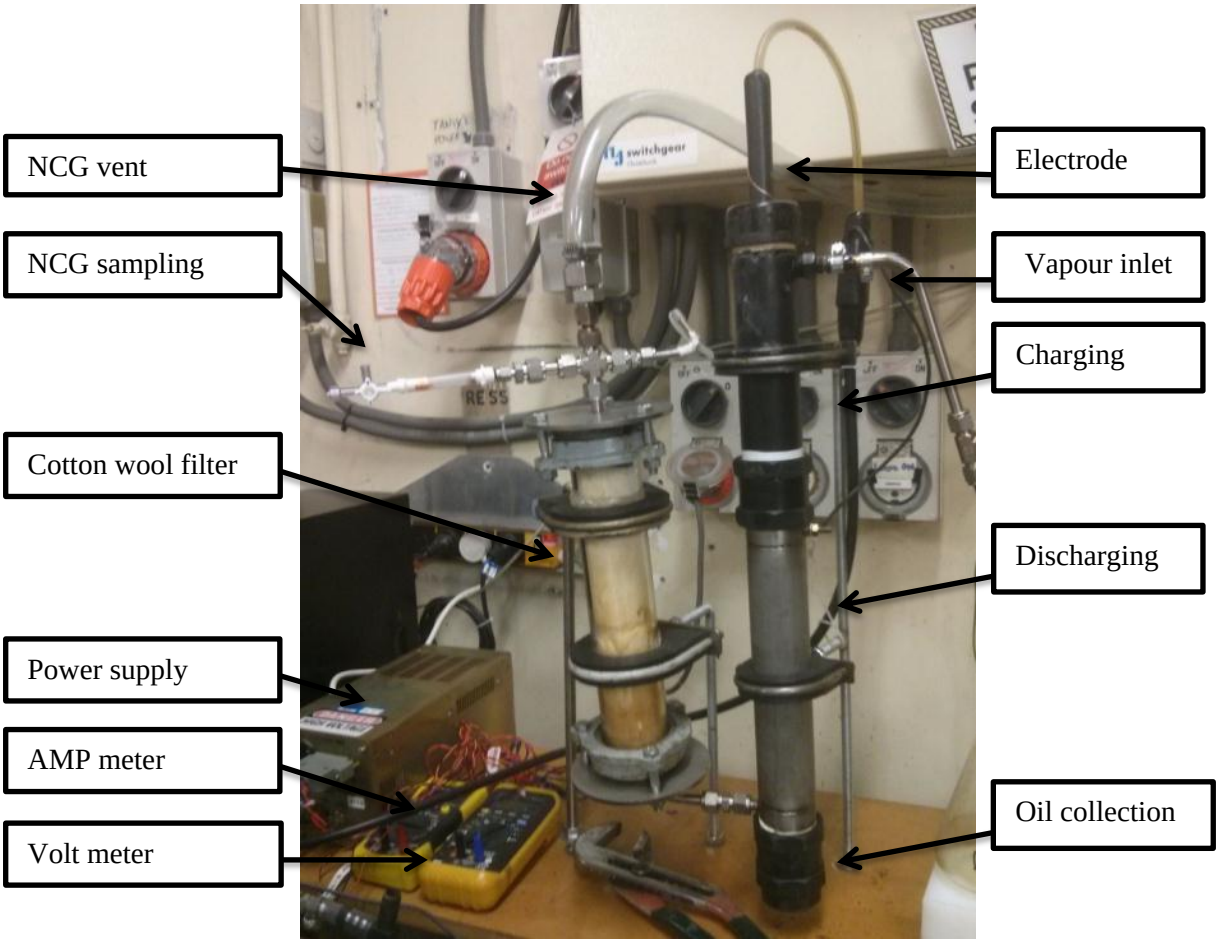

Figure 3-15: Electrostatic precipitator and cotton wool filter

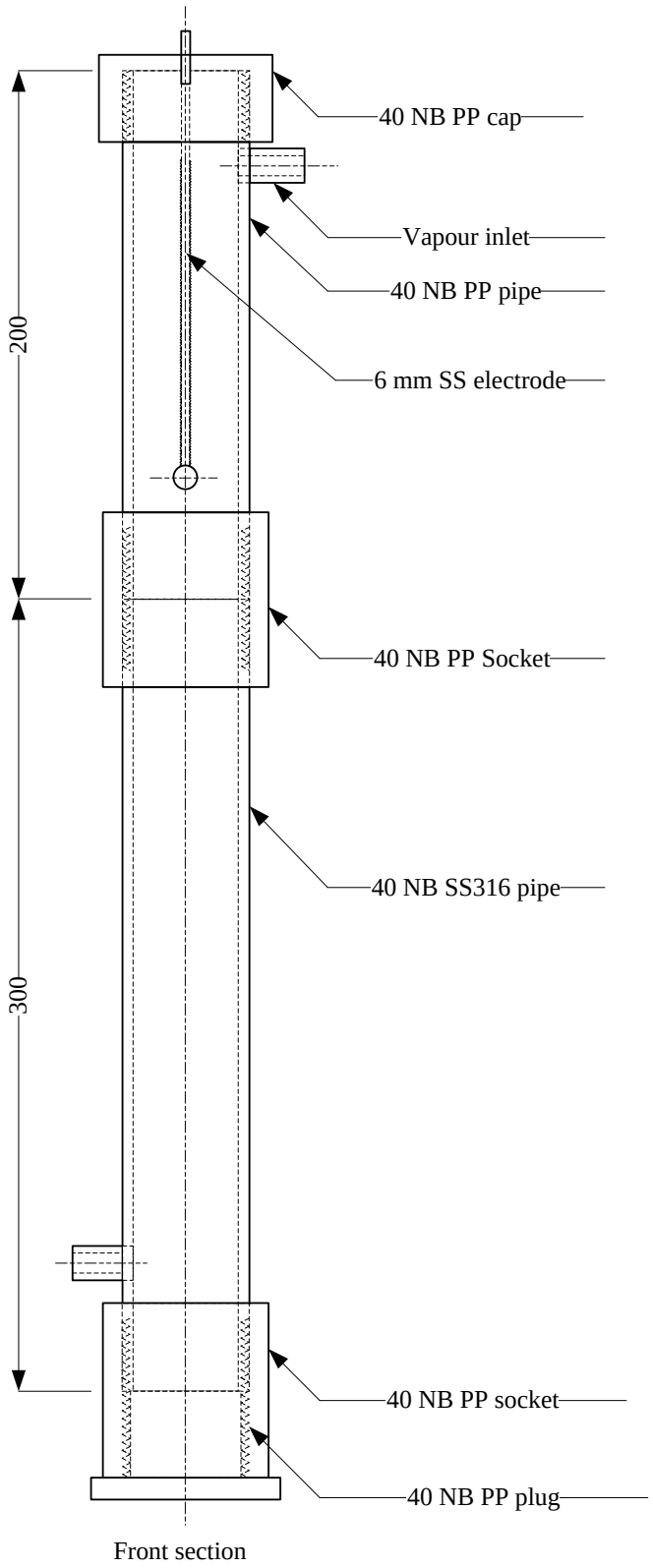

Figure 3-16: Schematic of the electrostatic precipitator for aerosol collection. SS is stainless steel, PP is polypropylene, and NB is nominal bore

3.1.6.2 Filtering and gas sampling

Remaining vapours pass through a cotton wool filter after the ESP, as displayed in Figure 3-15. The filter was constructed from a 305 mm long and 45 mm ID glass pipe. It was experimentally determined that 40 g

of cotton-wool provided sufficient packing to prevent saturation and breakthrough during a typical pyrolysis run. After a run, the bio-oil was recovered from the cotton wool by hydrolytically pressing at 350 bar, as displayed in Figure 3-17(a). Cotton wool could not be re-used after pressing.

A Swagelok cross on the filter exit acted as a bled line for NCG gas analysis before they were vented. Vapours were pulled through a 1 mL silica solid phase extraction (SPE) column using a Luer lock syringe. 40 mL of gas was collected for analysis, and the SPE column increase in weight was used as an indication for the overall vapour collection efficiency. NCGs were analysed using the mini-GC shown in Figure 3-17(b), with analytical details in Section 3.2.3.

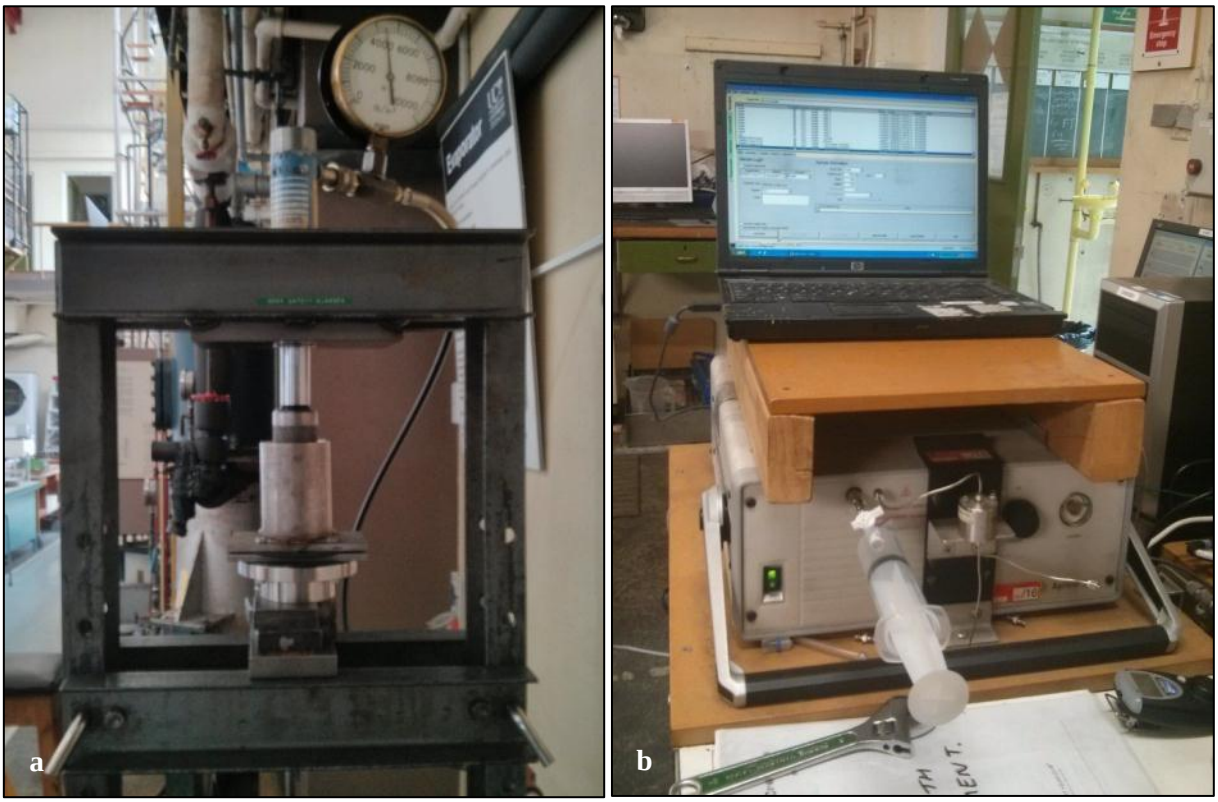

Figure 3-17(a-b): (a) pressing of cotton wool to recover bio-oil, (b) mcro-GC for NCG analysis

3.1.7 System control

Temperatures and pressures in the pyrolysis system were either controlled or logged using TracerDAQ Pro software during experiments, as indicated in Table 3-13. The fluidised bed and cyclone temperatures were PID controlled (solid state relay), while the preheater temperature was manually controlled. The fluidised bed's temperature was controlled at 3 internal points along the fluidised bed, using 2 Omron E5CSZ and 1 Shimaden SR91 controllers. The cyclone temperature was set based on the internal inlet vapour temperature, also using a Shimaden SR91 controller. The temperature of the N_2 exiting preheater was measured, and this was used to manually alter the preheater furnace temperature.

Other temperatures and pressures were measured and logged throughout the system. K type thermocouples were used with Measurement Computing USB-TEMP modules. Differential pressure was monitored by

attaching 1/4" tubing to the pyrolysis system and having the other port open to atmosphere, the pressure was determined using silicon pressure sensors from Honeywell. Pressure sensors were calibrated by measuring the pressure transducer voltage reading [42], when various nitrogen flow rates were applied and manually determining the pressure using a U-tube manometer.

Table 3-13: Temperature and pressure control/analysis for the pyrolysis system

Location	Type	Tag (Figure 3-3)
Temperature		
Outlet of N_2 preheater	Logged	T1
Fluidised bed 1	Controlled	T2
Fluidised bed 2	Controlled	T3
Fluidised bed 3	Controlled	T4
Cyclone entrance	Controlled	T5
Cyclone exit	Logged	T6
Condenser 1 entrance	Logged	T7
Condenser 2 entrance	Logged	T8
Condenser 3 entrance	Logged	T9
Condenser 3 exit	Logged	T10
Char pot	Logged	T11
Pressure		
Between auger 1 and 2	Logged	P1
Bottom of the fluidised bed	Logged	P2
Top of the fluidised bed	Logged	P3
Cyclone exit	Logged	P4
Condenser 3 exit	Logged	P5
Filter exit	Logged	P6

3.2 Analytical techniques

Physical and chemical tests were conducted to determine the properties of the biomass feedstock, NCG, char, and bio-oil. *Pinus radiata* wood chips (<6 mm) were obtained from the SRS Sawmill in Rolleston, New Zealand. After the chips were received, they were dried in a controlled room with a relative humidity of 50% and temperature of 40 °C, after which the final biomass moisture content was 8.4 wt% (dry basis). The dried biomass was then knife-milled to <2 mm and sieved to remove the fines under 295 µm. The removal of fines reduced errors during the pretreatments, as these could become embedded in/or permeate through the filters. For investigating the effect of the particle size during leaching, particles <6 mm, as received were also used. Finally, the dried biomass was stored in air-tight containers until use.

Uncertainties were determined using a 95% confidence interval. This indicates the range within the true value lies and the accuracy of the reported value [43]. During calculations, uncertainties were determined using Equation 3.3 for addition or subtraction and Equation 3.4 for multiplication or division.

$$(X_1 \pm \Delta X_1) +/- (X_{21} \pm \Delta X_2) = \sqrt{\Delta X_1^2 + \Delta X_2^2} \quad (3.3)$$

$$(X_1 \pm \Delta X_1) \times/\div (X_{21} \pm \Delta X_2) = (X_1 \times/\div X_2)\sqrt{\frac{\Delta X_1^2}{X_1} + \frac{\Delta X_2^2}{X_2}} \quad (3.4)$$

3.2.1 Feedstock, pretreated biomass, and char analysis

3.2.1.1 Moisture content of the biomass

The moisture content (MC) of biomass samples was determined by oven-drying at 105 °C for 24 hours. The MC was calculated using Equation 3.5 [1].

$$MC(wt\%) = \frac{m_{wet} - m_{dry}}{m_{dry}} \times 100 \quad (3.5)$$

Where m_{wet} is the mass of the sample before oven-drying and m_{dry} is the mass of the oven-dry sample. Biomass samples were stored in silica gel desiccators until use. Silica gel was periodically regenerated by heating to 105 °C for 5 hours.

3.2.1.2 Inorganic content and identification

Biomass or char samples were heated in a muffle furnace at 625±10 °C for at least 16 h to determine the total inorganic (ash) content. Due to the inherent variability in biomass and possible bark and stone contamination, the analysis result for each sample was an average value from 9 repetitions. The residence time was relatively long (approximately 6 h is common [44, 45]) because a constant weight could not be assessed without at least 2 h of cooling before removing the sample from the furnace.

The ash composition was analysed using inductively coupled plasma optical emission spectrophotometer (ICP-OES) and inductively coupled plasma mass spectrometry (ICP-MS). The solid samples were initially digested to solubilises the biomass's organic fraction [46]. ICP-OES can detect much higher concentrations of ions than the ICP-MS, which must have an ion concentration below 1000 ppm. Nitric acid was used for digestion in a 4748 Parr acid digestion vessel following the method originally developed by Zarcinas *et al.* [47] and modified by Zhelijazkov and Warman [48]. In brief, 0.25 g of biomass was placed in the digestion vessel with 2.5 mL of 70% nitric acid and digested at 150 °C for 4 h. The sample was then diluted 500 times to reduce the acid and inorganic concentration to levels suitable for ICP-MS.

Initial results showed large inconsistencies, possibly due to the extraction technique and dilution. Instead, 300±10 mg of biomass was digested in 2.5 mL of nitric acid and 2.5 mL of 30% hydrogen peroxide in a CEM MARS Xpress microwave digester at Lincoln University in Lincoln, New Zealand. The temperature was ramped to 90 °C over 15 min, held for 5 min, then ramped again to 180 °C over 10 min and held for 15 min. The digested samples were analysed using a Varian 720 ICP-OES, also at Lincoln University. Inorganics detected were: Li, Na, K, Mg, Ca, Ba, Cr, Cu, Fe, Mn, Ni, Zn, Cd, Co, V, Al, Pb, P, S, As, and B. Si and Cl are also found in biomass but could not be digested/detected. The Si content was based on the difference between the total ash content and the sum of the inorganic concentrations detected by ICP-OES. Cl was considered negligible, as X-ray fluorescence results of *P. radiata* by Bull [49] did not detect Cl.

3.2.1.3 Carbohydrate, acid, and lignin content of biomass

The structural composition of biomass and pretreated biomass was determined through complete hydrolysis of extractive free biomass to determine the Klason lignin content, followed by UV-Visible spectrophotometer (UV-Vis) and high performance liquid chromatography (HPLC) to determine the acid soluble lignin and carbohydrate content respectively.

Extraction: Extractives can interfere during hydrolysis, giving high predictions for acid insoluble lignin [50]. They were removed initially using a modified Soxhlet setup, and later with an automatic extractor. Ethanol was used as the solvent as hydrophilic solvents are superior to hydrophobic solvents [51], and less toxic compared to other commonly used solvents, such as dichloromethane [52] and acetone [53].

The modified Soxhlet extraction followed the standard NREL/TP-510-42619. Extraction in a Soxhlet extractor was compared to extraction in stirred flasks at 100 rpm for 6 hours at 45 °C. Acid hydrolysis of the samples indicated that the same acid insoluble lignin content could be obtained using the stirred flask as with the Soxhlet equipment as the solvent to biomass ratio was 30 times that of the standard procedure and samples were agitated. After extraction, samples were filtered with ethanol through a polycotton filter using a Buchner funnel then dried overnight to obtain the extractive yield.

Biomass samples were later extracted using an automatic Dionex ASE 350 extractor, as it was much faster technique but was not available at the start of this research. Conditions for extraction also followed standard NREL/TP-510-42619. In brief, samples were heated in 33 mL extraction cells to 100 °C at 1,500 psi for 7 min, followed by flushing with 150 vol% of ethanol. Three cycles were repeated for each sample. After this, samples were dried overnight to obtain the extractive yield. Since two different extractions techniques were used, there was a discrepancy between extractives yields, as the first technique was associated with a slight biomass loss during the filtering.

Hydrolysis: The standard hydrolysis procedure followed the standard NREL/TP-510-42618, with slight alterations. Due to the inaccessibility of glass pressure vessels for the hydrolysis at 121 °C (2 bar), experiments were done in a 4748 large capacity Parr acid digestion vessel to determine if the same hydrolysis results could be obtained at 113 °C (1.5 bar) using Duran® GL45 Pressure Plus laboratory glass bottles. Residence times were extended from 1 h to 1.5 h at the lower temperature. Results were comparable, thus it was assumed that this lower temperature was sufficient for hydrolysis to occur. Other authors have reported using temperatures down to 100 °C for acid hydrolysis [53, 54].

For hydrolysis, 300±10 mg of sample was added to 3 mL of 72% sulphuric acid in the Pressure Plus bottle, and maintained at 30 °C for 1 h, agitating every 10 min. Next, 84 mL of DI water was added, and the solution was heated to 113 °C for 1.5 h (sealed). After cooling for 1 h, the samples were filtered using Buchner funnels. The filtrate was reserved for further UV-Vis and HPLC analysis, while the remaining solids (Klason lignin) was washed with 100 mL of DI water before being dried overnight to determine the

Klason lignin yield. Some biomass ash dissolves during acid hydrolysis [55]; therefore the Klason lignin ash content was determined by complete combustion, following the same procedure as for biomass ashing.

UV-Vis: The hydrolysis filtrate was analysed for acid-soluble lignin by determining the absorbance at 240 nm with an absorptivity of 12 $Lg^{-1}cm^{-1}$. A wavelength of 280 nm is commonly used [56-58], but degraded carbohydrate products such as furfural and hydroxymethylfurfural strongly absorb at 280 nm, whereas a wavelength of 240 nm results in minimal absorbance interference. The total lignin content was the sum of Klason and acid-soluble lignin.

HPLC: The hydrolysis filtrate was neutralised with calcium carbonate and filtered through 0.22 µm nylon syringe filters prior to the HPLC analysis. A Supelcogel C-610H carbohydrate column was used for the sugar and organic acid analysis with a refractive index detector and a mobile phase of 0.1% phosphoric acid. The column temperature was maintained at 30 °C. The sample injection size was 17 µL with a residence time of 20 min. Standards were run for cellobiose, glucose, xylose, galactose, arabinose, mannose, acetic acid, formic acid, levulinic acid, and methanol, with residence times in Appendix 3.7. The column was chosen for optimal carboxylic acid analysis opposed to optimal sugar analysis, as accurately quantifying the acids content was deemed more important.

3.2.1.4 Elemental analysis

The carbon, hydrogen, oxygen, and nitrogen content of the solid samples was determined through complete oxidation [59], with the elementary analyser at CRL Energy Ltd. in Wellington, New Zealand. The carbon, hydrogen, and nitrogen content were determined using standard ISO 29541:2010, and the oxygen content was calculated by difference. Sulfur was also determined for some samples, using ASTM D4239. Ideally, elementary analysis should be repeated 3 times due to the inherent variability in biomass and the small sample size used [60]. Due to the cost per test, only selected samples were repeated, this provided an overall uncertainty for the analysis.

3.2.1.5 Heat of combustion

Many equations have been reported to calculate the higher heating value (HHV, $MJkg^{-1}$) based on the carbon, hydrogen, nitrogen, sulfur, ash, and oxygen content of a sample [61, 62]. Channiwala and Parikh [61] proposed a single, unified correlation that could be used for gases, liquids, coals, biomass, and char. The correlation is presented in Equation 3.6, and was used for all HHV calculations in the present study. It has an average error of ±1.45%.

$$\mathrm{HHV} = 0.3491 \times \mathrm{C} + 1.1783 \times \mathrm{H} + 0.1005 \times \mathrm{S} - 0.1034 \times \mathrm{O} - 0.0151 \times \mathrm{N} - 0.0211 \times \mathrm{A} \qquad (3.6)$$

Where C, H, S, O, N, and A represent dry mass (%) of carbon, hydrogen, sulphur, oxygen, nitrogen, and ash, respectively. The range for elements is: C:0-92.3%, H:0.43-25.2%, N:0-5.6%, S:0-94.08%, O:0-50% and A:0-71.4%.

3.2.1.6 Scanning electron microscope (SEM)

SEM was used to investigate char and biomass samples. Samples were gold plated prior to the analysis to improve conductivity. This was done in a Polaron E5000 in argon to produce a positive charge for gold deposition on the sample. Samples were then analysed using a JEOL JSM 7000F field emission, high resolution SEM. Samples were analysed at 3.0 kV at 100 and 250 times magnification.

3.2.2 Bio-oil analysis

Multiple techniques were required to determine the bio-oil composition. It is often necessary to group bio-oil compounds into families so these groups can be treated as a few compounds rather than hundreds of compounds, this allows for easier comparison between samples. Gas chromatography–mass spectrometry (GC-MS) is commonly used for bio-oil analysis; however GC-MS can only detect an average of 40% of the total compounds present in bio-oil [63-65]. Additionally, due to the abundance of peaks, overlapping peaks can reduce the accuracy. Since there are too many compounds to calibrate individually, quantification is normally done for a few representative compounds and it is assumed that the same signal area represent similar compounds [66]. Oasmaa and Meier [60] sent bio-oil samples to 12 laboratories for round-robin GC-MS analysis and reported large inconstancies in the liquid composition between laboratories. For these reasons, it was decided to use nuclear magnetic resonance (NMR) for determining the bio-oil composition as it can determine the entire, intact composition of the bio-oil [65]. Several other analytic procedures indicate the quality of bio-oil without the need for a detailed chemical composition analysis. These evaluate the bio-oil's acidity, water content, solids content, ash content, viscosity, density, and stability.

3.2.2.1 Nuclear magnetic resonance spectroscopy

Proton nuclear magnetic resonance (^{1}H-NMR) was used for an overall bio-oil analysis. Bio-oil was grouped into compounds with similar functional groups, additionally, major individual peaks were identified. Carbon NMR (^{13}C-NMR) was used to help identify individual compound shifts, for semi-quantification of major bio-oil compounds. 30 µL of bio-oil was dissolved in 300 µL of dimethyl sulfoxide-d6 (DSMO-d6); the sample was then filtered to 0.22 µm before being placed in the NMR tubes. Spectras were acquired at 26 °C on an Agilent 400 MR with Varian 7600-AS auto-sampler, equipped with OneNMR probe and variable temperature capabilities, operating at 400 MHz.

^{1}H-NMR: One-dimensional proton (^{1}H) spectra were acquired with 16384 data points, 128 scans, 16.0 ppm spectral width (6410.3 Hz), 2.0 s pulse delay time, 90° flip angle, with or without presaturation. Selected regions of the NMR spectra were used to group bio-oil compounds. Shifts used were similar to those of Mullen *et al.* [65] and Ingram *et al.* [67]: these are given in Table 3-14.

Table 3-14: Chemical shift range for ^{1}H-NMR of bio-oil

Shift	Functional groups present
0.5-1.6	Alkane (C-C)
1.6-2.2	Organic acids (R-C=OO-), alkane (R_2-CH_2), carbonyl (R_2-C=O)
2.2-3.0	Ketone (O=CH), methyl group attached to benzene ring (CH_3Ar)
3.0-4.2	Alcohols (C-OH), methoxy (O-CH_3), ether (R-CH_2O-R$^{'}$)
4.2-6.0	Ethers (lignin derived methoxyphenols) (C-O-C), carbohydrates, phenols
6.0-8.5	Aromatics (ArH), phenols (ArOH), olefins (HC=C)
9.5-10.1	Aldehydes (CH=O)

Individual compounds that are commonly present in bio-oil, as reported by Zhang and Kong [27], Diebold [68], and Huber *et al.* [25] and that were available to use, were identified in ^{1}H-NMR by determining the individual shift for each compound. The spectra for compounds is summarised in Table 3-15. Individual shifts were confirmed using a shift predicator supplied by the Institute of Chemical Sciences and Engineering [69], and shifts given by Hosoya *et al.* [70].

^{13}C-NMR: One-dimensional carbon (^{13}C) spectra were recorded with 32768 data points, 256 or 5120 scans, 248.7 ppm spectral width (25000 Hz), 1.0 s delay time, 45° flip angle. ^{13}C-NMR was only used to help confirm the presence of compounds in bio-oil. If they were present in both the ^{1}H-NMR and the ^{13}C-NMR spectra, they were considered to be present in the bio-oil, this was only done for a few bio-oil samples due the excessive cost of ^{13}C-NMR analysis. The sample compounds were tested for ^{13}C-NMR (as for ^{1}H-NMR) summarised in Table 3-15. Shifts were also confirmed using the predicator.

To confirm what compounds were present in bio-oil, two samples were compared in ^{13}C-NMR and ^{1}H-NMR. Compounds identified in both samples were considered present, while there was not sufficient data to confirm the presence of others; therefore they were not included in the ^{1}H-NMR analysis. Details for the peaks identified are given in Appendix 3.6, the results indicate that formic acid (8.10 ppm), acetaldehyde (9.58 and 2.08 ppm), levoglucosan (3.27,3.84-3.85,4.31-4.33, and 5.13 ppm), glycolaldehyde (9.55 ppm), hydroxyacetone (4.01 ppm), and acetic acid (1.88 ppm) can be identified. Peaks for aromatic compounds overlapped (phenol and furan derivatives such as syringol, guaiacol, phenol, methyl-2-furoate, furan, furfural, and hydroxymethylfurfural); therefore, were all grouped together and represented by the shift between 6.4-7.6 ppm as no olefins were identified after 6.4 ppm. Total aldehydes were represented by the shift between 9.5-10.5 ppm and alkanes between 0.5-1.6 ppm. Some of these shifts vary slightly from those of the ideal compounds given in Table 3-15 due to interactions in the actual bio-oil solution. Propanoic acid, octanoic acid, hexanoic acid, acetone, ethanol, glyoxal, methanol, 1-heptanol, and 1-pentanol were either not detected or present in too small of a quantity to accurately determine the peak above the baseline noise.

Table 3-15: Experimental ^{1}H-NMR and ^{13}C-NMR shifts for compounds

Compound	^{1}H-NMR	^{13}C-NMR
Formic acid	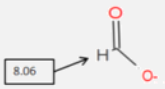	
Acetic acid	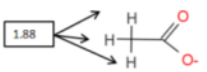	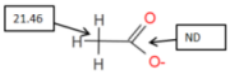
Propanoic acid	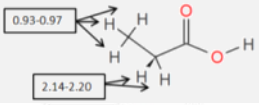	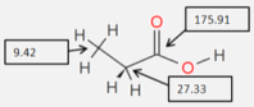
Hexanoic acid	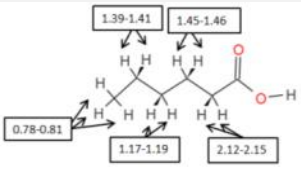	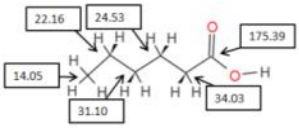
Octanoic acid	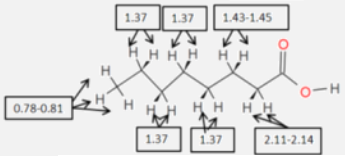	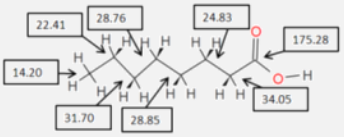
Methanol	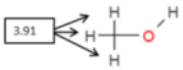	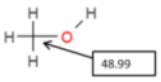
Ethanol	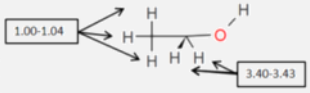	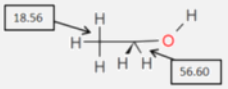
Acetaldehyde	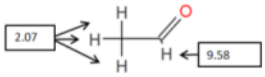	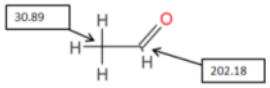
Glycolaldehyde	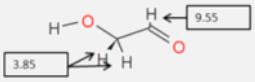	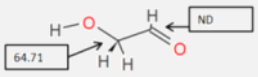
Acetone	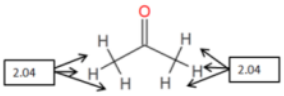	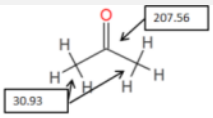
Hydroxyacetone (acetol)	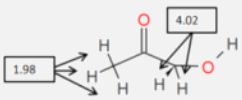	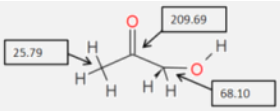
Glyoxal	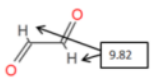	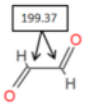
Levoglucosan	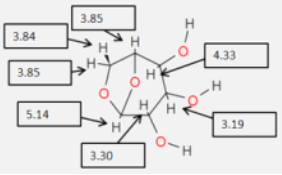	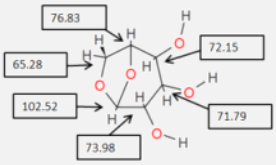
Hydroxymethylfurfural	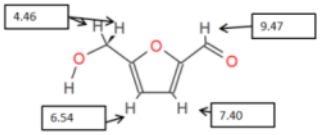	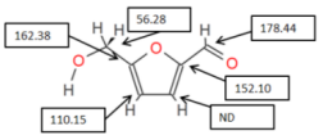

Table 3-15 continued

Furfural	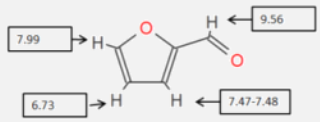	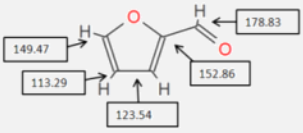
Furan	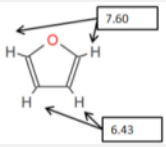	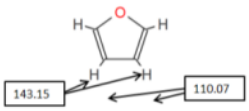
Methyl-2-furoate	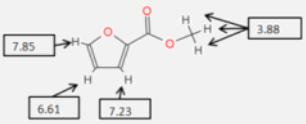	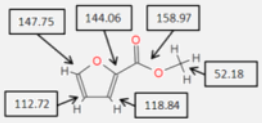
Guaiacol	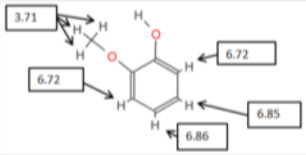	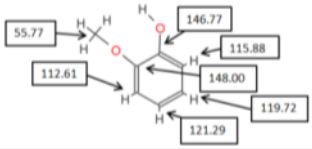
Phenol	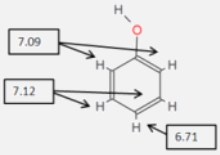	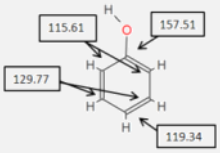
Syringol	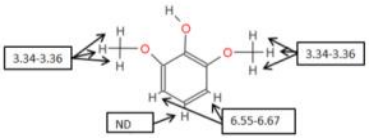	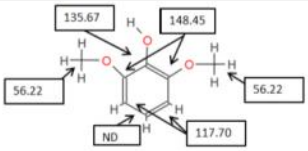
1-pentanol	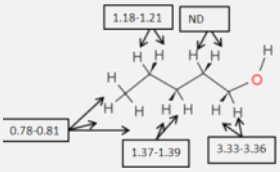	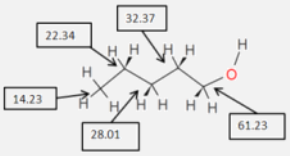
1-heptanol	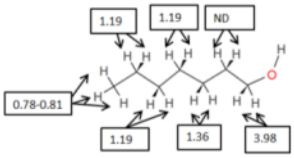	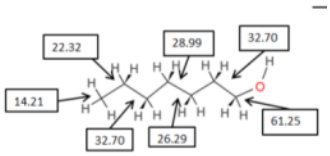

3.2.2.2 High performance liquid chromatography

High performance liquid chromatography (HPLC) was used to determine the bio-oil's acetic acid content [65]. The majority of the acids, furfural, sugar derivatives, and other organic compounds remain in the aqueous phase; this was separated from the non-aqueous phase to prevent blockages [71]. Samples were prepared by adding 0.5 mL of DI water, mixing using an ultrasonic bath for 20 min and then centrifuging for 20 min at 4000 rpm. A further 1 mL of DI water was then added, and the sample was mixed and centrifuged again, at the same conditions. The aqueous fraction was decanted and filtered to 0.22 µm for HPLC analysis. HPLC analysis followed the method used to determine the acetic acid content of hydrolysis liquor. Standards for acetic acid, acetol, acetone, ethanol, formic acid, glycolaldehyde, levoglucosan, glyoxal, hydroxyacetone, iso-propanol, methyl-2-furorate, methanol, octanoic acid, phenol, and 1-pentanol were also tested in the

HPLC, with residence times given in Appendix 3.8. Calibration curves were only formed after compounds were identified on the chromographs.

3.2.2.3 Water content

The water content of samples was determined by Karl Fisher titration, following ASTM E203 [72]. Karl Fisher titrant 5 was used (5 mg H_2O per mL) and titrations were carried out on a TitraLab TIM 550 Radiometer. 1% water standards were used to calibrate the titrator and for quality control checks. 0.1 mL of bio-oil was injected per test, and each sample was tested in triplicate.

3.2.2.4 Viscosity

Viscosity was determined using multiple techniques due to the high viscosity of some bio-oils. A Cannon-Fenske Routine (CFR) viscometer was mainly used, following the method by Li [72]. If bio-oil has a high viscosity and high solids content, then dynamic viscosity was determined as it is more accurate than kinematic (Newtonian behaviour) [60]. Viscosity was measured at 25 °C by placing the viscometer in a water bath. The CFR viscometer was filled with 8 mL of bio-oil, and was held in the bath for 10 min before measuring the viscosity. The viscosity of thick bio-oil samples was determined using a Haake viscometer. Here, 9 mL of bio-oil was injected into cup and the viscosity quantified.

3.2.2.5 Gel permeation chromatography

The high viscosity of some bio-oils made viscosity measurements inaccurate on the available equipment, thus gel permeation chromatography (GPC) was generally used instead. Samples were analysed by Scion in Rotorua, New Zealand and were prepared by adding tetrahydrofuran to bio-oil to make a 5 $mgmL^{-1}$ solution. These were filtered to 0.45 µm before analysing at 30 °C in a Knauer/Polymer Standards Service GPC with a PSS SDV Lux 1000Å column with a refractive index detector. The system was calibrated using polystyrene standards. The average number, molecular weight, and the size were determined using Polymer Standards Service Win GPC Unichrom software.

3.2.2.6 Stability

To test the bio-oil's stability, a 5 mL sample was heated in an air tight container to 80 °C for 25 h [60, 68], which is similar to aging at 25 °C for 6 months. Aging was quantified by an increase in the molecular weight, pyrolytic lignin formation, change in the NMR spectra, and the increase in water content. Equation 3.7 was used to calculate the stability index [73].

$$Index = \frac{(P_2 - P_1)}{P_1} \tag{3.7}$$

Where *P* is the parameter of interest (water content, pyrolytic lignin, NMR compounds, or molecular weight) and subscript 1 indicates the value before aging while 2 indicates the value after aging. Lower stability indexes indicate higher stability.

3.2.2.7 Density

Density was determined using two methods. These were using and digital density meter and by manual determination. Manual determination was required for viscous samples that could not be injected into the density meter.

Digital density meter: An Anton Parr DMA60 was used for digital density measurements. The system was calibrated by measuring the density of water and air prior to injecting bio-oil samples. 1 mL of bio-oil was injected into the U-tube and the change in oscillations was measured. Then, Equation 3.8 was used to calculate the density.

$$\rho = 998.2 + \left(\frac{998.2-1.21}{\tau^2-0.259572^2}\right)(\tau^2 - 0.338741^2) \quad (3.8)$$

Where ρ is the density measured in kgm^{-3} and τ is the oscillation period of the bio-oil, this equation is only valid for densities measurements at 20 °C. Three density measurements were taken for each sample.

Manual determination: Bio-oil was injected into a 1 mL syringe. The weight of the syringe was recorded before and after the injection and the difference was divided by the volume of bio-oil in the syringe to obtain the density. The procedure was repeated three times for each sample.

3.2.2.8 Solids content

It was important to quantify the solids in bio-oil as they may enhance bio-oil aging, corrosion, and equipment blockages [74]. Oasmaa and Meier [60] recommend using filters under 1 µm when filtering bio-oil, and to use ethanol as the solvent as it is less toxic than other common solvents, such as methanol. The solids content was the residue after filtering bio-oil through a 0.45 µm polyethersulfone syringe filter followed by flushing with 50 mL of ethanol to wash through any bio-oil residue. The filter was dried overnight to calculate the increase in weight and the solids content was calculated using Equation 3.9.

$$\boldsymbol{Solids}\ (\boldsymbol{wt}\%) = \frac{\boldsymbol{m_{filter+solids} - m_{filter}}}{\boldsymbol{m_{bio-oil}}} \times \mathbf{100} \quad \textbf{(3.9)}$$

Where $m_{filter+solids}$ is the mass of the filter plus the solids entrained after filtration, m_{filter} is the initial filter weight, and $m_{bio-oil}$ is the mass of bio-oil filtered. Syringe filters were dried and stored in a descanter prior to the analysis. Complex interactions occur between char and pyrolytic lignin, this mixture can form a gel like phase that can hinders filtration [75]. Therefore, some samples had to be diluted with ethanol before filtering. The weight of the bio-oil before dilution was recorded and taken into account in calculations.

3.2.2.9 Other bio-oil properties

Other properties and the corresponding techniques used, that either did not require a long procedure or were only done for a few samples are listed here:

- Acidity: this was quantified with the pH values [59], and was determined using an automatic pH meter. Total acid number (TAN) was not used due to issues in distinguishing the titration end point [76]

- Pyrolytic lignin: cold water precipitation is commonly used to determine the pyrolytic lignin content in bio-oil [77-79]. Scholze and Meier [80] found that the average molecular weight of pyrolytic lignin is between 650 and 1300 $gmol^{-1}$; therefore it was estimated from the GPC fraction above 650 $gmol^{-1}$.

- Ash and inorganics: both were determined using the same method as for solids

- Elementary analysis and heating value: both were determined using the same method as for solids but samples were sent to Scion in Rotorua, New Zealand, for analysis instead of CRL energy limited.

3.2.3 Non-condensable gas analysis

Gas chromatography (GC) is normally used to determine the composition of the non-condensable gas (NCG) produced during pyrolysis. Gas samples were taken every 10 minutes during pyrolysis experiments and injected directly into an Agilent 3000A micro-GC. The method used was previously setup by Bull [49] and calibrated by Penniall [81] to analyse gasification products. Two capillary columns were used to detect for H_2, O_2, N_2, CO, CO_2, CH_4, C_2H_6, and C_2H_4, with details given in Table 3-16. Quality checks were done by initially injecting air and analysing its composition and also repeating the last injection of the run. The GC only analysed a fraction of the overall NCG stream. The total mass flow rate flow rate of each gas component was found by determining the total gas flow rate based on the fraction of N_2 in the gas stream. The exact amount to N_2 entering the system was controlled using a mass flow controller, thus component flow rates could be determined.

Table 3-16: Configuration and operating conditions of the micro-GC

Configuration	**Channel 1**	**Channel 2**
Column type	Molecular sieve 5A plot	Plot Q
Carrier gas	Argon	Helium
Injector	Backflush	Fixed vol.
Detector	Thermal conduct.	Thermal cond.
Operation conditions		
Sample inlet temp. (°C)	95	95
Injector temp. (°C)	95	55
Column temp. (°C)	85	60
Sampling time (s)	15	15
Injection time (ms)	10	15
Run time (s)	180	240
Column pressure (kPa)	206.8	137.5
Backflush time (s)	10	10
Analysing for	H_2, N_2, CH_4, CO, O_2	CO_2, C_2H_4, C_2H_6

NGC's can be burnt for process heat; therefore the heating value needed to be quantified. The lower heating value can be estimated from the sum of the individual heating values using Equation 3.10 from Marosky [1].

$$LHV_{gas} = X_{H_2}LHV_{H_2} + X_{CH_4}LHV_{CH_4} + X_{CO}LHV_{CO} + X_{C_2H_4}LHV_{C_2H_4} + X_{C_2H_6}LHV_{C_2H_6} \quad (3.10)$$

Where X is the mass fraction (%) of that component in the gas stream. The lower heating values for the main gas components were taken from Perry *et al.* [82]. These were 120.0, 50.0, 10.1, 47.5, 47.2 $MJkg^{-1}$ for H_2, O_2, N_2, CO, CO_2, CH_4, C_2H_4, and C_2H_6 respectively. NCG analysis was not operational during preliminary experiments, but these were generally screening experiments, where it was not necessary to know the gas composition or heating value.

3.3 Comparison of yields with other systems

The pyrolysis system was initially tested using raw *P. radiata* biomass. This was to compare yields with values reported in literature for woody biomass. The system was operated at the standard pyrolysis conditions of 500 °C, and 10 wt% moisture in the feed. The yields are reported and compared to that of literature in Table 3-17. The advantage of smaller particle sizes can clearly be seen in Table 3-17, as the bio-oil yield was higher for researchers using smaller biomass particles. Yields obtained in this research were similar to those reported by Westerhof *et al.* [78] and Salehi *et al.* [9], who used similar sized particle. Decreasing the particle size has implications on the overall process costs, and would not be economical at large scale; therefore it was decided stay with particles between 0.295-2 mm to represent a more realistic particle size for a commercial pyrolysis system.

The char yield at 15.4±0.7 wt% was within the reported range of 9.3 to 23 wt%. The NCG yield was calculated based on difference, thus was higher than reported values as the mass balance was likely less than 100%. Uncertainties were determined using a 95% confidence interval over the three repeats. The low errors indicate the system's repeatability and stability. Experiments in proceeding sections that were determining a trend, such as the effect of various reactor temperatures, used a base case error to reduce the repeats required [83].

Table 3-17: Experimentally determined and reported yields from pyrolysis of woody biomass

Ref.	Biomass	Reactor Temp.	Feed rate ($kghr^{-1}$)	Feed size (mm)	Feed MC (%)	Wet basis (wt%)			Dry basis (wt%)			Total (%)	Oil MC
						Bio-oil	Char	NCG	Bio-oil	Char	NCG		
This work	*P.radiata*	500	0.300	0.3-2	10 ±1	51.8 ±0.4	14.0 ±0.7	34.2 ±1.0[1]	46.9 ±0.5	15.4 ±0.7	37.6 ±1.2[1]	100	24.0 ±1.2
[84]	Pine	500	1.0	0.09-0.6	0				63	15	14	92	17
[78]	Pine	450		<2	9-10				46	15	23	84	33
[52]	*P. sylvestris*	520	20	sawdust	4-11				74				10.3
[85]	Northern oak	529	0.82	<0.75	5.9	66	22	12	62	23	13	98	
[9]	Mixed wood	500	0.1	1-1.4	6	53	17	32	50	18	34	102	
[86]	Willow	507	0.15	0.25-0.36	7.8				68.9	9.3	20.9	99.1	17.4
[33]	Pine	480	1.0	<1	10	62.7	14	18.4	57	15.4	20.2	93	

[1]*Determined by difference as the gas sampling system was not yet operational*

3.4 References

1. Marosky, A., *Liquid fuels from woody biomass pyrolysis*, in *Department of Chemical and Process Engineering*. 2008, University of Canterbury: Berlin. p. 144.
2. Green, A., *Fixed bed pyrolysis optimisation, part 1*, S. Pang, Editor. 2009, Chemical and Process Engineering: University of Canterbury. p. 36.
3. Green, A., *Fixed bed pyrolysis optimisation, part 2*, S. Pang, Editor. 2009, Chemical and Process Engineering: University of Canterbury. p. 40.
4. Lede, J. *Temperature and heating rate of solid particles undergoing a thermal decomposition. Which criteria for characterising fast pyrolysis?* . in *20th International Symposium on Analytical and Applied Pyrolysis*. 2014. Bridgwater.
5. Aguado, R., et al., *Pyrolysis of sawdust in a conical spouted bed reactor. Yields and product composition.* Industrial & Engineering Chemistry Research, 2000. **39**(6): p. 1925-1933.
6. Butler, E., et al., *A review of recent laboratory research and commercial developments in fast pyrolysis and upgrading.* Renewable and Sustainable Energy Reviews, 2011. **15**(8): p. 4171-4186.
7. Briens, C., Piskorz, J., and Berruti, F., *Biomass valorization for fuel and chemicals production - a review*, in *International Journal of Chemical Reactor Engineering*. 2008. p. 1-52.
8. Holman, J.P., *Empirical and practical relations for forced-convection heat transfer*, in *Heat transfer*, J.P. Holman, Editor. 1992, McGraw-Hill: UK. p. 279-330.
9. Salehi, E., Abedi, J., and Harding, T., *Bio-oil from sawdust: effect of operating parameters on the yield and quality of pyrolysis products.* Energy & Fuels, 2011. **25**(9): p. 4145-4154.
10. Bull, D.R., *Performance improvements to a fast internally circulating fluidised bed (FICFB) biomass gasifier for combined heat and power plants*, in *Chemical and Process Engineering*. 2008, University of Canterbury: New Zealand. p. 232.
11. Rath, J., et al., *Heat of wood pyrolysis.* Fuel, 2003. **82**(1): p. 81-91.
12. Bridgwater, A.V., *Principles and practice of biomass fast pyrolysis processes for liquids.* Journal of Analytical and Applied Pyrolysis, 1999. **51**(1–2): p. 3-22.
13. Holman, J.P., *Steady state conduction - multiple dimenstions*, in *Heat tansfer*, J.P. Holman, Editor. 1992, McGraw-Hill: UK. p. 71-133.
14. Luo, Z., Wang, S., and Cen, K., *A model of wood flash pyrolysis in fluidized bed reactor.* Renewable Energy, 2005. **30**(3): p. 377-392.
15. Kunii, D. and Lvenspiel, O., *Fluidization engineering*. 2 ed. Vol. 1. 1991, U.S.A: Butterworth-Heinemann. 534.
16. Haider, A. and Levenspiel, O., *Drag coefficient and terminal velocity of spherical and nonspherical particles.* Powder Technology, 1989. **58**(1): p. 63-70.
17. Zhang, H., et al., *Catalytic fast pyrolysis of biomass in a fluidized bed with fresh and spent fluidized catalytic cracking (FCC) catalysts.* Energy & Fuels, 2009. **23**(12): p. 6199-6206.
18. Boateng, A.A., et al., *Bench-scale fluidized-bed pyrolysis of switchgrass for bio-oil production.* Industrial & Engineering Chemistry Research, 2007. **46**(7): p. 1891-1897.
19. Patwardhan, P.R., et al., *Distinguishing primary and secondary reactions of cellulose pyrolysis.* Bioresour Technol, 2011. **102**(8): p. 5265-5269.
20. Meng, J., et al., *The effect of torrefaction on the chemistry of fast-pyrolysis bio-oil.* Bioresour Technol, 2012. **111**(0): p. 439-446.
21. Liaw, S.-S., et al., *Effect of pyrolysis temperature on the yield and properties of bio-oils obtained from the auger pyrolysis of Douglas Fir wood.* Journal of Analytical and Applied Pyrolysis, 2012. **93**(0): p. 52-62.
22. Piskorz, J.W., CA), Majerski, Piotr (Waterloo, CA), Radlein, Desmond (Waterloo, CA), *Energy efficient liquefaction of biomaterials by thermolysis*. 1998, RTI Resource Transforms International Ltd. (Waterloo, CA): United States.
23. Scott, D.S., et al., *A second look at fast pyrolysis of biomass - the RTI process.* Journal of Analytical and Applied Pyrolysis, 1999. **51**(1–2): p. 23-37.
24. Bridgwater, A.V., *Renewable fuels and chemicals by thermal processing of biomass.* The Chemical engineering journal, 2003. **91**(2): p. 87.
25. Huber, G.W., Iborra, S., and Corma, A., *Synthesis of transportation fuels from biomass: chemistry, catalysts, and engineering.* Chemical Reviews, 2006. **106**(9): p. 4044-4098.
26. Xu, R., et al., *Bio-oil production by flash pyrolysis of sugarcane residues and post treatments of the aqueous phase.* Journal of Analytical and Applied Pyrolysis, 2011. **91**(1): p. 263-272.
27. Zhang, L. and Kong, S.-C., *Multicomponent vaporization modeling of bio-oil and its mixtures with other fuels.* Fuel, 2012. **95**(0): p. 471-480.
28. Economopoulou, A.A. and Economopoulos, A.P., *Rapid performance evaluation and optimal sizing of dry cyclone separators.* Journal of Environmental Engineering, 2002: p. 275-285.
29. Hoffmann, A. and Stein, L., *Gas cyclones and swirl tubes*. Vol. 1. 2002, Principles, Design and Operation: Springer. 1-334.

30. Schnelle, K. and Brown, C., *Cyclone Design*, in *Air pollution control technology handbook*. 2001, CRC Press. p. 1-11.
31. Leith, D. and Licht, W. *The collection efficiency of cyclone type particle collectors: a new theoretical approach*. in *AIChE Symp. Ser*. 1972.
32. Chen, T., Deng, C., and Liu, R., *Effect of selective condensation on the characterization of bio-oil from pine sawdust fast pyrolysis using a fluidized-bed reactor.* Energy & Fuels, 2010. **24**(12): p. 6616-6623.
33. Westerhof, R.J.M., et al., *Fractional condensation of biomass pyrolysis vapors.* Energy & Fuels, 2011. **25**(4): p. 1817-1829.
34. Chan, R., *Development of a condenser for the developed marine florae pyrolysis reactor*, in *Department of Mechanical Engineering*. 2011, University of San Carlos: University of San Carlos. p. 156.
35. Hewitt, G.F., *Handbook of heat exchanger design*, ed. G.F. Hewitt. 1992, New York: Belgell Housr, INC.
36. ACS. *SciFinder*. 2013 [cited 2012 07/06/12]; Available from: https://www.cas.org/products/scifinder.
37. Holman, J.P., *Condensation and boiling heat transfer*, in *Heat Transfer*. 1992, McGraw-Hill Book Co: UK. p. 505-528.
38. Chato, J.C., *Laminar condensation inside horizontal and inclined tubes*, in *Mechanical engineering*. 1960, Massachusetts Institute of Technology: Massachusetts. p. 1-204.
39. Chen, G., et al., *Biomass pyrolysis/gasification for product gas production: the overall investigation of parametric effects.* Energy Conversion and Management, 2003. **44**(11): p. 1875-1884.
40. Parker, K.R., *Applied electrostatic precipitation*. 1 ed, ed. K.R. Parker. 1997, UK: Blackie academic & Professional.
41. Bedmutha, R.J., et al., *Single and two-stage electrostatic demisters for biomass pyrolysis application.* Chemical Engineering and Processing: Process Intensification, 2009. **48**(6): p. 1112-1120.
42. Xu, R., et al., *Flash pyrolysis of grape residues into biofuel in a bubbling fluid bed.* Journal of Analytical and Applied Pyrolysis, 2009. **86**(1): p. 58-65.
43. Streiner, D.L., *Maintaining standards: differences between the standard deviation and standard error, and when to use each.* Can J Psychiatry, 1996. **Vol 41**: p. 498-501.
44. Vispute, T.P. and Huber, G.W., *Production of hydrogen, alkanes and polyols by aqueous phase processing of wood-derived pyrolysis oils.* Green Chemistry, 2009. **11**(9): p. 1433-1445.
45. ASTM, *Standard test method for ash in biomass*. 2007, ASTM International: United States. p. 1-3.
46. Hseu, Z.-Y., *Evaluating heavy metal contents in nine composts using four digestion methods.* Bioresour Technol, 2004. **95**(1): p. 53-59.
47. Zarcinas, B.A., Cartwright, B., and Spouncer, L.R., *Nitric acid digestion and multi-element analysis of plant material by inductively coupled plasma spectrometry.* Soil Science Plant Analysis, 1987. **18**(1): p. 131-146.
48. Zhelijazkov, V.D. and Warman, P.R., *Comparison of three digestion methods for the recovery of 17 plant essential nutrients and trace elements from six composts.* Compost Science & Utilization, 2002. **10**(3): p. 197-197.
49. Bull, D.R., *Performance improvements to a fast internally circulating fluidised bed (FICFB) biomass gasifier for combined heat and power plants*, in *Chemical and Process Engineering*. 2008, University of Canterbury. p. 1-243.
50. Rabemanolontsoa, H., Ayada, S., and Saka, S., *Quantitative method applicable for various biomass species to determine their chemical composition.* Biomass and Bioenergy, 2011. **35**(11): p. 4630-4635.
51. Speaks, J., Campbell, R., and Veal, M., *Pretreatment of wood particulates for removal of wood extractives*, in *United States Patent*. 1997. p. 20.
52. Oasmaa, A., Kuoppala, E., and Solantausta, Y., *Fast pyrolysis of forestry residue. 2. Physicochemical composition of product liquid.* Energy & Fuels, 2003. **17**(2): p. 433-443.
53. Yang, H., et al., *In-depth investigation of biomass pyrolysis based on three major components: hemicellulose, cellulose and lignin.* Energy & Fuels, 2005. **20**(1): p. 388-393.
54. Hosoya, T., Kawamoto, H., and Saka, S., *Cellulose-hemicellulose and cellulose-lignin interactions in wood pyrolysis at gasification temperature.* Journal of Analytical and Applied Pyrolysis, 2007. **80**(1): p. 118-125.
55. Chen, W.-H., Tu, Y.-J., and Sheen, H.-K., *Impact of dilute acid pretreatment on the structure of bagasse for bioethanol production.* International Journal of Energy Research, 2010. **34**(3): p. 265-274.
56. Dence, C.W., *The determination of lignin*, in *Methods in Lignin Chemistry*, S. Lin and C. Dence, Editors. 1992, Springer Berlin Heidelberg. p. 33-61.
57. Maekawa, E., Ichizawa, T., and Koshijima, T., *An evaluation of the acid-soluble lignin determination in analyses of lignin by the sulfuric acid method.* Journal of Wood Chemistry and Technology, 1989. **9**(4): p. 549-567.
58. Iiyama, K. and Wallis, A.F.A., *An improved acetyl bromide procedure for determining lignin in woods and wood pulps.* Wood Science and Technology, 1988. **22**(3): p. 271-280.
59. Nowakowski, D.J., et al., *Lignin fast pyrolysis: results from an international collaboration.* Journal of Analytical and Applied Pyrolysis, 2010. **88**(1): p. 53-72.
60. Oasmaa, A. and Meier, D., *Norms and standards for fast pyrolysis liquids: 1. Round robin test.* Journal of Analytical and Applied Pyrolysis, 2005. **73**(2): p. 323-334.
61. Channiwala, S.A. and Parikh, P.P., *A unified correlation for estimating HHV of solid, liquid and gaseous fuels.* Fuel, 2002. **81**(8): p. 1051-1063.
62. Friedl, A., et al., *Prediction of heating values of biomass fuel from elemental composition.* Analytica Chimica Acta, 2005. **544**(1–2): p. 191-198.

63. Meier, D., *New methods for chemical and physical characterization and round robin testing*, in *Fast Pyrolysis of Biomass: A Handbook*, A.V. Bridgwater, Editor. 1999, CPL Press: Newbury Berkshire UK. p. 92-101.
64. Garcia-Perez, M., et al., *Characterization of bio-oils in chemical families.* Biomass and Bioenergy, 2007. **31**(4): p. 222-242.
65. Mullen, C.A., Strahan, G.D., and Boateng, A.A., *Characterization of various fast pyrolysis bio-oils by NMR spectroscopy.* Energy & Fuels, 2009. **23**(5): p. 2707-2718.
66. Wang, Z., Cao, J., and Wang, J., *Pyrolytic characteristics of pine wood in a slowly heating and gas sweeping fixed-bed reactor.* Journal of Analytical and Applied Pyrolysis, 2009. **84**(2): p. 179-184.
67. Ingram, L., et al., *Pyrolysis of wood and bark in an auger reactor: physical properties and chemical analysis of the produced bio-oils.* Energy & Fuels, 2007. **22**(1): p. 614-625.
68. Diebold, J.P., *A review of the chemical and physical mechanisms of the storage stability of fast pyrolysis bio-oils*. 2000, National Renewable Energy Laboratory: Lakewood, Colorado. p. 1-59.
69. EPFL. *Institute of chemical sciences and engineering ISIC* 2013 [cited 2014.
70. Hosoya, T., Kawamoto, H., and Saka, S., *Different pyrolytic pathways of levoglucosan in vapor- and liquid/solid-phases.* Journal of Analytical and Applied Pyrolysis, 2008. **83**(1): p. 64-70.
71. Li, Q., et al., *The addition of water to extract maximum levoglucosan from the bio-oil produced via fast pyrolysis of pretreated loblolly pinewood.* BioResources, 2013. **8**(2): p. 1868-1880.
72. Li, J., *Pyhsical properties of biomass pyrolysis oil and analysis methods*. 2012, University of Canterbury: Christchurch. p. 1-12.
73. Chiaramonti, D., et al., *Development of emulsions from biomass pyrolysis liquid and diesel and their use in engines-part 1 : emulsion production.* Biomass and Bioenergy, 2003. **25**(1): p. 85-99.
74. Bridgwater, A.V., *Production of high grade fuels and chemicals from catalytic pyrolysis of biomass.* Catalysis Today, 1996. **29**(1–4): p. 285-295.
75. Bridgwater, A.V., *Review of fast pyrolysis of biomass and product upgrading.* Biomass and Bioenergy, 2012. **38**: p. 68-94.
76. Oasmaa, A., Elliott, D.C., and Korhonen, J., *Acidity of biomass fast pyrolysis bio-oils.* Energy & Fuels, 2010. **24**(12): p. 6548-6554.
77. Mourant, D., et al., *Mallee wood fast pyrolysis: effects of alkali and alkaline earth metallic species on the yield and composition of bio-oil.* Fuel, 2011. **90**(9): p. 2915-2922.
78. Westerhof, R.J.M., et al., *Effect of temperature in fluidized bed fast pyrolysis of biomass: oil quality assessment in test units.* Industrial & Engineering Chemistry Research, 2009. **49**(3): p. 1160-1168.
79. Scholze, B. and Meier, D., *Characterization of the water-insoluble fraction from pyrolysis oil (pyrolytic lignin). Part I. PY–GC/MS, FTIR, and functional groups.* Journal of Analytical and Applied Pyrolysis, 2001. **60**(1): p. 41-54.
80. Scholze, B., Hanser, C., and Meier, D., *Characterization of the water-insoluble fraction from fast pyrolysis liquids (pyrolytic lignin): part II. GPC, carbonyl goups, and 13C-NMR.* Journal of Analytical and Applied Pyrolysis, 2001. **58–59**(1): p. 387-400.
81. Penniall, C.L., *Fischer-Tropsch based biomass to liquid fuel plants in the New Zealand wood processing industry based on microchannel reactor technology*, in *Chemical and Process Engineering*. 2013, University of Canterbury. p. 1-265.
82. Perry, R.H., Green, D.W., and Maloney, J.O., *Perry's chemical engineers' handbook*. 6th ed. McGraw-Hill chemical engineering series. Vol. 1. 1984, New York: McGraw-Hill. 1-1846.
83. Hoekstra, E., et al., *Heterogeneous and homogeneous reactions of pyrolysis vapors from pine wood.* AIChE Journal, 2012. **58**(9): p. 2830-2842.
84. Garcia-Perez, M., et al., *Fast pyrolysis oil of mallee woody biomass: effect of temperature on the yield and quality of pyrolysis products.* Industrial & Engineering Chemistry Research, 2008. **47**(6): p. 1846-1854.
85. Brown, J., *Development of a lab-scale auger reactor for biomass fast pyrolysis and process optimization using response surface methodology*, in *Mechanical Engineering*. 2009, Iowa State University: Ames.
86. Fahmi, R., et al., *The effect of lignin and inorganic species in biomass on pyrolysis oil yields, quality and stability.* Fuel, 2008. **87**(7): p. 1230-1240.
87. Holman, J.P., *Heat transfer*. Vol. 5. 1992, UK: McGraw-Hill Book Co.
88. Smith, J.M., Van Ness, H.C., and Abbott, M.M., *Introduction to chemical engineering thermodynamics*. McGraw-Hill chemical engineering series. Vol. 7. 2005: McGraw-Hill. 1-817.
89. Rihani, D. and Doraiswamy, L., *Estimation of heat capacity of organic compounds from group contributions.* I&EC Fundamentals, 1965. **4**(1): p. 5.

4 Pretreatment development for bio-oil upgrading

The pyrolysis product yields and the bio-oil characteristics are affected by the properties of the biomass and the fast pyrolysis conditions; limiting repeatability at large scale and between systems. Large scale systems are prone to high levels of secondary reactions which reduces bio-oil quality. In this research, pretreatments were implemented with the aim of directly producing a higher quality bio-oil by limiting secondary reactions. The higher quality crude bio-oil could then be upgraded more efficiently using upgrading techniques such as catalytic cracking and hydroprocessing. Improving the repeatability and consistency of the bio-oil produced would occur concurrently with reduced secondary reactions. Three naturally inherent constituents in biomass have been identified from the literature review as potential pyrolysis catalysis for promoting secondary reactions, and are: inorganics, moisture, and organic acids.

4.1 Inorganic catalysts

Biomass inorganics have been identified as the foremost pyrolysis catalyst [1, 2], by increasing the reactivity of biomass, thus lowering the activation energy of certain pyrolysis reactions [3]. Ring opening reactions are catalysed through fragmentation, depolymerisation, and cracking reactions of primary pyrolysis vapours; which decreases the liquid yield and increases the NCG yield. Among the biomass inorganics, alkali metals are thought to be the most catalytic [4], although alkaline earth, transition metals, and non-metals can also be catalytic [5, 6]. Oasmaa *et al* [7] investigated pyrolysis of 12 different biomasses and concluded that feedstocks with higher contents of alkali metals produce more pyrolytic water but produce less total bio-oil. As reviewed in Chapter 2, Section 2.5.2.5, certain inorganics may enhance desirable, deoxygenation reactions to reduce the oxygen content of the bio-oil; therefore are desirable in biomass. Oxides such as ZnO, CuO, Fe_2O_3, MgO, and CaO have shown potential as desirable catalysts [8-10]. For simplicity, the catalytic fraction is referred to as the total inorganic or ash fraction; however the removal of individual elements was evaluated using ICP-OES.

Inorganics become concentrated in the char fraction, so vapour residence times should be minimised as inorganics in the char catalyse the vapour phase until it is separated from the char [11]. This limits reactor configurations and means fluidised bed must be shallow, thus increasing the fluidising gas requirements. Inorganics in bio-oil (predominantly in entrained char) cause high temperature corrosion and hard deposits in engines; possibly contribute to bio-oil aging; and hinder secondary upgrading processes [12, 13]. Therefore the concentration of inorganics in bio-oil has to be reduced to meet fuel standard either before, during, or following pyrolysis:

- Removing inorganics before pyrolysis requires biomass leaching. Although it can be more expensive than removing the inorganics later, higher bio-oil yields are obtained and the bio-oil quality improves.

- Removing inorganics during pyrolysis with hot gas filters reduces the bio-oil yield by 5-20% due to the catalytic filter cake formed, that vapours then pass through [14, 15]
- Removing inorganics from the bio-oil after pyrolysis is expensive due to difficulties filtering bio-oil and is associated with bio-oil loss [16]

4.2 Moisture

Physical desorption of biomass moisture during pyrolysis affects reaction mechanisms. Water appears to have an auto-catalytic role during pyrolysis [17], but results reported in literature have been varied for pyrolysis of dry biomass with in terms on the bio-oil yield and compositional changes [18-20]. This indicates that moisture in biomass clearly affects pyrolysis, possibly by causing hydrolytic scission of glucosidic bonds, which lowers of the degree of polymerisation in cellulose [21].

Removing excess moisture from biomass reduces its thermal conductivity; therefore if inorganics are present, the reduced water content may increase the time required to heat biomass particles, and thus increase catalytic inorganic activity. This was demonstrated by Gary *et al* [22] who showed that wet biomass (and inorganic free) produced significantly less volatiles and more char at approximately 500 °C, suggesting that some chemical interaction with water occurred compared to dry and inorganic free biomass. Conversely, if inorganics were not removed, then wet biomass gave higher bio-oil yields compared to dry biomass due to faster biomass heating, indicating that inorganics are more catalytic than moisture.

4.3 Acid catalysts

Primary acids are produced during the initial stages of pyrolysis through low temperature cleavage of carboxyl compounds and breakdown of extractives; therefore acids are present to catalytically interact with vapours during formation or after. Carboxyl groups associated with hemicellulose produce carboxylic acids while extractives remain as resin acids; form an esterified versions [23]; or breakdown to form acetone, formic acid, and methanol [24]. The main organic acid in bio-oil is acetic acid, produced from acetyl cleavage (from hemicellulose) and during secondary reactions. Research into the catalytic effect of organic acids is limited, but they are thought to affect pyrolysis because acids are catalytically active during bio-oil storage.

Acid catalysts favour dehydration reactions over depolymerisation reactions [21], which increases water yields. Karimi *et al* [25] stated that the acid catalysed condensation reactions lead to resin formation and phase separation of the bio-oil. Even in the presence of weak organic acids, the reactions rates for certain compounds increased, such as enhanced homolysis cracking reactions [26]. Catalytic pyrolysis with acidic H-ZSM-5 and Al-MCM-41 decreased bio-oil yields, indicating that the presence of strong acids caused a decrease in the bio-oil yield [27]. Britt *et al* [28] added acidic silica-alumina to pyrolysis, this enhanced the

rate of decomposition during pyrolysis of lignin. Acid catalysed cracking and polymerisation reactions altered the products produced with less alkenes and increased large aromatics, char, and coke. The effect of impregnating biomass with phosphoric acid was studied by Dobele *et al* [29] to increase the production of levoglucosenone by enhancing dehydration reactions. Overall volatile yields decreased from 91.4 to 64.8% as the concentration of phosphoric acid increased from 0 to 10.2%. The reduction in yields could partially be due to the presence of phosphorous; therefore a conclusion about the acidic effect could not be taken from this work.

4.4 Preliminary experiments to develop pretreatments

Preliminary experiments were conducted by pretreating biomass to remove/reduced the three catalysts naturally present in biomass (inorganics, water, and organic acids). Table 4-1 indicates the target for each experiment and the change in the biomass composition following the pretreatment. In terms of the organic acid reduction, uronic acid groups breakdown to form formic acid, acetone, and methanol during pyrolysis and hydrolysis [24, 30, 31], these were not detected in the biomass carbohydrate analysis and only minimal amounts of formic acid relative to acetic acid were detected in the bio-oil; therefore pretreatments targeted primarily acetyl compounds in biomass. Reduction/removal of biomass catalysts was accomplished following procedures given in Appendix 4.1, but in brief:

- Moisture was removed through complete drying at 105 °C overnight
- Inorganics were reduced by leaching with 1% nitric acid (HNO_3) for 4 h at 30 °C. The mild leaching conditions were not strong enough to alter the biomass's structure or to significantly reduce the acetyl content
- Acetyl groups were removed by leaching with 1% sodium hydroxide (NaOH) for 4 h at 30 °C. Acetyl and formyl side-branches are much more easily cleaved by alkali than by acid [32]. This also targets uronic acid removal [33].

Table 4-1: Combinations of biomass catalysts removed/reduced

Exp. no.	Catalyst/s targeted	Sample pretreatment	Inorganics (wt%)	Moisture (wt%)	Acetyl content[1] (wt%)	Biomass analysis		
						Lignin (wt%)	Cellulose (wt%)	Hemi. (wt%)
1	Raw biomass	Raw biomass	0.41±0.04	10.2±1.0	1.51±0.03	28.2±0.8	43.0±2.3	26.1±0.6
2	Inorganics	1% HNO_3 leached	0.12±0.01	9.8±1.8	1.48±0.05	28.1±1.7	43.6±1.7	26.8±3.6
3	Water	Dried	0.41±0.04	0	1.51±0.03	28.2±0.8	43.0±2.3	26.1±0.6
4	Acids	1% NaOH leached	1.35±0.10	9.9±0.3	0	27.5±0.7	45.7±2.3	26.9±2.3
5	Inorganics and water	1% HNO_3 leached and dried	0.12±0.01	0	1.48±0.05	28.1±1.7	43.6±1.7	26.8±3.6
6	Inorganics and acids	1% NaOH and 1% HNO_3 leached	0.08±0.02	9.2±0.9	0	27.5±2.0	44.2±2.8	26.1±3.2
7	Water and acids	1% NaOH washed and dried	1.35±0.10	0	0	27.5±0.7	45.7±2.3	26.9±2.3
8	Inorganics, water, and acids	1% NaOH leached, 1% HNO_3 leached, and dried	0.08±0.02	0	0	27.5±2.0	44.2±2.8	26.1±3.2

[1]*Acetyl content was reported as only acetic acid was detected in HPLC analysis*

4.4.1 Removal of one catalyst by leaching or drying

The experimental runs 2-4 in Table 4-1 reduced/removed only 1 biomass catalyst. This was to determine the influence of the individual biomass catalysts. Leaching with HNO_3 reduced inorganic content from 0.41±0.04 to 0.12±0.01 wt% and reduced the acetyl content of the biomass slightly; but did not alter the biomass's lignin or sugar composition. Leaching with NaOH removal all acetyl branches and slightly reduced the lignin content, which is characteristic for alkali pretreatments [34, 35]. The biomass structure may also have been altered by glucoside bond breakage and bond breakage between polymers. The inorganic content increased significantly to 1.35±0.10 wt% as Na was incorporated into the biomass after leaching, which could not be removed through rinsing.

Biomass samples with one catalyst reduced/removed were pyrolysed at the standard pyrolysis conditions given in Section 3.3. Yields from pyrolysis and key bio-oil properties are displayed in Table 4-2. Reducing the inorganic content in biomass gave a higher bio-oil and lower char yield. The acetic acid and water content in the bio-oil decreased. These results indicate secondary reactions were reduced. Pyrolysis of dry biomass produced a similar trend but to a lesser extent, indicating moisture in biomass enhances secondary reactions slightly. *P. radiata* has a naturally low inorganic content compared to other biomasses; therefore the moisture in biomass had a more significant catalytic effect than reducing the biomass's thermal conductivity when dried (causing an increase in the particle heating time). Finally, when acetyl braches were removed through NaOH leaching, the bio-oil yield decreased while the water content increased from 24.0 to 42.6 wt%. Since Na ions became incorporated into the biomass structure following leaching, secondary reactions increased significantly and the effect of reduced organic acids could not be determined. Nevertheless, the acetic acid content in the bio-oil decreased compared to pyrolysis of raw bio-oil, confirming that acetic acid is a combination of acetyl branches and products of secondary reactions. Results were comparable to Wang *et al* [35] who pretreated loblolly pine with NaOH and noticed the inorganic content increased from 0.39 wt% for raw biomass to 2.49 wt% after leaching. This decreased the bio-oil yield from 54 to 49 wt% and increased that char from 19 to 24 wt%.

Table 4-2: Summary of yields and bio-oil properties from pyrolysis of pretreated biomass

Exp. no.	Catalyst/s targeted	Bio-oil (wt% dry)	Char (wt% dry)	NCG by diff (wt% dry)	pH	Acetic acid in bio-oil (wt%)	Water in bio-oil (wt%)	Organic yield (wt%)
1	Raw biomass	46.9±0.5	15.4±0.7	37.6±1.2	2.5±0.1	3.5±0.4	24.0±1.2	35.5±0.3
2	1% HNO_3 leached	56.8	10.1	33.1	3.0	1.0	14.3	48.7
3	Dried	49.6	14.9	35.5	2.3	3.3	12.0	43.7
4	1% NaOH leached	44.8	19.3	35.9	2.7	2.7	42.6	25.7
5	1% HNO_3 leached and dried	54.7	14.7	30.6	2.9	2.0	12.9	47.6
6	1% NaOH and 1% HNO_3 leached	50.2	7.5	42.3	2.9	0.6	16.4	42.0
7	1% NaOH washed and dried	43.5	22.6	33.9	3.0	3.1	27.4	31.6
8	1% NaOH leached, 1% HNO_3 leached, and dried	55.4	6.7	37.9	3.0	0.4	6.2	52.1

4.4.2 Removal of two or more catalysts by leaching and drying

The experimental runs 5-7 in Table 4-1 aimed to reduced/remove two or more catalysts from the biomass. When biomass with reduced inorganics was subsequently dried, the bio-oil yield decreased and the acetic acid and pyrolytic water production increased compared to biomass that was solely leached. This indicated that either water reduces secondary reactions for low inorganic biomasses or that the catalytic effect of organic acids was more pronounced for dry biomass. The same relationship was observed for NaOH leached and dried biomass: the yields and bio-oil quality were lower when biomass was leached and subsequently dried. This was likely due to the enhanced effect of the Na ions incorporated into the biomass after NaOH leaching for dry biomass.

When NaOH leaching was followed by HNO_3 leaching, the bio-oil yield was lower than for solely HNO_3 leached biomass, while the water content was higher, signifying increased secondary reactions. This indicates that NaOH may negatively alter the biomass structure. It is likely that the slightly disturbed biomass structure following NaOH leaching reacted to a further extent compared to solely HNO_3 leached biomass, thermally enhancing cracking of primary vapours. The acetic acid content in the bio-oil was lower as acetyl branches were removed during the pretreatment.

When all three catalysts were reduced/removed in the experimental run 8, the organic yield was the highest measured while the char, acetic acid, and water content were significantly lower than for all other experiments. These experiments demonstrate the complexity of pyrolysis reactions and the ease at which the reaction mechanism can be altered. Therefore, even though the effect of individual catalysts could not be established without divulging into detailed pyrolytic mechanisms, it is clear all three catalysts enhance secondary reactions and reduction/removal of these catalyst from biomass would improve the bio-oil quality and quantity from pyrolysis.

4.5 Pretreatment sequence

Leaching and passivation are two techniques to mitigate the catalytic effect of inorganics. Passivation requires complicated equipment for embedding the catalyst into the biomass particle and requires acidic inputs. Leaching may also require acidic solutions and subsequent drying of the biomass. Disposal of the leachate leads to further complications and must be considered.

Torrefaction can reduce the acetyl content in biomass as acetyl groups are highly reactive, and have low activation energies [36, 37]. It also acts as a complete drying stage and can reduce the oxygen content in biomass. Hydrothermal torrefaction produces acetic acid in the initial stages, which acts as a leaching reagent. Stephanidis *et al* [27] found that hydrothermal torrefaction at 190 °C for 8 min lead to a higher organic yield during pyrolysis and reduced the pyrolytic water and acetic acid production. The biomass still requires drying after hydrothermal torrefaction and requires pressurised equipment. Therefore a two stage leaching and torrefaction pretreatment sequence was developed in this study, which is shown in Figure 4-1.

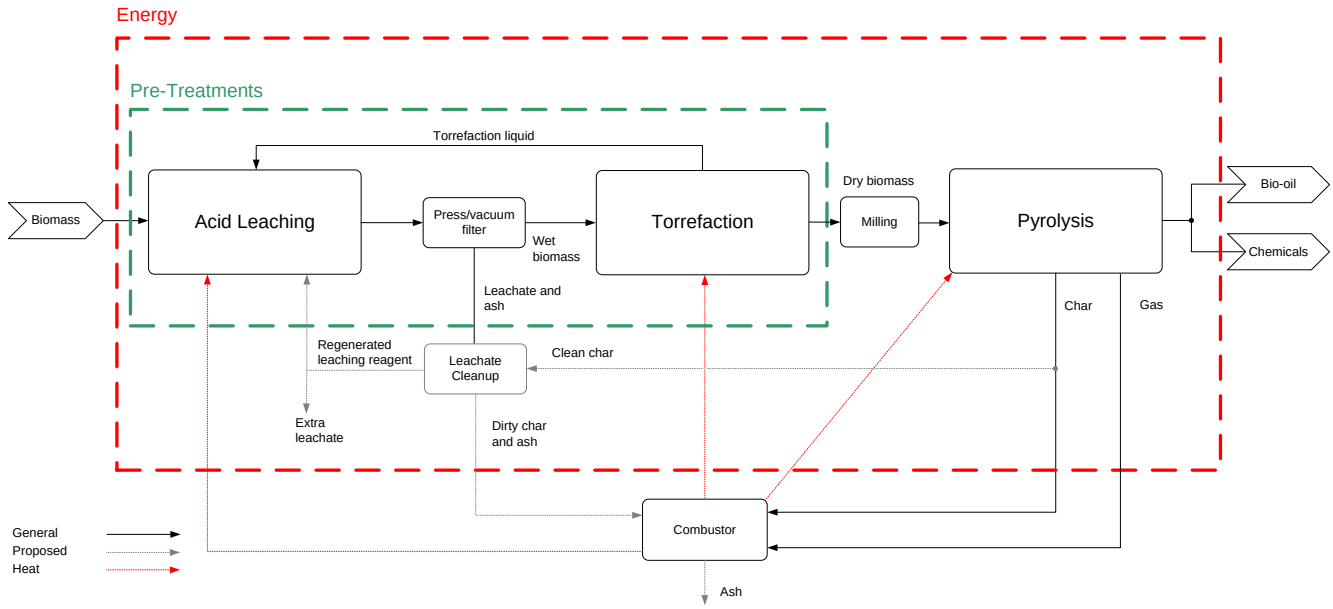

Figure 4-1: Biomass pretreatment sequence prior to fast pyrolysis, to improve the bio-oil quality

In the proposed process shown in Figure 4-1, biomass is initially demineralised via acid leaching, followed by the removal of excess moisture by pressing or vacuum filtering. Biomass is then torrefied, which also represents the drying stage. The liquid produced during torrefaction mainly contains water and organic acids; therefore this liquid can be recycled back into the demineralisation unit as the acid leaching reagent. The use of dilute organic acids (<1%) compared to commonly used mineral acids has not been reported in literature to date; although high concentrations of acetic acid (9.5 wt% and 5.7%) have been tested previously by Oudenhoven *et al* [38] and Davidsson *et al* [39], respectively; therefore biomass demineralisation using dilute organic acids was investigated in this study, with details presented in Chapter 5.

Demineralisation procedures require subsequent rinsing biomass to ensure complete removal of the leaching reagent. Rinsing is necessary because acids reduce bio-oil yields during pyrolysis and increase pyrolytic water through dehydration, condensation, and polymerisation reactions [40]. Rinsing is also required as acids in the feed material directly influence the bio-oil's pH. This could lead to economical drawbacks at larger scales due to the amount of water required for rinsing and disposal of the contaminated water solution produced during rinsing. No rinsing step is required in the proposed pretreatment sequence, as any remaining organic acids will volatise during torrefaction, and thus, will not enter the pyrolysis reactor.

Torrefaction does not produce an adequate volume of liquid to leach an equivalent amount of biomass; therefore the leachate would need to be recycled from acid leaching, with possible regeneration using pyrolysis chars as their hydrophilic surface is suitable for removing ions from water [41]. A portion of the leachate is lost during regeneration: this would be replenished with the new torrefaction liquor. The recycling and regeneration of leachate would minimise environmental issues concerning the disposal of the

mobile phase after leaching due to possible trace amounts of hazardous elements. Other benefits of the biomass pretreatment sequence include:

- Torrefaction reduces biomass grinding costs by <90% [42], thus it would be beneficial for leaching and torrefaction to be carried out on larger chips, afterward, a final size reduction could be implemented if necessary. Experiments will be performed to examine the difference between pretreating <6 mm chips and the standardly used <2 mm chips

- With reduced catalyst present during pyrolysis, there is potential to increase vapour residence times which would improve the flexibility of reactor configurations

- There is potential to use lower quality feedstocks such as forest residues with higher extractives, inorganics, and acetyl contents. The higher acetyl content would produce a stronger leaching solution to improve inorganic reduction. Increased methyl groups in biomass residues would mean additional methanol is produced during torrefaction, which would increase extractive removal during leaching.

Preliminary studies have been conducted by Saddawi *et al* [3] for combing leaching and torrefaction to improve the properties of biomass for co-combustion with coal. Water, ammonium acetate, and hydrochloric acid were used for the leaching. Results from the study indicated that leaching decreases the severity of torrefaction through the removal of alkali metals; therefore the combined effect of these pretreatments was investigated. The pretreated biomasses were analysed in terms of the combustion characteristics, such as the ash fouling behaviour and heating value. Insight into the influence of leaching and torrefaction on the biomass polymers is still required.

4.6 References

1. Scott, D. S., Paterson, L., Piskorz, J., & Radlein, D. (2001). Pretreatment of poplar wood for fast pyrolysis: rate of cation removal. *Journal of Analytical and Applied Pyrolysis, 57*(2), 169-176.
2. Hallen, R. T., Sealock, L. J., & Cuello, R. (1985). Influence of alkali carbonates on biomass volatilization. In R. P. Overend, T. A. Milne & L. K. Mudge (Eds.), *Fundamentals of Thermochemical Biomass Conversion* (pp. 157–166): Elsevier Applied Science Publishers.
3. Saddawi, A., Jones, J. M., Williams, A., & Le Coeur, C. (2011). Commodity fuels from biomass through pretreatment and torrefaction: Effects of mineral content on torrefied fuel characteristics and quality. *Energy & Fuels, 26*(11), 6466-6474.
4. Nowakowski, D., Jones, J., Brydson, R., & Ross, A. (2007). Potassium catalysis in the pyrolysis behaviour of short rotation willow coppice. *Fuel, 86*(15), 2389-2402.
5. Encinar, J. M., Beltrán, F. J., Ramiro, A., & González, J. F. (1997). Catalyzed pyrolysis of grape and olive Bagasse. influence of catalyst type and chemical treatment. *Industrial & Engineering Chemistry Research, 36*(10), 4176-4183.
6. Di Blasi, C., Galgano, A., & Branca, C. (2009). Influences of the chemical state of alkaline compounds and the nature of alkali metal on wood pyrolysis. *Industrial & Engineering Chemistry Research, 48*(7), 3359-3369.
7. Oasmaa, A., Solantausta, Y., Arpiainen, V., Kuoppala, E., & Sipilä, K. (2010). Fast pyrolysis bio-oils from wood and agricultural residues. *Energy & Fuels, 24*(2), 1380-1388.
8. Lin, Y., Zhang, C., Zhang, M., & Zhang, J. (2010). Deoxygenation of bio-oil during pyrolysis of biomass in the presence of CaO in a fluidized-bed reactor. *Energy and Fuels, 24*(10), 5686-5695.
9. Torri, C., Reinikainen, M., Lindfors, C., Fabbri, D., Oasmaa, A., & Kuoppala, E. (2010). Investigation on catalytic pyrolysis of pine sawdust: catalyst screening by Py-GC-MIP-AED. *Journal of Analytical and Applied Pyrolysis, 88*(1), 7-13.

10. Veses, A., Aznar, M., Martínez, I., Martínez, J. D., López, J. M., Navarro, M. V., et al. (2014). Catalytic pyrolysis of wood biomass in an auger reactor using calcium-based catalysts. *Bioresour Technol, 162*(0), 250-258.
11. Hoekstra, E., Westerhof, R. J. M., Brilman, W., Van Swaaij, W. P. M., Kersten, S. R. A., Hogendoorn, K. J. A., et al. (2012). Heterogeneous and homogeneous reactions of pyrolysis vapors from pine wood. *AIChE Journal, 58*(9), 2830-2842.
12. Zhang, Q., Chang, J., Wang, T., & Xu, Y. (2007). Review of biomass pyrolysis oil properties and upgrading research. *Energy Conversion and Management, 48*(1), 87-92.
13. Dayton, D. C., Jenkins, B. M., Turn, S. Q., Bakker, R. R., Williams, R. B., Belle-Oudry, D., et al. (1999). Release of inorganic constituents from leached biomass during thermal conversion. *Energy & Fuels, 13*(4), 860-870.
14. Bridgwater, A. V. (2003). Renewable fuels and chemicals by thermal processing of biomass. *The Chemical engineering journal, 91*(2), 87.
15. Hoekstra, E., Hogendoorn, K. J. A., Wang, X., Westerhof, R. J. M., Kersten, S. R. A., van Swaaij, W. P. M., et al. (2009). Fast pyrolysis of biomass in a fluidized bed reactor: In situ filtering of the vapors. *Industrial & Engineering Chemistry Research, 48*(10), 4744-4756.
16. Bridgwater, A. V. (2012). Review of fast pyrolysis of biomass and product upgrading. *Biomass and Bioenergy, 38*, 68-94.
17. Kasparbauer, R. D. (2009). *The effects of biomass pretreatments on the products of fast pyrolysis.* Iowa State University, Ames, Iowa.
18. Gary, M. (1984). *The effect of moisture and ash content on the pyrolysis of a wood derived material.* California Institute of technology, Pasadena.
19. Westerhof, R. J. M., Kuipers, N. J. M., Kersten, S. R. A., & van Swaaij, W. P. M. (2007). Controlling the water content of biomass fast pyrolysis oil. *Industrial & Engineering Chemistry Research, 46*(26), 9238-9247.
20. Kawamoto, H., Saito, S., Hatanaka, W., & Saka, S. (2007). Catalytic pyrolysis of cellulose in sulfolane with some acidic catalysts. *Journal of Wood Science, 53*(2), 127-133.
21. Scheirs, J., Camino, G., & Tumiatti, W. (2001). Overview of water evolution during the thermal degradation of cellulose. *European Polymer Journal, 37*(5), 933-942.
22. Gray, M. R., Corcoran, W. H., & Gavalas, G. R. (1985). Pyrolysis of a wood-derived material. Effects of moisture and ash content. *Industrial & Engineering Chemistry Process Design and Development, 24*(3), 646-651.
23. Alén, R., Kuoppala, E., & Oesch, P. (1996). Formation of the main degradation compound groups from wood and its components during pyrolysis. *Journal of Analytical and Applied Pyrolysis, 36*(2), 137-148.
24. Demirbas, A. (2007). Products from lignocellulosic materials via degradation processes. *Energy Sources, Part A: Recovery, Utilization, and Environmental Effects, 30*(1), 27-37.
25. Karimi, E., Gomez, A., Kycia, S. W., & Schlaf, M. (2010). Thermal decomposition of acetic and formic acid catalyzed by red mud - implications for the potential use of red mud as a pyrolysis bio-oil upgrading catalyst. *Energy & Fuels, 24*(4), 2747-2757.
26. Hsiang-Hui, K., & Stock, L. M. (1984). Aspects of the chemistry of donor solvent coal dissolution: promotion of the bond cleavage reactions of diphenylalkanes and the related ethers and amines. *Fuel, 63*(6), 810-815.
27. Stephanidis, S., Nitsos, C., Kalogiannis, K., Iliopoulou, E. F., Lappas, A. A., & Triantafyllidis, K. S. (2011). Catalytic upgrading of lignocellulosic biomass pyrolysis vapours: effect of hydrothermal pre-treatment of biomass. *Catalysis Today, 167*(1), 37-45.
28. Britt, P. F., Buchanan Iii, A. C., Thomas, K. B., & Lee, S.-K. (1995). Pyrolysis mechanisms of lignin: surface-immobilized model compound investigation of acid-catalyzed and free-radical reaction pathways. *Journal of Analytical and Applied Pyrolysis, 33*(0), 1-19.
29. Dobele, G., Rossinskaja, G., Telysheva, G., Meier, D., & Faix, O. (1999). Cellulose dehydration and depolymerization reactions during pyrolysis in the presence of phosphoric acid. *Journal of Analytical and Applied Pyrolysis, 49*(1–2), 307-317.
30. Yaman, S. (2004). Pyrolysis of biomass to produce fuels and chemical feedstocks. *Energy Conversion and Management, 45*(5), 651-671.
31. Stuart, P. R., El-Halwagi, M. M., & Ebooks, C. (2013). *Integrated biorefineries: design, analysis, and optimization* (Vol. 1). Boca Raton, FL: CRC Press.
32. Hayes, D. (2013). Advanced biomass research for beyond the petroleum age. *Important Compositional Parameters* Retrieved 07/09/2013, 2013, from http://www.carbolea.ul.ie/composition.php
33. Hassan, M., Steele, P. H., & Ingram, L. (2009). Characterization of fast pyrolysis bio-oils produced from pretreated pine wood. *Appl Biochem Biotechnol, 154*(1-3), 3-13.
34. McMillan, J. D. (1994). Pretreatment of lignocellulosic biomass *Enzymatic Conversion of Biomass for Fuels Production* (Vol. 566, pp. 292-324): American Chemical Society.
35. Wang, H., Srinivasan, R., Yu, F., Steele, P., Li, Q., & Mitchell, B. (2011). Effect of acid, alkali, and steam explosion pretreatments on characteristics of bio-oil produced from pinewood. *Energy & Fuels, 25*(8), 3758-3764.
36. Chew, J. J., & Doshi, V. (2011). Recent advances in biomass pretreatment – torrefaction fundamentals and technology. *Renewable and Sustainable Energy Reviews, 15*(8), 4212-4222.

37. Chen, Q., Zhou, J., Liu, B., Mei, Q., & Luo, Z. (2011). Influence of torrefaction pretreatment on biomass gasification technology. *Chinese Science Bulletin, 56*(14), 1449-1456.
38. Oudenhoven, S. R. G., Westerhof, R. J. M., Aldenkamp, N., Brilman, D. W. F., & Kersten, S. R. A. (2013). Demineralization of wood using wood-derived acid: towards a selective pyrolysis process for fuel and chemicals production. *Journal of Analytical and Applied Pyrolysis, 103*(0), 112-118.
39. Davidsson, K. O., Korsgren, J. G., Pettersson, J. B. C., & Jäglid, U. (2002). The effects of fuel washing techniques on alkali release from biomass. *Fuel, 81*(2), 137-142.
40. Di Blasi, C., Branca, C., & Galgano, A. (2008). Thermal and catalytic decomposition of wood impregnated with sulfur- and phosphorus-containing ammonium salts. *Polymer Degradation and Stability, 93*(2), 335-346.
41. Savova, D., Apak, E., Ekinci, E., Yardim, F., Petrov, N., Budinova, T., et al. (2001). Biomass conversion to carbon adsorbents and gas. *Biomass and Bioenergy, 21*(2), 133-142.
42. Meng, J., Park, J., Tilotta, D., & Park, S. (2012). The effect of torrefaction on the chemistry of fast-pyrolysis bio-oil. *Bioresour Technol, 111*(0), 439-446.

5 Pyrolysis of acid leached biomass

Torrefaction produces a significant quantity of organic acids, consisting primarily of acetic and formic acid and traces of higher carboxylic, lactic, and oxalic acids. It would be beneficial to use this solution for biomass leaching instead of commonly used mineral acids. Organic acids are less corrosive and prevent the addition of minerals to the biomass as carboxyl and phenolic hydroxyl groups in biomass provide anionic groups, which have the potential for ion exchange reactions. These sites act as binding sites for sorption of inorganics in biomass [1]. Bound inorganics are present in biomass as silicates (SO_4-), sulfates (SO_4^{2-}), oxides (R-O_i), hydroxides (R-OH), phosphates (PO_4^{3-}), carbonates (CO_3^{3-}), chlorides (Cl^{1-}), and nitrates (NO_3^-). Inorganics are also present as complex ions; dissolved salts in the biomass's free moisture; cations attached to carboxylic and other function groups; and chemisorbed material [2]. These can be divided in to three categories when leaching: water soluble ions, acid soluble ions, and insoluble ions.

Oudengoven *et al.* [3] extracted the acidic fraction from bio-oil and tested it as a leaching reagent. The solution contained 9.5 wt% acetic acid and was used as the leaching reagent to reduce the inorganics in pine wood from 0.53 to 0.02 wt%, when leaching at 90 °C for 2 h at a 1:10 ratio of biomass to leaching solution. Secondary reaction were likely reduced during pyrolysis of the leached biomass as less pyrolytic water and acetic acid were formed; sugar derivatives increase; and the bio-oil yield increased while the char yield decreased. In a separate study, Davidsson *et al* [4] also used acetic acid to leach biomass, this was to reduce alkali emissions during pyrolysis. Leaching with 1 M acetic acid solution (5.7%) was accomplished at room temperature for 4 h and with a biomass to solution ratio of 1:50. This reduced the alkali metal release during pyrolysis at 600 °C by 70% while water washing only reduced the release by 32%.

5.1 Leaching procedures

5.1.1 Small scale for leaching optimisation

Small scale leaching was used to optimise the leaching reagent, residence time, and temperature. Prior to acid leaching, the biomass was dried overnight at 105 °C to remove residual moisture, and then cooled in a desiccator. Leaching experiments were carried out in capped 2 L conical flasks, as indicated in Figure 5-1. A total of 700 mL of leaching solution was added to the flask, and 70 g of oven-dry biomass was added to this solution. The flasks containing biomass and leaching solution were heated using magnetic hot plates with a stirring speed of 250 rpm. The leaching temperature was controlled at 30 °C for 4 h in all runs, unless otherwise stated. After the leaching was completed, samples were neutralised by rinsing with deionised (DI) water using a Buchner funnel with a poly-cotton filter. Neutralised biomass was dried overnight at 105 °C and then the polymer composition and inorganic elements were analysed. Three duplicates were averaged for each reagent.

Figure 5-1: Small scale acid leaching apparatus

5.1.2 Large scale leaching

Once the acid leaching procedure was optimised, large scale leaching was used to produce greater quantities of leached biomass. The 25 L vessel, displayed in Figure 5-2 was modified to allow for a mechanically driven impeller to be mounted, which operated at 350 rpm. The vessel's temperature was controlled at 30 °C using two 60 W fish tank heaters. After the leaching was completed, the biomass was washed *in-situ* by adding a cotton wool filter to the outlet and circulating DI water through the vessel until a neutral pH was obtained.

Figure 5-2: Large scale leaching apparatus

5.1.3 Leaching procedure at elevated temperatures

In order to investigate the effect of elevated temperatures during biomass leaching runs at 150 °C were carried out in a modified Gallenkamp bomb calorimeter; displayed in Figure 5-3. A gas inlet and outlet, pressure sensor, internal thermocouple, and magnetic stirrer were added to the bomb. The saturated vapour pressure for water and acetic acid were calculated up to 150 °C, with results shown in Figure 5-4. These results indicate the vapour pressure for acetic acid leaching solutions reaches 0.47 MPa at 150 °C. Therefore, system was pressure tested to a maximum of 5 MPa, and was equipped with a pressure relief valve in case of higher pressures. Biomass was heated using a magnetic stirring plate, with a concentric aluminium block placed on top to aid heat transfer. After leachings were completed, samples were neutralised with DI water, analogous to leachings at 30 °C. Three duplicates were averaged for each reagent.

Figure 5-3: Modified Gallenkamp bomb calorimeter for high temperature leachings

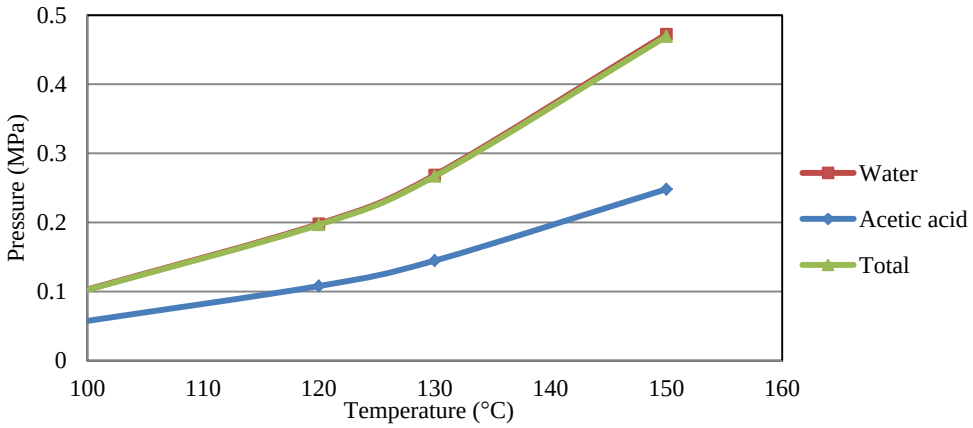

Figure 5-4: Vapour pressure system for high temperature leachings

5.2 Comparison between different leaching reagents

The efficiency of leaching with the two main organic acids identified in the solution produced during torrefaction, namely acetic and formic acid, were compared to leaching with water and three mineral acids: hydrochloric, sulfuric, and nitric acid. The total yields and structural analysis of biomass samples following leachings with different reagents are given in Table 5-1. The lignin composition of 28±1% for raw *P. radiata* was comparable to that reported previously of 26-29% by Evans *et al* [5], Green [6], Iiyama and Willis [7], and Johnsson and Packer [8]. The acid soluble lignin was 1.0±0.2%, this was slightly higher than typical values of <1% for softwoods [9, 10][7]. The cellulose composition was measured in the present study as 43±1%, which is comparable to reported values of 42 and 42.5% by Uprichard and Lloyd [11] and Berrocal *et al* [12], respectively. The hemicellulose content was measured in the present study as 26±1%, which is also within the reported range of 22.9% [12] to 29% [11]. The hemicellulose content varies significantly between studies, possibly due to the tree's age as the wood chemical composition varies with age: the cellulose content increases and hemicellulose content decreases [11]. Boonstra and Tjeerdsma [13] analysed *P. radiata* and found that the raw acetyl content was 1.48%, which was close to the 1.51±0.03% measured in this work. Overall, the hydrolysis procedure used to determine the biomass's chemical composition was considered reliable.

During the leachings, biomass sugar polymers depolymerised if conditions were severe enough for hydrolysis to proceed. The high mass yields indicate that hydrolysis was minimal for all leachings; the slight decreased in the acetyl content for sulfuric and hydrochloric acid leached biomass represent mild hydrolyses but the polymer composition did not vary.

The inorganic fraction in biomass was reduced from 0.45 to 0.27 wt% with water washing alone. This indicates that approximately 40% of the inorganics in biomass are present as soluble metal salts, such as alkali metal chlorides, sulfates, and carbonates [14]. Reduction of the acid soluble salts, such as alkaline earth carbonates and sulfates, was accomplished through dilute acid leachings. Inorganics remaining after acid leaching were inaccessible within the wood matrix and could not be removed even with severe leaching procedures for *P. radiata*. These could be either as organically bound salts, that require oxidation or dissolution of the organic matter for removal (using ammonium acetate or sodium hydroxide leaching solutions), or present as silicates which have limited removal during acid leachings [14]. Further reductions in the inorganic content have been reported by other researchers using different feedstocks [3, 15].

The reduction in biomass inorganics during leachings at 30 °C was slightly more effective with mineral acids than organic acids; this may be correlated with the pH of the leaching solution, as shown in Figure 5-5. From the figure, it was observed that the inorganic content in leached biomass decreased as the pH of the leaching solution was decreased, regardless of the actual acid type. This confirmed that organic acids can be used for

leaching biomass rather than mineral acids. Figure 5-5 can be used to predict the inorganic content after leaching for any given acid leaching reagent under the same leaching conditions.

Table 5-1: Biomass composition after leaching with different leaching reagents

	Leaching yield (%)	Inorganic content (%)	Acetyl content (%)	Lignin (%)	Cellulose (%)	Hemicellulose (%)
Raw wood	-	0.41±0.04	1.51±0.03	28±1	43±1	26±1
DI water	99.3±0.2	0.27±0.03	1.53±0.17	30±1	42±2	26±1
1% acetic acid	99.3±0.1	0.16±0.02	1.48±0.30	28±4	43±1	27±1
1% formic acid	99.0±0.3	0.14±0.02	1.53±0.15	28±1	42±1	26±1
1% sulfuric acid	99.3±0.9	0.11±0.02	1.36±0.05	29±2	42±2	27±1
1% hydrochloric acid	98.4±0.8	0.11±0.02	1.38±0.17	29±1	42±1	27±1
1% nitric acid	99.0±0.4	0.12±0.02	1.48±0.05	28±2	44±3	27±4

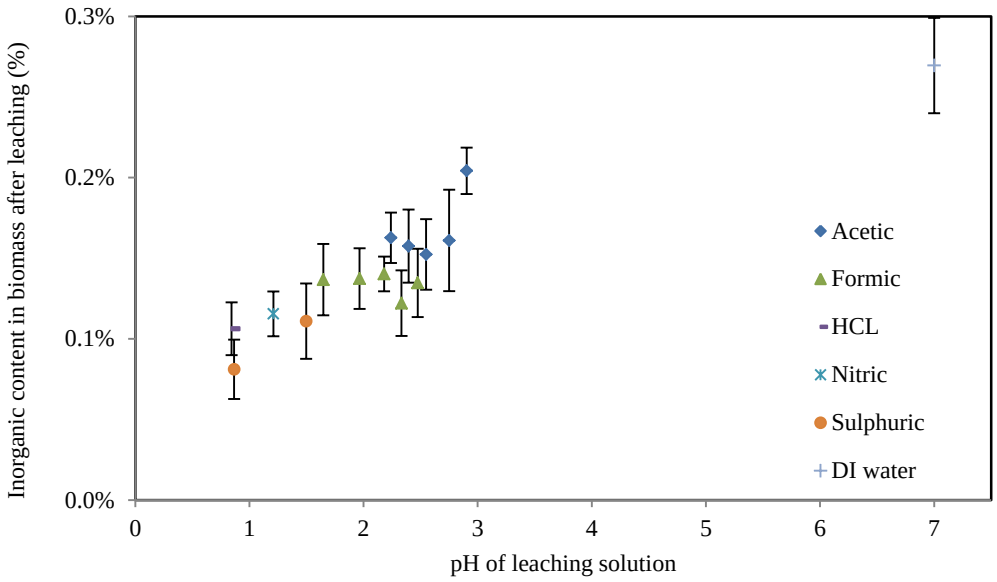

Figure 5-5: Inorganic content in biomass after leaching with varying reagent type and concentrations

The ICP-OES results given in Table 5-2 indicate that only S, P, Na (and Zn for formic acid) were reduced to the same degree by organic acids as by mineral acids for leachings at 30 °C. The higher concentration of alkaline earth metals (Mg and Ca) in the organic acid leached biomass could be beneficial as alkaline earth metals have been used as catalysts for deoxygenation during pyrolysis [16, 17], by favouring depolymerisation reactions over dehydration reactions [18]. Sulfuric acid leaching caused a large increase in S, indicating that either some of the acid was not washed out during the neutralising step or S became incorporated into the biomass, and thus could not be removed through water washing alone. Organic acids contain no inorganics, which is a potential benefit of leaching with organic acids compared to mineral acids.

A mass balance for the elements in biomass leached with 1% acetic acid at 30 °C is given in Table 5-3. The discrepancy between the calculated mass balance for the elements removed from the biomass and the experimentally measured values in the leachate indicate that additional ions were present in the leachate which

were not generated from the biomass. These could originate from the acetic acid or DI water, but both would be minimal based on the assay of the raw solutions. The most likely introduction of additional ions would be from either the vessel in which the leaching solution was collected or stored. For example, the Na and Si content can increase due to glassware leaching [19].

Table 5-2: ICP-OES results for biomass leached at 30 °C

Element[1] (ppm)	Al	B	Ca	Fe	K	Mg	Mn	Na	P	S	Zn	Si[2]
Raw wood	70.9	3.1	756.0	81.5	524.9	204.0	51.4	60.3	146.6	63.0	6.8	2126.7
DI water	48.3	2.2	647.6	44.6	142.1	173.1	45.6	50.7	107.2	40.5	6.1	1389.4
1% acetic acid	58.2	2.1	198.6	76.9	18.1	38.6	9.1	42.7	111.8	41.2	2.7	998.2
1% formic acid	54.6	1.9	133.8	63.8	19.2	18.5	3.4	44.8	114.5	43.7	1.4	898.7
1% sulfuric acid	42.1	1.2	52.8	44.3	9.5	12.3	1.4	42.4	112.0	82.8	2.4	677.7
1% nitric acid	48.9	0.8	47.5	51.3	10.5	11.9	1.3	42.4	111.3	45.6	1.2	825.1
1% hydrochloric acid	62.8	0.9	84.3	68.4	11.6	18.4	1.8	43.4	115.2	46.3	0.8	644.9

[1]*Elements below 2 ppm are not displayed, these include Ba, Cd, Cr, Cu, Li, Ni and V. Elements tested and not detected were As, Co and Pd.* [2]*Si was calculated as the difference between the total inorganic content and the sum of the total ions measured*

Table 5-3: Mass balance of elements for 1% acetic acid leached biomass at 30 °C

Element (mg)	Al	B	Ca	Fe	K	Mg	Mn	Na	P	S	Zn
In 70 g of raw biomass	5.0	0.2	52.9	5.7	36.7	14.3	3.6	4.2	10.3	4.4	0.5
In 70 g of 1% acetic acid leached biomass	4.1	0.1	13.9	5.4	1.3	2.7	0.6	3.0	7.8	2.9	0.2
Calculated mass balance for ion removal	0.9	0.1	39.0	0.3	35.5	11.6	3.0	1.2	2.4	1.5	0.3
Measured amount in the leachate	1.7	2.0	44.9	0.6	46.6	12.6	3.0	9.6	3.3	1.9	0.5

Figure 5-6 displays the ash of leached biomass produced after combustion at 620 °C. The colour and density of the ash were different for samples leached with different reagents. Raw biomass produced a darker and denser ash, water washed biomass produced a slightly lighter and less dense ash, while biomass leached with an acid produced the very pale and light ash. Wood ash is a complex mixture of oxides ($-O_i$), hydroxides (-OH), carbonates ($-CO_i$), and silicates ($-SiO_4$). For example, Etiégni and Campbell [20] proposed that calcium was present as mainly lime (CaO), calcite ($CaCO_3$), portlandite ($Ca(OH)_2$), and calcium silicate ($CaSiO_4$). They also observed that average particle diameter of ash was 230 µm. Ash can contain irregularly shaped inorganic particles as well as porous carbon particles. Therefore, the difference ash characteristics were due to complex mixture of compounds formed from the inorganics in biomass. For example, compounds such as MnO are black; therefore a reduction in Mn would alter the ash's colour.

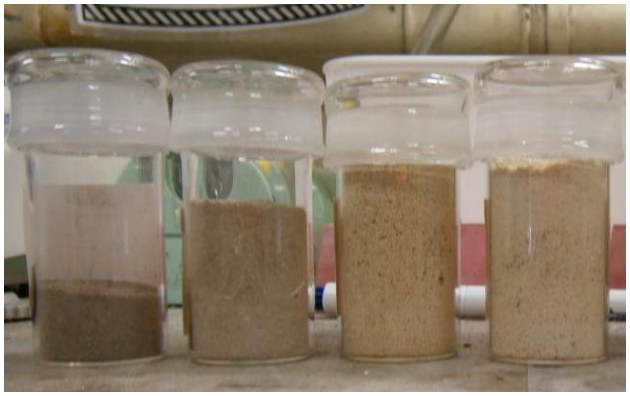

Figure 5-6: 1.5 g of biomass ash after acid leaching, from the left: raw wood, water washed, 1% acetic acid leached, and 1% formic acid leached

5.2.1 Pyrolysis of leached biomass

Raw biomass and the leached biomass listed in Table 5-1 was pyrolysed at the standard pyrolysis conditions described in Section 3.3. Pyrolysis yields are displayed in Figure 5-7, from which it was found that the bio-oil yield increased from 46.9 wt% for raw biomass to 51.2 wt% for DI water washed biomass. This was contradictory to other reports [21, 22] that stated the removal of water soluble ions did not affect pyrolysis yields. Acid soluble ions are thought to be more catalytic during pyrolysis as they are bound tightly to the biomass, thus interact during vapour formation more readily; however water soluble ions could catalyse secondary reactions during char and vapour entrainment from the reactor. During pyrolysis, repeated desorption and adsorption of inorganics allows inorganics to reform into a thermally stable form in the char; either bonded to the char or as non-volatile compounds such as silicates [23]. This concentrates water soluble and water insoluble inorganics in the char fraction, which could enhance heterogeneous vapour phase reactions as vapours exit through the outer char layer of a pyrolysing biomass particle or after entrainment. The extended length of the fluidised bed used in this research prolongs char and vapour interactions compared to other systems.

It was observed from Figure 5-7 that the bio-oil yield increased from 46.9 wt% for pyrolysis of raw biomass to 54.6 and 54.8 wt% for acetic and formic acid leached biomass respectively. This was only slightly lower than the bio-oil yields for nitric and hydrochloric leached biomass of 56.8 and 55.8 wt% respectively. Leaching with sulfuric acid only increased the bio-oil yield to 52.4 wt% and gave the highest char yield. Sulfur that became incorporated into the biomass following the leaching may have catalysed char formation through polymerisation of primary vapours. Char from acid leached biomass appeared to agglomerate more than char produced from raw or water leached biomass, as indicated in Figure 5-8. This phenomenon was also reported by Brown [24]. Biomass with very low concentration of inorganics produces more aerosols, which can be reflected by the percentage of bio-oil not captured in the condensers; this was 29% for raw bio-oil but 42-45% for the acid leached bio-oils. Collisions between aerosols and aerosols with other char particles as may cause adhesion of char particles and the agglomeration observed.

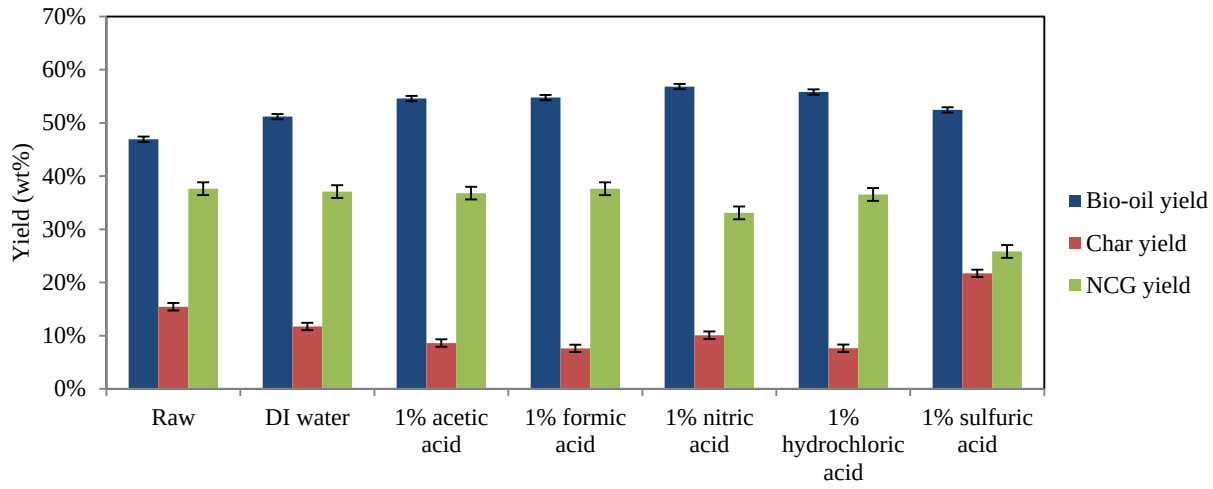

Figure 5-7: Yields from pyrolysis of leached biomass

Figure 5-8: Char from pyrolysis of acid leached biomass containing agglomerations (left) and char from pyrolysis of raw biomass (right)

Analysis of the bio-oils indicated the water and acetic acid content in the bio-oil decreased with all leachings, with the concentrations displayed in Figure 5-9. It is believed that inorganics catalyse the formation of carbonyl compounds such as acetic acid [25], with acetic acid formed from alkali catalysed ring opening reactions [26]. The pyrolytic water decreased due to reduced dehydration reactions of vapours. The reduction could also be due to removal of inorganics that formed a crosslink between biomass polymers. Removing these inorganics would slightly reduce the crosslinking severity of the biomass. If these crosslinks are not removed, they will continuously be broken and reformed in pyrolysis, thus extending the reaction time for volatiles associated with the inorganic crosslinks. This increases cracking reactions which typically produce water as a by-product [22].

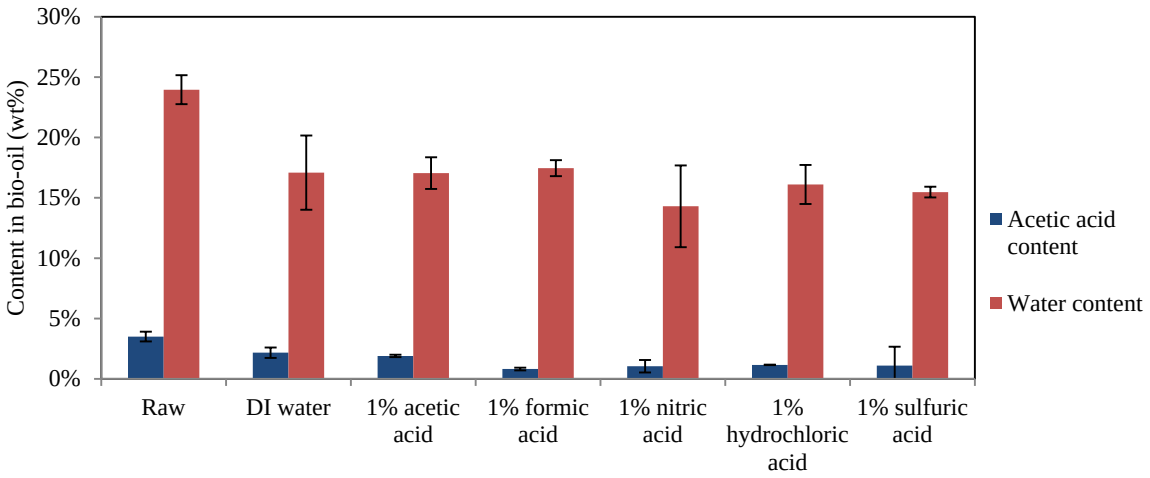

Figure 5-9: Acetic acid and water content in bio-oil produced from leached biomass

5.3 Effect of leaching temperature

5.3.1 Leaching at 90 °C

Yields and the biomass composition following leachings at 90 °C are given in Table 5-4. From the results it was found that increasing the leaching temperature to 90 °C slightly increased the leaching severity for DI water, acetic acid, and formic acid. There was a large increase in severity for leachings with the mineral acids. The mass yields were related to the pH of the leaching solution (in decreasing order: hydrochloric, nitric, sulfuric, formic, and acetic acid). Mineral acids all reduced the biomass yield. Leaching with hydrochloric acid was the most severe, with hemicellulose being partially hydrolysed and the acetyl concentration significantly reduced. Mass yields when leaching with organic acids and water at 90 °C were approximately the same, indicating that water soluble extractives were removed and minimal polymer degradation occurred.

It was mentioned in the previous section that the reduction in inorganics was slightly higher when leaching with mineral acids compared to the organic acids at 30 °C. However, increasing the leaching temperature to 90 °C improved the inorganic removal for the organic acids but only had a minor effect for the mineral acids. This was partially due to the high mass loss associated with the mineral acids concentrating the remaining inorganics in the biomass. Therefore, there was no advantage when leaching with mineral acids at 90 °C compared to 30 °C, in terms of the inorganic reduction. It was reported that acetyl groups associated with hemicellulose and even cellulose can function as weak ion exchange sites to exchange cations with a strong acid relatively quickly and do not require elevated temperatures [21].

Table 5-4: Composition of biomass after leaching with different leaching reagents at 90 °C

	Leaching yield (%)	Inorganic content (%)	Acetyl content (%)	Lignin (%)	Cellulose (%)	Hemi-cellulose (%)
Raw wood	- -	0.41±0.04	1.51±0.03	28±1	43±1	26±1
DI water	97.7±1.1	0.29±0.04	1.50±0.05	28±4	42±2	27±2
1% acetic acid	98.0±0.4	0.12±0.06	1.46±0.06	28±3	42±3	27±3
1% formic acid	97.9±0.6	0.11±0.04	1.41±0.02	31±3	42±3	26±1
1% sulfuric acid	92.0±1.5	0.10±0.02	0.80±0.13	32±3	43±2	22±1
1% hydrochloric acid	85.0±2.1	0.10±0.02	0.40±0.07	32±1	49±0	17±1
1% nitric acid	88.0±2.9	0.13±0.03	0.54±0.03	32±1	46±1	21±1

The ICP-OES results for the inorganic composition following leachings at 90 °C are given in Table 5-5. Similar trends were observed to those displayed for leachings at 30 °C given in Table 5-2 in terms of elements reduced with respect to the organic acids compared to the mineral acids. The removal of Al, B, K, Mg, Mn, and P was improved for all samples leached at 90 °C compared to 30 °C. The removal of Ca and Fe was also improved for all samples except for DI water leached biomass. There were minimal changes in the Na and S removal for all samples, indicating high temperatures do not enhance the removal for these elements.

Table 5-5: ICP-OES results for biomass leached at 90 °C

Element[1] (ppm)	Al	B	Ca	Fe	K	Mg	Mn	Na	P	S	Zn
Raw wood	70.9	3.1	756.0	81.5	524.9	204.0	51.4	60.3	146.6	63.0	6.8
DI-water	46.7	1.3	685.2	48.5	99.8	172.6	45.2	51.7	100.9	41.9	9.8
1% acetic acid	39.8	0.5	190.9	32.2	15.5	30.1	8.4	43.8	100.7	41.1	4.6
1% formic acid	47.6	0.3	90.4	23.9	9.4	14.4	2.0	43.5	102.6	44.2	1.2
1% sulfuric acid	40.6	0.3	32.6	12.9	7.7	7.3	0.7	42.9	91.2	71.1	1.3
1% nitric acid	39.6	0.3	33.6	11.7	7.9	7.4	1.0	42.7	88.1	47.5	1.2
1% hydrochloric acid	48.0	0.3	32.2	12.8	9.6	7.7	0.9	43.2	86.9	46.4	1.1

[1]*Elements below 2 ppm are not displayed, these include Ba, Cd, Cr, Cu, Li, Ni and V. Elements tested and not detected were As, Co and Pd*

Pyrolysis yields and the bio-oil properties were determined for all the leachings at 90 °C, with the results given in Table 5-6. Similar trends to pyrolysis of biomass leached at 30 °C were noticed: the higher S in the 1% sulfuric acid leached biomass caused an increase in the char yield. Also, mineral acids gave slightly higher bio-oil yields compared to the organic acids. Leaching with acetic acid was very similar to leaching with DI water; it was thought the rinsing was not sufficient for this sample and some acetic acid remained on the biomass to catalyse dehydration reactions. The low char yield indicates that acetic acid has minimal effect on char formation but does increase water formation at the expense of bio-oil.

Table 5-6: Pyrolysis yields and key bio-oil properties for leached biomass at 90 °C

Leaching reagent	DI water	1% acetic acid	1% formic acid	1% sulfuric acid	1% hydrochloric acid	1% nitric acid
Pyrolysis yields (wt%)						
Bio-oil	54.9	54.5	56.1	57.3	59.7	59.5
Char	11.4	8.6	6.8	13.0	6.7	7.8
NCG, by difference	33.7	36.9	37.1	29.7	33.6	32.7
Bio-oil properties						
Acetic acid conc.	2.0±0.1	1.4±0.0	0.7±0.2	0.8±0.1	0.5±0.2	0.5±0.1
Water	14.0±0.0	15.2±0.0	13.3±0.0	13.38±0.3	15.9±0.3	12.9±1.3
Density	1178.2	1298.7	1298.4	-	1303.3	1314.0
Organic yield (wt%)	47.2	46.22	48.6	49.6	50.3	51.8

^{1}H-NMR was carried out on bio-oil from raw biomass and the organic acid leached samples at both 30 and 90 °C. Figure 5-10 and Figure 5-11 displays the calculated concentrations of various organic compounds. Figure 5-10 indicates that raw bio-oil had a higher concentration of alkanes: a desirable compound in bio-oil, but when relative to biomass feed rate as shown in Figure 5-11, there was no obvious increase in alkane yield. Leaching the biomass decreased the acetic acid and formic acid content in the bio-oil, while significantly increasing the levoglucosan, hydroxyacetone, and aromatic content. Aromatics increased due to reduced secondary reactions of primary aromatic compounds, such as ring opening reactions. No peak for hydroxyacetone was present for the raw bio-oil; this was unexpected as it is a secondary product of levoglucosan decomposition [27]. The raw samples were stored for 2 months before analysis, and it is probable that the hydroxyacetone reacted during storage.

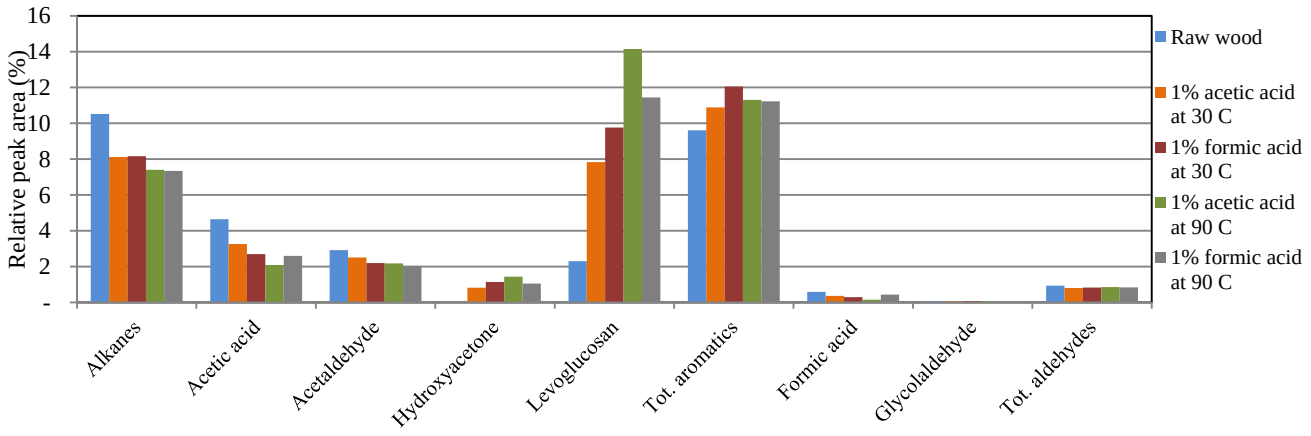

Figure 5-10: ^{1}H-NMR peak area for bio-oil composition, water free basis

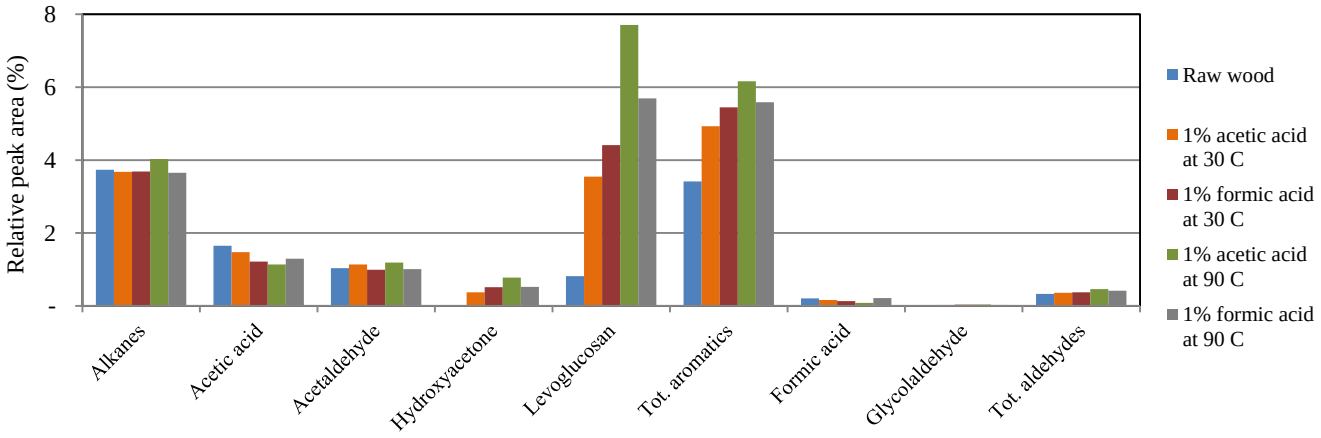

Figure 5-11: ^{1}H-NMR peak area for bio-oil compounds, relative to the biomass feed

5.3.2 Leaching at 150 °C

Leaching at 150 °C was only accomplished for DI water, 1% acetic acid, and 1% formic acid. During the 1% nitric acid leaching at 150 °C, the experiment was terminated shortly after reaching 150 °C as the system's pressure rapidly reached 2 MPa, theoretically it should have only reached 0.49 MPa. This was because nitric acid led to severe decomposition of the biomass, which produced additional vapours to pressurise the bomb calorimeter; therefore the experiment was terminated early and hydrochloric and sulfuric acids were not investigated as these are stronger than nitric acid.

The mass loss and biomass composition for DI water, acetic acid, and formic acid leached biomass at 150 °C are given in Table 5-7. All mass losses were significant, especially compared to leachings at 30 and 90 °C. There was also a larger variance for repeats, thus the uncertainties were larger. The significant variations observed during high temperature leachings were due to the fact that even slight temperature fluctuations had a substantial impact on the biomass breakdown. The partial decomposition of hemicellulose during the leachings indicated biomass hydrolysis was enhanced at the elevated temperatures, and hydrothermal torrefaction occurred. Hydrothermal torrefaction has rapid heating rates as conductive heat transfer dominates [28]. Due to the high mass loss and the initiation of hydrolysis, high temperature leaching was not researched further: hydrolysis of biomass was not desirable during the leaching stage and pressurised leaching would incur economic penalties.

Table 5-7: Solids yield and composition of biomass after leaching at 150 °C

Leaching reagent	Leaching yield (%)	Inorganic content (%)	Acetyl content (%)	Lignin (%)	Cellulose (%)	Hemi-cellulose (%)
Raw wood	-	- 0.41±0.04	1.51±0.03	28±1	43±1	26±1
DI water	88.4±4.3	0.19±0.05	1.24±0.26	26±3	49±4	23±2
1% acetic acid	83.3±5.6	0.12±0.04	0.97±0.30	33±2	47±3	17±2
1% formic acid	77.1±3.3	0.14±0.06	0.54±0.18	36±3	51±2	12±1

5.4 Effect of leaching residence time

The leaching residence time for 1% acetic acid samples was assessed between 1-8 h. The total inorganic fraction of the biomass after leaching for the various residence times is shown in Figure 5-12. Results indicate that at least 4 h is required to reduce the ion concentration significantly. Residence times shorter than 4 h were not sufficient for the leaching solution to penetrate deeply into all biomass micropores, thus allowing sufficient ion exchange to occur. Shorter residence times did not reach equilibrium between the leaching solution and the inorganic concentration of the biomass. Increasing the residence time to 6 h gave a slight decrease in the inorganic content from 0.16±0.03 to 0.14±0.02 wt% but increasing up to 8 h gave no further reduction.

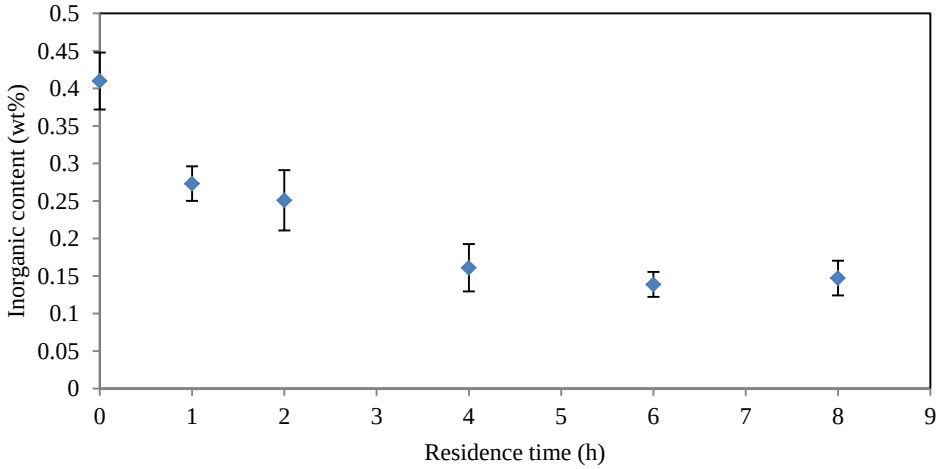

Figure 5-12: Inorganic fraction in biomass after leaching with 1% acetic acid for various residence times

Biomass leached with 1% acetic acid for various residence times was pyrolysed at the standard pyrolysis conditions, with results given in Table 5-8. From these results it was found that increasing the residence time past 4 h had a similar effect to increasing the concentration of the leaching solution: the bio-oil yield increased slightly and the pyrolytic water concentration decreased. This was possibly due to the biomass morphology being modified during extended leachings. In general, increasing the leaching residence time had minimal effect on the bio-oil composition, as determined by ^{1}H-NMR results given in Table 5-8. However, noticeable trends observed were increased alkanes and levoglucosan, and decreased formic acid concentrations. Based on these results, residence times of 4 h were considered the shortest residence time acceptable to reduce the inorganic content while minimising pretreatment costs.

Table 5-8: Results from pyrolysis of 1% acetic acid leached biomass for varying residence times

Leaching residence time (h)		**1**	**2**	**4**	**6**	**8**
Pyrolysis yields (wt%)						
Bio-oil		49.5	50.4	54.6	54.5	57.7
Char		6.7	6.0	8.6	6.1	7.1
NCG, by difference		43.8	43.5	36.8	36.8	35.2
Bio-oil properties						
Acetic acid conc. (%)		1.8±0.4	1.3±0.1	1.9±0.1	0.7±0.2	1.3±0.3
Water (wt%)		18.8±0.5	17.3±0.8	17.1±1.3	16.1±0.1	13.3±0.71
Density (kgm^{-3})		1289.3	1292.6	1268.9	1290.4	1306.7
Organic yield (wt%)		40.2	41.7	45.3	45.7	50.0
^{1}H-NMR results, relative to the biomass feed						
Compound/s	**Shift, ppm**	**wt% in bio-oil[1], in brackets: wt% relative to the organic yield**				
Alkanes	0.5-1.6	7.53 (3.03)	7.76 (3.24)	8.12 (3.68)	7.88 (3.60)	7.49 (3.75)
Acetic acid	1.88	3.48 (1.40)	3.13 (1.31)	3.26 (1.48)	2.72 (1.24)	2.79 (1.40)
Acetaldehyde	9.58 and 2.08	2.38 (0.96)	2.77 (1.16)	2.51 (1.14)	2.12 (0.97)	2.39 (1.20)
Hydroxyacetone	4.01	1.23 (0.49)	1.36 (0.57)	0.82 (0.37)	0.67 (0.31)	1.07 (0.54)
Levoglucosan	3.27,3.84-3.85,4.31-4.33, and 5.13	8.88 (3.57)	9.00 (3.75)	7.83 (3.55)	8.42 (3.85)	9.56 (4.78)
Tot. phenol and furan derivatives[2]	6.4-7.6	9.82 (3.95)	10.53 (4.39)	10.89 (4.93)	10.41 (4.76)	10.84 (5.42)
Formic acid	8.10	0.36 (0.14)	0.30 (0.13)	0.36 (0.16)	0.33 (0.15)	0.30 (0.15)
Glycolaldehyde	9.55	0.10 (0.04)	0.08 (0.03)	0.06 (0.03)	0.07 (0.03)	0.10 (0.05)
Tot. aldehydes	9.5-10.5	0.75 (0.30)	0.77 (0.32)	0.80 (0.36)	0.75 (0.34)	0.81 (0.41)

[1]In the organic fraction of the bio-oil. [2]Includes phenol, syringol, guaiacol, furan, furfural, methyl-2-furoate, and hydroxymethylfurfural

5.5 Effect of acid strength

The concentrations of acetic and formic acid were varied from 0.5 to 10% (leached at 30 °C for 4 h) to determine the minimal acid concentration required to reduce the biomass's inorganic content. The results are shown in Figure 5-13, which indicate the effect of low acid concentrations was more pronounced for acetic acid compared to formic acid; however increasing the concentration above 1% had minimal effect for both acids when the biomass was leached at 30 °C for 4 h. This result implies that a fraction of the inorganics present in biomass cannot be removed at 30 °C with formic or acetic acid under the given leaching conditions.

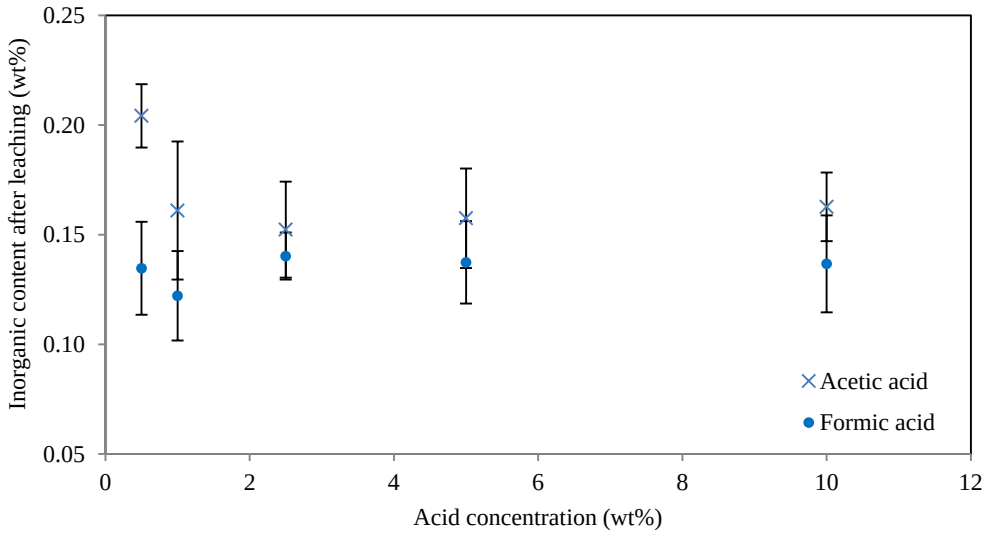

Figure 5-13: Inorganic reduction after leaching with varying acetic and formic acid concentrations

Yields and properties from pyrolysis of the biomass leached with 0.5, 1, and 5% acetic and formic acid solutions are presented in Table 5-9. The inorganic content did not vary when leaching with >1% solutions, and there was no additional mass loss during the leaching. However, the yields from pyrolysis and properties of the bio-oil did vary. The improvement is likely due to the stronger leaching conditions slightly altering the biomass's structure. Radlein *et al* [29] leached Avicel cellulose for 5.5 h at 90 °C using 5% H_2SO_4, the inorganic content remained the same following the leaching. After the pretreatment, organic yield changed from 87.1 to 86.3 wt%, but the levoglucosan yield increased from 26.9 to 38.4 wt%; indicating that pyrolysis reactions and the product distribution are not only affected by the inorganics but possibly by the morphology, porosity, and degree of hydrogen bonding in cellulose [30]. These properties may be altered during leaching pretreatments.

Pyrolysis of biomass leached with 1% acetic acid produced a higher concentration of acetic acid in the bio-oil compared to all other samples in Table 5-9. This was most likely due insufficient washing following the leaching and a small amount of acetic acid remaining in the biomass, indicating that the presence of acetic acid during pyrolysis catalysed char and water formation. Rinsing biomass to neutralise the pH after leachings was an ineffective method to remove all residue acids; it was observed during experiments that even when the leachate reached a neutral pH, pH paper pressed on to biomass indicated it was still acidic. Acid deep within biomass pores was hard to remove during the subsequent rinsing stage, and would require soaking in DI water to ensure full removal.

^{1}H-NMR results for the bio-oil samples are given in Table 5-9. The samples were analysed in two batches; initially both the samples pretreated using 1% acetic and formic acid leaching were analysed, then the remaining samples were all analysed at a later date. The water suppression technique was slightly improved to reduce the suppression of other compounds around 3.3 to 4.0 ppm during this time; therefore due to the analytical method,

both the 1% acetic acid formic acid leached samples were repressed in levoglucosan and hydroxyacetone but comparatively rich in all other compounds. Taking this into account, the general trends observed were, relative to the organic yield, levoglucosan, aldehydes, and alkanes yields increased when leaching with stronger solutions. The actual inorganic content in biomass did not decrease with acid leaching solutions stronger than 1%, and thus changes in the bio-oil properties were likely associated with changes in the morphology of the biomass. Therefore, 1% was considered the optimal leaching concentration. Changes in the biomass's morphology would instead be targeted during torrefaction.

Table 5-9: Results from pyrolysis of acetic and formic acid leached biomass at varying acid concentrations

		Acetic acid			**Formic acid**		
Leaching strength (%)		**0.5**	**1**	**5**	**0.5**	**1**	**5**
Pyrolysis yields (wt%)							
Bio-oil		52.6	54.6	57.0	52.6	54.8	56.7
Char		8.1	8.6	7.4	7.3	7.6	11.1
NCG, by difference		39.3	36.8	35.7	40.1	37.6	32.0
Bio-oil properties							
Acetic acid conc.		1.6±0.1	1.9±0.1	0.5±0.1	1.0±0.2	0.8±0.1	0.6±0.2
Water		21.1±0.9	17.1±1.3	16.2±0.2	18.9±0.8	14.7±0.7	15.8±0.0
Density		1265.6	1268.9	1299.3	1289.9	1296.0	1300.5
Organic yield (wt%)		41.5	45.3	47.7	42.7	45.0	47.9
[1]H-NMR results, relative to the biomass feed							
Compound/s	**Shift, ppm**	**wt% in bio-oil[1], in brackets: wt% relative to the organic yield**					
Alkanes	0.5-1.6	6.36 (2.64)	8.12 (3.68)	5.86 (2.80)	5.71 (2.44)	8.16 (3.67)	5.71 (2.74)
Acetic acid	1.88	2.71 (1.12)	3.26 (1.48)	2.04 (0.97)	2.17 (0.93)	2.69 (1.21)	2.27 (1.09)
Acetaldehyde	9.58 and 2.08	1.44 (0.60)	2.51 (1.14)	1.5 (0.72)	1.47 (0.63)	2.19 (0.99)	1.35 (0.65)
Hydroxyacetone	4.01	1.65 (0.68)	0.82 (0.37)	1.27 (0.61)	1.31 (0.56)	1.14 (0.51)	1.19 (0.57)
Levoglucosan	3.27,3.84-3.85,4.31-4.33, and 5.13	8.54 (3.54)	7.83 (3.55)	10.16 (4.85)	11.2 (4.78)	9.76 (4.39)	12.88 (6.17)
Tot. phenol and furan derivatives[1]	6.4-7.6	7.26 (3.01)	10.89 (4.93)	7.56 (3.61)	7.6 (3.25)	12.05 (5.42)	6.75 (3.23)
Formic acid	8.10	0.22 (0.09)	0.36 (0.16)	0.18 (0.09)	0.22 (0.09)	0.29 (0.13)	0.21 (0.10)
Glycolaldehyde	9.55	0.06 (0.02)	0.06 (0.03)	0.04 (0.02)	0.05 (0.02)	0.08 (0.04)	0.04 (0.02)
Tot. aldehydes	9.5-10.5	0.61 (0.25)	0.80 (0.36)	0.59 (0.29)	0.62 (0.26)	0.83 (0.36)	0.57 (0.29)

[1]*Includes phenol, syringol, guaiacol, furan, furfural, methyl-2-furoate, and hydroxymethylfurfural*

5.6 References

1. Su, P., Sorption of metal ions to wood, pulp and bark materials, in Chemistry Engineering 2012, Abo Akademi University: Finland. p. 93.
2. Vassilev, S.V., et al., An overview of the organic and inorganic phase composition of biomass. Fuel, 2012. **94**(0): p. 1-33.
3. Oudenhoven, S.R.G., et al., Demineralization of wood using wood-derived acid: Towards a selective pyrolysis process for fuel and chemicals production. Journal of Analytical and Applied Pyrolysis, 2013. **103**(0): p. 112-118.
4. Davidsson, K.O., et al., The effects of fuel washing techniques on alkali release from biomass. Fuel, 2002. **81**(2): p. 137-142.
5. Evans, P.D., P.D. Thay, and K.J. Schmalzl, Degradation of wood surfaces during natural weathering. Effects on lignin and cellulose and on the adhesion of acrylic latex primers. Wood Science and Technology, 1996. **30**(6): p. 411-422.
6. Green, A., Fixed bed pyrolysis optimisation, part 1, S. Pang, Editor. 2009, Chemical and Process Engineering: University of Canterbury. p. 36.
7. Iiyama, K. and A.F.A. Wallis, An improved acetyl bromide procedure for determining lignin in woods and wood pulps. Wood Science and Technology, 1988. **22**(3): p. 271-280.
8. Johnsson, S. and J. Packer, Introduction to the forestry industry, Carter Holt Harvry.

9. Browning, B.L., Determination of lignin, in Methods of wood chemistry. 1967, Interscience Publishers: Appleton. p. 785-823.
10. Maekawa, E., T. Ichizawa, and T. Koshijima, An evaluation of the acid-soluble lignin determination in analyses of lignin by the sulfuric acid method. Journal of Wood Chemistry and Technology, 1989. **9**(4): p. 549-567.
11. Uprichard, J.M. and L. J.A, Influence of tree age on the chemical composition of radiata pine. New Zealand Journal of Forestry Science, 1980. **1**(3): p. 551-557.
12. Berrocal, A., et al., Effect of the tree and on variation of Pinus Radiata: Chemical composition. Journal of the Chilean Chemical Society, 2004. **49**: p. 251-256.
13. Boonstra, M.J. and B. Tjeerdsma, Chemical analysis of heat treated softwoods. Holz als Roh- und Werkstoff, 2006. **64**(3): p. 204-211.
14. Saddawi, A., et al., Commodity fuels from biomass through pretreatment and torrefaction: Effects of mineral content on torrefied fuel characteristics and quality. Energy & Fuels, 2011. **26**(11): p. 6466-6474.
15. Piskorz, J., et al., Pretreatment of wood and cellulose for production of sugars by fast pyrolysis. Journal of Analytical and Applied Pyrolysis, 1989. **16**(2): p. 127-142.
16. Lin, Y., et al., Deoxygenation of bio-oil during pyrolysis of biomass in the presence of CaO in a fluidized-bed reactor. Energy and Fuels, 2010. **24**(10): p. 5686-5695.
17. Scott, D.S., J. Piskorz, and D. Radlein, Liquid products from the continuous flash pyrolysis of biomass. Industrial & Engineering Chemistry Process Design and Development, 1985. **24**(3): p. 581-588.
18. Scheirs, J., G. Camino, and W. Tumiatti, Overview of water evolution during the thermal degradation of cellulose. European Polymer Journal, 2001. **37**(5): p. 933-942.
19. Diebold, J.P., A review of the chemical and physical mechanisms of the storage stability of fast pyrolysis bio-oils. 2000, National Renewable Energy Laboratory: Lakewood, Colorado.
20. Etiégni, L. and A.G. Campbell, Physical and chemical characteristics of wood ash. Bioresour Technol, 1991. **37**(2): p. 173-178.
21. Scott, D.S., et al., Pretreatment of poplar wood for fast pyrolysis: rate of cation removal. Journal of Analytical and Applied Pyrolysis, 2001. **57**(2): p. 169-176.
22. Mourant, D., et al., Mallee wood fast pyrolysis: Effects of alkali and alkaline earth metallic species on the yield and composition of bio-oil. Fuel, 2011. **90**(9): p. 2915-2922.
23. Okuno, T., et al., Primary release of alkali and alkaline earth metallic species during the pyrolysis of pulverized biomass. Energy & Fuels, 2005. **19**(5): p. 2164-2171.
24. Brown, R.C. Selective thermal depolymerisation of biomass. in 20th International Symposium on Analytical and Applied Pyrolysis. 2014. Birmingham, UK.
25. Aho, A., et al., Catalytic pyrolysis of biomass in a fluidized bed reactor: Influence of the acidity of H-beta zeolite. Process Safety and Environmental Protection, 2007. **85**(5): p. 473-480.
26. Nowakowski, D., et al., Potassium catalysis in the pyrolysis behaviour of short rotation willow coppice. Fuel, 2007. **86**(15): p. 2389-2402.
27. Shen, D.K. and S. Gu, The mechanism for thermal decomposition of cellulose and its main products. Bioresour Technol, 2009. **100**(24): p. 6496-6504.
28. McMillan, J.D., Pretreatment of lignocellulosic biomass, in Enzymatic Conversion of Biomass for Fuels Production. 1994, American Chemical Society. p. 292-324.
29. Radlein, D., et al., Fast pyrolysis of pre-treated wood and cellulose, D.o.F.C. American Chemical Society, Editor. 1987, University of Waterloo: Ontario. p. 29-35.
30. Dobele, G., et al., Cellulose dehydration and depolymerization reactions during pyrolysis in the presence of phosphoric acid. Journal of Analytical and Applied Pyrolysis, 1999. **49**(1–2): p. 307-317.

6 Pyrolysis of torrefied biomass

Torrefaction targets a reduction in the free moisture, acetyl content, and oxygen content of biomass, while acid leaching targets the inorganic content. Torrefaction, as a biomass pretreatment method, also breaks hydrogen bonds between biomass polymers to reduce polymeric interactions during subsequent pyrolysis. When torrefaction conditions are severe, water is produced from cleavage of polymer hydroxyl groups. Removal of hydroxyl groups creates carbon-carbon double bonds. Adjacent crosslinks form a stable structure that will not decompose at pyrolysis conditions, but instead undergoes further polycondensation reactions to form char [1]. Crosslinked fragments of cellulose and hemicellulose appear as lignin in the fibre analysis; therefore the degree of crosslinking can be determined by the increase in acid insoluble fibres after biomass hydrolysis [2, 3]. Torrefaction was optimised to improve the biomass properties while limiting carbon-carbon crosslinking. This was achieved by controlling the torrefaction temperature and residence time.

6.1 Torrefaction procedures

6.1.1 Small scale torrefaction for optimisation

Small scale experiments optimised the torrefaction temperature and residence time. A 300 mL Gallenkamp bomb calorimeter, which was also used for high the temperature leaching experiments, was modified for torrefaction experiments. Two ¼ inch Swagelok fittings were welded to the top of the bomb, and these were used to attach carrier gas and exit vapour tubes. A single pass glass condenser was used to condense vapours exiting the reactor; vapours were then filtered into a 100 mL flask with a cotton wool filter at the top to capture any remaining condensables before the non-condensable gases (NCGs) were vented. The piping and instrumental diagram is shown in Figure 6-1 and the actual equipment is displayed in Figure 6-2. The operational temperature and pressure limits for the bomb were 316 °C and 5 MPa respectively, determined by the upper temperature limit of the Kalrez O-ring. The reactor was heated from below using a heated magnetic stirrer. A standard Teflon flea was not strong enough to provide agitation of the biomass, thus a new flea was constructed using 6, 5 mm thick and 15 mm in diameter Samarium cobalt magnets. These have a service temperature up to 250 °C, since the torrefaction temperature exceeded this in various experiments, the magnets were periodically replaced. A paddle was added to the stirrer to provide agitation of the biomass during torrefaction. Without the stirrer, only 20 g of biomass could evenly be reacted, while employment of the stirrer increased this to 30 g per run.

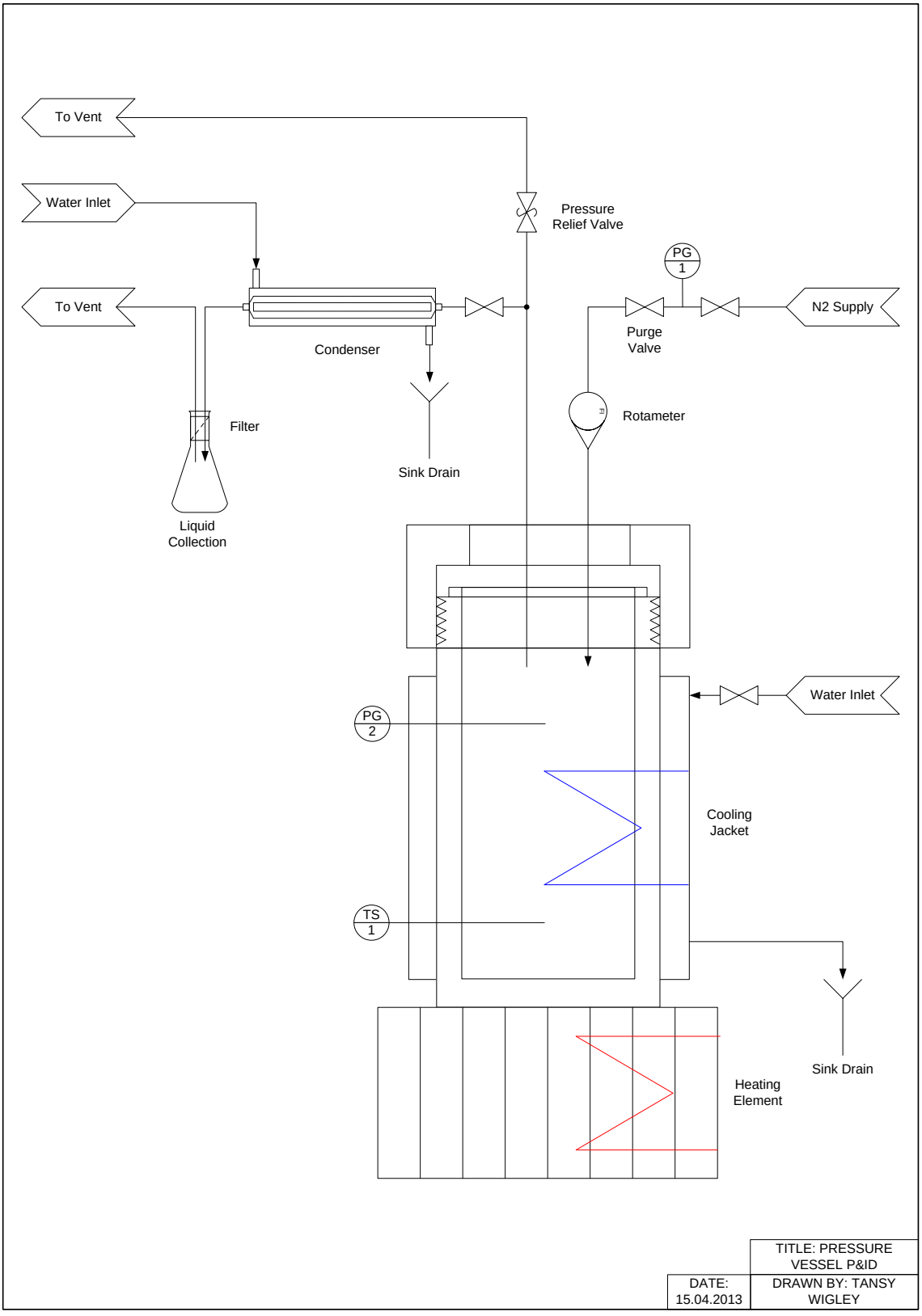

Figure 6-1: Piping and instrumental diagram of modified bomb calorimeter for biomass torrefaction

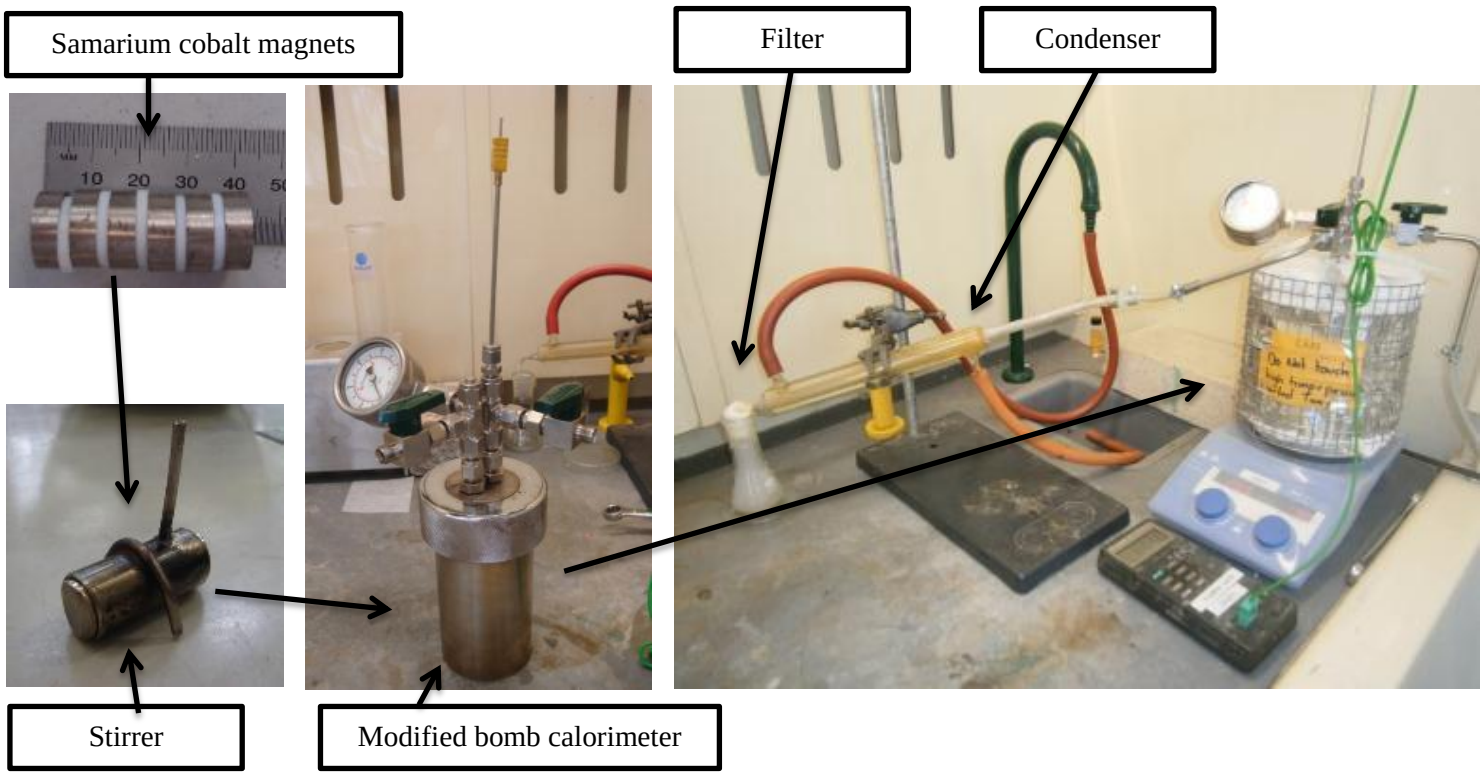

Figure 6-2: Modified bomb calorimeter for torrefaction experiments

6.1.2 Large scale torrefaction

Once torrefaction was optimised, a larger scale torrefaction reactor was designed and constructed to process 200-250 g of biomass per run. A schematic of the scaled-up system is shown in Figure 6-3. The vessel was constructed from schedule 40, nominal bore 125 stainless steel 316 pipe. A 152.4 mm diameter Kleanflow tri ferrule was welded to the top of the vessel to allow a Kleanflow tri clamp to be used for sealing the vessel. The vessel was heated in an oven to the required torrefaction temperature. The 1/4" N_2 feed tube was coiled within the oven to preheat the N_2 before it entered the vessel.

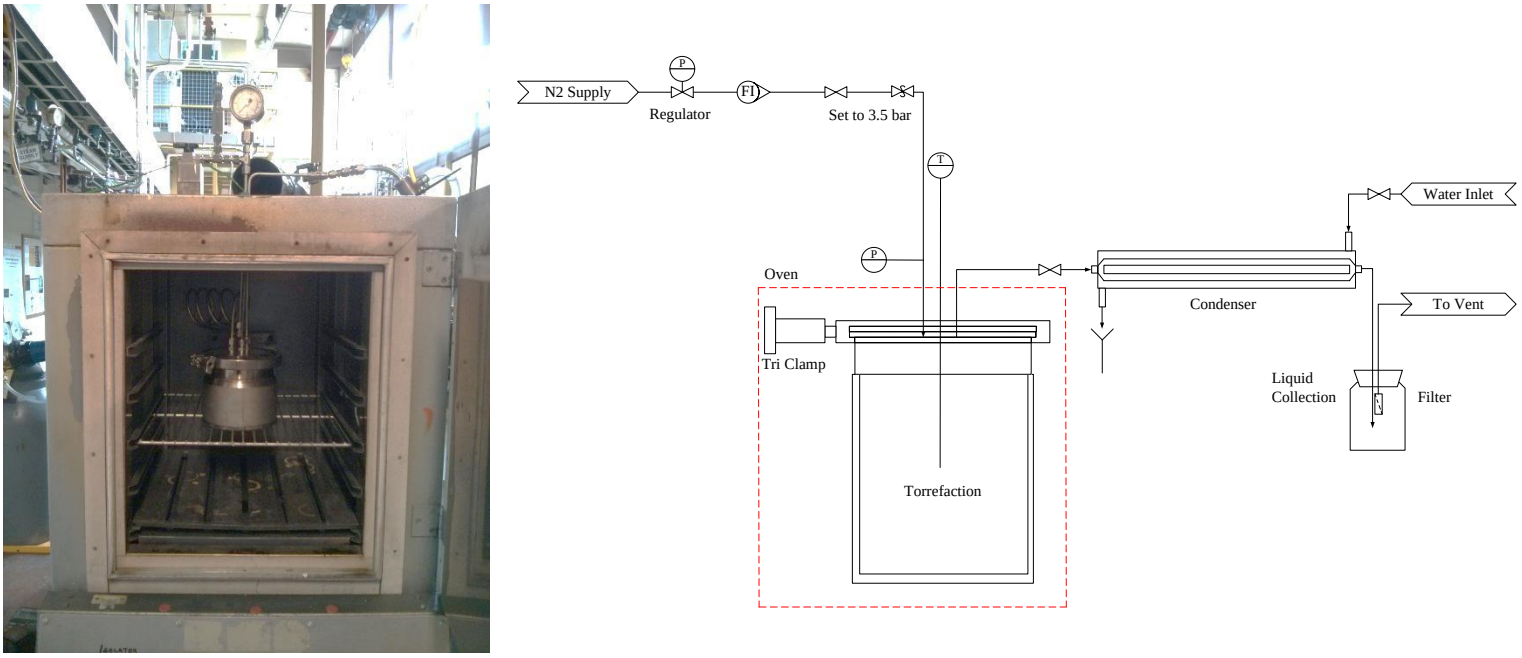

Figure 6-3: Picture and schematic of large scale torrefaction setup

6.2 Biomass moisture content

The moisture content (MC) of biomass should to be mechanically reduced after acid leaching; this reduces the energy required during torrefaction. The majority of free moisture in biomass can be removed mechanically by filtering or pressing [4], while complete drying occurs during torrefaction. The water in biomass can be present either as free water in the cell lumina that is held through capillary forces; as hygroscopic (bound) water which is attached by hydrogen bonds; or as vapour in the cell lumina, but the vapour is minimal at standard conditions. Hydrogen bonds in bound water form between water and negatively charged hydroxyl groups associated with biomass polymers. During drying, the biomass's physical properties change when the moisture content is reduced below the fibre saturation point (approximately 30% at room temperature). Rapid moisture removal at high drying temperatures can cause the cell wall to collapse and irreversible close biomass pores [5], which hinders volatile escape during pyrolysis.

The initial MC in biomass affects the torrefaction severity. Medic *et al.* [6] investigated the effect of the biomass's initial MC on torrefaction and found that moisture increased the torrefaction severity. The yield of condensables produced during torrefaction (excluding water originating from the moisture in the biomass) with MCs of 22 and 44 wt% were not significantly different but were twice that of 3 wt% MC. Medic *et al.* developed Equation 6.1 to predict the mass loss from torrefaction, with respect to temperature and the initial biomass MC. This indicates that torrefaction of biomass with a higher MC can be operated at a lower temperature to obtain the same mass loss. For example, torrefaction at 250 °C with a moisture content of 10 wt% produces a mass loss of 15.7%. This same mass can be achieved for torrefaction at 235 °C when the

initial MC is 30 wt%. Therefore the energy to evaporate the additional moisture can be somewhat offset by the lower torrefaction temperature required.

$$\text{Predicated mass loss (\%)} = 95.68 - 1.0396\text{T} + 0.2491\text{MC} + 0.00284\text{T}^2 \quad (6.1)$$

Where T is the temperature in °C and MC is the biomass initial MC in wt%. This equation was developed for corn stover, thus extrapolating to predict the behaviour of *P. radiata* during torrefaction would incur errors. Corn stover contains more hemicellulose (27.6%) and inorganics (5.2%), but less cellulose (37.4%) and lignin (18.0%) compared to pine [7], making it a more reactive species during torrefaction.

In the present study, torrefaction of biomass was performed at 240 °C for 20 min using *P. radiata* with MCs of 7.5 wt% (humidity in storage) and 25 wt% (assumed as the MC following acid leaching and pressing). Results for the biomass solids yield and structural composition are given in Figure 6-4. These results indicate a slightly higher solids yield was obtained for biomass with a MC of 25 wt%. A high MC could delay the initiation of torrefaction due to the energy required to heat and vaporise water. The sugar yield was lower and lignin yield was higher for biomass with a MC of 25 wt%, which indicates increased severity during torrefaction. The additional moisture may increase the rate of torrefaction reactions due to expansion of water vapour inside the polymer matrix during the temperature ramping stage. This would loosen the material and make it less resistant to heat transfer [6]. But in this case, it would be expected that the biomass yield decreased; therefore it is most likely that variations were minimal within the uncertainty range. Water may also catalyse cleavage of the oxygenated branches associated with hemicellulose and lignin; although this appears minimal as the acetyl yield remained constant. Based on the above observations, it was concluded that biomass moisture has negligible effect during torrefaction of *P. radiata* due to the lower inorganic and hemicellulose content compared to corn stover. A MC of 25 wt% was therefore used for all subsequent torrefaction experiments to represent achievable MCs after acid leaching. Consistency was required as the MC effects the liquid properties and may have an effect on the biomass's structure.

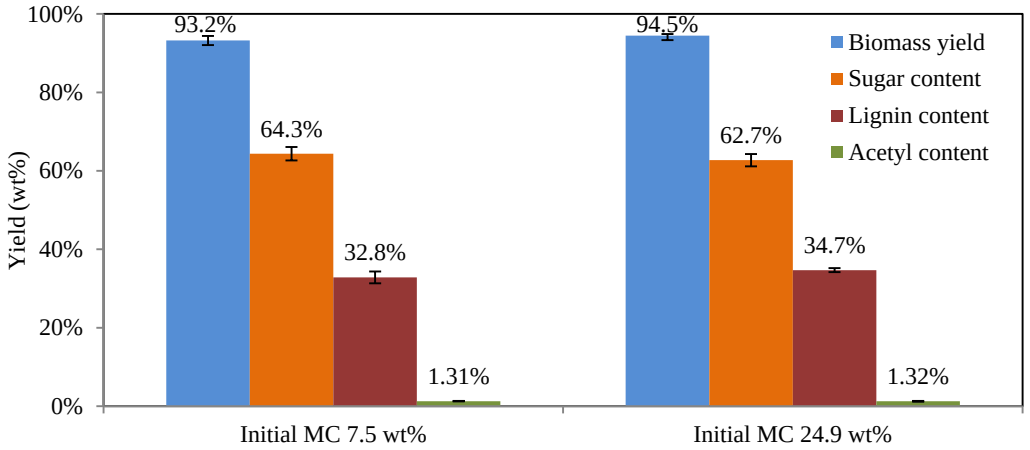

Figure 6-4: Torrefaction at 240 °C of biomass with a low and high moisture content

6.3 Optimising torrefaction residence time

The residence time for biomass torrefaction at 245 °C was varied between 15-120 min. Results displayed in Figure 6-5 give the biomass yield and the structural composition of the biomass following torrefaction. In the figure, results for 0 residence time represent raw biomass. It was found that the acetyl content decreased as the residence time was extended up to 120 min; however the decrease was not sufficiently large to warrant an extension beyond 20 min due to the additional heating costs and a decrease in the biomass carbohydrate content. Incomplete moisture removal may occur when residence times are short, thus 20 min was considered the optimal residence time during torrefaction.

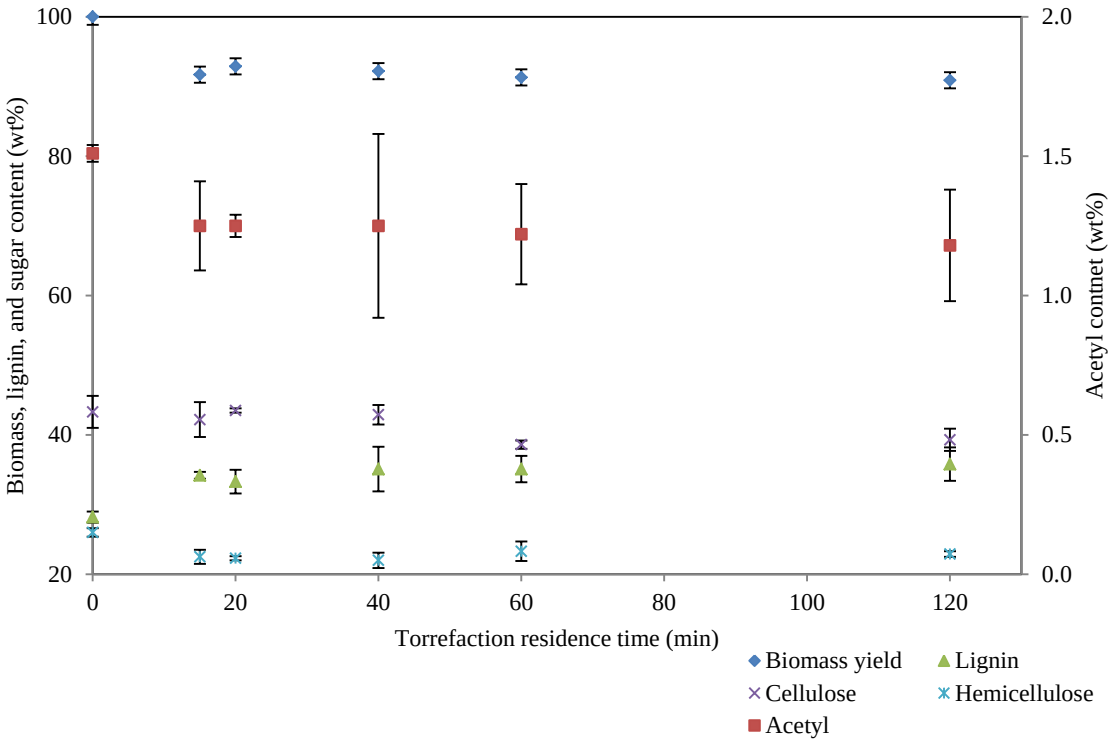

Figure 6-5: Torrefaction yields and biomass fibre analysis when varying the residence time of torrefaction at 245 °C

6.4 Optimising torrefaction temperature

One of the torrefaction targets was to reduce the highly oxygenated side braches associated with hemicellulose and lignin, particularly carboxyl compounds. It was reported that a higher torrefaction severity, achieved by increasing the reaction temperature, would enhance cleavage of acetyl branches associated with hemicellulose galactoglucomannans [8, 9]. In the present study, torrefaction temperature was investigated and optimised between 220-290 °C for 20 min. Biomass yields and the structural composition following torrefaction are shown in Figure 6-6. The results indicate that the acetyl content was reduced from 1.51 wt% in raw biomass to 0.43 wt% for biomass torrefied at 290 °C for 20 min. Mild pyrolysis occurs when torrefaction conditions are

severe, thereby decreasing the overall potential bio-oil yield during subsequent pyrolysis. Furthermore, severe torrefaction causes the formation of crosslinked carbohydrate polymers that are stable during pyrolysis conditions, leading to char formation instead of further polymeric breakdown to bio-oil vapours. This effect was quantified by the 'apparent' increase in lignin after a full acid hydrolysis of the biomass as crosslinked sugar polymers are acid insoluble. At 290 °C, the total 'apparent lignin' content reached 59 wt%. True lignin is hard to depolymerise during torrefaction, with only a small release of phenolic compounds [5], thus the high 'apparent' lignin content was the combinations of true lignin and crosslinked carbohydrate polymers.

The biomass yield decreased significantly as the torrefaction severity increased. Minimal polymer degradation occurred for mild torrefaction (<220 °C), which was dominated by non-reactive drying and particle shrinkage. This was followed by reactive drying; bond breaking; volatilisation of lipophilic extractives [10]; and volatilisation of other light compounds that did not hydrogen bond such as fatty acids, sterols, and terpenes [5]. When the severity of torrefaction was increased to the moderate range (220-250 °C), hydrogen, C-O, and C-C bonds started to break. Higher molecular weight compounds started to form. Typical compounds released included water, light volatiles, alcohols, aldehydes, ethers, organic acids, and NCGs [5]. Severe torrefaction (>250 °C) was associated with the majority of hemicellulose decomposing, with cellulose and slight lignin decomposition initiating [11]. When the temperature reached 290 °C, hemicellulose was completely decomposed.

Results from the structural analysis of torrefied biomass show that the acid-soluble fraction of lignin increased from 1.0±0.2% for raw biomass to 2-3% for torrefied biomass. This was possibly due to the formation of compounds during hydrolysis that had the same UV-Visible absorbance as acid soluble lignin but were produced from hydrolysis of crosslinked cellulose and hemicellulose polymers. Alternatively, the acid soluble lignin content could indicate the partial degradation of lignin during torrefaction, which may increase the acid soluble fraction. Compound such as syringic, vanillic, and *p*-hydroxybenzoic acids represent a significant part of the acid soluble fraction [12], and cleavage during hydrolysis of these compounds may increase after lignin was partially depolymerised during torrefaction.

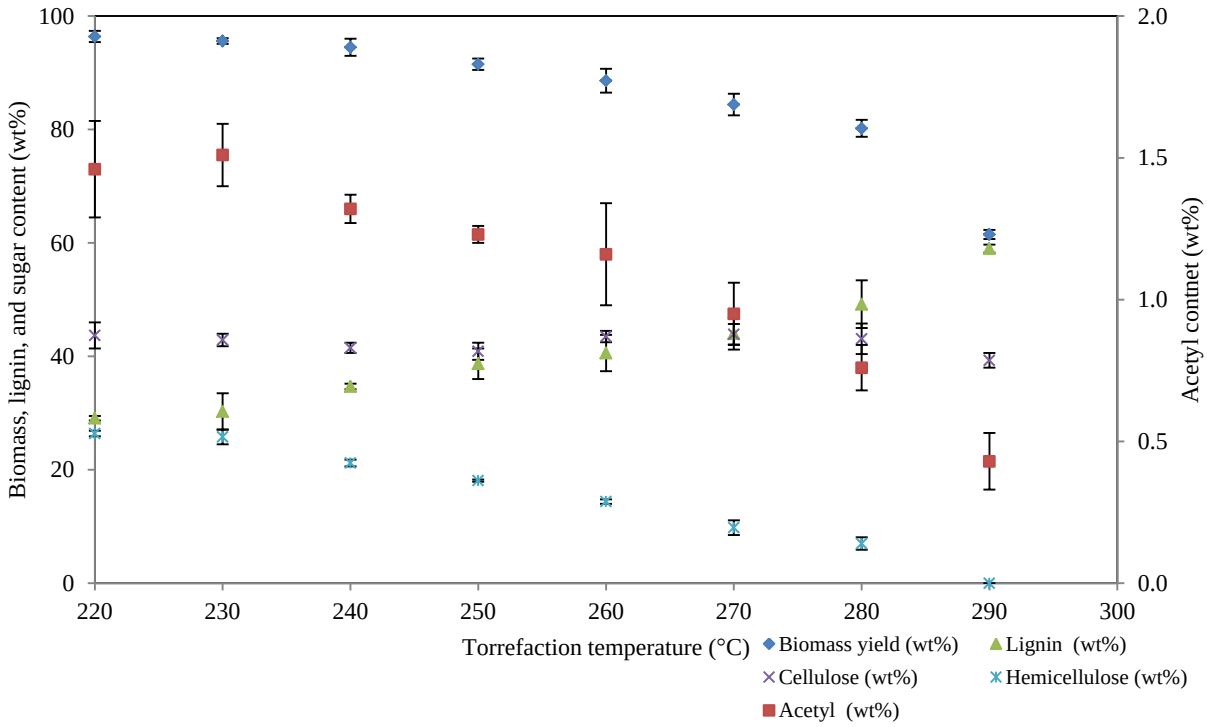

Figure 6-6: Effect of temperature during torrefaction for 20 min

The results from this research were compared to results for torrefaction of pine reported by Zheng *et al.* [13], Haoxi and Ragauskas [14], and Westover *et al.* [10] as shown in Figure 6-7. All results follow similar trends; with any discrepancies though to originate from the biomass type and the method for measuring the reactor temperature. Westover *et al.* [10] stated that 95% of the biomass was within 10 °C of the specified torrefaction temperature, but Figure 6-6 indicates that 10 °C change can have a significant impact on the torrefaction yields and biomass composition following torrefaction.

To illustrate the effect of different reactor systems, preliminary torrefaction experiments were carried out in two different reactors. These were the fast pyrolysis reactor used in this research operating as a fixed bed (operating at torrefaction temperatures) and a torrefaction auger at CRL Energy, Upper Hutt, New Zealand. For torrefaction at 300 °C for 20 min, the fixed bed yielded 61.6 wt% of torrefied biomass, while the auger reactor yielded 55.7 wt% of torrefied biomass. The variance in the yields between these systems was significant, which was attributed to the non-uniform internal temperature distribution in the auger reactor. These results were excluded in this thesis; however they indicate the variability across systems and emphasises limits when comparing results from different processes.

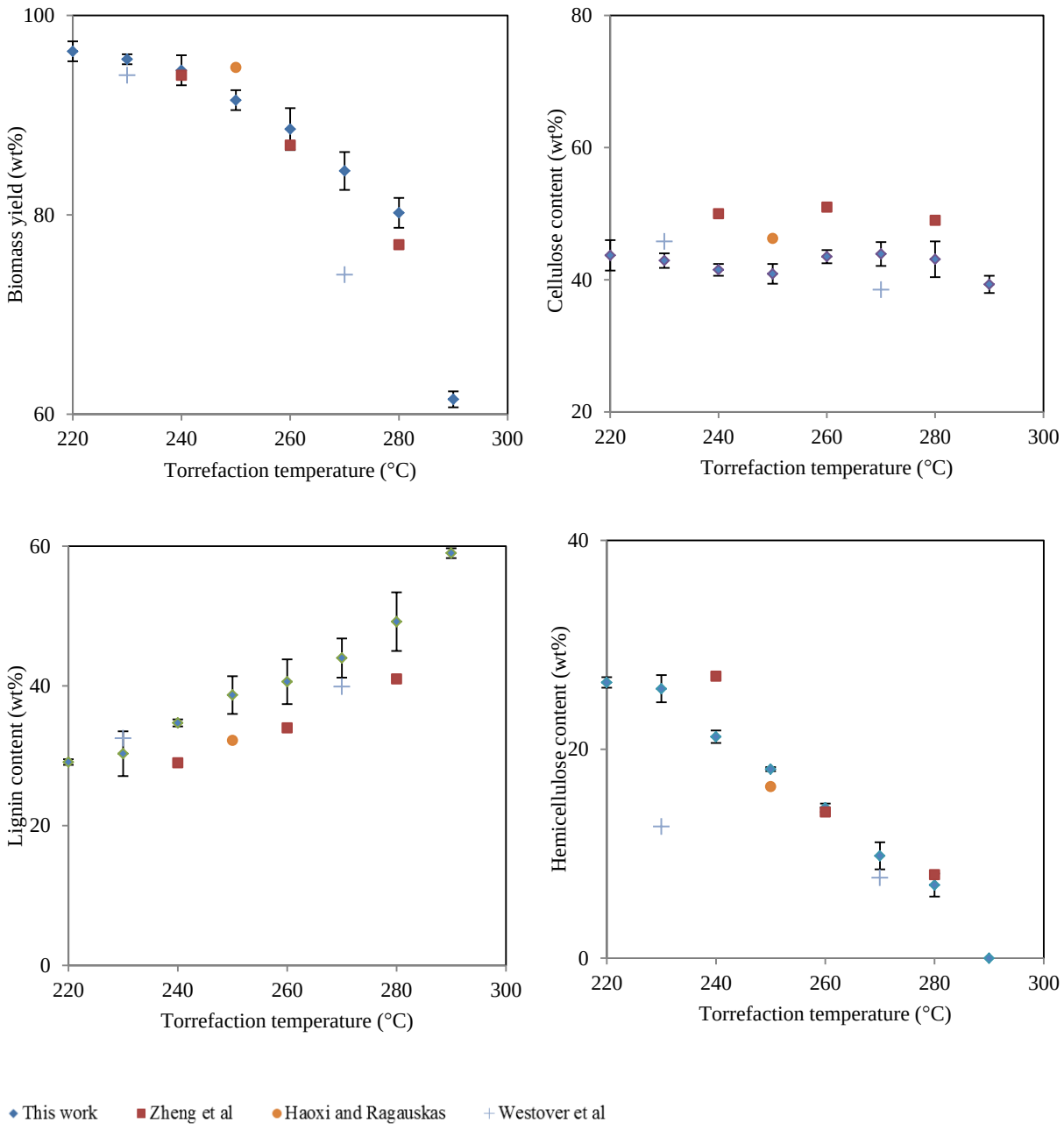

Zheng et al. [13]: torrefaction of pine for 40 min, results on wet basis. Haoxi and Ragauskas [14]: torrefaction of Loblolly pine for 25 min, results dry basis. Westover et al. [10]: torrefaction of Southern pine for 30 min, results dry basis.

Figure 6-7: Comparison of torrefaction yield and biomass composition for torrefied pine wood

An elemental analysis of the torrefied biomass is given in Table 6-1 at the different torrefaction temperatures. Elemental analysis was another method used to quantify the severity of torrefaction and also provides an indication on the oxygen reduction relative to the hydrogen reduction. Because pyrolysis is a hydrogen deficient process [15], the removal of oxygen through the production of water is undesirable during pretreating; furthermore, such removal leads to severely crosslinked biomass. Most research suggests that there is no chemical elimination of water from biomass when torrefied below 220 °C [16], thus hydroxyl groups are not

removed from sugar polymers to produce a crosslinked structure. However, carboxyl cleavage from hemicellulose and oxygen reduction was minimal in this low temperature regime. Higher torrefaction temperatures were required for significant acetyl reduction and oxygen reduction, as well as to breakdown the fibrous biomass structure. The optimum torrefaction temperature was proposed to be approximately 250 °C to prevent significant biomass loss during torrefaction (<10%) and to minimise the char yield from pyrolysis of the torrefied biomass. The torrefaction temperature could be increased to a maximum of 280 °C (before hydrogen loss becomes significant) if oxygen reduction and acetyl removal were considered more important than maintaining high bio-oil yields during subsequent pyrolysis. Significant oxygen reduction, however, was difficult to achieve during torrefaction without severe biomass loss. For example, after torrefaction at 290 °C with a biomass yield of 65.3 wt%, the oxygen content only decreased to from 43.1 to 35.7%. Therefore, it is suggested that torrefaction alone is not a suitable method to obtain a low oxygen bio-oil at reasonable yields.

Table 6-1: Elemental analysis of biomass after torrefaction at varying temperatures

Temperature (°C)	Carbon (%)	Hydrogen (%)	Nitrogen (%)	Oxygen (%)
Raw	50.4 ± 0.7	6.0 ± 0.2	0.10 ± 0.00	43.1 ± 0.8
220	51.1	5.9	0.09	42.9
230	51.1	6.0	0.11	42.8
240	51.5	5.9	0.11	42.5
250	52.4	5.9	0.11	41.6
260	53.4	5.9	0.11	40.6
270	54.8	5.9	0.11	39.3
280	55.9	5.8	0.11	38.2
290	58.7	5.6	0.09	35.7

6.4.1 Liquid and NCG composition

The solids, liquid, and NGC yields from torrefaction are displayed in Figure 6-8 for torrefaction between 230-280 °C, for 20 min. The liquid yield was underestimated due to residue remaining in the condenser following torrefaction, leading to large uncertainties when analysing torrefaction liquor. During torrefaction, hemicellulose was decomposed thermally and chemically via acid and free radical reactions [5]. These reactions produced many compounds, such as furfural, acetic acid, and water. Boardman *et al.* [5] stated that the water released may enhance further depolymerisation of hemicellulose, but results in Section 6.2 for varying the MC of *P. radiata* indicate minimal change to the severity of torrefaction in the presence of water; therefore decomposition was predominately through acid enhanced cleavage and thermal decomposition. The compounds produced during torrefaction at 240 °C for 20 min were determined qualitatively for 4 different samples using GS-MS, with results given in Table 6-2. Solid-phase microextraction (SPME) was used for sample injection, thus results are not quantitative, but do indicate the presence of hexanoic, heptanoic, octanoic, and nonanoic acid, which would enhance the ion exchange capacity of the torrefaction liquor when it is recycled as the leaching reagent.

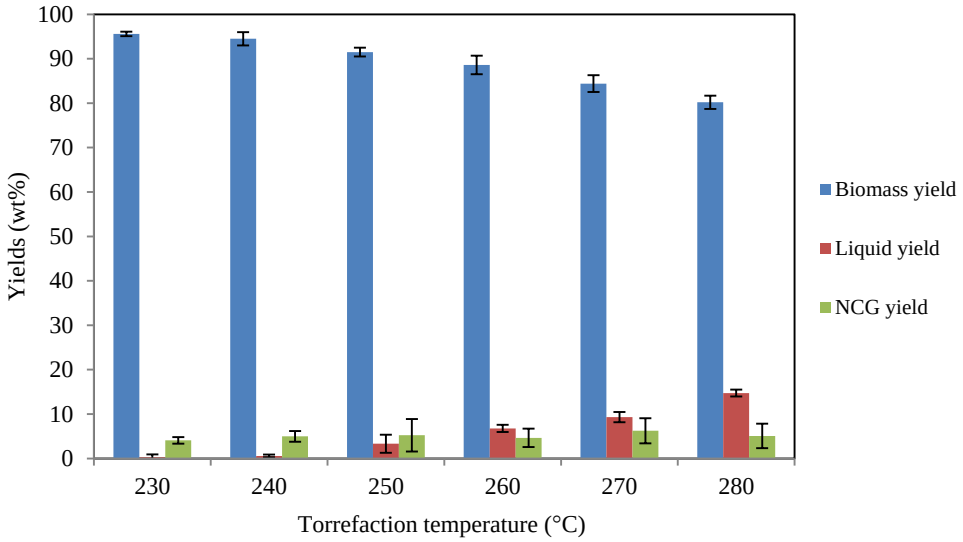

Figure 6-8: Torrefaction yields at different reaction temperatures

The torrefaction liquid composition is highly dependent on the biomass type, as biomass sources with a higher hemicellulose and inorganic content react at lower temperatures. Softwoods have a proportionally lower acetyl content compared to hardwoods; therefore would be expected to produce less acetic acid during torrefaction, and decomposition would be expected to be less significant. The acidity of the torrefaction liquors was quantified by pH. Additionally, the acetic acid, formic acid, and methanol concentration was quantified by HPLC, with results displayed in Figure 6-9. From the figure, it was found that the acetic acid, formic acid, and methanol concentrations in the torrefaction liquor increased with increasing torrefaction temperature.

The acetic acid concentration in the torrefaction liquor is dependent on the quantity of acetyl groups present in hemicellulose. Chang *et al.* [2] used Spruce (softwood) for torrefaction. No formic acid was detected but the acetic acid concentration in the torrefaction liquor was 6.06 wt% for torrefaction at 280 °C, compared to 17.2 wt% measured in this research. Spruce wood has an average acetyl content of 1.3% [17] which is comparable to 1.51 wt% for *P. radiata*. The large discrepancy between the acetic acid concentrations can be related to the severity of the torrefaction processes. Chang *et al.* used an auger reactor with a residence time of 10 min, from which the biomass yield for torrefaction at 280 °C was 93%; this is comparable to torrefaction at 250 °C in this research, which contained 7.8 wt% acetic acid, this is similar to the 6.06 wt% observed by Chang *et al.*. Prins *et al.* [18] used Larch (softwood) for torrefaction and noted that more formic acid was produced than acetic acid. The formic acid concentrations were 0.3, 0.7, and 0.9% for torrefaction at 230, 250 and 270 °C, respectively. These values are comparable to those found in this research, as shown in Figure 6-9 of 0.2, 0.7, and 1.0 wt% for the same torrefaction temperatures, respectively. Larch has an acetyl content of only 0.5% [17]; therefore a lower acetic acid concentration in the liquid would be expected.

Table 6-2: Qualitative results for GS-MS of torrefaction liquor produced at 240 °C for 20 min

	Sample 1		Sample 2		Sample 3		Sample 4	
Compound	Area (%)	Match (%)	Area (%)	Match (%)	Area (%)	Match (%)	Area (%)	Match (%)
Methyl acetate	1.61	98	1.99	98	1.44	97	1.41	97
Methanol	0.67	99	0.73	99	0.48	99	0.46	100
Ethanol	0.00	98	0.70	98	2.65	98	2.54	98
2,3-Butanedione	3.20	98	4.07	98	1.41	98	1.34	98
2-Butenal	2.09	98	2.32	98	1.35	98	1.43	98
2,3-Pentanedione	1.62	97	1.75	98	-	-	0.96	98
Hexanal	0.50	94	0.54	96	1.16	96	1.12	96
2-Pentenal, (E)-	1.02	95	1.09	96	0.79	96	0.87	96
1-Pentanol	1.04	97	1.05	97	0.96	97	1.01	97
Acetic acid	2.54	98	2.64	98	3.52	98	2.07	98
1-Heptanol	1.96	93	1.78	95	1.69	94	1.82	93
Furfural	30.03	97	31.48	98	25.42	96	25.34	96
Benzaldehyde	2.01	98	1.83	98	1.59	98	1.87	99
Furfuryl acetate	0.56	92	0.53	93	0.82	95	1.06	95
1-Octanol	1.75	97	1.50	97	1.22	96	1.29	97
5-Methyl furfural	5.17	94	4.89	94	5.66	95	5.91	95
Methyl 2-furoate	0.89	97	0.83	97	1.33	96	1.49	97
Nopinone	1.54	88	1.32	89	1.17	87	1.20	88
Myrtenal	1.16	96	1.17	95	1.04	97	1.12	96
Furfuryl alcohol	2.28	87	2.24	87	6.07	93	5.99	93
α-Terpineol	2.54	96	2.18	96	1.62	96	1.72	96
Myrtenol	1.48	96	1.35	96	0.96	96	1.02	96
Hexanoic acid	2.32	94	2.14	93	1.93	98	2.06	98
Guaiacol	1.28	98	1.11	98	3.07	98	3.26	98
Octanoic acid	1.84	97	1.33	97	1.63	97	1.59	97
Nonanoic acid	1.14	92	0.79	94	0.89	94	1.05	95

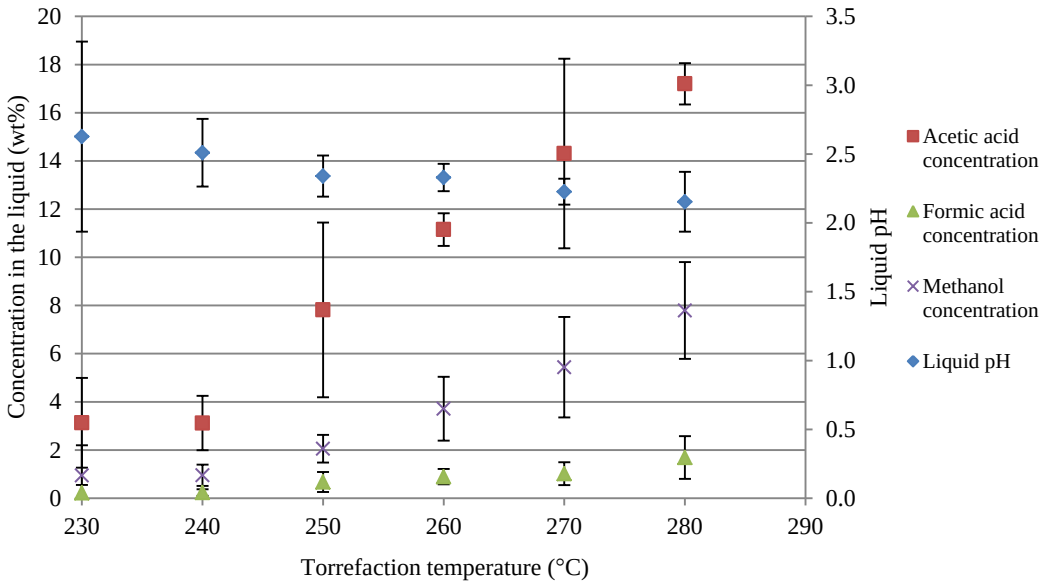

Figure 6-9: pH and concentration of compounds in the torrefaction liquor

The NCG produced during torrefaction was analysed for torrefaction temperatures between 230 and 270 °C. The NCG compositions are displayed in Figure 6-10. From the figure, it was observed that the CO concentration in the gas stream increased and the CO_2 concentration decreased at higher torrefaction temperatures. These same trends were reported by Chang *et al.* [2]. CO_2 is primarily formed through decarboxylation of hemicellulose while CO is formed from secondary reactions of CO_2 with steam or from the decarbonylation of liquids produced during torrefaction [2].

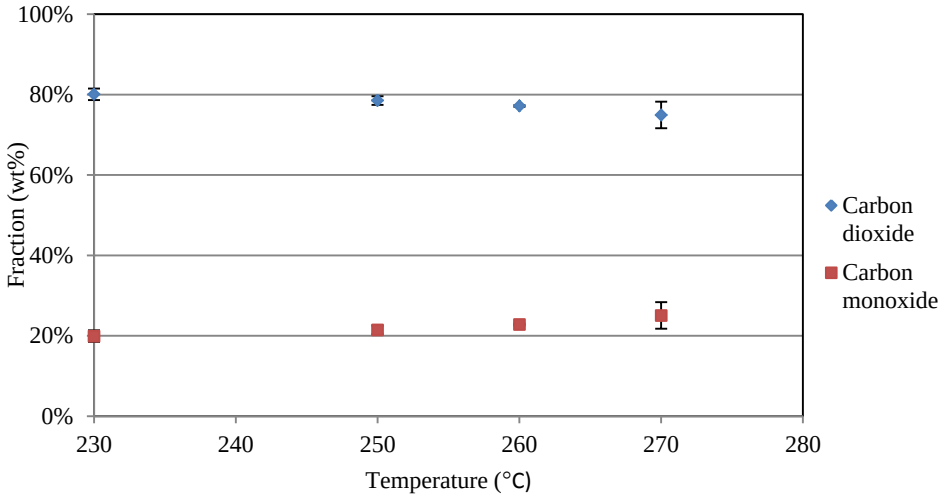

Figure 6-10: NCG composition for torrefaction between 240-270 °C

6.4.2 Pyrolysis of torrefied biomass

It has been reported that pyrolysis of torrefied biomass improves the bio-oil's quality by reducing the water, oxygen, organic acids, and light compounds in bio-oil [19]. Meng *et al.* [20] observed that the bio-oil was rich in pyrolytic lignin and anhydrosugars, while low in light oxygenates and aldehydes. Chang *et al.* [2] reported that the levoglucosan yield increased with torrefaction, and speculated that this was caused by the reduction of catalytic interactions between the major biomass components resulting from a reduction in hydrogen bonds between polymers. Westerhof *et al.* [21] pyrolysed torrefied pine wood and found that the sum of the torrefaction liquid and the bio-oil yield was equal the bio-oil yield of raw wood when torrefaction temperatures were below 290 °C.

In the present study, biomass torrefied between 230-290 °C for 20 min was pyrolysed at the standard pyrolysis conditions, as described in Section 3.3. The yields of bio-oil, NCGs, and char are given in Figure 6-11. From the figure it was found that, in general, increasing the torrefaction temperature decreased the bio-oil yield and increased the char yield. The bio-oil yield increased slightly with mild torrefaction in comparison with bio-oil produced from raw biomass. This was probably due to reduced catalytic interactions between the biomass polymers during pyrolysis of torrefied biomass [2].

Pyrolysis of torrefied biomass between 250-280 °C yielded approximately the same bio-oil as pyrolysis of raw biomass, but increasing the torrefaction temperature to 290 °C decreased the bio-oil yield. The char yield increased for all torrefied samples, due to carbon-carbon crosslinks formed during dehydration of carbohydrate polymers during torrefaction. Overall and total yields of bio-oil, char, and NCGs are given in Figure 6-12. The overall bio-oil yield takes into account the mass loss during torrefaction while the total yields are the sum of the torrefaction and pyrolysis liquid products. The bio-oil production decreased with increasing torrefaction temperature but the overall liquid yield increased for most torrefaction temperatures, indicating again, that torrefaction altered the structure of the biomass to reduce interactions between biomass polymers. Volatiles exiting the biomass particle interact less with other polymers and vapours when the biomass structure is slightly disturbed [22].

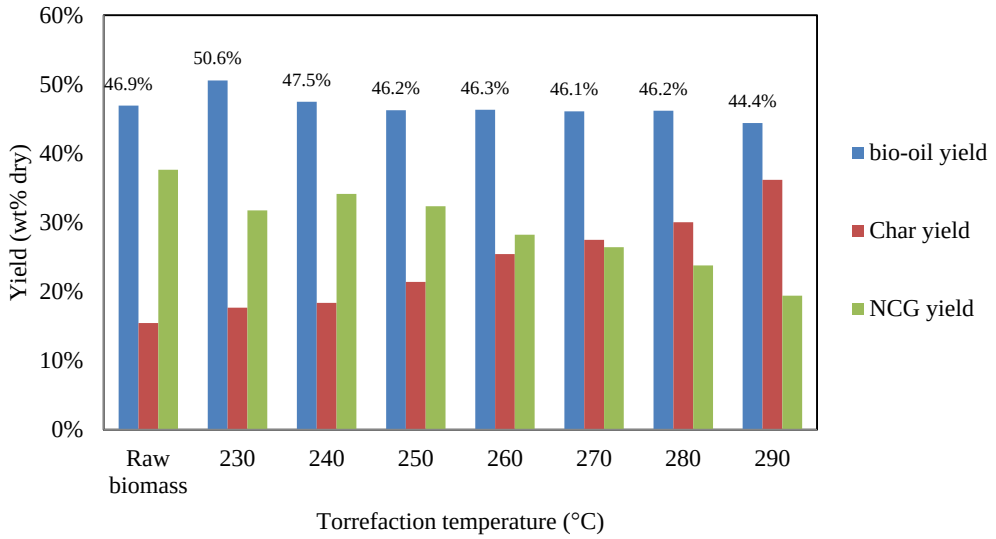

Figure 6-11: Yield from pyrolysis of torrefied biomass

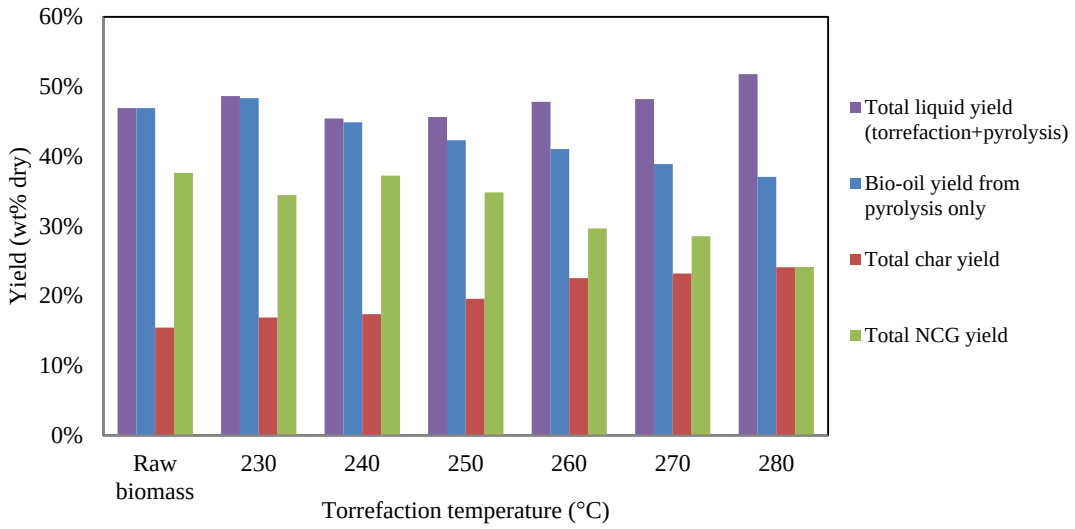

Figure 6-12: Overall yields, taking into account the mass loss during torrefaction

The reduction in bio-oil for pyrolysis of torrefied biomass is partly due to the removal of light organics during torrefaction. However, the reduction is acceptable if the bio-oil quality improves. This was assessed in terms of the composition, molecular weight distribution, and oxygen content of the bio-oil. Key bio-oil properties are given in Table 6-3. The acetic acid concentration in the bio-oil decreased significantly after the torrefaction temperature increased to 260 °C. The acetic acid in bio-oil may come from reactions of moisture in biomass; cleavage of the acetyl content in the biomass; secondary interactions between sugar polymers; and possibly from hemicellulose decomposing to form acetic acid.

As previously discussed in Section 6.4 for Figure 6-6, torrefaction up to 230 °C did not reduce the biomass's acetyl content. However, there was still a decrease in the acetic acid content of the bio-oil from pyrolysis of biomass torrefied at 230 °C. Bio-oil from pyrolysis of dry, raw biomass contained 3.6 wt% acetic acid

(Chapter 4); therefore moisture removal from the torrefied biomass cannot be the reason for reduced acetic acid concentration in the bio-oil. Torrefaction up to 230 °C also had minimal effect on the biomass composition: indicating that reduced interactions between biomass polymers following torrefaction decreased secondary reactions. The reduction in pyrolytic water to under 10 wt% following torrefaction confirms a reduction in secondary reactions, as the water content of bio-oil produced from dry biomass was 12.0 wt%, although dehydration of the sugar polymers during torrefaction could also account for this [1]. Cellulose and hemicellulose are sealed by lignin in raw biomass, and primary products such as levoglucosan are diffusionally restricted from escaping the reaction zone [23]. Torrefaction can enhance biomass pores size, reduce hydrogen bonding between polymers to facilitate volatile removal during pyrolysis, thus reduce secondary reactions that produce water as a by-product.

Pyrolysis of biomass torrefied at 290 °C produced a bio-oil with the lowest water and acetic acid content. Due to the high viscosity of this bio-oil, not all analytical tests could be carried out. The organic yield for this bio-oil was still high, but due to the significant mass loss during torrefaction, the overall organic yield was only 27.1 wt%; therefore torrefaction at or above 290 °C is not recommended. Torrefaction temperatures up to 280 °C produced the same overall organic yields as for pyrolysis for raw biomass, but the highest organic yields were found from pyrolysis of torrefied biomass between 230-270 °C.

Carbon-carbon crosslinking during torrefaction may increase the average molecular weight of bio-oil samples. The molecular number (Mn), molecular weight (Mw) and the molecular size (Mz) were assessed using GPC, with average values in Table 6-3 and Mw distribution curves given in Figure 6-13. These results indicate that there was no substantial change to the average number, weight, or size of the bio-oil compounds following torrefaction but the Mw distribution curves in Figure 6-13 indicate a slightly different relationship between torrefied and raw samples. The fraction of the bio-oil with a molecular weight of 174 $gmol^{-1}$ was less for all torrefied samples compare to that of raw bio-oil, and the small peak at 222 $gmol^{-1}$ was observed for raw bio-oil disappeared for torrefied samples. On the other hand, a peak at 255 $gmol^{-1}$ was present for torrefied samples. The compounds >650 $gmol^{-1}$, which were considered the pyrolytic lignin fraction, decreased. This decrease was reported previously [21, 24]. Westerhof *et al.* [21] though it was due to lignin partially crosslinking during torrefaction, and forming char during pyrolysis, instead of vapour. When biomass polymers form adjacent carbon-carbon crosslinks during torrefaction, it is thought that this structure is stable at pyrolysis conditions and will not break down further; therefore forms char and prevents the formation of large molecular weight compounds that would have otherwise formed [22]. The decrease could also be due to reduced secondary polymerisation reactions occurring for pyrolysis of raw biomass, probably due to the reduction of acetic acid and water in the vapour stream.

The results from an ultimate analysis of the bio-oil samples are given in Table 6-3. These results show an increased carbon content but decreased hydrogen and oxygen contents in the bio-oil following torrefaction. The

decrease in hydrogen and oxygen originates predominately from the reduced MC of the biomass, the bio-oil oxygen content only decreases from 41.9 to 40.5% (dry basis) for torrefaction at 280 °C. This indicates that even severe torrefaction only reduces the oxygen content slightly in the organic bio-oil fraction, although the total oxygen content does decrease, and this is what the bio-oil actually contains.

Table 6-3: Analysis of bio-oil produced from pyrolysis of torrefied biomass

Torrefaction temp. (°C)	**0 (raw)**	**230**	**240**	**250**	**260**	**270**	**280**	**290**
Bio-oil properties								
Acetic acid conc. (%)	3.5±0.4	2.6±0.3	2.6±0.1	2.7±0.5	1.5±0.2	0.6±0.4	0.7±0.1	0.6±0.2
Water (wt%)	24.0±1.2	9.8±1.2	9.9±1.2	9.5±0.8	8.1±0.8	6.1±0.3	3.7±1.8	1.1±0.2
Density (kgm^{-3})	1210	1270	1268	1251	1286	1281	1290	-
Dynamic viscosity (cP)	37.0	214.6	245.1	371.1	414.2	571.4	783.1	-
Organic yield (wt%)	35.5	45.6	42.8	41.9	42.6	43.3	44.5	43.9
Overall organic yield[1] (wt%)	35.5	43.6	40.4	38.3	37.7	36.5	35.7	27.1
GPC results								
Average number, Mn ($gmol^{-1}$)	246.4±3.1	244.5	245.4	238.9	241	238.4	242.5	-
Weight average, Mw ($gmol^{-1}$)	327.6±11.0	323.3	321.8	324	325	310.7	321.7	-
Size average, Mz ($gmol^{-1}$)	470.9±33.5	459.3	444.9	501.8	504.5	429.9	467.4	-
>650 $gmol^{-1}$ (%)	8.10±1.06	7.08	7.12	7.66	7.09	6.02	6.76	-
Ultimate analysis								
Wet basis								
Carbon (%)	39.1±1.4	48.3	47.0	46.7	49.4	49.1	51.0	-
Hydrogen (%)	7.3±0.6	6.5	6.8	6.6	6.6	6.7	6.6	-
Nitrogen (%)	0.3±0.2	0.3	0.7	0.3	1.0	0.7	0.1	-
Oxygen, by difference (%)	53.2±1.2	44.9	45.5	46.4	43.0	43.5	42.3	-
Dry basis								
Carbon (%)	51.5	53.5	52.2	51.6	53.7	52.3	52.9	-
Hydrogen (%)	6.2	6.0	6.3	6.2	6.3	6.4	6.4	-
Nitrogen (%)	0.4	0.3	0.8	0.3	1.1	0.7	0.1	-
Oxygen, by difference (%)	41.9	40.2	40.7	42.0	39.9	40.5	40.5	-
Higher heating value ($MJkg^{-1}$)	20.9±0.8	21.6	21.4	20.9	22.1	21.6	21.9	-
Overall energy in bio-oil[2] (MJ)	7.4	9.4	8.6	8.0	8.3	7.9	7.8	-

[1]Taking into account the mass loss during torrefaction [2]Per kg of biomass feed

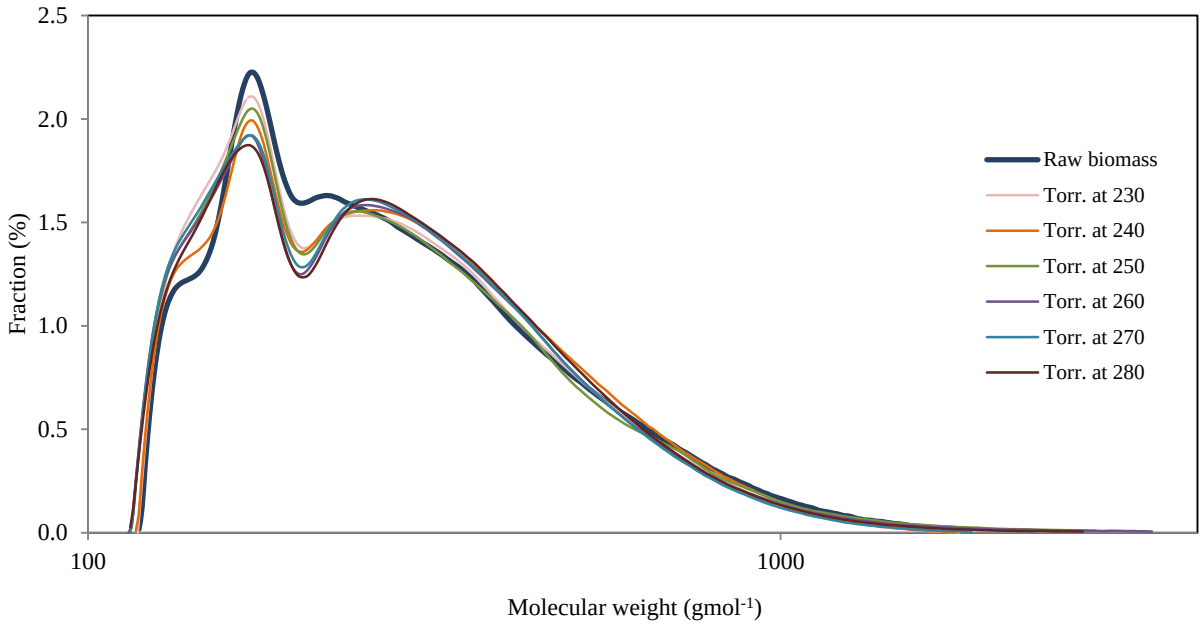

Figure 6-13: Molecular weight distribution curves for raw and torrefied bio-oil samples

The bio-oil's composition from pyrolysis of raw and torrefied biomass was determined by ^{1}H-NMR. The ^{1}H-NMR results for compound concentrations are given in Figure 6-14 on a water free basis and in Figure 6-15 relative to the dry biomass feed rate. Yields relative to the biomass feed (Figure 6-15) indicate that acetic acid, hydroxyacetone, and formic acid decreased with increasing torrefaction temperature while levoglucosan and total aromatics compounds increased. Similar results were reported by Westerhof *et al.* [21] for pyrolysis of torrefied pine wood and Ren *et al.* [25] for pyrolysis of torrefied Douglas fir. Aromatics increased due to the higher lignin fraction in the biomass following torrefaction and dehydrated cellulose forming furans during pyrolysis. Slight depolymerisation of lignin may also enhance thermal decomposition to encourage aromatic release over char formation. There was no significant change to the aldehyde fraction, which was also observed by Zheng *et al.* [1]. Overall, the composition of the bio-oil was improved following biomass torrefaction.

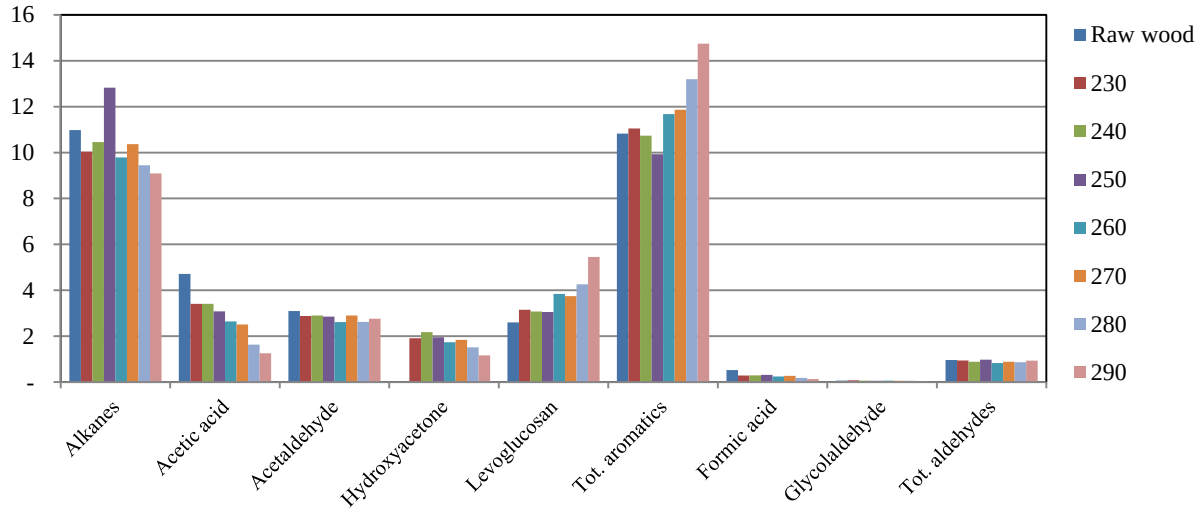

Figure 6-14: ^{1}H-NMR peak area for bio-oil composition, water free basis

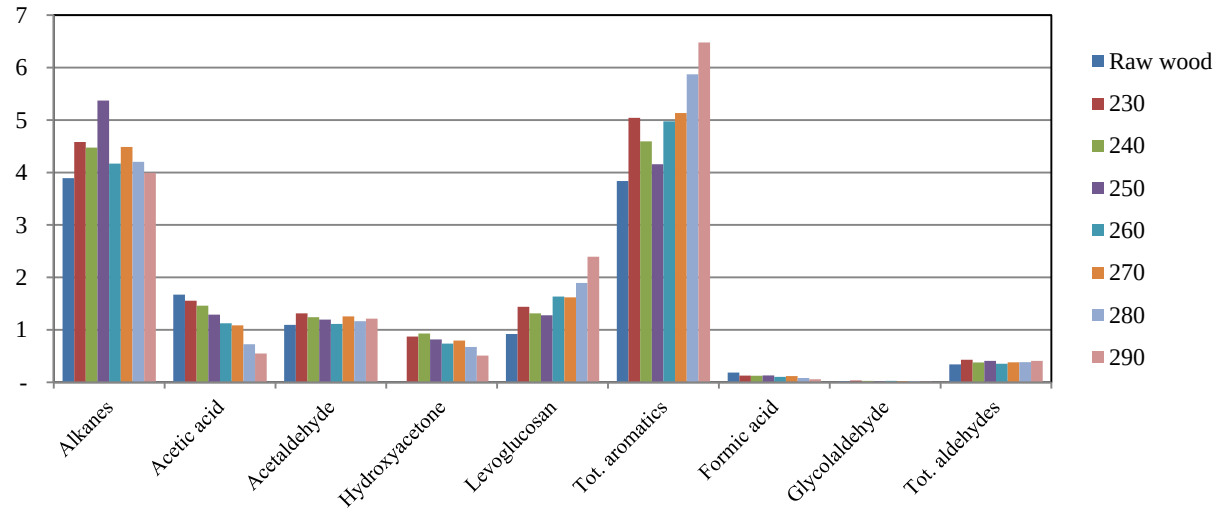

Figure 6-15: ^{1}H-NMR peak area for bio-oil compounds, relative to biomass feed

6.5 References

1. Zheng, A., Zhao, Z., Chang, S., Huang, Z., Wang, X., He, F., *et al.*. (2012). Effect of torrefaction on structure and fast pyrolysis behavior of corncobs. *Bioresour Technol, 128*(0), 370–377.
2. Chang, S., Zhao, Z., Zheng, A., He, F., Huang, Z., & Li, H. (2012). Characterization of products from torrefaction of sprucewood and bagasse in an auger reactor. *Energy & Fuels, 26*(11), 7009-7017.
3. Yan, W., Acharjee, T. C., Coronella, C. J., & Vásquez, V. R. (2009). Thermal pretreatment of lignocellulosic biomass. *Environmental Progress & Sustainable Energy, 28*(3), 435-440.
4. Brown, R. C. (2003). *Biorenewable resources: engineering new products from agriculture*: Iowa State Press.
5. Boardman, R. D., Hess, J. R., Sokhansanj, S., Tumuluru, J. S., & Wright, C. T. (2011). A review on biomass torrefaction process and product properties for energy applications. [Report]. *Industrial Biotechnology, 7*(5), 384+.
6. Medic, D., Darr, M., Shah, A., Potter, B., & Zimmerman, J. (2012). Effects of torrefaction process parameters on biomass feedstock upgrading. *Fuel, 91*(1), 147-154.
7. Huang, H.-J., Ramaswamy, S., Al-Dajani, W., Tschirner, U., & Cairncross, R. A. (2009). Effect of biomass species and plant size on cellulosic ethanol: a comparative process and economic analysis. *Biomass and Bioenergy, 33*(2), 234-246.

8. Aho, A., Kumar, N., Eränen, K., Salmi, T., Hupa, M., & Murzin, D. Y. (2007). Catalytic pyrolysis of biomass in a fluidized bed reactor: influence of the acidity of H-beta zeolite. *Process Safety and Environmental Protection, 85*(5), 473-480.
9. Hayes, D. (2013). Advanced biomass research for beyond the petroleum age. *Important Compositional Parameters* Retrieved 07/09/2013, 2013, from http://www.carbolea.ul.ie/composition.php
10. Westover, T. L., Phanphanich, M., Clark, M. L., Rowe, S. R., Egan, S. E., Zacher, A. H., *et al.*. (2012). Impact of thermal pretreatment on the fast pyrolysis conversion of southern pine. *Biofuels, 4*(1), 45-61.
11. Kasparbauer, R. D. (2009). *The effects of biomass pretreatments on the products of fast pyrolysis.* Iowa State University, Ames, Iowa.
12. Browning, B. L. (1967). Determination of lignin *Methods of wood chemistry* (Vol. 2, pp. 785-823). Appleton: Interscience Publishers.
13. Zheng, A., Zhao, Z., Chang, S., Huang, Z., He, F., & Li, H. (2012). Effect of torrefaction temperature on product distribution from two-staged pyrolysis of biomass. *Energy & Fuels, 26*(5), 2968-2974.
14. Haoxi, B., & Ragauskas, A. J. (2012). Torrefaction of loblolly pine. *Green Chemistry, 14*(1), 72-76.
15. Barth, T., & Kleinert, M. (2008). Motor fuels from biomass pyrolysis. *Chemical Engineering & Technology, 31*(5), 773-781.
16. Scheirs, J., Camino, G., & Tumiatti, W. (2001). Overview of water evolution during the thermal degradation of cellulose. *European Polymer Journal, 37*(5), 933-942.
17. Rowell, R. M. (2005). *Handbook of wood chemistry and wood composites* (Vol. 2). Boca Raton, Fla. : CRC Press.
18. Prins, M. J., Ptasinski, K. J., & Janssen, F. J. J. G. (2006). Torrefaction of wood: part 2. Analysis of products. *Journal of Analytical and Applied Pyrolysis, 77*(1), 35-40.
19. Wannapeera, J., & Worasuwannarak, N. (2012). Upgrading of woody biomass by torrefaction under pressure. *Journal of Analytical and Applied Pyrolysis, 96*(0), 173-180.
20. Meng, J., Park, J., Tilotta, D., & Park, S. (2012). The effect of torrefaction on the chemistry of fast-pyrolysis bio-oil. *Bioresour Technol, 111*(0), 439-446.
21. Westerhof, R. J. M., Brilman, D. W. F., Garcia-Perez, M., Wang, Z., Oudenhoven, S. R. G., & Kersten, S. R. A. (2012). Stepwise fast pyrolysis of pine wood. *Energy & Fuels, 26*(12), 7263–7273.
22. Chaiwat, W., Hasegawa, I., Kori, J., & Mae, K. (2008). Examination of degree of crosslinking for cellulose precursors pretreated with acid/hot water at low temperature. *Industrial & Engineering Chemistry Research, 47*(16), 5948-5956.
23. Bartek, R., Brady, M., & Stamires, D. (2012). United States Patent No.
24. Liaw, S.-S., Zhou, S., Wu, H., & Garcia-Perez, M. (2013). Effect of pretreatment temperature on the yield and properties of bio-oils obtained from the auger pyrolysis of Douglas fir wood. *Fuel, 103*(0), 672-682.
25. Ren, S., Lei, H., Wang, L., Bu, Q., Chen, S., Wu, J., *et al.*. (2013). The effects of torrefaction on compositions of bio-oil and syngas from biomass pyrolysis by microwave heating. *Bioresour Technol, 135*(0), 659-664.

7 Pyrolysis of leached and torrefied biomass

Chapter 5 indicated that leaching biomass prior to pyrolysis increased the bio-oil yield and reduced secondary reactions, thus the bio-oil quality and quantity improved. Chapter 6 showed that torrefaction has the potential to significantly reduce the water and acetic acid content in bio-oil; however the bio-oil yield may decrease following severe torrefaction. Combining these pretreatments is expected to further improve the bio-oil quality while maintaining acceptable bio-oil yields.

In this chapter, the effects of combining the pretreatments were investigated and the sequence was optimised. Practical implementation of the optimised pretreatment sequence was investigated. The pyrolysis system was optimised for both raw biomass and pretreated biomass; allowing differences between the two processes to be examined. Next, selective condensation was implemented to fractionate the bio-oil into four streams, and finally, the potential for using pyrolysis chars to regenerate the leaching leachate to reduce effluent from the pretreatment sequence was investigated. For simplicity, bio-oil produced from pyrolysis of raw biomass is referred to as 'raw bio-oil' while bio-oil produced from pyrolysis of leached and torrefied biomass is referred to as 'pretreated bio-oil'.

7.1 Procedure for combined leaching and torrefaction

Torrefaction of biomass following leaching was carried out by torrefying the biomass leached with DI water and acetic, formic, hydrochloric, nitric, and sulfuric acid, as described in Sections 5.2 and 5.3. Samples were dried after leaching to obtain accurate leaching yields but the moisture content (MC) was then increased to 25 wt% (dry basis) prior to torrefaction. All of these samples were torrefied at 240 °C for 20 min. Next, the 1% acetic acid leached samples (leached at 30 °C for 4 h) were torrefied between 240-280 °C at 10 °C increments in order to optimise the torrefaction temperature. Figure 7-1 gives a representation of the small scale pretreatment sequence, using the apparatus described in Chapters 5 and 6. While this diagram indicates how torrefaction liquor was recycled for acid leaching, during experiments, the torrefaction liquor was only recycled after the pretreatment sequence was optimised. Additionally, the biomass was dried following leaching to obtain the leaching yield, rather than torrefying the wet, leached biomass directly. The moisture content was manually increased to 25 wt% prior to torrefaction.

Once the pretreatment sequence was optimised, the large scale leaching vessel and torrefaction reactor described in Chapters 5 and 6 respectively were used to produce pretreated biomass at a larger scale. The pretreated biomass was combined to produce 5 kg of feedstock. This was used when optimising the pyrolysis reactor conditions which are discussed in Section 7.5.

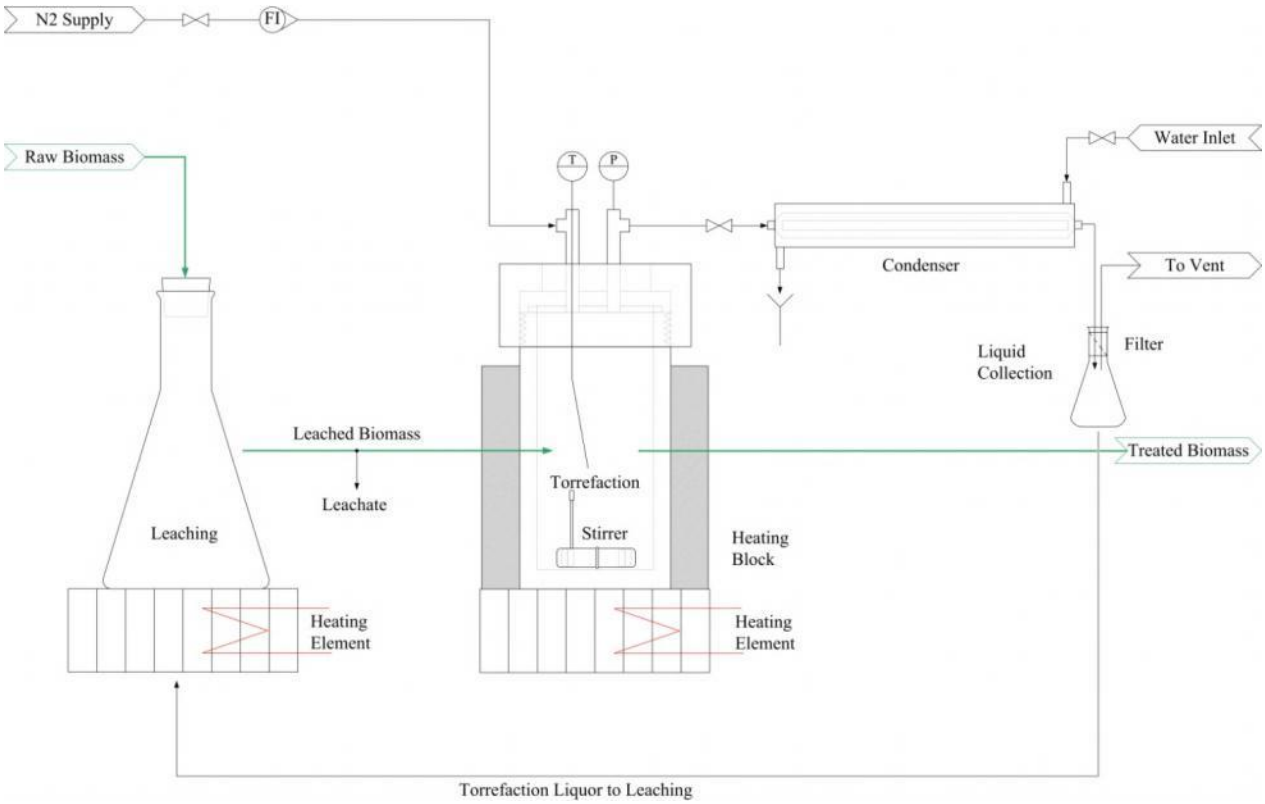

Figure 7-1: Schematic for combined leaching and torrefaction of biomass prior to pyrolysis

7.2 Effect of varying leaching conditions but constant torrefaction conditions

7.2.1 Leaching and torrefaction of biomass

In this part of the study, biomass samples were leached at 30 °C and 90 °C with DI water and acetic, formic, hydrochloric, nitric, and sulfuric acid. The leached samples were then torrefied at a fixed temperature of 240 °C for 20 min. This allowed the effects of the leaching temperature and reagent on torrefaction and pyrolysis to be determined.

The yields after torrefaction are given in Figure 7-2 for leachings at 30 °C and Figure 7-3 for leachings at 90 °C. From these results, it was found that the torrefaction liquid yields varied on a dry basis, possibly due a fraction of the condensate been retained in the condenser. The mass balance for the 1% nitric acid solution at 90 °C indicates no liquid was produced but a solution was still collected due to the high initial moisture content of the biomass. The collected solution still had a low pH and was the normal light yellow colour. Yield deviations from the torrefaction of raw wood were minimal for leaching procedures at 30 °C, although slight deviations were observed for torrefaction of biomass leached at 90 °C. When torrefaction succeeded leaching, there was a general trend of decreased torrefaction severity, with slightly higher biomass yields and a higher pH of the torrefaction liquid compared to torrefaction of raw biomass.

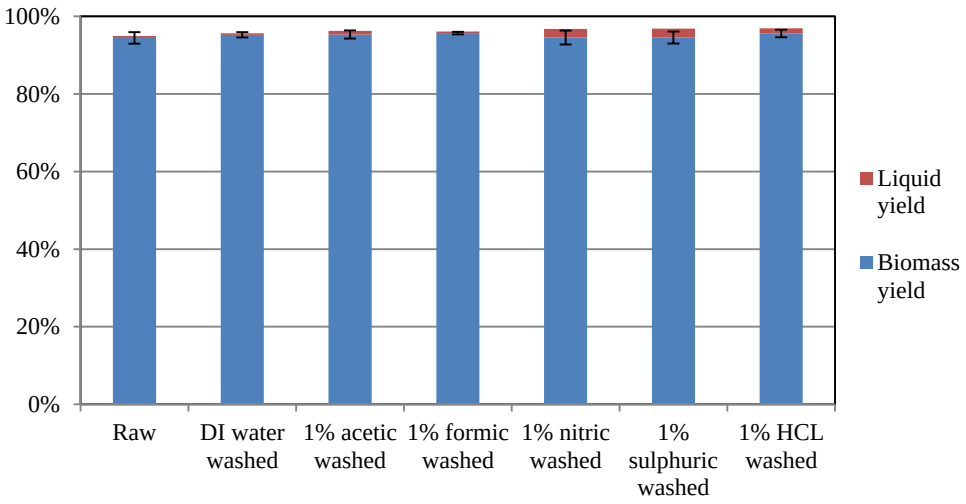

Figure 7-2: Biomass and liquid yields from torrefaction of biomass leached at 30 °C

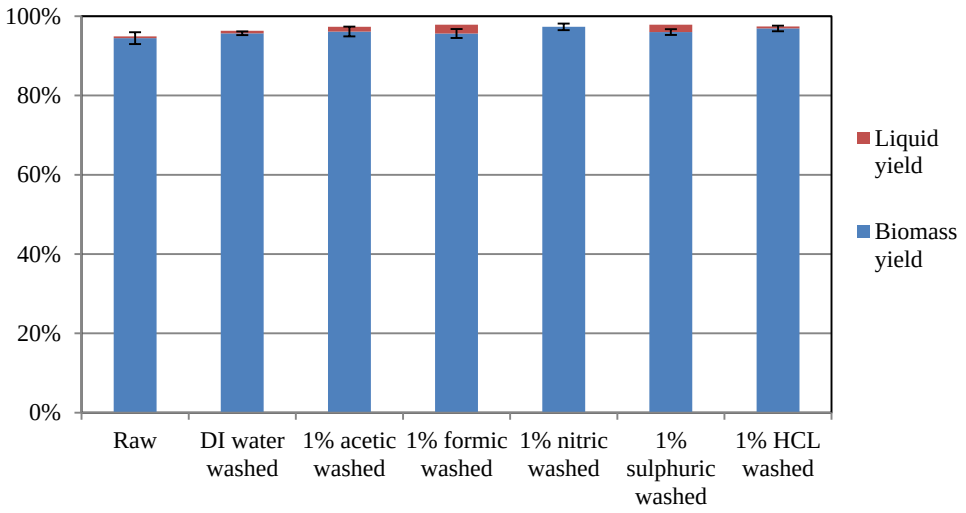

Figure 7-3: Biomass and liquid yields from torrefaction of biomass leached at 90 °C

The acetic acid, formic acid, and methanol concentrations in the torrefaction liquid are given in Figure 7-4 for torrefaction of biomass leached at 30 °C and Figure 7-5 for torrefaction of biomass leached at 90 °C. There was a general trend of decreasing acetic acid and methanol concentrations in the torrefaction liquor, but slightly more formic acid when the leaching temperature was at 90 °C. Structural changes to the biomass polymers during leachings at 90 °C may have stabilised compounds that would normally decomposed during torrefaction to produce acetic acid and methanol (not associated with carbonyl cleavage). Differences in the acetic acid, formic acid, and methanol concentrations for the different leaching reagents could originate from the removal of compounds during leaching procedures, such as extractives. Especially for mineral acids at 90 °C as a large percentage of acetyl branches were removed during the leaching. Acids or inorganic minerals remaining in the biomass after leaching may also alter the product formation by catalysing the formation of certain compounds.

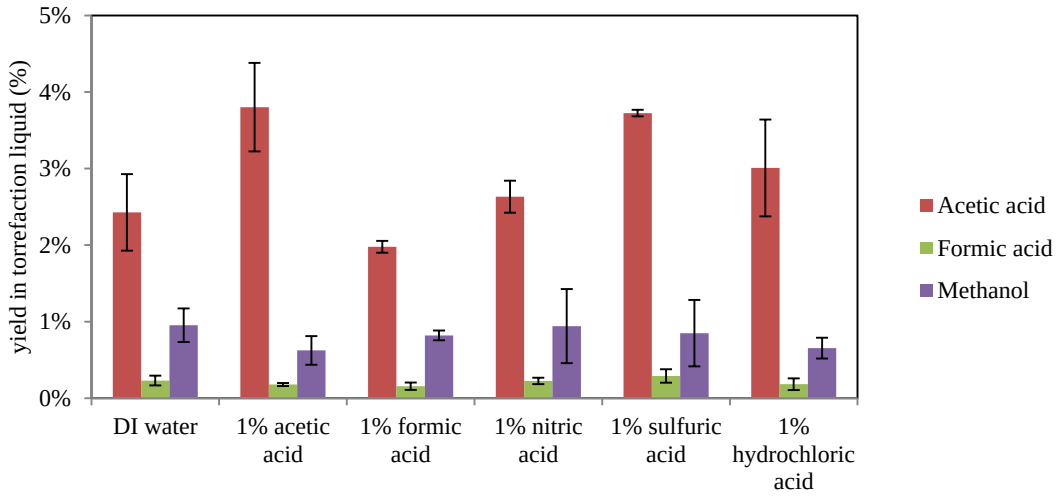

Figure 7-4: Concentrations of major compounds in the torrefaction liquor following leachings at 30 °C

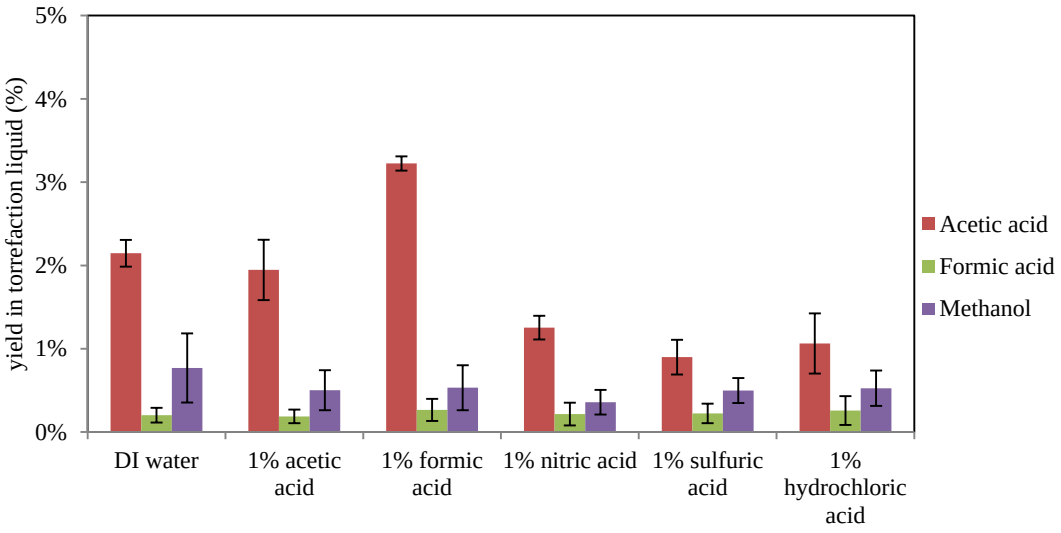

Figure 7-5: Concentrations of major compounds in the torrefaction liquor following leachings at 90 °C

The biomass acetyl content after the combined pretreatments (leaching and torrefaction) is given in Table 7-1. The relative reduction in acetyl compounds during torrefaction was lower for samples leached at 90 °C compared to samples leached at 30 °C, or biomass not previously leached. Torrefaction may appear less severe due to the loss of easily cleavable compounds during the leaching, especially for mineral acids. There was no reduction in the acetyl content for DI water leached biomass at 90 °C; therefore the decreased acetyl removal cannot be solely attributed to previous cleavage. Inorganics could play a catalytic role in acetyl cleavage during torrefaction. Acetyl side branches of galactoglucomannan are easily cleaved by alkali species during leaching [1]; a similar mechanism may apply during torrefaction. However, the inorganic reduction for DI water leached biomass at 90 °C was considerably less than the reduction by all of the acid leaching reagents at 30 °C. Therefore, elevated leaching temperatures must alter the morphology of the biomass and make it less susceptible to acetyl degradation during torrefaction, which explains the lower acetic acid concentration for torrefaction liquor that was previously leached at 90 °C. Performing torrefaction following biomass leaching at 90 °C would provide minimal benefits; therefore biomass

leaching at 30 °C is recommended when both acid leaching and torrefaction are employed as biomass pretreatments.

Table 7-1: Biomass yield and structural analysis after leaching and torrefaction

	Overall biomass yield (%)		**Acetyl after leaching (%)**		**Acetyl after torr. (%)**		**Acetyl change[1] (%)**		**Lignin (%)**		**Cellulose (%)**		**Hemi-cellulose (%)**	
Torrefaction only	94.5 ± 1.5		1.51 ± 0.03		1.32 ± 0.05		14.4		34.7 ± 0.5		41.5 ± 0.9		21.2 ± 0.6	
Torrefaction after leaching														
Leaching temp. (°C)	*30*	*90*	*30*	*90*	*30*	*90*	*30*	*90*	*30*	*90*	*30*	*90*	*30*	*90*
DI water	94.5	93.5	1.53	1.50	1.34	1.39	14.2	7.9	35.0	32.6	39.0	42.2	23.8	23.5
1% acetic acid	94.6	94.3	1.48	1.46	1.29	1.40	14.7	4.3	34.5	37.0	40.9	37.1	23.2	23.5
1% formic acid	94.8	92.9	1.53	1.41	1.31	1.24	16.8	13.7	36.3	38.0	39.7	38.1	23.9	22.9
1% nitric acid	93.7	85.6	1.48	0.54	1.29	0.54	14.7	0.0	35.9	38.6	41.6	39.4	22.1	20.5
1% sulphuric acid	93.8	88.3	1.36	0.80	1.23	0.73	10.6	9.6	36.7	36.8	42.1	41.0	20.4	19.7
1% hydrochloric acid	94.1	82.4	1.38	0.40	1.18	0.42	16.9	-4.8	37.4	41.7	39.6	41.1	21.3	14.9

[1]*Change in acetyl content following torrefaction of leached biomass: relative to the acetyl content after leaching*

7.2.2 Pyrolysis of leached and torrefied biomass

After acid leaching and torrefaction, samples were pyrolysed and the pyrolysis yields and bio-oil properties were determined. As described in Chapter 5, solely leaching biomass with different reagents had a small influence on the pyrolysis yields and bio-oil properties. However, the difference between the leaching reagents may have a noticeable effect when subsequent torrefaction was implemented.

The pyrolysis yields and the bio-oil properties from biomass leached and then torrefied are given in Table 7-2 for leachings at 30 °C and in Table 7-3 for leachings at 90 °C. From these results, it was found that the bio-oil yield from formic and acetic leached and torrefied biomass was higher than for biomass that was solely leached at 30 or 90 °C. However, all torrefied biomass that was leached with DI water or minerals acids (except for biomass leached with hydrochloric acid at 30 °C and torrefied) exhibited a decrease in the bio-oil yield compared to solely leached biomass. This indicated biomass leached with acetic acid and formic acid benefit from subsequent torrefaction to volatise acid residues. It also indicates the role organic acids to catalyses secondary pyrolysis reactions.

It was also observed from the results in Table 7-2 that sulfuric acid leaching gave a lower bio-oil yield and higher char yield compared to the other acid leached samples. This was due to the increased sulfur content in the biomass following the sulfuric acid leaching. The low water and acetic acid content in this bio-oil indicates the mechanism for char formation did not enhance water or acetic acid formation. Leaching with hydrochloric acid produced high bio-oil yields but the water and acetic acid content in the bio-oil were increased, indicating that chloride became incorporated into the biomass and enhanced secondary reactions or altered the primary reaction pathway to enhance the production of low molecular weight compounds such as water and acetic acid. When hydrochloric acid leaching was not followed by torrefaction, the water and acetic acid yields were comparable to samples leached with other reagents; this was likely due to the more

Cl ions incorporated into the second biomass sample or torrefaction enhanced Cl ions interactions during vapour formation by transforming Cl into a stable form.

From Table 7-2 and Table 7-3, it was found that pyrolysis yields were approximately the same for leachings at 30 °C and 90 °C. There was a slight trend of decreasing water and acetic acid content in the bio-oil from pyrolysis of biomass leached at 90 °C compared to samples leached at 30 °C. Sulfuric acid leached samples at 90 °C still produced lower bio-oil yields compared to the samples leached with other acid reagents. Hydrochloric acid leached biomass had a water and acetic acid content much lower compared to those for pyrolysis of biomass leached at 30 °C: confirming that the increased water and acetic acid in the sample leached at 30 °C was from insufficient rinsing following the leaching. Overall the differences in the bio-oil yield and properties between biomass leached at 30 and 90 °C were relatively small. However, the results did indicated how sensitive pyrolysis is to additional ions incorporated into the biomass's structure following the leaching; acetic, formic, and nitric acid (assuming nitrogen is not catalytic) do not leave minerals in the biomass following leachings: a portion of the acids may remain but these would volatise during torrefaction. Therefore pyrolysis results from torrefaction of biomass leached with acetic, formic, and nitric acid are more consistent compared to biomass torrefied and leached with sulfuric and hydrochloric acid. This is a positive benefit for using organic acids compared to some mineral acids.

Table 7-2: Yields and bio-oil properties for pyrolysis of acid leached (30 °C) and torrefied biomass

Leaching reagent	DI water	1% acetic acid	1% formic acid	1% sulfuric acid	1% hydrochloric acid	1% nitric acid
Pyrolysis yields[1] (wt%)						
Bio-oil	52.8	58.7	58.1	50.2	58.3	56.0
Char	15.1	10.6	9.4	9.4	10.4	10.1
NCG, by difference	32.1	30.7	32.6	35.3	31.3	33.9
Bio-oil properties						
Acetic acid conc. (%)	1.7±0.5	0.6±0.1	0.3±0.1	0.2±0.1	1.6±0.2	0.4±0.1
Water content (wt%)	9.4±1.4	7.1±0.2	5.0±0.8	2.0±0.2	11.1±1.5	3.5±0.1
Organic yield (wt%)	47.7	54.5	55.2	49.2	51.8	54.1

[1]*Acid leaching was carried out at 30 °C for 4 h and torrefaction was at 240 °C for 20 min*

Table 7-3: Yields and bio-oil properties for pyrolysis of acid leached (90 °C) and torrefied biomass

Leaching reagent	DI water	1% acetic acid	1% formic acid	1% sulfuric acid	1% hydrochloric acid	1% nitric acid
Pyrolysis yields[1] (wt%)						
Bio-oil	53.2	57.9	59.6	52.5	56.5	58.2
Char	13.6	9.9	9.8	12.3	9	33.2
NCG, by difference	33.2	32.1	30.6	35.1	34.4	13.6
Bio-oil properties						
Acetic acid conc. (%)	0.5±0.1	0.5±0.0	0.3±0.0	0.4±0.3	0.2±0.0	0.3±0.1
Water content (wt%)	6.4±0.3	4.7±1.6	1.5±0.0	1.4±0.0	4.1±0.9	3.4±1.9
Organic yield (wt%)	49.8	55.2	58.8	51.8	54.3	56.2

[1]*Acid leaching was carried out at 90 °C for 4 h and torrefaction was at 240 °C for 20 min*

For comparison amongst the various pretreatment combinations, Table 7-4 presents a summary for the yield and properties of bio-oil produced from:

- Pyrolysis of raw biomass
- Pyrolysis of biomass that was leached with 1% acetic acid at 30 or 90 °C
- Pyrolysis of biomass that was torrefied at 240 °C
- Pyrolysis biomass that was leached with 1% acetic acid at 30 or 90 °C and then torrefied at 240 °C.

From the results in Table 7-4, it was found that the bio-oil yield was the highest for the combined acid leaching and torrefaction pretreatments. It was thought that the combined pretreatments would decrease the bio-oil yield compared to bio-oil produced from solely acid leached biomass, due to the carbon-carbon crosslinks formed during torrefaction. The increase in the bio-oil yield shows how sensitive pyrolysis is to natural catalytic compounds in biomass and the benefit of controlling their presence.

The results indicate the bio-oil properties were improved from the combined use of acid leaching and torrefaction in terms of the acetic acid and water content in the bio-oil. The overall organic bio-oil yield was much higher when both pretreatments were implemented. These results provide evidence that inorganics, acetic acid, and water all contribute to secondary reactions of pyrolysis vapours and that removal/reduction is required to significantly improve the bio-oil properties. When comparing the samples leached at 30 °C to samples leached at 90 °C, there were only small improvements in the bio-oil quality for the higher temperature leaching. For this reason, it was decided to carry out leaching at 30 °C as minimising heating during the pretreatments reduces the process costs.

Acid catalysed reactions can enhance the formation of large aromatics and char [2]. It is reported that pyrolysis at temperatures above 375 °C is dominated by these acid catalysed reactions over free radical reactions [3]. Average GPC results in Table 7-4 indicate a reduction in the weight and size average of bio-oil compounds produced from acid leached and torrefied biomass. The pyrolytic lignin content (fraction >650 $gmol^{-1}$) nearly halved, and this confirms that secondary, acid catalysed polymerisation reactions were reduced: both from a reduction in the acetic acid present in bio-oil and possibly due to more pathways present for the volatiles to escape from the biomass particle. The GPC distribution curves are displayed in Figure 7-6, from which a large peak 157 $gmol^{-1}$ was observed for bio-oil produced from leached and torrefied biomass.

Inorganics in biomass predominantly catalyse primary vapours as they escape biomass particles [4], and catalyse products as they are formed. Polymer fragmentation is dominant in the presence of inorganic cations [5], which enhances the formation of small oxygenated compounds at the expense of levoglucosan. Both these mechanisms were reduced for pyrolysis of pretreated biomass as leaching reduced the inorganic content and torrefaction loosened the biomass structure to reduce interactions between immobilised inorganics in the biomass or primary vapours. Rapid moisture removal from the amorphous regions of cellulose during torrefaction can rupture the biomass structure to reduce interactions [6] as well as breaking hydrogen bonds between biomass polymers.

Table 7-4: Comparison between pyrolysis of raw biomass and pretreated biomass

Pretreatment[1]	Raw	Leached at 30 °C	Leached at 90 °C	Torr. at 240 °C	Leached at 30 °C and torr. at 240 °C	Leached at 90 °C and torr. at 240 °C
Pyrolysis yields (wt%)						
Bio-oil	46.9	54.6	54.5	47.5	58.7	57.9
Char	15.4	8.6	8.6	18.4	10.6	9.9
NCG, by difference	37.6	36.8	36.9	34.1	30.7	32.1
Bio-oil properties						
Acetic acid conc. (%)	3.5±0.4	1.9±0.1	1.4±0.0	2.6±0.1	0.6±0.1	0.5±0.0
Water (wt%)	24.0±1.2	17.0±1.3	15.2±0.0	9.9±1.2	7.1±0.2	4.7±1.6
Density (kgm^{-3})	1210	1269	1299	1268	-	-
Dynamic viscosity (cP)	37.0	190.1	861.9	245.1	1953.5	-
Organic yield (wt%)	35.5	45.3	46.22	42.8	54.51	55.2
Overall organic yield[2] (wt%)	35.5	45.0	42.3	40.4	51.6	52.0
GPC results						
Average number, Mn ($gmol^{-1}$)	246.4±3.1	211.3	-	245.4	218.3	-
Weight average, Mw ($gmol^{-1}$)	327.6±11.0	325.8	-	321.8	280.9	-
Size average, Mz ($gmol^{-1}$)	470.9±33.5	505.4	-	444.9	390.8	-
>650 $gmol^{-1}$ (%)	8.10±1.06	9.9	-	7.12	4.6	-
[1]H-NMR results, relative to the biomass feed						
Compound/s	**Shift, ppm**	**wt% in bio-oil[1], in brackets: wt% relative to the organic yield**				
Alkanes	0.5-1.6	10.52 (3.74)	7.53 (3.03)	7.40 (4.03)	10.46 (4.47)	9.18 (5.00)	8.30 (4.58)
Acetic acid	1.88	4.64 (1.65)	3.48 (1.40)	2.09 (1.14)	3.41 (1.46)	2.05 (1.12)	2.40 (1.33)
Acetaldehyde	9.58 and 2.08	2.92 (1.04)	2.38 (0.96)	2.18 (1.19)	2.9 (1.24)	2.54 (1.38)	2.03 (1.12)
Hydroxyacetone	4.01	-	1.23 (0.49)	1.43 (0.78)	2.17 (0.93)	1.56 (0.85)	1.33 (0.73)
Levoglucosan	3.27,3.84-3.85,4.31-4.33, and 5.13	2.30 (0.82)	8.88 (3.57)	14.15 (7.71)	3.07 (1.31)	15.68 (8.55)	10.48 (5.79)
Tot. aromatics[3]	6.4-7.6	9.61 (3.41)	9.82 (3.95)	11.31 (6.17)	10.74 (4.59)	11.37 (6.20)	12.39 (6.84)
Formic acid	8.10	0.59 (0.21)	0.36 (0.14)	0.15 (0.08)	0.29 (0.12)	0.07 (0.04)	0.30 (0.17)
Glycolaldehyde	9.55	0.06 (0.02)	0.10 (0.04)	0.07 (0.04)	0.06 (0.03)	0.06 (0.03)	0.10 (0.06)
Tot. aldehydes	9.5-10.5	0.93 (0.33)	0.75 (0.30)	0.85 (0.46)	0.88 (0.38)	0.9 (0.49)	0.84 (0.46)

[1]Leaching reagent was 1% acetic acid and leached was carried out for 4 h. [2]Taking into account the mass loss during torrefaction and leaching. [3]Includes phenol, syringol, guaiacol, furan, furfural, methyl-2-furoate, and hydroxymethylfurfural

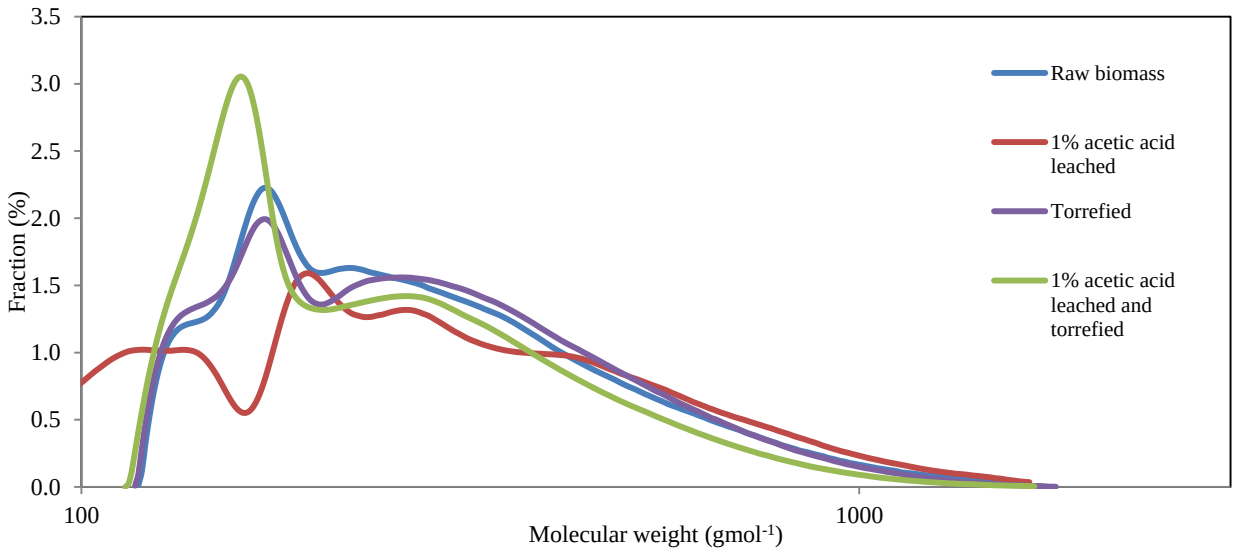

Figure 7-6: Molecular weight distribution curves for bio-oils from pyrolysis of for raw and pretreated biomass. Acid leaching was at 30 °C and torrefaction was at 240 °C

7.3 Effect of constant leaching conditions but varying torrefaction conditions

7.3.1 Leaching and torrefaction of biomass

In this part of the study, samples were first leached with 1% acetic acid and then torrefied between 240-280 °C for 20 min. The torrefaction yields and the structural composition on the biomass were determined. Table 7-5 compares the results to the torrefaction of raw biomass in the same temperature range. From Table 7-5, it was found that the severity of torrefaction appeared to be less affected by the leaching pretreatment as the torrefaction temperature increased. The overall biomass loss from combined acid leaching and torrefaction was still less than the loss from torrefaction alone, but the acetyl removal increased, possibly due to the weakening of biomass polymers facilitating acetyl cleavage during torrefaction. Sugar degradation was reduced during torrefaction for samples had been previously leached, and therefore, the oxygen content was higher due to the high oxygen content in cellulose and hemicellulose; approximately 49 wt% and 54 wt% respectively [7]. When acetic acid leaching precedes torrefaction, the temperature of torrefaction can be increased to 260 °C while still maintaining high overall biomass yields, but with a further reduction in acetyl content to 0.83 wt% and lower lignin and oxygen contents in the biomass compared to biomass solely torrefied at 250 °C or above.

Table 7-5: Comparison between torrefaction of raw biomass and 1% acetic acid leached biomass

Torrefied biomass (no leaching prior)							
Temperature (°C)	**Biomass loss (wt%)**	**Acetyl (wt%)**	**Lignin (wt%)**	**Total sugars (wt%)**	**Carbon (wt%)**	**Hydrogen (wt%)**	**Oxygen (wt%)**
240	5.5 ± 1.5	1.32 ± 0.05	34.7 ± 0.5	62.7 ± 1.1	51.5	5.9	42.5
250	8.6 ± 1.0	1.23 ± 0.03	38.7 ± 2.7	59.0 ± 1.5	52.4	5.9	41.6
260	11.4 ± 2.1	1.16 ± 0.18	40.6 ± 3.2	57.9 ± 1.1	53.4	5.9	40.6
270	15.6 ± 2.0	0.95 ± 0.11	44.0 ± 2.8	53.8 ± 2.2	54.8	5.9	39.3
280	19.8 ± 1.5	0.76 ± 0.08	49.2 ± 4.2	50.1 ±2.9	55.9	5.8	38.2
1% acetic acid leached and torrefied biomass							
Temperature (°C)	**Biomass loss[1] (wt%)**	**Acetyl (wt%)**	**Lignin (wt%)**	**Total sugars (wt%)**	**Carbon (wt%)**	**Hydrogen (wt%)**	**Oxygen (wt%)**
240	5.4 ± 1.1	1.29 ± 0.13	34.5 ± 3.9	64.0 ± 1.7	51.4	5.9	42.6
250	7.6 ± 0.7	1.12 ± 0.16	34.9 ± 1.8	64.2 ± 1.8	52.2	5.9	41.8
260	10.3 ± 2.1	0.83 ± 0.15	35.5 ± 1.1	62.5 ± 2.5	53.4	5.8	40.7
270	14.0 ± 0.6	0.74 ± 0.03	39.5 ± 3.3	59.1 ± 1.9	53.6	5.8	40.6
280	17.8 ± 1.5	0.71 ±0.05	45.8 ± 4.4	51.8 ±1.8	55.2	5.8	39.0

[1]*Overall mass loss from leaching and torrefaction*

The torrefaction liquor was collected and analysed from torrefaction of leached biomass, with the concentrations of acetic acid, formic acid, and methanol displayed in Figure 7-7. In comparison with the results presented in Chapter 6, it was found that concentration of all the compounds detected was lower than for biomass that was solely torrefied. The decrease indicates that the inorganics enhanced formation of these compounds by decreasing the activation energy required for bond cleavage during torrefaction. The lower

biomass loss, given in Table 7-5, for samples that were leached and torrefied compared to solely torrefied biomass confirms that activation energies for bond cleavage were reduced in the presence of inorganics.

From Table 7-5, it was found that the acetyl removal was slightly better when biomass was leached and torrefied compared to solely torrefied; therefore the activation energy for acetyl branch removal was not affected by the present of inorganics in biomass. This indicates the higher concentration of acetic acid, formic acid, and methanol in the liquor produced from solely torrefied biomass was from polymer decomposition, which was enhanced in the presence of inorganics. Since degradation of biomass polymers is not desirable during torrefaction, torrefaction of leached biomass was considered superior to torrefaction of raw biomass; in terms of reducing the biomass acetyl content and maintaining high biomass yields. Prins *et al.* [8] investigated torrefaction of beech, willow, larch, and straw. Their results indicated that feedstocks with a high content of inorganics (straw) produced higher concentrations of acetic acid, formic acid, and methanol compared to feedstocks with a lower inorganic content. Larch, with the lowest inorganic content, produced the least acetic acid, formic acid, and methanol, which agrees with the results observed in this research.

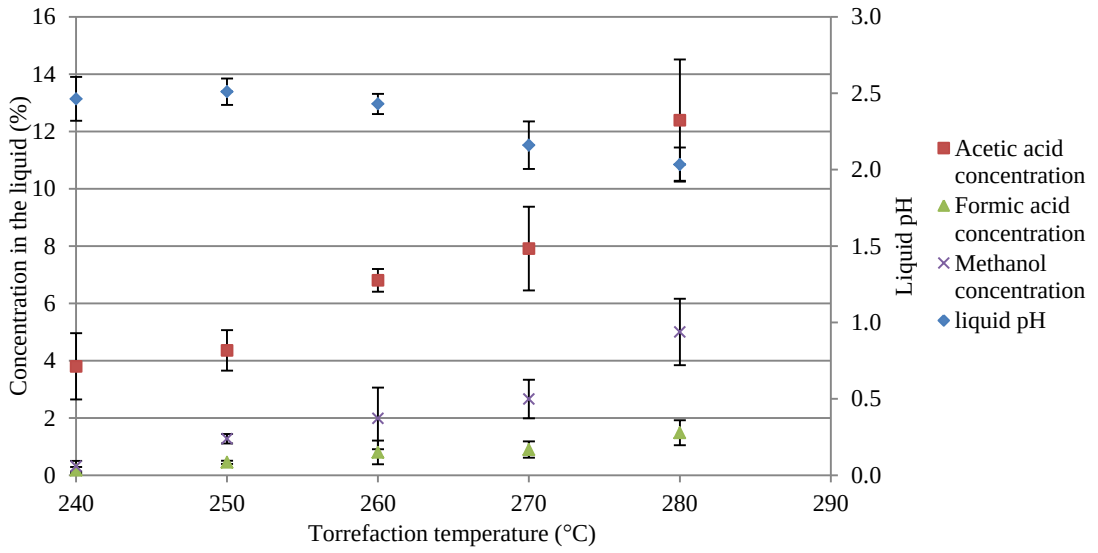

Figure 7-7: pH and concentration of the main compounds in liquor produced by torrefaction of leached biomass

The composition of the non-condensable gases (NCGs) was determined for torrefaction of 1% acetic acid leached biomass. Results for the NCG composition are shown in Figure 7-8; this figure includes data from torrefaction of raw biomass for a comparison. The lower CO yield for torrefaction of leached biomass was partly from the decreased torrefaction severity, but this alone could not account for the entire difference as torrefaction of raw biomass still produced 19.9±0.6 wt% of CO for torrefaction at 230 °C. Therefore the reduction must be partly from reduced secondary reactions of CO_2 with steam and reduced decarbonylation of the torrefaction vapours [9]. These reactions were likely catalysed by inorganics since the reactions were reduced for torrefaction of leached biomass.

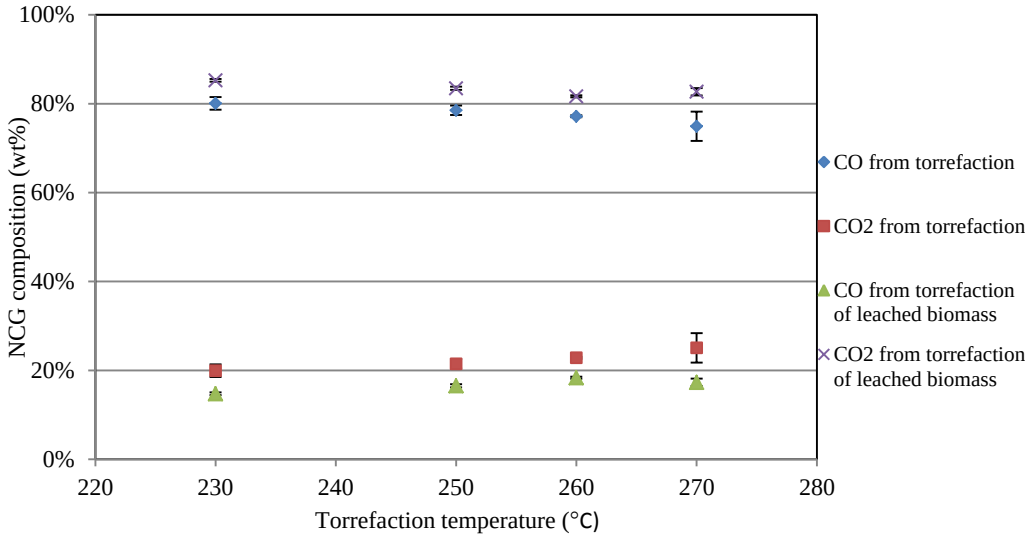

Figure 7-8: NCG composition from torrefaction of raw biomass and 1% acetic acid leached biomass

7.3.2 Pyrolysis of leached and torrefied biomass

Pyrolysis yields for biomass samples that were acetic acid leached and then torrefied between 240-280 °C are shown in Figure 7-9. From this, it was observed that pyrolysis of severely torrefied biomass at 280 °C still had a higher bio-oil yield than for pyrolysis of raw biomass (52.4 wt% compared to 46.9 wt% dry basis). When taking into account the mass loss during the pretreatments, the overall bio-oil yields were reduced; however the yields were still higher than those from pyrolysis of raw biomass for torrefaction temperatures between 240-270 °C. When the torrefaction temperature reached at 280 °C, the overall yield dropped to 43.4 wt%. Torrefaction at 280 °C was associated with a sudden increase in char. Thus, severe carbon-carbon crosslinking of the biomass carbohydrates occurred during torrefaction at 280 °C; reducing the degradation potential during pyrolysis as a larger proportion of the crosslinked carbohydrates formed char instead of decomposing to produce volatiles.

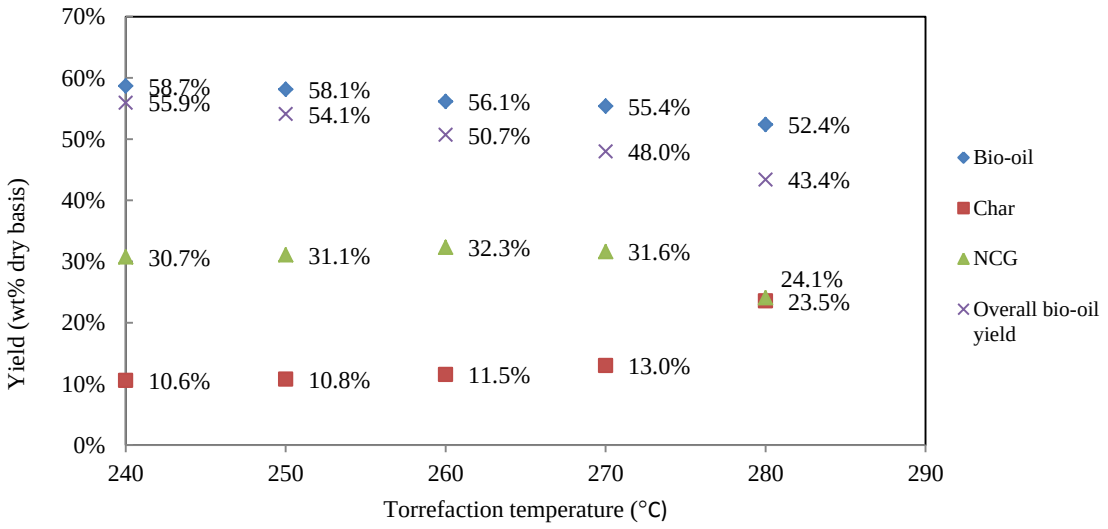

Figure 7-9: Yields from pyrolysis of acetic acid leached and torrefied biomass

The properties of leached and torrefied biomass were analysed: the results are given in Table 7-6 and GPC distribution curves are given in Figure 7-10. From Table 7-6, it can be seen that increasing the torrefaction temperature decreased the acetic acid and water content in the bio-oil due to reduced acid catalysed reactions. The organic yield was much higher than that of bio-oil from raw biomass, even when the mass loss due to the pretreatments was taken into account. The average GPC results indicate a small decrease in the average bio-oil molecular weight as the torrefaction temperature increased. This was associated with a general trend of decreasing pyrolytic lignin content. The decrease was probably due to reduced secondary polymerisation reactions, such as oligomerisation of levoglucosan [10]. The elementary analysis of the pretreated samples show the bio-oil's oxygen content slightly decreased; while torrefaction reduced the biomass's oxygen content, significant decreases cannot be accomplished without severe carbohydrate loss. Additionally, acid leaching increased the bio-oil's oxygen content (to 51.8 wt% wet basis and 44.2 wt% (dry basis) for 1% acetic acid leached samples at 30 °C for 4 h), this offsets the decrease accomplished by torrefaction. Therefore when combining the pretreatments, only a marginal decrease in the bio-oil oxygen content was obtained on a dry basis.

Samples were evaluated over the range of torrefaction temperatures investigated to determine the highest torrefaction temperature acceptable. Temperatures above 270 °C were required for a large decrease in the bio-oil's acetic and formic acid concentration. It has been reported that organic acids cause bio-oil to be corrosive and promote aging reactions, such as aldol reactions to form carbon-carbon bonds between compounds, leading to the formation of high molecular weight compounds [11]. Bio-oils produced from biomass torrefied at 270 and 280 °C were compared to raw biomass in terms of the yields and bio-oil properties. Full details can be found in Appendix 7.1. The analysis indicated torrefaction at 270 °C was preferable over torrefaction at 280 °C as the bio-oil had a similar water, acetic acid, pyrolytic lignin, and oxygen content. The molecular weight was also similar but the bio-oil yield was higher following torrefaction at 270 °C.

Table 7-6: Properties of bio-oil produced from pyrolysis of pretreated biomass

Torrefaction temp.[1](°C)	Raw	240	250	260	270	280
Bio-oil properties						
Acetic acid conc. (%)	3.5±0.4	0.56 ±0.06	0.50±0.04	0.51±0.05	0.15±0.07	0.14±0.02
Water (wt%)	24.0±1.2	7.1±0.2	4.8±1.1	4.5±0.1	4.3±0.0	4.4±0.2
Organic yield (wt%)	35.5	54.5	55.3	56.6	53.0	50.1
Overall organic yield[2] (wt%)	35.5	51.6	51.2	48.1	45.6	41.2
GPC results						
Average number, Mn ($gmol^{-1}$)	246.4±3.1	218.3	225.9	226.1	215.2	214.2
Weight average, Mw ($gmol^{-1}$)	327.6±11.0	280.9	295.4	295.4	273.7	274.8
Size average, Mz ($gmol^{-1}$)	470.9±33.5	390.8	419.8	416.2	375.3	385.4
>650 $gmol^{-1}$ (%)	8.10±1.06	4.6	5.6	5.6	4.0	4.3
Ultimate analysis						
Wet basis						
Carbon (%)	39.1	48.7	49.1	50.0	50.4	49.6
Hydrogen (%)	7.3	6.2	6.4	6.3	6.4	6.5
Nitrogen (%)	0.3	0.9	0.7	0.8	0.7	1.1
Oxygen, by difference (%)	53.2	44.2	43.8	42.8	42.5	42.9
Dry basis						
Carbon (%)	51.5	52.4	51.5	52.4	52.6	51.9
Hydrogen (%)	6.2	5.8	6.1	6.1	6.2	6.2
Nitrogen (%)	0.4	1.0	0.8	0.9	0.7	1.1
Oxygen, by difference (%)	41.9	40.8	41.6	40.7	40.4	40.8
Higher heating value ($MJkg^{-1}$)	20.9±0.8	20.9	20.9	21.3	21.5	21.2
Overall energy in bio-oil[3] (MJ)	7.4	10.8	10.7	10.2	9.8	8.7

[1]All samples were leached with 1% acetic acid for 4 h prior to torrefaction. [2]Taking into account the mass loss during torrefaction and leaching. [3]Per kg of biomass feed

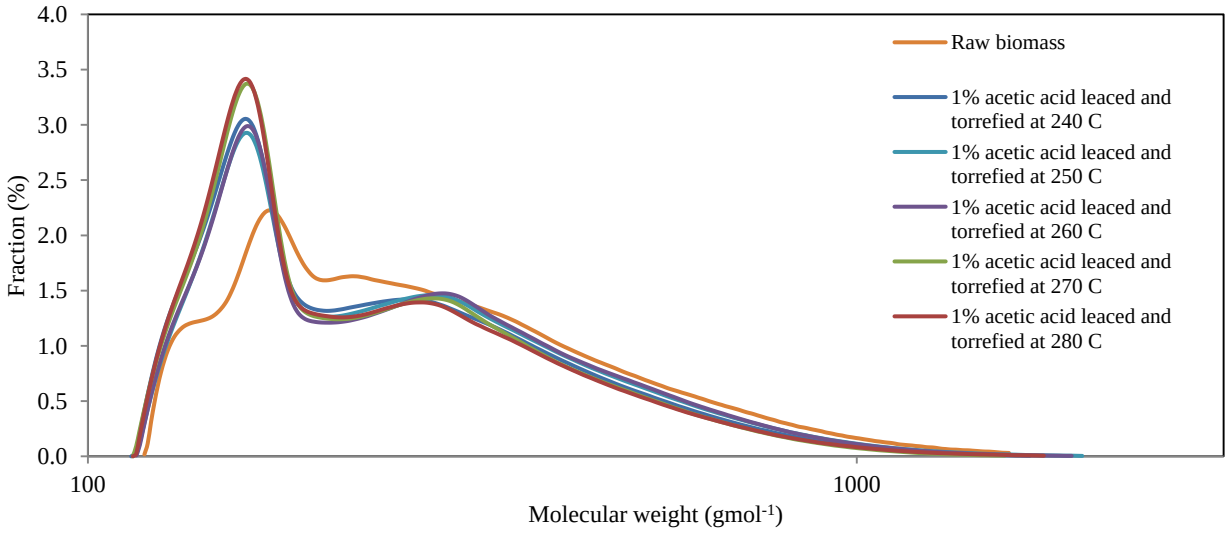

Figure 7-10: Molecular weight distribution curves for raw and pretreated bio-oil samples

^{1}H-NMR results for the bio-oils are given in Figure 7-11 for concentrations of compounds on a water-free basis and Figure 7-12 for concentrations relative to the biomass feed rate. From Figure 7-12, a large increase in levoglucosan production was observed for pretreated bio-oil compared to raw bio-oil. Total aromatics also increased while the alkane, acetic acid, acetaldehyde, and formic acid concentrations decreased. The levoglucosan concentration of acid leached and torrefied bio-oil was higher than for samples that were either solely leached or torrefied; indicating a reduced breakdown of primary products when both pretreatments were implemented. The reduction in alkanes was most likely from the removal of hydroxyl groups during

torrefaction, which produced a carbon-carbon double bond opposed to a single carbon-carbon bond. The reduction may also be due to reduced cleavage of primary products to produce low molecular weight alkanes.

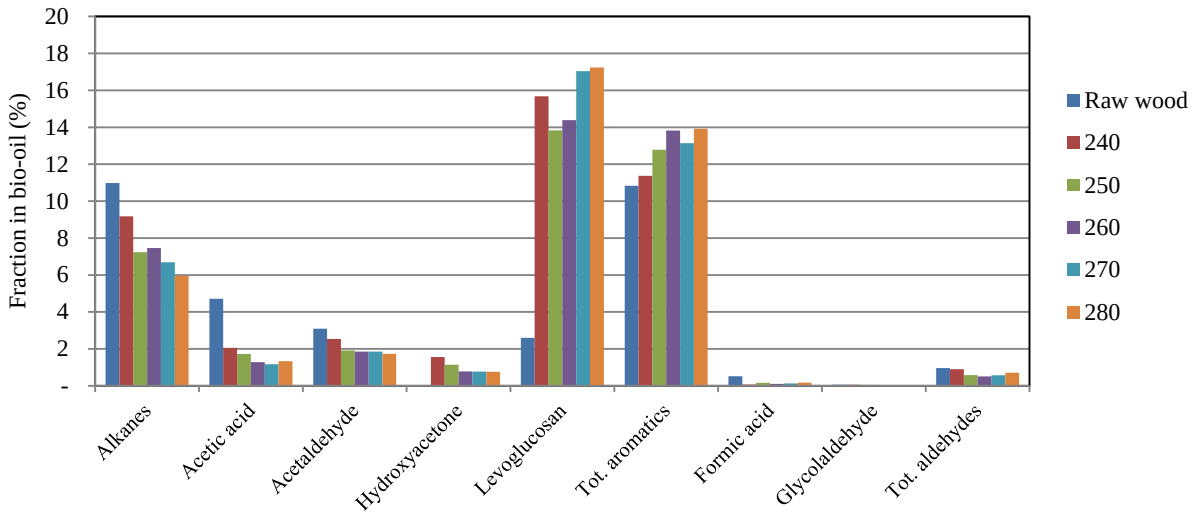

Figure 7-11: ^{1}H-NMR peak area for bio-oil composition, water free basis

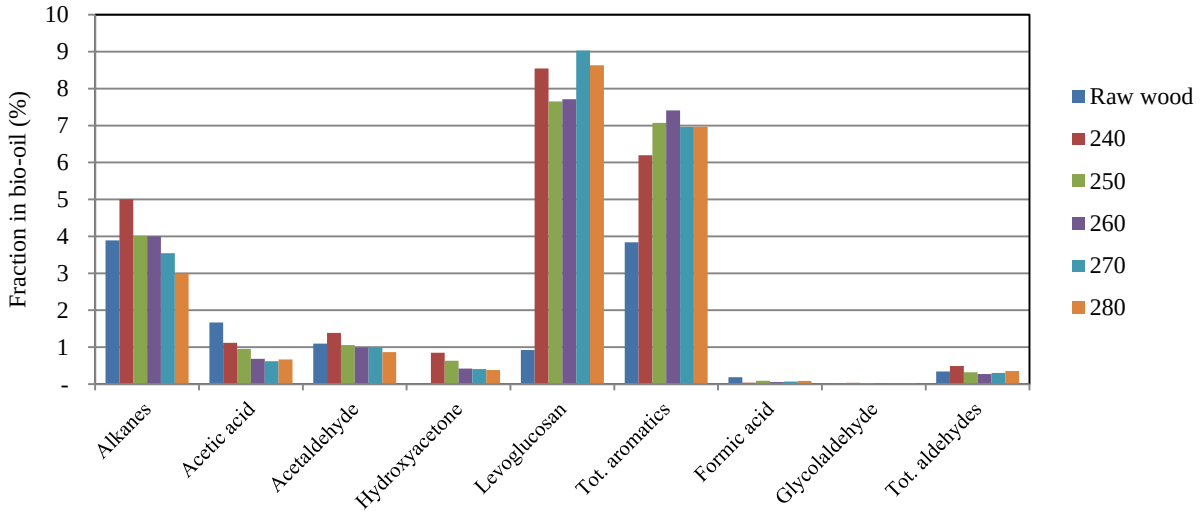

Figure 7-12: ^{1}H-NMR peak area for bio-oil compounds, relative to the biomass feed

In order to investigate the effect of the combined acid leaching and torrefaction pretreatments on biomass, Table 7-6 was modified to produce Table 7-7. Table 7-7 compares bio-oil produced from raw biomass; biomass that was solely leached with 1% acetic acid at 30 °C; biomass solely torrefied at 270 °C; and biomass leached with 1% acetic acid at 30 °C then torrefied at 270 °C. These results can be used to identify if the bio-oil improvements originate from the leaching, torrefaction, or a combination of both.

Speculative reactions pathways were developed based on the results in Table 7-7 and shown in Figure 7-13. These were developed to explain how the product formation alters following the different pretreatments. Figure 7-13 predicts the bio-oil's water content decreased following the pretreatments due to reduced water in the feed and reduced secondary reactions of volatiles that produce water as a by-product. The acetic acid

production decreased for pyrolysis of pretreated biomass due to the reduced acetyl content in the biomass and reduced production during pyrolysis. Pyrolysis of pure cellulose produces no acetic acid [10]; therefore it originates from secondary reactions of primary products; inorganic catalysed reactions; or hemicellulose pyrolysis. Reducing the inorganic and acetyl content in biomass limited these reactions.

Table 7-7: Comparison between pyrolysis of raw biomass and pretreated biomass

Pretreatment[1]		**Raw**	**Leached at 30 °C**	**Torr. at 270 °C**	**Leached at 30 °C and torr. at 270 °C**
Bio-oil properties					
Acetic acid conc. (%)		3.5±0.4	1.9±0.1	0.6±0.4	0.15±0.07
Water (wt%)		24.0±1.2	17.0±1.3	6.1±0.3	4.3±0.0
Dynamic viscosity (cP)		37.0	190.1	571.4	1005.5
Organic yield (wt%)		35.5	45.3	43.3	55.4
Overall organic yield[2] (wt%)		35.5	45.0	36.5	47.9
GPC results					
Average number, Mn ($gmol^{-1}$)		246.4±3.1	211.3	238.4	215.2
Weight average, Mw ($gmol^{-1}$)		327.6±11.0	325.8	310.7	273.7
Size average, Mz ($gmol^{-1}$)		470.9±33.5	505.4	429.9	375.3
>650 $gmol^{-1}$ (%)		8.1±1.1	9.9	6.02	4.0
H-NMR results, relative to the biomass feed					
Compound/s	**Shift, ppm**	**wt% in bio-oil[1], in brackets: wt% relative to the organic yield**			
Alkanes	0.5-1.6	10.52 (3.74)	7.53 (3.03)	10.37 (4.49)	6.69 (3.54)
Acetic acid	1.88	4.64 (1.65)	3.48 (1.40)	2.51 (1.09)	1.17 (0.62)
Acetaldehyde	9.58 and 2.08	2.92 (1.04)	2.38 (0.96)	2.90 (1.25)	1.85 (0.98)
Hydroxyacetone	4.01	-	1.23 (0.49)	1.84 (0.80)	0.77 (0.41)
Levoglucosan	3.27,3.84-3.85,4.31-4.33, and 5.13	2.30 (0.82)	8.88 (3.57)	3.74 (1.62)	17.04 (9.03)
Tot. aromatics[3]	6.4-7.6	9.61 (3.41)	9.82 (3.95)	11.87 (5.13)	13.14 (6.96)
Formic acid	8.10	0.59 (0.21)	0.36 (0.14)	0.27 (0.12)	0.13 (0.07)
Glycolaldehyde	9.55	0.06 (0.02)	0.10 (0.04)	0.05 (0.02)	0.04 (0.02)
Tot. aldehydes	9.5-10.5	0.93 (0.33)	0.75 (0.30)	0.88 (0.38)	0.57 (0.30)
Ultimate analysis					
Wet basis					
Carbon (%)		39.1±1.4	40.5	49.1	50.4
Hydrogen (%)		7.3±0.6	7.6	6.7	6.4
Nitrogen (%)		0.3±0.2	0.1	0.7	6.7
Oxygen, by difference (%)		53.2±1.2	51.8	43.5	42.5
Dry basis					
Carbon (%)		51.5	48.8	52.3	52.6
Hydrogen (%)		6.2	6.9	6.4	6.2
Nitrogen (%)		0.4	0.1	0.7	0.7
Oxygen, by difference (%)		41.9	44.2	40.5	40.4
Higher heating value ($MJkg^{-1}$)		20.9±0.8	20.6	21.6	21.5
Overall energy in bio-oil[4] (MJ)		7.4	9.3	7.9	9.8

[1]Leaching reagent was 1% acetic acid and leached was carried out for 4 h. [2]Taking into account the mass loss during torrefaction and leaching. [3]Includes phenol, syringol, guaiacol, furan, furfural, methyl-2-furoate, and hydroxymethylfurfural. [4]Per kg of biomass feed

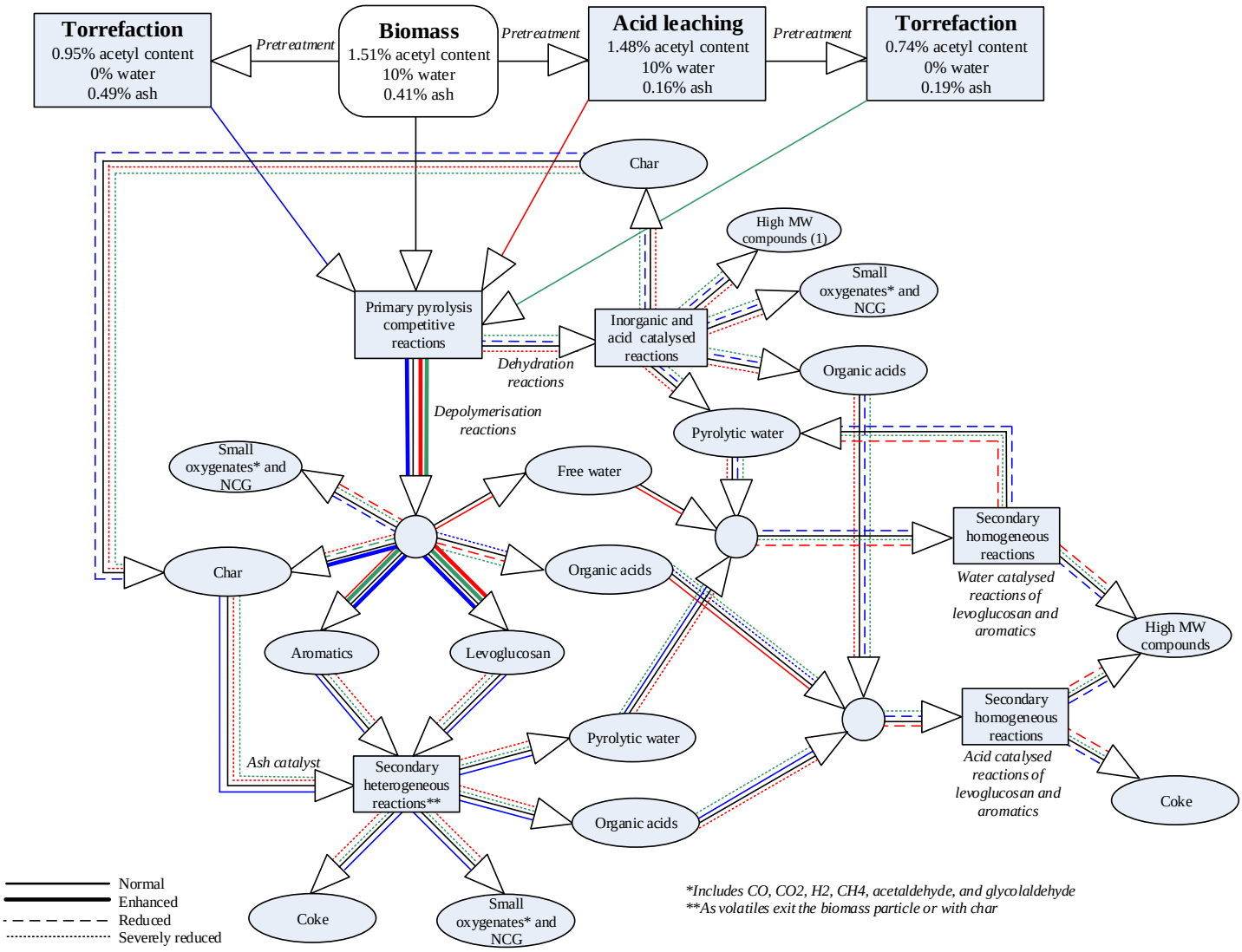

Figure 7-13: Proposed reaction pathways for pyrolysis of raw and pretreated biomass

SEM was used to visually investigate changes to the biomass's structure following the pretreatments. SEM images of raw and pretreated biomass are displayed in Figure 7-14. The pretreated biomass displayed was leached with 1% acetic acid at 30 °C followed by torrefaction at 270 °C for 20 min. No obvious differences were observed between the raw and pretreated biomass. Chen *et al.* [12] used SEM to obtain images of Lauan torrefied at 280 °C for 1 h. The images indicated surface damage, with a tubular shaped surface formed instead of the characteristic cell shape. However, torrefaction between 220-250 °C for 1 h did not significantly alter the biomass's surface. Lauan would be expected to be less reactive compared to *P. radiata* during torrefaction due to the high lignin content of Lauan (43.8 wt%), low hemicellulose content (15.7 wt%), and the low inorganic content (0.25 wt%). Perhaps reduced reactivity of leached *P. radiata* prevented surface alterations in the pretreated biomass so it reacted more like Lauan during torrefaction at 250 °C for 1 h.

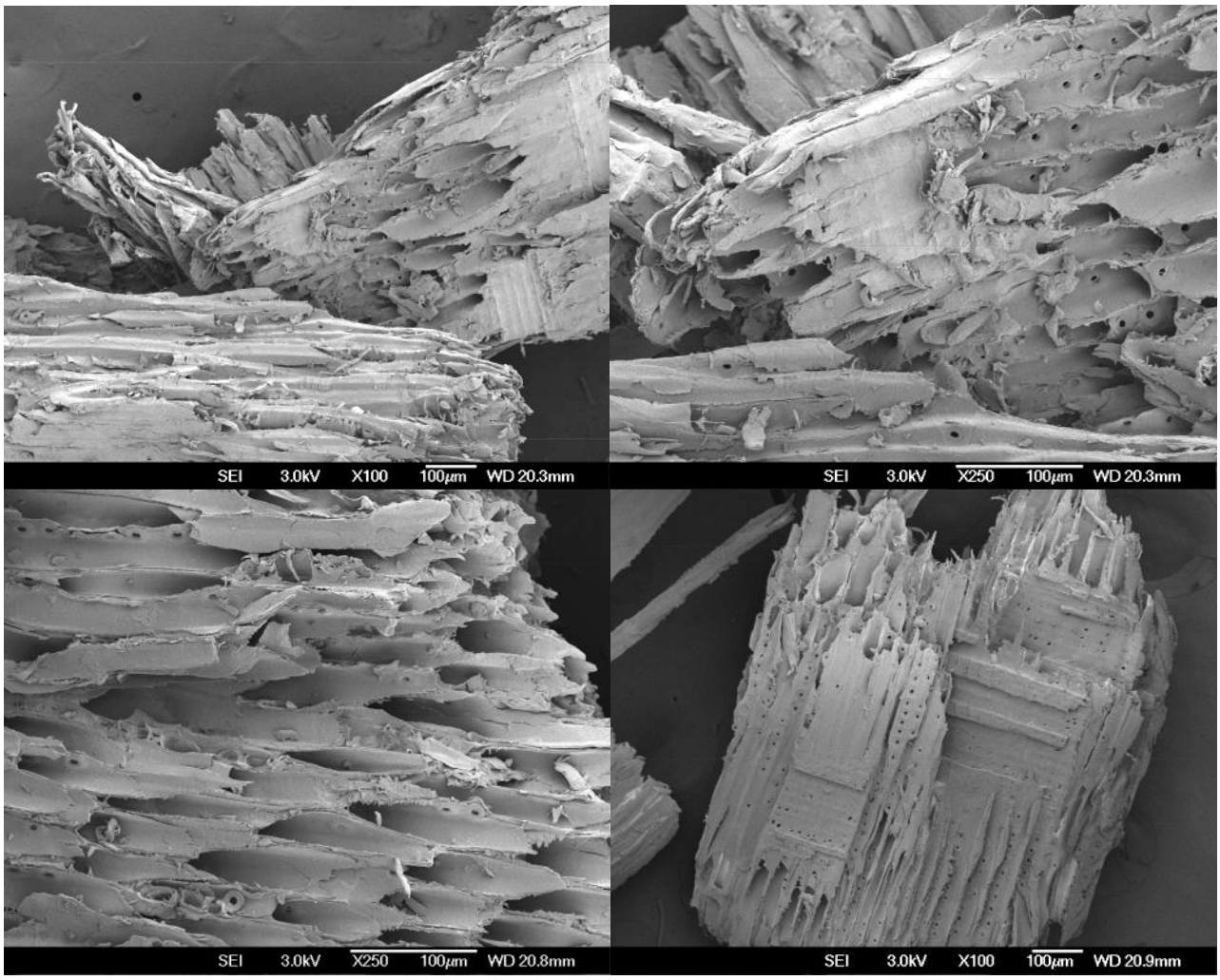

Figure 7-14: SEM images of raw biomass (top) and pretreated biomass (bottom)

7.4 Practical implementation of the biomass pretreatments

For the pretreatment of biomass to be commercially viable, the treatments need to be economical by reducing process effluent, decreasing energy inputs, and improving the bio-oil quality. Three options were explored:

- The pretreatment sequence was optimised using acetic and formic acid to represent the torrefaction liquor; therefore the leaching efficiency when using actual torrefaction liquor was compared to the synthetic solutions.
- Biomass was rinsed after leaching to remove the majority of the leaching acid. It was proposed that no rinsing step would be implemented commercially as torrefaction would volatise the remaining organic acids.
- Pretreatments were carried out on <2 mm wood chips; however pretreating larger wood chips would reduce the pretreatment costs for commercial systems, with a final milling employed after torrefaction.

7.4.1 Recycling torrefaction liquor for acid leaching

Recycling the torrefaction liquor for leaching reduces the requirement for a leaching reagent, whilst reducing the torrefaction effluent. However, torrefaction of biomass does not produce an adequate volume of liquid to leach an equivalent amount of biomass; therefore the leachate would need to be recycled from acid leaching, with possible regeneration using pyrolysis chars investigated later in this chapter, as char's hydrophilic surface is suitable for removing ions from water [13]. A portion of the leachate is lost during regeneration; this would be replenished with the new torrefaction liquor. The recycling and regeneration of leachate would minimise environmental issues concerning the disposal of the mobile phase after leaching due to possible trace amounts of hazardous elements.

Experiments were conducted by recycling the torrefaction liquor as the leaching solution. The results obtained from these experiments were compared to those obtained using 1% acetic acid solutions. The liquid was collected from 5 large scale leaching and torrefaction experiments; these aliquots were combined to yield a solution with an acetic acid concentration of 5.2%. The liquid was then diluted to a pH of 2.75 which was equivalent to the pH of the 1% acetic acid solution, and biomass was leached in this solution at 30 °C for 4 h. The actual acetic acid content in the solution after dilution was determined through HPLC as 0.54% and the formic acid concentration was 0.13%. Small amounts of hexanoic, octanoic, and nonanoic acid in the torrefaction liquor were not quantified by HPLC but would have contributed to the solution's acidity. These were detected when the torrefaction liquor was qualitatively analysed using gas chromatography-mass spectrometry (GC-MS) as described in Section 6.4.1.

The inorganic content in the biomass leached with recycled leachate was reduced to 0.15±0.02 wt%, which was slightly lower than for biomass leached with 1% acetic acid and slightly higher than biomass leached with 1% formic acid. This was expected as the solution's pH was higher than 1% formic acid solutions (pH of 2.33). The leached biomass samples were then torrefied at 270 °C for 20 min, with results compared to 1% acetic acid leached biomass in Table 7-8. Both samples were torrefied in the larger scale system (250 g per run), this produced biomass with a slightly different composition to small scale torrefaction, which will be discussed later in the Section 7.5. Torrefaction of biomass leached with recycled torrefaction liquor had a marginally higher biomass loss, indicating that torrefaction was slightly more severe. This was confirmed by the higher lignin and lower carbohydrate content in the biomass leached with recycled torrefaction liquor compared to biomass leached with 1% acetic acid. The increased severity was because torrefaction reached an average of 2 °C above the set-point temperature. Therefore, it was concluded that torrefaction liquor can be recycled as the leaching reagent.

Table 7-8: Comparison between biomass leached with 1% acetic acid and with recycled leachate

Leaching regent	1% acetic acid	Recycled torr. liquor
Torrefaction yields[1] (wt%)		
Biomass loss	12.2±1.4	13.4±1.3
Liquid yield	8.1±1.8	7.3±0.4
NCG yield	5.1±1.5	6.1±1.6
Liquid composition (%)		
Acetic acid	4.8±0.7	5.1±0.5
Formic acid	0.9±0.1	1.0
Methanol	2.1±0.4	2.3
Biomass properties following acid leaching and torrefaction (wt%)		
Acetyl content	0.71±0.13	0.75±0.27
Lignin	41.8±1.8	44.0±2.6
Hemicellulose	12.9±0.9	10.8±2.2
Cellulose	43.2±1.2	43.6±2.5
Inorganic content	0.14±0.02	0.14±0.02
Ultimate analysis of biomass (wt%)		
Carbon	52.5	52.1
Hydrogen	5.5	5.5
Nitrogen	0.1	0.1
Oxygen by diff.	41.9	42.4

[1]*Torreafaction was at large scale (250 g per run) for both samples*

7.4.2 Replacing biomass rinsing with mechanical dewatering after leaching

Demineralisation procedures require subsequent biomass rinsing to ensure complete removal of the leaching reagent. Rinsing is necessary because residual acids in the leached biomass reduce yields during pyrolysis and increase pyrolytic water through dehydration, condensation, and crosslinking reactions [14]. Additionally, residual acids in the feed material directly influence the bio-oil's pH. However, rinsing leached biomass could lead to economical drawbacks for commercial processes due to the large quantity of water required for rinsing and disposal of the contaminated water. Therefore, it would be beneficial if leached biomass did not have to be washed, instead, only vacuum filtered/pressed to remove the bulk of the leachate. This means that a proportion of the leaching reagent would remain in the biomass and enter torrefaction reactor where it would volatise; however the inorganics associated with leaching solution would remain in the biomass.

Biomass was leached with 1% acetic acid for 4 h at 30 °C. The biomass was vacuum filtered using a Buchner funnel to remove the bulk of the moisture. After this, the inorganic content of the leached biomass was 0.15±0.03 wt%. This is equivalent to the inorganic content of rinsed biomass; therefore a negligible amount of inorganics remain in the unrinsed biomass. Theoretical calculations agree with this result: if 2.5% of the leaching solution remains in the biomass (25% MC (dry basis) of the biomass following vacuum filtering) and 0.175 g of inorganics were removed from the biomass during the leaching. Assuming that the

0.175 g of inorganics were evenly distributed within the leachate, then there would only be 0.006 wt% additional inorganics in the biomass if rinsing was omitted.

7.4.3 Pretreatment of larger sized wood chips

Grinding biomass consumes a significant amount of energy. Torrefaction of biomass significantly reduces the grinding energy, thus it would be beneficial for leaching and torrefaction to be carried out on larger chips; afterward, a final size reduction can be implemented if necessary. Wood chips with a particle size of <6 mm were leached to compare the ion removal efficiency with that of standard wood particles with a particle size of <2 mm.

The <6 mm chips were leached using 1% acetic acid at the standard conditions (30 °C for 4 h). It was interesting to find that leaching was marginally more efficient with the larger chips and reduced the biomass's inorganic content to 0.15±0.02 wt%, indicating that the system was not limited by internal mass transfer. This finding could be because the <6 mm chips were milled predominantly in the longitudinal direction (with the grain), whereas the <2 mm particles were knife milled equally in the longitudinal, radial and tangential directions. Knife milling against the grain could close elongated tracheid cell ends, thereby reducing the mass transfer rate of leaching solution into the biomass and the rate of ion transfer out, especially if the knife blades were not sharp. Figure 7-15 provides a representation of the two different biomass sizes. The <6 mm chips could reach 20 mm in the longitudinal direction due to the chipping technique used, whereas the <2 mm particles were approximately equal in all directions.

SEM was used to determine if the tracheid cells became crushed during knife milling. Images of <2 mm wood particles are shown in Figure 7-16 for biomass that was knife milled and in Figure 7-17 for biomass that was simply sieved to <2 mm. There is a clear indication of crushing in Figure 7-16 while Figure 7-17 shows the cells retained their original shape. This confirms why the <6 mm chips could be leached with the same efficiency as the <2 mm particles. The leached <6 mm wood chips were torrefied at 270 °C for 20 min and then knife milled. Figure 7-18 compared the microstructure of raw biomass knifed milled (left) and biomass that was pretreated prior to the knife milling (right). The biomass knife milled prior to the pretreatments displayed slightly crushed cells, while the biomass milled after the pretreatments retained the original cell shape. Reducing polymeric interactions during torrefaction produces a more brittle biomass that is prone to shattering rather than compressing during milling. Biomass that retains the cell shape would have a higher surface area available for volatiles to escape during pyrolysis.

Figure 7-15: Wood chips <6 mm (left) and biomass knife-milled to <2 mm (right)

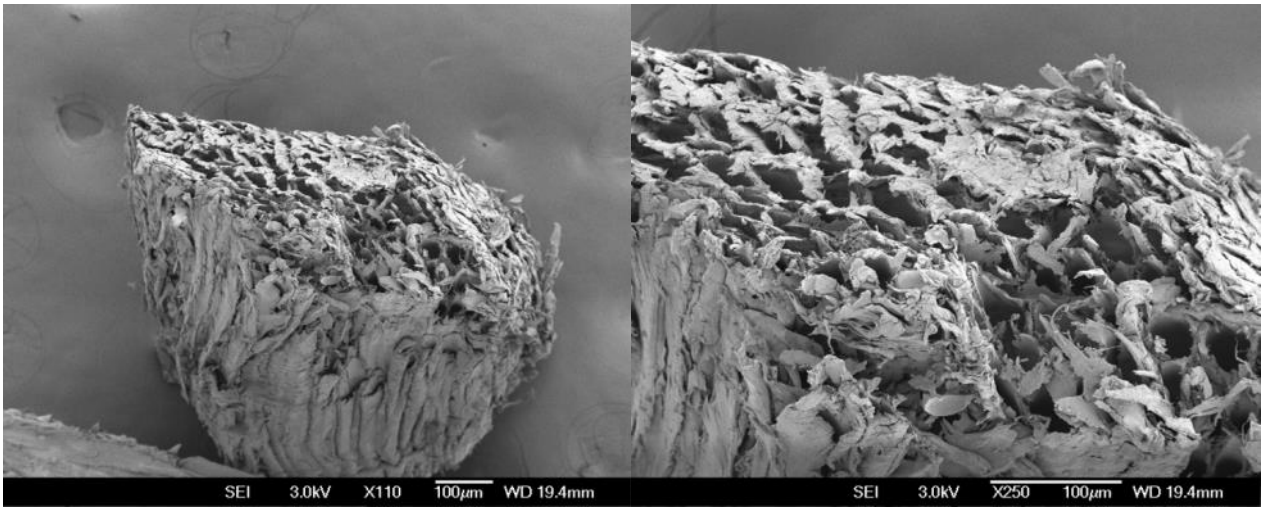

Figure 7-16: Biomass knife milled to <2 mm

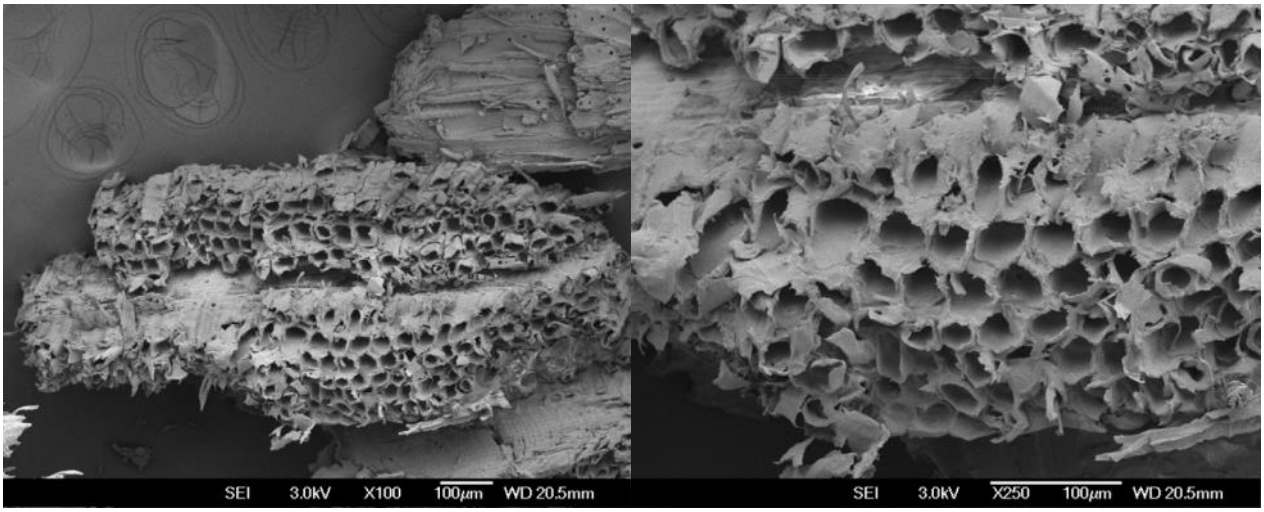

Figure 7-17: Biomass predominantly milled in the longitudinal direction to <6 mm then sieved to <2 mm

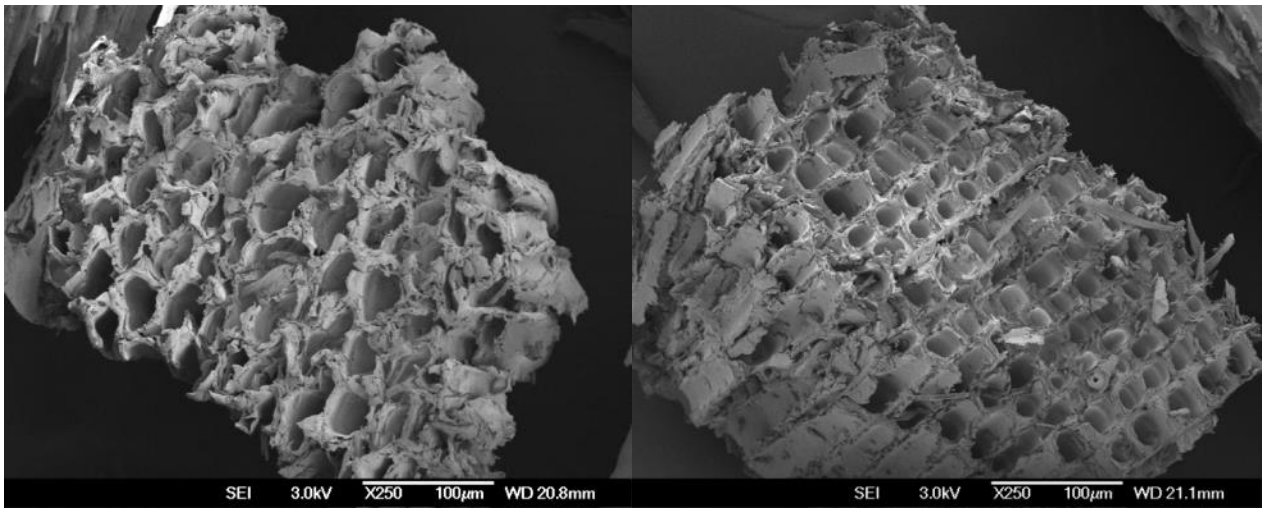

Figure 7-18: Biomass knife milled to <2 mm before pretreating (left), and biomass knife milled to <2 mm after pretreating (right)

The particle size distribution for biomass milled before and after pretreating is compared in Figure 7-19. Milling after torrefaction moved the particle size distribution curve to the left, indicating smaller particles were produced on average. This may be beneficial during pyrolysis as smaller particles reduce secondary reactions by decreasing the time for the entire particle to be heated to the pyrolysis temperature. Also, the time for pyrolysis vapours to exit the pyrolysing particle would be reduced for smaller particles. However, for consistency when comparing pyrolysis results to raw biomass, all subsequent experiments were conducted using biomass which was knife-milled prior to the pretreatments.

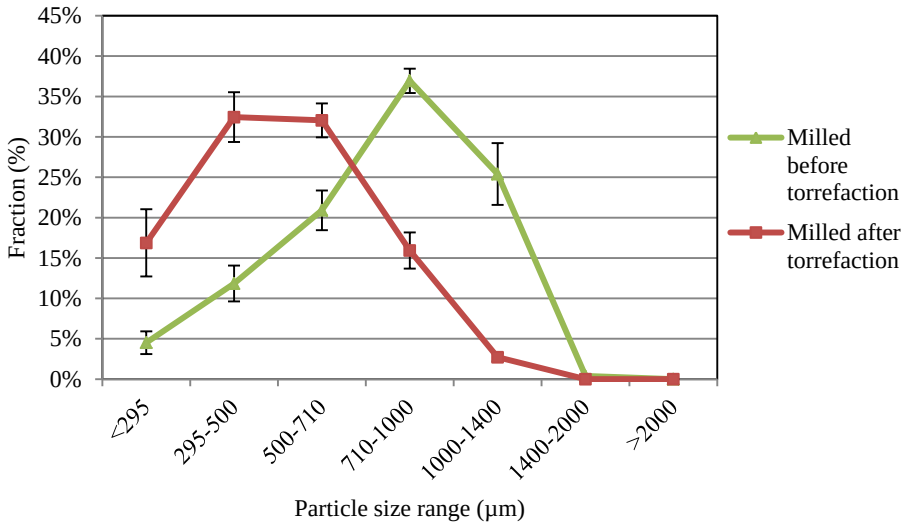

Figure 7-19: Particle size distribution for biomass milled prior to torrefaction and after torrefaction

7.5 Pyrolysis optimisation

7.5.1 Improvements to the pyrolysis system

The optimal pretreatment sequence was summaries as 1% acetic acid leaching at 30 °C for 4 h followed by torrefaction at 270 °C for 20 min from the discussion in Section 7.3. 5 kg of pretreated biomass was produced using the optimal pretreatment sequence and used during the pyrolysis experiments to optimise the pyrolysis conditions. Pyrolysis of raw biomass was also performed for a comparison with pyrolysis of pretreated biomass. Torrefaction at large scale took significantly longer to heat up compared to small scale (210 min compared to 40 min). It was shown in Section 6.3 that torrefaction residence time has minimal effect on the torrefaction severity. It was experimentally determined that dropping the torrefaction temperature to 264 °C, with a heat up time of 210 min was equivalent to torrefaction at 270 °C with a heat up time of only 40 min.

The properties of the pretreated biomass produced at small and large scales are compared in Table 7-9. The biomass loss was slightly lower in the scaled up pretreatment sequence, although the acetyl reduction remained approximately the same. There were small discrepancies between the two systems but the differences were within the uncertainty range. The acetic acid content in the torrefaction liquor was lower for the scaled up system since the severity of the scale up sequence was slightly less severe due to the marginally lower biomass loss.

Table 7-9: Comparison between pretreated biomass produced at small and large scale

	Small scale	**Large scale**
Biomass properties following acid leaching and torrefaction (wt%)		
Biomass loss during torrefaction	14.0±0.6	12.2±1.4
Acetyl content	0.74±0.03	0.71±0.13
Lignin	39.5±3.3	41.8±1.8
Hemicellulose	12.0±0.6	12.9±0.9
Cellulose	46.3±1.2	43.2±1.2
Total sugars	59.1±1.9	56.1±3.0
Inorganic content	0.14±0.04	0.14±0.02
Ultimate analysis of biomass (wt%)		
Carbon	53.6	52.5
Hydrogen	5.8	5.5
Nitrogen	0.1	0.1
Oxygen by diff.	40.6	41.9
Liquid composition (%)		
Acetic acid	7.9±1.5	4.8±0.7
Formic acid	0.9±0.3	0.9±0.1
Methanol	2.7±1.3	2.1±0.4
NCG composition (wt%)		
Carbon dioxide	-	82.7±0.4
Carbon monoxide	-	17.3±0.4

For the pyrolysis system, improvements were made to the temperature control on the fluidised bed and the electrostatic precipitator (ESP) before the system optimisation experiments commenced. The temperature control over the fluidised bed was improved by adding an additional temperature controller to bottom heating band. The cooling jacket around the auger feeding biomass into the fluidised bed acted as a heat sink to reduce the heat supplied to the reactor at this point; therefore adding a separate temperature controller to the lower heating band regulated the temperature profile over the fluidised bed to a higher degree.

It was noticed that the electric current produced in the ESP was between 0.1 and 0.5 µA during pyrolysis of pretreated biomass compared to 15 and 20 µA during pyrolysis of raw bio-oil. The low current indicated the collection efficiency of the ESP was significantly lower for pretreated bio-oil; therefore the liquid yield collected in the ESP was much lower, with a greater proportion of the liquid being captured in the filter instead. It was observed that bio-oils with a higher water content produced higher currents, thus it was thought the negative corona charges water molecules that either attach to aerosols or collide with aerosols as the water molecules are drawn to the positive collection plate. The collection mechanism is represented in Figure 7-20 (left).

Bedmutha *et al.* [15] stated that nitrogen, which is the main component in the vapour stream when used as the fluidising gas, does not form negative ions; therefore a positive corona was instead produced. To improve the ESP collection efficiency of pretreated bio-oil, changing the electrode to supply a positive voltage to produce a positive corona was investigated. However, this had no effect on the collection efficiency and actually decreased the current produced, indicating that there was no benefit to a positive corona, thus it was changed back to the negative electrode. It was established that bombardment of water molecules attracted to the positive plate was the main mechanism for vapour collection. Based on this theory, it was thought that purposeful drainage for ions to the positive collection plate could produce a similar effect for the collection of pretreated vapours that have low moisture content. The ESP was modified to extend the negative electrode to the full length of the ESP and the positive collection plate was also extended to the full length of the ESP system. This meant the positive collection plate was much closer to the negative electrode to provide constant drainage. The proposed mechanism for the collection of pretreated bio-oil is displayed in Figure 7-20 (right).

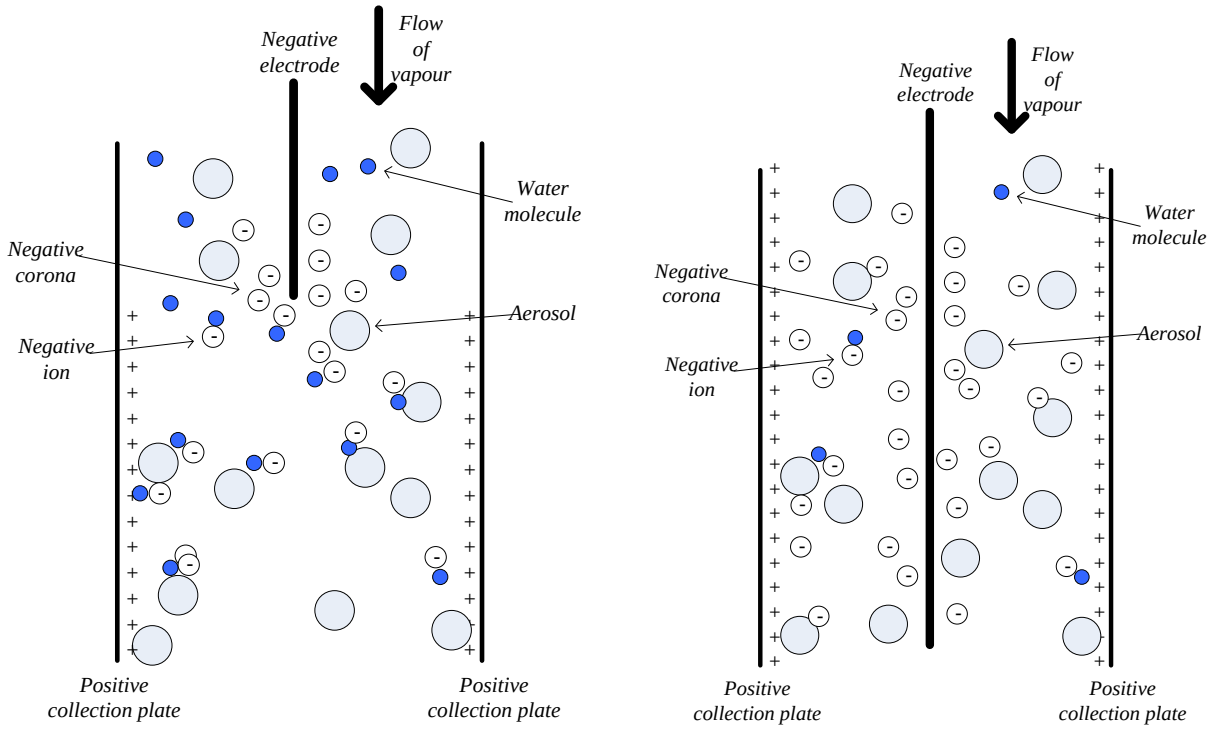

Figure 7-20: Proposed mechanism for vapour collection in the presence of moisture (left) and for near dry vapours (right)

7.5.2 Optimising the fluidised bed temperature

The fluidised bed temperature was varied between 400-525 °C at 25 °C increments to investigate the effect of the pyrolysis temperature on the bio-oil yield and properties. The advantages for using lower pyrolysis temperatures include:

- Lower the process costs
- Reduce the pyrolytic lignin content in bio-oil [16]
- Reduce inorganic volatilisation [17, 18]
- Reduced secondary polymerisation reactions [16, 19]
- Decrease the bio-oil's oxygen content due to increased CO_2 formation [17, 20].

The yields from pyrolysis of raw and pretreated biomass over the range of temperatures investigated are displayed in Figure 7-21. Both samples produced a maximum bio-oil yield at 500 °C but only slight decreases were observed over the temperature range investigated.

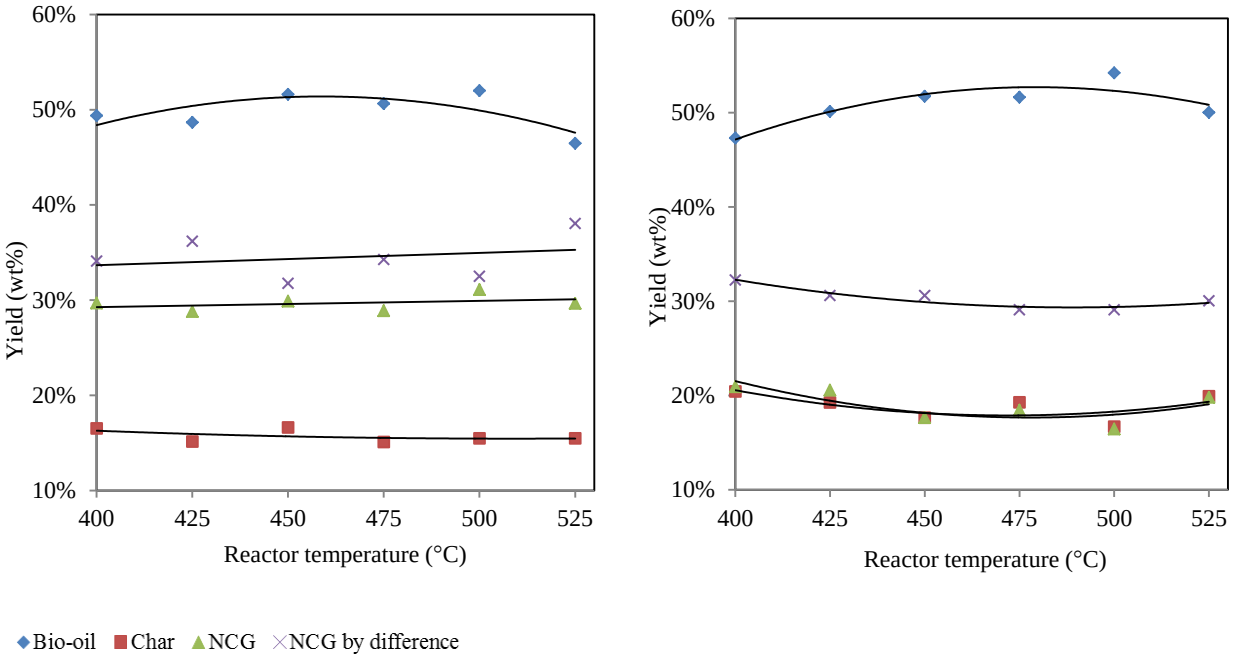

Figure 7-21: Yields for pyrolysis of raw biomass (left), and yields for pyrolysis of pretreated biomass (right)

An overall system mass balance was performed based on the measured yields of bio-oil, NCG, and char. The difference between the actual NCG measured and that calculated by difference can be seen in Figure 7-21. Typical mass balances discrepancies for pyrolysis systems are 10-20% due to the low accuracy when determining the product yields. For example, possible leaks when measuring the gas composition, which would alter the NCG yields measured. Oxygen was detected in the micro-GC, it was thought that this was from the injection technique. Additionally, bio-oil remaining in transfer lines, condensers, and the ESP all had to be accounted for. The equipment could not be accurately weighted due to its initial high weight; therefore the collection system was washed with acetone preceding a run to determine the total weight of bio-oil after the acetone was evaporated. The majority of the char was collected in the char pot but a small amount remained in the fluidised bed, cyclone, and transfer lines. The amount of char in the fluidised bed was determined by combusting the sand and char mixture collected at the end of a run. The cyclone and transfer lines were cleaned with an extended brush; however a small amount of char adhered the walls and required combustion for removal, and was not accounted for as weighting the parts accurately was not possible.

The NCG compositions are given in Figure 7-22 for pyrolysis of raw and pretreated biomass over the pyrolysis temperature range investigated. The cyclone temperature was maintained at 450 °C throughout the experiments; therefore pyrolysis reactor temperatures <450 °C would have been influenced by the further reactions occurring in the cyclone. Only one variable at a time was altered for consistency: the subsequent section investigates the effect of lowering the cyclone temperature. This means trends for the NCG composition were obscured and unreliable to predict at this stage. Variations between pyrolysis of raw and pretreated biomass can, however, be established. Pretreating biomass decreased the total NCG production. The CO, CO_2, H_2, and C_2H_2 formation decreased while the CH_4 and C_2H_6 remained approximately constant.

This was very similar to trends reported by Ren *et al.* [21] for microwave pyrolysis of torrefied biomass, who reported an increase in the H_2, CH_4, and CO fractions (in terms of the fraction in the NCG stream) and a decrease in the CO_2 fraction of the NCG.

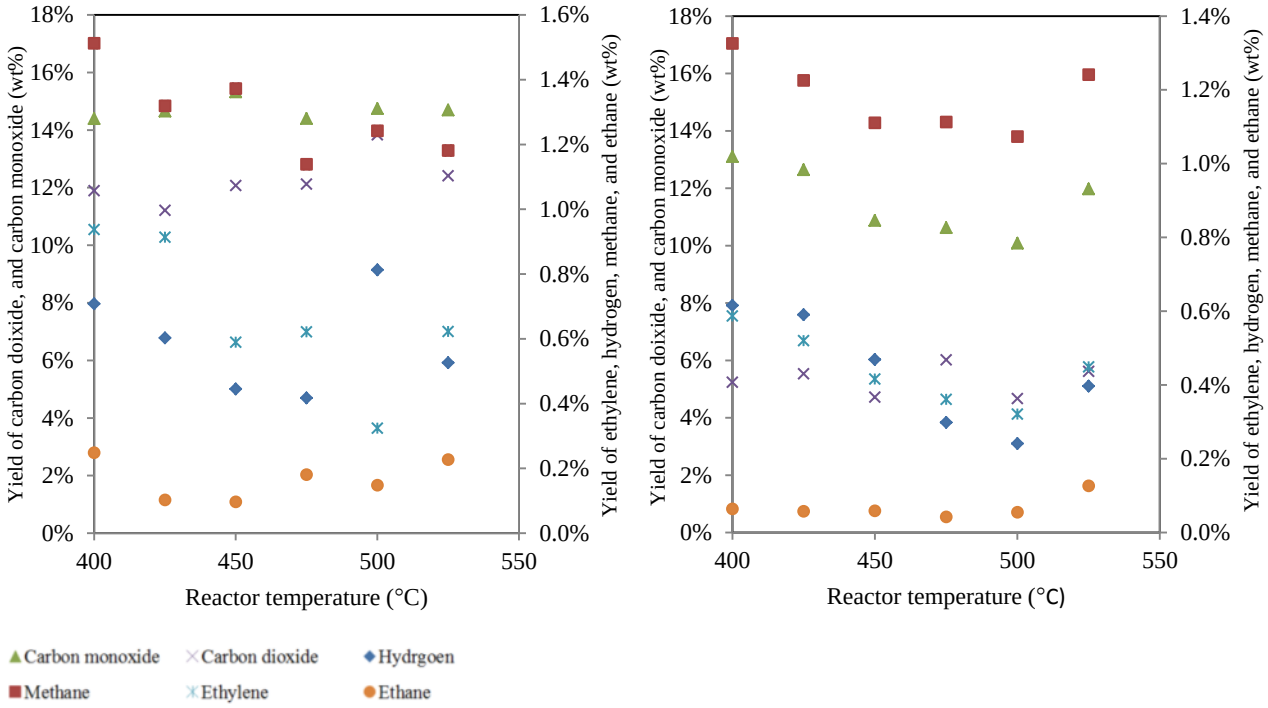

Figure 7-22: NCG yields from pyrolysis of raw biomass (left) and pretreated biomass (right)

The bio-oil compositions were analysed in detail, with results given in Table 7-10 for raw bio-oil and in Table 7-11 for pretreated bio-oil. The NCG heating values are also displayed in these tables. Similarly to NCG yields, the cyclone temperature operating at 450 °C reduced the viability of obtaining reliable trends from the data. It was desirable to operate at the lowest reactor temperature possible without hindering the bio-oil quality or quantity. For both the raw and pretreated bio-oil, reducing the pyrolysis temperature to 450 °C only had minimal effect on the organic bio-oil yield. Decreasing the pyrolysis temperature for pretreated biomass reduced the water content in the bio-oil, likely from reduced secondary reactions. The GPC (molecular weight distribution curves are given in Figure 7-23) and CHN results indicated minimal variance within the temperature range investigated; this was also reported by Westerhof *et al.* [19] for pyrolysis of pine wood between 450-530 °C. GPC results may fluctuate with changing pyrolysis temperatures as the concentration of phenol and its derivatives varies: higher temperatures tend to increase secondary reactions and break down phenol oligomers, however, their formation is increased due to further lignin degradation [16, 20].

Table 7-10: Properties of bio-oil produced from raw biomass at varying pyrolysis temperatures

Pyrolysis temperature (°C)	400	425	450	475	500	525
Bio-oil properties						
Acetic acid conc. (%)	3.2±0.0	3.1±0.1	3.1±0.0	3.2±0.7	3.0±0.0	3.0±0.0
Water (wt%)	22.1±1.8	19.1±1.1	24.6±2.7	22.0±2,5	21.1±2.9	23.8±2.4
Organic yield (wt%)	38.5	39.4	38.9	39.5	41.0	35.4
Overall organic yield[1] (wt%)	38.5	39.4	38.9	39.5	41.0	35.4
NCG heating value (MJm^{-3})	12.2	11.6	10.4	10.1	10.6	10.5
GPC results						
Average number, Mn ($gmol^{-1}$)	193.0	202.6	197.2	198.6	210.1	199.3
Weight average, Mw ($gmol^{-1}$)	286.0	304.6	296.0	297.0	316.9	298.3
Size average, Mz ($gmol^{-1}$)	457.1	490.5	476.9	475.4	502.9	472.8
>650 $gmol^{-1}$ (%)	6.8	8.14	7.6	7.6	8.2	7.7
Ultimate analysis						
Wet basis						
Carbon (%)	38.7	42.3	39.1	40.6	40.4	40.6
Hydrogen (%)	7.6	7.2	7.61	7.7	7.4	7.4
Nitrogen (%)	0.6	0.5	0.6	0.9	0.6	0.5
Oxygen, by difference (%)	53.1	50.1	52.7	50.9	51.7	51.4
Dry basis						
Carbon (%)	49.7	52.2	51.8	52.0	51.2	53.3
Hydrogen (%)	6.6	6.2	6.5	6.7	6.4	6.3
Nitrogen (%)	62.8	62.9	67.7	63.8	60.4	65.4
Oxygen, by difference (%)	42.9	40.9	41.0	40.1	41.7	39.7
Higher heating value ($MJkg^{-1}$)	20.7	21.3	21.5	21.9	21.1	21.9
Overall energy in bio-oil[2] (MJ)	8.0	8.4	8.4	8.7	8.7	7.8

[1]Taking into account the mass loss during torrefaction and leaching. [2]Per kg of biomass feed

Table 7-11: Properties of bio-oil produced from pretreated biomass at varying pyrolysis temperatures

Pyrolysis temperature[1] (°C)	400	425	450	475	500	525
Bio-oil properties						
Acetic acid conc. (%)	0.7±0.0	0.4±0.2	0.3±0.0	0.2±0.0	0.3±0.1	0.3±0.1
Water (wt%)	3.2±0.9	2.9±0.9	2.7±0.9	2.3±0.6	4.1±0.3	4.5±0.7
Organic yield (wt%)	45.8	48.7	50.3	50.5	52.0	47.8
Overall organic yield[2] (wt%)	39.9	42.5	43.9	44.0	45.3	41.7
NCG heating value (MJm^{-3})	14.5	14.0	13.8	11.8	12.3	13.0
GPC results						
Average number, Mn ($gmol^{-1}$)	191.4	196.1	190.1	192.3	186.7	192.6
Weight average, Mw ($gmol^{-1}$)	262.0	267.4	257.5	256.2	251.7	261.9
Size average, Mz ($gmol^{-1}$)	391.8	396.1	380.1	372.7	367.4	390.6
>650 $gmol^{-1}$ (%)	4.4	4.5	4.1	3.8	3.6	4.4
Ultimate analysis						
Wet basis						
Carbon (%)	50.3	49.8	51.2	49.8	50.0	48.9
Hydrogen (%)	6.2	6.1	6.2	6.1	6.3	6.4
Nitrogen (%)	0.3	0.3	0.3	0.3	0.4	0.3
Oxygen, by difference (%)	43.2	43.8	42.2	43.8	43.4	44.5
Dry basis						
Carbon (%)	52.0	51.3	52.7	51.0	52.1	51.1
Hydrogen (%)	6.0	6.0	6.0	6.0	6.1	6.2
Nitrogen (%)	0.3	0.3	0.4	0.3	0.4	0.3
Oxygen, by difference (%)	41.7	42.4	40.9	42.7	41.4	42.4
Higher heating value ($MJkg^{-1}$)	21.0	20.6	21.3	20.4	21.0	20.7
Overall energy in bio-oil[3] (MJ)	8.4	8.8	9.4	9.0	9.5	8.6

[1]Biomass was leaching with 1% acetic acid at 30 °C for 4 h. [2]Taking into account the mass loss during torrefaction and leaching. [3]Per kg of biomass feed

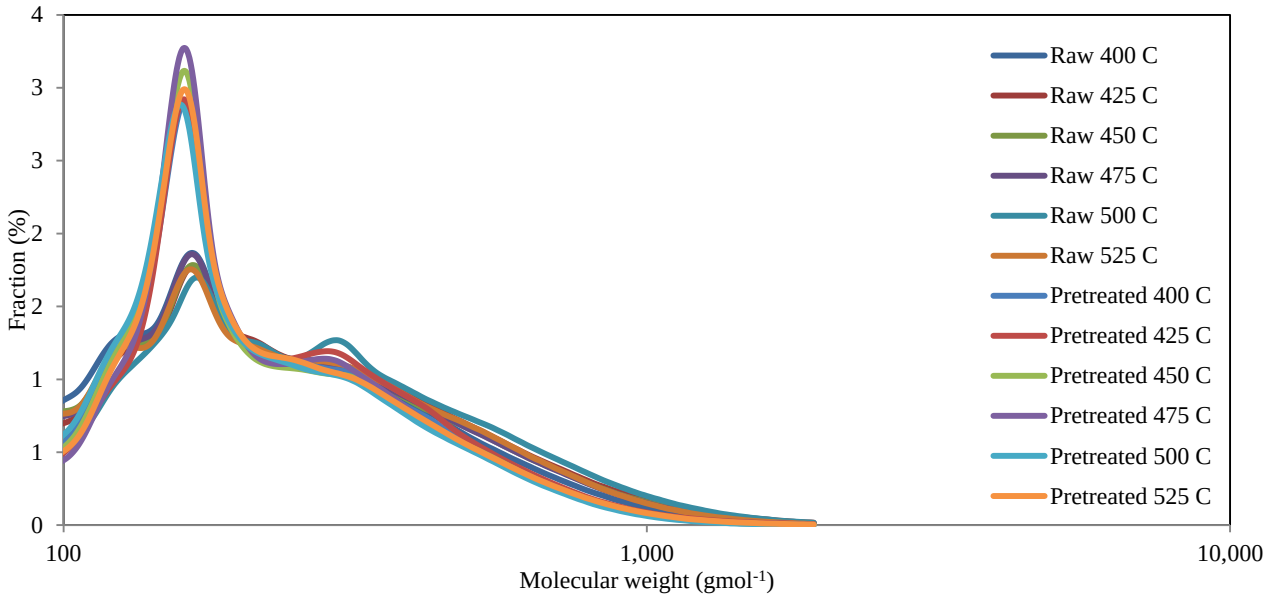

Figure 7-23: Molecular weight distribution curves for raw and pretreated bio-oil samples at different pyrolysis temperatures

The bio-oil compositions were analysed using ^{1}H-NMR, with results given in Figure 7-24 on a water free basis and in Figure 7-25 relative to the feed rate of biomass. Relative the biomass feed rate, lower pyrolysis temperatures produced slightly less alkanes, acetaldehyde, acetic acid, and aromatics. Increased aromatics at higher pyrolysis temperature was reported by DeSisito *et al.* [17] due to further lignin degradation. The maximum levoglucosan concentration was in the middle temperature range as lower temperatures encourage the production of alternative compounds while higher temperatures are associated with increased secondary degradation of levoglucosan. This indicated there was a change in the pyrolysis mechanism at different temperatures which slightly altered the pyrolysis products.

The bio-oil compositions did not vary significantly for pyrolysis temperatures between 450-525 °C, similar results were reported by Westerhof *et al.* [19], who stated there was minimal change to the bio-oil when lowering the pyrolysis temperature from 530 to 450 °C. Pyrolysis temperatures <450 °C lead to a decrease in the organic yield and increased water and acetic acid in the pretreated bio-oil; therefore the optimal pyrolysis temperature was 450 °C.

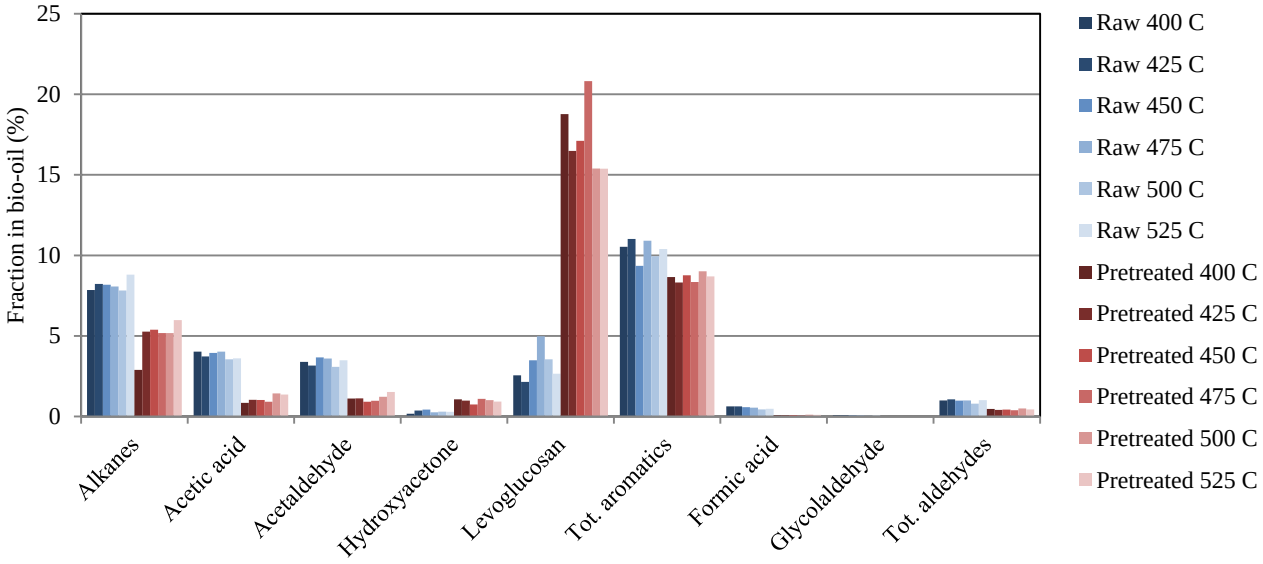

Figure 7-24: ^{1}H-NMR peak area for bio-oil composition, water free basis

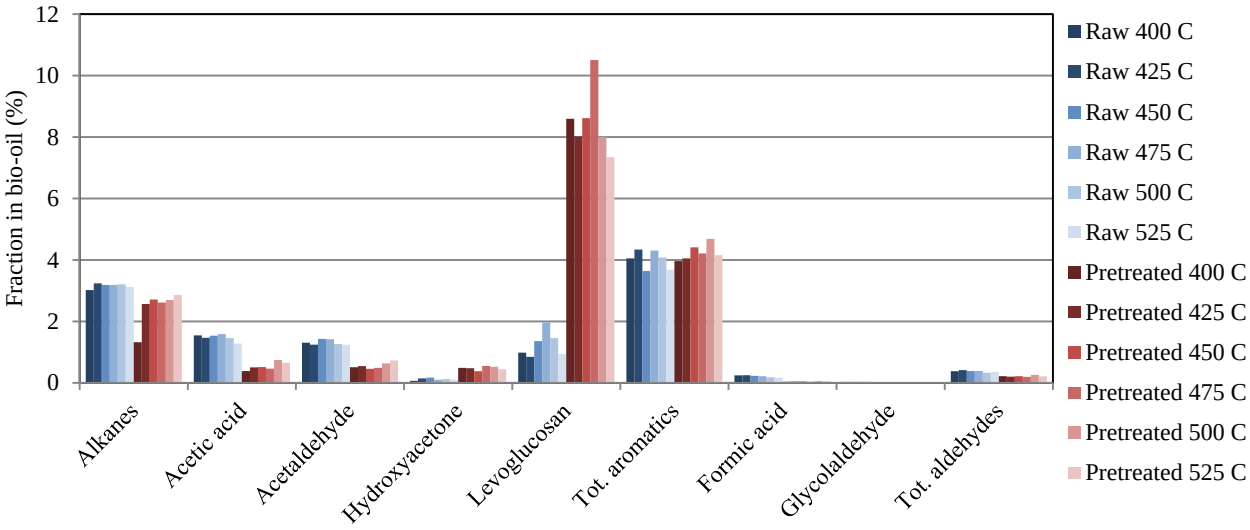

Figure 7-25: ^{1}H-NMR peak area for bio-oil composition, relative to the biomass feed

7.5.3 Optimising the cyclone temperature

The cyclone temperature was originally set at 450 °C to ensure no vapour condensation occurred in the cyclone. Lowering the temperature to 350 °C was investigated to determine the lowest practical cyclone temperature when the pyrolysis reactor operated at 450 °C. Pyrolysis yields from raw and pretreated biomass over the range of cyclone temperatures (350 to 450 °C) are given in Figure 7-26. Reducing the cyclone temperature from 450 to 400 °C increased the bio-oil yield and decreased the NCG yield for pyrolysis of both raw and pretreated biomass. This indicated the cyclone temperature at 450 °C caused either homogeneous or heterogeneous secondary reactions with char by reaching the activation temperature for secondary gasification reactions. The cyclone was trace heated with the temperature controlled at the inlet, thus, the temperature in the cyclone body may have varied from the set-point. The cyclone exit was modified to allow for a temporary thermocouple to be inserted down the cyclone's length. When the cyclone inlet temperature was set to 450 °C, a maximum of 510 °C was measured in the cyclone, confirming hot spots

within the cyclone were above the set-point temperature. Unless the cyclone heating mechanism was changed to a jacketed type supply, the temperature profile was unavoidable, thus the cyclone temperature was still optimised using the inlet temperature.

Bio-oil yields suddenly dropped when the cyclone temperature was lowered to 350 °C. Condensation of vapours occurred at this temperature and bio-oil adhered to the char; therefore exited the system as char. Operating the cyclone at or lower than 350 °C is not recommended due to premature vapour condensation.

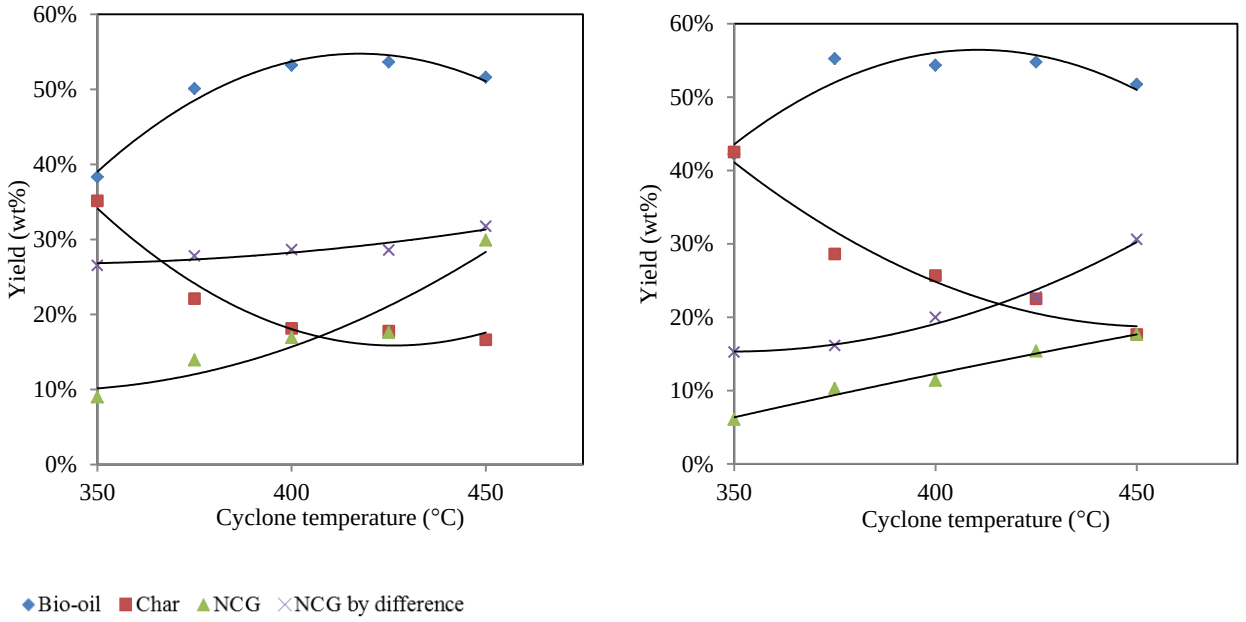

Figure 7-26: Pyrolysis yields when varying the cyclone temperature for raw biomass (left), and pretreated biomass (right)

The NCG compositions were analysed over the cyclone temperature range examined (350-450 °C), with the individual gas yields reported in Figure 7-27 for raw and pretreated biomass. When operating the cyclone at 400 °C, the CO and CO_2 productions were approximately equal. Lower temperatures produced a NCG rich in CO_2, while higher cyclone temperatures caused the CO yield to surpass the CO_2 yield. The production of CO increases when pyrolysis gases are held at high temperatures for extended residence times or exposed to higher temperatures due to thermal cracking of cellulose and hemicellulose derived vapours [22].

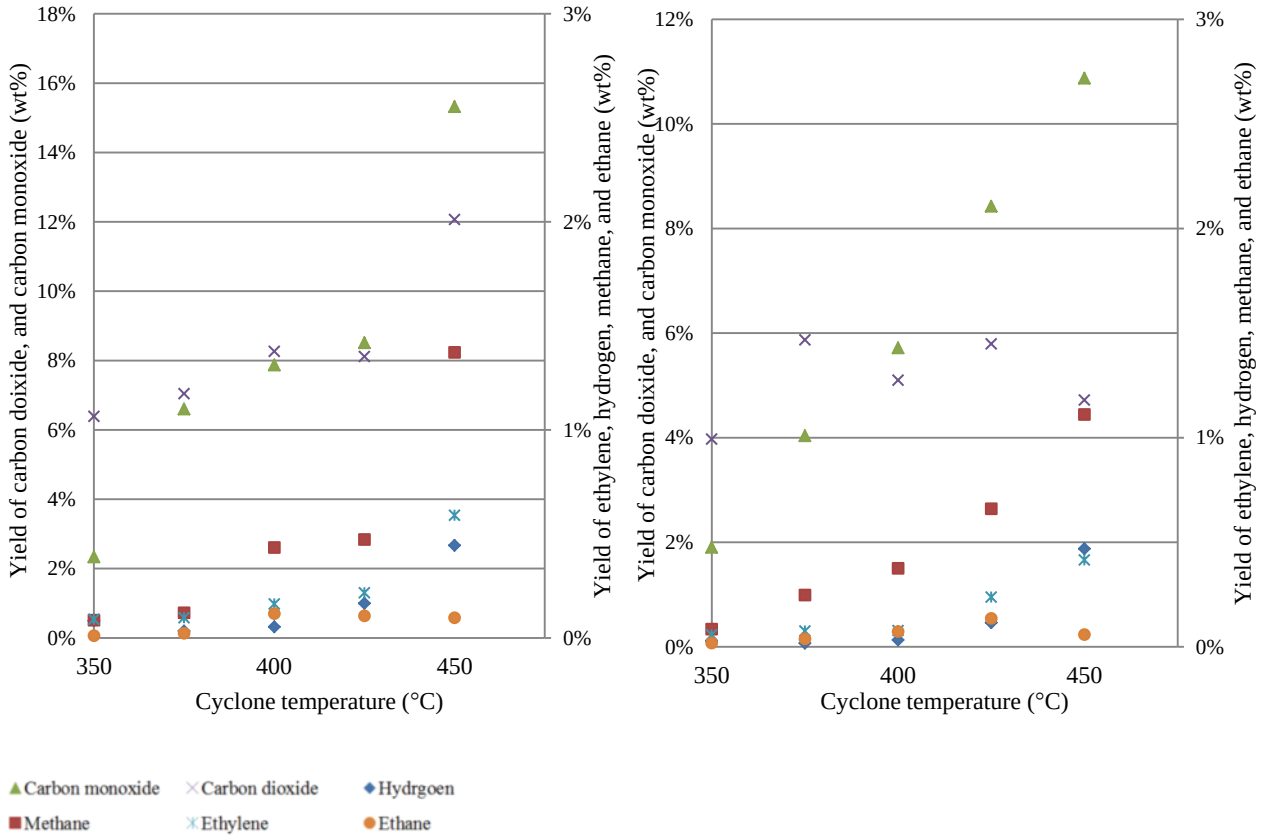

Figure 7-27: NCG yields from pyrolysis of raw biomass (left) and pretreated biomass (right)

The NCG yields were also expressed in terms of the fractions of each component in the stream, with the results displayed in Figure 7-28. From the figure, it was found that CO_2 was the main component in the NCG stream at lower cyclone temperatures but with an increase in the cyclone temperature, the CO_2 fraction decreased and the fractions CO and other compounds increased. Thus, the heating value of the gas stream increased at higher cyclone temperatures. The fraction of CO in the NCG stream for pyrolysis of pretreated biomass was higher compared to that for raw biomass since a portion of the easily cleavable CO_2 groups were volatised during torrefaction. The effect of torrefying biomass is beneficial in terms of NCG end usage as the increased heating value makes gas more useful.

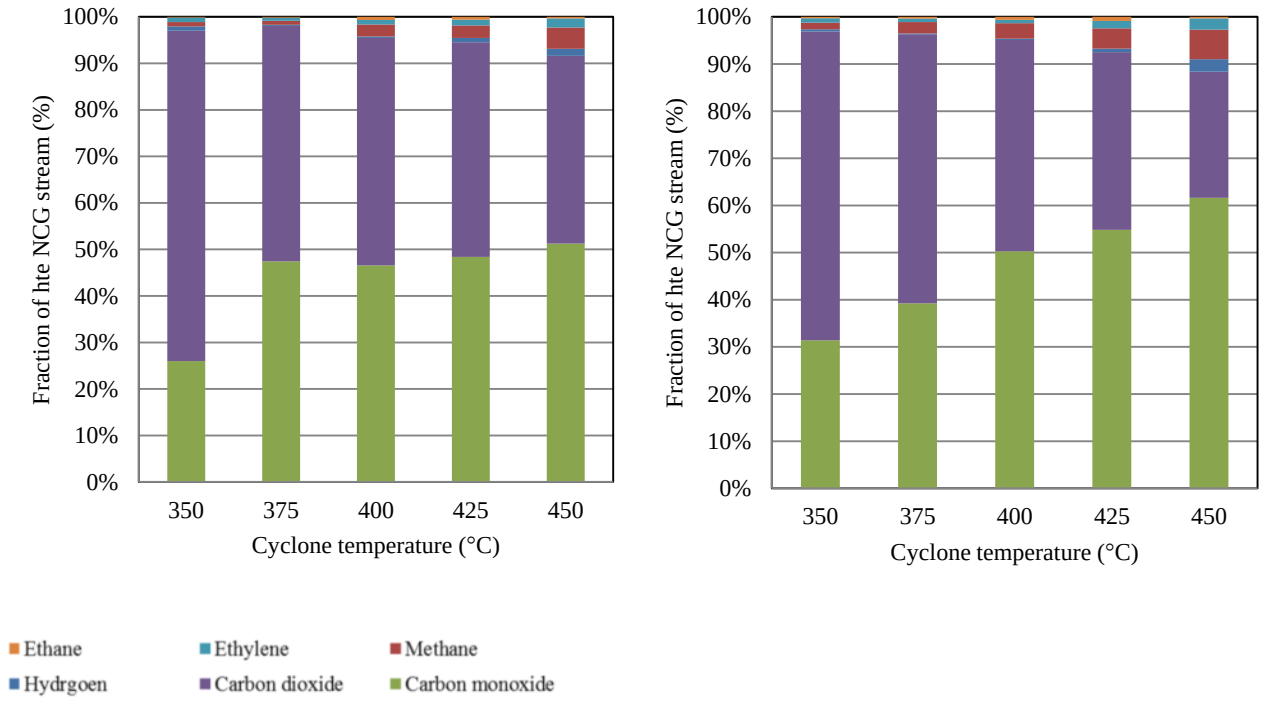

Figure 7-28: Gas component fraction in the NCG stream from pyrolysis of raw biomass (left), and pretreated biomass (right)

Key bio-oil properties were determined and results are given in Table 7-12. GPC, CHN, and ^{1}H-NMR were not carried out on the bio-oil samples in this part of the study due to the cost of the tests and small variance in results when the pyrolysis reactor temperature was altered in the preceding section. The bio-oil's acetic acid content was highest at both the lowest and highest cyclone temperatures (350 and 450 °C). It is understood that high temperatures enhance secondary reactions and increase the production of acetic acid. However, the increase at low temperatures was partially due to the lower overall bio-oil yield: large compounds with high boiling points were thought to condense in the cyclone rather than in the condensers while small compounds such as acetic acid would still exit the cyclone.

The large increase in NCG yields as the cyclone temperature increased was partially from secondary reactions. The bio-oil's quality and yield only marginally decreased at high cyclone temperatures, but the char yield decreased significantly. This indicated biomass was still partially decomposing in the cyclone; therefore the residence time for biomass particles in the fluidised bed was too short. Increasing the residence time in the fluidised bed could be accomplished by the addition of more fluidising sand. A low biomass to sand ratio of 75:1 sand to biomass was used in experiments to replicate ratios used at industrial scale; therefore increasing the sand to biomass ratio was investigated in the subsequent section. The optimal cyclone temperature was considered as 425 °C for pyrolysis of both pretreated and raw biomass as this produced the lowest water and acetic acid content in the bio-oil while providing the highest liquid yield. When increasing the sand loading in the fluidised bed, the cyclone temperature was set to 400 °C as it was thought that extended residence times and higher temperature in the cyclone would decrease the bio-oil yield and enhance secondary vapour reactions in the cyclone.

Table 7-12: Bio-oil properties from raw and pretreated biomass at varying cyclone temperatures

Cyclone temperature (°C)	350	375	400	425	450
Pyrolysis of raw biomass					
Acetic acid conc. (%)	3.2±0.1	2.3±0.1	2.5±0.1	1.9±0.1	3.1±0.0
Water (wt%)	19.1±0.6	22.0±2.2	18.9±2.4	17.1±0.2	24.6±2.7
Organic yield (wt%)	31.0	39.1	43.2	44.5	38.9
Overall organic yield[1] (wt%)	31.0	39.1	43.2	44.5	38.9
NCG heating value (MJm^{-3})	4.7	5.9	7.2	9.63	10.4
Pyrolysis of pretreated biomass					
Acetic acid conc. (%)	0.6±0.1	0.1±0.0	0.1±0.0	0.1±0.0	0.3±0.1
Water (wt%)	5.2±0.3	5.01±1.6	4.6±0.2	3.0±0.1	2.7±0.9
Organic yield (wt%)	40.1	52.5	51.9	53.2	50.3
Overall organic yield[1] (wt%)	35.0	45.8	45.2	46.4	43.9
NCG heating value (MJm^{-3})	5.0	5.9	7.7	9.8	13.8

[1]*Taking into account the mass loss during torrefaction and leaching*

7.5.4 Optimising the sand volume in the fluidised bed

The standard sand loading in the fluidised bed was 12.5 g. This was increased to 25, 50, and 75 g to investigate if the biomass's residence time (RT) in the fluidised bed has and effect on the pyrolysis yields and bio-oil composition. The sand to biomass ratios investigated and the corresponding residence times in the fluidised bed are given in Table 7-13. The residence time was still theoretically short at 0.066 s with 75 g of sand in the fluidised bed as the calculation only considers the void volume in the bed and the gas flow rate upwards (RT=bed voidage/gas flow rate). The actual time would be longer as interactions with other biomass particles, sand, char, and the reactor wall were not taken into consideration in the calculation.

Table 7-13: Sand to biomass ratio and biomass residence time in the fluidised bed

Sand mass (g)	Sand to biomass ratio	Biomass RT in bed (s)
12.5	75:1	0.012
25.0	150:1	0.023
50.0	300:1	0.044
75.0	450:1	0.066

The pyrolysis yields from both raw and pretreated biomass over the range of sand loadings considered are given in Figure 7-29. The pyrolysis temperature was set to 450 °C and the cyclone temperature to 400 °C for all experiments. From Figure 7-29, it was found that the sand loading in the reactor had a lesser influence on the pyrolysis yield compared to altering the pyrolysis or cyclone temperature, especially for pyrolysis of raw biomass. Increasing the sand loading from 12.5 to 25 g for pyrolysis of raw biomass increased the bio-oil yield as the biomass's exposure with hot sand was extended. However, further increasing the sand loading promoted secondary reactions, thus the bio-oil yield decreased while the char yield increased slightly.

It was mentioned in Chapter 5 that pyrolysis of acid leached biomass tended to agglomerate in the fluidised bed. All runs with pretreated biomass had a larger portion of char remaining within the system compared to pyrolysis of raw biomass. This remaining char was found to be distributed over the fluidised bed walls, transfer lines, and in the cyclone. Increasing the sand loading in the fluidised bed decreased the char accumulation within the system, probably through reduced biomass, aerosol, and char impactions in the fluidised bed and the higher sand loading scouring the fluidised bed. Char and aerosols adhered to the

system walls reacted further in the hot environment to produce additional vapours at the expense of char. These reactions were not desirable as they are uncontrolled and the products were more typical of secondary type products, such as water and small oxygenates; therefore pyrolysis of pretreated biomass required 75 g of sand to reduce char accumulation in the system. To compensate for the lower yield, the cyclone temperature was operated at 425 °C.

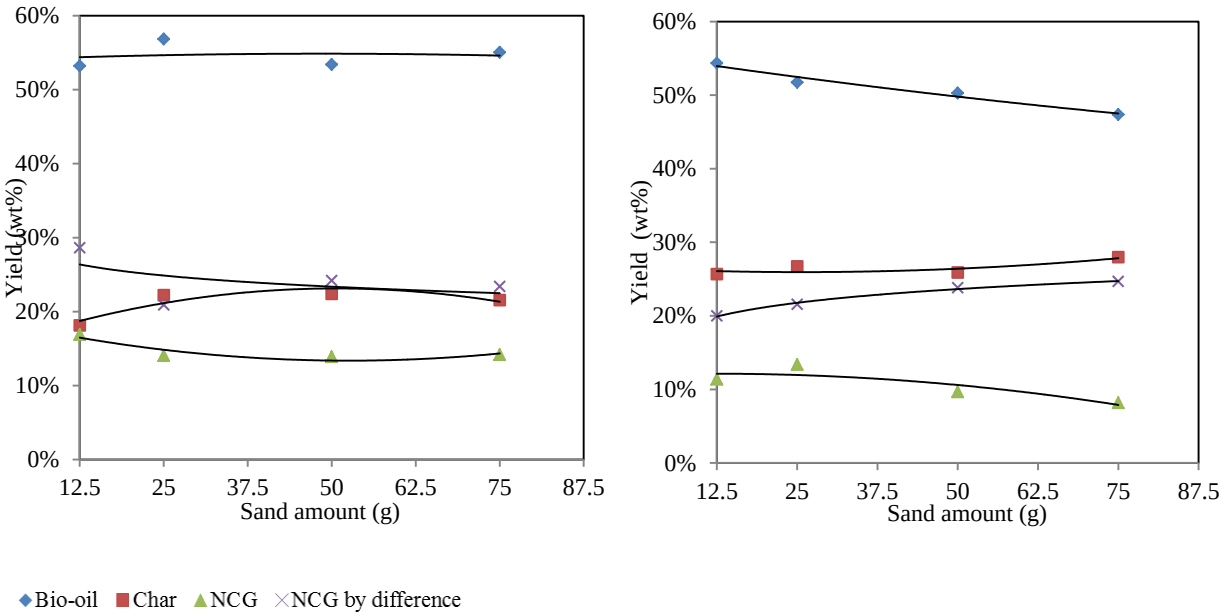

Figure 7-29: Pyrolysis yields as a function of sand loading for raw biomass (left), and pretreated biomass (right)

The yields of gas compounds in the NCG are displayed in Figure 7-30 for pyrolysis of raw and pretreated biomass. From the figure, C_2H_6 and CH_2 were only detected for raw biomass with sand loadings of 12.5 and 25 g in the fluidised bed. The yields for C_2H_4, CO, and CO_2 remained approximately constant for pyrolysis of raw biomass, except were higher with 12.5 g of sand. The lower yields at higher sand loadings may be from faster particle heating times in the presence of more sand, as conductive heat transfer increases. When increasing the sand loading was above 25 g, the increased heat transfer rate might be offset by the longer particle/vapour residence times enhancing secondary reactions of vapours.

Pyrolysis of pretreated biomass produced higher gas yields for most gas compounds when the sand mass was increased to 25 g, but then the yields decreased when the sand loading was increased further. The initial increase for 25 g of sand may be associated with the change in the heating rate of the biomass, while higher sand loadings led to a reduction in agglomeration, and therefore reduced secondary cracking reactions.

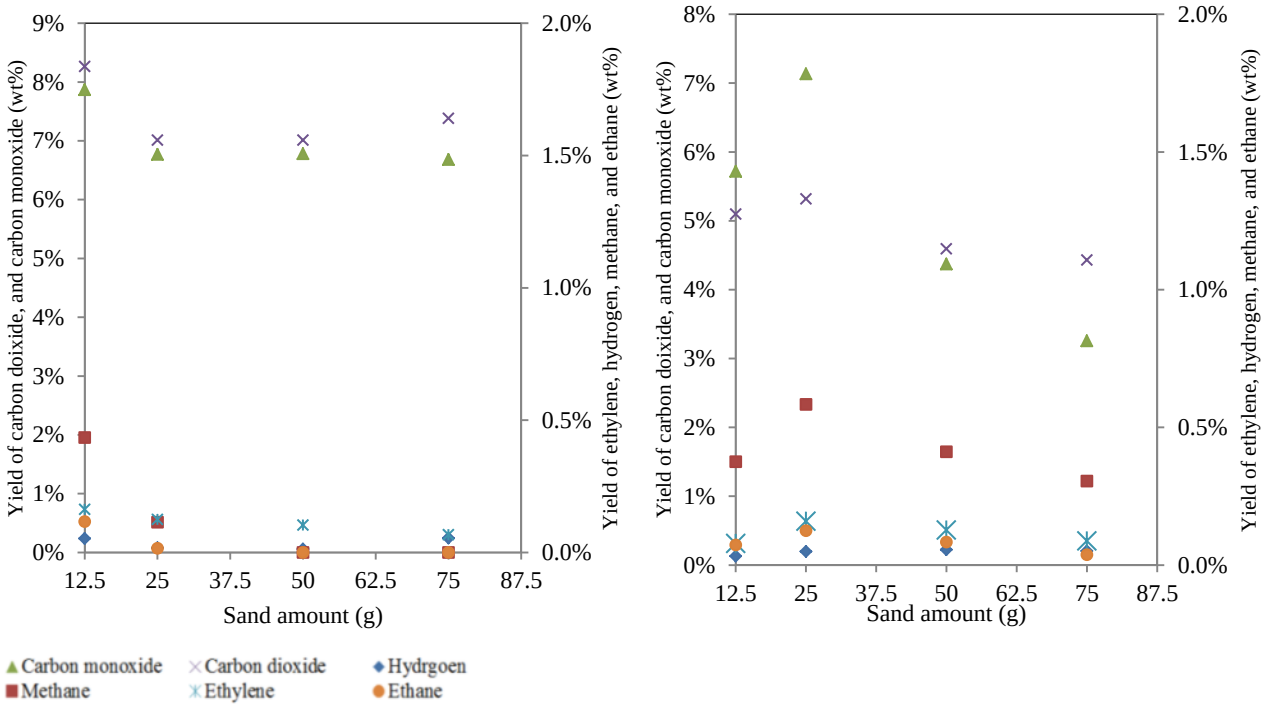

Figure 7-30: NCG yields for pyrolysis of raw biomass (left), and pretreated biomass (right)

The total inorganic content in the char was quantified for the different sand loadings to determine if sand may abrade and exit with the char. Results are given in Figure 7-31, these indicate a significant increase in the total inorganic content of the char as the sand loading increased. Per 1 kg of raw biomass fed into the reactor, there was 4.1 g of ash in the biomass. The ash in the raw char was 3.8, 3.5, 7.5, and 8.6 g for sand masses of 12.5, 25, 50, and 75 g respectively. Per 1 kg of pretreated biomass fed into the reactor, there was 1.5 g of ash in the biomass. The ash in the pretreated char was 1.9, 5.9, 8.4, and 12.5 g for sand masses of 12.5, 25, 50, and 75 g respectively. This indicated a huge increase in inorganics for both biomass types when more sand mass was used, especially for pyrolysis of pretreated biomass. While pure silica is reported to be inert during pyrolysis [23], the silica sand used for fluidising was off-white; therefore was not pure silica. ICP-OES of the sand was used to determine the composition of other elements present. Results are given in Table 7-14. These indicate sand was 99.92% silica. Other elements present in significant quantities were Al, Ca, Fe, K, Mg, Mn, Na, P, S, and Zn, with traces of Cr and Cu.

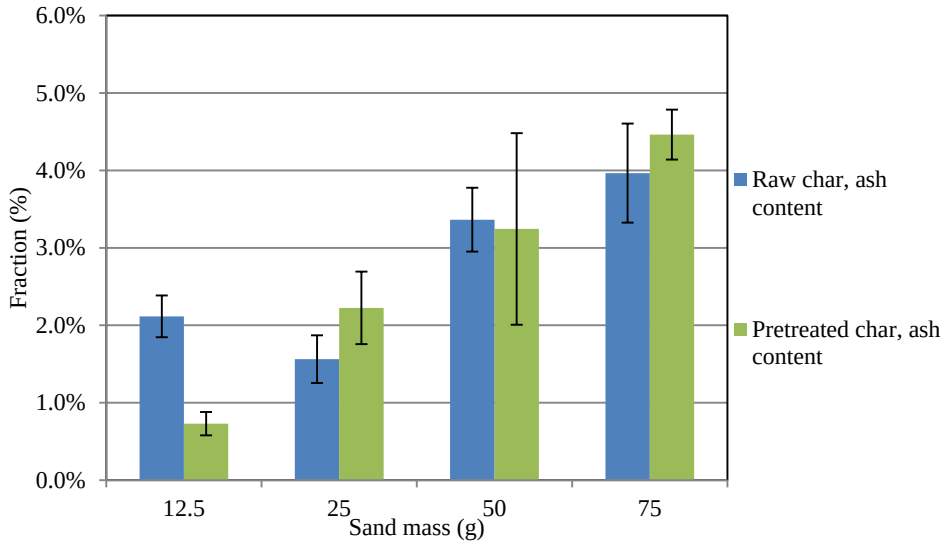

Figure 7-31: Fraction of inorganics in the pyrolysis char when the sand loading varied between 12.5-75 g

Table 7-14: Inorganic content in the silica sand used for fluidisation

Element[1]	**Al**	**Ca**	**Cr**	**Cu**	**Fe**	**K**	**Mg**	**Mn**	**Na**	**P**	**S**	**Zn**
Amount (ppm)	338.99	63.68	0.49	0.68	317.89	80.81	7.89	42.65	10.40	10.16	4.66	2.33
Error (ppm)	119.65	-	0.16	0.10	306.07	18.72	1.75	3.27	3.65	0.61	3.48	1.21

[1]*Elements not detected were B, Ba, Ni, Cd, Li, V, As, Co, and Pd*

The key bio-oil properties are reported in Table 7-15 for pyrolysis of raw and pretreated biomass at the different sand loadings in the fluidised bed. From these results, the acetic acid content in the bio-oil samples varied slightly with the sand loading for raw bio-oil but did not vary with the sand loading for pretreated bio-oil. For pretreated bio-oil, the water content in the bio-oil was low at 4.6 wt% for 12.5 g of sand, and decreased further as the sand loading increased. The lower water content was from reduced secondary reactions of char agglomerates in the system. Since the acetic acid content did not increase, this indicates the secondary reactions of char agglomerates did not promote organic acid production. The low water content for high sand loadings also indicates that impurities in the silica sand did not interact with the pyrolysis vapours to enhance heterogeneous secondary reactions to form acetic acid or water. However, the slightly higher char yields observed at higher sand loadings indicates polymerisation reactions may have been enhanced by catalytic inorganics in the sand, such as S.

Table 7-15: Bio-oil properties from raw and pretreated biomass at varying sand loadings

Sand mass (g)	12.5	25	50	75
Pyrolysis of raw biomass				
Acetic acid conc. (%)	2.5±0.1	2.6±0.7	2.6±0.1	2.4±0.0
Water (wt%)	18.9±2.4	16.2±3.0	18.1±0.4	15.1±0.2
Organic yield (wt%)	43.2	47.6	43.7	46.7
Overall organic yield[1] (wt%)	43.2	47.6	43.7	46.7
NCG heating value (MJm^{-3})	7.2	5.9	5.4	5.5
Pyrolysis of pretreated biomass				
Acetic acid conc. (%)	0.1±0.0	0.1±0.0	0.1±0.0	0.1±0.0
Water (wt%)	4.6±0.2	2.7±0.7	2.7±1.5	2.3±0.4
Organic yield (wt%)	51.9	50.4	48.9	46.3
Overall organic yield[1] (wt%)	45.2	43.9	42.6	40.4
NCG heating value (MJm^{-3})	7.7	9.0	8.5	7.4

[1]*Taking into account the mass loss during torrefaction and leaching*

7.6 Extensive analysis of the pyrolysis products from raw and pretreated biomass

After determining the optimal fluidised bed temperature, cyclone temperature, and sand loading in the fluidised bed, bio-oil was produced from raw and pretreated biomass and analysed in depth. For pyrolysis of raw biomass, the reactor temperature was set to 450 °C, the cyclone to 400 °C, and the sand loading to 25 g. For pretreated biomass, the reactor temperature was set to 450 °C, the cyclone to 425 °C, and the sand loading to 75 g. For pyrolysis of pretreated biomass, a higher sand loading was used to prevent char agglomeration, thus the cyclone temperature was set to a slightly higher temperature to improve the bio-oil yield.

Yields from pyrolysis at the optimal conditions are displayed in Figure 7-32. From the figure, it was found that pyrolysis of both raw and pretreated biomass had similar mass balance closures of approximately 93%. The pyrolysis yields were also quite similar but pyrolysis of pretreated biomass had a slightly higher bio-oil yield (57.8 wt%) compared to pyrolysis of raw biomass (55.3 wt%). Both biomass feedstocks had higher char yields (23.7 to 25.0 wt%) than those reported in the literature review of 10-20 wt%. Since the reactor temperature was dropped to 450 °C, less lignin in the biomass volatised during pyrolysis. It was expected that increasing the pyrolysis temperature would improve the bio-oil yield slightly but also increase the NCG production and enhance both heterogeneous and homogeneous secondary reactions; therefore it was acceptable to have higher char yields.

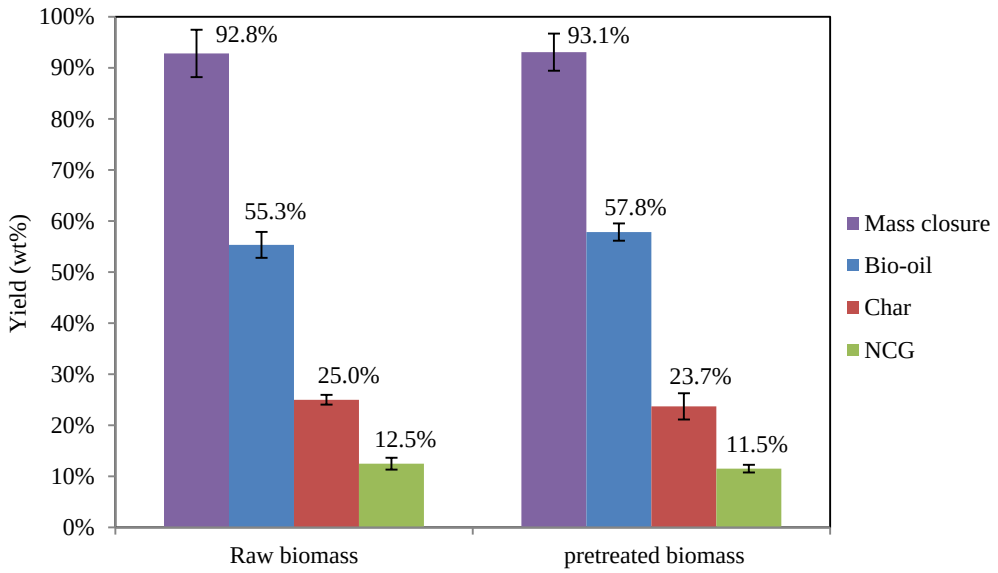

Figure 7-32: Mass closure and yields (dry basis) from pyrolysis at the optimal conditions

7.6.1 Bio-oil properties

Six bio-oils (three raw bio-oil and three pretreated bio-oil) were analysed in more detail. The basic bio-oil properties are displayed in Table 7-16, where the uncertainties indicate each system's stability and reproducibility. The uncertainties for raw bio-oil were typically much higher than for pretreated bio-oil, indicating the system was not as stable. Pretreated biomass was less prone to catalytic secondary reactions during pyrolysis, and hence small fluctuations in the operating conditions had minimal effect on the pyrolysis products. The organic fraction in pretreated bio-oil was much higher compared to the organic fraction in raw bio-oil, even when taking into account the mass loss from the pretreatments. This was due to the reduced secondary reactions to produce NCG, char, and water.

The average GPC values in Table 7-16 indicate the pretreated bio-oil contained significantly smaller compounds compared to raw bio-oil. The pyrolytic lignin content was under half that of the raw bio-oil; therefore the pyrolytic vapours from pyrolysis of raw biomass may have been prone to polymerisation reactions. Polymerisation reactions could be due to inorganics [2], or acidic compounds catalysing polymerisation reactions. A small reduction in the pyrolytic lignin fraction was noticed in Chapter 6 for pyrolysis of solely torrefied biomass while a large reduction was shown in Chapter 5 for pyrolysis of solely leached biomass. This indicates inorganics are the predominate catalyst for secondary polymerisation reactions. Even though the pretreated bio-oil had a lower average molecular weight compared to raw bio-oil, the viscosity was much higher and the bio-oil was denser. Branched compounds in the bio-oil interlock when there is no solvent for dissociation. This leads to a denser oil and an exponential increase in the viscosity when the water content is decreased. If the high viscosity is problematic, adding a solvent such as ethanol or methanol to the pretreated bio-oil as it condenses would reduce the viscosity. The addition of 5% methanol to bio-oil can reduce its viscosity by 35% [24, 25]. The molecular weight distribution curves are

given in Figure 7-33, multiple curves are shown for raw and pretreated bio-oils from different pyrolysis runs; the close proximity of the curves for pretreated bio-oil indicates high repeatability.

For the ultimate analysis, all previous bio-oil samples were sent to Scion. However, the samples in this part of the thesis were sent to CRL Energy Ltd instead. It was noticed that the values were varied from the usual. A few of the same samples were sent to Scion and retested for a comparison. The comparison between both laboratories results for the same samples are shown in Figure 7-34. Differences were noted for the carbon and hydrogen contents when both laboratories were analysing the same samples. This led to inclusive trends for the effect of the biomass pretreatments on the oxygen content. The carbon fraction for raw bio-oil was 42.1% from CRL Energy Ltd but 45.2% from Scion. The carbon fraction for pretreated bio-oil was 43.8% from CRL Energy Ltd and 45.6% from Scion. These discrepancies limit the reliability of the ultimate analysis results and will lead to uncertainties in the elemental balances.

Table 7-16: Properties of raw and pretreated bio-oil produced at the optimal reactor conditions

Biomass source	Raw	Pretreated
Bio-oil properties		
Acetic acid conc. (%)	2.46±0.13	0.16±0.05
Water (wt%)	16.8±1.6	3.6±0.3
Density (kgm^{-3})	1236.4±15.4	1371.8±9.1
Viscosity (cP)	156.0±39.2	4836.0±158.7
Organic yield (wt%)	46.1±2.0	55.7±1.8
Overall organic yield[1] (wt%)	46.1	48.6
GPC results		
Average number, Mn ($gmol^{-1}$)	221.6±39.7	176.3±1.8
Weight average, Mw ($gmol^{-1}$)	337.4±57.5	251.9±5.2
Size average, Mz ($gmol^{-1}$)	523.7±54.1	378.0±12.8
>650 $gmol^{-1}$ (%)	10.2±4.6	4.2±0.4
Ultimate analysis		
Wet basis		
Carbon (%)	42.1±0.6	43.8±1.6
Hydrogen (%)	7.8±0.2	7.5±0.5
Nitrogen (%)	0.03±0.04	0.04±0.00
Oxygen, by difference (%)	50.1±0.7	48.7±1.5
Dry basis		
Carbon (%)	50.5±0.5	45.4±1.7
Hydrogen (%)	7.1±0.2	7.4±0.5
Nitrogen (%)	0.03±0.05	0.04±0.00
Oxygen, by difference (%)	42.3±0.3	47.2±1.5
Higher heating value (MJm^{-3})	21.6±0.1	19.6±0.7
Overall energy in bio-oil[2] (MJ)	10.0	9.5

[1]Taking into account the mass loss during torrefaction and leaching. [2]Per kg of biomass feed

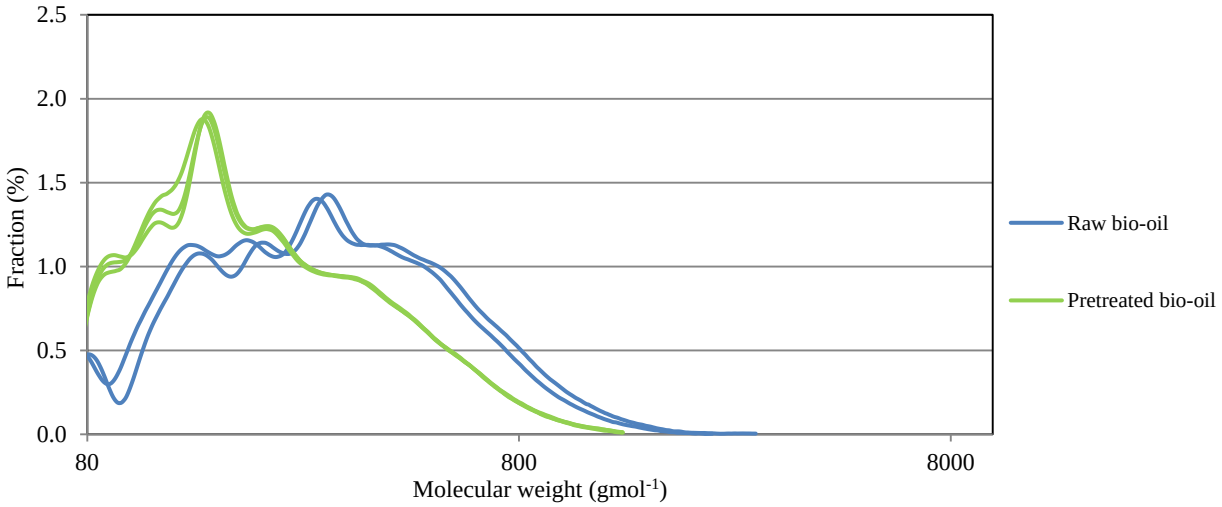

Figure 7-33: Molecular weight distribution curves for raw and pretreated bio-oil

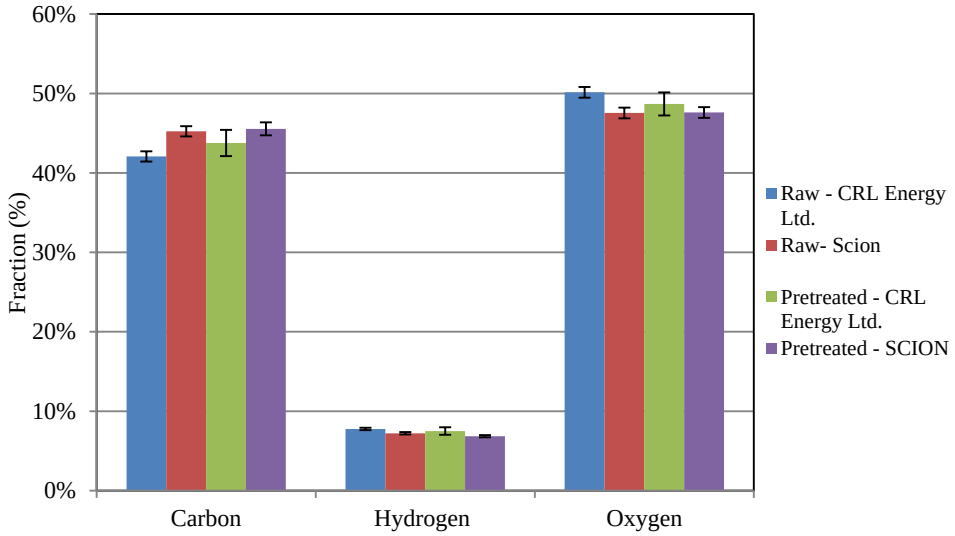

Figure 7-34: Comparison between the ultimate analysis results from Scion and CRL Energy Ltd.

^{1}H-NMR results for raw and pretreated bio-oil on a water free basis and relative to the biomass feed rate are displayed in Figure 7-35. The ^{1}H-NMR spectrums are shown in Appendix 7.3 and Appendix 7.4 for the 6 bio-oils. Relative to the biomass feed rate, raw bio-oil contained more alkanes, acetic acid, acetaldehyde hydroxyacetone, formic acid, glycolaldehyde, and aldehydes than pretreated bio-oil. The pretreated bio-oil was much richer in levoglucosan compared to the raw bio-oil. The total aromatic content was approximately equal for both bio-oils; therefore carbohydrates crosslinked during torrefaction did not increase the aromatic production. Raw bio-oil was rich in compounds from secondary reactions, produced from the breakdown of levoglucosan and other primary products.

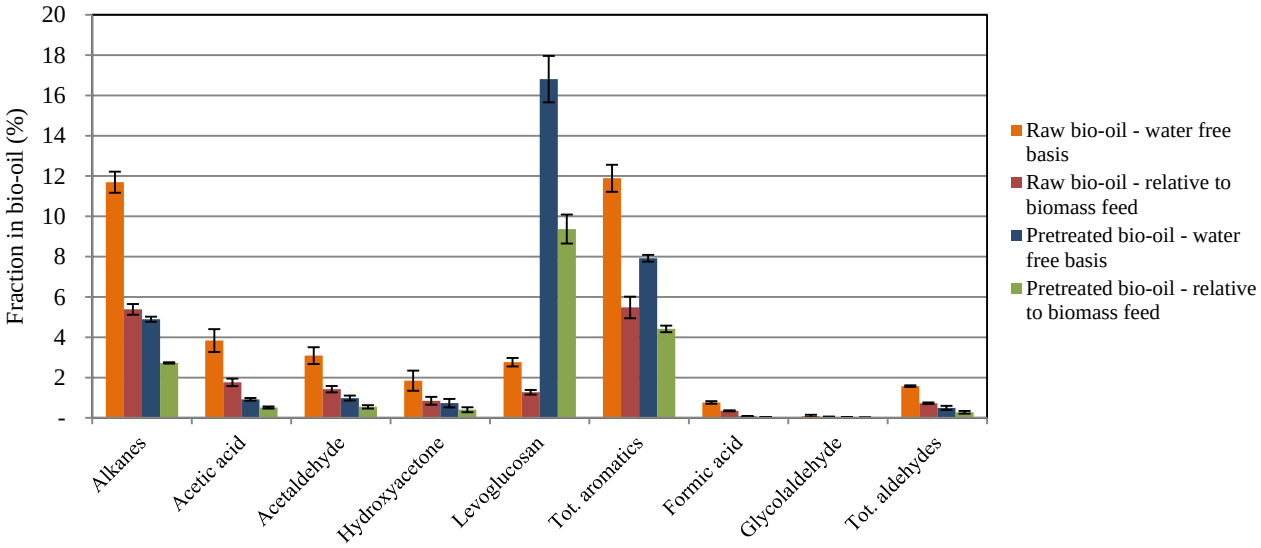

Figure 7-35: ^{1}H-NMR peak areas for raw and pretreated bio-oil

The pretreated bio-oil from this study was compared to upgraded bio-oil produced by other researchers, with the results given in Table 7-17. The bio-oils from other researchers shown in Table 7-17 were either upgraded by the addition of catalysts to the pyrolysis reactor or bio-oil vapours were catalytically upgraded. Pretreated bio-oil from this study had the lowest water content, and the bio-oil yield was in the higher range. However, a significant difference between the pretreated bio-oil and the catalytically upgraded bio-oils was the lower oxygen content for the catalytically upgraded bio-oils. Therefore, there is potential to add catalysts to the pyrolysis reactor to decrease the oxygen content of pretreated bio-oil. The most promising catalyst is CaO, which was added to an auger reactor by Veses *et al.* [26]. There was no decrease in the bio-oil yield with the addition of CaO but a slight decrease in the water content and CO_2 yield in the NCG, indicating oxygen was predominantly removed as CO and $CaCO_3$.

Table 7-17: Comparison between pretreated bio-oil and catalytically upgraded bio-oil

	This research, raw biomass	**This research, pretreated biomass**	**Catalytic upgrading[1] [27]**	**Catalytic pyrolysis[2] [26]**	**Catalytic pyrolysis[3] [28]**	**Catalytic pyrolysis[4] [29]**
Biomass type	*P. radiata*	*P. radiata*	*P. sylvestris*	*P. halepensis*	Spruce	Pine
Bio-oil yield, wt%	55.3±2.5	57.8±1.7	57±2	49	34.4	60
Char/coke yield, wt%	25.0±1.0	23.7±2.6	18.7	28	42.1	10
NCG yield, wt%	12.7±1.1	11.6±0.7	20±2	27	8.8	30
Bio-oil properties						
Acetic acid conc. (%)	2.46±0.13	0.16±0.05		4.5 (tot. acids)	1.3 (tot. acids)	0.82
Water (wt%)	16.8±1.6	3.6±0.3	24.8±0.8	12	14.7 (tot. aqueous)	28.8
Density (kgm^{-3})	1236.4±15.4	1371.8±9.1		1233		
Ultimate analysis						
Wet basis						
Carbon (%)	42.1±0.6	43.8±1.6	42	67.9		67.9
Hydrogen (%)	7.8±0.2	7.5±0.5	8	7.6		8.4
Nitrogen (%)	0.03±0.04	0.04±0.00	<0.1	0.3		
Oxygen, by difference (%)	50.1±0.7	48.7±1.5	51	24.2		23.7

[1]Pyrolysis at 525 °C followed by vapour upgrading over ZnO catalyst at 400 °C. [2]Catalytic pyrolysis at 450 °C using CaO as the fluidising medium. [3]Catalytic pyrolysis using FCC catalyst. [42]Catalytic pyrolysis at 450 °C using HZSM-5.

7.6.1.1 Inorganic content

The total inorganic content in bio-oil samples was determined by complete combustion of bio-oil samples. Bio-oil was filtered to 0.45 µm prior to combustion to remove char. The results indicated that raw bio-oil contained an average of 0.017±0.009 wt% char while pretreated bio-oil contained 0.080±0.032 wt% char. The pretreated bio-oil had a higher solids content because higher abrasion levels for pretreated biomass increased the fraction of small char particles produced (to be discussed in Section 7.6.3), which increased the char entrainment from the cyclone. The addition of a second cyclone or a hot gas filter to the process would decrease char entrainment, and therefore reduce the solids content in the bio-oils.

Following complete combustion of the filtered bio-oils, the inorganic content was determined as 0.162±0.056 wt% for raw bio-oil and as 0.091±0.030 wt% for pretreated bio-oil. The filtered bio-oil samples were analysed using ICP-OES to determine the inorganic composition, with results given in Table 7-18. Inorganics in the bio-oil may originate from inorganic volatilisation during pyrolysis; leaching of char entrained in the bio-oil; corrosion of stainless steel (SS) 316 by pyrolysis vapours or bio-oil after condensation; or leached from the storage vessel. The char content in both bio-oil samples was low, thus inorganics leached from char would be minimal.

SS-316 contains 0.08% C, 2.00% Mn, 0.045% P, 0.030% S, 0.75% Si, 16.0-18.0% Cr, 10.0-14.0% Ni, 2.0-3.0% Mo, 0.10% N, and 62.0-69.0% Fe [30]. The Mo in SS-316 gives it superior strength at elevated temperatures and improves the corrosion resistance compared to SS-304. Raw bio-oil contained a significant quantity of Fe, and traces of Mn and Ni (ignoring S as this was most likely from the biomass or storage vessel, as discussed below). Conversely, pretreated bio-oil only contained a minor amount of Fe and no Mn or Ni was detected. The Fe reduction was limited for leaching with 1% acetic acid at 30 °C (Section 5.2); therefore pretreated biomass still contained a significant amount of Fe, indicating raw bio-oil created a more corrosive environment. SS-316 has a high corrosion resistance to organic acids, but both acetic and formic acid at elevated temperatures do slightly corrode SS-316 [31]. Therefore, the higher organic acid concentration in raw bio-oil compared to pretreated bio-oil lead to mild corrosion of the system, which needs to be considered when designing and operating commercial plants.

The Na concentration in bio-oil has been reported to increase during storage from glass leaching [32]. A solution was produced to represent the leaching solution from high grade, representative chemicals. This was stored in a glass vessel identical to the bio-oil's storage container. Results in Table 7-18 indicate Al, Cr, Cu, Fe, K, Na, S, and Zn were leached from the container, with significant leakage of Na and S. This would have led to the high Na and S content in the bio-oil samples and may have influenced the trace amounts of other compounds detected in the bio-oils.

Inorganic volatilisation should be minimal at pyrolysis temperatures [33]. Since any elements present in significant quantities were most likely from corrosion or leaching, it can be assumed that there was minimal

inorganic volatilisation during pyrolysis. Alkali and alkaline earth metals may be released during pyrolysis but are typically re-adsorbed onto the char in a stable form, such as silicates [33].

Table 7-18: ICP-OES results for the inorganic composition of raw and pretreated bio-oil

Element[1]	**Al**	**B**	**Ca**	**Cr**	**Cu**	**Fe**	**K**	**Mg**	**Mn**	**Na**	**Ni**	**P**	**S**	**Zn**
Raw bio-oil														
Conc. (ppm)	1.10	0.79	BDL	BDL	BDL	37.84	1.57	0.90	0.27	38.14	0.63	BDL	71.24	1.36
Error (mg)	0.48	0.11				6.36	0.30	0.22	0.15	8.94	0.33		9.03	0.22
Pretreated bio-oil														
Conc. (ppm)	0.75	BDL	BDL	0.19	BDL	5.22	3.34	BDL	BDL	67.16	BDL	BDL	63.04	1.43
Error (mg)	0.29			0.00		1.63	1.29			22.62			29.10	0.09
Ions leached from storage containers														
Conc. (ppm)	4.56	BDL	BDL	0.37	0.09	1.87	2.67	BDL	BDL	34.33	BDL	BDL	69.43	6.13

7.6.1.2 Stability

The raw and pretreated bio-oil samples were aged at 80 °C for 25 h, which represents storage at 25 °C for 6 months [32, 34]. ^{1}H-NMR, water content, and GPC were carried out on the aged samples. The ^{1}H-NMR results for fresh and aged bio-oils are compared in Figure 7-36. From the figure, it was founds that raw bio-oil experienced significant changes in the composition during the aging compared to pretreated bio-oil. It was reported in Chapter 2 that aldehydes are most reactive in bio-oil, and with aging, readily undergo homo-polymerisation reactions to form oligomers and polymers; react with phenols to form hemiformal or polymers; oxidise to form organic acids; or undergo acetalisation with alcohols to form acetals or cyclic diether [32, 35]. Homo-polymerisation reactions are favoured in an acidic environment while polymerisation reactions between a phenol and aldehydes require metal ions or acid catalysts to promote the reaction. The large decrease in aromatics for raw bio-oil indicates a high degree of polymerisation reactions with aldehydes. Furan and furan derivatives can undergo condensation reactions to produce polymers, which are also catalysed by an acid; this would decrease the aromatic content further. Pretreated bio-oil, containing less inorganic and acid catalysts, underwent fewer of these reactions.

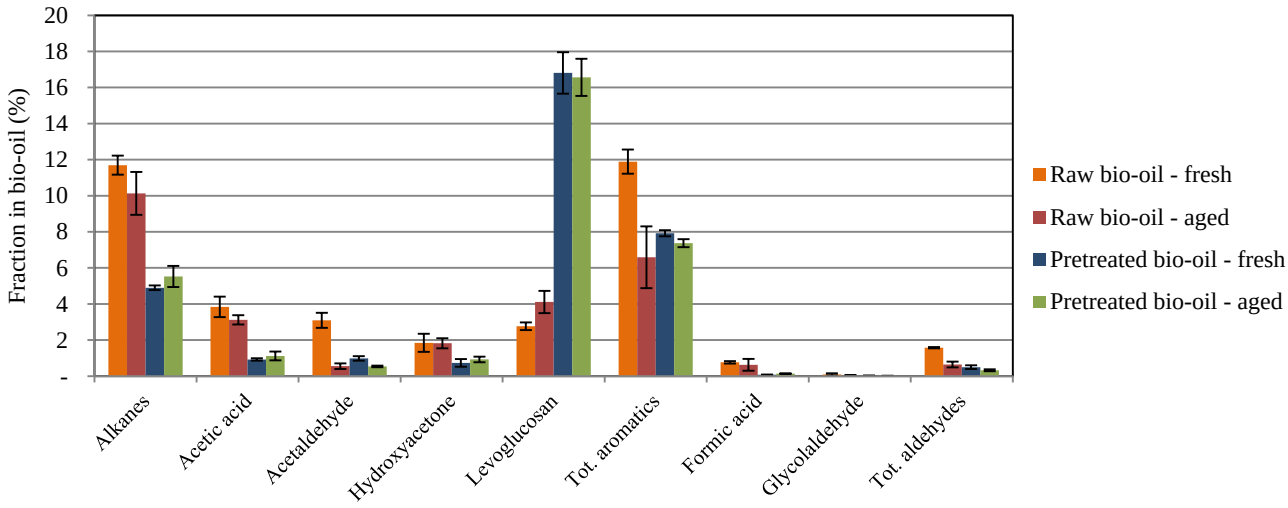

Figure 7-36: ^{1}H-NMR spectrum for fresh and aged bio-oil samples

The water content of raw bio-oil increased from 16.8±1.6 to 20.0±2.0 wt% after aging, while water content of the pretreated bio-oil increased from 3.6±0.3 to 5.8±0.3 wt% after aging. The water index, calculated using Equation 3.2, indicates the relative change in the water content; this was 0.19±0.02 for raw bio-oil and 0.59±0.20 for pretreated bio-oil. The index was larger for pretreated bio-oil as the initial water content was much lower than that of raw bio-oil. The absolute change in the water content was 3.2 wt% for raw bio-oil and 2.2 wt% for pretreated bio-oil. This means there were fewer aging reactions in the pretreated bio-oil that produced water as a by-product. The acetalisation, polymerisation, and furan condensations reactions typically produce water.

GPC gives an indication of the degree of polymerisation reactions that occur during aging. The average GPC results are given in Table 7-19, along with the stability index. The stability index indicated that both raw and pretreated bio-oil underwent similar increases in the average number, weight average, and size average of molecules. The pyrolytic lignin fraction index was slightly higher for pretreated bio-oil, but this was still lower than pyrolytic content of fresh raw bio-oil. Similarly to the water index, the absolute increase in pyrolytic lignin was lower for pretreated bio-oil (3.0%) compared to raw bio-oil (4.6%). The molecular weight distribution curves for the fresh and aged bio-oils are displayed in Figure 7-37. The aged curves are shifted to the right for both bio-oil samples. The pretreated bio-oil still displayed a molecular weight distribution lower than fresh raw bio-oil. Boateng and Mullen [36] reported similar results: the after storing bio-oil produced from torrefied biomass at 80 °C for 24 h, the average molecular weight of the sample increased but was still lower than that of fresh bio-oil produced from raw biomass.

The properties of the aged pretreated bio-oil were improved in terms of the average molecular weight and the pyrolytic lignin, water, inorganic, aldehyde, and acetic acid content but the bio-oil was still prone to a certain degree of aging. This indicates aging is a complex phenomenon. Zheng and Wei [37] used reduce

pressure distillation to fractionate bio-oil. 62 wt% of the distilled product was considered the upgraded fraction and termed the "distilled oil", while 29 wt% went to the water phase which contained water, acids, and phenols. The remaining 10 wt% was residue. The distilled oil was stable and did not increase in viscosity when aged. The distilled oil had a higher inorganic content than raw bio-oil produced in this research (0.13 wt% compared to 0.1 wt% initially); indicating inorganics did not contribute to the instability of the bio-oil. The acetic acid content of the distilled oil was 0.36 wt% (initially 4.56 wt%) and the formic acid content was 0.6 wt% (initially 7.69 wt%). These are similar to that of the pretreated bio-oil produced in this research; therefore can be assumed to be low enough to prevent aging. The distilled oil produced by Zheng and Wei contained 0.1 wt% water (initially 25.2 wt%), this was lower than that of pretreated bio-oil; thus is it possible that water in the bio-oil enhanced aging reactions. However, the main difference between the pretreated bio-oil produced in this research and the distilled oil produced by Zheng and Wei was the oxygen content. The distilled oil had a low oxygen content of 9.2 wt% (initially 50.3 wt%) while the oxygen content in the pretreated bio-oil was still 48.7±1.5%. Oxygenated compounds such as aldehydes, ketones, carboxylic acids and ethers, and substituted furans or phenols are thought to reduce the bio-oil's stability [38], thus a reduction in the oxygen content would reduce the presence of reactive oxygenates. A reduction in the oxygen content could be accomplished by the addition of CaO to the fluidised bed reactor, as discussed in the Section 7.6.1.

Table 7-19: GPC results for fresh and aged bio-oil

Biomass source	Raw - fresh	Raw - aged	Raw - index	Pretreated - fresh	Pretreated - aged	Pretreated - index
Average number, Mn ($gmol^{-1}$)	221.6±39.7	234.7±2.5	0.06	176.3±1.8	189.4±7.1	0.07
Weight average, Mw ($gmol^{-1}$)	337.4±57.5	390.0±1.2	0.16	251.9±5.2	286.5±23.1	0.14
Size average, Mz ($gmol^{-1}$)	523.7±54.1	645.4±3.3	0.23	378.0±12.8	459.5±49.8	0.22
>650 $gmol^{-1}$ (%)	10.2±4.6	15.8±0.1	0.56	4.2±0.4	7.2±1.9	0.73

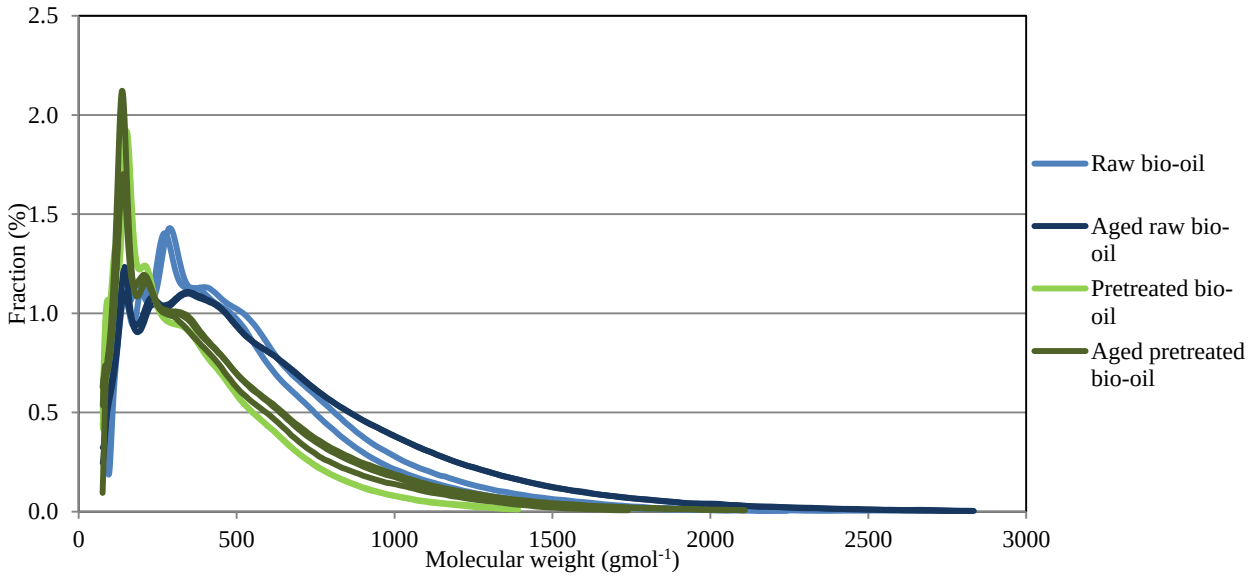

Figure 7-37: Molecular weight distribution for fresh and aged bio-oil from raw and pretreated biomass

7.6.1.3 Selective condensation to separate bio-oil fractions

The pyrolysis system designed and constructed in the research had the capability to fractionate the bio-oil into four categories, based on the components' boiling point. Pyrolysis vapours from raw and pretreated biomasses were selectively separated into 4 fractions during condensation. The 4th fraction comprised of the bio-oil captured in the electrostatic precipitator (ESP) and the filter. The percentage of bio-oil in each fraction is displayed in Figure 7-38, the residue that was recovered from the condensers and ESP is also displayed. There was more residue for pretreated bio-oil due to the higher viscosity leading to a larger retention in the system. The largest fraction for both bio-oils was captured in the ESP and filter. Oasmaa *et al.* [39] reported similar results from experiments on a 1 kghr^{-1} pyrolysis system. This indicates the efficiently of shell and tube condensers are limited for vapour condensation/collection. Condensers with larger surface areas would improve the collection but would be prone to fouling.

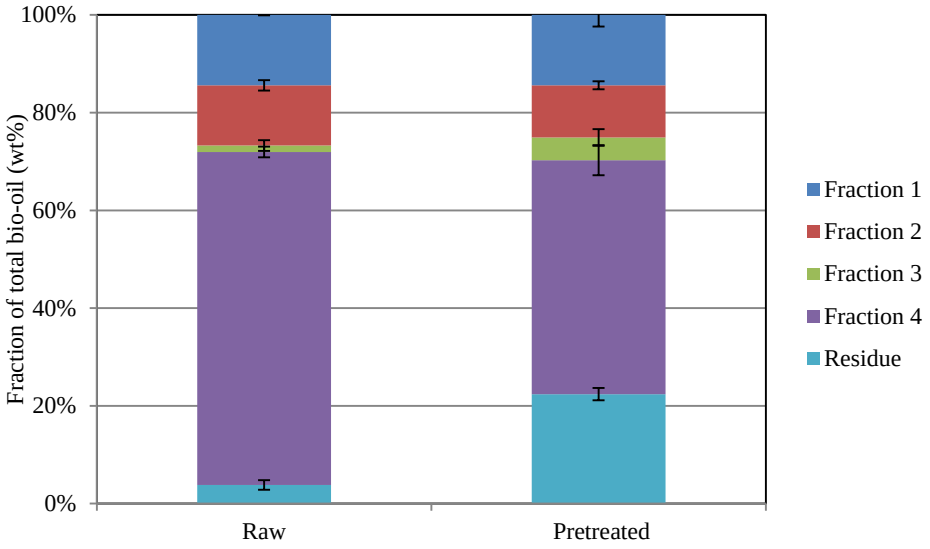

Figure 7-38: Fraction of bio-oil in each condenser/ESP, and the residue remaining in the system

Key properties of the bio-oil fractions from this research are given in Table 7-20. The first fraction had the lowest acetic acid and water content, which was expected as vapour entered the condenser at 120±21°C for pyrolysis of raw biomass and 140±11 °C for pyrolysis of pretreated biomass. Westerhof *et al.* [40] reported a similar tread when using selective condensation to collect pine wood vapours following pyrolysis at 480 °C. With the temperature of the first condenser was set a 80 °C, acetic acid in the first fraction was minimal and was mainly collected in the second condenser, which operated at 20 °C. The temperature drops obtained in this research for the cyclone exit and through each condenser are given in Table 7-21, with raw data in Appendix 7.2. The condenser model predicated a temperature drop from 400 to 200 °C over the first condenser; 200 to 120 °C over the second condenser; and 120 to 40 °C over the third condenser. The vapour temperature entering condenser 1 was lower than that predicted by the model as the cooling in the cyclone exit was not taken into account and there was 40 mm of tubing between each condenser.

GPC results in Table 7-20 indicate that faction 4 for pyrolysis of both raw and pretreated biomass had the highest pyrolytic lignin content. These bio-oil fractions contained aerosols that could not be captured in the

condensers and required electrostatic precipitation or filtering for collection. The first fractions, which were too thick to flow, still had a low average molecular weight. This indicates the reduction in water and other small compounds had a significant impact on the viscosity. It was interesting that fraction 3 for pretreated bio-oil had a higher average molecular weight and pyrolytic lignin content compared to the fraction 2. The thicker oil may have increased the capture of aerosols if they impacted and adhered to the condensed residue on the condenser walls, these aerosols would have otherwise been captured in the ESP.

Table 7-20: Properties of raw and pretreated bio-oil fractions

Biomass source	**Raw**				**Pretreated**			
Condenser fraction	**1**	**2**	**3**	**4**	**1**	**2**	**3**	**4**
Bio-oil properties								
Acetic acid conc. (%)	1.4±0.1	3.6±0.5	3.9±0.2	2.6±0.1	0.0±0.0	0.5±0.1	0.8±0.0	0.3±0.0
Water (wt%)	10.0±0.5	21.7±1.0	34.8±0.4	18.0±0.1	1.7±0.1	2.9±0.1	7.6±0.2	5.0±0.1
pH	2.2	2.1	2.0	2.5	2.4	2.8	2.7	2.9
GPC results								
Average number, Mn ($gmol^{-1}$)	204.6	213.4	179.7	235.6	176.15	172.7	181.3	191.9
Weight average, Mw ($gmol^{-1}$)	289.8	299.9	275.7	353.6	249.8	242.0	258.3	276.8
Size average, Mz ($gmol^{-1}$)	421.9	437.1	443.9	526.0	369.4	360.2	383.2	401.9
>650 $gmol^{-1}$ (%)	6.0	6.9	6.4	11.2	3.9	3.6	4.5	5.3

Table 7-21: Temperature drop over the cyclone exit and condensers for raw and pretreated bio-oil

Biomass source	**Raw**		**Pretreated**	
Condenser fraction	**In (°C)**	**Out (°C)**	**In (°C)**	**Out (°C)**
Cyclone exit	317	113	350	137
Condenser 1	113	80	137	100
Condenser 2	80	60	100	60
Condenser 3	25	25	60	27

The composition of each bio-oil fraction was determined using ^{1}H-NMR, with results displayed in Figure 7-39. The composition varied less for pretreated bio-oil, indicating that the efficiency of selective would be limited when fractionating vapours from pyrolysis of pretreated biomass. It was thought that thicker bio-oil from pretreated biomass stuck to the condenser walls, which passing vapours adhered to. High temperature selective condensation provides superior separation compared to cooling vapours instantly to ambient temperature then separating based on the heat of vaporisation of compounds. However, pretreated bio-oil is of high enough quality that selective condensation may not be required. This would allow for spray condensers to be used at large scale.

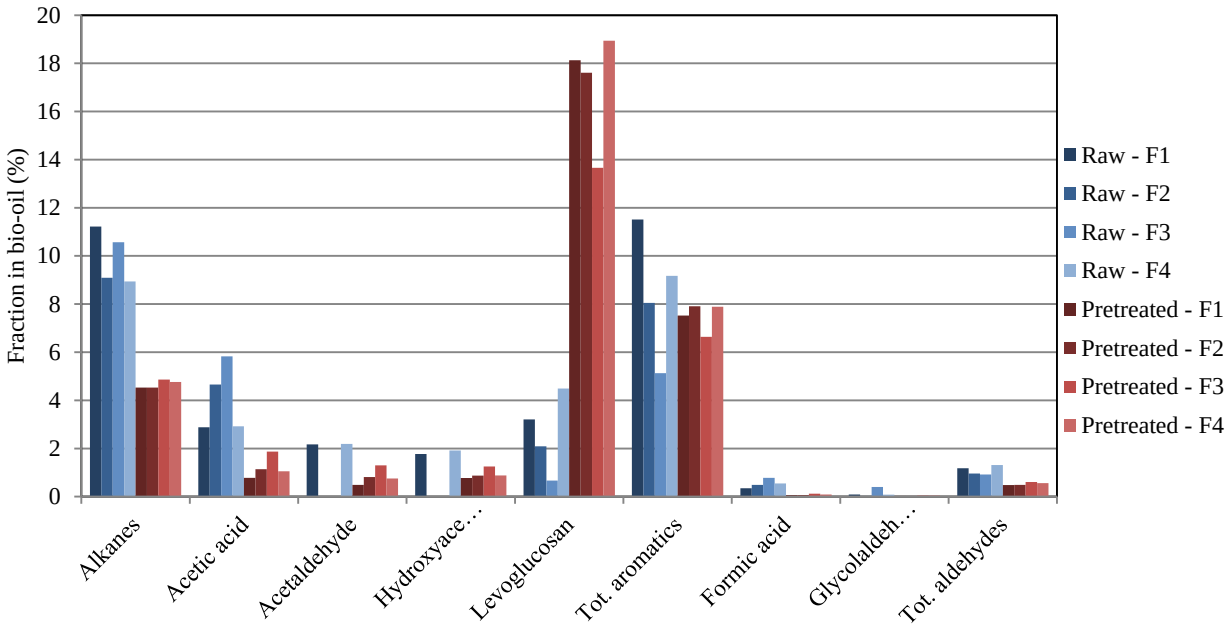

Figure 7-39: ^{1}H-NMR results for raw and pretreated bio-oil fractions

7.6.2 NCG properties

The NCG yield for pyrolysis of raw biomass was 12.5±1.2 wt% and was 11.5±0.7 wt% for pyrolysis of pretreated biomass. Pyrolysis of raw biomass produced more NCG due to heterogeneous cracking of pyrolysis vapours, catalysed by inorganic in the char [41]. The results for the individual gas yields are displayed in Figure 7-40 and the results for the NCG composition are displayed in Figure 7-41. Pyrolysis of raw biomass produced less CO, CH_4, H_2, C_2H_6, and C_2H_4 but more CO_2 compared to pyrolysis of pretreated biomass. This relationship was also noticed by Stephanidis *et al.* [42] who investigated pyrolysis of biomass that was hydrothermal torrefied. Due to acetyl cleavage during hydrothermal torrefaction, results from Stephanidis *et al.* [42] can be compared to pyrolysis of acid leached and torrefied biomass produced in this study. It was observed that pyrolysis of hydrothermally treated biomass increased the yield of all gases except CO_2. Hemicellulose produces predominantly CO_2 during pyrolysis due to cracking and reforming of carboxyl groups [43], but a portion of these groups are removed during torrefaction; therefore the CO_2 yield was expected to reduce during pyrolysis of the pretreated biomass. Cellulose produces proportionally more CO due to cracking of carboxyl and carbonyl groups, while lignin produces proportionally more H_2 and CH_4 from the cracking of aromatic rings and methoxy groups respectively [43].

NCGs are typically combusted to supply process heat. For this purpose, the lower heating value of the NCG produced was determined based on the NCG composition. The lower heating value for NCGs produced from pyrolysis of raw biomass was 5.7±0.5 MJm^{-3} while that for pyrolysis of pretreated biomass was 8.9±1.0 MJm^{-3}. The larger heating value for the NCG produced from pretreated biomass makes it more useful as an energy source.

In this study, pyrolysis experiments were carried using N_2 as the fluidising gas; therefore the NCG stream was diluted by N_2. However, pyrolysis at commercial scale typically recycles a portion of the NCG as the fluidising gas to prevent dilution and reduce processing costs [44]. CO promotes the conversion of oxygen from the bio-oil fraction into CO_2, while H_2 promotes oxygen conversion to water [45]; therefore the effect of using the NCGs as the fluidising agent would require investigating on this system.

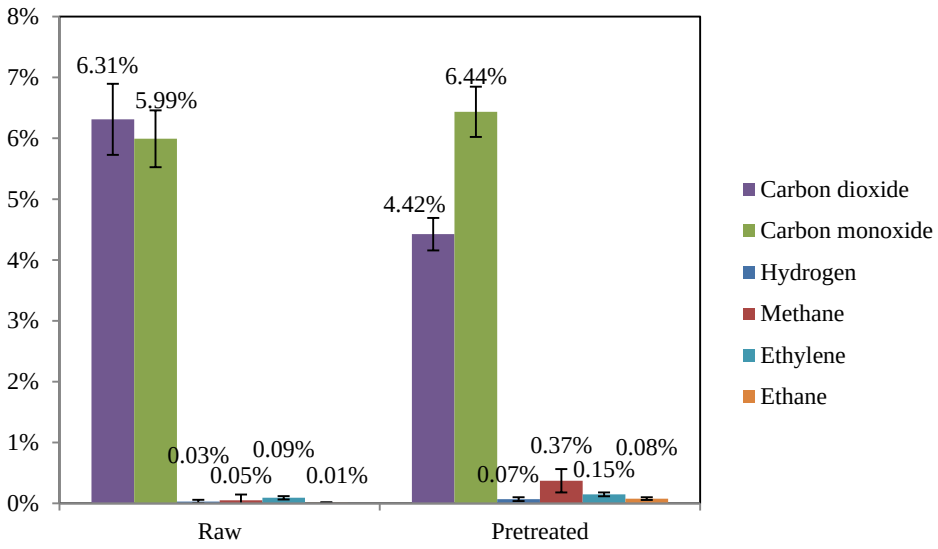

Figure 7-40: Gas yields from pyrolysis from pyrolysis of raw and pretreated biomass

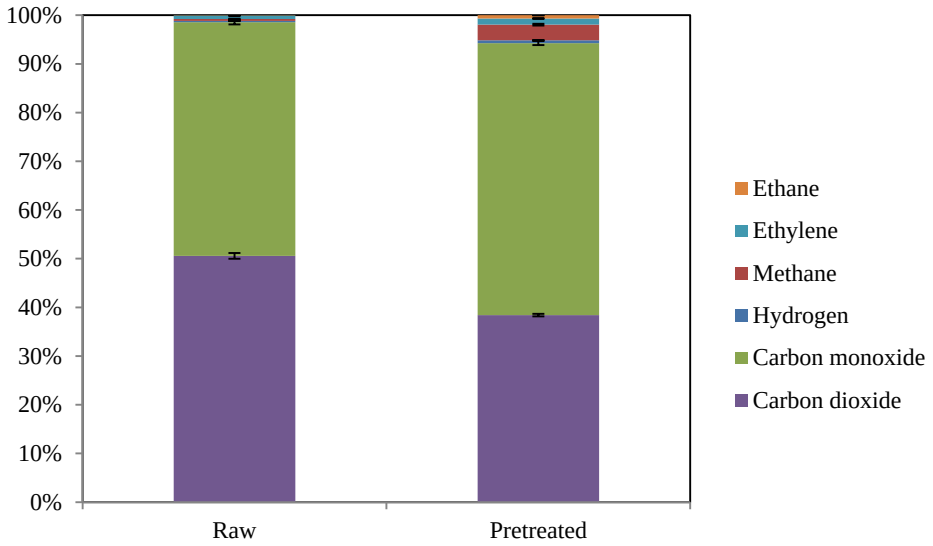

Figure 7-41: Concentration of compounds in the NCG from pyrolysis of raw and pretreated biomass

7.6.3 Char properties

Ultimate analysis was used to determine the elemental composition of chars from pyrolysis of both raw and pretreated biomass. The result for the inorganic, carbon, hydrogen, nitrogen, and oxygen content are given in Table 7-22, along with the calculated heating values. From these results, it was found that pretreated biomass produced chars with a higher carbon content but lower hydrogen and oxygen compared to chars produced from raw biomass. The char from pretreated biomass had a higher heating value of 27.3 $MJkg^{-1}$,

while the chars from raw biomass had at higher heating value of 24.7 $MJkg^{-1}$. The chars produced had higher a heating value larger than the average values for lignite (16.7 $MJkg^{-1}$), sub-bituminous coals (16.7-24.3 $MJkg^{-1}$), and within the range of bituminous coals (24.3-33.5 $MJkg^{-1}$) [46]. This indicates the chars have the potential to be used as low-ash coal substitutes.

ICP-OES was carried out on the chars from both raw and pretreated biomass, with the results reported in Table 7-23. From the table, it was seen that pretreated biomass produced char with a higher overall inorganic content compared to char from raw biomass, this was due to the increased sand loading in the fluidised bed. ICP-OPS results in Table 7-23 indicate that char from pretreated biomass contained more Al, Cr, Cu, Fe, Na, Ni, Zn, and Si but less B, Ca, K, Mg, Mn, P, and S compared to char from raw biomass. During pyrolysis of pretreated biomass, the sand loading (75 g) was 3 times more than the sand loading (25 g) used for pyrolysis of raw biomass, thus there was the potential for more sand to be incorporated into the char, either through abrasion of sand to produce fines or sand entrainment at the pyrolysis conditions. Sand contained Al, Fe, and Si in significant quantities that could have led to the higher inorganic content of these elements in the char from pretreated biomass. From the discussion in Section 7.6.1, there was no Ca, Cr, Cu, or P detected in the pretreated bio-oil. This indicates these species did not volatise during pyrolysis; therefore should have remained in the char.

Table 7-22: Char properties from pyrolysis of raw and pretreated biomass

Biomass source	**Raw**	**Pretreated**
Inorganic content (wt%)	1.4±0.1	2.1±0.2
Heating value ($MJkg^{-1}$)	24.7±0.9	27.3±0.3
Ultimate analysis of biomass (wt%)		
Carbon	64.3±1.9	72.9±0.6
Hydrogen	4.7±0.2	3.6±0.3
Nitrogen	0.3±0.1	0.2±0.2
Oxygen by diff.	30.8±1.9	23.3±0.3

Table 7-23: Inorganic content in the fluidising sand and char from raw and pretreated biomass

Element[1]	**Al**	**B**	**Ca**	**Cr**	**Cu**	**Fe**	**K**	**Mg**	**Mn**	**Na**	**Ni**	**P**	**S**	**Zn**	**Si**
Raw char															
Amount (mg)	24.3	1.8	686.0	0.7	2.1	32.5	599.4	191.4	57.3	7.7	0.7	61.8	29.4	5.3	1824.7
Error (mg)	22.3	0.1	245.4	0.4	1.2	37.0	410.0	55.8	7.0	0.6	0.4	19.2	6.4	1.3	912.9
In 25 of sand used for pyrolysis of raw biomass															
Amount (mg)	8.5	BDL	1.6	0.01	0.02	8.0	2.0	0.2	1.1	0.26	BDL	0.25	0.12	0.06	24978.8
Error (mg)	3.0	-	0.0	-	0.00	7.7	0.5	0.0	0.1	0.09	-	0.02	0.09	0.03	8.2
Pretreated char															
Amount (mg)	40.5	1.3	229.7	3.1	4.1	64.9	44.1	32.2	9.7	11.3	2.2	36.5	11.6	6.7	3931.4
Error (mg)	20.4	0.1	475.2	0.2	1.1	47.5	26.6	1.05	14.1	10.0	0.1	13.3	4.9	2.6	1031.6
In 75 of sand used for pyrolysis of pretreated biomass															
Amount (mg)	25.4	BDL	4.8	0.04	0.05	23.8	6.1	0.59	3.20	0.78	BDL	0.76	0.35	0.17	74936.3
Error (mg)	9.0	-	0.00	0.01	0.01	23.0	1.4	0.13	0.24	0.27	-	0.05	0.26	0.09	24.7

[1]*Elements not detected were Ba, Cd, Li, V, As, Co, and Pd*

As char can potentially be used as a fuel source, char pelletisation was investigated. Char from raw and pretreated biomass was pelletised at a pressure of 27.6 MPa at ambient temperature. The pellets produced are displayed in Figure 7-42. From the figure, it can be seen that char pellets from raw biomass retained the pellet shape and formed a solid disc while char pellets from pretreated biomass were friable and slightly elastic. Pellet strength is heavily dependent on the char moisture content, pressing temperature, char type, and the char particle size [47]. Char from pretreated biomass had a MC of 3.2±0.6% compared to 3.8±0.6% for char from raw biomass: this slightly lower moisture content may have slightly increased the pellets friability. Additionally, the pelletisation pressure was relatively low compared to commercial pelletising, which commonly use pressures up to 200 MPa [47] at ambient temperatures.

The density of char pellets from raw biomass was 879.1±23.6 kgm^{-3} and the density of char pellets from pretreated biomass was 550.2±25.7 kgm^{-3}. The lower density of the char pellets from pretreated biomass was due to the slightly elastic properties.

Figure 7-42: Pelletised char from raw biomass (left) and pretreated (right)

The particle size distribution of biomass particles and the corresponding pyrolysis chars were analysed, with the results displayed in Figure 7-43. From the figure, it was observed that pretreated biomass produced char with a size distribution curve shifted to the left compared to char from raw biomass, indicating the average particle size for chars from pretreated biomass were smaller than char from raw biomass. Torrefied biomass was brittle and would be prone to abrasion and breakage in the feeding augers and in the fluidised bed, thus the average particle size was reduced.

The bulk density of the particles was analysed and the results are given in Table 7-24. Interestingly, the char from pretreated biomass had a bulk density (172.1 kgm^{-3}) similar to that of raw biomass (182.7 kgm^{-3}), whilst the bulk density of char from raw biomass was lower (115.2 kgm^{-3}). Although at similar bulk densities, the smaller char particles from pyrolysis of pretreated biomass would pack closer together compared to the larger raw biomass particles. Therefore, particle densities of these two materials should be different; however determining particles densities was outside the scope of the present study. Higher bulk densities are desirable when utilising char as an energy source and it reduces the throughput volume for a given energy output.

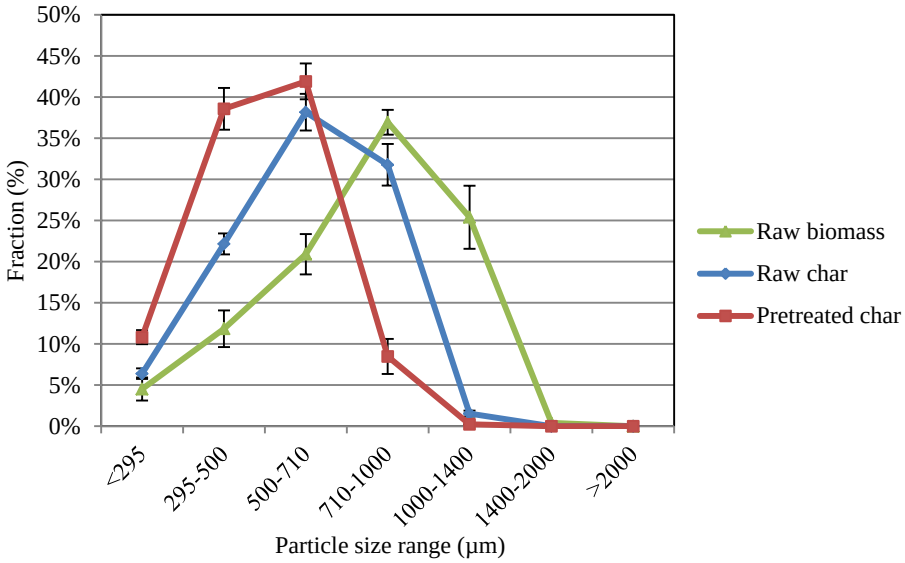

Figure 7-43: Particle size distribution for raw biomass and pyrolysis chars

Table 7-24: Bulk density of raw biomass and chars

	Bulk density (kgm^{-3})
Raw biomass	182.7±6.3
Raw char	115.2±3.0
Pretreated char	172.1±3.9

The microstructure of raw biomass, pretreated biomass and pyrolysis chars were compared using SEM, with images displayed in Figure 7-44. For a comparison, Figure 7-45 displays what was believed to be coke; this is produced from secondary polymerisation reactions of pyrolysis vapours. It was expected that fast pyrolysis chars retain the shape of biomass particle [48], and as observed in Figure 7-44, the particle shape of the biomass remained after pyrolysis for both samples. However, the morphological changes to the biomass were less for char from pretreated biomass compared to char from raw biomass. The severity of biomass deformation was higher for char from raw biomass as product vapours violently exited the particle in the initial stages of pyrolysis. Deformation to the biomass structure in the early stages of pyrolysis may limit further volatile release if elongated tracheid cell openings are damaged. Stable carbon-carbon crosslinks formed during torrefaction may also help stabilise the structure of char from pretreated biomass.

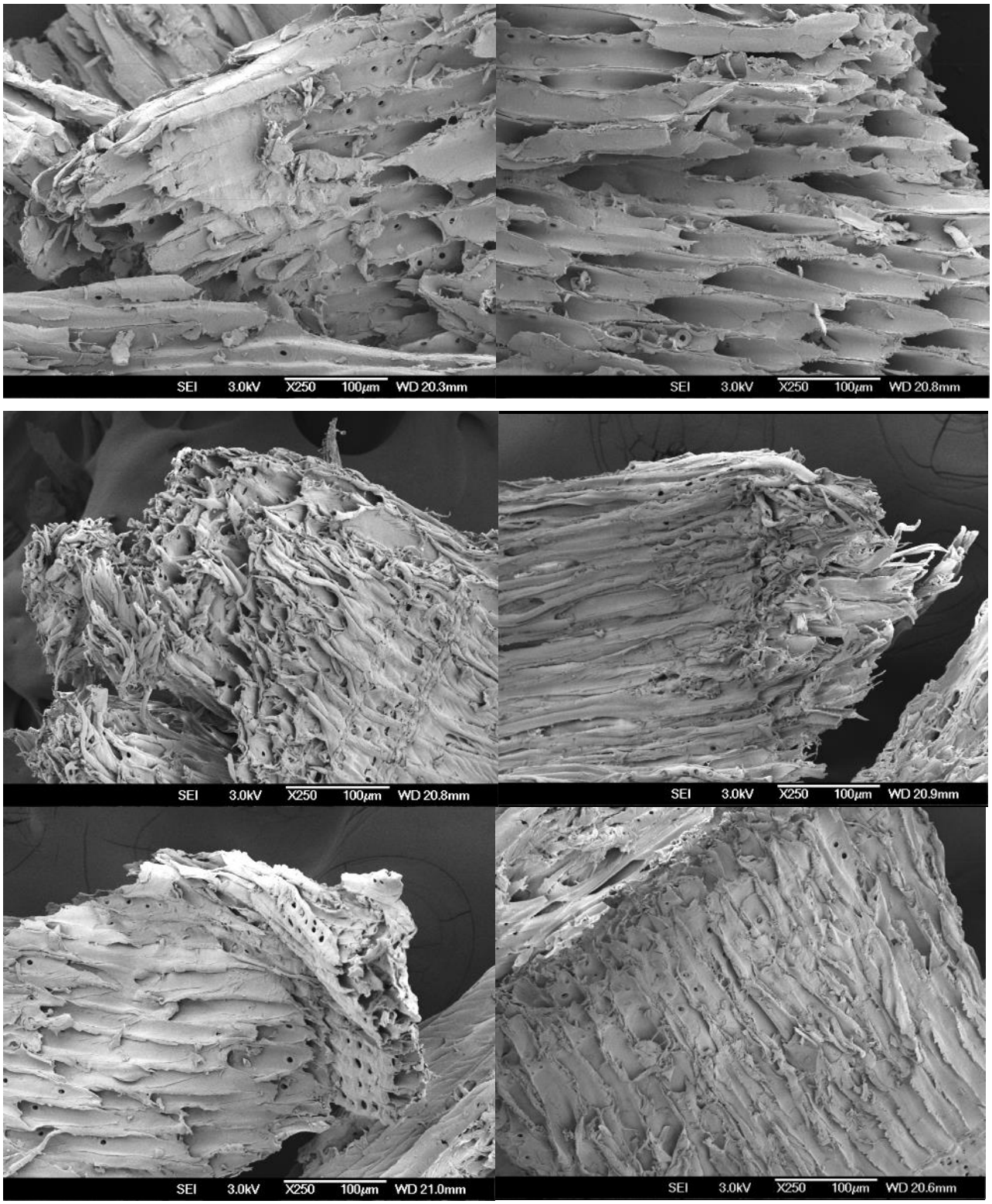

Figure 7-44: SEM images of raw biomass (top left), pretreated biomass (top right), char from raw biomass (middle), and char from pretreated biomass (bottom)

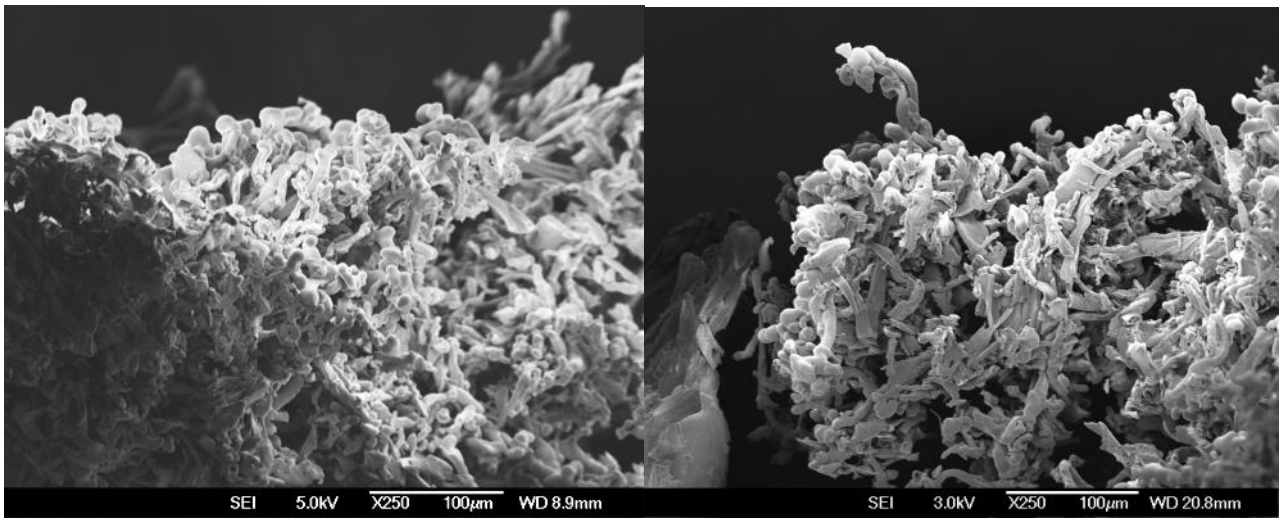

Figure 7-45: SEM images of coke found in the char pot

7.7 Leaching leachate regeneration using pyrolysis chars

Torrefaction of biomass does not produce sufficient liquor to leach an equivalent amount of biomass; therefore the leachate would need to be recycled from acid leaching. Ions from the leachate would need to be reduced/removed prior to recycling to achieve similar acid leaching results. Regeneration of the leachate may be possible using pyrolysis chars, as their hydrophilic surface is suitable for removing ions from liquids [13]. A portion of the leachate would be lost during regeneration; this leachate would be replenished with the new torrefaction liquor. The recycling and regeneration of leachate would minimise environmental issues concerning the disposal of the mobile phase after leaching due to possible trace amounts of hazardous elements and organic acids.

Filtering leachate through chars produced from raw and pretreated biomass was investigated to determine the potential for pyrolysis chars to be used for leachate regeneration. The char pore size, surface area, and ion exchange capabilities affects its ability for leachate regeneration [49]. The biomass moisture content prior to pyrolysis influences the char surface area, with dry biomass reported to have double the surface area compared to biomass with an initial moisture content of 16% [50]. Pyrolysis temperatures also affect the char structure: high temperatures increase the surface area, micro-porosity, and hydrophobicity of char to aid organic sorption while lower pyrolysis temperatures enhance the removal of inorganics and organic polar compounds through electrostatic attraction, precipitation, and oxygen containing functional groups [49].

During leachate regeneration, it is desirable to adsorb the inorganic compounds, especially alkali metals but to limit adsorption of the organic acids. Char is typically negatively charged [49], which indicates alkali, alkaline, and transition metals may be adsorbed. Inorganic removal via other mechanisms is displayed in Figure 7-46, which indicates anionic metal attraction, ion exchange, and precipitation may all contribute to inorganic removal.

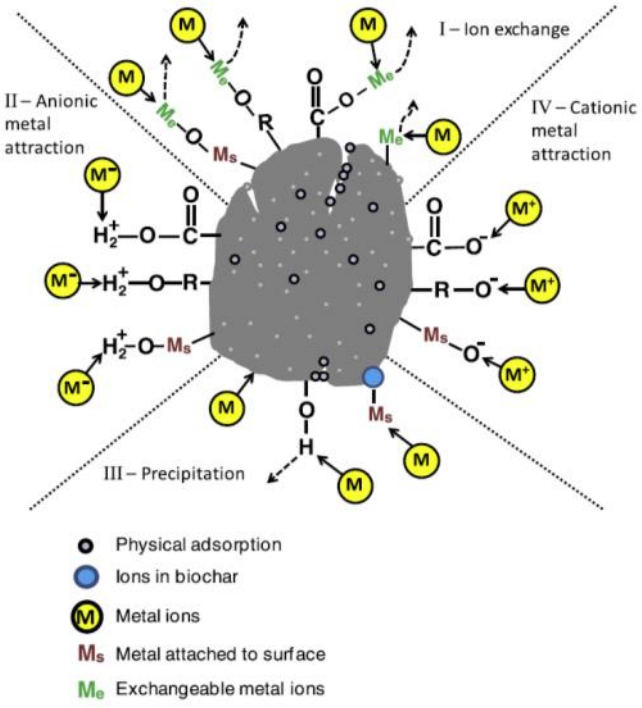

Figure 7-46: Proposed mechanism for inorganic removal using char, extracted from Ahmad *et al.* [49]

Preliminary experiments were carried out by Yaki [51] at the University of Canterbury. Yaki used the char from pyrolysis of raw and pretreated biomass with pyrolysis between 400-500 °C (Section 7.5.1, chars produced at 525 °C were not included). Since the sand loading in the fluidised bed was lower for these experiments, the char had an average inorganic content of 0.92±0.21 wt% from pretreated biomass. Some chars were soaked for 30 min in DI water prior to regeneration to saturate the char; this reduced the inorganic content to 0.40±0.12 wt%. Wet char was thought to reduce channelling that occurred when dry char was undergoing leachate saturation. Dry or soaked char was packed to a height of 30 mm in syringes 12.57 mm in diameter. The inorganic content in the dry char did not change following regeneration while that of the soaked char increased to 1.01±0.04 wt%. Therefore char with a lower inorganic content adsorbed ions, while char with a higher original inorganic content did not.

Leachate regeneration using chars from raw and pretreated biomass at the optimal conditions (Section 7.5) was carried out to investigate the ion adsorption process in more detail. The leachate used for regeneration in experiments was obtained using the pretreatment method described in Section 7.4.1, when leaching with the recycled torrefaction liquor. Initially, leachate was regenerated using the same method as for acid leaching, this was stirred at 250 rpm for 4 hr at 30 °C. Next, 1.09 g of wet or dry char was packed into syringes of either 13.5 mm or 21 mm in diameter. This equated to approximately 5 mL of char when compressed by hand to form a bed. 50 mL of leachate recovered from acid leaching was run through the char bed. The char to leachate ratio required was determined from the mass balance for the maximum available char from pyrolysis for regeneration (Chapter 8).

Results for the leachate pH following regeneration and the char inorganic content are given in Table 7-25 for chars from raw and pretreated biomass. All variations of the regeneration process had minimal impact on the pH of the leachate when using char from pretreated biomass, while char from raw biomass lead to an increase in the pH of the leachate. Increased leachate pH indicates organic acids were removed from the solution which is undesirable as it means more acid is required to reduce the pH to 2.75 for subsequent leaching. Although, removal of organic acids that have ion exchanged with a cation has been reported to enhance inorganic removal [52]. For all chars samples from raw biomass, the inorganic content in the char decreased following leachate regeneration; therefore ions were desorbed from the char. This indicates char from raw biomass could not be used for liquid regeneration. The inorganic content in char from pretreated biomass either increased or decreased slightly following leachate regeneration. The decrease in the inorganic content was due to the high initial inorganic content of the char from pretreated biomass associated with the higher sand mass in the fluidised bed.

The actual ions removed were determined using ICP-OES. Only the 13.5 mm diameter syringe with dry chars (from raw and pretreated biomass) were analysed. The results are given in Table 7-26. These results indicate certain ions were removed from the leachate while other ions actually increased in concentration. Regeneration with chars from both raw and pretreated biomass decreased the Al, B, Cr, and Na concentrations in the leachate but increased the concentration of all other species. Leachate regenerated with char from raw biomass had a proportionally higher concentration of ions leached into the solution compared to regeneration with char from pretreated biomass. The leachate is an acidic solution; therefore leaching of ions could occur from the storage vessel. Results for compounds leached for vessels during storage were determined in Section 7.6.1.1. These were replicated in Table 7-26, and indicate Al, Cr, Cu, Fe, K, Na, S, and Zn were leached from the container, with significant leakage of Na and S. Na is typically associated with glass leaching [32].

Mohan and Chander [53] studied the removal of Fe, Mn, and Zn using activated carbon in individual and multicomponent systems. The multicomponent systems did not hinder the adsorption of other ions until the column was saturated. If ion exchange was the main mechanism for removal, then ions must be released during ion adsorption. It was noted that P and K were released from the activated carbon. However, it is likely that the inorganic removal is through multiple mechanisms, as described in Figure 7-46. Overall, it was concluded that char modifications would be required for satisfactory inorganic reduction, ideally by increasing ion attraction and precipitation removal. Activating the char thermally or chemically may improve ion adsorption as it exposes additional functional groups with negative charges [54]. Ion reductions using techniques such as ion exchange resins could also be implemented if necessary.

Table 7-25: Change in leachate pH and char inorganic content following regeneration

Initial leachate pH	3.30±0.03				
	Final leachate pH	Discrepancy (%)	Initial inorganic content (wt%)	Final inorganic content (wt%)	Discrepancy (%)
Stirred in vessel					
Raw char	3.52±0.03	6.53±0.13	1.41±0.07	0.76±0.13	-45.95±1.06
Pretreated char	3.31±0.12	0.26±0.02	2.14±0.26	0.97±0.15	-54.92±1.31
21 mm diameter syringe, dry					
Raw char	3.46±0.01	4.69±0.07	1.41±0.07	0.95±0.13	-33.00±0.48
Pretreated char	3.35±0.01	1.51±0.03	2.14±0.26	2.67±0.43	24.60±0.78
21 mm diameter syringe, soaked					
Raw char	3.44±0.02	4.08±0.08	1.11±0.11	0.77±0.11	-31.06±0.51
Pretreated char	3.33±0.01	0.89±0.02	1.10±0.18	1.10±0.28	0.32±0.01
13.5 mm diameter syringe, dry					
Raw char	3.61±0.03	9.44±0.21	1.41±0.07	0.77±0.09	-45.19±0.51
Pretreated char	3.32±0.02	0.63±0.01	2.14±0.26	2.12±0.33	-1.06±0.03
13.5 mm diameter syringe, soaked					
Raw char	3.62±0.02	9.71±0.57	0.84±0.07	0.66±0.31	-22.05±0.57
Pretreated char	3.33±0.02	0.84±0.02	1.21±0.23	1.06±0.23	-12.72±0.39

Table 7-26: Inorganic content in leachate before and after regeneration

Element[1]	**Al**	**B**	**Ca**	**Cr**	**Cu**	**Fe**	**K**	**Mg**	**Mn**	**Na**	**Ni**	**P**	**S**	**Zn**
Leachate														
Conc. (ppm)	1.737	2.010	44.892	0.004	0.084	0.643	46.617	12.554	2.967	9.638	0.019	3.316	1.901	0.548
Error (ppm)	0.177	0.499	1.825	0.001	0.006	0.167	0.527	0.339	0.128	2.704	0.016	0.818	0.394	0.111
Leachate after regeneration with raw char														
Conc. (ppm)	1.613	0.243	87.027	BDL	0.140	1.406	195.76	35.881	8.408	6.738	0.022	9.312	7.364	1.030
Error (ppm)	0.170	0.026	11.059	0	0.005	0.091	22.006	4.220	1.126	0.796	0.021	1.308	2.853	0.051
Discrepancy (%)	7.2	87.9	-93.9	100.0	-67.6	-118.5	-320.0	-185.8	-183.4	30.1	-12.0	-180.8	-287.4	-88.1
Error (%)	1.4	31.3	-114.2	0	-1.7	-26.3	-503.9	-132.1	-72.5	27.8	-2.2	-112.3	-313.1	-14.0
Leachate after regeneration with pretreated char														
Conc. (ppm)	1.530	0.242	66.579	BDL	0.356	1.847	71.075	24.541	5.743	7.422	0.053	6.042	6.010	1.060
Error (ppm)	0.234	0.120	9.536	0	0.056	0.391	9.472	1.672	0.285	2.019	0.000	1.007	1.031	0.117
Discrepancy (%)	11.9	87.9	-48.3	100.0	-324.7	-187.1	-52.5	-95.5	-93.6	23.0	-175.2	-82.2	-216.1	-93.6
Error (%)	2.8	37.7	-58.0	0	-31.4	-66.5	-59.1	-33.5	-13.1	26.3	-20.3	-50.0	-109.9	-17.6
Ions leached from storage containers														
Conc. (ppm)	4.555	BDL	BDL	0.368	0.085	1.868	2.674	BDL	BDL	34.331	BDL	BDL	69.434	6.129

[1]*Elements not detected were Ba, Cd, Li, V, As, Co, and Pd*

7.8 References

1. Hayes, D. (2013). Advanced biomass research for beyond the petroleum age. *Important Compositional Parameters* Retrieved 07/09/2013, 2013, from http://www.carbolea.ul.ie/composition.php
2. Hoekstra, E., Westerhof, R. J. M., Brilman, W., Van Swaaij, W. P. M., Kersten, S. R. A., Hogendoorn, K. J. A., et al. (2012). Heterogeneous and homogeneous reactions of pyrolysis vapors from pine wood. *AIChE Journal, 58*(9), 2830-2842.
3. Britt, P. F., Buchanan Iii, A. C., Thomas, K. B., & Lee, S.-K. (1995). Pyrolysis mechanisms of lignin: surface-immobilized model compound investigation of acid-catalyzed and free-radical reaction pathways. *Journal of Analytical and Applied Pyrolysis, 33*(0), 1-19.
4. Agblevor, F. A., & Besler, S. (1996). Inorganic compounds in biomass feedstocks. 1. Effect on the quality of fast pyrolysis oils. *Energy & Fuels, 10*(2), 293-298.

5. Scott, D. S., Paterson, L., Piskorz, J., & Radlein, D. (2001). Pretreatment of poplar wood for fast pyrolysis: rate of cation removal. *Journal of Analytical and Applied Pyrolysis, 57*(2), 169-176.
6. Boardman, R. D., Hess, J. R., Sokhansanj, S., Tumuluru, J. S., & Wright, C. T. (2011). A review on biomass torrefaction process and product properties for energy applications. [Report]. *Industrial Biotechnology, 7*(5), 384+.
7. Bridgwater, A. V., & Diebold, J. P. (1999). Overview of fast pyrolysis of biomass for the production of liquid fuels. In A. V. Bridgwater (Ed.), *Fast Pyrolysis of Biomass: A Handbook* (Vol. 1, pp. 14-32). Newbury: CPL Press
8. Prins, M. J., Ptasinski, K. J., & Janssen, F. J. J. G. (2006). Torrefaction of wood: part 2. Analysis of products. *Journal of Analytical and Applied Pyrolysis, 77*(1), 35-40.
9. Chang, S., Zhao, Z., Zheng, A., He, F., Huang, Z., & Li, H. (2012). Characterization of products from torrefaction of sprucewood and bagasse in an auger reactor. *Energy & Fuels, 26*(11), 7009-7017.
10. Patwardhan, P. R., Dalluge, D. L., Shanks, B. H., & Brown, R. C. (2011). Distinguishing primary and secondary reactions of cellulose pyrolysis. *Bioresour Technol, 102*(8), 5265-5269.
11. Tang, Z., Lu, Q., Zhang, Y., Zhu, X., & Guo, Q. (2009). One step bio-oil upgrading through hydrotreatment, esterification, and cracking. *Industrial & Engineering Chemistry Research, 48*(15), 6923-6929.
12. Chen, W.-H., Hsu, H.-C., Lu, K.-M., Lee, W.-J., & Lin, T.-C. (2011). Thermal pretreatment of wood (Lauan) block by torrefaction and its influence on the properties of the biomass. *Energy, 36*(5), 3012-3021.
13. Savova, D., Apak, E., Ekinci, E., Yardim, F., Petrov, N., Budinova, T., et al. (2001). Biomass conversion to carbon adsorbents and gas. *Biomass and Bioenergy, 21*(2), 133-142.
14. Di Blasi, C., Branca, C., & Galgano, A. (2008). Thermal and catalytic decomposition of wood impregnated with sulfur- and phosphorus-containing ammonium salts. *Polymer Degradation and Stability, 93*(2), 335-346.
15. Bedmutha, R. J., Ferrante, L., Briens, C., Berruti, F., & Inculet, I. (2009). Single and two-stage electrostatic demisters for biomass pyrolysis application. *Chemical Engineering and Processing: Process Intensification, 48*(6), 1112-1120.
16. Garcia-Perez, M., Wang, X. S., Shen, J., Rhodes, M. J., Tian, F., Lee, W.-J., et al. (2008). Fast pyrolysis oil of mallee woody biomass: effect of temperature on the yield and quality of pyrolysis products. *Industrial & Engineering Chemistry Research, 47*(6), 1846-1854.
17. DeSisto, W. J., Hill, N., Beis, S. H., Mukkamala, S., Joseph, J., Baker, C., et al. (2010). Fast pyrolysis of pine sawdust in a fluidized-bed reactor. *Energy & Fuels, 24*(4), 2642-2651.
18. Salehi, E., Abedi, J., & Harding, T. (2011). Bio-oil from sawdust: effect of operating parameters on the yield and quality of pyrolysis products. *Energy & Fuels, 25*(9), 4145-4154.
19. Westerhof, R. J. M., Brilman, D. W. F., van Swaaij, W. P. M., & Kersten, S. R. A. (2009). Effect of temperature in fluidized bed fast pyrolysis of biomass: oil quality assessment in test units. *Industrial & Engineering Chemistry Research, 49*(3), 1160-1168.
20. Horne, P. A., & Williams, P. T. (1996). Influence of temperature on the products from the flash pyrolysis of biomass. *Fuel, 75*(9), 1051-1059.
21. Ren, S., Lei, H., Wang, L., Bu, Q., Chen, S., Wu, J., et al. (2013). The effects of torrefaction on compositions of bio-oil and syngas from biomass pyrolysis by microwave heating. *Bioresour Technol, 135*(0), 659-664.
22. Shen, D. K., & Gu, S. (2009). The mechanism for thermal decomposition of cellulose and its main products. *Bioresour Technol, 100*(24), 6496-6504.
23. Jensen, A., Dam-Johansen, K., Wójtowicz, M. A., & Serio, M. A. (1998). TG-FTIR study of the influence of potassium chloride on wheat straw pyrolysis. *Energy & Fuels, 12*(5), 929-938.
24. Zhang, Q., Chang, J., Wang, T., & Xu, Y. (2007). Review of biomass pyrolysis oil properties and upgrading research. *Energy Conversion and Management, 48*(1), 87-92.
25. Güllü, D., & Demirbaş, A. (2001). Biomass to methanol via pyrolysis process. *Energy Conversion and Management, 42*(11), 1349-1356.
26. Veses, A., Aznar, M., Martínez, I., Martínez, J. D., López, J. M., Navarro, M. V., et al. (2014). Catalytic pyrolysis of wood biomass in an auger reactor using calcium-based catalysts. *Bioresour Technol, 162*(0), 250-258.
27. Nokkosmäki, M. I., Kuoppala, E. T., Leppämäki, E. A., & Krause, A. O. I. (2000). Catalytic conversion of biomass pyrolysis vapours with zinc oxide. *Journal of Analytical and Applied Pyrolysis, 55*(1), 119-131.
28. Adam, J., Antonakou, E., Lappas, A., Stöcker, M., Nilsen, M. H., Bouzga, A., et al. (2006). In situ catalytic upgrading of biomass derived fast pyrolysis vapours in a fixed bed reactor using mesoporous materials. *Microporous and Mesoporous Materials, 96*(1–3), 93-101.
29. Olazar, M., Aguado, R., Bilbao, J., & Barona, A. (2000). Pyrolysis of sawdust in a conical spouted-bed reactor with a HZSM-5 catalyst. *American Institute of Chemical Engineers. AIChE Journal, 46*(5), 1025-1025.
30. AK-Steel. (2007). 316/316L stainless steel (Vol. UNS S31600, pp. 1-2). West Chester: AK Steel Corporation.
31. The-international-nickel-company. (1963). *Corrosion resistance of the austenitic chromium-nickel stainless steel in chemical environments*. New York: The international nickel company;.
32. Diebold, J. P. (2000). *A review of the chemical and physical mechanisms of the storage stability of fast pyrolysis bio-oils*. Lakewood, Colorado: National Renewable Energy Laboratory.
33. Okuno, T., Sonoyama, N., Hayashi, J.-i., Li, C.-Z., Sathe, C., & Chiba, T. (2005). Primary release of alkali and alkaline earth metallic species during the pyrolysis of pulverized biomass. *Energy & Fuels, 19*(5), 2164-2171.

34. Oasmaa, A., & Meier, D. (2005). Norms and standards for fast pyrolysis liquids: 1. Round robin test. *Journal of Analytical and Applied Pyrolysis, 73*(2), 323-334.
35. Huber, G. W., Iborra, S., & Corma, A. (2006). Synthesis of transportation fuels from biomass: chemistry, catalysts, and engineering. *Chemical Reviews, 106*(9), 4044-4098.
36. Boateng, A. A., & Mullen, C. A. (2013). Fast pyrolysis of biomass thermally pretreated by torrefaction. *Journal of Analytical and Applied Pyrolysis, 100*(0), 95-102.
37. Zheng, J.-L., & Wei, Q. (2011). Improving the quality of fast pyrolysis bio-oil by reduced pressure distillation. *Biomass and Bioenergy, 35*(5), 1804-1810.
38. Aho, A., Kumar, N., Eränen, K., Salmi, T., Hupa, M., & Murzin, D. Y. (2007). Catalytic pyrolysis of biomass in a fluidized bed reactor: influence of the acidity of H-beta zeolite. *Process Safety and Environmental Protection, 85*(5), 473-480.
39. Oasmaa, A., Solantausta, Y., Arpiainen, V., Kuoppala, E., & Sipilä, K. (2010). Fast pyrolysis bio-oils from wood and agricultural residues. *Energy & Fuels, 24*(2), 1380-1388.
40. Westerhof, R. J. M., Brilman, D. W. F., Garcia-Perez, M., Wang, Z., Oudenhoven, S. R. G., van Swaaij, W. P. M., et al. (2011). Fractional condensation of biomass pyrolysis vapors. *Energy & Fuels, 25*(4), 1817-1829.
41. Boroson, M. L., Howard, J. B., Longwell, J. P., & Peters, W. A. (1989). Heterogeneous cracking of wood pyrolysis tars over fresh wood char surfaces. *Energy & Fuels, 3*(6), 735-740.
42. Stephanidis, S., Nitsos, C., Kalogiannis, K., Iliopoulou, E. F., Lappas, A. A., & Triantafyllidis, K. S. (2011). Catalytic upgrading of lignocellulosic biomass pyrolysis vapours: effect of hydrothermal pre-treatment of biomass. *Catalysis Today, 167*(1), 37-45.
43. Yang, H., Yan, R., Chen, H., Lee, D. H., & Zheng, C. (2007). Characteristics of hemicellulose, cellulose and lignin pyrolysis. *Fuel, 86*(12–13), 1781-1788.
44. Steinberg, M., Fallon, P. T., & Sundaram, M. S. (1986). Flash pyrolysis of biomass with reactive and non-reactive gas. *Biomass, 9*(4), 293-315.
45. Zhang, H., Xiao, R., Wang, D., He, G., Shao, S., Zhang, J., et al. (2011). Biomass fast pyrolysis in a fluidized bed reactor under N2, CO2, CO, CH4 and H2 atmospheres. *Bioresour Technol, 102*(5), 4258-4264.
46. Gunn, P. (2015). Coal marketing international Pty Ltd. *Coal Rank* Retrieved 21.5.2015, 2015
47. Stelte, W., Holm, J. K., Sanadi, A. R., Barsberg, S., Ahrenfeldt, J., & Henriksen, U. B. (2011). Fuel pellets from biomass: the importance of the pelletizing pressure and its dependency on the processing conditions. *Fuel, 90*(11), 3285-3290.
48. Cetin, E., Gupta, R., & Moghtaderi, B. (2005). Effect of pyrolysis pressure and heating rate on radiata pine char structure and apparent gasification reactivity. *Fuel, 84*(10), 1328-1334.
49. Ahmad, M., Rajapaksha, A. U., Lim, J. E., Zhang, M., Bolan, N., Mohan, D., et al. (2014). Biochar as a sorbent for contaminant management in soil and water: a review. *Chemosphere, 99*(1), 19-33.
50. Gray, M. R., Corcoran, W. H., & Gavalas, G. R. (1985). Pyrolysis of a wood-derived material. Effects of moisture and ash content. *Industrial & Engineering Chemistry Process Design and Development, 24*(3), 646-651.
51. Yaki, N. A. (2014). Pretreatments of biomass and application of fast pyrolytic char for acid regeneration. University of Canterbury.
52. Faur-Brasquet, C., Kadirvelu, K., & Le Cloirec, P. (2002). Removal of metal ions from aqueous solution by adsorption onto activated carbon cloths: adsorption competition with organic matter. *Carbon, 40*(13), 2387-2392.
53. Mohan, D., & Chander, S. (2001). Single component and multi-component adsorption of metal ions by activated carbons. *Colloids and Surfaces A: Physicochemical and Engineering Aspects, 177*(2–3), 183-196.
54. Lima, I. M., Boateng, A. A., & Klasson, K. T. (2010). Physicochemical and adsorptive properties of fast-pyrolysis bio-chars and their steam activated counterparts. *Journal of Chemical Technology & Biotechnology, 85*(11), 1515-1521.

8 System balances and economics

8.1 Mass and elemental balances

Mass balances were performed for the optimal raw and pretreated pyrolysis systems based on the results given in Section 7.6. Balances were also performed on an elementary basis to determine the closure for carbon, hydrogen, nitrogen, and oxygen. Balances assumed a feed rate of 2 kg of wet biomass with a moisture content of 50% wet basis (equal to 100 wt% dry basis), which is close to measured values of 53 wt% wet basis for freshly milled *P. radiata* in summer [1]. The mass balance results can be scaled up for larger systems.

8.1.1 Pyrolysis of raw biomass

The procedure for pyrolysis of raw biomass is given in Figure 8-1. The mass and elementary flows during each stage in Figure 8-1 are detailed below in the bullet points 1-4. The biomass moisture content was reduced from 100 to 10 wt% (dry basis) in the drying process. It was assumed there was no biomass loss during the milling stage; this stage was only present for economic analysis later in the chapter due to the energy cost associated with the milling.

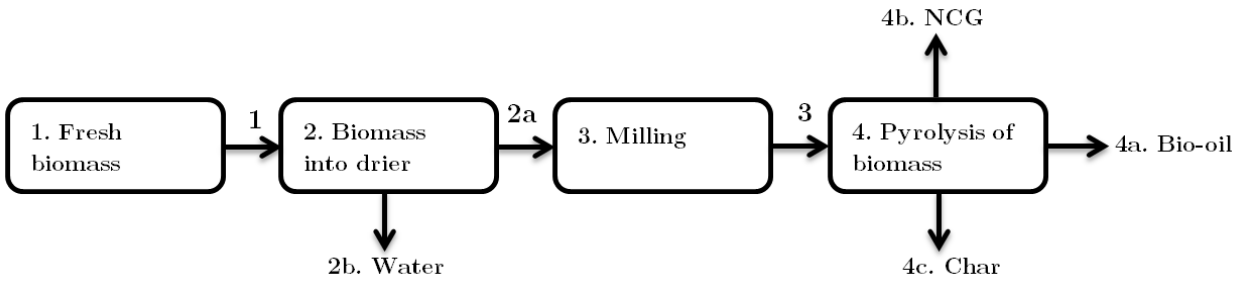

Figure 8-1: Flow diagram of raw biomass pyrolysis as a reference for the mass balance sheets

1) Fresh biomass

1. Fresh biomass	Value	Error
Wet biomass in (kg)	2	-
Moisture content (wt% wet basis)	50	-
Water in biomass (kg)	1	-
Dry biomass weight (kg)	1	-
Inorganic content (wt%)	0.41	0.04
Inorganic content (kg)	0.0041	0.00003
Inorganics as soluble salts	0.0014	-
Elemental composition (% dry basis)		
Carbon	50.30	0.67
Hydrogen	6.06	0.18
Nitrogen	0.10	0.00
Oxygen	43.54	0.80

2) Biomass into drier

2a. Dried biomass	Value	Error
Dry biomass weight (kg)	1	-
Moisture content (wt% dry basis)	10	-
Inorganic content (kg)	0.0041	0.00003
Water mass (kg)	0.1	
Total mass (kg)	1.1	-
Elemental composition (% dry basis)		
Carbon	50.30	0.67
Hydrogen	6.06	0.18
Nitrogen	0.10	0.00
Oxygen	43.54	0.80

2b. Water removed	Value	Error
Water (kg)	0.9	-

3) Milling: same as stream 2a

4) Pyrolysis of biomass

4a. Bio-oil	Value	Error
Liquid yield (wt%)	55.3	1.0
Liquid produced (kg)	0.553	0.007
Inorganics (wt%)	0.16	0.06
Inorganic content (kg)	0.000896	0.0012
Water mass (kg)	0.1	
Total mass (kg)	1.1	-
Elemental composition (% wet basis)		
Carbon	42.07	0.65
Hydrogen	7.76	0.15
Nitrogen	0.03	0.04
Oxygen	50.15	0.68

4b. NCG	Value	Error
NCG yield (wt%)	12.5	1.2
NCG produced (kg)	0.125	0.004
NCG composition (%)		
Hydrogen	0.24	0.23
Methane	0.39	0.00
Carbon monoxide	48.01	0.44
Carbon dioxide	5.57	0.63
Ethylene	0.73	0.00
Ethane	0.0007	0.000
Density of the gas (kgm^{-3})	1.56	0.01
Elemental composition (% dry basis)		
Carbon	35.28	0.45
Hydrogen	0.44	0.01
Nitrogen	0.00	0.00
Oxygen	64.21	0.82

4c. Char	Value	Error
Char yield (wt%)	**25.0**	1.0
Char produced (kg)	0.25	0.005
Inorganic content (kg)	0.00353	0.00004
Inorganics (wt%)	1.41	0.05
Elemental composition (% dry basis)		
Carbon	64.27	1.90
Hydrogen	4.65	0.20
Nitrogen	0.25	0.10
Oxygen	30.83	1.90

The overall mass, inorganic, and elemental balances were calculated based on the mass and elemental flows detailed above, with the results given in Table 8-1. The overall mass balance indicates that 7.20±0.27% of the dry biomass fed into the system was not account for in product streams; most likely due to difficulties in accounting for all the pyrolysis products accurately, as discussed in Chapter 7. The discrepancy for the elemental balance indicates a loss in all species; this was partly due to the errors associated with the elementary analysis techniques as the solids samples were analysed at a different laboratory to the liquid samples. The discrepancy between identical samples sent to both laboratories for analysis (see Section 7.6.1 for details) was 7.51% for carbon, 7.48% for hydrogen, and 5.47% for oxygen. The nitrogen discrepancy was unknown as the nitrogen detector at Scion was faulty. While these discrepancies could account for the hydrogen and oxygen losses, it could not account for the carbon loss. The most likely source for carbon loss was residue in the pyrolysis system that required combustion for removal. This would have had high carbon content due to its extended residence time in the hot zone.

The overall inorganic balance in Table 8-1 indicates a discrepancy of -7.83±0.02%, which shows additional inorganics became incorporated into the bio-oil or char. A balance on the actual inorganic elements was accomplished using ICP-OES to test the likely origin of the additional inorganic elements. The balance is displayed in Table 8-2. Inorganics are presents in low concentrations in woody biomass, leading to large discrepancies associated with most elements, although the error was higher than the discrepancy for all elements

except B. This means the variance in the elementary analysis is the main source of error and reduces the reliability of the data. In the overall inorganic balance K, Mn, Ni, S, and Si all increased compared to the initial content in the biomass; while Al, Ca, B, Cr, Cu, Fe, Mg, Na, P, and Zn all decreased.

Table 8-1: Overall mass, inorganic, and elemental balances for pyrolysis of raw biomass

System balance	Balance	Discrepancy (%)
Total mass (kg)	0.072±0.003	7.20±0.27
Inorganics (kg)	-0.00032±0.00004	-7.83±0.018
Elemental balance		
Carbon (%)	6.56±2.60	13.05±1.11
Hydrogen (%)	0.55±0.31	9.15±0.39
Nitrogen (%)	0.02±0.11	22.91±1.61
Oxygen (%)	0.08±2.32	0.18±0.15

Table 8-2: Inorganic mass balance for pyrolysis of raw biomass

Element[1]	Al	B	Ca	Cr	Cu	Fe	K	Mg	Mn	Na	Ni	P	S	Zn	Si
Biomass															
Amount in stream (mg)	70.9	3.1	756.0	0.9	2.7	81.5	524.9	204.0	51.5	60.3	0.5	146.6	63.1	6.8	2127.0
Error (mg)	10.2	0.5	17.3	0.3	0.5	30.2	1.2	0.1	0.5	3.2	0.0	4.2	1.8	0.1	36.7
Char															
Amount in stream (mg)	24.3	1.8	686.0	0.7	2.1	32.5	599.4	191.4	57.3	7.7	0.7	61.8	29.4	5.3	1824.7
Error (mg)	22.3	0.1	245.4	0.4	1.2	37.0	410.0	55.8	7.0	0.6	0.4	19.2	6.4	1.3	912.9
Bio-oil															
Amount in stream (mg)	0.6	0.4	-	-	-	20.9	0.9	0.5	0.2	21.1	0.4	-	39.4	0.8	810.2
Error (mg)	0.3	0.1	-	-	-	21.6	0.2	0.1	0.0	30.5	0.2	-	42.2	0.1	301.3
System balance															
Balance (mg)	46.0	0.9	69.9	0.2	0.6	28.1	-75.4	12.1	-6.0	31.5	-0.5	84.8	-5.7	0.8	-508.0
Error (mg)	24.5	0.5	246.0	0.5	1.3	52.4	410.0	55.8	7.1	30.7	0.4	19.6	42.7	1.3	962.0
Discrepancy (%)	64.9	27.9	9.3	21.7	23.3	34.5	-14.4	5.9	-11.6	52.2	-83.9	57.9	-9.1	11.3	-23.9
Error (%)	247.1	18.2	272.2	24.6	39.6	359.9	-678.0	95.1	-33.5	286.4	-50.9	124.9	-162.1	16.7	-1019.5

[1]*Elements below the detection limit were As, Cd, Co, Pb, V, Ba, and Li*

8.1.2 Pyrolysis of pretreated biomass

The procedure for pyrolysis of raw biomass is given in Figure 8-2. The mass and elementary flows during each stage in Figure 8 are detailed below in the bullet points 1-8. For the mass balance, it was assumed that biomass was initially milled to <6 mm followed by torrefaction. Then the hot torrefied biomass was directly fed into the pyrolysis reactor, during which the biomass was further milled to <2 mm by a sharpened feeding auger (secondary milling). The organic acids used for leaching were represented by a 1% acetic acid solution in the balance. The acetic acid removed during leachate regeneration was assumed to be the amount required to maintain a 1% acetic acid leaching solution. Regeneration also assumed complete removal of inorganics, although this still requires further development to achieve: possibly with the use of ion exchange resins or through modifications to the char. It was also assumed that char contained 50 wt% (dry basis) of moisture following regeneration. This reduced the energy obtained from char combustion in the subsequent section. Finally, it was assumed in calculations that 100% of the char was used for regeneration.

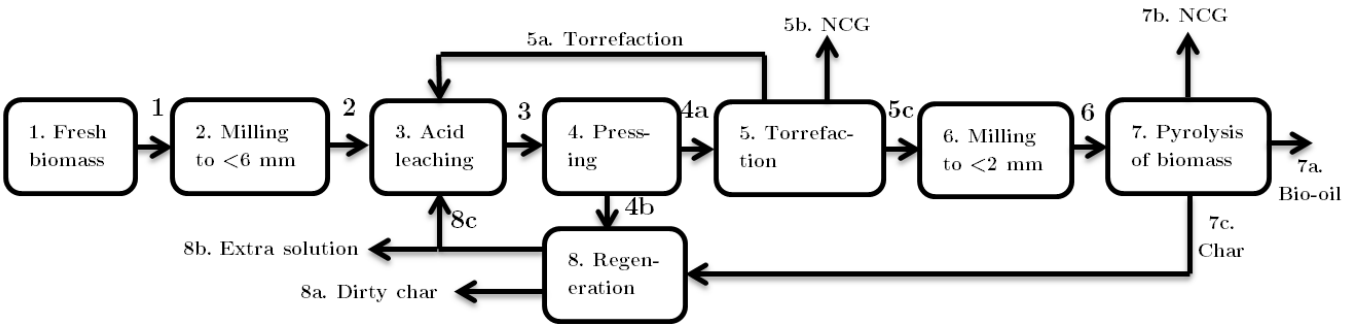

Figure 8-2: Flow diagram of pretreated biomass pyrolysis as a reference for the mass balance sheets

1) Fresh biomass

1. Fresh biomass	Value	Error
Wet biomass in (kg)	2	-
Moisture content (wt% wet basis)	50	-
Water in biomass (kg)	1	-
Dry biomass weight (kg)	1	-
Inorganic content (wt%)	0.41	0.04
Inorganic content (kg)	0.0041	0.00003
Inorganics as soluble salts	0.0014	-
Elemental composition (% dry basis)		
Carbon	50.30	0.67
Hydrogen	6.06	0.18
Nitrogen	0.10	0.00
Oxygen	43.54	0.80

2) Milling to <6 mm: same as stream 1

3) Acid leaching

3. Acid leaching	Value	Error
Dry biomass weight (kg)	1	-
Total leaching reagent (kg)	10	-
Inorganic content (kg)	0.0041	0.00003
Inorganics as soluble salts	0.0014	-
Acetic acid conc. (wt%)	1	-
Acetic acid mass (kg)	0.10	-
Water mass (kg)	9.90	-
Elemental composition (% dry basis)		
Carbon	50.30	0.67
Hydrogen	6.06	0.18
Nitrogen	0.10	0.00
Oxygen	43.54	0.80

4) Pressing

4a. Wet biomass	Value	Error
Biomass loss (%)	0.72	0.13
Dry biomass weight (kg)	0.993	0.015
Moisture content (wt% dry basis)	50	-
Liquid in biomass (kg)	0.496	0.008
Total mass (kg)	1.489	0.017
Inorganic content (wt%)	0.15	0.02
Inorganic content (kg)	0.0015	0.00002
Acetic acid mass (kg)	0.0050	0.0001
Water mass (kg)	0.491	0.008
Elemental composition (% dry basis)		
Carbon	50.30	0.67
Hydrogen	6.06	0.18
Nitrogen	0.10	0.00
Oxygen	43.54	0.80

4b. Leachate	Value	Error
Total mass (kg)	9.51	0.02
Dry biomass (extractives) (kg)	0.0072	0.0001
Total liquid mass (kg)	9.50	0.023
Inorganic content (kg)	0.00264	0.00003
Soluble salts (kg)	0.0014	-
Ion exchanged inorganics (kg)	0.00124	0.00003
Acetic acid conc. (wt%)	1	-
Acetic acid mass (kg)	0.0950	0.0001
Water mass (kg)	9.409	0.008

5) Torrefaction

5a. Liquid	Value	Error
Liquid yield (wt%)	8.05	1.83
Liquid produced (kg)	0.080	0.005
Water in feed (kg)	0.496	0.006
Acetic acid from feed (kg)	0.00496	0.00005
Acetic acid conc. (wt%)	3.59	0.03
Amount of acid (kg)	0.0207	0.0001

5b. NCG	Value	Error
NCG yield (wt%)	4.03	1.50
NCG produced (kg)	0.040	0.003
NCG composition (mass%)		
Carbon monoxide	17.31	0.36
Carbon dioxide	82.69	0.36
Density of the gas (kgm^{-3})	1.774	0.006
Elemental composition (% dry basis)		
Carbon	29.97	0.51
Oxygen	70.03	0.51

5c. Torrefied biomass	Value	Error
Biomass yield (wt%)	**87.85**	1.35
Biomass produced (kg)	0.87	0.02
Moisture content (wt%)	0.0	0.0
Inorganic content (kg)	0.00146	0.00002
Inorganics (wt%)	0.168	0.003
Elemental composition (% dry basis)		
Carbon	52.05	0.53
Hydrogen	5.50	0.53
Nitrogen	0.09	0.35
Oxygen	42.37	0.61

6) Milling to <2 mm: same as stream 5c

7) Pyrolysis of biomass

7a. Bio-oil	Value	Error
Liquid yield (wt%)	57.8	1.7
Liquid produced (kg)	0.50	0.015
Inorganics (wt%)	0.091	0.030
Inorganic content (kg)	0.00046	0.00023
Water mass (kg)	0.018	0.003
Elemental composition (% wet basis)		
Carbon	43.77	1.65
Hydrogen	7.50	0.47
Nitrogen	0.04	0.00
Oxygen	48.69	1.45

7b. NCG	Value	Error
NCG yield (wt%)	11.50	0.70
NCG produced (kg)	0.1003	0.0029
NCG composition (%)		
Hydrogen	0.59	0.12
Methane	3.21	0.79
Carbon monoxide	55.85	0.11
Carbon dioxide	38.41	2.00
Ethylene	1.28	0.05
Ethane	0.007	0.000
Density of the gas (kgm^{-3})	1.44	0.003
Elemental composition (% dry basis)		
Carbon	37.91	0.82
Hydrogen	1.57	0.03
Nitrogen	0.00	0.00
Oxygen	59.85	1.29

7c. Char	Value	Error
Char yield (wt%)	**23.7**	2.6
Char produced (kg)	0.207	0.012
Inorganic content (kg)	0.0044	0.0001
Inorganics (wt%)	2.14	0.19
Elemental composition (% dry basis)		
Carbon	72.87	0.16
Hydrogen	3.64	0.17
Nitrogen	0.15	0.10
Oxygen	23.34	0.16

8) Regeneration

8a. Dirty char	Value	Error
Moisture content (wt%)	50.0	-
Liquid mass (kg)	0.107	0.012
Inorganic removal (%)	100	-
Acetic acid removed (%)	13.93	-
Acetic acid (kg)	0.0133	0.0002
Inorganic content (kg)	0.0071	0.0001
Mass char and extractives (kg)	0.214	0.012

8b. Extra solution	Value	Error
Extra solution (kg)	0.973	0.021
Acetic acid (kg)	0.0085	0.0002

8c. To acid leaching	Value	Error
Total liquid (kg)	9.40	0.02
Acetic acid (kg)	0.0818	0.0002
Acetic acid (%)	0.870	0.006
Inorganic content (kg)	0.0	0.00

8c+5a. Leaching solution	Value	Error
Amount of solution (kg)	9.00	-
Acetic acid (kg)	0.0990	0.0002
Acid concentration (%)	1.100	0.021
Inorganic content (kg)	0.00	-
Water from feed (kg)	1.00	-
Total solution (kg)	10.00	-
Over all acetic acid conc. (%)	1.00	-

The overall mass, inorganic, and elemental balances were calculated based on the mass and elemental flows detailed above, with results given in Table 8-3. The mass balance closure indicated 6.17±0.49% of the biomass fed into the system was not accounted for. The discrepancy originated predominately from pyrolysis: the mass balance closure around pyrolysis was 93.2±3.7%. The discrepancy of 6.17±0.49% was due to limitations when measuring the pyrolysis products, as discussed in Chapter 7. The elementary balance indicated a loss in all elements. Similarly to pyrolysis of raw biomass, the loss was associated with errors in the analytical technique. Again, the carbon loss was the highest; indicating unaccounted for mass in the system was likely carbon rich.

The discrepancy of -83.53±0.38% for the overall inorganic mass balance suggested a significant addition of inorganics in the leachate, bio-oil, or char. Char had a high inorganic content of 2.14±0.19 wt%, which was thought to be due to silica sand in the fluidised bed becoming incorporated into the char fraction, as discussed in Section 7.6.3. A balance on the actual inorganic species was accomplished using ICP-OES to test the likely origin of the additional inorganic species. The balance is displayed in Table 8-4. Inorganics that increased in quantity were Si, P, Mg, Mn, Fe, and Al, which likely originated from silica sand entrainment in the char or from leaching of glassware during storage. Similarly to the discrepancy on the inorganic balances for the raw biomass pyrolysis system; the error in the analysis was larger than the discrepancy for most elements, indicating the variance in the ICP-OES analysis for repeated samples was high and limited the reliability of the data.

Table 8-3: Mass, inorganic, and elemental balance for pyrolysis of pretreated biomass

System balance	Balance	Discrepancy (%)
Total mass (kg)	0.0617±0.0195	6.17±0.49
Inorganics (kg)	-0.00342±0.00027	-83.53±0.38
Elemental balance		
Carbon (%)	7.81±2.03	15.52±1.14
Hydrogen (%)	1.33±0.54	21.90±1.03
Nitrogen (%)	0.05±0.10	48.08±2.08
Oxygen (%)	5.06±2.17	11.61±1.13

Table 8-4: Inorganic balance for pyrolysis of pretreated biomass

Element[1]	Al	B	Ca	Cr	Cu	Fe	K	Mg	Mn	Na	Ni	P	S	Zn	Si
Biomass															
Amount in stream (mg)	70.9	3.1	756.0	0.9	2.7	81.5	524.9	204.0	51.5	60.3	0.5	146.6	63.1	6.8	2127.0
Error (mg)	10.2	0.5	17.3	0.3	0.5	30.2	1.2	0.1	0.5	3.2	0.0	4.2	1.8	0.1	36.7
Leachate															
Amount in stream (mg)	23.6	27.3	609.9	0.1	1.1	8.7	633.4	170.6	40.3	131.0	0.3	45.1	25.8	7.4	908.7
Error (mg)	1.9	5.7	99.3	0.0	0.0	1.1	29.3	9.8	1.8	68.2	0.0	12.1	4.4	0.7	2.5
Torrefaction liquor															
Amount in stream (mg)	0.28	0.48	0.72	0.00	0.00	0.08	0.22	0.03	0.01	2.17	0.01	0.01	1.81	0.22	0.28
Char															
Amount in stream (mg)	40.5	1.3	229.7	3.1	4.1	64.9	44.1	32.2	9.7	11.3	2.2	36.5	11.6	6.7	3931.4
Error (mg)	20.4	0.1	475.2	0.2	1.1	47.5	26.6	1.05	14.1	10.0	0.1	13.3	4.9	2.6	1031.6
Bio-oil															
Amount in stream (mg)	0.4	0.0	0.0	0.1	0.0	2.6	1.7	0.0	0.0	33.9	0.0	0.0	31.8	0.7	159.7
Error (mg)	0.1	0.0	0.0	0.0	0.0	0.9	0.6	0.0	0.0	46.7	0.0	0.0	58.2	0.0	165.6
System balance															
Balance (mg)	6.1	-26.0	-84.4	-2.3	-2.5	5.1	-154.4	1.2	1.5	-118.0	-1.9	65.0	-7.9	-8.3	-2872.8
Error (mg)	22.9	5.8	485.7	0.4	1.2	56.3	39.6	19.82	14.2	83.3	0.1	18.5	58.6	2.7	522.7
Discrepancy (%)	8.6	-847.3	-11.2	-244.6	-94.0	6.3	-29.4	0.6	2.9	-195.7	-351.9	44.3	-12.6	-122.1	-135.1
Error (%)	80.4	-991.5	-590.2	-59.3	-75.9	158.1	-93.7	5.35	33.7	-1503.2	-23.1	102.6	-262.1	-114.7	-1321.6

[1]*Elements below the detection limit were As, Cd, Co, Pb, V, Ba, and Li*

8.2 Energy balances

The total energy required for biomass drying, milling, and pyrolysis was determined for pyrolysis of raw and pretreated biomass. For pyrolysis of pretreated biomass, the energy required for the pretreatments was also calculated. Next, the potential energy from combustion of the NCG and char was determined and compared to the total energy demand. Pyrolysis requires energy to heat the biomass and to drive reactions. The energy required to drive pyrolysis reactions can be exothermic or endothermic depending on the pyrolysis temperature and the products produced. Char formation is an exothermic reaction, while NCG and bio-oil formation are endothermic processes [2]. Higher char yields may indicate a shift from a typically endothermic system to more of an exothermic system. The energy required for the pyrolysis reactions was predicated using Equation 8.1, developed by Rath *et al.* [2].

$$H_{rxn} = -3827 \times Y_{char} + 1277 \times (1 - Y_{char}) \qquad 8.1$$

Where H_{rxn} is the energy required to drive pyrolysis reactions in kJkg^{-1} and Y_{char} is the yield of char from pyrolysis in wt%. The energy required for biomass drying was a combination of heating the biomass and water to 100 °C plus the heat of vaporisation for water removal. The energy required for grinding biomass was reported but not added to the total energy requirements as the heat from char or NCG combustion cannot be used directly for milling.

Since combustion of the NCG and char was for heating purposes, the higher heating value was used for calculations as hot NGC would be initially used to heat the pyrolysis reactor and then used for other means such

as heating or drying biomass. This allows the heat of vaporisation of water to be taken into account as the combusted gas eventually reaches near atmospheric temperature before being released. This maximises the energy extracted from the combusted NCG or char.

The energy for grinding used data produced by Miao *et al.* [3]. Miao *et al.* used raw chips that were 6-58 mm×6-76 mm×5-25 mm before milling. The comminution energy required to reduce biomass to <6 and <2 mm particles was 200 and 1400 $kJkg^{-1}$ (dry basis), respectively, when using knife milling. Only Miscanthus and Switchgrass were both hammer and knife milled by Miao *et al*. Hammer milling generally requires less energy and is typically used for industrial processes, thus milling energy was divided by the average reduction in energy consumption for hammer milling compared to knife milling. The results indicated that the energy requirements were 81.5 and 570.4 $kJkg^{-1}$ (dry basis) for hammer milling to reduce particles to <6 and <2 mm respectively.

8.2.1 Pyrolysis of raw biomass

For pyrolysis of raw biomass, biomass was assumed to have an initial MC of 100 wt% (dry basis), which was reduced to 10 wt% prior to milling and pyrolysis. Milled biomass entered the pyrolysis at 20 °C. The energy flows in the 5 stages described in Figure 8-1 are given in Table 8-5. The energy balance assumed 1 kg of dry feed entered the system. Biomass drying required 2.42 MJ of energy and pyrolysis required 1.29±0.02 MJ of energy. Combustion of NCG can produce 0.45±0.03 MJ of heat and combustion of the char produces 6.17±1.11 MJ of heat. This indicated there was a surplus of energy produced, and only 52.7% of the char was required to provide the heat required. Additional char would be required to compensate for heat loss from the system, which was estimated to be 1% of the biomass's lower heating value, as reported by Dutta *et al.* [4] for a commercial scale system with a biomass feeding rate of 82567 $kghr^{-1}$ (dry basis). This equates to approximately 0.2 MJ. The remaining char could be used for production of co-products such as pellets or activated carbon.

Table 8-5: Energy balance for pyrolysis of raw biomass

	Energy in $MJkg^{-1}$	Energy in MJ[1]	Type
1. Fresh biomass	20.19±0.71	20.19±3.19	In stream
2. Biomass drying	-2.42	-2.42	Required
3. Milling	-0.57	-0.57	Required[2]
4. Pyrolysis	-1.29±0.02	-1.29±0.02	Required
4a. Bio-oil	+21.60±0.10	+9.94±0.24	In stream
4b. NCG	+5.68±0.06	+0.43±0.03	Available
4c. Char	+24.69±0.89	+6.17±1.11	Available
Total energy required		3.71±0.02	
Total energy available		6.63±1.11	
Balance		+2.87±1.11	

[1]Per kg of dry biomass feed [2]Not included in the energy balance as heat from combustion cannot be utilised

8.2.2 Pyrolysis of pretreated biomass

For pyrolysis of pretreated biomass, fresh biomass was assumed to have a MC of 100 wt% (dry basis). This was milled to <6 mm, leached, pressed, torrefied, and then milled to <2 mm in the feeding auger before pyrolysis. Milled biomass entered the pyrolysis reactor with a MC of 0 wt% (dry basis) and at 270 °C as torrefaction was represented by a heated feeding auger. The energy flows for the 8 stages described in Figure 8-2 are given in Table 8-6. In the energy balance calculations, it was assumed that 1 kg of dry biomass feed entered the system. There was a surplus of energy of 3.65±0.03 MJ following char and NCG combustion, this indicated only 53.4% of the char was required for combustion, plus additional char to compensate for heat loss. Torrefaction, which also acts as the drying stage required the most energy at 2.06 MJ. Without considering the energy required for drying during torrefaction, the energy required to drive torrefaction reactions may be exothermic as torrefaction of hemicellulose, cellulose, and lignin are typically exothermic [5]. The energy required for torrefaction was assumed to be solely the energy required for heating the biomass and moisture removal; therefore the total energy for torrefaction was likely overestimated. Pyrolysis of pretreated biomass required less energy compared to pyrolysis of raw biomass as the biomass entered the reactor dry; there was less biomass entering the reactor; and the biomass entered the reactor at 270 °C. However, less energy was harnessed from char combustion as the char was wet prior to combustion due to the additional 50 wt% (dry basis) of moisture from leachate regeneration.

The total energy required for milling, which were not taken into account in the energy balance, indicated pretreated biomass required 0.15±0.001 MJ to produce <2 mm particles, while raw biomass milling required significantly more energy at 0.57 MJ. Due to the high moisture content of raw biomass, there was 0.973±0.021 kg of leachate containing 0.87±0.001% acetic acid to dispose of per kg of dry biomass fed into the system.

Table 8-6: Energy balance for pyrolysis of pretreated biomass

	Energy in MJkg^{-1}	Energy in MJ[1]	Type
1. Fresh biomass	20.19±0.71	20.19±3.19	In stream
2. Milling to <6 mm	-0.082	-0.082	Required[2]
3. Acid leaching	20.19±0.71	20.19±3.19	In stream
4. Pressing	20.19±0.71	20.05±3.71	In stream
5. Torrefaction	-2.07	-2.06	Required
5a. Torr. liquor	-	-	-
5b. Torr. NCG	+1.42±0.01	+0.057±0.001	Available
5c. Torr. biomass	20.26±0.02	17.67±0.36	In stream
6. Milling to <2 mm	-0.074±0.001	-0.064±0.001	Required[2]
7. Pyrolysis	-0.583±0.012	-0.508±0.001	Required
7a. Bio-oil	19.65±0.07	9.55±0.25	In stream
7b. NCG	+5.95±0.12	+0.60±0.03	Available
7c. Char	27.26±0.17	5.64±0.24	In stream
8a. Dirty char	+26.02±0.69	+5.56±0.02	Available
8b. Extra solution	-	-	-
8c. To acid leaching	-	-	-
8c+5a. Leaching solution	-	-	-
Total energy required		2.57±0.01	
Total energy available		6.22±0.03	
Balance		+3.65±0.03	

[1]Per kg of dry biomass feed. [2]Not included in the energy balance as heat from combustion cannot be utilised

8.3 Economics for raw and pretreated bio-oil production

An extensive economic evaluation using Aspen Plus for biofuel production was developed by Puladian [6] and reported in her PhD thesis at the University of Canterbury. Her research compared two scenarios for the production of Fischer-Tropsch liquid fuels from *P. radiata*. Scenario 1 used biomass gasification to directly produce a syngas for later Fischer-Tropsch synthesis. Scenario 2 investigated initially densifying the biomass using pyrolysis to reduce transportation costs, followed by bio-oil gasification at a central plant to produce a syngas. In Scenario 2, bio-oil was produced from five, 20 MW pyrolysis reactors. Capital and operational costs for each 20 MW pyrolysis reactor were given by Puladian [6], and was used in the present study for pyrolysis of raw biomass. The costs were slightly modified and used for an economic evaluation comparing pyrolysis of raw biomass to pyrolysis of pretreated biomass.

In order to reduce transportation costs of woody biomass, multiple smaller pyrolysis plants located near the logging site can be used to densify the biomass before upgrading in a central refinery. A logging truck can carry approximately 30 tonnes of logs and it costs \$0.18-0.24 to truck one m^3 of wood per km. The conversion of wood chips to bio-oil via pyrolysis increases the energy density by around 4 times and the volume reduction by around 7 times. On-site pyrolysis would decrease the transportation costs of bio-oil to a central refinery [7].

The pyrolysis system modelled by Puladian [6] in Aspen was a fluidised bed reactor. A piping and instrumental diagram of the system is given in Appendix 8.1. The biomass enters the system as chips with a particle size of

<35 mm. A slip stream from the NCG production was recycled as the fluidising gas during fast pyrolysis. The char was separated using a cyclone and the bio-oil vapours were condensed in two quenches. A portion of the light bio-oil collected from the second quencher was recycled as the quenching liquid. The remaining NCGs and a portion of the char were sent to a combustor, which produced a flue gas at 1000 °C for biomass heating, drying, and fast pyrolysis. The process in Puladian's system produced a bio-slurry for further gasification; therefore the char was mixed with the bio-oil. The 20 MW plant required 30,096 $t.yr^{-1}$ of dry biomass. Since the capacity of the pyrolysis system was designed to process this biomass feed rate, the feed rate to the pyrolysis reactor was kept constant. The output in MJ of bio-oil for the raw and pretreated bio-oil was calculated by using the mass balances given in Section 8.1, but with constant biomass feed rate of 30,096 $t.yr^{-1}$ of dry biomass into the pyrolysis reactor. Based on this feed rate, it was calculated that pyrolysis of raw biomass produced 10.39 MW of bio-oil while the pretreated system produced 11.44 MW of bio-oil. This was partly due to the biomass loss during torrefaction allowing for a higher overall raw biomass input into the pretreated system, as indicated in Table 8-7.

8.3.1 Capital costs

Raw biomass required drying and milling to <2 mm while pretreated biomass required an acid leaching vessel, a filter press, and a torrefaction reactor. Acid leaching was assumed to be a 4 batch vessels stirred using a heavy duty ribbon mixer. After leaching, the biomass was pressed using a filter press and then torrefied. Torrefaction was envisioned as simply heating the first feed auger to the fluidised bed. This would operate at a rate to allow sufficient torrefaction residence time. Feeding augers are typically water jacketed to prevent premature pyrolysis during the feeding, instead, that heat can be used to supplement the torrefaction heating requirements. This reduces the water requirements and improves the system's energy efficiency. To prevent hot spots in the torrefaction reactor, a jacket with circulating hot air would be required. Also, a double valve system before the pyrolysis reactor would be required to prevent torrefaction vapours entering the pyrolysis reactor.

For the acid leaching process, the power consumption of mixer in the acid leaching vessel was determined using equations given by Furukawa *et al.* [8]. The leaching vessel was assumed to be 4 m in diameter by 4 m in length. The ribbon impeller was 3.7 m in diameter and 3.1 m in length. The power consumption of the impeller was 9.04 kW. The cost for 4 vessels plus motors was estimated using the first approximation costing technique (FACT), which was calculated as $53,771. The cost of the filter press was determined assuming a continuous, automated press with a nominal filter area of 4 m^2; the capital cost for this was $24,470. The power consumption for the auger reactor used for torrefaction was determined assuming the auger was 0.46 m in diameter and 4 m long. It was assumed a 20 kW motor was required to drive the auger, using results reported by Nicolai *et al.* [9]. The total capital cost was for the torrefaction auger and motor was $16,666. It was assumed the inflation rate was of 2.3 between 2004 and 2015 for calculations [10].

The total capital investment for the raw and pretreated pyrolysis systems is given in Table 8-7. Results in the table indicate the raw pyrolysis system requires a capital investment of $NZ 53,793,407 while the pretreated pyrolysis system requires $NZ 46,334,375. The higher cost for the raw pyrolysis system originated from the cost of the biomass dryer and grinder. The total capital investment takes into account the offsite capital costs of 40% of the total capital costs and a contingency of 10% of the total capital costs [6]. The total cost were much higher than those estimated by Puladian [6] of $NZ 29,506,800 for a pyrolysis plant with the same biomass feed rate. This was because the offsite costs were taken into account and higher cost factors were used.

Table 8-7: Total capital costs for raw and pretreated bio-oil production

	Tag	Raw biomass	Pretreated biomass	Comments	Ref.
Operating hours per yr	-	8000	8000		[6]
Plant capacity (MW bio-oil)	-	10.39	11.44		Cal.
Biomass required for pyrolysis (odt.yr^{-1})	-	30,096	30,096	Set based on the capacity of [6]	[6]
Capital costs ($NZ)					
Biomass dryer	A	1,271,000	-	Rotary dryer	[6]
Grinder	B	80,906	-	Hammer mill, reducing to 2-3 mm	[6]
Acid leaching	C	-	53,771	4 heavy duty ribbon mixers	Calc.
Filter press	D	-	24,470		Calc.
Torrefaction	E	-	16,666	Auger acts as the grinder	Calc.
Pyrolysis reactor	F	4,086,126	4,086,126		[6]
Air coolers	G	469,087	469,087		[6]
Quench system	H	131,982	131,982		[6]
Tanks	I	1,131,993	1,131,993		[6]
Fan	J	1,360,271	1,360,271		[6]
Pumps	K	13,757	13,757		[6]
Storage tank	L	520,164	520,164		[6]
Major equipment costs ($NZ)	J	9,065,286	7,808,287	SUM(A-L)	
Instrumentation and control systems ($NZ)	K	1,359,793	1,171,243	15% of J	[11]
Minor materials ($NZ)	L	6,255,047	5,387,718	60% of J+K	[11]
Total equipment costs ($NZ)	M	16,680,126	14,367,248	L+K+J	
Installation costs ($NZ)					
Freight insurance and handling	N	2,502,019	2,155,087	15% of M	[11]
Engineering	O	3,336,025	2,873,450	20% of M	[11]
Construction labour	P	10,008,076	8,620,349	60% of M	[11]
Construction equipment	Q	1,668,013	1,436,725	10% of M	[11]
Construction supervision	R	1,668,013	1,436,725	10% of M	[11]
Total installation costs ($NZ)	S	19,182,145	16,522,335	SUM(N-R)	
Total capital costs ($NZ)	T	35,862,271	30,889,583	M+S	
Offsite capital costs	U	14,344,909	12,355,833	40% of T	[12]
Contingency ($NZ)	V	3,586,227	3,088,958	10% of T	[6]
Total capital investment (TCI) ($NZ)	W	53,793,407	46,334,375	T+U+V	

8.3.2 Production costs

Forest residues are the cheapest biomass option for bio-oil production. It was assumed that chipped forest residues (<35 mm) were used for bio-oil production. The cost of procuring, harvesting, handling, processing (chipping), and transporting forest residues to a central location in the North Island of New Zealand (Kinleith

Pulp and Paper Mill) was $NZ 70 per dry tonne in 2006 [13]. Taking an average inflation rate into account, this was assumed to be $NZ 85.89 per oven-dry tonne in 2015.

Results for the total annual production costs are given in Table 8-8. The results in this table indicate the cost to produce raw bio-oil was $NZ 29.87 per GJ compared to $NZ 29.67 per GJ to produced pretreated bio-oil. The pretreated pyrolysis system required additional biomass feed but also had a higher plant capacity; this was due to the biomass feed into the pyrolysis reactor being held constant for the two systems. The raw pyrolysis system had a significantly higher electricity cost associated with grinding the biomass to <2 mm. This system also had higher maintenance, local tax on property, insurance, and depreciation costs due to the higher capital investment. The production costs in this study were significantly higher than those reported by Puladian [6] of $NZ 6,575,635 for a pyrolysis reactor of the same capacity (or $NZ 231 per tonne of bio-oil). The lower production costs reported by Puladian were primarily from the lower biomass cost used in her research of $NZ 21.2 per tonne (100% MC). Additionally, a higher maintenance cost factor was used in this research and the electricity cost associated with biomass grinding was higher.

The energy balance indicated that 52.74% of the raw char was required to supply the system's energy, and 53.37% of the pretreated char was required for the pretreated system. This equates to 2.69 and 4.47 MW respectively for the two systems, which is available as a by-product. The char could be pelletise and sold as a coal substitute. The coal price in 2015 was $NZ 0.00297 per MJ [14]. This equates to additional revenue of $NZ 229,375 p.a. for raw char and $NZ 373,510 p.a. for pretreated char if the char was used directly as a coal substitute. The char pellets could be sold for domestic use as a substitute to coal or wood pellets, or for commercial combustion applications.

While the economic analysis only used the first approximation costing technique, it does indicate that there are no economic penalties for pretreating biomass prior to pyrolysis. Therefore, pretreatments can be effectively used to improve the properties of crude bio-oil by significantly reducing secondary reactions during pyrolysis. The pretreated bio-oil could then be upgraded to a transportation fuel or potentially used directly as a marine fuel substitute with small modifications, as discussed later. Upgrading to a transportation type fuel may be easier than upgrading traditional bio-oil due to the lower water, organic acid, inorganic, and pyrolytic lignin content. Water attacks the catalyst's support [15]; decreases the catalytic activity; adsorbs onto acids sites [16]; and causes dealumunation of the catalyst [17], which can irreversibly deactivate upgrading catalysts [18]. Acetic acid and pyrolytic lignin enhance coke formation [19, 20], once formed, coke causes reversible catalyst deactivation [18]. Heavy metals and sulfur are major contributors to FCC catalyst deactivation [21]. Therefore a reduction in these compounds should improve the efficiency of catalytic cracking or hydrotreating the bio-oil.

Table 8-8: Total annual production costs for raw and pretreated bio-oil

	Tag	Raw biomass	Pretreated biomass	Comments	Ref.
Operating hours per yr	-	8000	8000		[6]
Plant capacity (MW)	-	10.39	11.44		Cal.
Biomass feed required (t.yr^{-1} dry)	-	30,096	34,507	Set based on the capacity of [6]	[6]
Biomass cost (per dry tonne)	X	85.89	85.89		[13]
Annual production costs ($NZ.yr^{-1})					
Grinding and milling electricity	Y	524,513	153,350	Assumes electricity is 0.11 kJ/sH	Calc.
Electricity for pretreatments	Z	-	25,555	Assumes electricity is 0.11 kJ/sH	Calc.
Other electricity	AA	348,480	348,480		[6]
Biomass	AB	2,585,161	2,964,042		Calc.
Supervision	AC	340,000	340,000	1 person per shift, $40 per h	[6]
Operating labour	AD	774,162	774,162	4 people per shift, $24 per h	[6]
Maintenance	AE	1,793,114	1,544,479	5% of TCI	[12]
Laboratory charges	AF	193,000	193,000		[6]
Operating supplies	AG	300,000	300,000		[6]
Depreciation	AH	1,668,013	1,436,725	Straight line deprecation	[12]
Local tax on property	AI	382,623	332,896	1% TCI	[12]
Insurance	AJ	573,934	499,344	1% TCI	[12]
Plant overheads	AK	735,000	735,000		[6]
General and administrative expenses	AL	400,000	400,000		[6]
Total annual production costs ($NZ.yr^{-1})		10,737,310	10,141,408	Sum(Y-AL)	Calc.
Bio-oil produced (t.yr^{-1})		16,643	17,396	From Section 8.1	Calc.
Production costs ($NZ.t^{-1})		645	583		Calc.
Production costs per GJ ($NZ.GJ^{-1})		29.87	29.67		Calc.

The cost to produce bio-oil per GJ was compared to the price of Brent and WTI crude oils and No. 6 residue fuel (residual fuel oil) over the second quarter of 2015. The prices per barrel of Brent crude oil, WTI crude oil, and residual fuel oil were $US 61.66, 57.85, and 150.00, respectively [14]. These prices were converted to $NZ using the exchange rate of $NZ 1 to $US 0.7314, which was the average over the second quarter of 2015 [22]. When converting the fuel to an energy content basis, the prices were $NZ 13.78, 12.78, and 30.92 per GJ for Brent crude oil, WTI crude oil, and No. 6 heavy fuel oil, respectively. The calculations assumed each barrel of crude oil contained 6.119 GJ and each barrel of residual fuel oil contained 6.633 GJ.

From the cost analysis, both the raw and pretreated bio-oils were cheaper than residual fuel oil on a GJ basis. This was impressive as crude fuel prices were very low at the time of analysis, for example, in the same quarter of 2014, the prices for Brent crude oil, WTI crude oil, and residual fuel oil were $US 103.35, 109.70, and 244.00, respectively [14]. This would have made the crude fuels $NZ 19.60, 20.81, and 42.69 per GJ of Brent crude oil, WTI crude oil, and No. 6 heavy fuel oil respectively: assuming an exchange rate of $NZ 1 to $US 0.862 in the second quarter of 2014.

While pretreated bio-oil cannot be used directly as a transportation fuel without further upgrading, there is potential to use it as a marine fuel substitute without upgrading or with minimal upgrading. The short term use

of this bio-oil as a marine fuel is advantageous as bio-oil upgrading (via catalytic cracking or hydrotreating) is currently expensive and yields are low. Bio-oil from pyrolysis of woody biomass has a much lower sulfur content compared to residual fuel oil, which contains 3.5-4.5% sulfur. Current sulfur regulations limit the sulfur content in a marine fuel to a maximum of 3.5%, with some countries' regulations requiring <0.1% sulfur [23]. This makes bio-oil attractive compared to residue fuels that would otherwise require desulfurisation. However, the lower energy content of bio-oil increases the volume required to obtain the same energy as residue fuel oils (hence, the price for the fuels is reported per GJ instead of per L). The stability of the bio-oil may also be an issue during storage or upon heating. The addition of a catalyst to the pyrolysis fluidised bed (primarily CaO) could reduce the oxygen content in the pretreated bio-oil without reducing the bio-oil yield, which may improve the bio-oil's stability and heating value [24], as discussed in Section 7.6.1.3.

8.3.3 Sensitivity analysis

A sensitivity analysis was carried out around four production variables that were associated with costs of over $NZ 1,000,000 per year. These variables were the biomass price, the electricity price, plant maintenance costs, and the depreciation level. Results for the sensitivity analysis are given in Figure 8-3, from which it was found that both the raw and pretreated systems were most sensitive to the biomass price. The pretreated system was more sensitive to fluctuations in the biomass price compared to the raw system. This was because the biomass feed rate into the pretreated system was higher. A 20% increase in the biomass price would make pretreated bio-oil production slightly more expensive than raw bio-oil production.

Both the raw and pretreated systems were least sensitive to the electricity price. The pretreated system was less sensitive to the electricity price than the raw system as milling pretreated biomass requires substantially less electricity. Variations in the maintenance costs and the depreciation level were very similar for both systems.

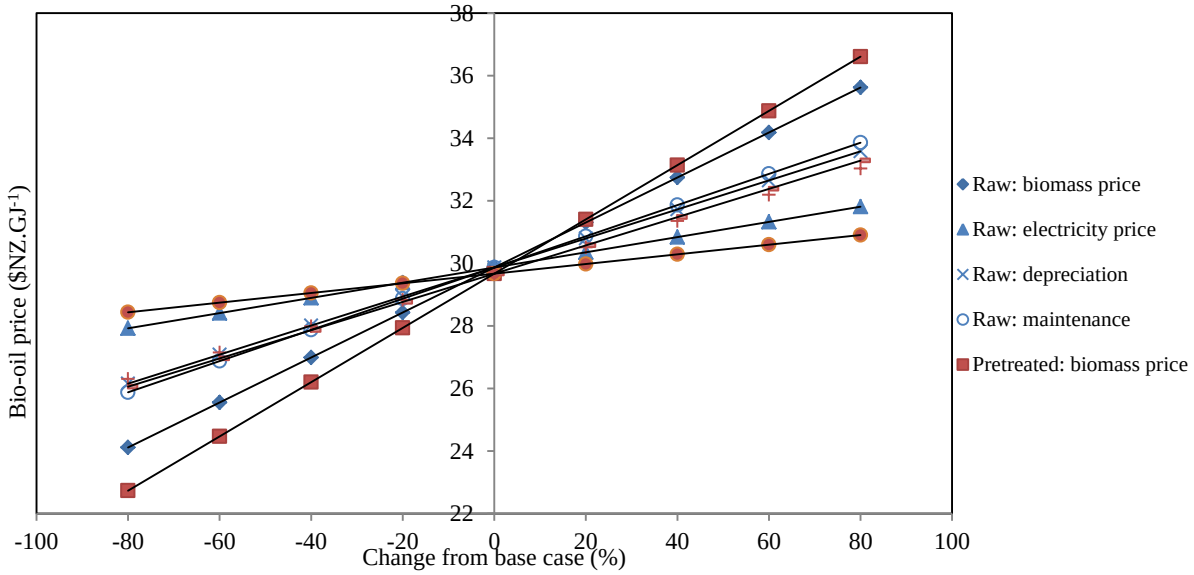

Figure 8-3: Sensitivity analysis for the production of raw and pretreated bio-oil

8.4 References

1. Visser, R., Berkett, H., & Spinelli, R. (2014). Determining the effect of storage conditions on the natural drying of radiata pine logs for energy use. *New Zealand Journal of Forestry Science, 44*(1), 1-8.
2. Rath, J., Wolfinger, M. G., Steiner, G., Krammer, G., Barontini, F., & Cozzani, V. (2003). Heat of wood pyrolysis. *Fuel, 82*(1), 81-91.
3. Miao, Z., Grift, T. E., Hansen, A. C., & Ting, K. C. (2011). Energy requirement for comminution of biomass in relation to particle physical properties. *Industrial Crops and Products, 33*(2), 504-513.
4. Dutta, A., Sahir, A., Tan, E., Humbird, D., Snowden-Swan, L., Meyer, P., et al. (2013). *Process design and economics for the conversion of lignocellulosic biomass to hydrocarbon fuels*. NREL/TP-5100-51400: National Renewable Energy Laboratory.
5. Chen, W.-H., & Kuo, P.-C. (2011). Torrefaction and co-torrefaction characterization of hemicellulose, cellulose and lignin as well as torrefaction of some basic constituents in biomass. *Energy, 36*(2), 803-811.
6. Puladian, N. (2015). *Development of an integrated system model for production of Fischer-Tropsch liquid fuels from woody biomass.* Unpublished Ph.D., University of Canterbury, University of Canterbury.
7. Green, A. (2009). *Fixed bed pyrolysis optimisation, part 1*. University of Canterbury: Chemical and Process Engineering.
8. Furukawa, H., Kato, Y., Y., I., Kato, T., Tada, Y., & Hashimoto, S. (2012). Correlation of power consumption for several kinds of mixing impellers. *International Journal of Chemical Engineering, 2012*, 6.
9. Nicolai, R., Dittbenner, A., & Pasikanti, S. (2006). *Large portable auger power and throughput analysis.* Paper presented at the American Society of Agricultural and Biological Engineers
10. Reserve-bank. (2015). Inflation calculator. Retrieved 07.07.2015, 2015, from http://www.rbnz.govt.nz
11. Bouman, R., Jesen, S., & Wake, M. (2005). *Process capital cost estimation for New Zealand 2004*. Society of Chemical Engineers New Zealand: Society of Chemical Engineers New Zealand.
12. Towler, G., & Sinnott, R. (2013). *Chemical engineering design* (2 ed. Vol. 1). United Kingdom: Elsevier.
13. Li, J., & Pang, S. (2009). *Existing biomass resources*. Chemical and Process Engineering: University of Canterbuty.
14. U.S-department-of-energy. (2015). Short-term energy outlook. Retrieved 7.8.2015, 2017, from http://www.eia.gov
15. Bridgwater, A. V. (1996). Production of high grade fuels and chemicals from catalytic pyrolysis of biomass. *Catalysis Today, 29*(1–4), 285-295.
16. Gunawardena, D. A., & Fernando, S. D. (2013). *Methods and applications of deoxygenation for the conversion of biomass to petrochemical products* (Vol. 16).
17. Wang, H., Male, J., & Wang, Y. (2013). Recent advances in hydrotreating of pyrolysis bio-oil and its oxygen-containing model compounds. *ACS Catalysis, 3*(5), 1047-1070.
18. Al-Sabawi, M., Chen, J., & Ng, S. (2012). Fluid catalytic cracking of biomass-derived oils and their blends with petroleum feedstocks: a review. *Energy & Fuels, 26*(9), 5355-5372.
19. Wildschut, J., Arentz, J., Rasrendra, C. B., Venderbosch, R. H., & Heeres, H. J. (2009). Catalytic hydrotreatment of fast pyrolysis oil: model studies on reaction pathways for the carbohydrate fraction. *Environmental Progress & Sustainable Energy, 28*(3), 450-460.
20. Hilten, R. N., Speir, R. A., Kastner, J. R., Mani, S., & Das, K. C. (2013). Effect of torrefaction on bio-oil upgrading over HZSM-5. Part 1: product yield, product quality, and catalyst effectiveness for benzene, toluene, ethylbenzene, and xylene production. *Energy & Fuels, 27*(2), 830-843.
21. Samolada, M. C., Baldauf, W., & Vasalos, I. A. (1998). Production of a bio-gasoline by upgrading biomass flash pyrolysis liquids via hydrogen processing and catalytic cracking. *Fuel, 77*(14), 1667-1675.
22. Reserve-bank. (2015). B1 exchange rates & TWI. Retrieved 07.08.2015, 2015, from http://www.rbnz.govt.nz/statistics
23. Wells, P. (2014). *Renewable fuels for marine transport*. Paper presented at the Bioenergy Association of New Zealand.
24. Veses, A., Aznar, M., Martínez, I., Martínez, J. D., López, J. M., Navarro, M. V., et al. (2014). Catalytic pyrolysis of wood biomass in an auger reactor using calcium-based catalysts. *Bioresour Technol, 162*(0), 250-258.

9 Conclusions and recommendations

A fast pyrolysis reactor was designed, commissioned, and used to produce bio-oil from woody biomass. The pyrolysis reactor was a fluidised bed with nitrogen as the fluidising gas and silica sand as the fluidising medium. Char was separated in a high efficiency cyclone and bio-oil vapours were condensed in a series of three shell and tube condensers. Remaining aerosols in the vapour stream were collected in an electrostatic precipitator.

Pyrolysis of raw *Pinus radiata* yielded 46.9±0.5 wt% (dry basis) bio-oil when the reactor operated at 500 °C. The bio-oil contained 3.5±0.4 wt% acetic acid and 24.0±1.2 wt% water. The low quality of the crude bio-oil limits its direct use to stationary combustion applications and reduces the efficiency of subsequent upgrading (catalytic cracking and hydrotreating processes). Therefore, producing a high quality crude bio-oil was investigated by pretreatment biomass prior to pyrolysis.

Three catalysts naturally inherent in biomass were identified from the literature review as the key contributors for undesirable primary and secondary reactions during fast pyrolysis. These were inorganics, organic acids (from acetyl compounds), and water. Experimental studies were conducted to reduce/remove these catalytic compounds. The results indicated all three catalysts should be targeted to significantly reduce the bio-oil's water and acetic acid content. A pretreatment sequence integrating both acid leaching and torrefaction was developed to reduce/remove these three catalytic components from raw biomass.

Acid leaching biomass

The viability of leaching biomass with the liquor produced during torrefaction was investigated. Torrefaction liquor contains mainly acetic and formic acid; therefore leaching with acetic and formic acid was compared to leaching with nitric, sulfuric, and hydrochloric acid. It was found that the mineral acids had a slightly higher removal efficiency compared to the organic acids when leachings were carried out at 30 °C, but the organic acids were equally as efficient for leachings at 90 °C.

Leaching biomass increased the bio-oil yield for all acid reagents investigated. Char yields were also reduced, except for biomass leached with sulfuric acid as sulfur became incorporated into the biomass and catalysed charring reactions. The water and acetic acid content in the bio-oil decreased when samples were leached prior to pyrolysis, indicating less secondary reactions of the pyrolysis vapours. Pyrolysis of biomass leached at 90 °C slightly improved the bio-oil yield and properties compared to pyrolysis of biomass leached at 30 °C; however the improvements were not sufficient to warrant leaching elevated at temperatures. The optimal leaching conditions were summarised as leaching at 30 °C with 1% acetic acid for 4 h. This reduced the inorganic content from 0.41±0.04 wt% for raw biomass to 0.16±0.02 wt% for leached biomass. Leaching did not change the biomass's structural composition. Pyrolysis of biomass leached at the optimal conditions yielded 54.6 wt% (dry basis) bio-oil which contained 1.9±0.1 wt% acetic acid and 17.1±1.3 wt% water. Thus, undesirable pyrolysis

reactions were reduced in the inorganic limited environment, which was confirmed by the higher levoglucosan yield of 7.83% for leached bio-oil opposed to 2.30% for raw bio-oil.

Torrefaction of biomass

Raw biomass was torrefied at 245 °C for 15 to 120 min. It was found that increasing the torrefaction residence time beyond 20 min had minimal benefit, but torrefaction residence times less than 20 min may not be sufficient to ensure complete moisture removal from the biomass; thus 20 min was considered optimal residence time. The torrefaction temperature was optimised between 220 and 290 °C. The biomass's acetyl content was reduced from 1.51 wt% for raw biomass to 0.43 wt% for biomass torrefied at 290 °C for 20 min. The oxygen content also decreased from 43.1 to 35.7%. However, the mass loss during torrefaction at 290 °C was significant at 38.5 wt%.

Bio-oil yields from pyrolysis of the biomass torrefied between 220 to 270 °C increased compared to yields obtained from pyrolysis of raw biomass. This was due to reduced interactions between biomass polymers and reduced water and acid catalysed reactions. However, when the mass loss during torrefaction was taken into account, only torrefaction at 230 °C produced more liquid compared to pyrolysis of raw biomass. Pyrolysis of biomass torrefied at 270 °C for 20 min yielded 46.1 wt% bio-oil, which was equivalent to an overall yield of 38.9 wt% bio-oil when the mass loss during torrefaction was taken into account. The bio-oil from pyrolysis of the torrefied biomass contained 0.6±0.4 wt% acetic acid and 6.1±0.3 wt% water. The bio-oil was slightly enriched in levoglucosan (3.64%) and aromatics compared to raw bio-oil. The char yield was higher following torrefaction due to stable carbon-carbon crosslinks; formed by dehydration of biomass polymers during torrefaction.

Integrated acid leaching and torrefaction

Acid leached biomass was torrefied to investigate the effect of combining the pretreatments. Torrefaction of leached biomass indicated that leaching at 90 °C changed the morphology of the biomass to make it less susceptible to acetyl cleavage during torrefaction. Biomass leached with hydrochloric acid or sulfuric acid and then torrefied was prone to increased chlorine or sulfur ions in the biomass. This changed the reaction mechanism during pyrolysis to increase the acetic acid and water content in the bio-oil (for chlorine rich biomass) or the char yield (sulfur rich biomass). Therefore, leaching with organics acids was superior as no ions were incorporated into the biomass.

Bio-oil produced from acid leached and torrefied biomass had a similar oxygen content to that of raw bio-oil (40.5% (dry basis) for bio-oil produced from pyrolysis of biomass torrefied at 270 °C for 20 min; compared to 41.9% for bio-oil produced from raw biomass). Torrefaction decreased the oxygen content in raw biomass to produce a slightly oxygen depleted bio-oil; however the bio-oil's oxygen content increased to 44.2% for

pyrolysis of 1% acetic acid leached biomass. The overall effect when integrating the pretreatments was minimal change to the bio-oil's oxygen content on a dry basis but a decrease on a wet basis.

Based on the bio-oil yield and composition changes, the optimal pretreatment sequence was summarised as 1% acetic acid leaching at 30 °C for 4 h followed by torrefaction at 270 °C for 20 min. This yielded 55.4 wt% bio-oil, which equated to an overall bio-oil yield of 48.0 wt%, taking into account the mass loss during the pretreatments. The bio-oil contained 0.15±0.07 wt% acetic acid and 4.3±0.0 wt% water. Reducing the biomass's acetyl content limited organic acid formation in the early stages of pyrolysis; this reduced acid catalysed reactions, and therefore the pyrolytic lignin content in the bio-oil was lower. Inorganics in biomass promote fragmentation reactions reactions, which enhances the production of organic acids, thus, reducing the inorganic content during leaching can further reduce acid catalysed reactions during pyrolysis. The water content in the bio-oil was extremely low as less water entered the system. Also, water is thought to play an auto-catalytic role to promote the production of pyrolytic water; therefore dry biomass decreased pyrolytic water formation. Finally, less water was produced from secondary condensation or dehydration reactions due to the lower inorganic content. The high levoglucosan yield of 17.0% confirms that secondary reactions were limited to a much higher degree when both pretreatments were implemented and all three catalysts (organic acids, water, and inorganics) were reduced/removed.

Pyrolysis optimisation

Pyrolysis of biomass pretreated at the optimal acid leaching and torrefaction conditions was compared to pyrolysis of raw biomass at varying pyrolysis temperatures, cyclone temperatures, and silica sand loadings in the fluidised bed. Based on the bio-oil yields and composition, the optimal conditions for pyrolysis of raw biomass were found to be pyrolysis at 450 °C; the cyclone operating at 400 °C; and 25 g sand loading in the fluidised bed. The optimal conditions for pyrolysis of pretreated biomass were pyrolysis at 450 °C; the cyclone operating at 425 °C; and 75 g sand loading in the fluidised bed. Pyrolysis of raw biomass yielded 55.3±2.5 wt% bio-oil, 25.0±1.0 wt% char, and 12.5±1.2 wt% non-condensable gas (NCG). Pyrolysis of the pretreated biomass yielded 57.8±1.7 wt% bio-oil, 23.7±2.6 wt% char, and 11.5±0.7 wt% NCG. Pretreating the biomass significantly reduced both heterogeneous and homogeneous secondary reactions, and instead primary reactions were dominant. This was observed by the reduction in secondary products such as organic acids (2.46±0.13 to 0.16±0.05%), water (16.8±1.6 to 3.6±0.3 wt%), acetaldehyde (3.09±0.42 to 0.98±0.13%), hydroxyacetone (1.84±0.50 to 0.73±0.21%), aldehydes (1.58±0.04 to 0.50±0.10%), high molecular weight compounds (10.2±4.6 to 4.2±0.4%), char, and NCG. The bio-oil's inorganic content was reduced from 0.162±0.056 wt% for raw bio-oil to 0.091±0.030 wt% for pretreated bio-oil. Pretreated bio-oil contained less inorganics as some were removed during acid leaching and the less acidic pyrolysis vapours reduced hot corrosion of the reactor. It is recommended to implement a hot gas filter to reduce the inorganic content further in a large scale system.

The stability of raw and pretreated bio-oil was accessed by aging the samples for 25 h at 80 °C. It was found that pretreated bio-oil was more stable, as the increase in pyrolytic lignin, water, and compositional changes were less for pretreated bio-oil compared to raw bio-oil. However, it was concluded that the oxygen content in the pretreated bio-oil should be reduced to further improve its stability; it is recommended to investigate the use of calcium oxide as the fluidising medium during pyrolysis. This would remove oxygen by calcium carbonate formation instead of via dehydration reactions to produce additional water and further deplete hydrogen.

The bio-oil vapours were selectively condensed in four stages. Selective condensation would be complicated at industrial scale and high temperature condensation would be extremely prone to condenser fouling. However, the improved quality of the pretreated bio-oil is sufficient that selective condensation is not required, which allows for quench system to be implemented at industrial scale.

The NCGs produced from pyrolysis pretreated biomass were depleted in carbon dioxide but enriched in carbon monoxide, methane, hydrogen, ethylene, and ethane. The NCG heating value from pyrolysis of raw biomass was 5.7±0.5 MJm^{-3} and 8.9±1.0 MJm^{-3} from pyrolysis of pretreated biomass. Char from pretreated biomass was enriched in carbon but depleted in hydrogen and oxygen compared to char from raw biomass. The higher heating values for char from raw and pretreated biomass were 24.7±0.9 and 27.3±0.3 $MJkg^{-1}$ respectively. These values are higher than that of lignite (16.7 $MJkg^{-1}$), sub-bituminous coals (16.7-24.3 $MJkg^{-1}$), and within the range of some bituminous coals (24.3-33.5 $MJkg^{-1}$). Tests indicated that there was potential to pelletise char, which could then be sold for domestic use to replace wood pellets or for commercial use to substitute coal. The ability for char to remove inorganics from the acid leaching leachate was also investigated. Results indicated that an equilibrium was reached between adsorption of ions from the leachate and desorption from the char. It is likely that modifications to thermally or chemically activate the char would be required for efficient inorganic removal. Further research in this area is recommended.

It was experimentally shown that the liquor produced during torrefaction could be recycled for acid leaching, with the same efficiency as the synthetic 1% acetic acid leaching solution. Leaching wood chips <6 mm produced the same inorganic reduction as leaching with <2 mm particles. This indicated there were no mass transfer limitations when leaching with larger chips. This means larger wood chips can be leached and torrefied; then comminution can be implemented to significantly reduce the grinding costs. Finally, torrefaction of biomass that was leached but not subsequently rinsed to remove the remaining leaching solution indicated no rinsing step was required as any remaining organic acids volatised during torrefaction so did not alter pyrolysis.

Mass and energy balances

Mass balances were carried out for the optimised raw and pretreated systems. Mass discrepancies were 7.20±0.27 and 6.17±0.49% for pyrolysis of raw and pretreated biomass respectively. The discrepancies arose due to limitations when measuring the pyrolysis products.

Energy balances around both systems indicated the pyrolysis of raw biomass required 3.71±0.02 $MJkg^{-1}$ of energy but there was 6.63±1.11 $MJkg^{-1}$ available in the NCG and char, giving a surplus of 2.87±1.11 $MJkg^{-1}$. Therefore, 52.74% of the char generated was required to supply the systems energy. Pyrolysis of pretreated biomass required 2.57±0.01 $MJkg^{-1}$ of energy but there was 6.22±0.03 $MJkg^{-1}$ available in the NCG and char, giving a surplus of 3.65±0.03 $MJkg^{-1}$. In this case, only 53.37% of the char was required to supply the systems energy.

Economics analysis

An economic evaluation using the first approximation costing technique for raw and pretreated bio-oil production indicated that pretreated bio-oil was slightly cheaper to produce than raw bio-oil. This was due to the reduced grinding costs, redundancy of the dry stage, and a higher biomass through-put into the system for a given biomass feed rate of 30,096 $t.yr^{-1}$ (oven-dry) into the pyrolysis reactor. The system's bio-oil energy capacities from the pyrolysis reactors were 10.39 and 11.44 MW for pyrolysis of raw and pretreated biomass respectively. The raw bio-oil pyrolysis plant required a capital investment of $NZ 53,800,000 while the pretreated bio-oil plant required $NZ 46,300,000. The cost to produce raw bio-oil was $NZ 29.87 per GJ compared to $NZ 29.67 per GJ to produced pretreated bio-oil. This was competitive with price of No. 6 heavy fuel oil ($NZ 30.92 per GJ) in the second quarter of 2015, but more expensive than Brent crude oil ($NZ 13.78 per GJ) and WTI crude oil ($NZ 12.78 per GJ). This indicates there is potential to use pretreated bio-oil as a No. 6 heavy fuel oil substitute in marine operations; however it is recommended to firstly investigate the use of calcium oxide in the fluidised bed to reduce the bio-oil's oxygen content to improve its stability and energy density. A sensitivity analysis indicated that the price of both raw and pretreated bio-oil was most sensitive to the price of the biomass and least sensitive to the price of electricity.

The economic evaluation suggested the pretreatment sequence does not incur economic penalties compared to the raw sequence, but produces a higher quality bio-oil. Acid leaching is required to improve the quality of crude bio-oil as inorganics are highly catalytic during pyrolysis; however, leaching biomass is expensive. Torrefaction reduces the costs of acid leaching by providing the leaching reagent and eliminating biomass rinsing preceding leaching. Torrefaction also reduces the biomass grinding costs, which is required to offset the additional process costs associated with pretreating biomass. Pyrolysis of solely torrefied biomass is constrained by the high torrefaction temperatures required to improve the bio-oil's quality. These leads to low yields due to the mass loss during torrefaction and carbon-carbon crosslinking in biomass polymers leading to char formation during pyrolysis. Finally, inorganics become concentrated in torrefied biomass and the reduced thermal conductivity of dry torrefied biomass increases the time for inorganic catalysed reactions. Therefore, the integration of acid leaching and torrefaction is required to reduce/remove catalytic components in biomass and economically improve the crude bio-oil quality.

Appendix 3

3.1 Reactor design and experimental development

The following tables supply additional data that was used in Chapter 3 for designing the pyrolysis reactor. Reliable data on some compounds could not be found; therefore was based on similar compounds.

Table A-1: Determining constants for Nusselt's equation [8]

Reynolds no.	C	n
0.4-4	0.989	0.330
4-40	0.911	0.385
40-4000	0.683	0.466
4000-40,000	0.193	0.618
40,000-400,000	0.0266	0.805

3.1.1 Vapour properties

Table A-2: Properties of nitrogen gas [87]

Temperature K	Temperature °C	Density kgm^{-3}	Heat capacity $kJkg^{-1}K^{-1}$	Viscosity $kgm^{-1}s^{-1}$	Thermal conductivity $Wm^{-1}K^{-1}$	Prandtl no. -
273	0.15	1.25	1.04	1.29E-05	0.02	0.56
300	27	1.14	1.04	1.28E-05	0.03	0.71
400	127	0.85	1.05	2.20E-05	0.03	0.69
500	227	0.68	1.06	2.57E-05	0.04	0.68
600	327	0.57	1.08	2.91E-05	0.05	0.69
700	427	0.49	1.10	3.21E-05	0.05	0.69
800	527	0.43	1.12	3.48E-05	0.06	0.70

Table A-3: Properties of hydrogen gas [35]

Temperature K	Temperature °C	Density kgm^{-3}	Viscosity $kgm^{-1}s^{-1}$	Thermal conductivity $Wm^{-1}K^{-1}$
200	-73	0.123	6.81E-06	0.13
300	27	0.082	8.96E-06	0.18
400	127	0.061	1.09E-05	0.23
500	227	0.049	1.26E-05	0.27
600	327	0.041	1.43E-05	0.32
700	427	0.035	1.59E-05	0.35
800	527	0.040	1.74E-05	0.38

Table A-4: Properties of carbon dioxide [35]

Temperature K	Temperature °C	Density kgm^{-3}	Viscosity $kgm^{-1}s^{-1}$	Thermal conductivity $Wm^{-1}K^{-1}$
223	-50	2.401	1.13E-05	0.011
273	0	1.960	1.37E-05	0.015
373	100	1.435	1.82E-05	0.022
473	200	1.132	2.22E-05	0.03
573	300	0.934	2.59E-05	0.038
673	400	0.796	2.93E-05	0.045
773	500	0.693	2.93E-05	0.052

Table A-5: Properties of carbon monoxide [35]

Temperature K	Temperature °C	Density kgm^{-3}	Viscosity $kgm^{-1}s^{-1}$	Thermal conductivity $Wm^{-1}K^{-1}$
223	-50	1.531	1.40E-05	0.019
273	0	1.250	1.66E-05	0.023
373	100	0.915	2.11E-05	0.03
473	200	0.722	2.51E-05	0.037
573	300	0.596	2.87E-05	0.043
673	400	0.507	3.20E-05	0.049
773	500	0.442	3.52E-05	0.055

Table A-6: Properties of ethane [35]

Temperature K	Temperature °C	Density kgm^{-3}	Viscosity $kgm^{-1}s^{-1}$	Thermal conductivity $Wm^{-1}K^{-1}$
223	-50	1.641	7.15E-06	0.013
273	0	1.340	8.60E-06	0.018
373	100	0.981	1.15E-05	0.034
473	200	0.774	1.42E-05	0.047
573	300	0.639	1.66E-05	0.064
673	400	0.544	1.90E-05	0.081
873	600	0.419	2.34E-05	0.118

Table A-7: Properties of methane [35]

Temperature K	Temperature °C	Density kgm^{-3}	Viscosity $kgm^{-1}s^{-1}$	Thermal conductivity $Wm^{-1}K^{-1}$
223	-50	0.882	8.45E-06	0.024
273	0	0.720	1.02E-05	0.03
373	100	0.527	1.33E-05	0.044
473	200	0.416	1.61E-05	0.061
573	300	0.343	1.86E-05	0.079
673	400	0.292	2.07E-05	0.099
873	600	0.225	2.49E-05	0.139

Table A-8: Properties of water vapour [35]

Temperature K	Temperature °C	Density kgm^{-3}	Viscosity $kgm^{-1}s^{-1}$	Thermal conductivity $Wm^{-1}K^{-1}$	Heat capacity $kJkg^{-1}K^{-1}$
380	107	0.05863	1.27E-05	0.0246	2.06
400	127	0.5542	1.34E-05	0.0261	2.01
500	227	0.4405	1.70E-05	0.0339	1.99
600	327	0.3652	2.07E-05	0.0422	2.03
700	427	0.314	2.43E-05	0.0505	2.09
800	527	0.2739	2.79E-05	0.0592	2.15

Table A-9: Properties of acetic acid vapour [35]

Temperature K	Temperature °C	Density kgm^{-3}	Viscosity $kgm^{-1}s^{-1}$	Thermal conductivity $Wm^{-1}K^{-1}$
273	0	2.680		0.0087
392	119	1.936		0.0076
473	200	1.548	1.35E-05	0.0260
573	300	1.278	1.66E-05	0.0370
673	400	1.088	1.98E-05	0.0490
873	600	0.839	2.63E-05	0.0740

Table A-10: Properties of phenol vapour [35]

Temperature K	Temperature °C	Density kgm^{-3}	Viscosity $kgm^{-1}s^{-1}$	Thermal conductivity $Wm^{-1}K^{-1}$
	0	4.200		
473	200	2.425	1.17E-05	0.0250
573	300	2.002	1.43E-05	0.0350
673	400	1.705	1.67E-05	0.0450
873	600	1.314	2.13E-04	0.0650

Table A-11: Properties of syringol, levoglucosan and isoeugenol vapour (used m-cresol) [35]

Temperature K	Temperature °C	Density kgm^{-3}	Viscosity $kgm^{-1}s^{-1}$	Thermal conductivity $Wm^{-1}K^{-1}$
	0	4.830		
573	300	2.302	1.25E-05	0.0330
673	400	1.960	1.47E-05	0.0420
873	600	1.511	1.88E-05	0.0610

Table A-12: Properties of furfural vapour [35]

Temperature K	Temperature °C	Density kgm^{-3}	Viscosity $kgm^{-1}s^{-1}$	Thermal conductivity $Wm^{-1}K^{-1}$
273	0	4.290		0.0050
360	87	3.477		0.0120
473	200	2.477	1.20E-05	0.0230
573	300	2.045	1.46E-05	0.0320
673	400	1.741	1.70E-05	0.0400
873	600	1.342	2.16E-05	0.0570

Table A-13: Properties of hydroxypropanone vapour (used proponic acid) [35]

Temperature K	Temperature °C	Density kgm^{-3}	Viscosity $kgm^{-1}s^{-1}$	Thermal conductivity $Wm^{-1}K^{-1}$
273	0	3.310		0.0046
473	200	1.911	1.22E-05	0.0260
573	300	1.578	1.48E-05	0.0360
673	400	1.343	1.72E-05	0.0460
873	600	1.036	2.17E-05	0.0670

Table A-14: Properties of hydroxyacetaldehyde vapour (used formic acid) [35]

Temperature K	Temperature °C	Density kgm^{-3}	Viscosity $kgm^{-1}s^{-1}$	Thermal conductivity $Wm^{-1}K^{-1}$
273	0	2.050		
473	200	1.184	1.53E-05	0.0270
573	300	0.977	1.84E-05	0.0360
673	400	0.832	2.15E-05	0.0450
873	600	0.641	2.69E-05	0.0620

3.1.2 Liquid properties

Table A-15: Properties of water [35]

Temperature K	Temperature °C	Density kgm^{-3}	Viscosity $kgm^{-1}s^{-1}$	Thermal conductivity $Wm^{-1}K^{-1}$
273	0	999.82	0.001792	0.569
293	20	998.29	0.001003	0.606
313	40	992.25	0.000653	0.634
333	60	983.13	0.000467	0.655
353	80	971.6	0.000355	0.671
373	100	958.05	0.000282	0.680

Table A-16: Properties of acetic acid [35]

Temperature K	Temperature °C	Density kgm^{-3}	Viscosity $kgm^{-1}s^{-1}$	Thermal conductivity $Wm^{-1}K^{-1}$
293	20	1049	1.21E-03	0.161
323	50	1018	7.92E-04	0.155
373	100	960	4.58E-04	0.142

Table A-17: Properties of phenol [35]

Temperature K	Temperature °C	Density kgm^{-3}	Viscosity $kgm^{-1}s^{-1}$	Thermal conductivity $Wm^{-1}K^{-1}$
323	50	1050	3.42E-03	0.156
373	100	973	1.05E-03	0.135
423	150	931	6.70E-04	0.130

Table A-18: Properties of syringol, levoglucosan and isoeugenol (used m-cresol) [35]

Temperature K	Temperature °C	Density kgm^{-3}	Viscosity $kgm^{-1}s^{-1}$	Thermal conductivity $Wm^{-1}K^{-1}$
293	20	1034	1.69E-02	0.150
323	50	1009	4.20E-03	0.148
373	100	973	1.20E-03	0.143
423	150	930	5.74E-04	0.135
473	200	882	3.47E-04	0.130

Table A-19: Properties of furfural [35]

Temperature K	Temperature °C	Density kgm^{-3}	Viscosity $kgm^{-1}s^{-1}$	Thermal conductivity $Wm^{-1}K^{-1}$
248	-25	1201	4.10E-03	0.184
273	0	1181	2.48E-03	0.178
323	50	1128	1.20E-03	0.167
373	100	1077	6.40E-04	0.155
423	150	1020	3.80E-04	0.142

Table A-20: Properties of hydroxypropanone (used proponic acid) [35]

Temperature K	Temperature °C	Density kgm^{-3}	Viscosity $kgm^{-1}s^{-1}$	Thermal conductivity $Wm^{-1}K^{-1}$
273	0	1015	1.54E-03	0.015
302	29	993	1.69E-03	0.150
323	50	963	7.38E-04	0.144
373	100	911	4.50E-04	0.136

Table A-21: Properties of hydroxyacetaldehyde (used formic acid) [35]

Temperature K	Temperature °C	Density kgm^{-3}	Viscosity $kgm^{-1}s^{-1}$	Thermal conductivity $Wm^{-1}K^{-1}$
293	20	1220	1.79E-03	0.261
323	50	1184	1.03E-03	0.250
373	100	1108	5.42E-04	0.232
293	20	1220	1.79E-03	0.261

3.2 Calculating the heat capacity of compounds from group contributions

3.2.1 Non-condensable gases

Heat capacity for varying temperatures was determined assuming an ideal gas and water and using the equation from Smith *et al.* [88]:

$$Cp = (A + B \times E^{-3} \times T + C \times E^{-6} \times T^2 + D \times E^5 \times T^{-2}) \times \text{Gas constant}$$

Table A-22: Determining the heat capacity of for the NCGs and water [88]

Gas constant ($JK^{-1}mol^{-1}$)	8.3144					
Temperature (K)	573					
Gas	**Constants**				**Heat capacity ($Jmol^{-1}K^{-1}$)**	**Heat capacity ($kJkg^{-1}K^{-1}$)**
	A	**B**	**C**	**D**		
Hydrogen	3.246	0.422		0.083	29.21	14.49
Methane	1.702	9.081	-2.164		51.51	3.21
Carbon dioxide	3.376	0.557		-0.031	30.64	1.09
Carbon monoxide	5.457	1.045		-1.157	47.42	1.08
Ethane	1.131	19.225	-5.561		85.81	2.85
Water	4.038	3.47		0.121	6.06	2.95

3.2.2 Other vapours

The heat capacity for the condensable bio-oil compounds (excluding water) was calculated from the contributing chemical groups and calculated using the equation from Rihani and Doraiswamy [89].

$$Cp = \sum A + \sum B \times E^{-2} \times T + \sum C \times E^{-4} \times T^2 + \sum D \times E^{-6} \times T^3$$

Table A-23: Calculating the heat capacity of compounds in bio-oil [89]

Phenol					
Chemical bonds	**Amount**	**A × Amount**	**B × Amount**	**C × Amount**	**D × Amount**
HC ring	5	-7.286	9.5735	-0.6165	0.014925
C ring	1	-1.3883	1.5159	-0.1069	0.002659
OH	1	6.5128	-0.1347	0.0414	-0.001623
Sum		-2.1615	10.9547	-0.682	0.015961
Heat capacity at 573 K	41.22	$calg^{-1}mol^{-1}K^{-1}$			
Heat capacity at 573 K	1.83	$kJkg^{-1}K^{-1}$			
Syringol					
Chemical bonds	**Amount**	**A × Amount**	**B × Amount**	**C × Amount**	**D × Amount**
HC ring	3	-4.3716	5.7441	-0.3699	0.008955
C ring	3	-4.1649	4.5477	-0.3207	0.007977
OH	1	6.5128	-0.1347	0.0414	-0.001623
O	2	5.6922	-0.02	0.0908	-0.005456
CH3	2	1.2174	4.2866	-0.1704	0.00227
Sum		4.8859	14.4237	-0.7288	0.012123
Heat capacity at 573 K	65.89	$calg^{-1}mol^{-1}K^{-1}$			
Heat capacity at 573 K	1.79	$kJkg^{-1}K^{-1}$			

Hydroxyacetaldehyde					
Chemical bonds	**Amount**	**A × Amount**	**B × Amount**	**C × Amount**	**D × Amount**
OH	1	6.5128	-0.1347	0.0414	-0.001623
CH2	1	0.3945	2.1363	-0.1197	0.002596
CH=O	1	1.4055	0.9437	0.0614	-0.006978
Sum		8.3128	2.9453	-0.0169	-0.006005
Heat capacity at 573 K	23.5	$calg^{-1}mol^{-1}K^{-1}$			
Heat capacity at 573 K	1.64	$kJkg^{-1}K^{-1}$			
Hydroxypropanone					
Chemical bonds	**Amount**	**A × Amount**	**B × Amount**	**C × Amount**	**D × Amount**
CH2	1	0.3945	2.1363	-0.1197	0.002596
OH	1	6.5128	-0.1347	0.0414	-0.001623
C=O	1	1.0016	2.0763	-0.1636	0.004494
CH3	1	0.6087	2.1433	-0.0852	0.001135
Sum		8.5176	6.2212	-0.3271	0.006602
Heat capacity at 573 K	34.67	$calg^{-1}mol^{-1}K^{-1}$			
Heat capacity at 573 K	1.96	$kJkg^{-1}K^{-1}$			
Acetic acid					
Chemical bonds	**Amount**	**A × Amount**	**B × Amount**	**C × Amount**	**D × Amount**
CH3	1	0.6087	2.1433	-0.0852	0.001135
OH-C=O	1	1.4055	3.4632	-0.2557	0.006886
Sum		2.0142	5.6065	-0.3409	0.008021
Heat capacity at 573 K	24.46	$calg^{-1}mol^{-1}K^{-1}$			
Heat capacity at 573 K	1.70	$kJkg^{-1}K^{-1}$			
2-Furanone (for furfural)					
Chemical bonds	**Amount**	**A × Amount**	**B × Amount**	**C × Amount**	**D × Amount**
C ring	1	-1.3883	1.5159	-0.1069	0.002659
HC ring	3	-4.3716	5.7441	-0.3699	0.008955
O ring	1	-3.7344	1.3727	-0.1265	0.003789
O	1	2.8461	-0.01	0.0454	-0.002728
Sum		-6.6482	8.6227	-0.5579	0.012675
Heat capacity at 573 K	26.83	$calg^{-1}mol^{-1}K^{-1}$			
Heat capacity at 573 K	1.34	$kJkg^{-1}K^{-1}$			
Isoeugenol					
Chemical bonds	**Amount**	**A × Amount**	**B × Amount**	**C × Amount**	**D × Amount**
HC ring	3	-4.3716	5.7441	-0.3699	0.008955
C ring	3	-4.1649	4.5477	-0.3207	0.007977
OH	1	6.5128	-0.1347	0.0414	-0.001623
O	1	2.8461	-0.01	0.0454	-0.002728
CH3	2	1.2174	4.2866	-0.1704	0.00227
CH=CH	1	0.9377	2.9904	-0.1749	0.003918
Sum		2.9775	17.4241	-0.9491	0.018769
Heat capacity at 573 K	75.19	$calg^{-1}mol^{-1}K^{-1}$			
Heat capacity at 573 K	1.92	$kJkg^{-1}K^{-1}$			
Levoglucosan					
Chemical bonds	**Amount**	**A × Amount**	**B × Amount**	**C × Amount**	**D × Amount**
C ring	5	-6.9415	7.5795	-0.5345	0.013295
O ring	1	-3.7344	1.3727	-0.1265	0.003789
OH	3	6.5128	-0.1347	0.0414	-0.001623
O	1	2.8461	-0.01	0.0454	-0.002728
Sum		-1.317	8.8075	-0.5742	0.012733
Heat capacity at 573 K	32.69	$calg^{-1}mol^{-1}K^{-1}$			
Heat capacity at 573 K	0.84	$kJkg^{-1}K^{-1}$			

3.3 Determining the condenser lengths

Table A-24 below, provides the full calculations for determining the three condenser lengths for selective condensation of pyrolysis vapours.

Table A-24: Determining the condensers lengths

Determining the condenser lengths						
Constants	**Sym.**	**Units**	**Equation**	**Value**		
Bio-oil yield	Y_{oil}	wt%	*System input*	70		
NCG yield	Y_{NCG}	wt%	*System input*	15		
Biomass feed rate	$\dot{m}_{bio}$	kgs^{-1}	*System input*	0.000278		
Mass flow of NCG	$\dot{m}_{NCG}$	kgs^{-1}	$\dot{m}_{NCG} = \dot{m}_{bio} \times Y_{NCG}$	0.000042		
Mass flow rate of N_2	$\dot{m}_{N2}$	kgs^{-1}	*Set in fluidisation*	0.00044		
Mass flow of bio-oil	$\dot{m}_{oil}$	kgs^{-1}	$\dot{m}_{oil} = \dot{m}_{bio} \times Y_{oil}$	0.000195		
Dimensions of condensers tubes						
Inner tube OD	OD_{in}	m	*3/8" tubing*	0.00953		
Inner tube wall thickness	W_{in}	m	-	0.0012		
Inner tube ID	ID_{in}	m	$ID_{in}=OD_{in}-2\times W_{in}$	0.00713		
Outer tube OD	OD_{out}	m	*3/4" tubing*	0.0191		
Outer tube wall thickness	W_{out}	m	-	0.0015		
Outer tube ID	ID_{out}	m	$ID_{out}=OD_{out}-2\times W_{out}$	0.0161		
Variables	**Sym.**	**Units**	**Equation**	**Cond. 1**	**Cond. 2**	**Cond. 3**
Vapour flow into cond.	$\dot{m}_{in-c}$	kgs^{-1}	*Cond. 1 from* ***Error! Reference source not found.****. Cond. 2 and 3 from* $\dot{m}_{out-c}$ *of preceding cond.*	0.00068	0.00064	0.00055
Percent of NCG in vapour	M_{NCG}	%	$M_{NCG} = \frac{\dot{m}_{NCG}}{\dot{m}_{in-c}}$	6.2	6.6	7.6
Percent of N_2 in vapour	M_{N2}	%	$M_{N2} = \frac{\dot{m}_{N2}}{\dot{m}_{in-c}}$	65.1	69.2	80
Percent of bio-oil in vapour	M_{oil}	%	$M_{oil} = 100\% - M_{N2} - M_{NCG}$	29	24	12
Inlet vapour temp.	T_{in-c}	°C	*Cond. 1 from* ***Error! Reference source not found.****. Cond. 2 and 3 from* T_{out-c} *of preceding cond.*	400	200	120
Outlet vapour temp.	T_{out-c}	°C	*System input*	200	120	40
Film temp.	T_{f-c}	°C	$T_{f-c} = \frac{T_{in-c} + T_{out-c}}{2}$	300	170	80

Heat required to cool vapours over condensers 1					
Variables	**Sym.**	**Units**	**Equation**	**Bio-oil vapours**	**NCG**

				Water	Hy. ace.	Ace. acid	Hy. Prop.	Levo.	Furf.	Iso.	Phen.	Syrin.	H_2	CH_4	CO	CO_2	C_2H_6	N_2
Comp. fraction in stream	F_c	%	*From Table 0-25*	25.0	28.2	7.2	15.7	12.1	3.0	2.1	0.1	6.5	2.4	8.2	38.1	49.4	2.0	-
Boiling point	bp	°C	*System input*	100	132	118.5	145.5	384	86.7	266	181.7	261	-	-	-	-	-	-
Molecular weight	MW	$gmol^{-1}$	*System input*	18.0	60.1	60.1	74.1	162.0	84.1	164.2	94.1	154.2	2.0	16.0	28.0	44.0	30.1	14.0
Heat of vap.	h_v	Jkg^{-1}	*System input [36]*	$2.3E^6$	$7.2E^5$	$3.9E^5$	$6.0E^5$	$4.5E^5$	$5.2E^5$	$3.2E^5$	$4.6E^5$	$3.4E^5$	-	-	-	-	-	-
Comp. flow in	$\dot{m}_{in-c1}$	kgs^{-1}	$\dot{m}_{in-c1} = IF(bp < T_{in-c}, \dot{m}_{oil} \times F_c, 0)$ OR $\dot{m}_{in-c1} = \dot{m}_{NCG} \times F_c$	$4.9E^{-5}$	$5.5E^{-5}$	$1.4E^{-5}$	$3.1E^{-5}$	$2.4E^{-5}$	$5.9E^{-6}$	$4.0E^{-6}$	$2.6E^{-7}$	$1.3E^{-5}$	$1.0E^{-6}$	$3.4E^{-6}$	$1.6E^{-5}$	$2.1E^{-5}$	$8.2E^{-7}$	$4.4E^{-4}$
Comp. flow out	$\dot{m}_{out-c1}$	kgs^{-1}	$\dot{m}_{out-c1} = IF(bp < T_{out-c}, \dot{m}_{oil} \times F_c, 0)$ OR $\dot{m}_{out-c1} = \dot{m}_{NCG} \times F_c$	$4.9E^{-5}$	$5.5E^{-5}$	$1.4E^{-5}$	$3.1E^{-5}$	0	$5.9E^{-6}$	0	$2.6E^{-7}$	0	$1.0E^{-6}$	$3.4E^{-6}$	$1.6E^{-5}$	$2.1E^{-5}$	$8.2E^{-7}$	$4.4E^{-4}$
Fraction of conden.	F_{con}	%	$F_{con} = \frac{(\dot{m}_{in-c1} - \dot{m}_{out-c1})}{\dot{m}_{con}}$	0	0	0	0	58.6	0	9.9	0	31.5	-	-	-	-	-	-
Comp. heat capacity at T_{f-c}	Cp_{c1}	$Jkg^{-1}K^{-1}$	*Value lookup at* T_{f-c}	2798	1638	1704	1958	844	1335	1916	1833	1788	14489	3210	1094	1077	2854	1056
Heat required	q_{c1}	W	$q_{c1} = \dot{m}_{in-c1}(Cp_{c1}(T_{in-c} - T_{out-c}) + IF(\dot{m}_{out-c1} = 0, h_v, 0)$	27.2	18.0	4.8	12.0	14.6	1.6	2.8	0.1	8.8	2.9	2.2	3.5	4.4	0.5	92.9
Heat required to cool vapours over condensers 2																		
Comp. flow in	$\dot{m}_{in-c2}$	kgs^{-1}	$\dot{m}_{in-c2} = \dot{m}_{out-c1}$	$4.9E^{-5}$	$5.5E^{-5}$	$1.4E^{-5}$	$3.1E^{-5}$	0	$5.9E^{-6}$	0	$2.6E^{-7}$	0	$1.0E^{-6}$	$3.4E^{-6}$	$1.6E^{-5}$	$2.1E^{-5}$	$8.2E^{-7}$	$4.4E^{-4}$
Comp. flow out	$\dot{m}_{out-c2}$	kgs^{-1}	$\dot{m}_{out-c2} = IF(bp < T_{out-c}, \dot{m}_{oil} \times F_c, 0)$ OR $\dot{m}_{out-c2} = \dot{m}_{NCG} \times F_c$	$4.9E^{-5}$	0	$1.4E^{-5}$	0	0	$5.9E^{-6}$	0	0	0	$1.0E^{-6}$	$3.4E^{-6}$	$1.6E^{-5}$	$2.1E^{-5}$	$8.2E^{-7}$	$4.4E^{-4}$
Fraction of conden.	F_{con}	%	$F_{con} = \frac{(\dot{m}_{in-c2} - \dot{m}_{out-c2})}{\dot{m}_{out}}$	0	64.1	0	0	35.6	0	0	0.3	0	-	-	-	-	-	-
Comp. heat capacity at T_{f-c}	Cp_{c2}	$Jkg^{-1}K^{-1}$	*Value lookup at* T_{f-c}	2601	1429	1453	1708	711	1080	1610	1528	1507	14333	2747	1071	1007	2366	1046
Heat required	q_{c2}	W	$q_{c2} = \dot{m}_{in-c2}(Cp_{c2}(T_{in-c} - T_{out-c}) + IF(\dot{m}_{out-c2} = 0, h_v, 0)$	12.7	47.2	2.0	23.6	0	0.6	0	0.2	0	1.4	0.9	1.7	2.1	0.2	46.0
Heat required to cool vapours over condensers 3																		
Comp. flow in	$\dot{m}_{in-c3}$	kgs^{-1}	$\dot{m}_{in-c3} = \dot{m}_{out-c2}$	$4.9E^{-5}$	0	$1.4E^{-5}$	0	0	$5.9E^{-6}$	0	0	0	$1.0E^{-6}$	$3.4E^{-6}$	$1.6E^{-5}$	$2.1E^{-5}$	$8.2E^{-7}$	$4.4E^{-4}$
Comp. flow out	$\dot{m}_{out-c3}$	kgs^{-1}	$\dot{m}_{out-c3} = IF(bp < T_{out-c}, \dot{m}_{oil} \times F_c, 0)$ OR $\dot{m}_{out-c3} = \dot{m}_{NCG} \times F_c$	0	0	0	0	0	0	0	0	0	$1.0E^{-6}$	$3.4E^{-6}$	$1.6E^{-5}$	$2.1E^{-5}$	$8.2E^{-7}$	$4.4E^{-4}$
Fraction of conden.	F_{con}	%	$F_{con} = \frac{(\dot{m}_{in-c3} - \dot{m}_{out-c3})}{\dot{m}_{out}}$	70.9	0	20.4	0	0	8.6	0	0	0	-	-	-	-	-	-
Comp. heat capacity at T_{f-c}	Cp_{c3}	$Jkg^{-1}K^{-1}$	*Value lookup at* T_{f-c}	2473	1270	1248	1508	599	866	1363	1277	1282	14276	2404	1053	925	1998	1041
Heat required[1]	q_{c3}	W	$q_{c3} = \dot{m}_{in-c3}(Cp_{c1}(T_{in-c} - T_{out-c}) + IF(\dot{m}_{out-c3} = 0, h_v, 0)$	119.4	0	6.9	0	0	3.5	0	0	0	1.1	0.7	1.3	1.5	0.1	36.6
Determining the heat transfer coefficient for water[2]																		
Constants	**Sym.**	**Units**	**Equation**	**Value**														

Ave. temp. water	T_{in-w}	°C	*System input*	20		
Heat capacity of water at T_{in-w}	Cp_{in-w}	$Jkg^{-1}K^{-1}$	*Value lookup at* T_{in-w}	4182		
Cross section area cond. for water	A_w	m^2	$A_w = \frac{\pi ID_{out}^2}{4} - \frac{\pi OD_{in}^2}{4}$	$1.31E^{-4}$		
Hydraulic dia.	D_h	m	$D_h = \frac{(ID_{out}^2 - OD_{in}^2)}{OD_{in}}$	0.0175		
Variables	**Sym.**	**Units**	**Equation**	**Cond. 1**	**Cond. 2**	**Cond. 3**
Total heat req. to cool stream	q_{tot-c}	W	$q_{tot-c} = \sum q_{co}\ comp.$	**196.3**	**138.6**	**171.3**
SS thermal conductivity	k_{ss}	$Wm^{-1}K^{-1}$	*Value lookup at* T_{f-c}	18.9	17.21	16.04
Flow of water	$\dot{m}_w$	kgs^{-1} ($Lmin^{-1}$)	*Set based on cond. Length desired*	0.00835 (0.5)	0.00835 (0.5)	0.0330 (2.0)
Temp. water out of cond.	T_{out-w}	°C	$T_{out-w} = \frac{q_{tot-c}}{\dot{m}_w Cp_{in-w}} + T_{in-w}$	25.6	24.0	21.2
Film temp. water	T_{f-w}	°C	$T_{f-w} = \frac{T_{in-w} + T_{out-w}}{2}$	22.8	22.0	20.6
Density of water	ρ_w	kgm^{-3}	*Value lookup at* T_{f-w}	998	998	998
Viscosity of water	μ_w	$kgm^{-1}s^{-1}$	*Value lookup at* T_{f-w}	0.010	0.010	0.010
Water thermal conductivity	k_w	$Wm^{-1}K^{-1}$	*Value lookup at* T_{f-w}	0.61	0.61	0.61
Superficial water velocity	v_{s-w}	$m.s^{-1}$	$v_{s-w} = \frac{\dot{m}_w}{\rho_w A_w}$	0.064	0.064	0.252
Reynolds no.	Re_w	-	$Re_w = \frac{\rho_w v_{s-w} D_h}{\mu_w}$	1113	1113	4398
Prandtl no.	Pr_w	-	$Pr_w = \frac{Cp_{in-w}\mu_w}{k_w}$	6.9	6.9	6.9
Nusselt no.	Nu_w	-	$Nu_w = 3.66 + \frac{0.0668 Re_w Pr_w (D_h/L_c)}{1 + 0.04(Re_w Pr_w (D_h/L_c))^{2/3}}$	20.7	18.4	*20.2 - Nu all for laminar flow as* Re_w*>10,000*
Heat transfer coff.	h_w	$Wm^{-2}K^{-1}$	$h_w = \frac{Nu_w k_w}{D_h}$	714.5	636.8	697.4

Calculating the condenser length[3]

Constants	**Sym.**	**Units**	**Equation**	**Value**
Angle of the condensers	θ	°	*System input*	20 - *Compared to the horizon*
Gravity	g'	$m.s^{-2}$	$\theta' = 9.81 \sin\theta$	8.96 - *correction for inclined condensers*

Heat transfer coefficient of the remaining vapours over condenser 1

Variables	**Sym.**	**Units**	**Equation**	**Bio-oil vapours**	**NCG**

				Water	Hy. ace.	Ace. acid	Hy. Prop.	Levo.	Furf.	Iso.	Phen.	Syrin.	H_2	CH_4	CO	CO_2	C_2H_6	N_2
Vapour density	ρ_{vap}	kgm^{-3}	*Value lookup at* T_{f-c}	0.93	0.98	1.28	1.58	2.30	2.05	2.30	2.00	2.30	0.05	0.34	0.60	0.93	0.64	0.68
Vapour viscosity	μ_{vap}	$kgm^{-1}s^{-1}$	*Value lookup at* T_{f-c}	$2.9E^{-5}$	$2.2E^{-5}$	$2.0E^{-5}$	$1.7E^{-5}$	$1.5E^{-5}$	$1.7E^{-5}$	$1.5E^{-5}$	$1.7E^{-5}$	$1.5E^{-5}$	$1.4E^{-5}$	$2.1E^{-5}$	$3.2E^{-5}$	$2.9E^{-5}$	$1.9E^{-5}$	$2.9E^{-5}$
Vapour thermal conductivity	k_{vap}	$Wm^{-1}K^{-1}$	*Value lookup at* T_{f-c}	0.038	0.036	0.037	0.036	0.033	0.032	0.033	0.035	0.033	0.272	0.079	0.043	0.038	0.064	0.040
Superficial vapour velocity	$v_{s\text{-}vap}$	$m.s^{-1}$	$v_{s-vap} = \frac{4\dot{m}_{out-c1}}{\rho_{vap}\pi ID_{in}^2}$	1.31	1.41	0.28	0.49	0	0.07	0	0.003	0	0.51	0.25	0.67	0.55	0.03	16.17
Reynolds no.	Re_{vap}	-	$Re_{vap} = \frac{\rho_{vap} v_{s-vap} ID_{in}}{\mu_{vap}}$	296.8	456.7	126.5	317.5	0	62.2	0.0	2.8	0	12.5	29.5	88.7	125.6	7.7	2701
Prandtl no.	Pr_{vap}	-	$Pr_{vap} = \frac{Cp_{c1}\mu_{vap}}{k_{vap}}$	1.53	0.98	0.91	0.94	0.38	0.71	0.85	0.87	0.80	0.76	0.84	0.81	0.83	0.85	0.68
Nusselt no.	Nu_{vap}	-	$Nu_{vap} = 3.66 + \frac{0.0668 Re_{vap} Pr_{vap} (ID_{in}/L_c)}{1+0.04\left(Re_{vap} Pr_{vap} (ID_{in}/L_c)\right)^{2/3}}$ *if* $Re_{vap-c1} < 2300$, *else* $Nu_{vap} = 0.023 Re_{vap}^{0.8} Pr_{vap}^{0.4}$	5.52	5.49	4.24	4.98	3.66	3.90	3.66	3.67	3.66	3.72	3.80	4.04	4.19	3.70	10.99
Vapour heat transfer coff.	h_{vap}	$Wm^{-2}K^{-1}$	$h_{vap} = \frac{Nu_{vap} k_{wvap}}{ID_{in}}$	29.4	27.7	22.0	25.2	0	17.5	0	18.1	0	141.8	42.1	24.4	22.4	33.2	61.4
Heat transfer coefficient of the condensing compounds for condenser 1																		
Overall film temp.	T_{f-o}	°C	$T_{f-o} = \frac{(T_{f-c} + T_{f-w})}{2}$	161.4	161.4	161.4	161.4	161.4	161.4	161.4	161.4	161.4	-	-	-	-	-	-
Conden. density	ρ_{con}	kgm^{-3}	*Value lookup at* T_{f-o}	958.1	1108.0	960.0	911.0	930.0	1020.0	930.0	931.0	930.0	-	-	-	-	-	-
Conden. viscosity	μ_{con}	$kgm^{-1}s^{-1}$	*Value lookup at* T_{f-o}	$2.8E^{-4}$	$5.4E^{-4}$	$4.6E^{-4}$	$4.5E^{-4}$	$5.7E^{-4}$	$3.8E^{-4}$	$5.7E^{-4}$	$6.7E^{-4}$	$5.7E^{-4}$	-	-	-	-	-	-
Conden. thermal conductivity	k_{con}	$Wm^{-1}K^{-1}$	*Value lookup at* T_{f-o}	0.680	0.232	0.142	0.136	0.135	0.142	0.135	0.130	0.135	-	-	-	-	-	-
Condensate heat transfer coff.	h_{con}	$Wm^{-2}K^{-1}$	$h_{con} = 0.555\left(\frac{\rho_{con}^2 g' k_{con}^3 (h_v + 0.68 Cp_c (bp - T_{out-c}))}{\mu_{con} ID_{in} (bp - T_{f-0})}\right)^{1/4} F_{con} M_{oil}$	-	-	-	-	173.0	-	32.8	0.0	105.4	-	-	-	-	-	-
Heat transfer coefficient of the remaining vapours over condenser 2																		
Variables	Sym.	Units	Equation	**Bio-oil vapours**									**NCG**					
				Water	Hy. ace.	Ace. acid	Hy. Prop.	Levo.	Furf.	Iso.	Phen.	Syrin.	H_2	CH_4	CO	CO_2	C_2H_6	N_2
Vapour density	ρ_{vap}	kgm^{-3}	*Value lookup at* T_{f-c}	1.44	-	1.94	-	-	3.48	-	-	-	0.06	0.53	0.92	1.44	0.98	0.85
Vapour viscosity	μ_{vap}	$kgm^{-1}s^{-1}$	*Value lookup at* T_{f-c}	$2.2E^{-5}$	-	$1.4E^{-5}$	-	-	$1.2E^{-5}$	-	-	-	$1.1E^{-5}$	$1.6E^{-5}$	$2.5E^{-5}$	$2.2E^{-5}$	$1.4E^{-5}$	$2.2E^{-5}$
Vapour thermal conductivity	k_{vap}	$Wm^{-1}K^{-1}$	*Value lookup at* T_{f-c}	0.022	-	0.008	-	-	0.012	-	-	-	0.228	0.044	0.030	0.022	0.034	0.033
Superficial vapour velocity	$v_{s\text{-}vap}$	$m.s^{-1}$	$v_{s-vap} = \frac{4\dot{m}_{out-c1}}{\rho_{vap}\pi ID_{in}^2}$	0.85	-	0.182	-	-	0.043	-	-	-	0.41	0.16	0.44	0.36	0.02	12.92
Reynolds no.	Re_{vap}	-	$Re_{vap} = \frac{\rho_{vap} v_{s-vap} ID_{in}}{\mu_{vap}}$	391.7	-	185.6	-	-	88.2	-	-	-	16.4	37.9	113.1	165.7	10.3	3576.7

Prandtl no.	Pr_{vap}	-	$Pr_{vap} = \frac{Cp_{c1}\mu_{vap}}{k_{vap}}$		2.03	-	2.60	-	-	1.08	-	-	-	0.68	1.01	0.90	1.02	0.99	0.69
Nusselt no.	Nu_{vap}	-	$Nu_{vap} = 3.66 + \frac{0.0668\,Re_{vap}Pr_{vap}(ID_{in}/L_c)}{1+0.04\left(Re_{vap}Pr_{vap}(ID_{in}/L_c)\right)^{2/3}}$ *if*	$Re_{vap-c1} <$ 2300, *else* $Nu_{vap} = 0.023Re_{vap}^{0.8}Pr_{vap}^{0.4}$	5.90	-	5.17	-	-	4.03	-	-	-	3.7	3.8	4.0	4.3	3.7	13.8
Vapour heat transfer coff.	h_{vap}	$Wm^{-2}K^{-1}$	$h_{vap} = \frac{Nu_{vap}k_{wvap}}{ID_{in}}$		18.2	-	5.5	-	-	6.8	-	-	-	118.6	23.6	17.0	13.2	17.7	64.7
Heat transfer coefficient of the condensing compounds for condenser 2																		
Overall film temp.	T_{f-o}	°C	$T_{f-o} = \frac{(T_{f-c} + T_{f-w})}{2}$		96.0	96.0	96.0	96.0	96.0	96.0	96.0	96.0	96.0	-	-	-	-	-	-
Conden. density	ρ_{con}	kgm^{-3}	*Value lookup at* T_{f-o}		971.6	1184.0	1018.0	963.0	1009.0	1128.0	1009.0	1050.0	1009.0	-	-	-	-	-	-
Conden. viscosity	μ_{con}	$kgm^{-1}s^{-1}$	*Value lookup at* T_{f-o}		$3.6E^{-4}$	$1.0E^{-3}$	$7.9E^{-4}$	$7.4E^{-4}$	$4.2E^{-3}$	$1.2E^{-3}$	$4.2E^{-3}$	$3.4E^{-3}$	$4.2E^{-3}$	-	-	-	-	-	-
Conden. thermal conductivity	k_{con}	$Wm^{-1}K^{-1}$	*Value lookup at* T_{f-o}		0.671	0.25	0.155	0.144	0.148	0.167	0.148	0.156	0.148		-	-	-	-	-
Condensate heat transfer coff.	h_{con}	$Wm^{-2}K^{-1}$	$h_{con} = 0.555\left(\frac{\rho_{con}^2 g' k_{con}^3 (h_v + 0.68\,Cp_c(bp - T_{out-c}))}{\mu_{con} ID_{in}(bp - T_{f-0})}\right)^{1/4} F_{con}$	M_{oil}	-	415.9	-	133.7	-	-	-	0.7	105.4	-	-	-	-	-	-
Heat transfer coefficient of the remaining vapours over condenser 3																		
Variables	**Sym.**	**Units**	**Equation**		**Bio-oil vapours**									**NCG**					
					Water	Hy. ace.	Ace. acid	Hy. Prop.	Levo.	Furf.	Iso.	Phen.	Syrin.	H_2	CH_4	CO	CO_2	C_2H_6	N_2
Vapour density	ρ_{vap}	kgm^{-3}	*Value lookup at* T_{f-c}		-	-	-	-	-	-	-	-	-	0.08	0.72	1.25	1.96	1.34	1.14
Vapour viscosity	μ_{vap}	$kgm^{-1}s^{-1}$	*Value lookup at* T_{f-c}		-	-	-	-	-	-	-	-	-	$0.9E^{-5}$	$1.3E^{-5}$	$2.1E^{-5}$	$1.8E^{-5}$	$1.2E^{-5}$	$1.3E^{-5}$
Vapour thermal conductivity	k_{vap}	$Wm^{-1}K^{-1}$	*Value lookup at* T_{f-c}		-	-	-	-	-	-	-	-	-	0.182	0.030	0.023	0.015	0.018	0.026
Superficial vapour velocity	v_{s-vap}	$m.s^{-1}$	$v_{s-vap} = \frac{4\dot{m}_{out-c1}}{\rho_{vap}\pi ID_{in}^2}$		-	-	-	-	-	-	-	-	-	0.31	0.12	0.32	0.26	0.02	9.66
Reynolds no.	Re_{vap}	-	$Re_{vap} = \frac{\rho_{vap} v_{s-vap} ID_{in}}{\mu_{vap}}$		-	-	-	-	-	-	-	-	-	19.9	45.8	134.6	202.2	12.7	6123
Prandtl no.	Pr_{vap}	-	$Pr_{vap} = \frac{Cp_{c1}\mu_{vap}}{k_{vap}}$		-	-	-	-	-	-	-	-	-	0.70	1.07	0.97	1.12	1.28	0.71
Nusselt no.	Nu_{vap}	-	$Nu_{vap} = 3.66 + \frac{0.0668\,Re_{vap}Pr_{vap}(ID_{in}/L_c)}{1+0.04\left(Re_{vap}Pr_{vap}(ID_{in}/L_c)\right)^{2/3}}$ *if*	$Re_{vap-c1} <$ 2300, *else* $Nu_{vap} = 0.023Re_{vap}^{0.8}Pr_{vap}^{0.4}$	-	-	-	-	-	-	-	-	-	3.7	3.7	3.8	4.0	3.7	21.5
Vapour heat transfer coff.	h_{vap}	$Wm^{-2}K^{-1}$	$h_{vap} = \frac{Nu_{vap}k_{wvap}}{ID_{in}}$		-	-	-	-	-	-	-	-	-	94.0	15.7	12.4	8.3	9.3	79.1

Heat transfer coefficient of the condensing compounds for condenser 3

Overall film temp.	T_{f-o}	°C	$T_{f-o} = \frac{(T_{f-c} + T_{f-w})}{2}$	50.3	50.3	50.3	50.3	50.3	50.3	50.3	50.3	50.3	-	-	-	-	-	-
Conden. density	ρ_{con}	kgm^{-3}	*Value lookup at* T_{f-o}	992.3	1184.0	1018.0	963.0	1009.0	1128.0	1009.0	1050.0	1009.0	-	-	-	-	-	-
Conden. viscosity	μ_{con}	$kgm^{-1}s^{-1}$	*Value lookup at* T_{f-o}	$6.5E^{-4}$	$1.0E^{-3}$	$7.9E^{-4}$	$7.4E^{-4}$	$4.2E^{-3}$	$1.2E^{-3}$	$4.2E^{-3}$	$3.4E^{-3}$	$4.2E^{-3}$	-	-	-	-	-	-
Conden. thermal conductivity	k_{con}	$Wm^{-1}K^{-1}$	*Value lookup at* T_{f-o}	0.634	0.250	0.155	0.144	0.148	0.167	0.148	0.156	0.148	-	-	-	-	-	-
Condensate heat transfer coff.	h_{con}	$Wm^{-2}K^{-1}$	$h_{con} = 0.555\left(\frac{\rho_{con}^2 g' k_{con}^3 (h_v + 0.68\,Cp_c(bp - T_{out-c}))}{\mu_{con} ID_{in} (bp - T_{f-0})}\right)^{1/4} F_{con} M_{oil}$	603.8	-	35.9	-	-	18.6	-	-	-	-	-	-	-	-	-	-

Determining the condenser length						
Variables	**Sym.**	**Units**	**Equation**	**Cond. 1**	**Cond. 2**	**Cond. 3**
Total heat transfer coff.	h_{tot}	$Wm^{-2}K^{-1}$	$h_{tot} = \sum (h_{con} + h_{vap})$	780.2	836.0	876.9
Log mean temp. diff.	ΔT_{log}	°C	$\Delta T_{log} = \frac{(T_{in-c} - T_{out-w}) - (T_{out-c} - T_{in-w})}{ln(T_{in-c} - T_{out-w})/(T_{out-c} - T_{in-w})}$	265.4	142.7	49.3
Flow vapours condensed	$\dot{m}_{con}$	kgs^{-1}	$\dot{m}_{con} = \sum (\dot{m}_{in-c} - \dot{m}_{out-c})$	0.00064	0.00055	0.00048
Percent of bio-oil condensed	-	%	-	21	44	35
Condenser length	L_c	m	$L_c = \frac{q_{tot-c}}{\pi \Delta T_{log}} \left(\frac{1}{OD_{in} h_w} + \frac{LN\left(\frac{OD_{in}}{ID_{in}}\right)}{2k_{ss}} + \frac{1}{ID_{in} h_{tot}} \right)$	0.079	0.105	0.357

N.B. value lookup tables can be found in Appendix 3 [1]Caluclation for heat required from [34] [2]Calculations based on those given by [8] [3]following the procedure in [37], but developed by [38]

3.4 P&IDs of the pyrolysis system

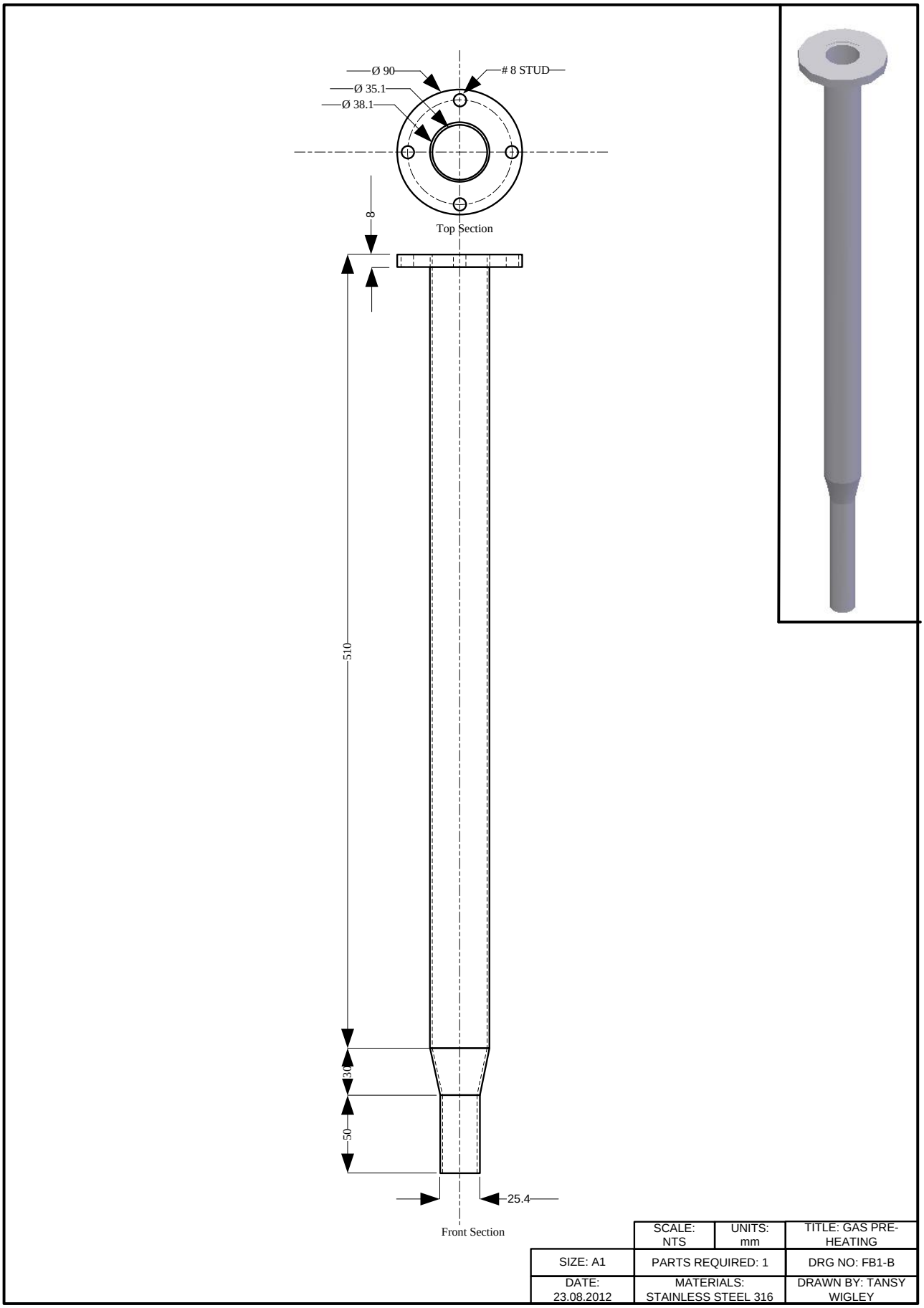

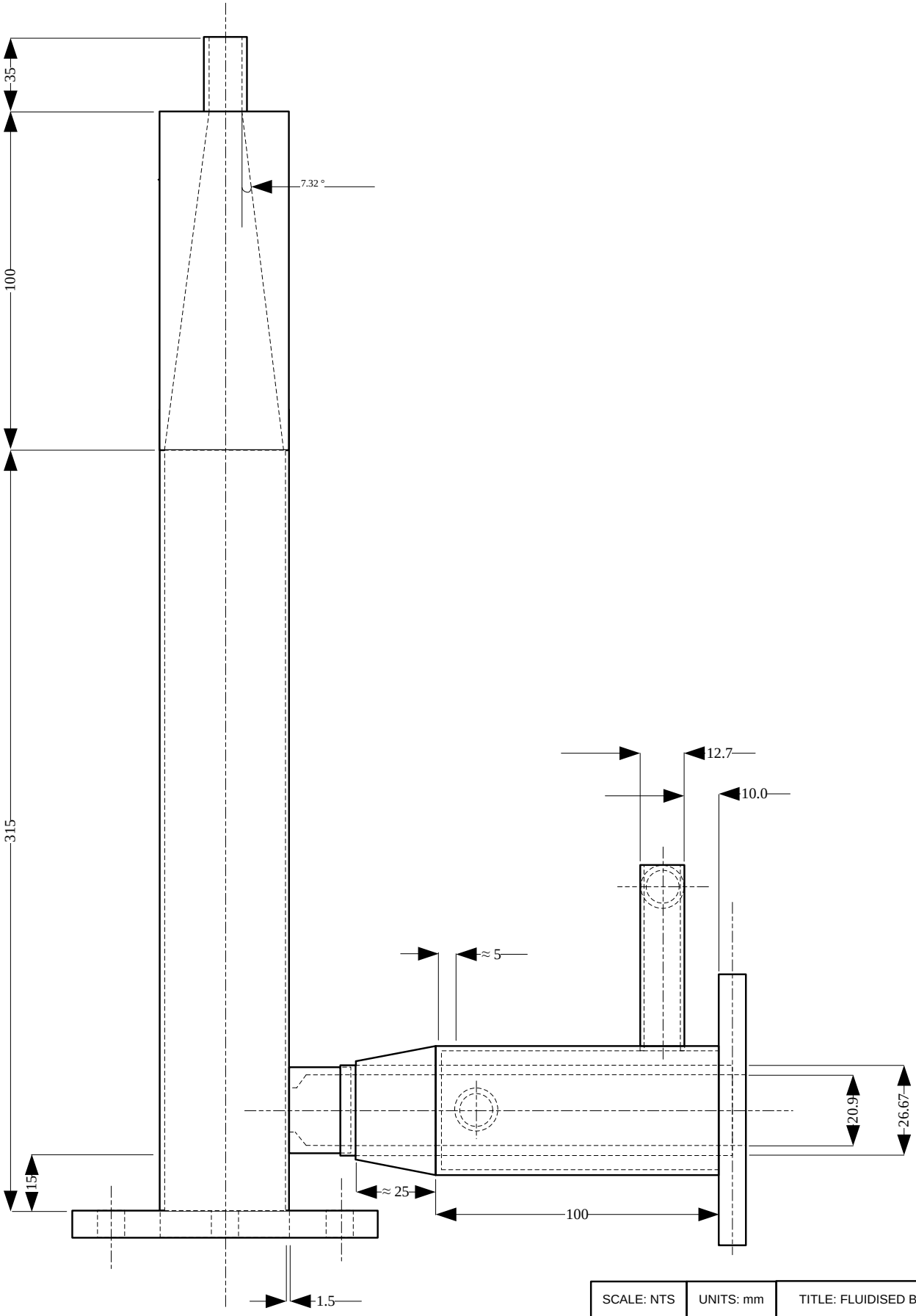

Front Section

	SCALE: NTS	UNITS: mm	TITLE: FLUIDISED BED
SIZE: A3	PARTS REQUIRED: 1		DRG NO: FB1-C
DATE: 24.08.2012	MATERIALS: STAINLESS STEEL 316		DRAWN BY: TANSY WIGLEY

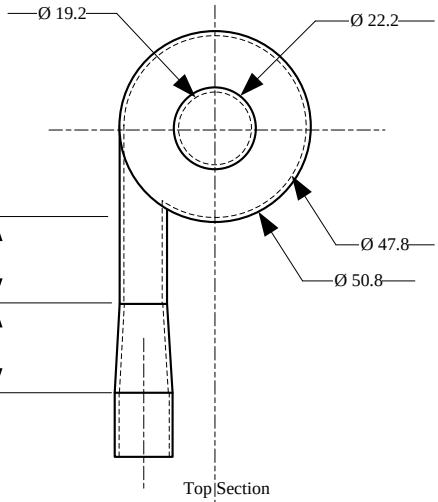

Top Section

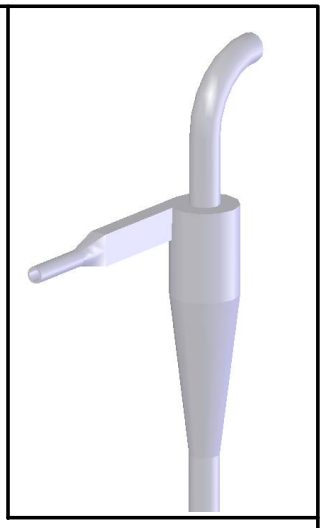

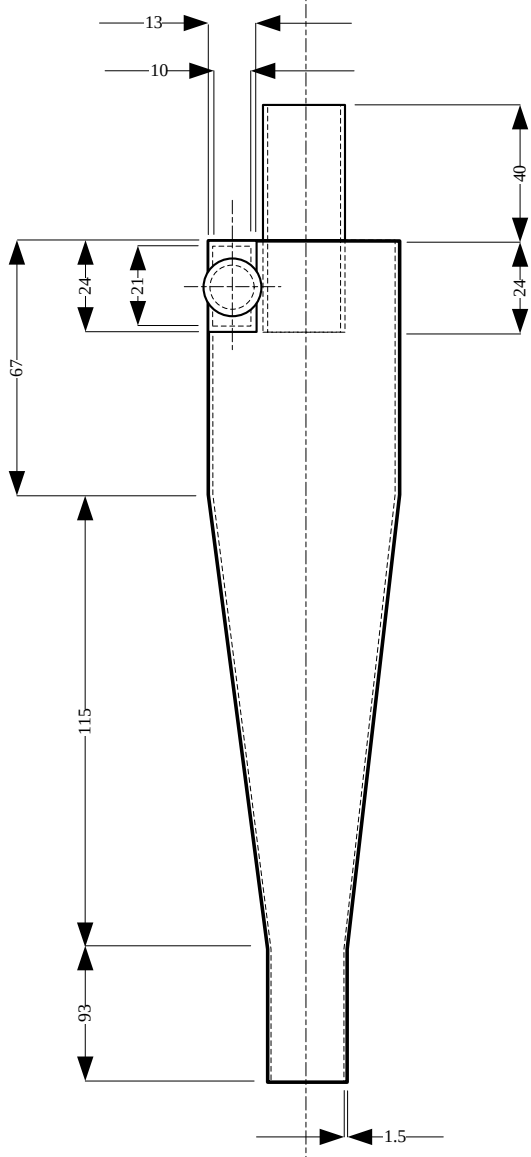

Front Section

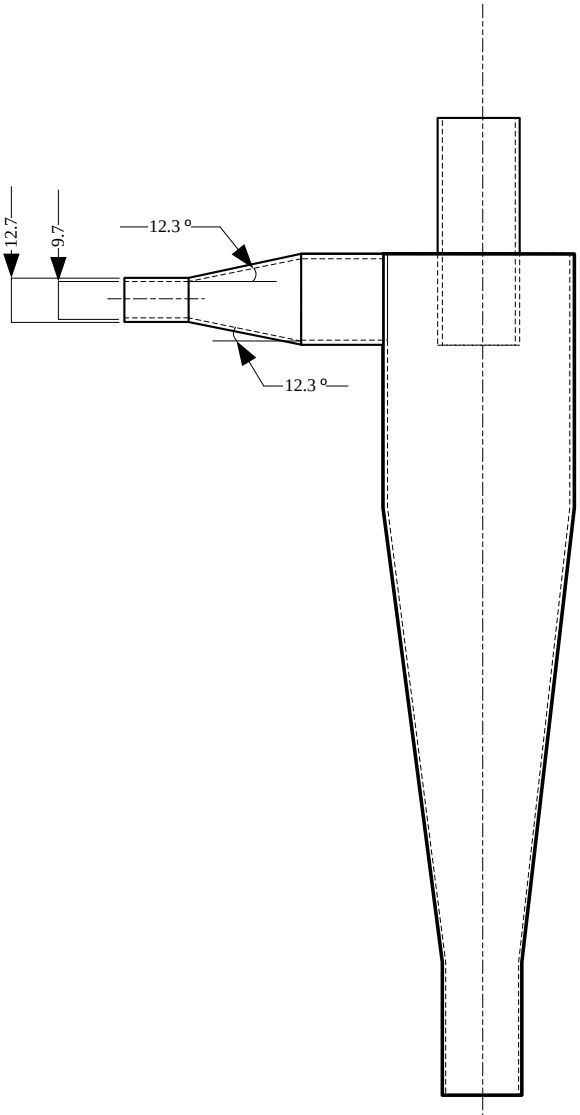

Side Section

PAPER SIZE: A3	SCALE: NTS	TITLE: CYCLONE
UNITS: mm	DATE: 27.07.2012	DRG NO: CY1-A
MATERIALS: STAINLESS STEEL 316		DRAWN BY: TANSY WIGLEY

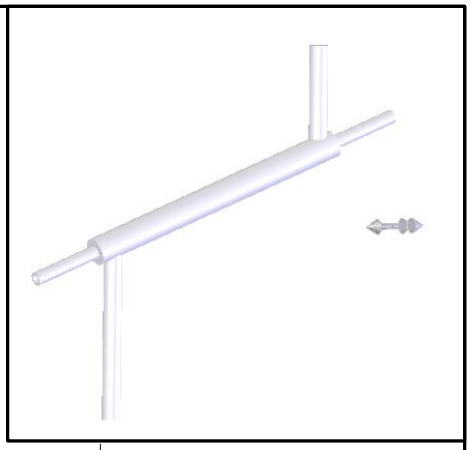

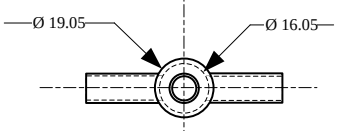

Top Section

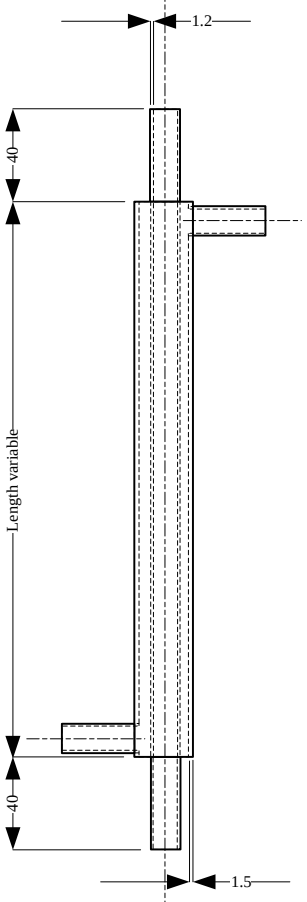

Front Section

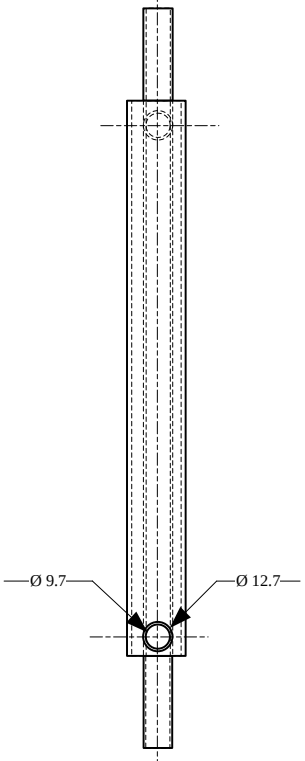

Side Section

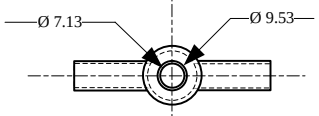

Botton Section

SCALE: NTS	TITLE: CONDENSER 1
DATE: 07.07.2012	DRG NO: C1-A
MATERIALS: STAINLESS STEEL 316	DRAWN BY: TANSY WIGLEY

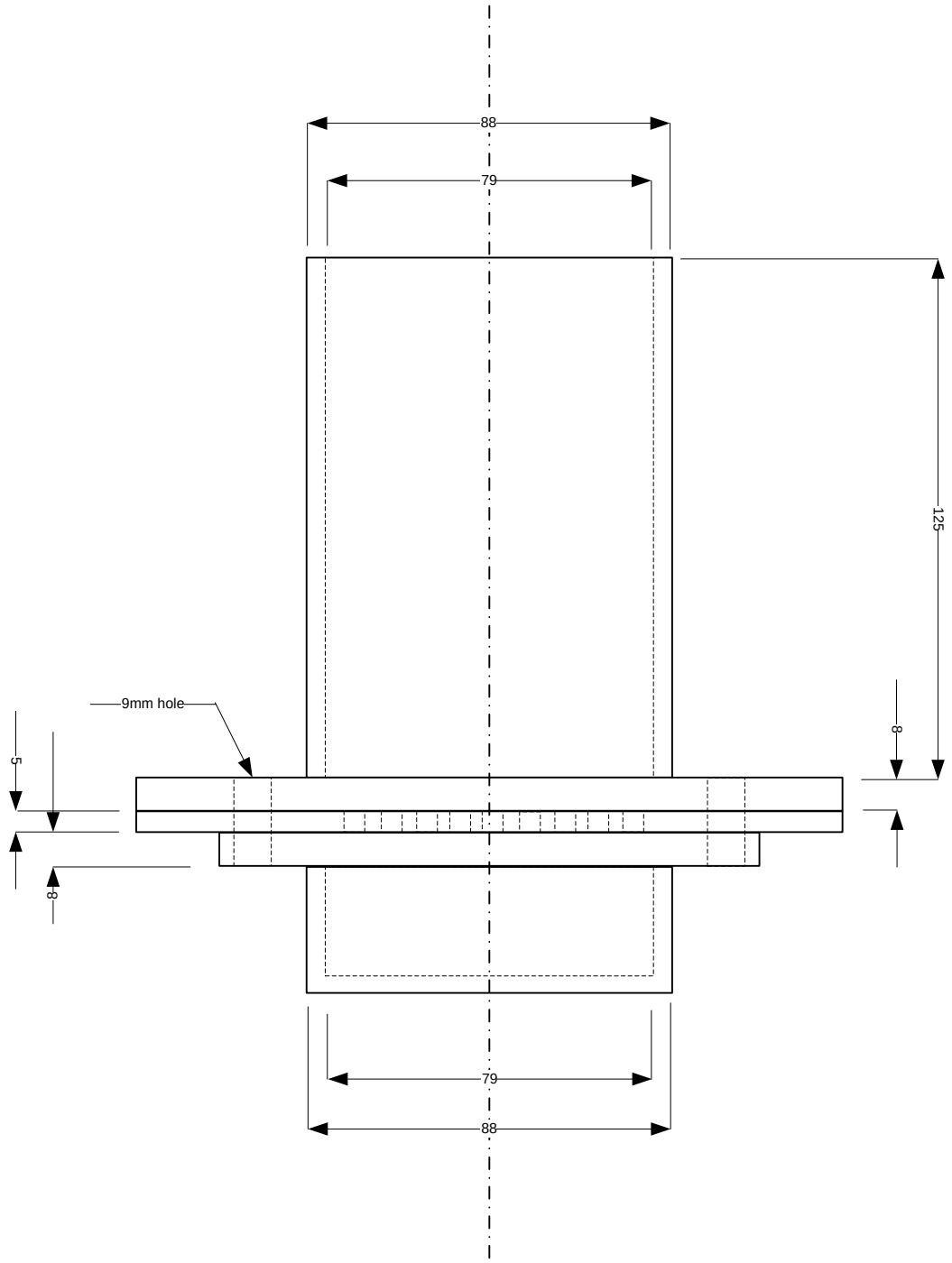

NTS	TITLE: PRESS
DATE: 6.03.2013	DRAWN BY: TANSY WIGLEY

3.5 Operating and cleaning for the pyrolysis reactor

3.5.1 Operating procedure

Setup and heating

1. Place the stainless steel fluidising mesh and copper gasket on top of the nitrogen gas preheater. Place the fluidised bed on top of this and tighten the 6 bolts
2. Line up auger 2 with the inlet of the fluidised bed. Push the feeder towards the reactor until the two flanges meet. Tighten the 4 bolts to connect the feeder to the fluidised bed
3. Add the required mass of leached, combusted, washed, and dried sand to the fluidised bed through the 1/2 inch Swagelok fitting on the exit of the fluidised bed
4. Connect the cyclone by placing its inlet on the exit of the fluidised bed (the 1/2 inch Swagelok fitting), only tighten loosely. The lab stand should be supporting the bottom of the char collector under the cyclone
5. Ensure the metal scrub attached to a 1/8 inch wire is clean and in the 7/8 inch fitting that attaches to the cyclone exit. Place the cyclone exit on top of the cyclone and tighten the 7/8 inch fitting loosely
6. Add condenser 1 to the exit of the cyclone. Ensure the thermocouple inlet is on the side closest to the cyclone. Join the condenser exit to the next condenser. This will already be in place
7. Now that everything is in line, go back and tighten the 1/2 inch fitting at the fluidised bed exit and the 7/8 inch fitting at the cyclones exit
8. Attach the thermocouple to the cyclone's exit and the pressure sensor after the cyclone
9. Attach the thermocouple to the entrance of condenser 1 and the inlet and outlet water hoses
10. Add insulation around the bottom of the fluidised bed, to the exit of it, and to the exit of the cyclone. Add the metal guard to the main body of the fluidised bed
11. Turn on the mini-GC and start a bake-out. Refer to the mini-GC manual for operation
12. Turn on the preheater furnace. Set this to 120 °C above the desired pyrolysis reactor temperature and leave to heat for 1 hour
13. After 1 hour, turn on the water mains and set the 3 rotameter flows (for each of the 3 condensers) to the desired level. Turn on the heating bands around the fluidised bed using the three labelled temperature controllers. Set to the desired temperature for pyrolysis. These control the internal temperature of the fluidised bed. If you are operating above 400 °C, then heat up in 2 stages to prevent over-heating due to the feed-back lag
14. If the mini-GC has completed the bake-out, load the required running method
15. While the system heats up, weigh the containers for bio-oil collection, record the weight and attached these to the system condensers

16. Attach the collection container to the bottom of the ESP

17. Weigh approximately 40 g of cotton wool (recording the exact weight) and add this to the glass filter after the ESP. Attach the entrance and exit of the filter using 3 bolts on each, there is a rubber gasket that goes between the glass and metal attachments. Do not over tighten or the glass tube will break

18. Weigh a silica SPE column to 4 dp and attach this to the fitting after the filter, attach the gas sampling system to this (the gas sampling system is made up a 50 mL syringe and valves)

19. Add weighed biomass to the hopper. If a MC of 0% is required, add it to the hopper at 105 °C to prevent moisture intake while purging the system

20. Tighten the 4 G-clamps on the hoppers lid

21. Turn on the N_2 gas supply and the flow controller. Set the flow rate to 10 $Lmin^{-1}$ and let the system purge for 5 min

22. While the system purges, turn on the computer and open the data logger software (TracerDAG pro). Open one window for the pressure sensors and one window for the temperature sensors. Start logging both and turn on the power to the ESP (ensure the electrode is safely connected)

23. While the system is purging, take an air reading using the mini-GC for calibration

24. After purging the system for 5 min, increase the gas flow rate to the required level, this depends on the reactor temperature as the same superficial gas velocity should be maintained in the fluidised bed. The table below can be used to determine the required flow rate:

Temperature (°C)	**N_2 flow rate ($Lmin^{-1}$)**
400	23.4
425	23.2
450	23.0
475	22.0
500	21.1
525	20.2
550	Not recommended

Running the reactor

1. Once the temperature of the gas exiting the preheater has increased to the required temperature, start both augers. Auger 1 is normally set to 12 Hz and auger 2 is normally set to 50 Hz. It is not recommended to vary from these setting significantly

2. Start timing once the pressure in the fluidised bed increases slightly (about 90 seconds after starting the augers). Over 50 g of sand in the fluidised will make the slight pressure increase hard to observe, instead timing can be started once vapours can be seen in the collection containers.

3. Ensure there are no vapour leaks, if one is found, place on a vapour gas mask and either tighten the fitting or add Teflon tape to the outside of the fitting. There is a CO monitor in the room that will alarm if the CO concentration in the room exceeded the set-point. In case of this, turn off the feeding system and heating, and then leave the room.

4. After 2 minutes of running, fill the gas sampling syringe with 45 mL of NCG, the first injection of the day is used as a flush only. The three way valve must be turned on while filling the syringe and then turned off after to prevent leaks. Eject the syringe contents to a vent line; the one on the muffle furnace is most suitable. Take another 45 mL sample and this time; inject a sample into the mini GC. Once the GC run is completed, dispose of the remaining gas out the vent line

5. Take gas samples every 10 minutes for the duration of the run

6. The pressure in the system slowly increases during a run due to the filter becoming saturated and char carry-over from the cyclone. To regenerate the metal scrub during a run, loosen the Swagelok fitting keeping the 1/8" rod in place and press this quickly down and up again to shake off char. Wear a mask while doing this as some pyrolysis vapours may be released

7. If the pressure in the fluidised bed reaches 550 mbar, stop the feeding system and end the run to prevent bursting the pressure sensors

8. Once the run is complete (this will be observed by a slight decrease in pressure), stop the timer but leave N_2 purging the system for 5 min. Then turn off the heating bands, the cyclone heating, and the preheater and reduce the nitrogen flow rate to 10 $Lmin^{-1}$ for another 5 min. Turn off the ESP and start the cool down of the mini-GC

9. Reduce the nitrogen flow rate to 3 $Lmin^{-1}$ and leave for 1 hour while the system cools, this is to prevent a vacuum forming due to the vent

10. Reduce the water flow rates through the condensers to 0.5 $Lmin^{-1}$ for the cool down

3.5.2 Collecting products and cleaning the reactor

Product collection

1. Once the system has cooled down for 1 hour, removed the insulation that was added at the start of the run

2. Wearing a vapour mask, collect and weigh the 3 bio-oil containers from the condensers, transfer to a fume-hood

3. Remove the collection container from the ESP, the cotton-wool from the filter, and the SPE column. Transfer to the fume-hood and weigh

4. Unscrew the cap at the bottom of the char collector to release the char into a container (still wearing the vapour mask), weigh and store in a sealed bag

5. Determine the gas yields based on the mini-GC results

Cleaning

1. Turn off the N_2 supply and turn off the gas flow controller

2. Loosen the 4 bolts connecting the feeder to the fluidised bed and remove auger 2, loosen the 4 G-clamps on the hoppers lid and vacuum clean the hopper and auger 2 to clean. Squirt compressed air down auger 1 while hold the vacuum cleaner near auger 2 to clean the transfer line

3. Remove condenser 1 from the exit on the cyclone and the rest of the condensers. Remove the thermocouple and the water inlet/outlet hoses. Remove the condenser from the support

4. Remove the cyclone exit from the cyclone by loosening the 7/8" connection. Remove the pressure sensor and thermocouple from the cyclone

5. Cook the cyclone exit and condenser 1 at 450 °C for 3 hours in the muffle furnace to remove any char/bio-oil residue. Once they are cool, run a pipe cleaner down both to remove any reside and squirt with compressed air

6. Run the extended cleaning brush down the cyclone to remove any char that may be in it and the smaller brush down the cyclone entrance. Check if there is any more char in the char pot

7. Disconnect the cyclone from the fluidised bed

8. Loosen the 6 bolts that connect the preheater to the fluidised bed and remove the fluidised bed. Collect the sand and any char remaining in the bed

9. Use the vacuum cleaner to clean up any sand that was not collected

10. Run the extended cleaning brush up the fluidised bed to remove any char that may be in it and collect this. Take the weight of the sand plus the char from the fluidised bed. Cook this at 620 °C overnight to determine the amount of char in the mixture

11. Re-attach the fluidised bed to the preheater and the cyclone to the fluidised bed add the metal guard to the fluidised bed. Do not attach the feeder or the condensers

12. Turn on the cyclone and fluidised bed temperature controllers and heat to 450 °C for 30 min to bake-out the reactor and the cyclone

13. Turn off the heaters and allow to cool, once cool, brush out both again with the extended cleaning brush to remove any ash, run compressed air though both to help remove the ash

14. To clean condensers 2 and 3, re-attach the collection containers once the bio-oil has been removed from them and wash with acetone or ethanol (use acetone if it is to be evaporated to determine the bio-oil residue). Wash until the liquid runs clear

15. Clean the ESP using the same technique. Wipe the glass filter tube clean using paper towels and ethanol

16. Waste bio-oil mixed with ethanol or acetone cannot be disposed of down the sink. Collect this in a storage container and dispose of it as a hazardous chemical

3.6 NMR peak identification

The four spectras given here are split into two figures each. Peaks are labelled with possible compounds based on ^{13}NMR of pure samples. Samples were only considered present if the compounds could be identified on both ^{13}C-NMR and ^{1}H-NMR.

^{13}C-NMR spectra for bio-oil 1

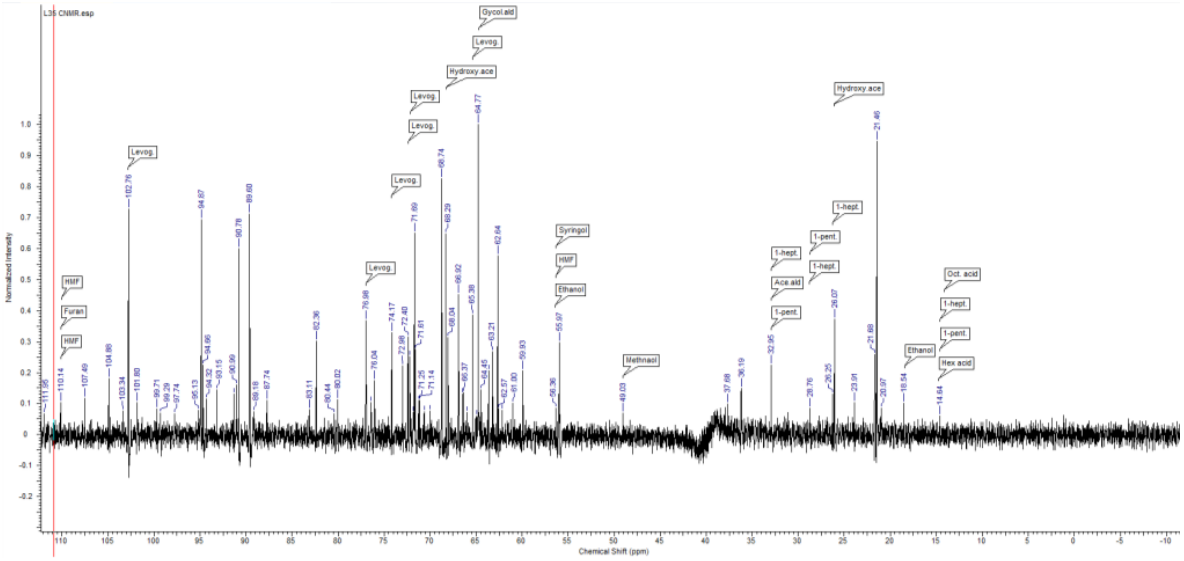

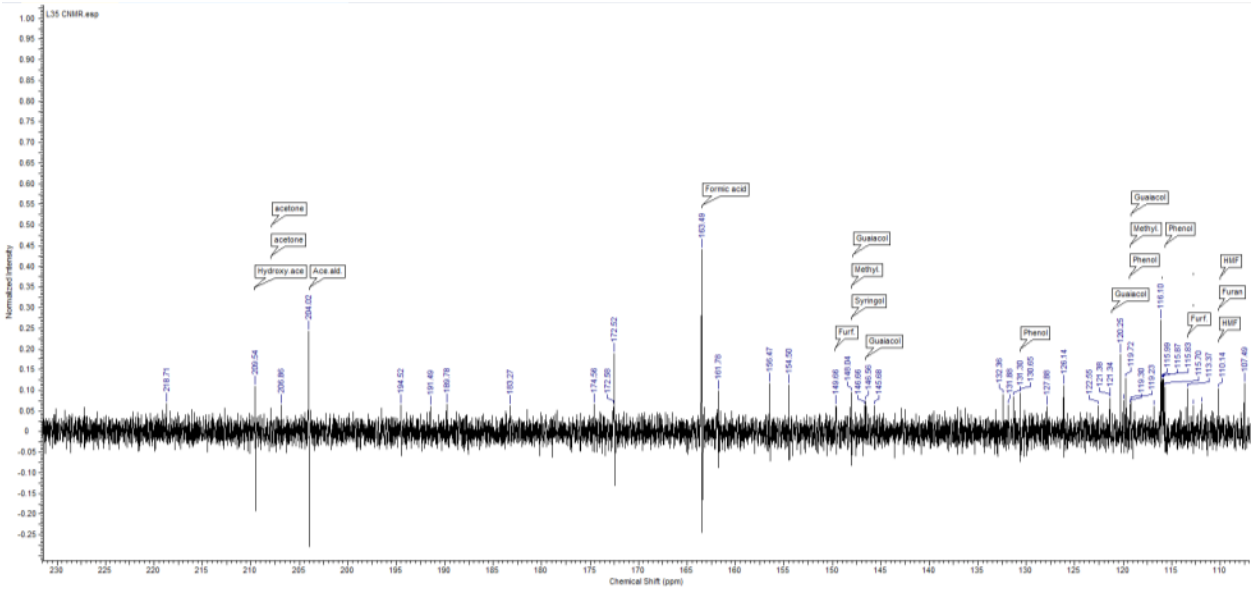

[1]H-NMR spectra for bio-oil 1

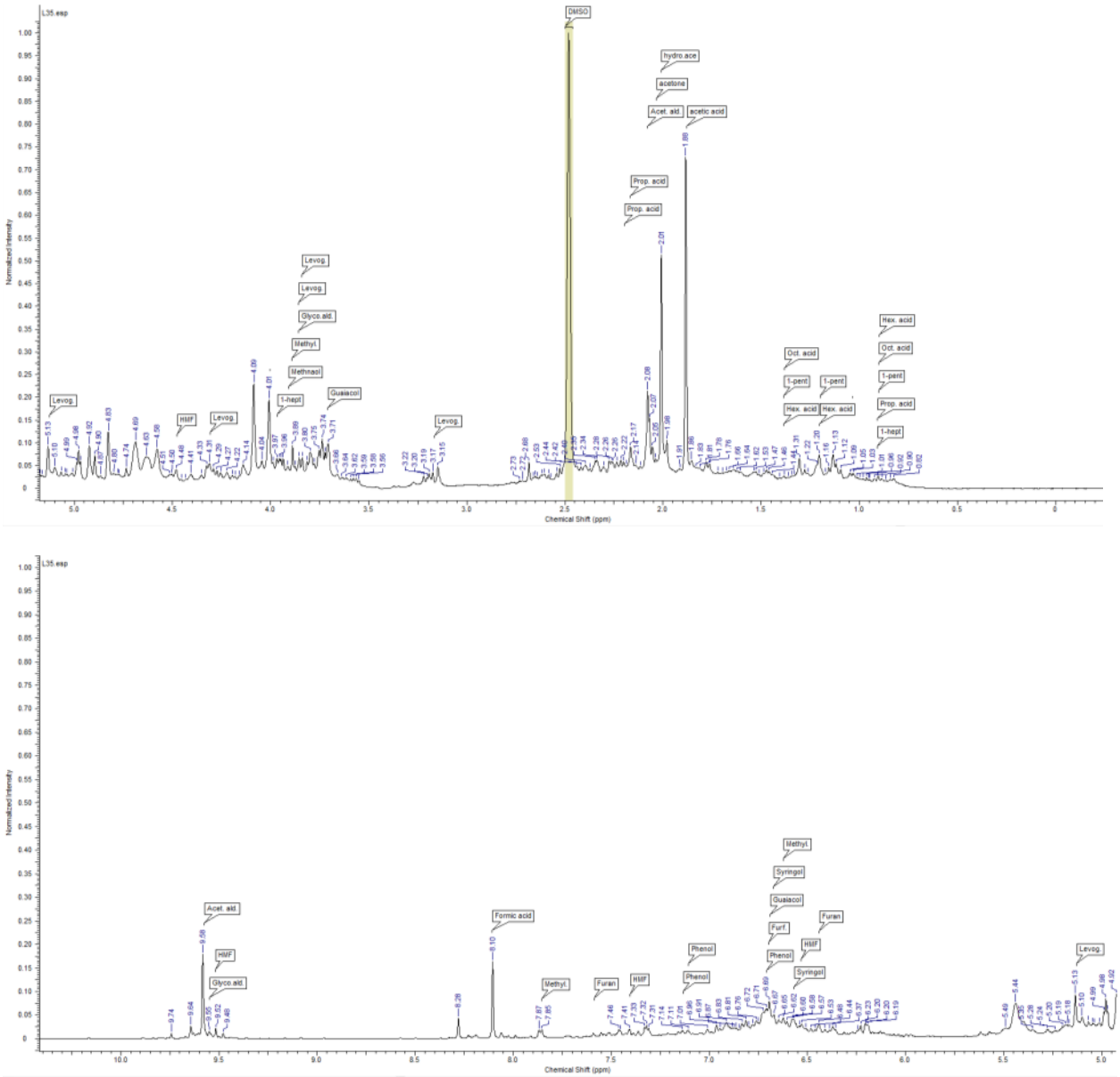

^{13}C-NMR spectra for bio-oil 2

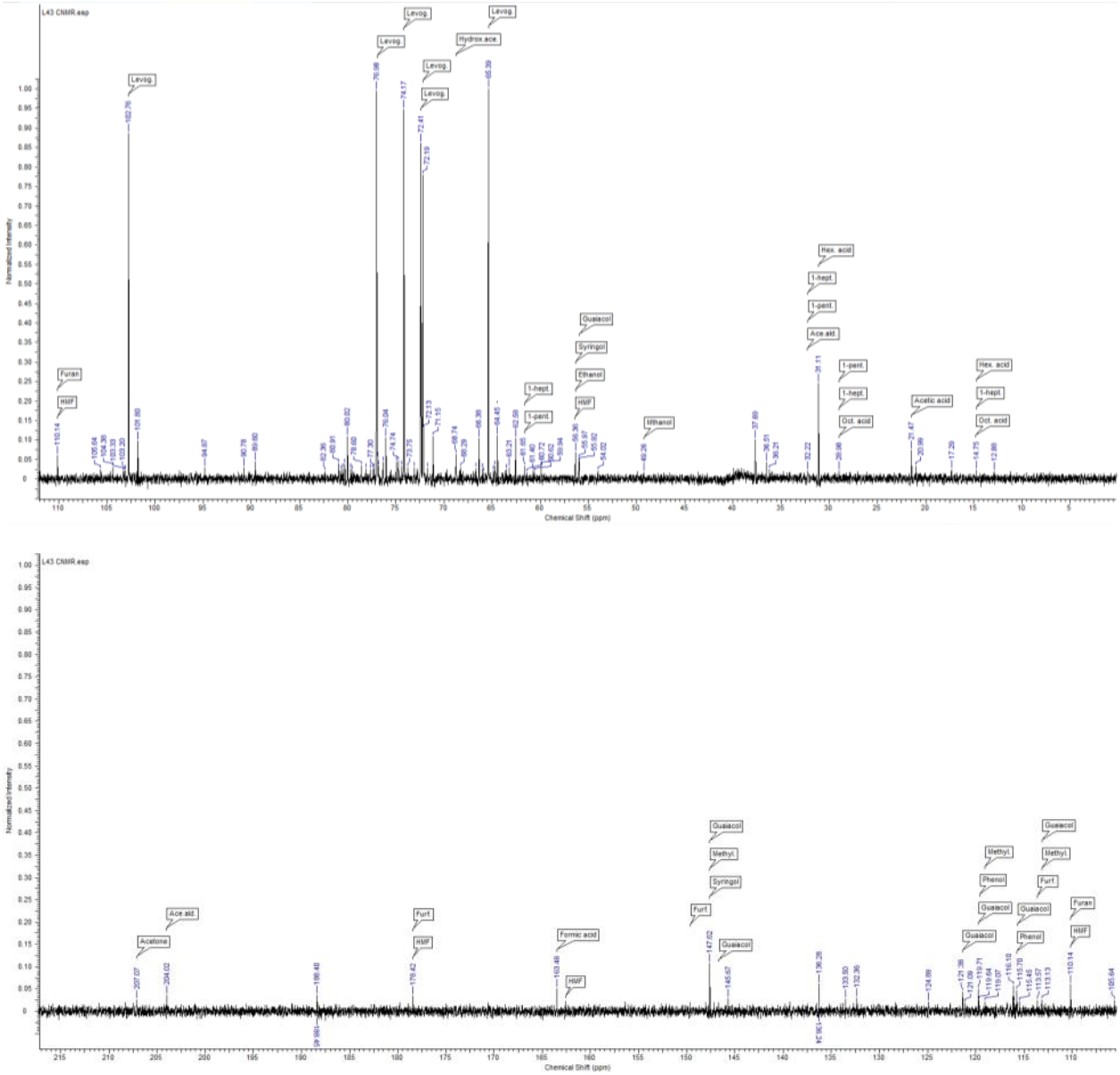

^{1}H-NMR spectra for bio-oil 2

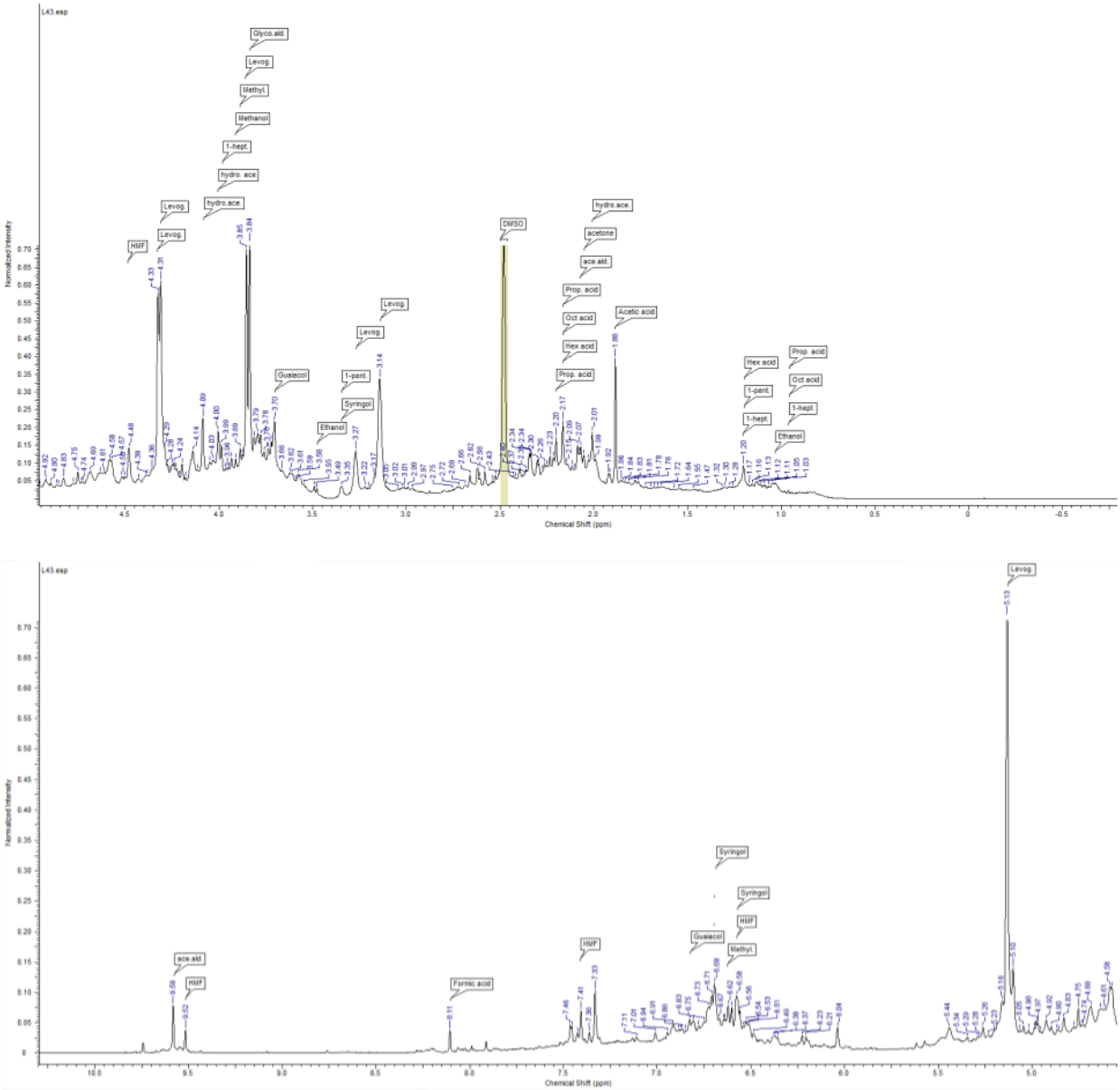

3.7 HPLC retention times and calibration for hydrolysis sugars and acids

The residence times for sugars and acids thought to be in biomass are listed in Table A-26. The chromographs are displayed in Figure A-1, Figure A-2, and Figure A-3. The peak at 5.55 min is associated with sulphuric acid and the one at 7.7 min is associated with water in the samples. The calibration curves for the compounds are given in Figure A-4, Figure A-5, and Figure A-6.

Table A-26: Residence time for hydrolysis sugars and acids

Compound	Retention time (min)
Acetic acid	13.34
Arabinose	9.67
Cellobiose	6.93
Formic acid	12.26
Galactose	8.90
Glucose	8.27
Levulinic acid	15.54
Mannose	8.80
Xylose	8.79

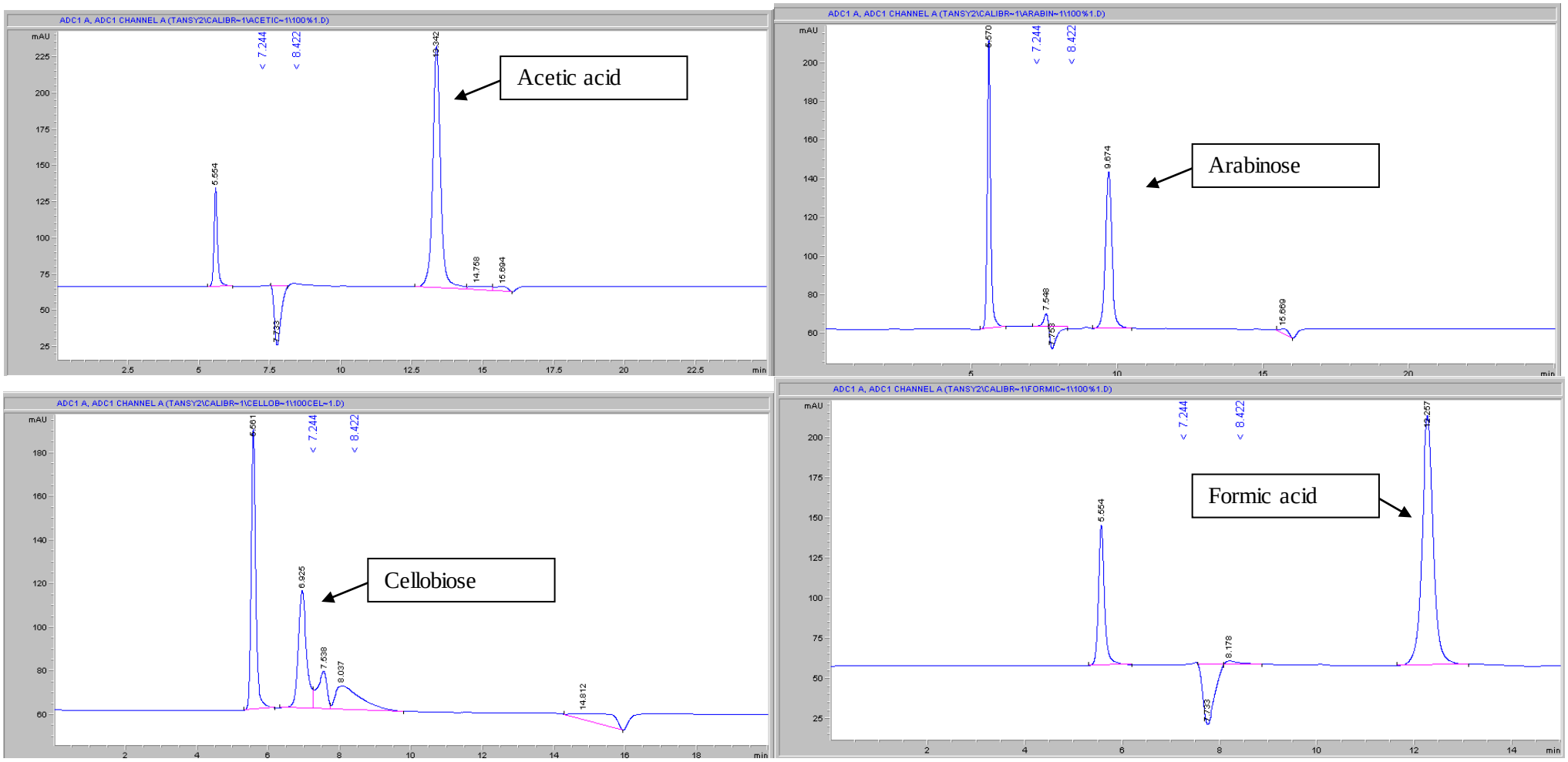

Figure A-1: Retention time for hydrolysis compounds

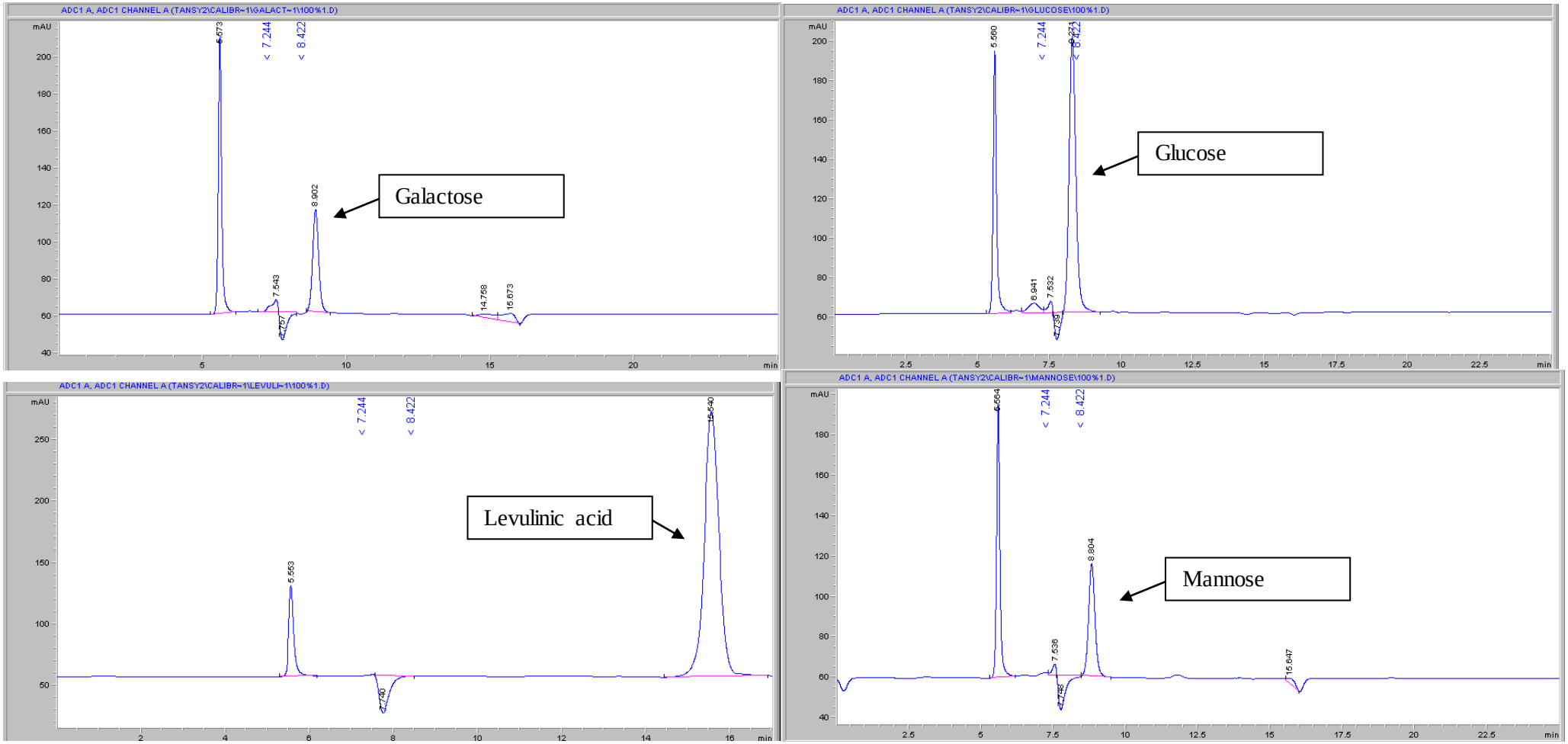

Figure A-2: Retention time for hydrolysis compounds

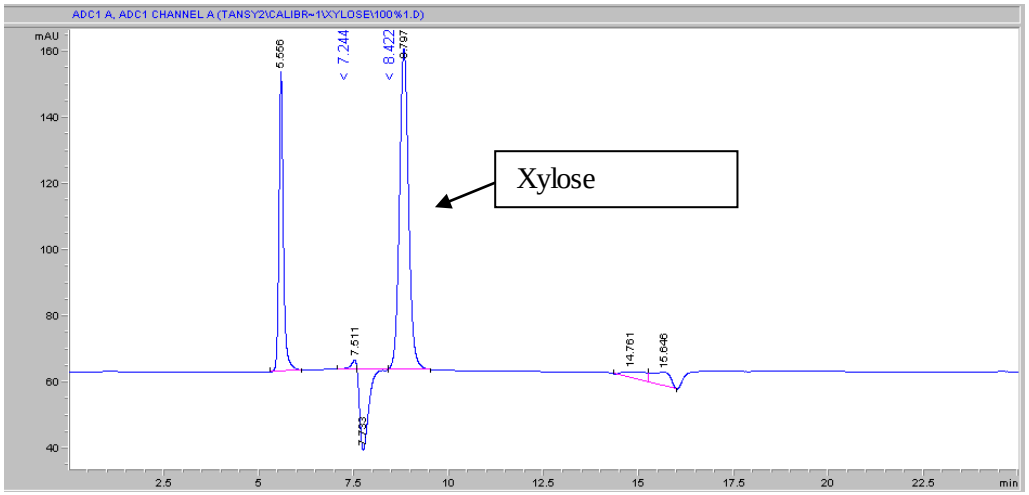

Figure A-3: Retention time for hydrolysis compounds

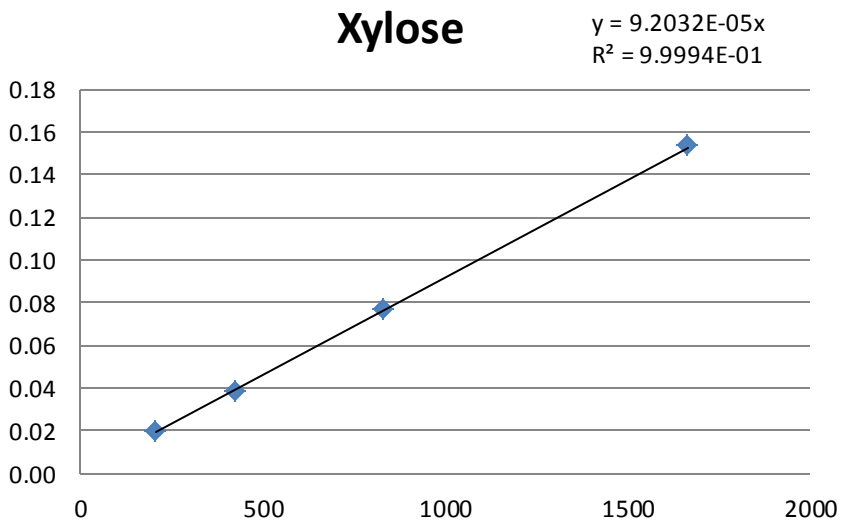
Xylose
y = 9.2032E-05x
R² = 9.9994E-01
0.18
0.16
0.14
0.12
0.10
0.08
0.06
0.04
0.02
0.00
0
500
1000
1500
2000

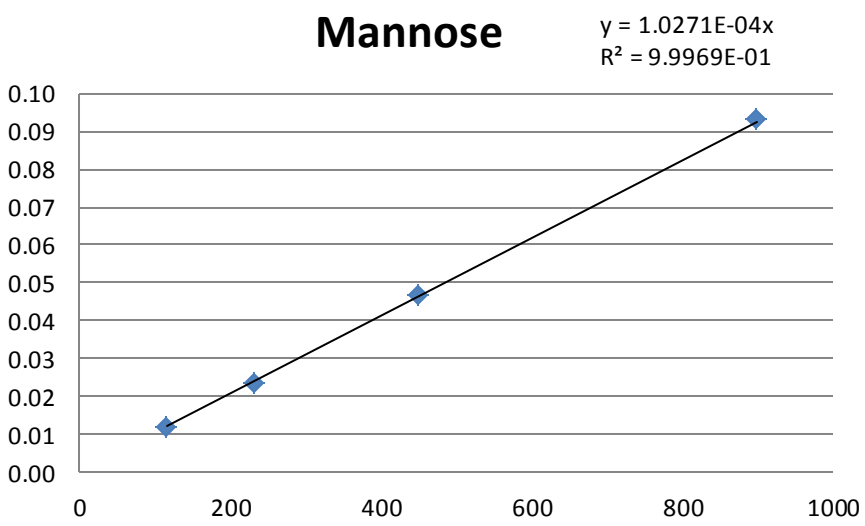
Mannose
y = 1.0271E-04x
R² = 9.9969E-01
0.10
0.09
0.08
0.07
0.06
0.05
0.04
0.03
0.02
0.01
0.00
0
200
400
600
800
1000

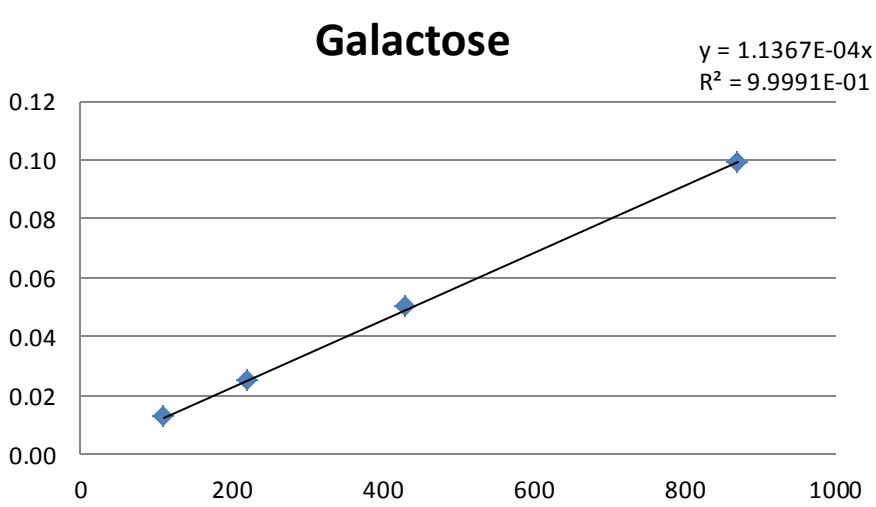
Galactose
y = 1.1367E-04x
R² = 9.9991E-01
0.12
0.10
0.08
0.06
0.04
0.02
0.00
0
200
400
600
800
1000

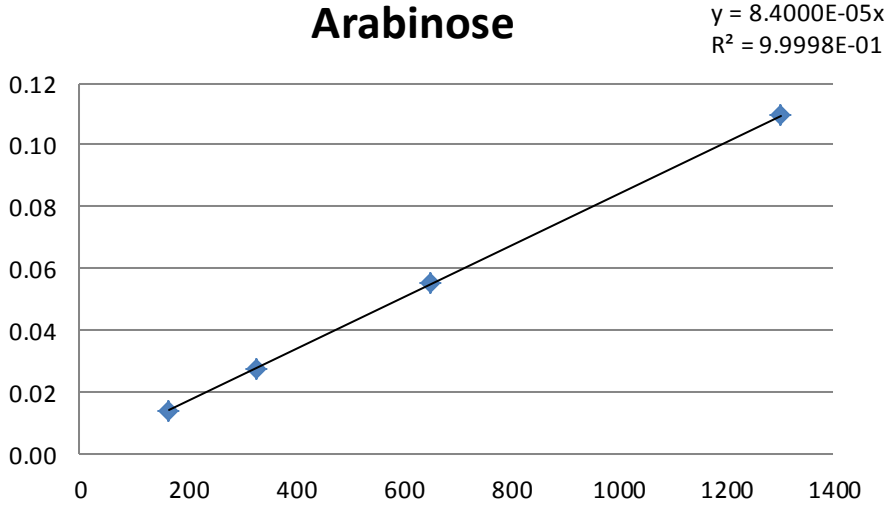
Arabinose
y = 8.4000E-05x
R² = 9.9998E-01
0.12
0.10
0.08
0.06
0.04
0.02
0.00
0
200
400
600
800
1000
1200
1400

Figure A-4: Calibration curves for hydrolysis compounds

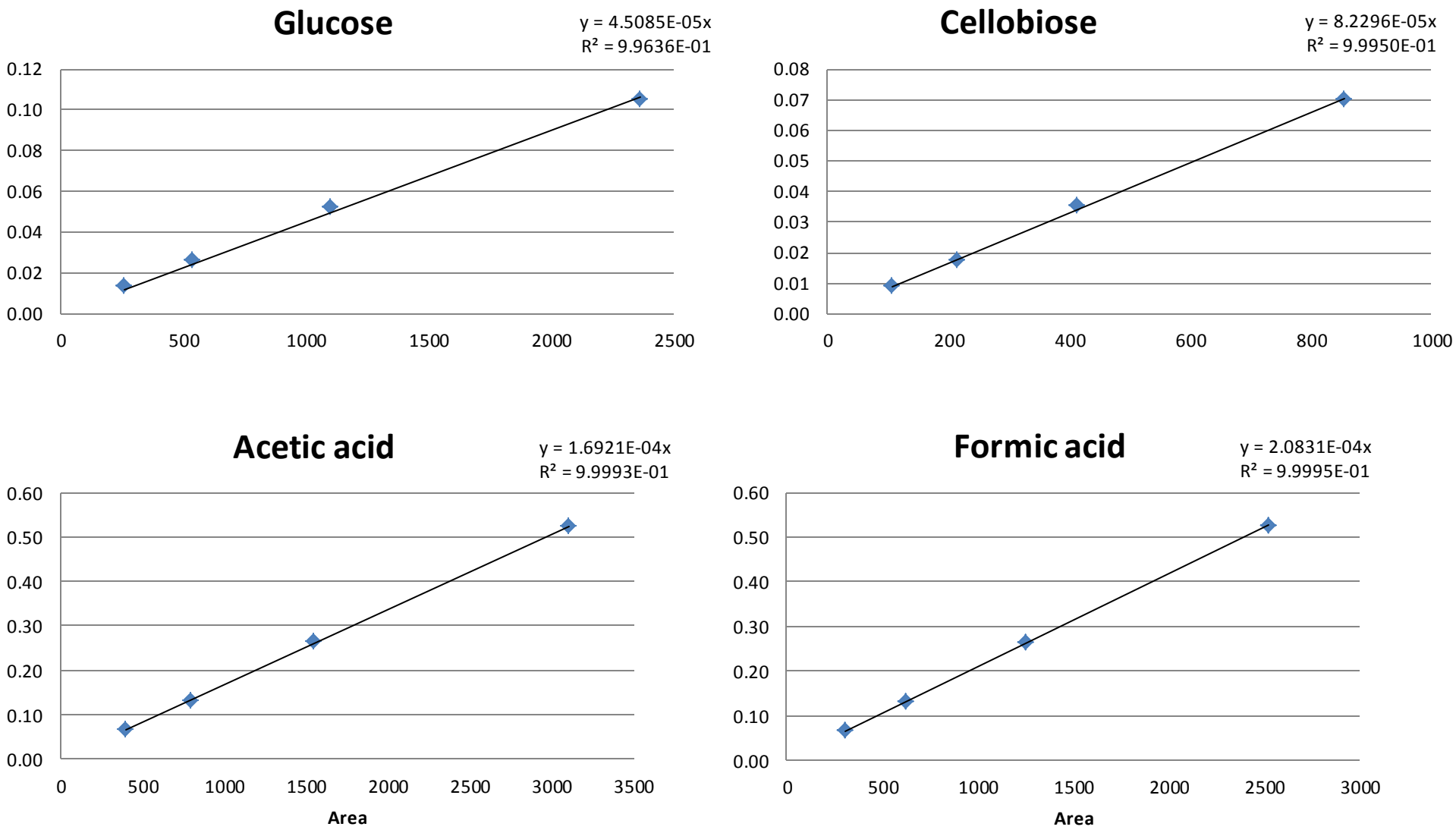

Figure A-5: Calibration curves for hydrolysis compounds

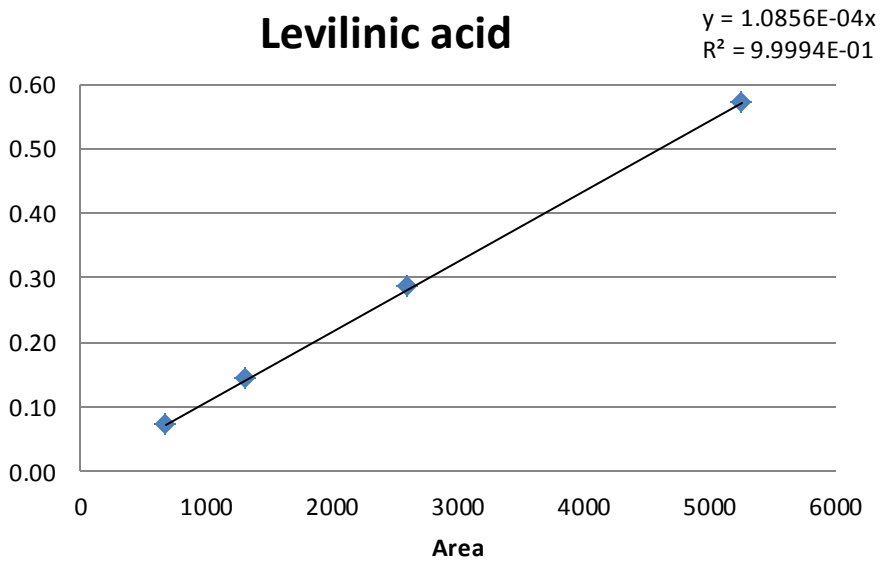

Figure A-6: Calibration curves for hydrolysis compounds

3.8 HPLC retention times for possible pyrolysis compounds

The residence times for compounds thought to be in bio-oil are listed in Table A-27. The chromographs are displayed in Figure A-7, Figure A-8, Figure A-9, and Figure A-10. The negative peak at 7.66 min is associated with water that most samples were diluted in. If they were not water soluble, samples were dissolved in ethanol or acetone.

Table A-27: HPLC residence time for bio-oil compounds

Compound	Retention time (min)
Acetic acid	13.40
Acetol (ethanol added)	14.78
Acetone	18.96
Ethanol	16.95
Formic acid	12.19
Glycolaldehyde	10.68
Levoglucosan	11.74
Glyoxal	9.13
Hydroxyacetone	15.50
Iso-propanol	18.36
Methyl-2-furorate	21.13
Methanol	15.36
Octanoic acid (ethanol and acetone added)	17.30
Phenol	54.49
1-pentanol (ethanol added)	47.20

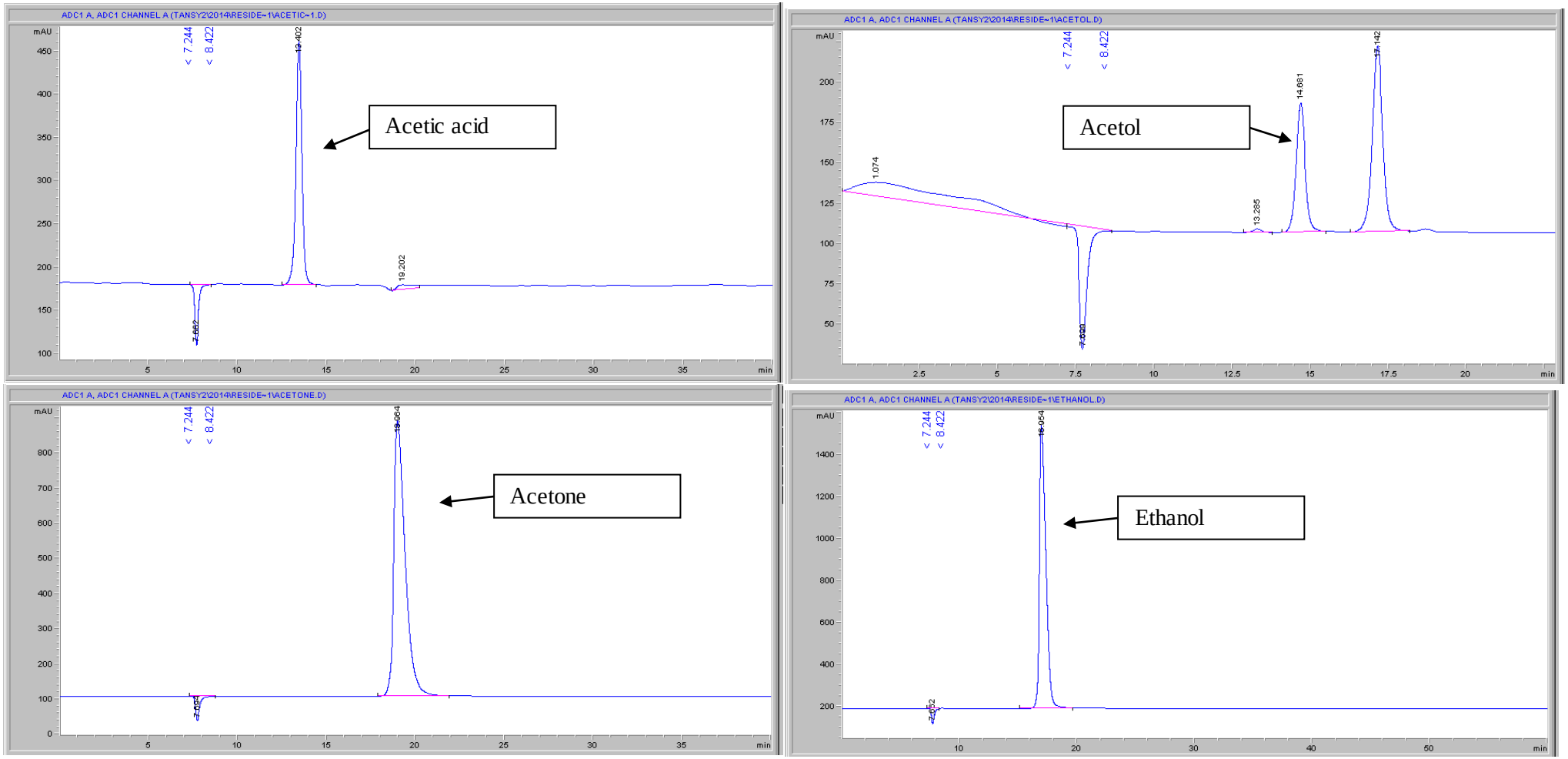

Figure A-7: Retention time for possible bio-oil compounds

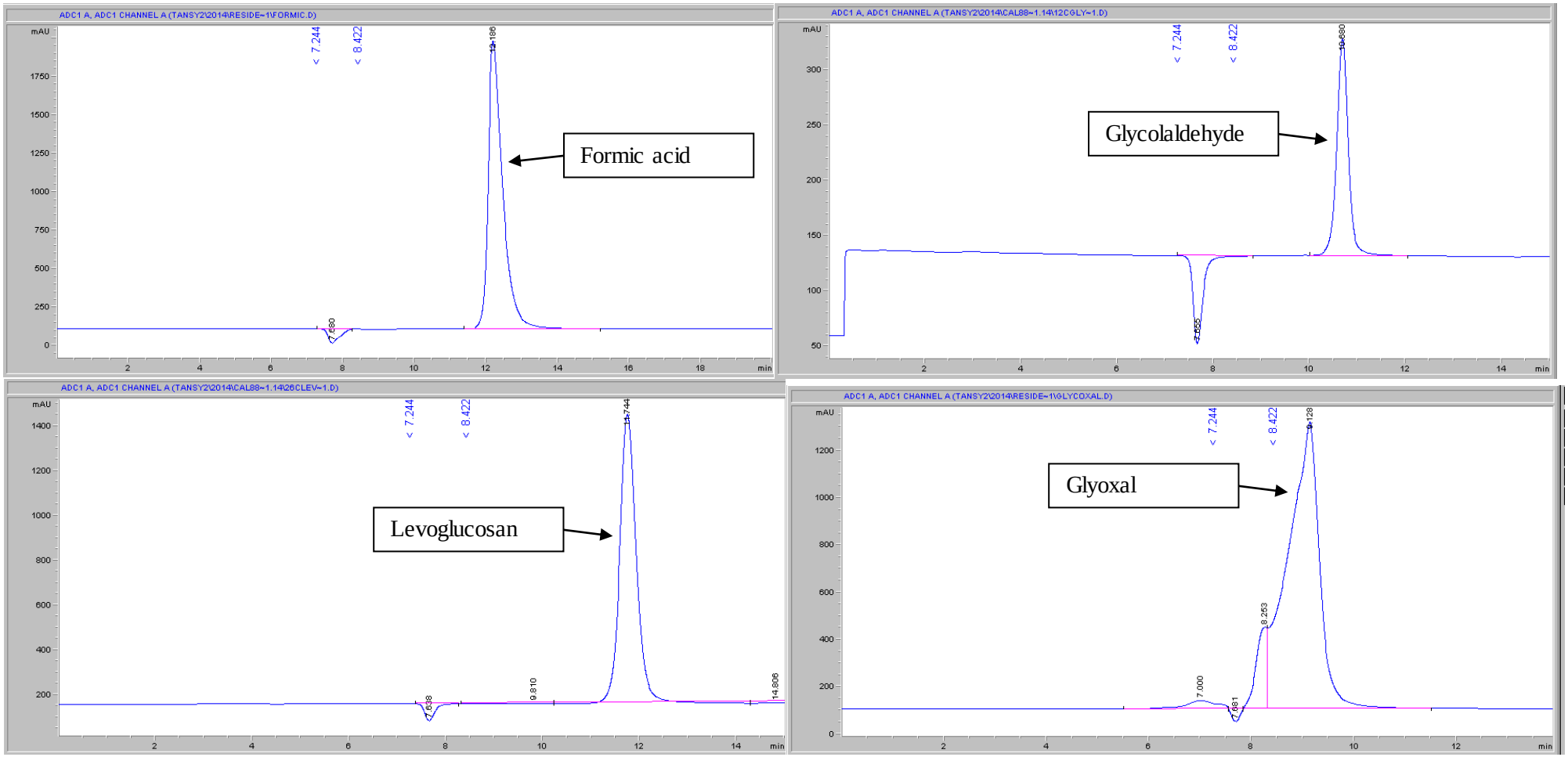

Figure A-8: Retention time for possible bio-oil compounds

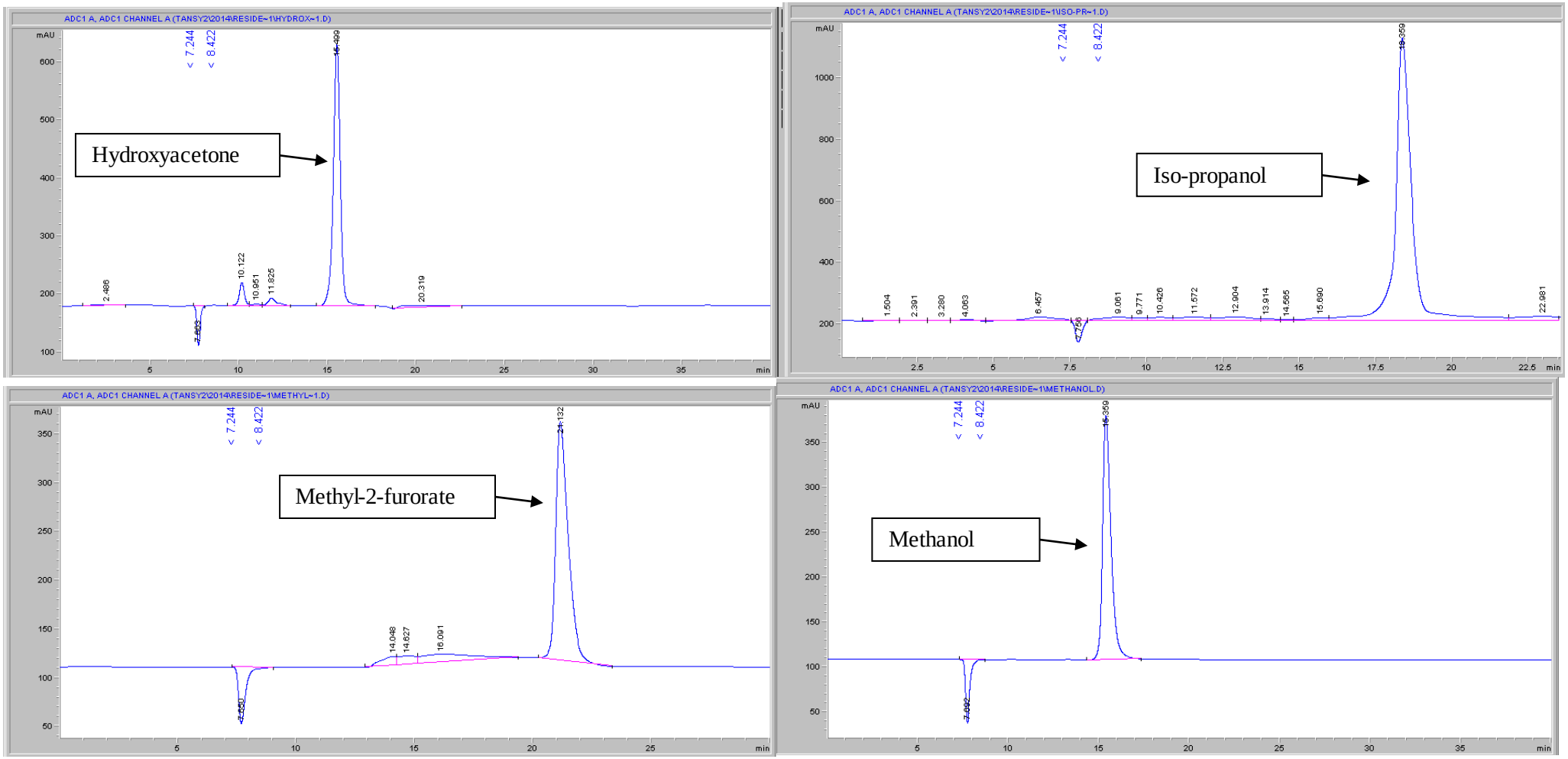

Figure A-9: Retention time for possible bio-oil compounds

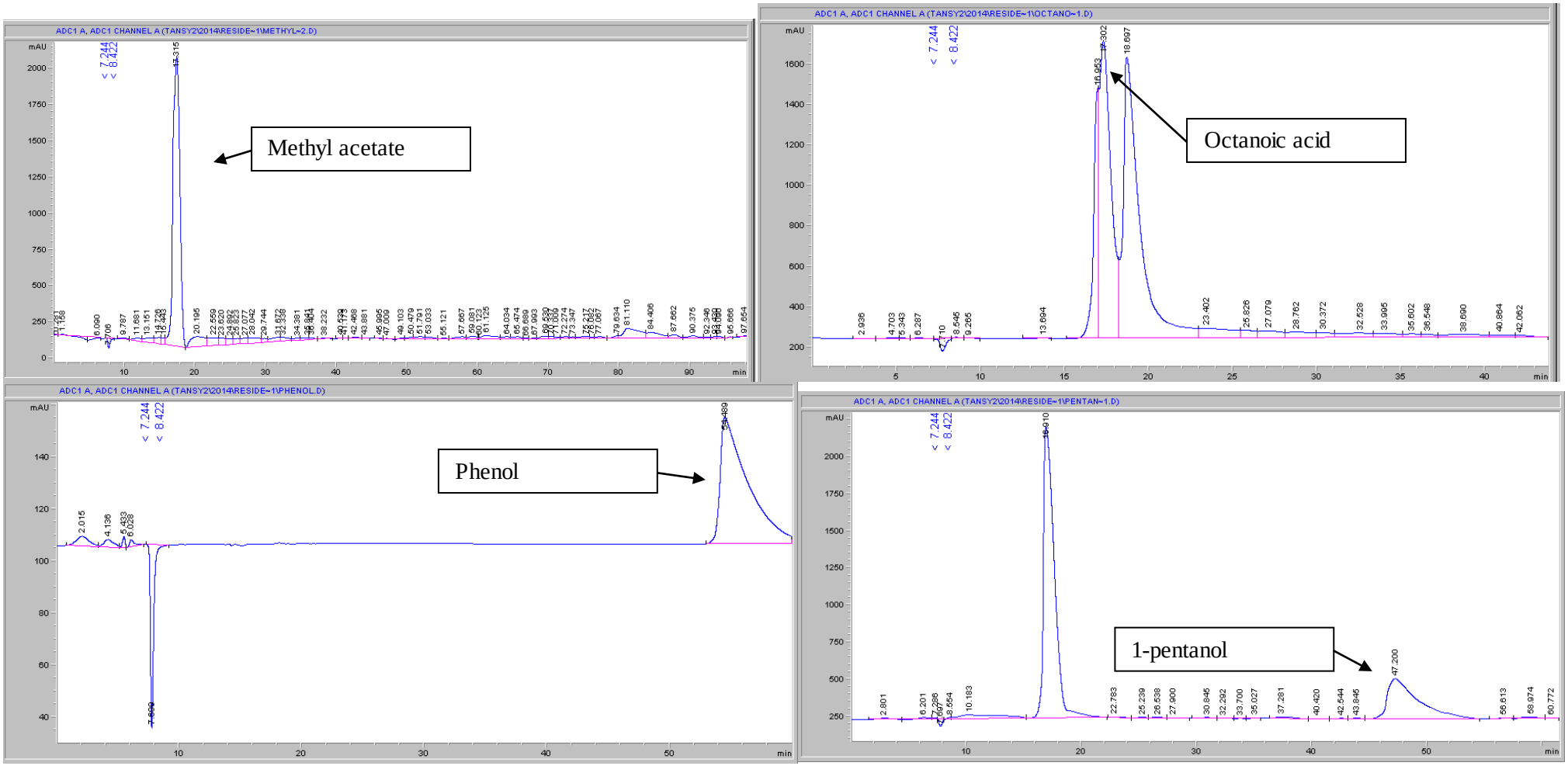

Figure A-10: Retention time for possible bio-oil compounds

Appendix 4

4.1 Leaching and torrefaction procedures

4.1.1 Leaching

1. Place 70 g of dry biomass in the 2 L conical flask with a 2 inch Teflon flea at the bottom
2. Add 700 mL of leaching solution (1 wt% concentration solution of either nitric acid or sodium hydroxide)
3. Bung the flask and place on the magnetic stirrer. Set the stirrer conditions to 30 °C at 250 rpm and leach for 4 h
4. Rinse the leached biomass with DI water until a neutral pH is obtained then dry overnight at 105 °C

4.1.2 Torrefaction

1. Clean all equipment using ethanol and dry
2. Place the concentric aluminium block on the hot plate and heat to 30 °C above the required temperature for 1 h
3. Place the 30 g of biomass in the batch vessel with the modified magnetic stirrer at the bottom
4. Ensure the O-ring in the top of the vessel is in good condition. Tighten the lid
5. Attach the nitrogen inlet, thermocouple, and gas outlet
6. Place the vessel in the concentric aluminium block situated on the hot plate, insulate around the top and then turn on the condenser water supply
7. Ensure that the inlet and outlet valves are open, then purge the system with 0.5 $Lmin^{-1}$ of nitrogen for 5 min, test for leaks with the Swagelok leak detector fluid
8. Set the hotplate to the required temperature (normally 260 °C). Monitor the internal temperature on the digital temperature sensor
9. Run the experiment for 20 min once it has reached the required internal temperature. Then turn off the heater and remove insulation from the vessel
10. Remove the vessel carefully from the concentric aluminium block and place on a ceramic brick to cool. Use thick leather gloves for this and only touch the top of the vessel
11. Once the reactor has cooled to 100 °C (monitor using internal thermocouple), remove the torrefied biomass and dry overnight at 105 °C.
12. Turn water supply off and nitrogen purge off, then collect the liquid product

Appendix 7

7.1 Comparison between pretreated and raw biomass

Table A-1: Comparison between pretreated and raw biomass

		Leaching and torrefaction	
Torrefaction	**Raw wood**	**Torrefaction temp: 270 °C**	**Torrefaction temp: 280 °C**
Liquid	0	9.1%	11.1%
Solid	100%	86.6%	82.8%
Gas	0	4.3%	6.0%
pH of torrefaction liquid	0	2.16	2.03
Acetic acid in torrefaction liquid	0	7.9%	12.4%
Biomass analysis			
Acetyl content	1.51%	0.74%	0.71%
Cellulose	43.0%	46.9%	44.9%
Hemi-cellulose	26.1%	12.2%	6.8%
Lignin	28.2%	39.5%	45.8%
Carbon	50.3%	53.6%	55.2%
Hydrogen	6.06%	5.75%	5.75%
Nitrogen	0.10%	0.10%	0.11%
Oxygen	43.5%	40.6%	39.0%
Pyrolysis			
Yields (dry basis)			
Liquid	46.9%	55.4%	52.4%
Gas	37.6%	31.6%	24.1%
Char	15.4%	13.0%	23.5%
Pyrolysis yields (pyrolysis taking into account torrefaction loss)			
Liquid	46.9%	48.0%	43.4%
Gas	37.6%	27.4%	19.9%
Char	15.4%	11.3%	19.5%
Overall system yields (pyrolysis plus torrefaction)			
Total liquid	46.9%	59.8%	57.4%
Total gas	37.6%	29.0%	23.1%
Total char	15.4%	11.3%	19.5%
Bio-oil analysis			
Water	24.0%	4.3%	4.4%
Non-water pyrolysis liquid yield	35.5%	53.0%	50.1%
Non-water overall yield (taking into account loss during torrefaction)	35.5%	45.9%	41.5%
Ultimate analysis, dry			
Carbon	51.5%	52.6%	51.9%
Hydrogen	6.15%	6.2%	6.2%
Nitrogen	0.45%	0.7%	1.1%

Oxygen, by diff	41.9%	40.4%	40.8%
GPC			
Average number, Mn [g/mol]	246.4	215.2	214.2
Weight average, Mw (g/mol)	327.6	273.7	274.8
Size average, Mz (g/mol)	470.9	375.3	385.4
Mw/Mn, D ()	1.33	1.27	1.28
Mp [g/mol]	173	161.1	161.1
% above 650 Mw (pyrolytic lignin)	8.10%	4.00%	4.34%
Max MW (g/mol)	1710	1558	1751
HPLC			
Acetic acid, wt %	3.50%	0.15%	0.14%
H-NMR normalised			
0.5-1.6 Alkanes (C-C)	4.43%	3.77%	3.22%
1.6-2.2 Organic acids (C=OO-), CH2, carbonyl (C=O)	8.43%	6.97%	5.68%
2.2-3.0 Ketone (O=CH), ArCH3, Ar=CH2	5.38%	7.89%	7.14%
3.0-4.2 Alcohols (C-OH), methoxy (O-CH3),	9.05%	13.27%	10.99%
4.2-6.0 Ethers (lignin derived methoxyphenols) (C-O-C), carbohydrates, phenols	8.26%	14.24%	15.33%
6.0-8.5 Aromatics (ArH), phenols (ArOH), olefins (HC=C)	5.43%	9.14%	10.73%
9.5-10.1 Aldehydes (CH=O)	0.38%	0.32%	0.38%

Yellow indicates important variables and the bio-oil samples with the best properties

7.2 Temperature profiles for pyrolysis of raw and pretreated biomass

The temperature profiles for raw biomass are displayed in Figure A-1, Figure A-2, and Figure A-3 for pyrolysis at the optimal conditions and in Figure A-4, Figure A-5, and Figure A-6 for pyrolysis of pretreated biomass at the optimal conditions. Channel 0 (PH tag) gives the temperature of the N_2 preheating gas entering the pyrolysis reactor. Channel 1 (FB tag) monitored the internal temperature at the bottom of the fluidised bed but this was later changed to a temperature controller so the port was redundant. Channel 2 (CY tag) gives the temperature of the vapours exiting the cyclone. Channel 3 (C1 tag) gives the temperature of the vapours entering condenser 1. Channel 4 (C2 tag) gives the temperature of the vapours entering condenser 2 and exiting condenser 1. Channel 5 (C3 tag) gives the temperature of the vapours entering condenser 3 and exiting condenser 2. Channel 6 (C4 tag) gives the temperature of the vapours exiting condenser 3 and entering the ESP. Channel 7 (Char tag) gives the temperature of the char in the char pot.

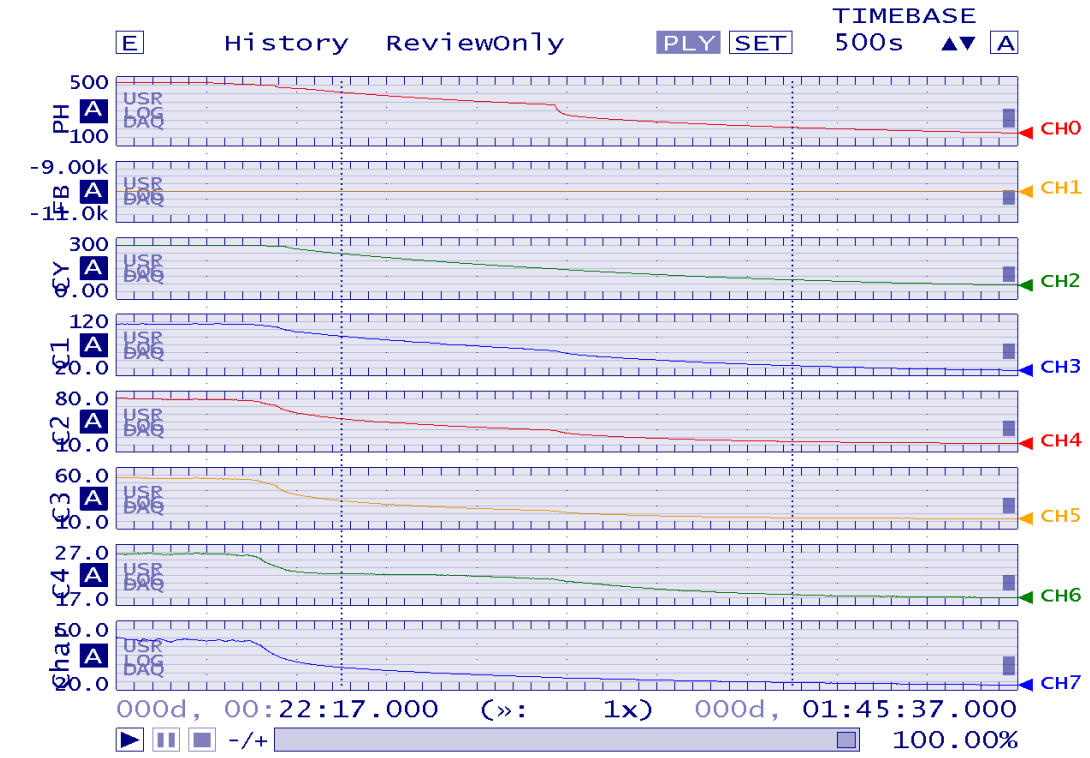

Figure A-1: Temperature profiles for pyrolysis of raw biomass at the optimal conditions

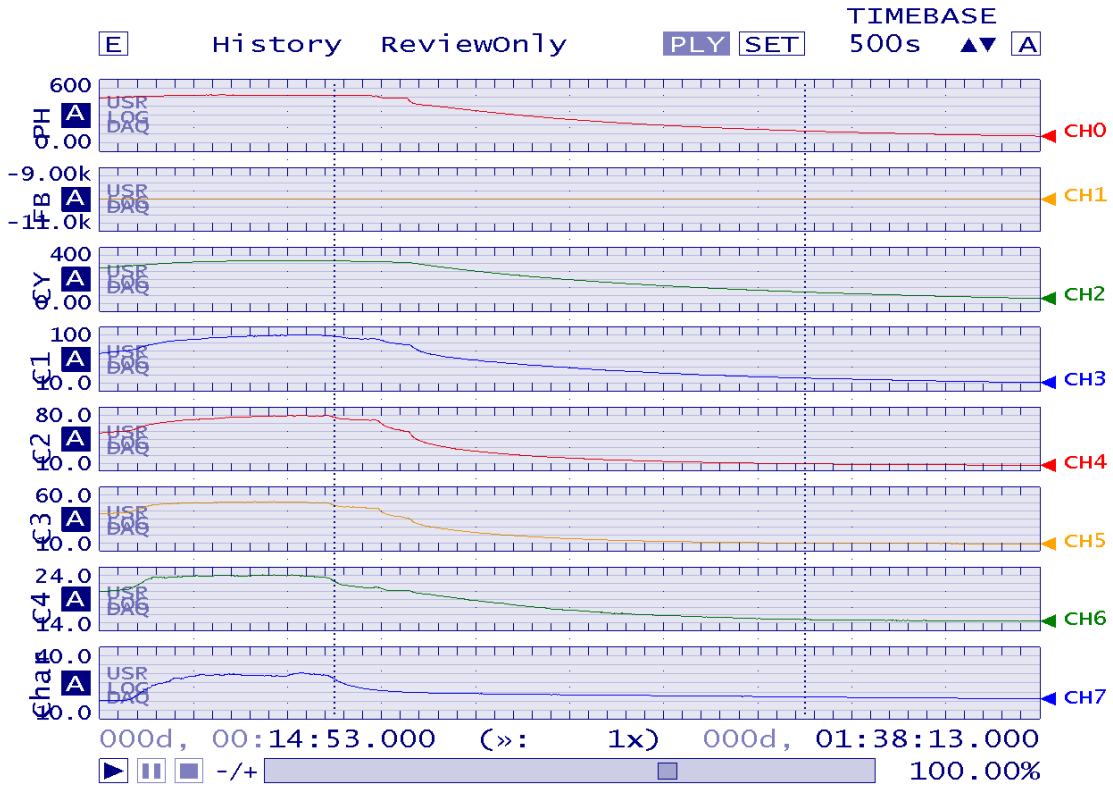

Figure A-2: Temperature profiles for pyrolysis of raw biomass at the optimal conditions

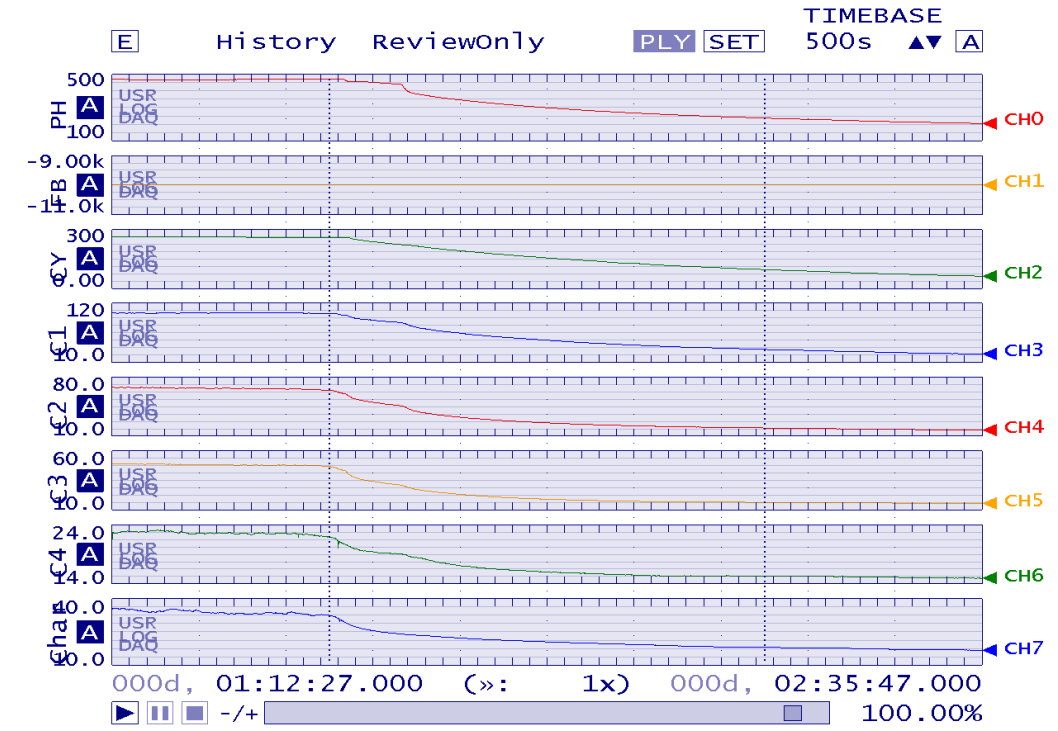

Figure A-3: Temperature profiles for pyrolysis of raw biomass at the optimal conditions

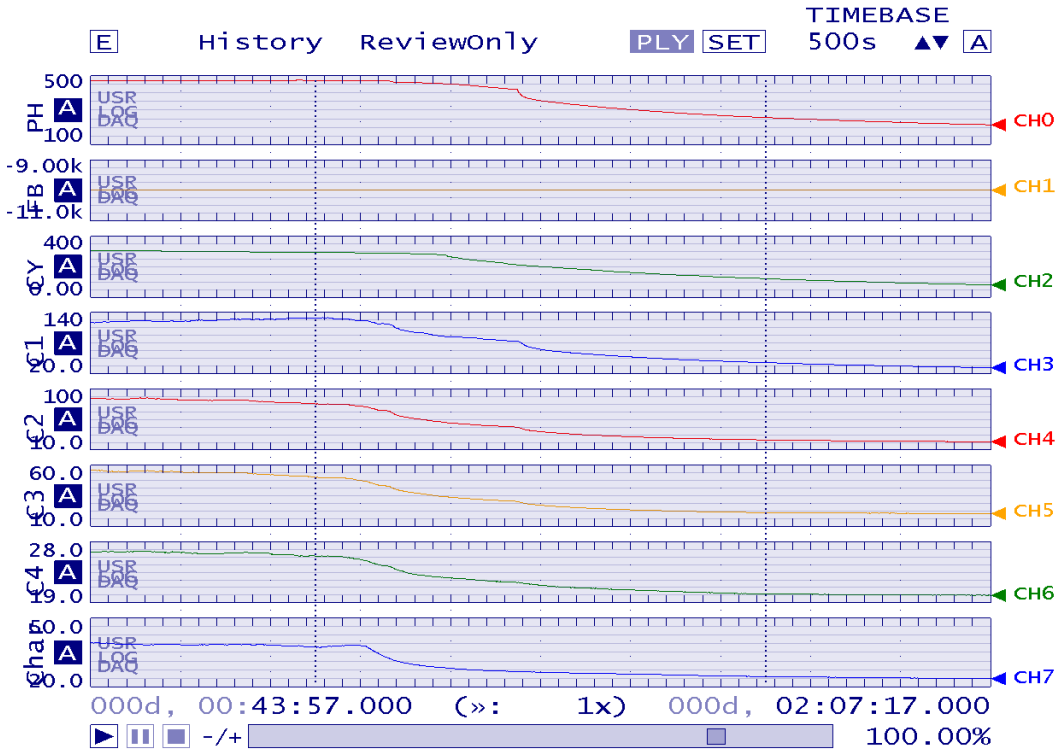

Figure A-4: Temperature profiles for pyrolysis of pretreated biomass at the optimal conditions

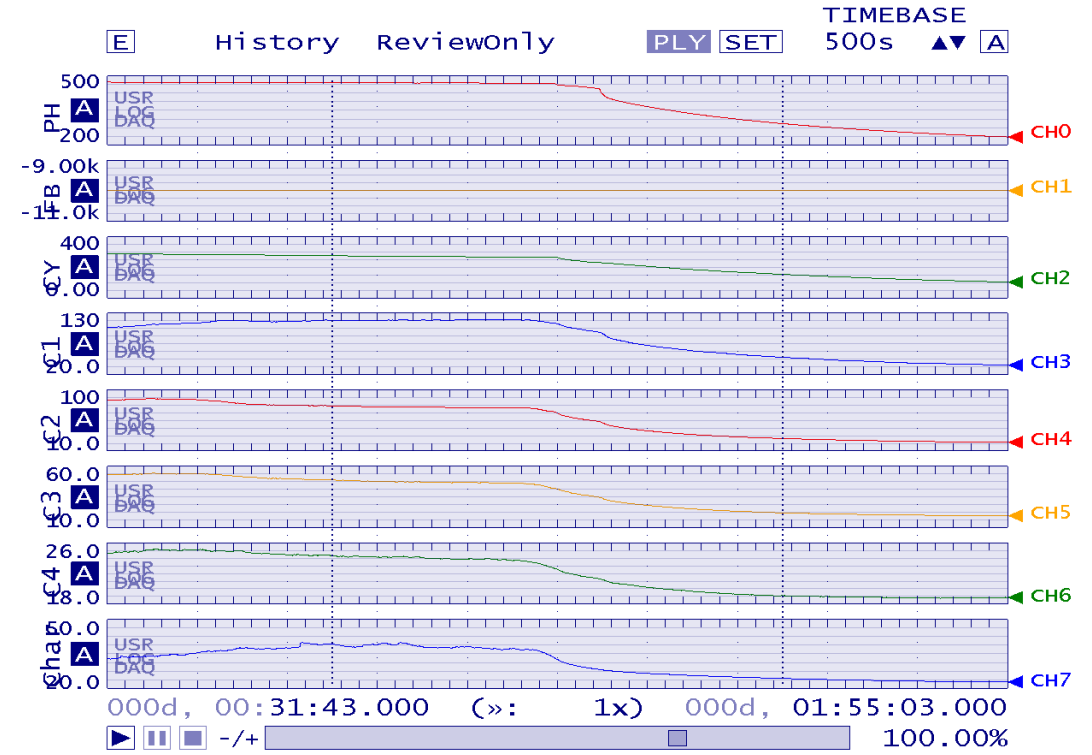

Figure A-5: Temperature profiles for pyrolysis of pretreated biomass at the optimal conditions

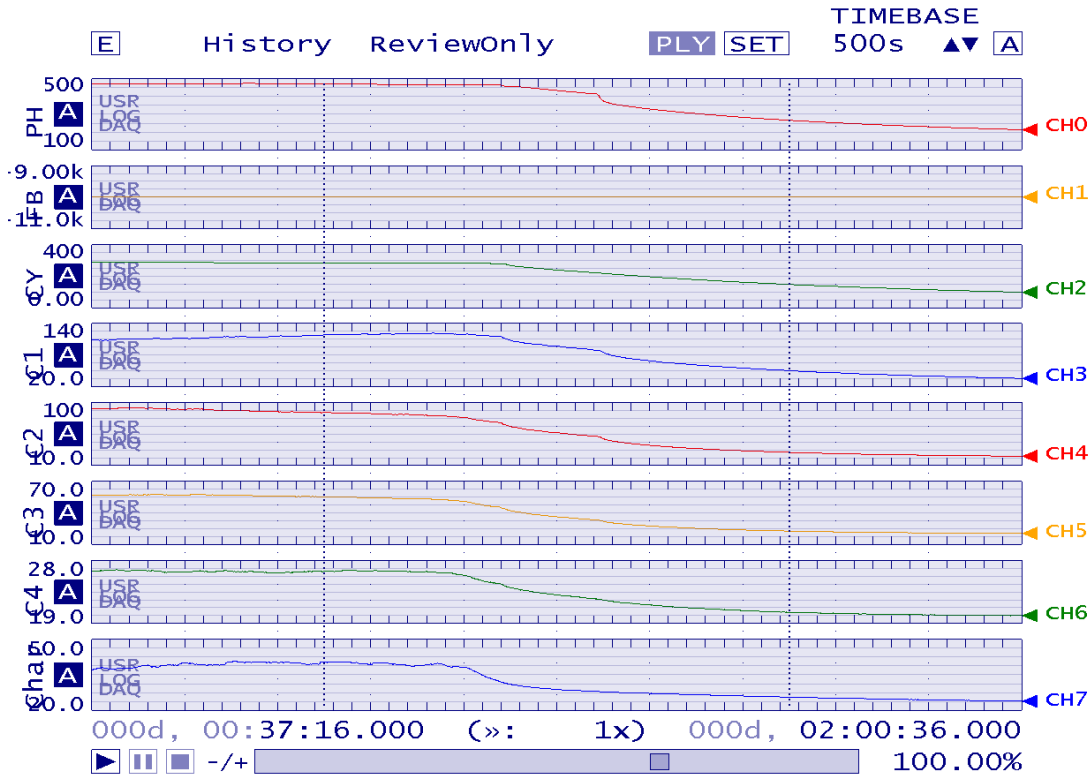

Figure A-6: Temperature profiles for pyrolysis of pretreated biomass at the optimal conditions

7.3 H-NMR spectrums for raw bio-oil

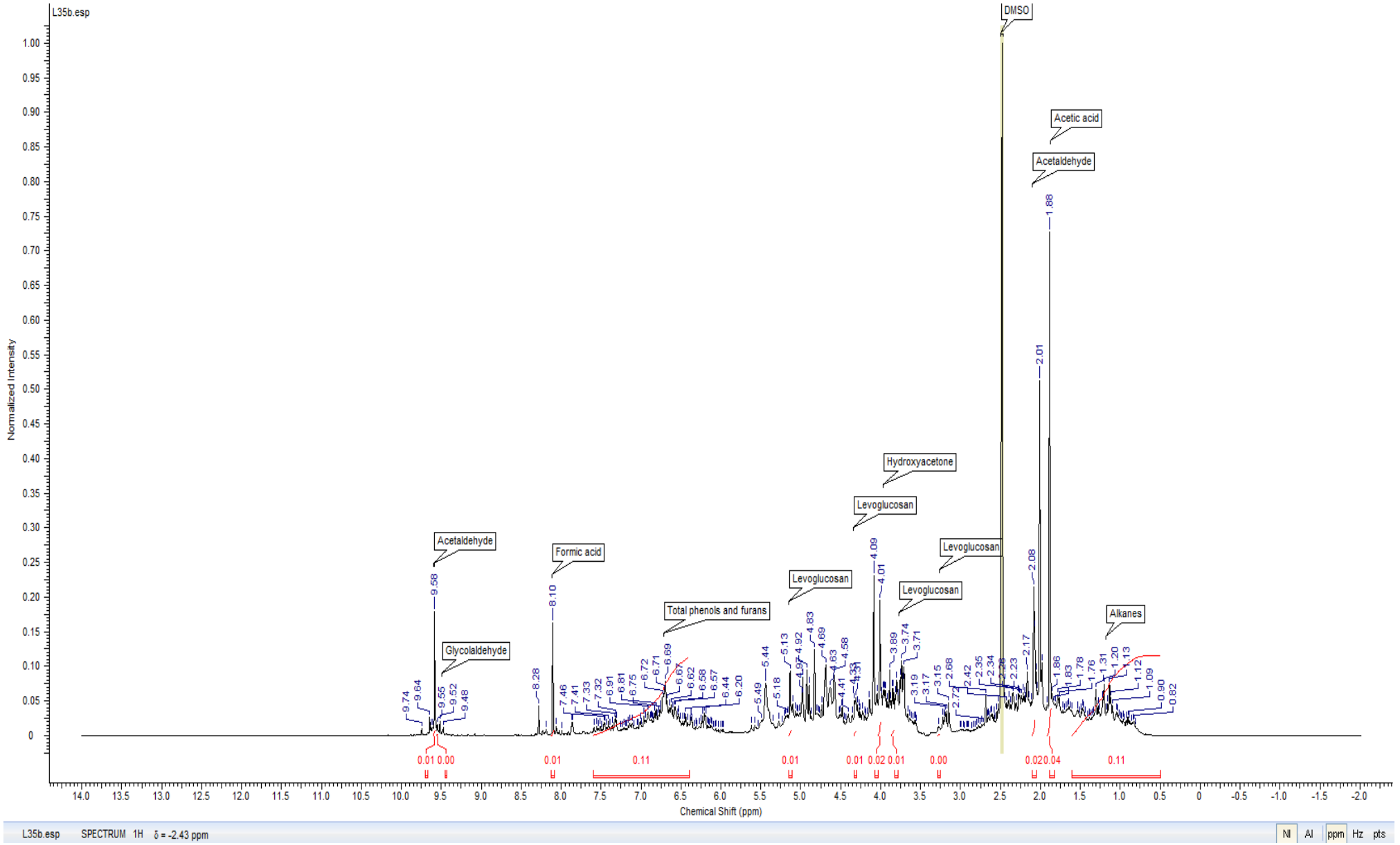

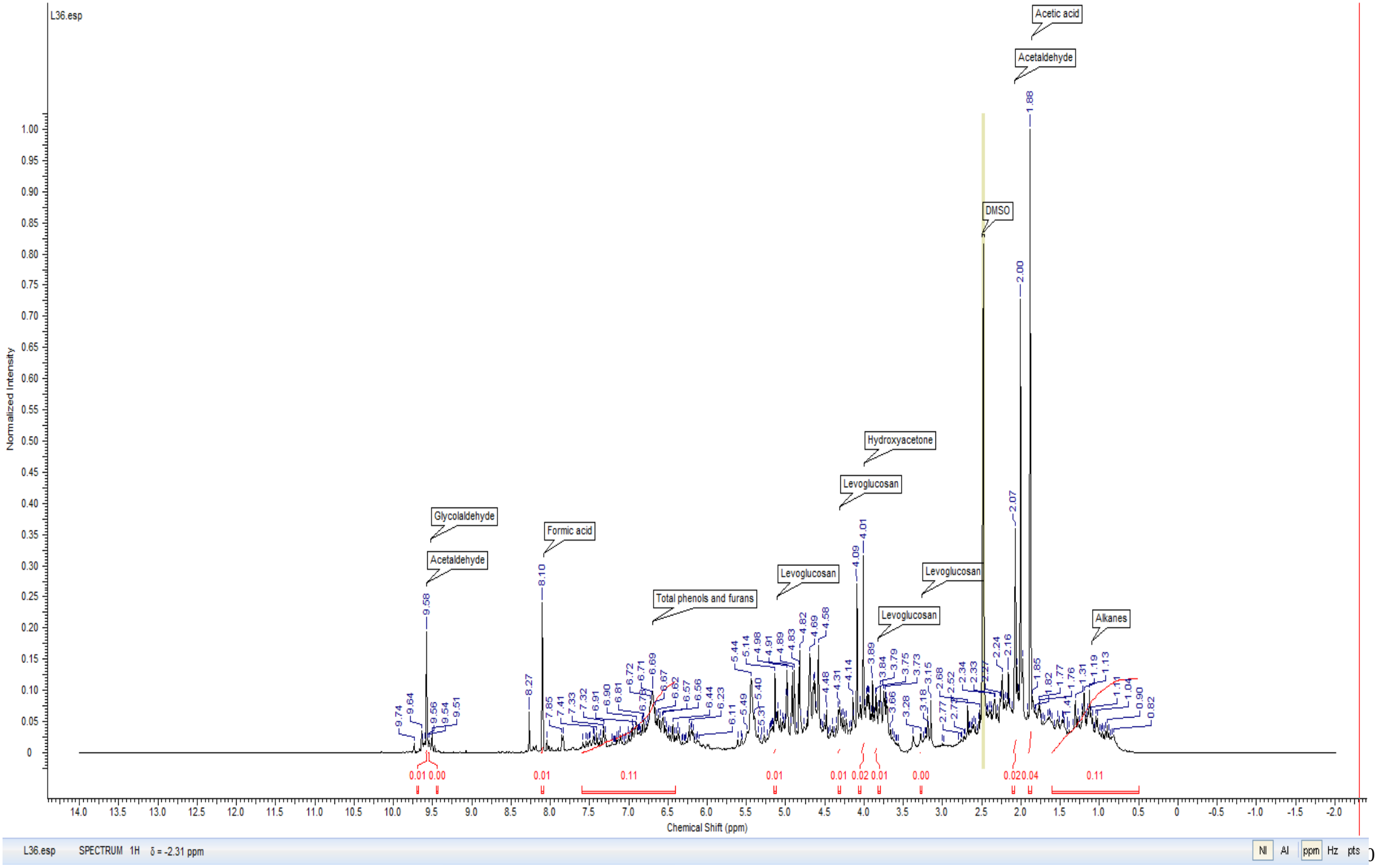
L36.esp
Acetic acid
Acetaldehyde
DMSO
Glycolaldehyde
Acetaldehyde
Formic acid
Total phenols and furans
Levoglucosan
Hydroxyacetone
Levoglucosan
Levoglucosan
Levoglucosan
Alkanes
Normalized Intensity
Chemical Shift (ppm)
L36.esp SPECTRUM 1H δ = -2.31 ppm

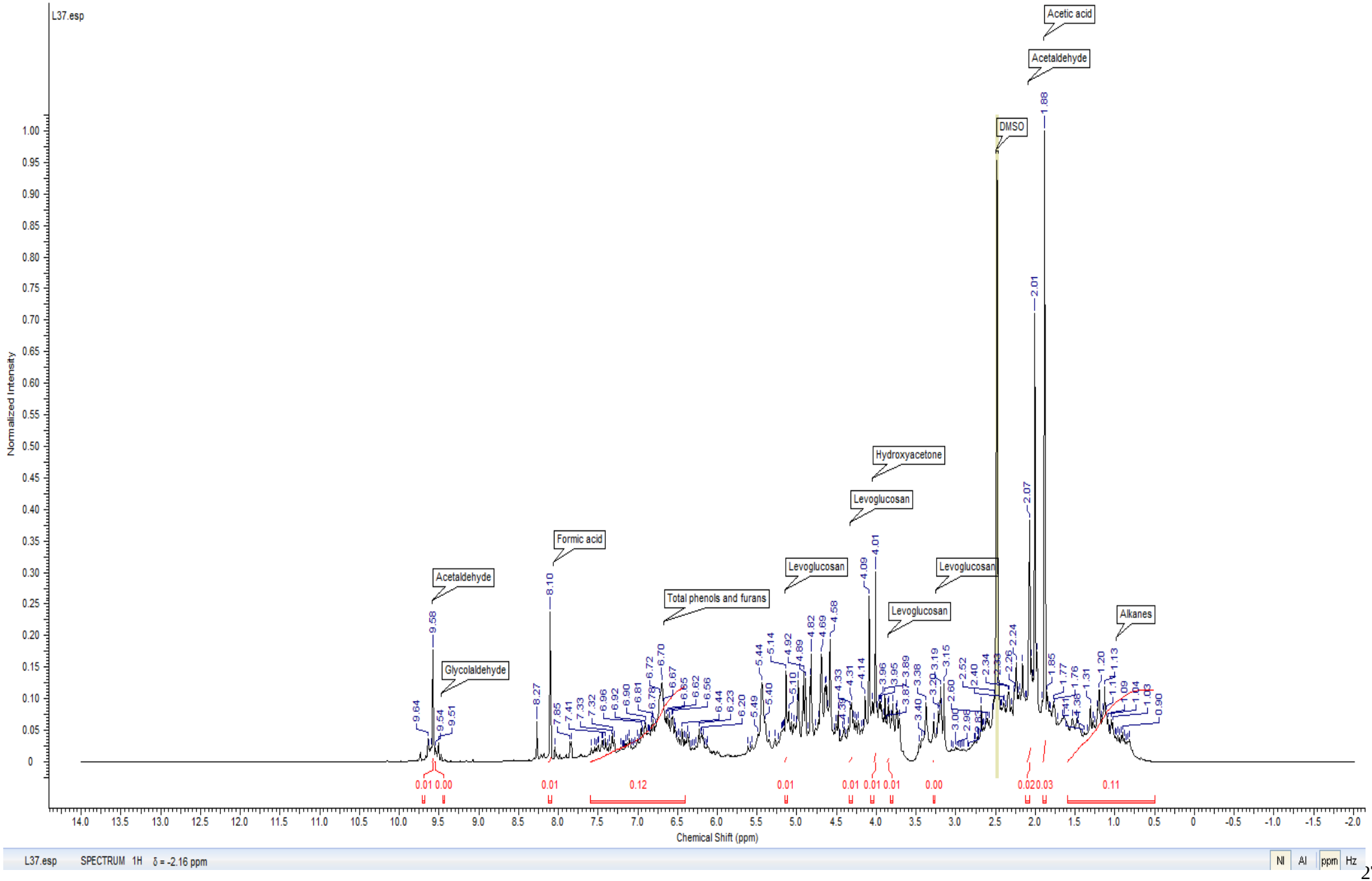
L37.esp
Acetic acid
Acetaldehyde
DMSO
Hydroxyacetone
Levoglucosan
Formic acid
Levoglucosan
Levoglucosan
Levoglucosan
Total phenols and furans
Acetaldehyde
Glycolaldehyde
Alkanes
Normalized Intensity
Chemical Shift (ppm)
L37.esp SPECTRUM 1H δ = -2.16 ppm
NI AI ppm Hz

7.4 H-NMR spectrums for pretreated bio-oil

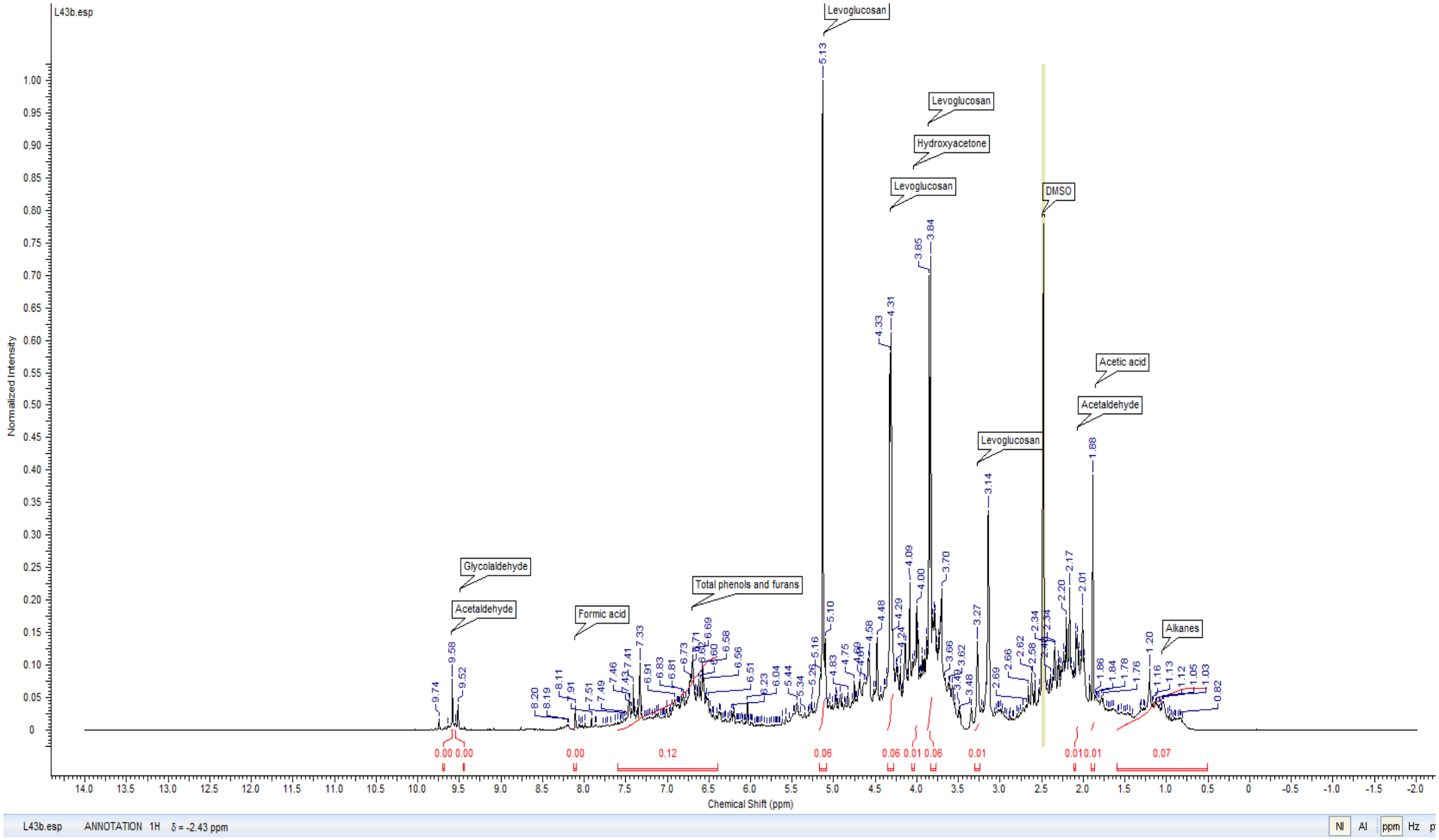

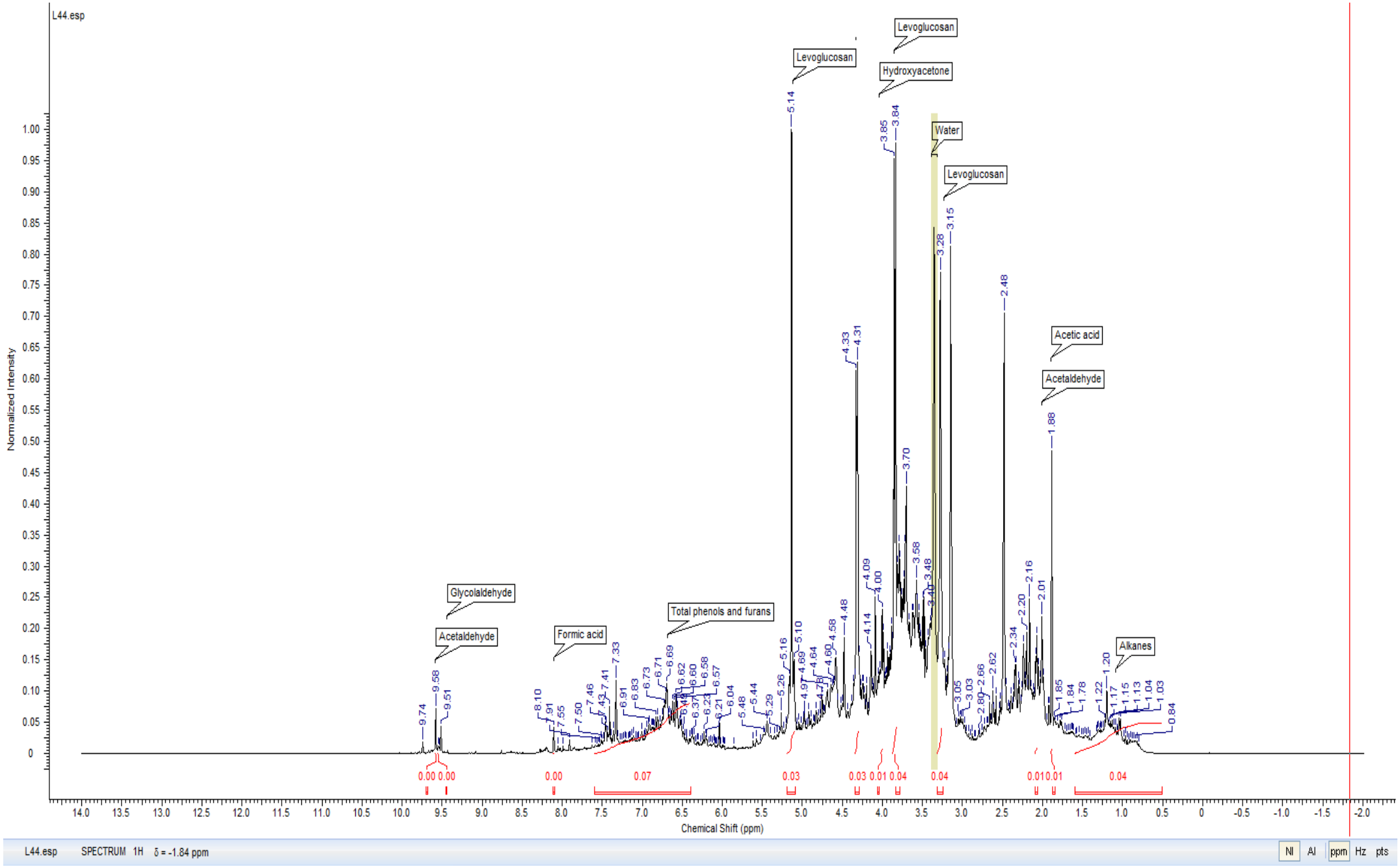
L44.esp
Levoglucosan
Levoglucosan
Hydroxyacetone
Water
Levoglucosan
Acetic acid
Acetaldehyde
Glycolaldehyde
Acetaldehyde
Formic acid
Total phenols and furans
Alkanes
Normalized Intensity
Chemical Shift (ppm)
L44.esp SPECTRUM 1H δ = -1.84 ppm
NI AI ppm Hz pts

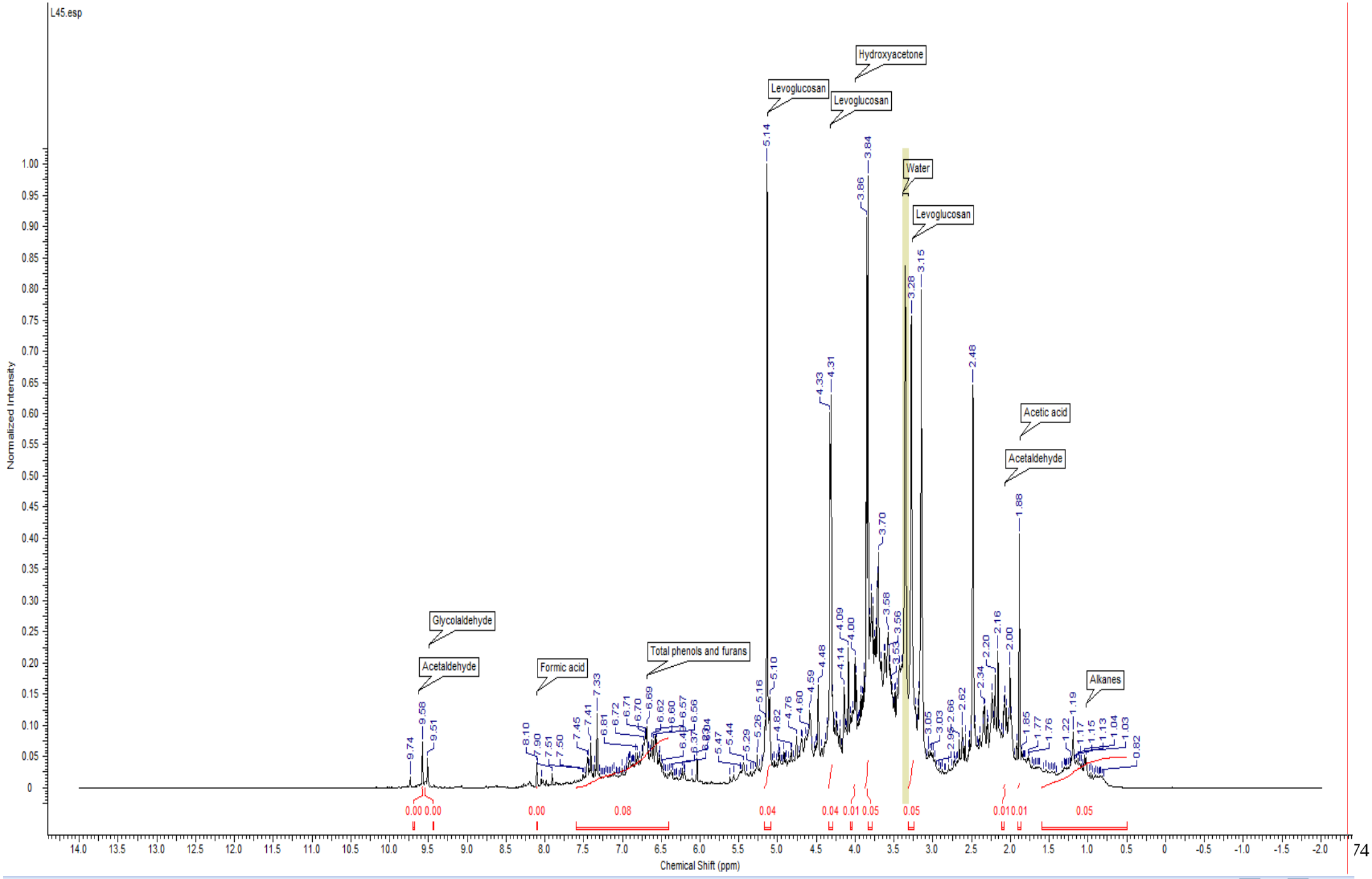
L45.esp
Hydroxyacetone
Levoglucosan
Levoglucosan
Water
Levoglucosan
Acetic acid
Acetaldehyde
Glycolaldehyde
Acetaldehyde
Formic acid
Total phenols and furans
Alkanes
Normalized Intensity
Chemical Shift (ppm)
L45.esp SPECTRUM 1H δ = -2.34 ppm
NI AI ppm Hz pts

Appendix 8

8.1 Economics

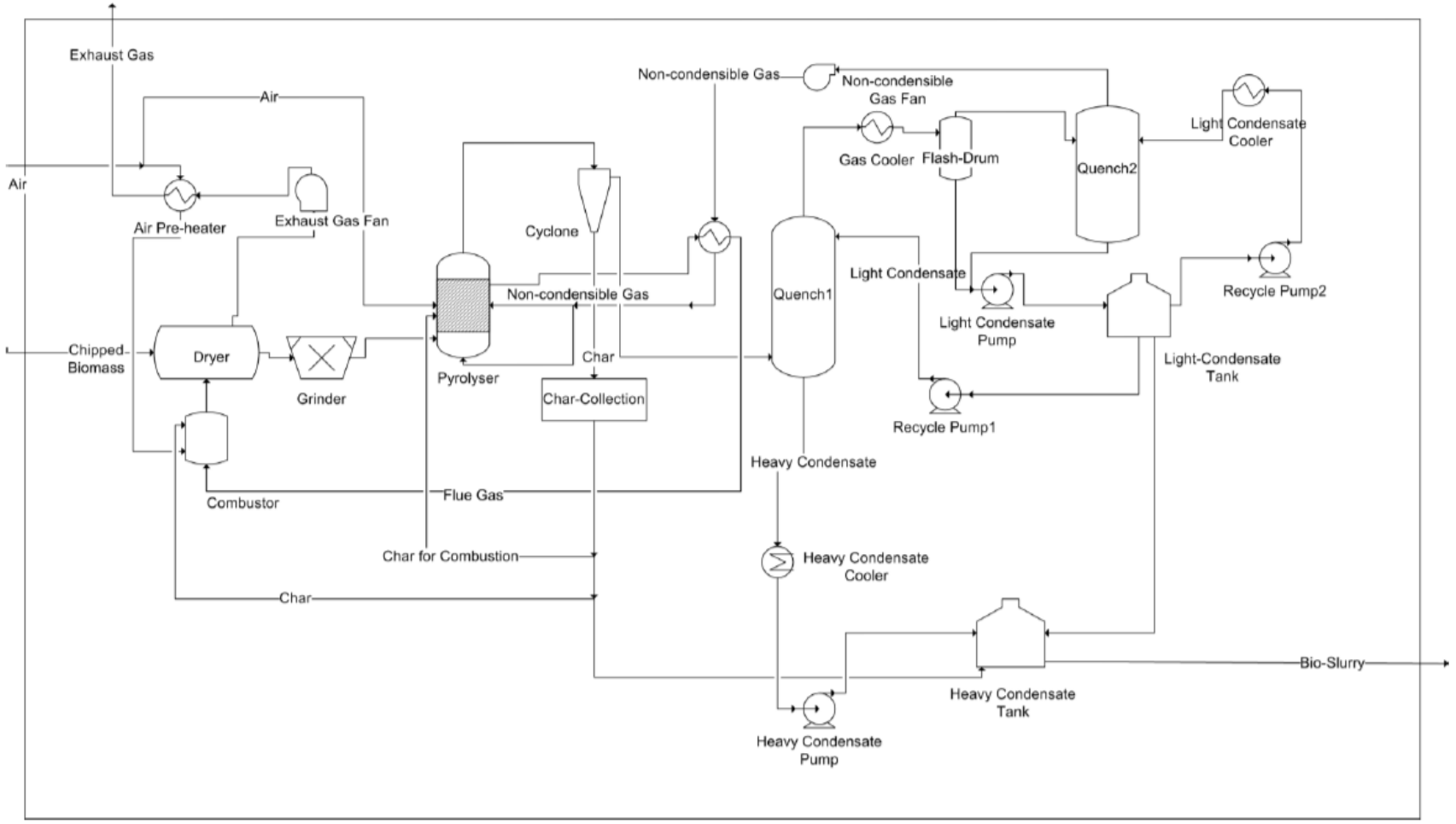

Figure A-1: Piping and instrumental diagram for pyrolysis of biomass, extracted from Puladian [6]